THE THERMOTECTONIC HISTORY OF THE GRENVILLE PROVINCE OF WESTERN LABRADOR

JAMES N. CONNELLY, B.Sc., M.Sc.

NOTICE

The quality of this microform is heavily dependent upon the quality of the original thesis submitted for microfilming. Every effort has been made to ensure the highest quality of reproduction possible.

If pages are missing, contact the university which granted the degree.

Some pages may have indistinct print especially if the original pages were typed with a poor typewriter ribbon or if the university sent us an inferior photocopy.

Reproduction in full or in part of this microform is governed by the Canadian Copyright Act, R.S.C. 1970, c. C-30, and subsequent amendments.

AVIS

La qualité de cette microforme dépend grandement de la qualité de la thèse soumise au microfilmage. Nous avons tout fait pour assurer une qualité supérieure de reproduction.

S'il manque des pages, veuillez communiquer avec l'université qui a conféré le grade.

La qualité d'impression de certaines pages peut laisser à désirer, surtout si les pages originales ont été dactylographiées à l'aide d'un ruban usé ou si l'université nous a fait parvenir une photocopie de qualité inférieure.

La reproduction, même partielle, de cette microforme est soumise à la Loi canadienne sur le droit d'auteur, SRC 1970, c. C-30, et ses amendements subséquents.

THE THERMOTECTONIC HISTORY OF THE GRENVILLE PROVINCE OF WESTERN LABRADOR

by

© JAMES N. CONNELLY, B.Sc., M.Sc.

A thesis submitted to the School of Graduate
Studies in partial fulfilment of the
requirements for the degree of
Doctor of Philosophy

Department of Earth Sciences
Memorial University of Newfoundland
May 1991

St. John's Newfoundland

ISBN 0-315-68275-2

Canada

ABSTRACT

The Grenville Orogen in western Labrador has been divided into three lithologically distinct terranes comprising, from the Grenville Front towards the southeast, the Gagnon, Molson Lake and Lac Joseph terranes. Of these terranes, only the Lac Joseph Terrane is devoid of lithologies that may be correlated with units to the north of the Grenville Front in the pre-Grenvillian, stable North American craton.

In the Lac Joseph Terrane, high grade polydeformed migmatitic pelitic supracrustal rocks contain two distinct leucosomes which have been dated at 1658+36/-8 Ma and 1639+12/-7 Ma by U/Pb geochronology; a third migmatitic sample which is retrogressed yielded an age of 1611+13/-6 Ma. These ages indicate that the gneisses in the Lac Joseph Terrane all formed during the Labradorian Orogeny, which must have been a protracted event. High grade metamorphism and migmatization of the supracrustal rocks was synchronous with folding and the development of localized shear zones, one of which has yielded a U-Pb age of 1634+13/-4 Ma. Sillimanite and/or kyanite-bearing mineral assemblages in the restite of the pelitic migmatites occur throughout Lac Joseph Terrane, and also formed during the Labradorian Orogeny. They yield P-T estimates (garnet - biotite geothermometry and garnet - plagioclase - aluminosilicate - quartz geobarometry) between 575-800°C and 3-8 kbar in the southern Lac Joseph Terrane to 700-850°C and 6-10 kbar in the northwestern part of the terrane. Granitoid rocks were emplaced into the Lac Joseph Terrane throughout the Labradorian Orogeny; a gabbroic pluton of the Ossokmanuan Intrusive Suite has yielded a U/Pb age of 1623±7 Ma.

Synchronous with Labradorian metamorphism in the Lac Joseph Terrane, granitoid rocks were emplaced into the adjacent Molson Lake Terrane, one body of which yielded a U-Pb zircon age of 1648±7 Ma. No evidence exists to suggest that these granitoid rocks, which are interpreted to represent a southwestern extension of the Trans Labrador Batholith, were tectonized during the Labradorian Orogeny. The Shabogamo Intrusive Suite, the only other unit in the Molson Lake Terrane, intruded

into the granitoid rocks at 1431 $\pm$ 7 Ma during a period of south-southeast - north-northwest crustal extension; this unit is correlated, on the basis of geochemistry and age, with the Michael Gabbro of eastern Labrador.

Retrogression of granulite facies basic gneisses in the Lac Joseph Terrane to amphibolite facies assemblages took place, at least locally, at about 1281 Ma, as recorded by U/Pb (titanite) and $^{40}Ar/^{39}Ar$ (hornblende) isotopic systematics. The tectonic significance of this event is not understood.

The Molson Lake Terrane was extensively recrystallized and deformed during the Grenvillian Orogeny (1001 Ma - 990 Ma; U/Pb sphene and zircon data), locally under high P - moderate T conditions, between 8-12 kbar and 650-850°C (garnet - clinopyroxene geothermometry and garnet - clinopyroxene - plagioclase - quartz geobarometry). The near coincidence of Grenvillian U-Pb and $^{40}Ar/^{39}Ar$ ages from the Molson Lake Terrane suggests that this terrane was rapidly exhumed after peak metamorphism, probably along a crustal scale, frontal thrust zone. The Lac Joseph Terrane experienced only minor heating and non-penetrative deformation during the Grenvillian Orogeny; the preservation of a pre-Grenvillian $^{40}Ar/^{39}Ar$ amphibole age in the Lac Joseph Terrane while Ar was reset in biotite and muscovite, indicates that temperatures during this event were between about 350°C and 530°C. The Lac Joseph Terrane is thought to have been emplaced as a pre-assembled, coherent package over the Molson Lake Terrane late in the Grenvillian Orogeny along a decollement at, or near, the brittle-ductile transition. Rocks in the Lac Joseph Terrane preserving Labradorian, deeper level P-T conditions were thus emplaced over freshly exhumed rocks, recording Grenvillian P-T conditions, in the Molson Lake Terrane.

ACKNOWLEDGEMENTS

I am indebted to Toby Rivers, the supervisor of this study. Toby's guidance, support and enthusiasm throughout this project have made an immeasurable difference to its outcome and are sincerely appreciated.

Much of the field work and sample collection were accomplished while I was employed by the Newfoundland Department of Mines and Energy; the support of the department and discussions with colleagues there, in particular, Richard Wardle, Ges Nunn, Charlie Gower, Brian O'Brien and Pat O'Neill were very helpful. Pam Scowen was responsible for approximately half the mapping in the first summer; I am grateful for her conscientious work and friendship in the first season. Field crew members are thanked for their competent, zealous assistance.

Discussions with Flemming Mengel about geology, in particular geothermobarometry, and other totally unrelated subjects have been of great benefit and enjoyment. His generosity with computer programs and programming skills was invaluable. The first aid skills of Henry Longerich and Geoff Vienott, as applied to the electron microprobe, were critical to the geothermobarometric work. David MacNeil's advice on the pitfalls of AutoCad and other related computer dilemmas was very useful. Valuable exchanges of information came about through discussions with Jeroen van Gool and Dennis Brown.

U-Pb geochronology was performed at the Royal Ontario Museum (ROM), Toronto, Ontario; Tom Krogh's enthusiasm for the project and generosity with laboratory resources are much appreciated. The U-Pb component of this thesis would certainly not have been possible without Larry Heaman at the ROM; his patience, perseverance and good company made for productive and enjoyable visits to Toronto. Discussions with and assistance by the technical staff and researchers at the ROM were invaluable. Ken Booth and Margaret Napier are thanked for their brilliant hospitality in Toronto, as are the GO train commuters for providing, daily amusement. John Hanes of Queen's University at Kingston is thanked for his interest and efforts in producing the

$^{40}Ar/^{39}Ar$ data reported in this work. Discussion with Greg Dunning, in part fueled by his fascination with problems in the Grenville Province, have been a tremendous asset; his comments on an earlier version of this thesis were most helpful.

A Memorial University Fellowship awarded for the duration of this study is gratefully acknowledged. The author's expenses while at the ROM were funded through NSERC grants to Toby Rivers.

Finally, I would like to thank Kathy Manser to whom I am indebted on many fronts; from field work in blizzard conditions, to the pasting of photographs, she has provided assistance and moral support far beyond the call of duty. I am most grateful for her help, patience and friendship throughout.

TABLE OF CONTENTS

LIST OF TABLES

LIST OF FIGURES

LIST OF PHOTOS

ABBREVIATIONS

Ab	albite	Al6	octahedral cooridinated Al
alm	almandine	°C	degrees Celcius
als	aluminosilicate	°K	degress Kelvin
amph	(or amp) amphibole	K	equilibrium constant
An	anorthite	kbar	kilobar
bio	biotite	P	pressure
chl	chlorite	P-T	pressure-temperature
cpx	clinopyroxene	T	temperature
epi	epidote	R	1.987 cal/°
gnt	garnet	W	Margules Parameter
gro	grossular	X	mole fraction
hbl	hornblende		
K-fsp	K-feldspar		
ky	kyanite		
l	liquid	$^{40}Ar/^{39}Ar$	$^{40}Argon/^{39}Argon$
mus	(or musc) muscovite	Ma	million years before present
opx	orthopyroxene	m.y.	million years
Or	orthoclase	U/Pb	Uranium - Lead
phl	phlogopite		
pla	(or plg; pl) plagioclase		
pyr	pyrope		
qtz	(or qz) quartz		
sil	sillimanite		
ttn	titantite		
v	vapour		
zir	zircon		

CHAPTER 1
INTRODUCTION

1.1 Preamble

The Grenville Orogen, with its extensions in Mexico and Scandinavia, flanks the eastern edge of the North American (Laurentian) and Baltic Shields. Early theories concerning the development of the Grenville Orogen envisaged the majority of the orogen as juvenile crust accreted to a previously stabilized North American craton at about 1.0 Ga (see Wynne-Edwards (1972) for review). Such theories were gradually abandoned as reworked extensions of older Precambrian orogenic belts were recognized within the orogen (Wynne-Edwards, 1972). The challenge to distinguish between Grenvillian and pre-Grenvillian rocks and thermotectonic events became and remains pivotal in determining the extent, intensity and style of the Grenvillian Orogeny. Such work must, therefore, precede the formulation of realistic models to describe the processes which occurred during this major orogenic event. In many areas, the nature and magnitude of Grenvillian tectonism relative to pre-Grenvillian events still remains uncertain.

In this study, three sub-disciplines of the earth sciences are integrated in an analysis of the tectonic history of part of the Grenville Orogen in western Labrador. The initial phase of field mapping provided the framework within which the other aspects of the project were conceived, planned and executed. Results of the mapping helped to elucidate the lithological patterns, terranes, terrane boundaries and distribution of structural elements and metamorphic mineral assemblages in the map area. These data provided first order constraints on the style and relative ages of major thermotectonic events. Further constraints were subsequently furnished by an analysis of metamorphic mineral assemblages and by geothermobarometry, which permitted quantification of absolute differences in the P-T conditions within and between terranes. At this stage, having established a relative chronology, geochronological techniques were employed to constrain and/or determine the absolute timing of these events. Precise U-Pb geochronology was employed to determine the ages of intrusive rocks, migmatite generation and mineral recrystallization. $^{40}Ar/^{39}Ar$ geochronology was

utilized to determine the ages of the last thermal events which affected the different parts of the study area. Since western Labrador is typical of much of the northeastern Grenville Orogen, insights gained in this work may be applicable to areas where detailed work is presently unavailable, and may be extrapolated to constrain tectonic models of the orogen as a whole. Furthermore, knowledge of the timing, mechanisms and consequences of tectonism in this relatively deep orogenic belt will complement information from the more numerous geological studies in younger orogenic belts and will, therefore, contribute to a better understanding of orogenesis as a whole.

1.2 Project Logistics

The first field season (1986) of this project was executed while the author was in the employ of the Geological Survey Branch of the Newfoundland Department of Mines (NFDM) and responsible for 1:100,000 scale mapping of seven 1:50,000 map sheets in western Labrador (Fig. 1-1). This mapping was accomplished with a crew of five and full helicopter support. A second field season (1987), with a two person field party, was spent examining critical areas in more detail, with particular focus on terrane boundaries. Approximately 25 hours of NFDM supported helicopter time were dedicated to examining the relatively inaccessible northern region in the second field season.

The topography in the area is varied; granulite facies migmatites and basic intrusive rocks tend to form prominent highlands with excellent exposure, whereas a significant part of the area is covered by extensive string-bog with only rare exposures. The area is traversed by two electric power lines which emanate from Churchill Falls, one to Wabush-Labrador City, the other to the Hydro Quebec electric grid to the south (Fig. 1-1). The Quebec North Shore and Labrador (Q.N.S. & L.) Railway traverses the western part of the map area and its services initially figured prominently in plans for logistical support. These plans were subsequently altered, however, with the realization that an organization which excels in delivering millions of tons of iron ore annually might not be too concerned about the fate of a few kilograms of groceries.

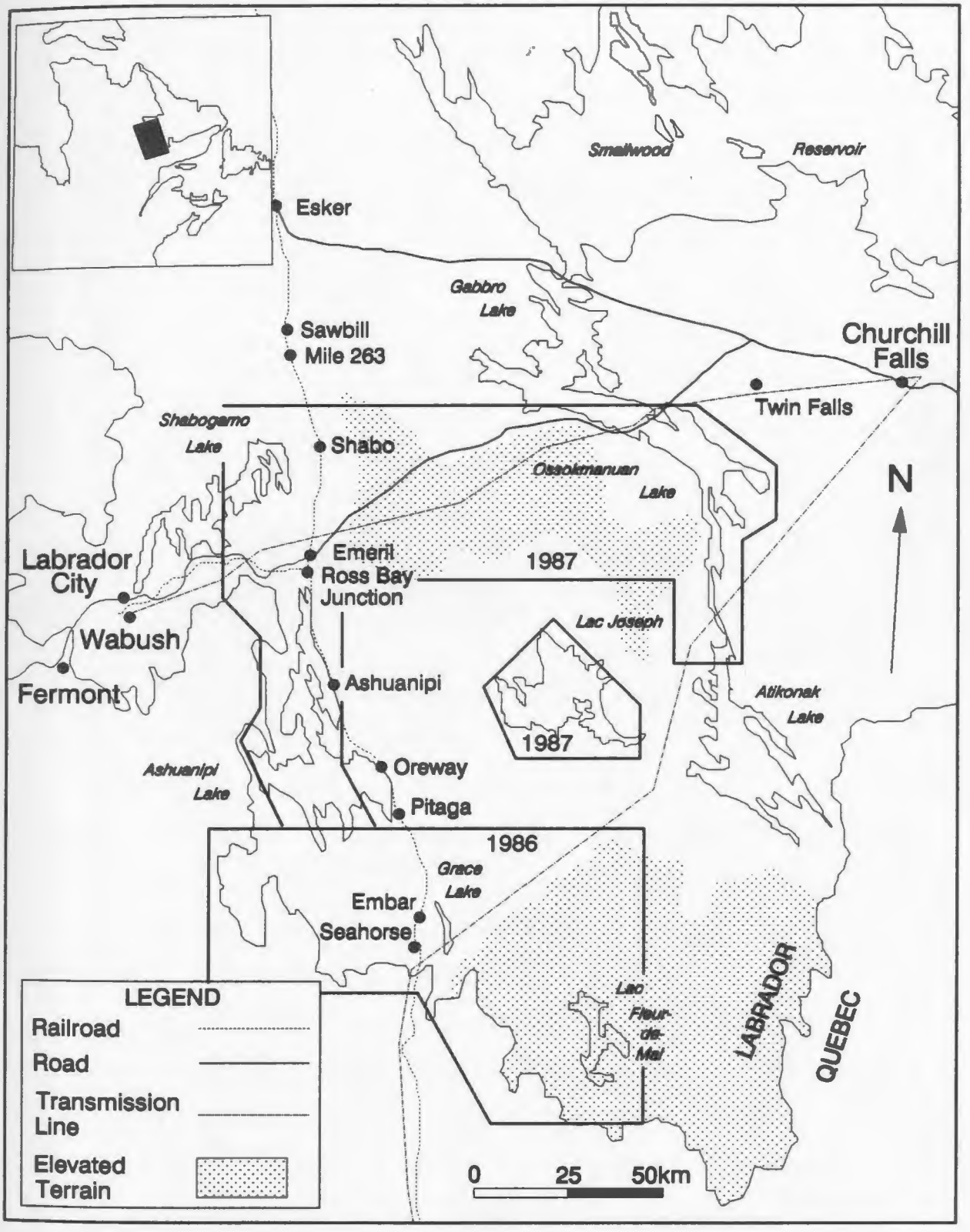

Figure 1-1: Location, physiography and access routes of western Labrador. Areas of study, with year of mapping, are outlined.

Electron microprobe analyses for geothermobarometry were performed at Memorial University. U-Pb geochronology was carried out during four visits to the Royal Ontario Museum (R.O.M.) in Toronto. The final steps in mineral separation of samples for $^{40}Ar/^{39}Ar$ analysis (initial steps performed at the R.O.M.) were performed by the author at Memorial University; analyses were conducted by Dr. J. Hanes at Queen's University at Kingston.

1.3 Synopsis of Previous Work

Figure 1.2 shows the locations of most recent previous mapping in western Labrador relevant to this project. The southeastern part of the area shown in Figure 1-2 was mapped at 1:250,000 scale and described briefly by Stevenson (1968) as part of the reconnaissance mapping during the 1960's by the Geological Survey of Canada (not shown on Fig. 1-2)). The southwestern part of the area was previously mapped by Jackson (1976) at 1:100,000 scale, but no report was issued (not shown on Fig. 1-2). The remaining areas, indicated in Figure 1.2, were mapped by personnel of the NFDM as part of their program to remap Labrador at 1:100,000 scale. Although most detailed reports have yet to be issued, preliminary or final maps as well as articles in Current Research of the NFDM are available for each map area.

Preliminary tectonic models for the Grenville Orogen in Labrador were proposed in the early to mid 1980's, mainly by NFDM personnel, based on mapping projects in western and eastern Labrador. This project was conceived in 1986 as a continuation of the regional mapping in western Labrador and the thesis research was to include related detailed work in order to test and refine these developing tectonic models.

1.4 Tectonic Framework of the Grenville Orogen

The northwestern boundary of the Grenville Orogen, the Grenville Front, is defined as the northwestern limit of penetrative Grenvillian metamorphic and deformational effects, beyond which lies the tectonic foreland consisting of a variety of pre-Grenvillian orogens (Rivers et al., 1989). In the Canadian Shield these comprise, from southwest to northeast, the Southern Province, Superior Province, Labrador

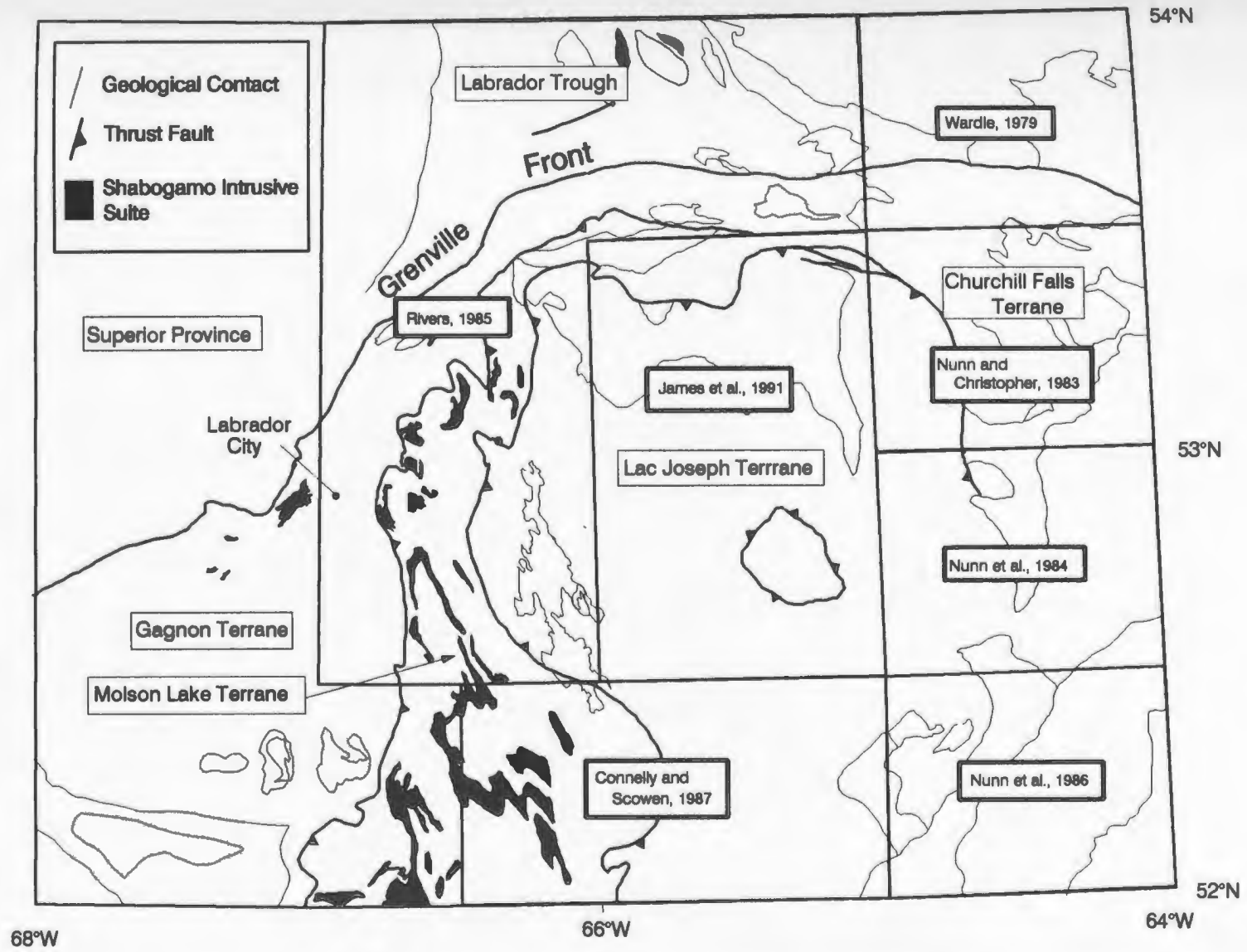

Figure 1-2: Location of previous geological mapping in western Labrador.

Trough or New Quebec Orogen, Churchill Province and Makkovik Province (Hoffman, 1989). The southeastern part of the Grenville Orogen is covered by upper Proterozoic and Paleozoic rocks of the Appalachian Orogen.

The exposed part of the Grenville Orogen has recently been subdivided into longitudinal, northeast-trending belts on the basis of tectonic history and relationship to the North American foreland (Fig. 1-3) (Rivers et al., 1989; see also Rivers, 1983; Rivers and Nunn, 1985; Thomas et al., 1985; Rivers and Chown, 1986; Wardle et al., 1986). These belts in turn are composed of terranes of distinct lithological and geophysical character. The Parautochthonous Belt adjacent the Grenville Front comprises terranes which exhibit links to the pre-Grenvillian foreland. The Allochthonous Monocyclic and Polycyclic Belts, situated within the interior of the orogen, contain terranes which lack demonstrable affinities with the foreland. The belts and terranes are characteristically bounded by ductile mylonite zones.

1.4.1 Parautochthonous Terranes of Western Labrador

The Parautochthonous Belt in southwestern Labrador is represented by three terranes known as the Gagnon, Molson Lake and Churchill Falls terranes (Fig. 1-3 and 1-4) (Rivers et al., 1989; Connelly et al., 1989a) which are distinguished on the basis of contrasting lithologies and pre-Grenvillian thermotectonic histories. Prior to this study, the Gagnon Terrane was thought to be immediately adjacent to the Lac Joseph Terrane. However, more detailed mapping during the course of this project revealed the existence of another terrane, referred to as the Molson Lake Terrane (Connelly et al., 1989a), which is composed of a lithologically distinct suite of rocks. The Molson Lake Terrane is separated from the Lac Joseph and Gagnon terranes by ductile mylonite zones.

The Gagnon Terrane predominantly comprises a continental margin sequence of metasedimentary rocks of the Knob Lake Group (part of the Kaniapiskau Supergroup in the New Quebec Orogen) which were largely undeformed in southwestern Labrador prior to the Grenvillian Orogeny (Rivers and Chown, 1986). These rocks were intruded by gabbros of the Middle Proterozoic Shabogamo Intrusive Suite and granitoid rocks of unknown age. The Molson Lake Terrane to the southeast, is characteristically devoid of supracrustal rocks, being composed principally of granitoid rocks and gabbro of the

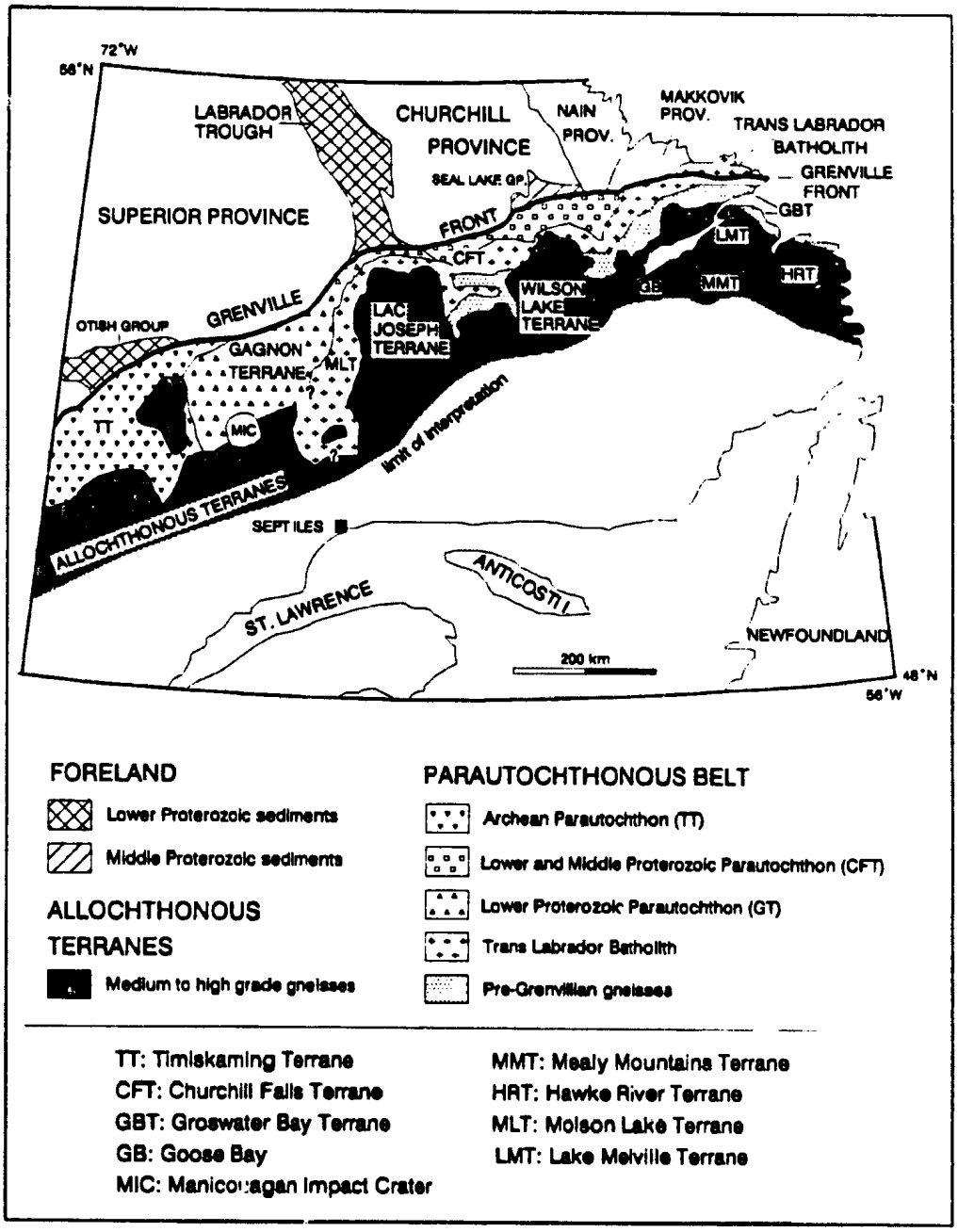

Figure 1-3: Tectonic subdivisions of the eastern Canadian Shield. Subdivisions in the Grenville Province modified from Rivers and Chown (1986).

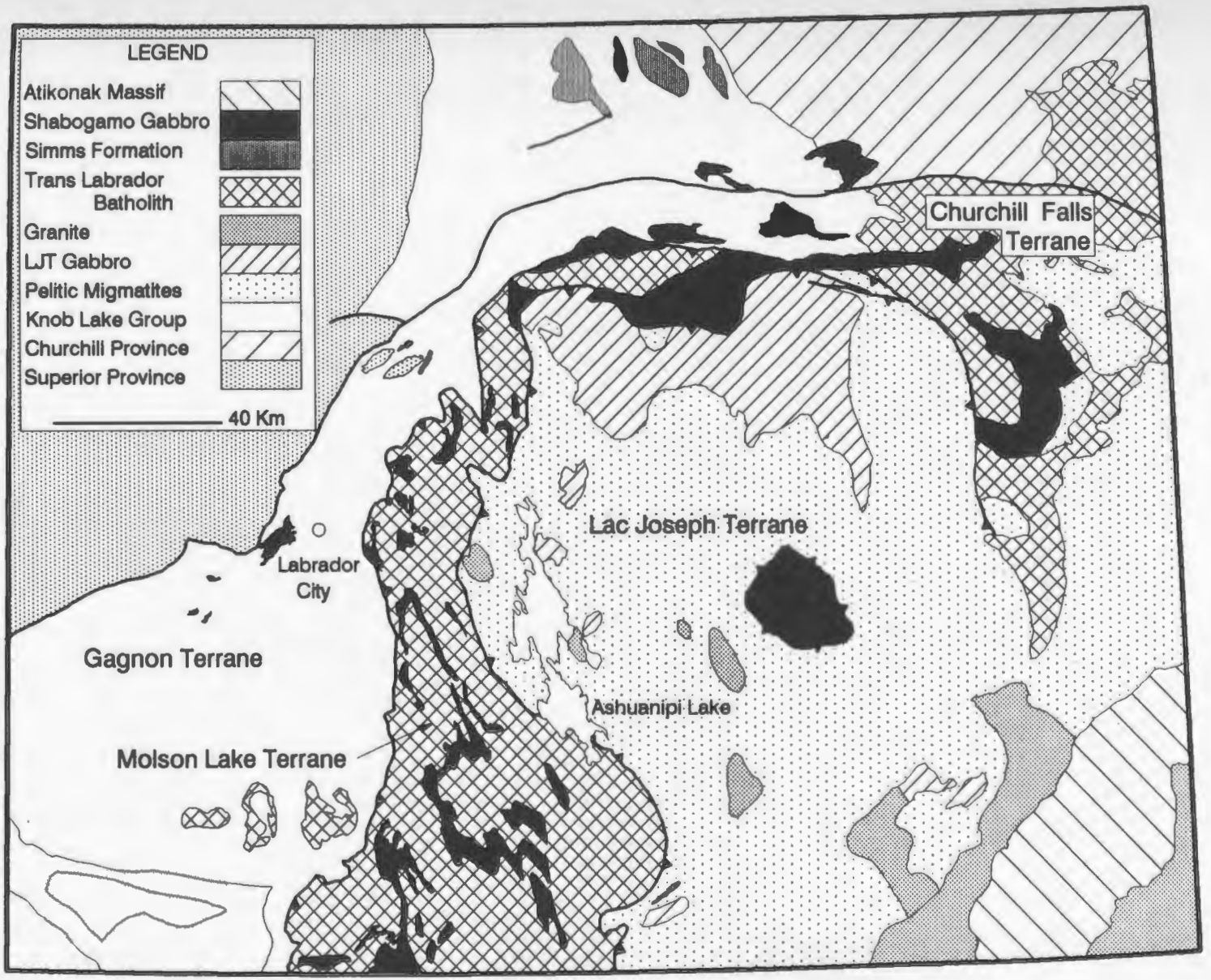

Figure 1-4: Simplified geology and major tectonic elements of western Labrador

Shabogamo Intrusive Suite. The Churchill Falls Terrane (Connelly and Nunn, 1988) lies to the east of the Molson Lake Terrane and consists of granite, granitic orthogneiss, gabbroic rocks and upper amphibolite-facies, sillimanite-bearing paragneiss. Some rock types in each of the parautochthonous terranes can be traced across the Grenville Front establishing a pre-Grenvillian link with the North American foreland.

1.4.2 The Allochthonous Terrane of Western Labrador

The Lac Joseph Terrane is one of a number of allochthonous terranes to the southeast of the Parautochthonous Belt that are composed of pre-Grenvillian amphibolite- to granulite-facies migmatites and intrusive mafic and felsic plutonic rocks. Nunn et al. (1985) reported that pre-Grenvillian metamorphism and deformation within the allochthonous terranes of Labrador occurred at about 1675 to 1600 Ma during an event they termed the Labradorian Orogeny. According to the tectonic models of Rivers et al. (1989) these allochthonous terranes were tectonically emplaced onto telescoping parautochthonous terranes during the Grenvillian Orogeny. The degree of thermal and structural reworking of the allochthonous terranes during this Grenvillian emplacement was uncertain prior to the present study.

1.4.3 The Allochthon-Parautochthon Boundary

The boundary between the allochthonous and parautochthonous terranes, referred to as the Allochthonous Boundary Front by Rivers et al. (1989), is marked by a zone of anastomosing shear zones in western Labrador which incorporate rock types of adjacent units (Connelly, 1988). However, in spite of well-developed ductile shear fabrics in these shear zones, kinematic indicators are relatively rare. Interpretation of sense of movement is further complicated by post-mylonite refolding. However, asymmetric fabrics and rotated inclusions in areas of minimal refolding around the Lac Joseph Terrane imply that it moved towards the northwest over the parautochthonous terranes along southeastwardly dipping thrust faults (Connelly, 1988).

CHAPTER 2
LITHOLOGICAL DESCRIPTIONS

2.1 Introduction

In this project, mapping was concentrated in the Lac Joseph and Molson Lake terranes with only minor forays into the Gagnon and Churchill Falls terranes. Reflecting this data collection bias, this chapter presents detailed lithological descriptions of the units in the Lac Joseph and Molson Lake terranes based on the author's observations of samples in the field and laboratory. An overview of the lithologies within the Gagnon and Churchill Falls terranes is presented for the sake of understanding the former terranes in a regional context; these latter sections are based primarily on the work of others. Map unit numbers are assigned, in a chronological order, to units mapped by the author in the Molson Lake and Lac Joseph terranes and correspond to the legend of Figure 2-1; since the units are discussed in the text by terrane rather than in chronological order, these unit numbers are not always referred to in numerical sequence in the text. Map units outside the Molson Lake and Lac Joseph Terranes are shown on the map and legend of Figure 2-1, but have not been assigned numbers. Figure 2-1 incorporates recent mapping of James et al. (1991) and therefore differs slightly from the more generalized maps throughout this thesis which were produced prior to the availability of these revisions. To relate the mapping coverage and results and to provide the structural measurements in spatial context, 1:100,000 scale field maps of the areas examined by the author are included in the back pocket. The southern maps are to be released by the Newfoundland Department of Mines in conjunction with a white cover report.

2.2 Lithologic Units in the Lac Joseph Terrane

2.2.1 Supracrustal Lithologies: Unit 1

Supracrustal rocks, which constitute a large part of the Lac Joseph Terrane, consist predominantly of metapelitic rocks with minor meta-semi-pelitic, metapsammitic and metabasic interlayers (Fig. 2-1) which are metamorphosed to upper amphibolite to granulite facies. Although the age of the sediments which constitute the supracrustal

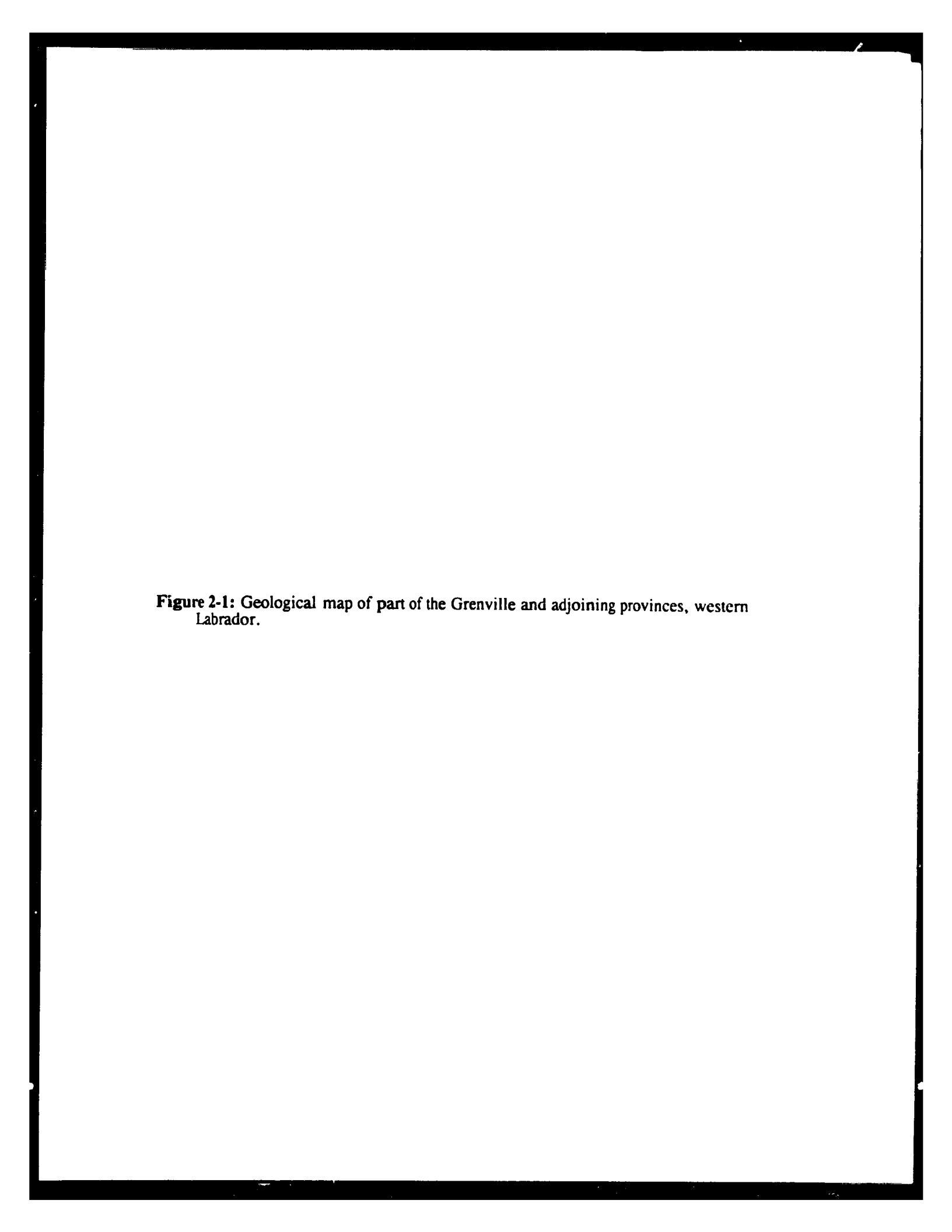

Figure 2-1: Geological map of part of the Grenville and adjoining provinces, western Labrador.

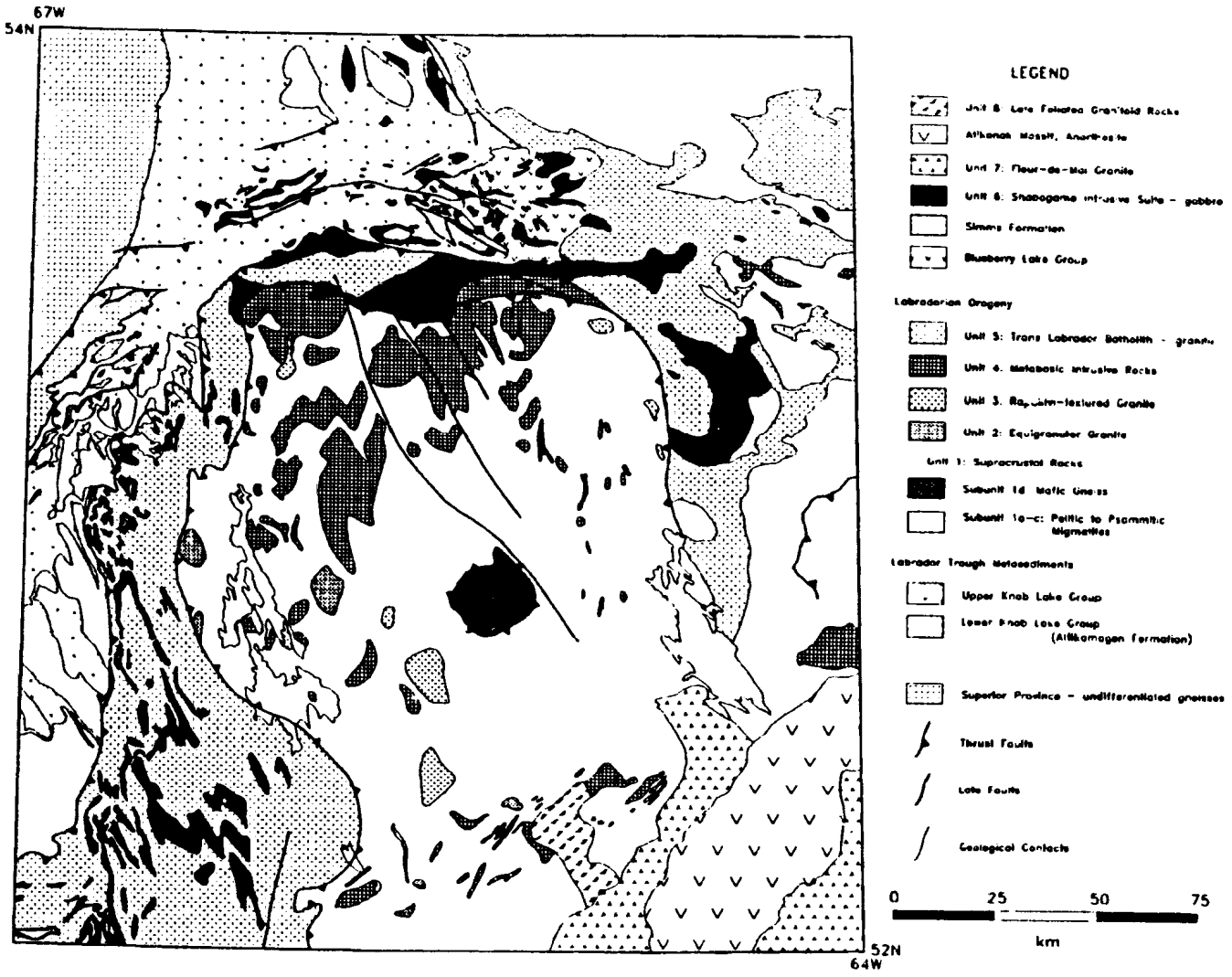
67W
54N
52N
64W
LEGEND
Unit 8: Late Foliated Granitoid Rocks
Athenian Massif, Anorthosite
Unit 7: Fleur-de-Mal Granite
Unit 6: Shabogamo intrusive Suite - gabbro
Simms Formation
Blueberry Lake Group
Labradorian Orogeny
Unit 5: Trans Labrador Batholith - granite
Unit 4: Metabasic intrusive Rocks
Unit 3: Rapakivi-textured Granite
Unit 2: Equigranular Granite
Unit 1: Supracrustal Rocks
Subunit 1d: Mafic Gneiss
Subunit 1a-c: Pelitic to Psammitic Migmatites
Labrador Trough Metasediments
Upper Knob Lake Group
Lower Knob Lake Group (Attikamagen formation)
Superior Province - undifferentiated gneisses
Thrust Faults
Late Faults
Geological Contacts
0
25
50
75
km

rocks of the Lac Joseph Terrane was known to be older that a 1672 Ma granite which intrudes the sediments (Krogh, 1983), no lower age limit has been established. The principal lithological varieties are discussed below.

2.2.1.1 Aluminosilicate-bearing Migmatites: Subunit 1a

The supracrustal rocks of the Lac Joseph Terrane are dominated by pelitic metasedimentary rocks (Fig. 2-1) which contain at least two generations of leucosomes, resulting in well-developed, often chaotic, gneissic layering (Photo 2-1). Two generations of leucosomes are distinct, and may be recognized in most outcrops. The early grey, medium-grained K-feldspar - plagioclase - quartz leucosomes (termed N_1 for first neosome) are cross-cut by, and sub-concordant with, a younger, coarser grained, pale pink leucosome phase (N_2) (Photo 2-1). The N_2 leucosomes do not appear to have been as intensely deformed as the N_1 leucosomes. Both leucosomes are interbanded with restite layers which vary from about .2 to 2 cm in width, are dark gray-blue in colour, and generally consist of sillimanite and/or kyanite, biotite, garnet and magnetite. Both leucosomes and the restite have experienced polyphase deformation. Minerals in the restite are typically aligned parallel to the folded gneissosity and define well-developed planar and linear mineral fabrics. The abundance of magnetite in the restite of this subunit results in a strong positive magnetic signature.

2.2.1.2 Muscovite-bearing Migmatites: Subunit 1a-m

Pelitic migmatites containing quartz - muscovite - biotite - garnet - hematite in the restite underlie two discrete areas of significant size in the southern Lac Joseph Terrane. As these rocks weather recessively, aeromagnetic maps (e.g. Geological Survey of Canada, 1977c) are locally the most useful method to differentiate the muscovite-bearing rocks (with a subdued magnetic expression) from the aluminosilicate-magnetite-bearing migmatites.

In the southeastern part of the Lac Joseph Terrane, muscovite-bearing migmatite occurs in spatial association with granitic intrusions. Within this area, subunit 1a-m comprises thin (.2 to 1 cm) gray restite bands composed of muscovite - biotite - garnet - hematite which are interlayered with white, medium-grained leucosome consisting of plagioclase - quartz - muscovite with minor amounts of K-feldspar (Photo 2-2). Subunit

Photo 2-1: Two-leucosome pelitic migmatites in the Lac Joseph Terrane; the earlier leucosome (N_1) is represented by thin grey bands which are cross-cut by pink, coarser-grained late leucosomes (N_2).

Photo 2-2: Muscovite-bearing pelitic migmatites of the Lac Joseph Terrane; the bleached weathered surface is typical in this subunit.

1a-m is separated from the aluminosilicate-bearing migmatites to the northwest by a wide belt of pelitic migmatites which contain both sillimanite and muscovite. Muscovite in this area does not exhibit a preferred orientation and cuts across earlier mineral fabrics defined by sillimanite - biotite - garnet - magnetite.

Muscovite-bearing migmatites also occur along the southwestern margin of the Lac Joseph Terrane in a belt which is approximately parallel to the boundary between the Lac Joseph and Molson Lake terranes. The muscovite - biotite - garnet - hematite restite is interlayered with white leucosomes consisting of quartz - plagioclase - muscovite similar to the southeastern muscovite-bearing migmatite described above except that muscovite exhibits a preferred orientation (Photo 2-3).

For reasons outlined in subsequent chapters, the muscovite-bearing migmatites are thought to be retrogressed equivalents of the aluminosilicate-bearing migmatites. This interpretation is reflected by the common subunit number 1a, suffixed by m (for muscovite); 1a and 1a-m are consequently shown as a single unit in Figure 2-1.

2.2.1.3 Semipelitic and Psammitic Migmatites: Subunits 1b and 1c

The pelitic migmatites are locally interlayered with minor amounts of semipelitic (subunit 1b) and psammitic (subunit 1c) migmatites. The semipelitic migmatites contain quartz - feldspar leucosomes which are interlayered with restite consisting principally of biotite - garnet - magnetite.

The rocks of psammitic composition are characterized by poorly defined layering (perhaps an enhanced sedimentary layering) and a distinctive light-gray to white color. Layering is defined by quartz - plagioclase - K-feldspar rich leucosomes interlayered with more biotite rich bands. Subunits 1b and 1c are spatially extensive enough to be shown in Figure 2-1; they are included only to provide a complete description of the compositional range of the supracrustal rocks in the Lac Joseph Terrane.

2.2.1.4 Mafic Gneiss: Subunit 1d

Mafic gneiss of subunit 1d is locally interlayered with subunits 1a to 1c on various scales ranging from metres to 100's of metres. It varies considerably in appearance from a straight, banded gneiss (Photo 2-4) to an agmatitic rock (Photo 2-5) in which the mafic component ranges in width from 10 to 50 cm. The scale of interlayering in the

Photo 2-3: Polished slab showing elongate clots of aligned muscovite (dark brown) in the pelitic migmatites from the southwest margin of the Lac Joseph Terrane.

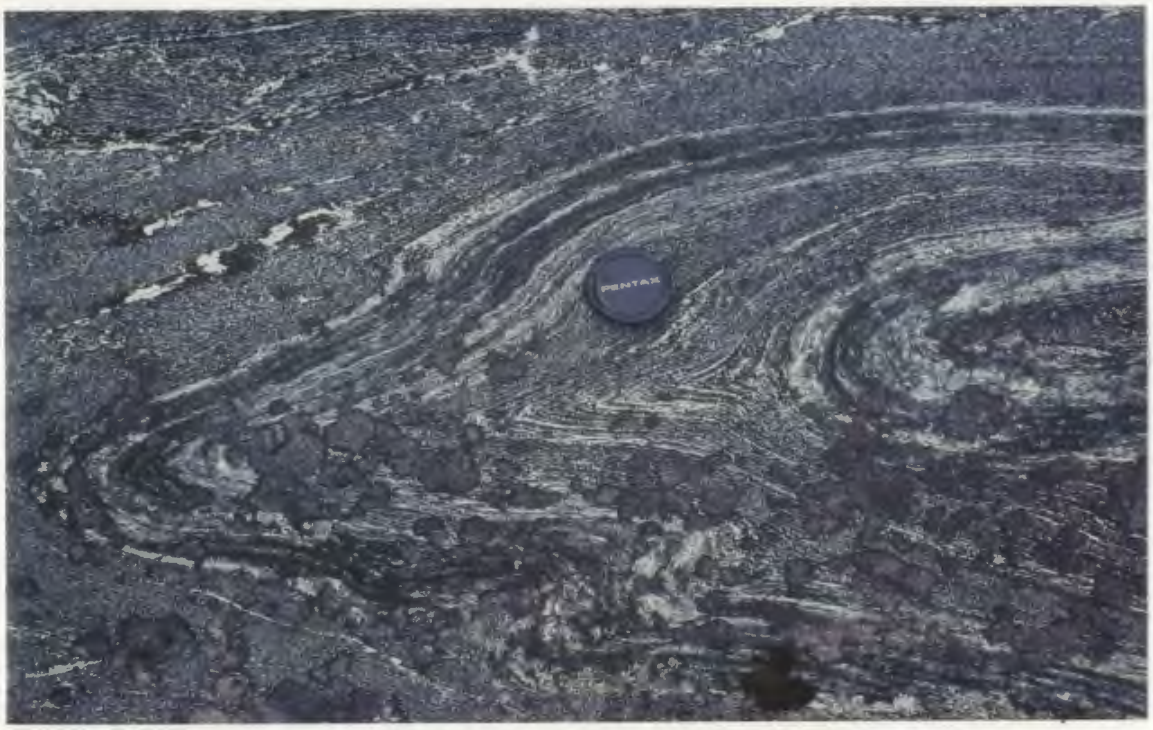

Photo 2-4: Layered mafic gneiss from the Lac Joseph Terrane.

Photo 2-5: Agmatitic gneiss from the Lac Joseph Terrane.

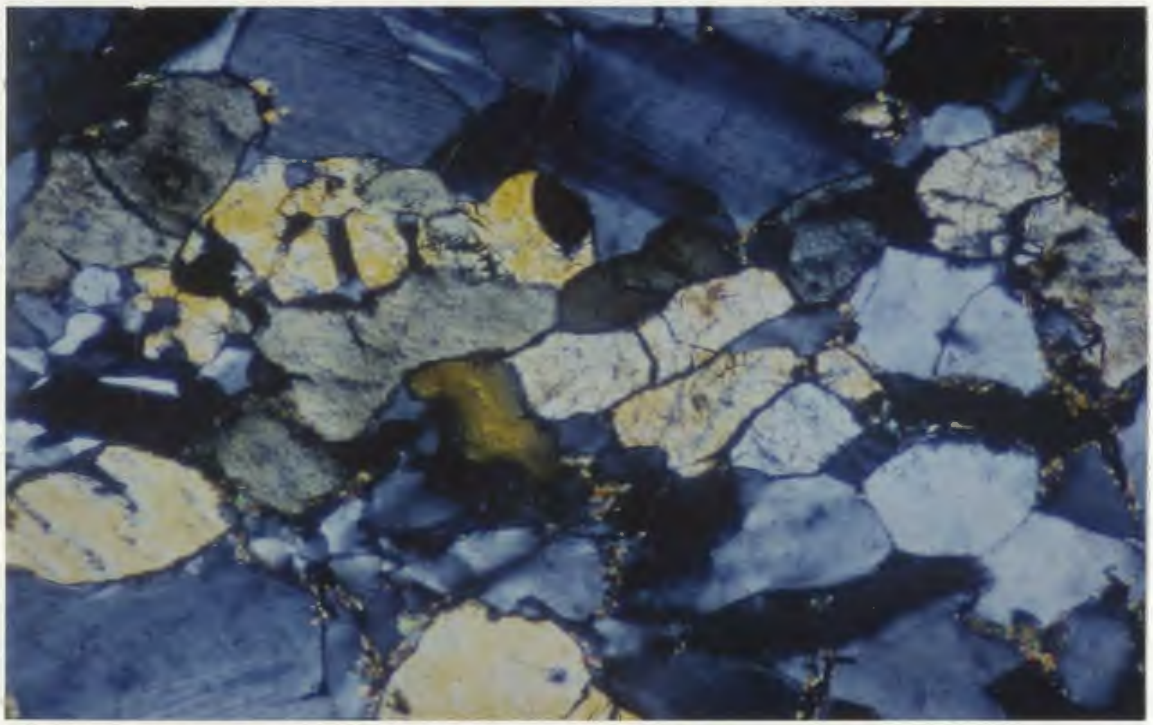

Photo 2-6: Orthopyroxene in rapakivi-textured granite from northeast of Grace Lake in the southern Lac Joseph Terrane. Cross polarized light.

banded gneiss and the diverse nature of this lithology suggests that it is a supracrustal unit with the layering possibly representing relict primary layering, within the predominantly pelitic metasedimentary terrane. In several places it is difficult to distinguish between weakly banded or layered supracrustal mafic gneiss and metamorphosed basic intrusive rocks. Mafic rocks which exhibit any layering or partial melting have been included in subunit 1d in this study, although it is acknowledged that some unlayered metabasic rocks (which have been mapped as metabasic intrusive rocks) may actually belong to subunit 1d.

Mineral assemblages in this unit indicate variations in local metamorphic conditions from amphibolite to granulite facies. Amphibolite facies assemblages predominantly underlie the lowland areas, in which paleosomes comprising hornblende - plagioclase - biotite - quartz - epidote - magnetite - titanite are interlayered with plagioclase - hornblende - biotite neosomes. Granulite facies assemblages dominate the upland terrain where paleosomes contain plagioclase - clinopyroxene - orthopyroxene - biotite with minor magnetite, quartz and/or garnet and the neosomes contain plagioclase - orthopyroxene - biotite.

2.2.2 Early Intrusive Rocks of the Lac Joseph Terrane

The early intrusive rocks contain a post-intrusive mineral assemblage indicative of high temperatures, a significant fabric and/or exhibit margins which are transitional with the host migmatites and are therefore thought to have been emplaced prior to or during the main thermotectonic event in the Lac Joseph Terrane. These units are designated early intrusive rocks of the Lac Joseph Terrane and are described below.

2.2.2.1 Equigranular Granite: Unit 2

Equigranular granite of Unit 2 comprises small dispersed granitic to granodioritic bodies which commonly appear to have been highly recrystallized; they are not megacrystic. Accessory minerals include biotite, sillimanite and magnetite, similar to the restite phases within the sillimanite-bearing migmatites. The margins of these intrusive bodies may be abrupt intrusive contacts but are commonly transitional with the host migmatites of Unit 1 such that the accessory phases gradually increase towards the margin of the intrusion.

2.2.2.2 Orthopyroxene-bearing Granite and Diorite: Unit 3

The meta-igneous rocks of Unit 3 (Fig. 2-1) are variably foliated granitoids characterized by the presence of metamorphic orthopyroxene and rapakivi-textured K-feldspar megacrysts (subunit 3a), which both intrude and are intruded by an equigranular granite phase (subunit 3b). This unit comprises plagioclase, K-feldspar, quartz and orthopyroxene with minor hornblende, biotite and magnetite. Orthopyroxene and hornblende exhibit a granular texture and are generally of smaller grain size than the phases that comprise the matrix to the megacrysts (Photo 2-6). Biotite is present in finer grained, partially aligned clusters interstitial to the matrix feldspar. A pluton of this unit on Ashuanipi Lake (Fig. 2-1) has yielded a U-Pb age of 1619 ± 2 Ma (Brooks, 1983) indicating a Labradorian emplacement age. This unit is typically massive to weakly foliated, but locally exhibits 1-2 centimetre wide shear zones containing pseudotachylyte. Locally this unit is fringed by an equigranular dioritic phase (subunit 3c) which is moderately foliated and in places contains chlorite.

2.2.2.3 Basic Intrusive Rocks in the Lac Joseph Terrane; Ossokmanuan Mountain Intrusive Suite: Unit 4

The basic rocks intruding the migmatites of the Lac Joseph Terrane are quite diverse in composition, texture and degree of post-intrusive recrystallization. A large basic intrusive complex which dominates the northern and northwestern part of the Lac Joseph Terrane, is referred to as the Ossokmanuan Mountain Intrusive Suite (James, 1991), whereas the southern part of the Lac Joseph Terrane typically contains only small intrusions (Fig. 2-1). In both areas, textural and compositional variations occur over very short distances.

The compositional variation of Unit 4 includes metamorphosed norite (subunit 4a), gabbronorite (subunit 4b), gabbro (subunit 4c), olivine gabbronorite (subunit 4d) and websterite (subunit 4e). The variable degree of recrystallization in these rocks has resulted in a range of textures being preserved, from primary igneous textures (including cumulate and ophitic textures) to granoblastic. Local variations in the degree of recrystallization precludes use of these criteria to establish a relative chronology.

The most pristine basic rocks are medium to coarse grained, contain primary mineralogy, except in narrow coronas, and do not exhibit penetrative fabrics although they are locally fractured. Three different corona textures are locally developed: (1) olivine rimmed by a narrow band of fibrous orthopyroxene; (2) olivine surrounded by a symplectic intergrowth of spinel and clinopyroxene; and (3) clinopyroxene rimmed by a pleochroic brown amphibole. Based on samples from the northwestern part of the Lac Joseph Terrane, Rivers and Mengel (1989) suggested that the development of coronas was a post-intrusive, subsolidus, cooling phenomenon.

At least one basic intrusive complex is cross-cut by a medium-grained, equigranular, massive to weakly foliated tonalitic phase (Subunit 4f). This subunit contains magnetite, hornblende and clinopyroxene as accessory minerals and is massive to weakly foliated. The spatial association of tonalite with the basic intrusive suite, and the presence of hornblende and clinopyroxene in the tonalite, may suggest that the tonalite represents a late differentiate of the gabbronorite suite.

At the other end of the textural spectrum, the most recrystallized mafic intrusive rocks in the Lac Joseph Terrane are characterized by a fine-grained granoblastic texture with all phases except plagioclase having been completely recrystallized. Samples from in this unit typically contain two metamorphic pyroxenes, plagioclase and biotite implying that recrystallization occurred under granulite facies conditions.

2.2.3 Late Equigranular Granitoid Rocks in the Lac Joseph Terrane

Intrusive granitoid rocks, which are interpreted to have been emplaced after the main thermotectonic event in the Lac Joseph Terrane, are categorized as late granitoid rocks. Evidence of their post-metamorphic nature includes overprinting metamorphic aureoles, lack of deformation, and cross-cutting relationships with deformed rocks. In addition, their mineralogy contrasts with granitoids in Unit 3, in that they are peraluminous, contain 2 micas and are orthopyroxene-free.

2.2.3.1 Fleur-de-Mai Granite: Unit 7

The Fleur-de-Mai granite (Unit 7) occurs along the southeastern boundary of the Lac Joseph Terrane and is marginal to the Atikonak Anorthosite Massif. The granite ranges from medium grained, equigranular to K-feldspar megacrystic and locally

exhibits a rapakivi texture (Nunn et al., 1986); it is typically xenolith free and contains muscovite, biotite, titanite and, locally, hornblende as accessory minerals. This unit exhibits abrupt cross-cutting contacts with the country rocks. Recrystallization in this body appears to be restricted to the margins where a weakly developed planar fabric is locally observed. Nunn et al. (1986) reported that this unit is transitional into the pyroxene-bearing monzonitic rim around the Atikonak Massif. Emslie and Hunt (1990) reported a U-Pb zircon age of 1133+10/-5 Ma for Unit 7 which is taken to represent the emplacement age of the massif.

2.2.3.2 Late Foliated Granitoid Rocks: Unit 8

Unit 8 is a two-mica granitoid rock which is massive to foliated, medium-grained and locally contains inclusions of mafic gneiss. The main occurrence of this unit lies to the northwest of the Atikonak Anorthosite Massif and its associated granitoid suite (Fig. 2.1). The composition typically ranges from granite to granodiorite and in places it becomes tonalitic. Unit 8 is not dated directly; the age of this unit is only constrained by the observation that the metamorphic aureole around the pluton overprints the sillimanite-bearing assemblage in the pelitic migmatites of Unit 1.

2.2.3.3 Granitoid Pegmatites in the Lac Joseph Terrane: Unit 9

Medium to coarse grained pegmatite dykes are found throughout the Lac Joseph Terrane in the map area. Since this unit does not appear in Figure 2-1, due to the inappropriate scale for showing such detail, it is not represented in the figure's legend. The pegmatites cross-cut all tectonic fabrics in the host rock, but may themselves be weakly foliated. In addition to K-feldspar, plagioclase and quartz, these pegmatites contain muscovite, biotite, monazite and apatite. The host rocks typically show signs of having been affected by the pegmatites in the vicinity of the intrusions; for instance, muscovite commonly overprints sillimanite up to a metre away from the pegmatite margin in the migmatites of Unit 1, suggesting that the pegmatites contributed water to the host to promote retrogression.

2.2.4 Post-tectonic Diabase Dykes in the Lac Joseph Terrane: Unit 10

Diabase dykes cross-cut all tectonic fabrics in both migmatites and intrusive rocks; as with Unit 9, diabase dykes do not appear on Figure 2-1. Diabase dykes contain

unrecrystallized plagioclase and clinopyroxene; no fabric was observed in this unit. Chilled margins along the contacts of many of these dykes, pristine textures and lack of a fabric all attest to the post tectonic nature of this unit. They are therefore assumed to be post-Grenvillian in age.

2.3 Lithologies of the Molson Lake Terrane

The Molson Lake Terrane, consisting exclusively of granitic and gabbroic rocks, are distinguished lithologically from the Lac Joseph Terrane by its lack of supracrustal rocks.

2.3.1 Granitoid Rocks - Unit 5

The granitoid rocks in the Molson Lake Terrane are medium-grained, equigranular rocks of granitic to tonalitic composition, with muscovite, biotite, chlorite, calcic amphibole, epidote, titanite, clinopyroxene and/or garnet as accessory minerals, the assemblage apparently depending on local metamorphic conditions. These rocks are characteristically partially recrystallized and possess well-developed metamorphic mineral fabrics defined by biotite, chlorite, muscovite and calcic amphibole. There is no evidence to suggest that they have been partially melted.

2.3.2 Shabogamo Intrusive Suite - Unit 6

The basic intrusive rocks in the Molson Lake Terrane are correlated, on the basis of texture, mineralogy and tectonometamorphic history, with the Shabogamo Intrusive Suite. This unit was formalized by Rivers (1980) and has been dated at 1375 ± 60 Ma (Rb-Sr and Sm-Nd whole rock and minerals; Brooks et al., 1981; Zindler et al., 1981) and 1353 ± 17 Ma ($^{40}Ar/^{39}Ar$ on biotite, Dallmeyer, 1982). A U/Pb age from this study indicate that this unit crystallized at 1431 ± 7 Ma (see Section 6.4.2).

The composition of this variably metamorphosed unit is restricted to gabbro (subunit 7a) and gabbronorite (subunit 7b). Olivine has been observed only locally in the map area. Igneous pyroxene and plagioclase are medium-grained and contrast with the finer grained, locally symplectic secondary minerals. Sub-solidus reactions have resulted in the widespread development of corona textures between igneous olivine or pyroxene and plagioclase. Corona mineralogy includes combinations of amphibole and/or garnet between the olivine or pyroxene core and plagioclase matrix. Detailed

petrographic work allows subdivision into three groups on the basis of corona textures and mineral relationships: (1) gabbro-gabbronorite with non-coronitic clinopyroxene - amphibole; (2) gabbro-gabbronorite with clinopyroxene - amphibole - garnet coronas and (3) gabbro-gabbronorite with clinopyroxene - garnet coronas. The corona relationships are discussed in more detail in Section 4.5.

2.4 Lithologies of the Western Churchill Falls Terrane

The Churchill Falls Terrane has not been extensively examined in this study, thus descriptions which follows are based largely on the work of Wardle, (1979), Wardle and Britton (1981), Wardle (1982), Nunn and Christopher (1983) and Nunn et al. (1984). The Churchill Falls Terrane contains rock types comparable to both the Molson Lake and Lac Joseph terranes.

2.4.1 Supracrustal Rocks of the Churchill Falls Terrane

Nunn and Christopher (1983) reported that the southwestern part of the Churchill Falls Terrane is dominated by pelitic migmatites with several generations of granitic leucosomes interlayered with aluminous restite. They described early pink to brown weathered leucosomes cross-cut by a pink, medium-grained late melt phase. Although sillimanite is the dominant aluminous phase in the restite, Wardle (1982) reported kyanite in the northern occurrences of this unit. These migmatites are thus identical to the pelitic migmatites in the Lac Joseph Terrane. Metabasic rocks are present as discontinuous layers, enclaves and trains of boudins similar to those in the Lac Joseph Terrane.

2.4.2 Granitoid Rocks of the Churchill Falls Terrane

A diverse suite of granitoid rocks intrudes the supracrustal rocks of the Churchill Falls Terrane. Compositions vary from diorite to granite with textures ranging from weakly foliated to gneissic (Nunn and Christopher, 1983 and Nunn et al., 1984). The orthogneisses in this unit are fine- to medium-grained rocks derived from hornblende-biotite granodiorite and tonalite; they exhibit a single melt phase, in contrast to the supracrustal rocks. Titanite analyses from granitoid rocks of this terrane plot on a line which defines upper and lower intercept U-Pb ages of 1654 Ma and 993 Ma respectively (Krogh, 1983).

2.4.3 Basic Intrusive Rocks of the Churchill Falls Terrane

The basic intrusive rocks of this terrane primarily comprise subophitic, layered and equigranular gabbro to leucogabbro which exhibits corona textures (Nunn and Christopher, 1983). On the basis of texture and composition, this unit has been correlated with the Shabogamo Intrusive Suite (Nunn and Christopher, 1983).

2.4.4 The Problematic Boundary Between the Molson Lake and Churchill Falls Terranes

The Churchill Falls and Molson Lake terranes were erected on the basis of perceived differences in lithologies, metamorphism and structural styles. However, the boundary zone between these two terranes, which is thought to be situated immediately south of Gabbro Lake (see Fig. 1-1), is not exposed. In the absence of a documented boundary fault between these two terranes, it is possible that they are in fact a single terrane with spatially distinct lithologies and contrasting thermotectonic histories. This would imply a lithological linkage between the Lac Joseph and Molson Lake terranes, the implications of which are discussed later.

2.5 Lithologies of the Gagnon Terrane

The Gagnon Terrane is distinguished from other terranes in the Parautochthonous Belt of western Labrador by the presence of metasedimentary rocks of the Kaniapiskau Supergroup, which extend across the Grenville Front from the New Quebec Orogen (Labrador Trough). These are intruded by granitoid and basic rocks.

2.5.1 Metasediments of the Kaniapiskau Supergroup of the Gagnon Terrane.

The metasedimentary rocks of the Knob Lake Group, the lower sequence of the Kaniapiskau Supergroup, in the Gagnon Terrane comprise, stratigraphically upwards, the Attikamagen, Denault, McKay River, Wishart, Nimish, Sokoman, Mehihek and Tamarack formations (Wardle and Bailey, 1981; Rivers, 1983). This continental margin sequence rests unconformably on the Superior Province margin and comprises metapelitic to semipelitic schist, marble, metavolcanic rocks, quartzite and iron

formation. Lower stratigraphic levels are exposed in the southern part of the Gagnon Terrane whereas the northern regions are dominated by formations higher in the succession.

2.5.2 Intrusive Rocks of the Gagnon Terrane

The Knob Lake Group in the Gagnon Terrane has been intruded by granitoid and gabbroic rocks. The granitoid rocks are present as relatively small, variably deformed bodies ranging in composition from granite to tonalite. Gabbro of the Shabogamo Intrusive Suite commonly exhibits relict igneous textures with coronitic textures (Rivers, 1980). Many of the gabbroic intrusions are sill-like structures concordant with the regional deformation trends. The areal exposure of Shabogamo Intrusive Suite is significantly less than in the Molson Lake Terrane.

CHAPTER 3
STRUCTURAL GEOLOGY

3.1 Introduction

In this study, structural measurements were principally made in the Lac Joseph and Molson Lake terranes and along the western margin of the Churchill Falls Terrane adjacent to the Lac Joseph Terrane. This chapter reflects this data collection bias by focussing on the Lac Joseph and Molson Lake terranes.

The fabrics in the Lac Joseph and Molson Lake terranes typically differ in definition, intensity, and in the southern part of the area, orientation, giving rise to contrasting structural styles in the two terranes. These contrasting structural styles may be attributable to differences in rock types, peak metamorphic conditions and/or tectonic histories. The structural observations from the two terranes will be presented separately. To facilitate the presentation of structural data, the Lac Joseph Terrane has been subdivided into several structural domains (Fig. 3.1).

3.2 Structural Geology of the Lac Joseph Terrane

3.2.1 Supracrustal Rocks

The supracrustal rocks of the Lac Joseph Terrane are polydeformed and metamorphosed resulting in a diversity of structural fabric types and orientations. The fabric notation employed here is designed to indicate the relative timing of fabric development where overprinting relationships permit distinction. Planar and linear fabrics, denoted by "S" and "L" respectively, are subscripted with a number which refers to the relative sequence of fabric development and the letter "J" to denote the Lac Joseph Terrane (eg. S_{1J} signifies the first planar fabric in the Lac Joseph Terrane). Mineral fabrics in the Lac Joseph Terrane are assigned a position in the progressive sequence of early flattening, subsequent mylonitization and, finally, folding fabrics. It is acknowledged that the mineral fabrics quite probably developed over a period of time which overlapped, in whole or in part, with the formation of flattening fabrics in the leucosomes, mylonitization and folding.

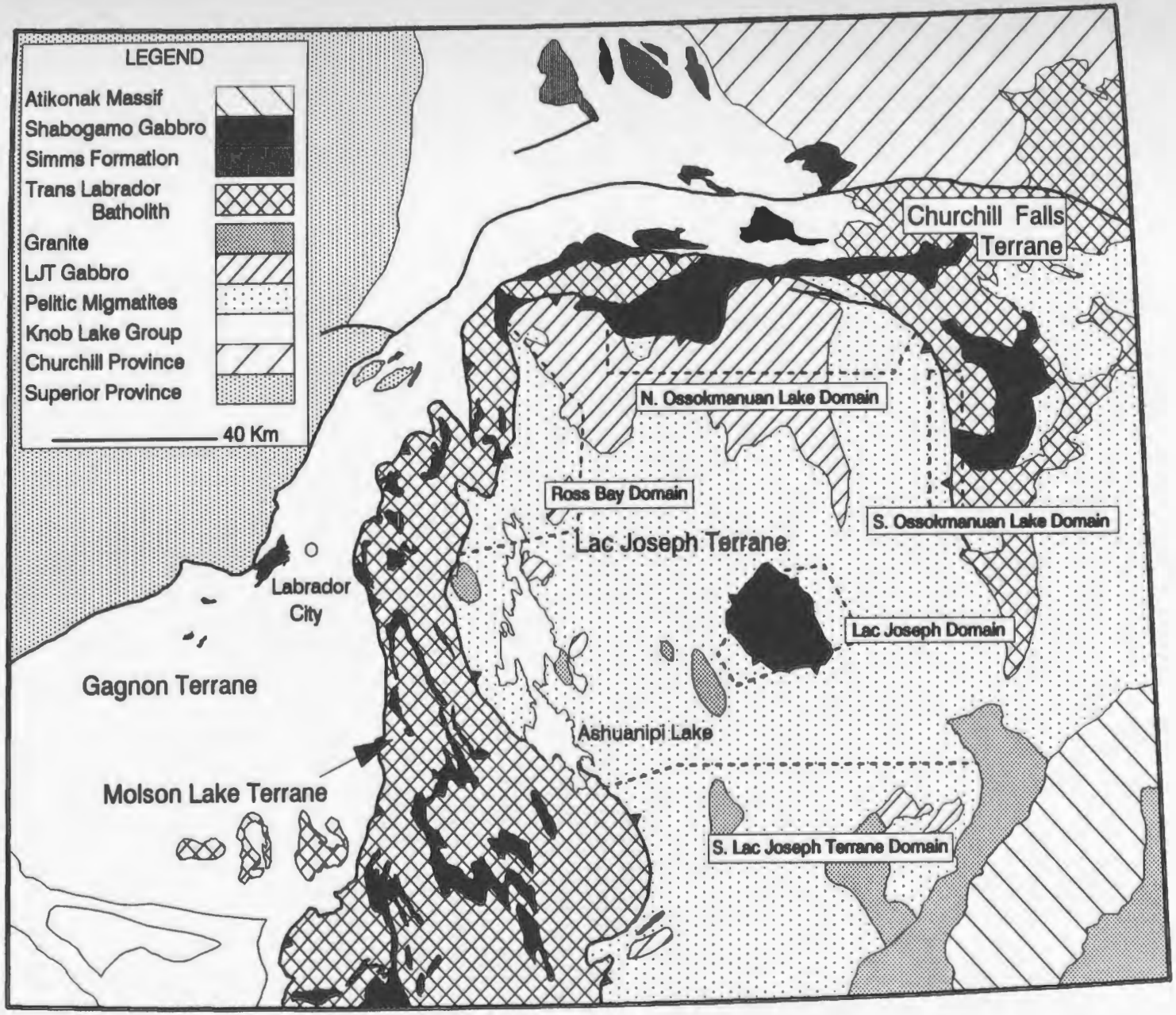

Figure 3-1: Structural domains in the Lac Joseph Terrane

3.2.1.1 Early Planar Fabrics in the Lac Joseph Terrane: S_{1J}

The earliest planar fabric recognized in the Lac Joseph Terrane is a penetrative gneissic fabric in the migmatites which is attributed to a deformation episode herein termed D_{1J}; no primary sedimentary layering was observed although the preservation of distinct supracrustal subunits presumably indicate its existence. Within the pelitic to psammitic migmatite (Subunits 1a-c) the gneissosity is defined by layering of the earliest leucosome (N_1) and thin restite seams (Photo 2-1). As previously mentioned, this N_1 leucosome is both cross-cut by, and is sub-parallel to, a coarser grained N_2 leucosome phase (Photo 2-1). Both N_1 and N_2 leucosomes contain a flattening fabric defined by quartz and feldspar which is parallel to the gneissic layering. This fabric is variably oriented throughout the Lac Joseph Terrane. Early fabrics in the southern Lac Joseph Terrane area exhibit a wide range of orientations with an overall northeast trend (Fig. 3-2a), whereas sparse data from the northern domains show variable orientations (Fig 3.3a).

Planar mineral fabrics in the restite are defined by biotite and matted sillimanite (Photo 3-1). These fabrics are parallel to the flattening fabric in N_1 and N_2 leucosomes suggesting that they developed approximately coevally.

The localized cross-cutting nature of the N_2 leucosome with respect to the earlier N_1 leucosomes suggests that the planar gneissic fabric began to form prior to N_2 crystallization. However, the general concordancy of the foliated N_2 and N_1 leucosomes suggests that flattening during D_{1J} continued throughout the crystallization of N_2. The common occurrence of flattening fabrics in the N_2 (Photo 3.2) suggests that D_{1J} affected most of the N_2 leucosomes and therefore probably out-lasted migmatization of the pelitic supracrustal rocks (Unit 1). Since mineral fabrics are parallel to the flattening fabric in the N_2 leucosomes, it is likely that they formed during the latter stages of D_{1J}. The gneissosity defined by N_1, N_2 and the restite layering, together with the flattening fabrics in the leucosome and the planar mineral fabrics in the restite are therefore collectively referred to as S_{1J}. U-Pb ages indicate that both leucosome phases and the mineral fabric formed during the Labradorian Orogeny (see Sections 3.2.1.3 and 6.5).

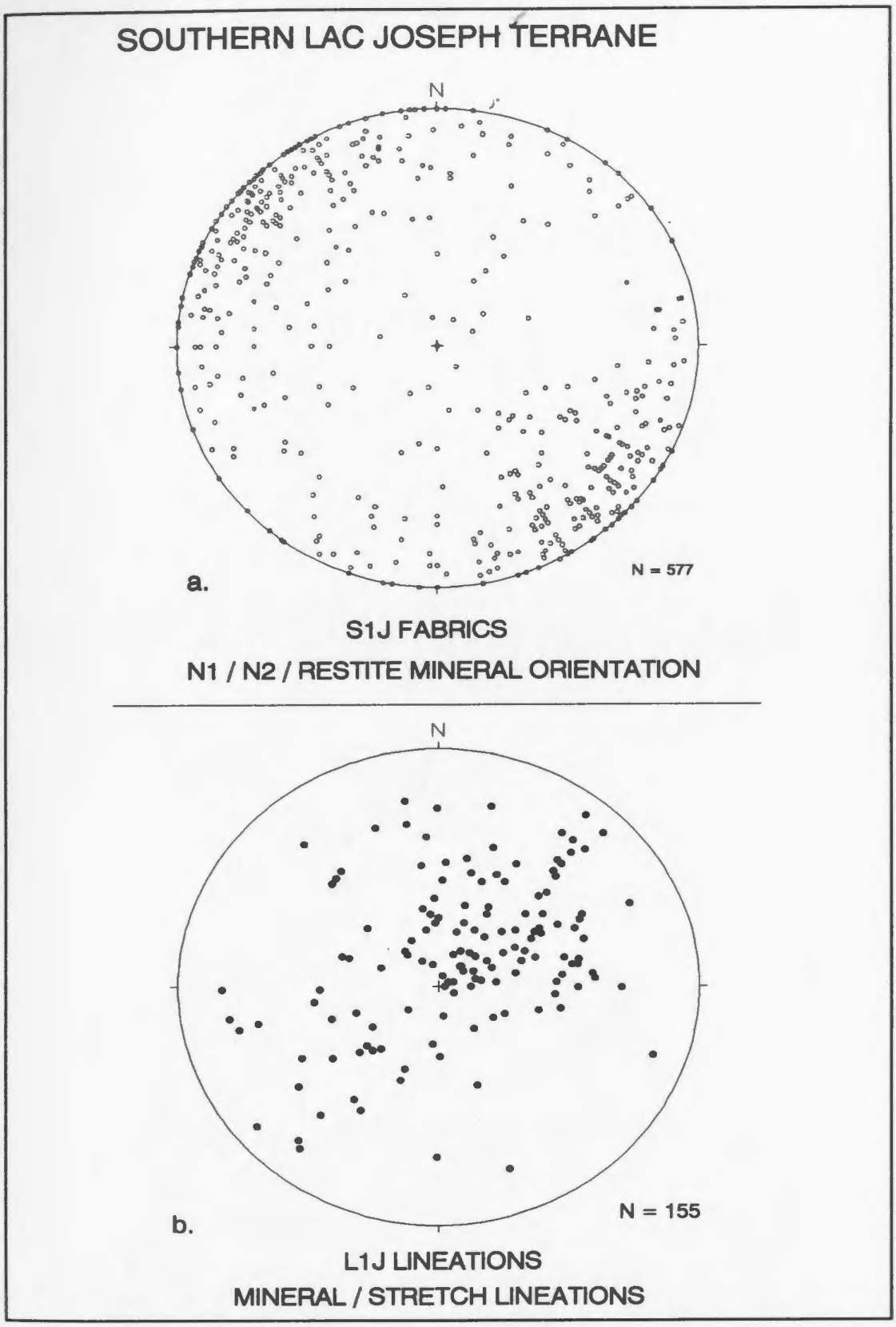

Figure 3-2: Orientations of S1J Planar and L1J linear fabrics in the pelitic migmatites of the southern Lac Joseph Terrane.

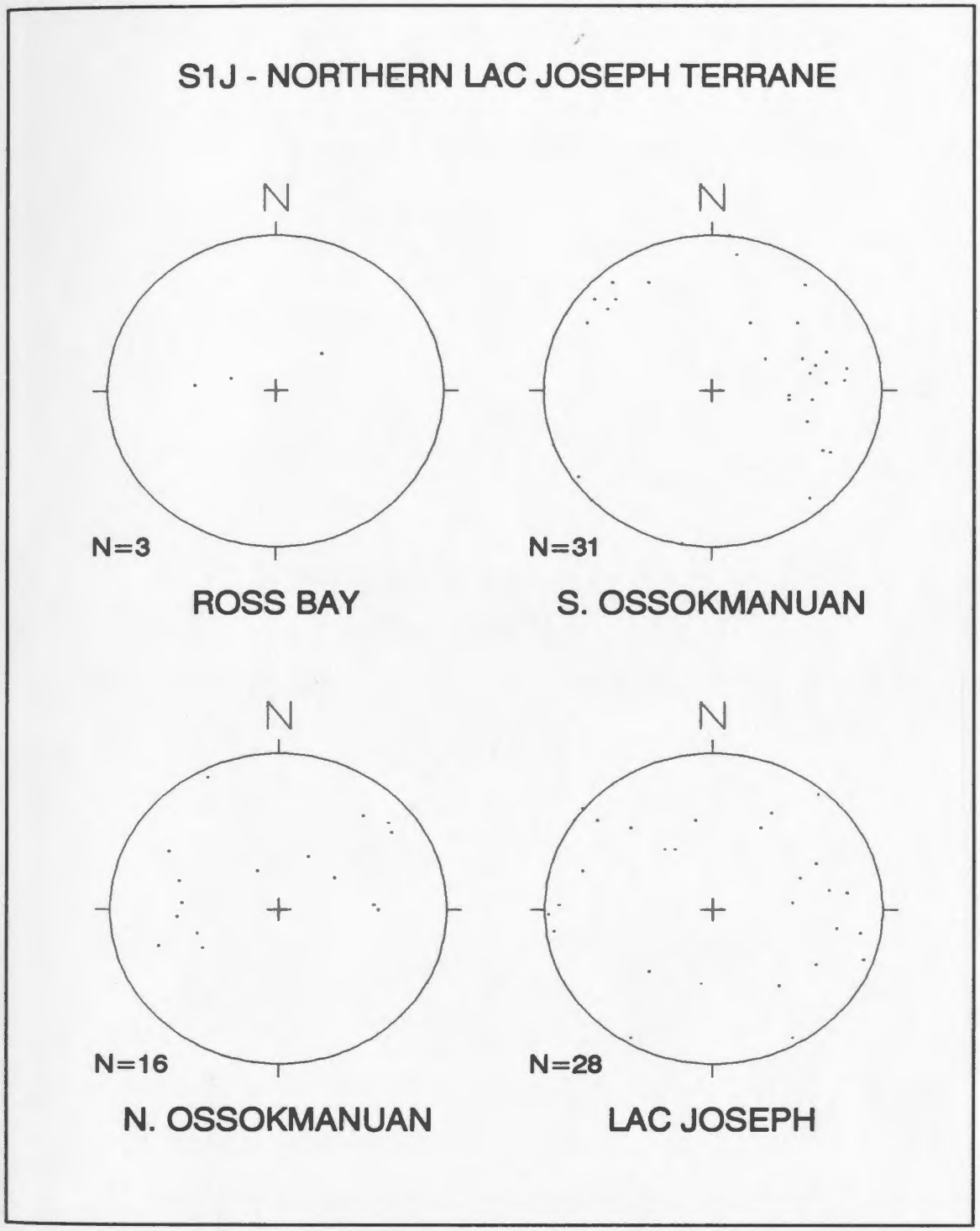

Figure 3-3: Orientations of S1J planar fabrics in pelitic migmatites in domains indicated in the Lac Joseph Terrane.

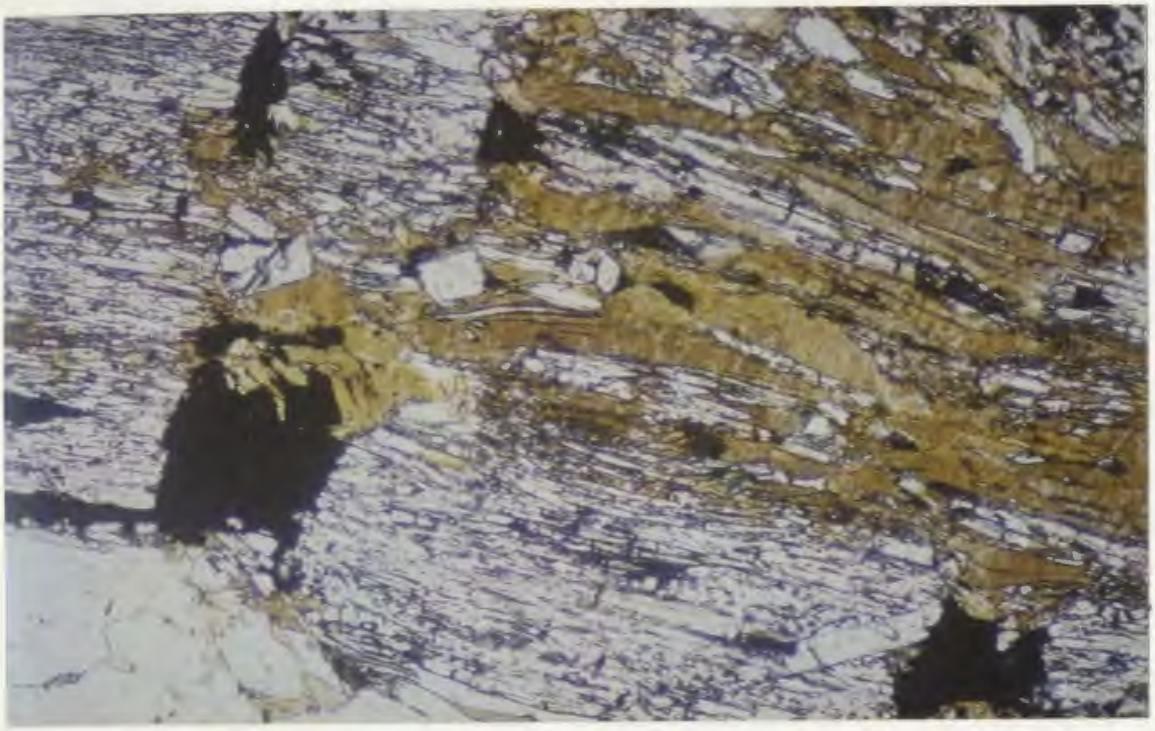

.2 mm

Photo 3-1: Sillimanite and biotite define S_{1J} in the restite of the pelitic migmatites in the Lac Joseph Terrane; sillimanite is preferentially aligned to define L_{1J} lineation. Plane polarized light.

Photo 3-2: N_2 leucosome exhibiting a penetrative flattening fabric which is parallel to the mineral alignment in the restite.

The gneissic layering in the mafic gneiss (Subunit 1d) is defined by interlayering of a single leucosome phase with the paleosome. Amphibole and/or clinopyroxene locally define a planar mineral fabric which is parallel to the gneissosity. The intensity of the planar fabric in the mafic gneiss is more variable than that in the pelitic migmatites. However, fabrics are compatible in orientation with the early gneissic layering in surrounding pelitic migmatites and are therefore similarly labelled as S_{1j}.

3.2.1.2 Early Linear Fabrics: L_{1j}

Lineations in the pelitic migmatites are defined by stretched quartz and plagioclase grains in the leucosomes and by the preferred orientation of sillimanite in the restite, all of which are aligned parallel to S_{1j}; lineations in both leucosome and restite are colinear suggesting that they formed approximately coevally and are therefore collectively referred to as L_{1j}. These stretching and mineral lineations generally plunge towards the northeast and southwest in the southern part of the Lac Joseph Terrane (Fig. 3-2b). Although fabric data are less abundant in the northern domains, the majority of data plunge towards the south and southwest in the north and south Ossokmanuan and Lac Joseph domains (Fig. 3-4). These linear fabrics are interpreted to be coeval with the S_{1j} planar fabrics and are therefore thought to have formed during the Labradorian Orogeny. In the muscovite-bearing migmatite, the lack of sillimanite results in a weaker expression of the lineation.

3.2.1.3 Shear Zones in the Lac Joseph Terrane

Although discontinuous bands with mylonitic fabrics were observed at several individual outcrops in the migmatites of the Lac Joseph Terrane, only one continuous mappable zone, located in the southern Lac Joseph Terrane, could be distinguished. The mylonitic fabric in this shear zone is defined by ribbon quartz, extensive sub-grain development in both quartz and feldspar, asymmetric planar fabrics, rotated inclusions and strong planar and linear fabrics. Sillimanite and biotite define the mineral fabrics in the restite layers of the mylonitic rocks, as in their unmylonitized equivalents, and appear to represent a synkinematic, stable mineral assemblage. U-Pb geochronology from one of these shear zones has established that mylonitization occurred during the Labradorian Orogeny (Section 6.5) thus implying that the stable synkinematic

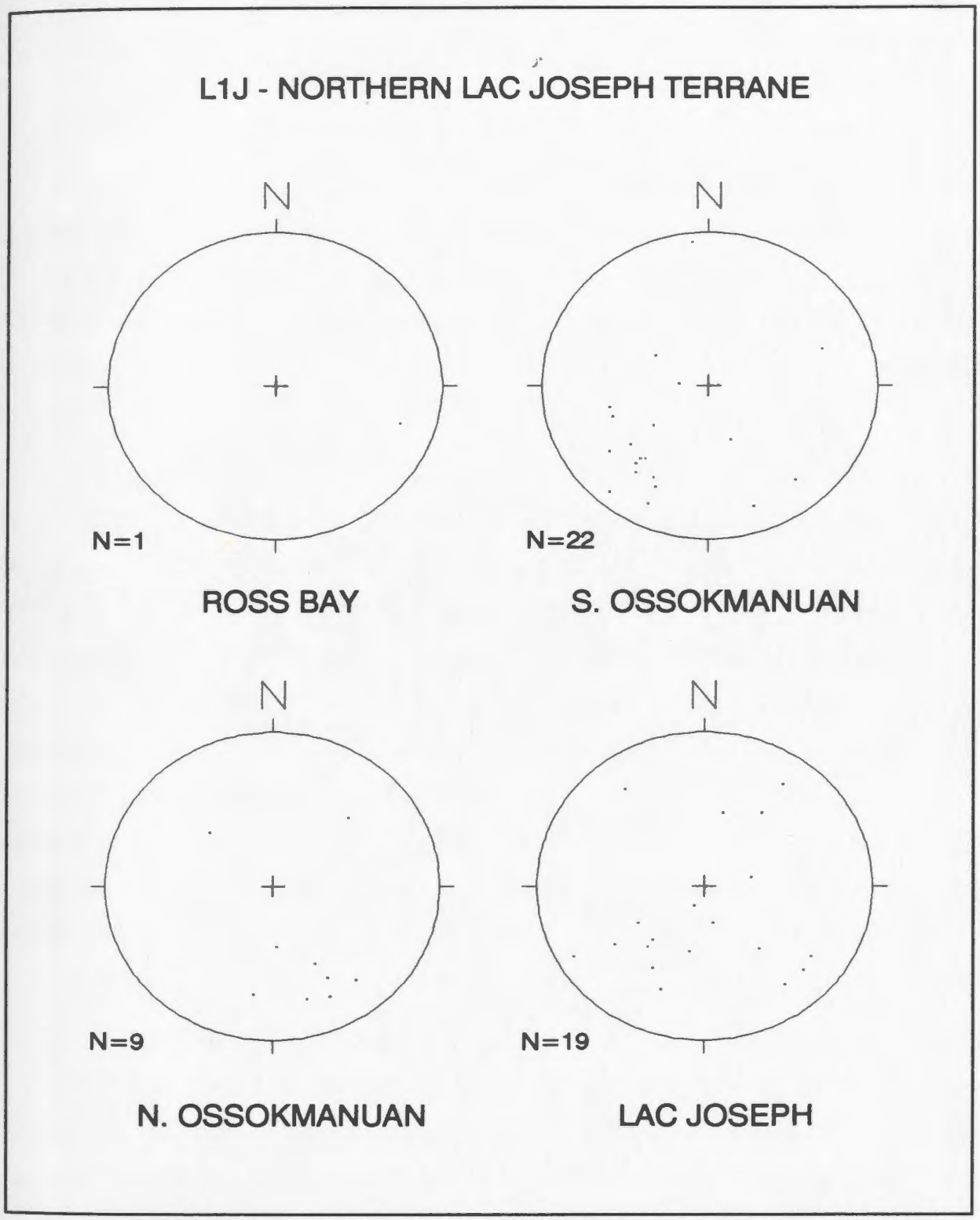

Figure 3-4: Orientations of L1J linear fabrics in the pelitic migmatites in domains indicated in the Lac Joseph Terrane.

aluminosilicate assemblage must also be Labradorian in age. Assuming that the aluminosilicate assemblages both in and away from the mylonitic zones formed during the same event, this indirectly establishes that the restite assemblage throughout the Lac Joseph Terrane is also Labradorian in age.

Sparse kinematic indicators in the southern mylonite zone (C/S fabrics, rotated feldspar inclusions) suggest that the northwest side moved up relative to the southeast side along this zone, which is presently steeply dipping towards the northwest. Since this shear zone formed early, the orientation and inferred direction of relative movement may not be directly meaningful for tectonic reconstructions if the shear zone was reoriented during subsequent deformation events.

3.2.1.4 F_{2J} Folding

The S_{1J} planar fabrics in the pelitic supracrustal rocks were reoriented and refolded during D_{2J} into tight to isoclinal F_{2J} folds (Photo 3-3) such that the early planar fabrics are subparallel to the F_{2J} axial planes. Mineral fabrics parallel to the F_{2J} axial planes are generally absent except where locally defined by biotite (Photo 3-4). The F_{2J} axial surfaces are oriented northeast-southwest in the southern part of the Lac Joseph Terrane (Fig. 3-5a) and are generally parallel to the S_{1J} planar fabrics (as expected since F_{2J} folds are isoclinal). The patterns of the F_{2J} folds in the northern domains are highly variable with a slight maximum in a north-northwest trending orientation (Fig. 3-6). The variable orientations of F_{2J} axial planes suggest that the area was affected by an F_{3J} deformation event (discussed below) which resulted in complex, large-scale folds.

Observations in many outcrops throughout the Lac Joseph Terrane indicate that the F_{2J} fold axes are subparallel to the L_{1J} mineral lineations (Photo 3-5). F_{2J} axes in the southern part of the area exhibit a very weak northeast-southwest preferred orientation (Fig. 3-5b). F_{2J} fold axes in the northern domains exhibit varied orientations (Fig. 3-7). Since the F_{2J} folding event can be shown to predate the 1133+10/-5 Ma old Fleur-de-Mai granite (Emslie and Hunt, 1990), it is thought to be Labradorian in age.

Photo 3-3: Both leucosomes and S_{1J} fabrics are folded around F_{2J} fold axial planes throughout the Lac Joseph Terrane.

Photo 3-4: Biotite aligned parallel to the F_{2J} axial planes in the pelitic migmatites of the Lac Joseph Terrane; this relationship is only locally observed.

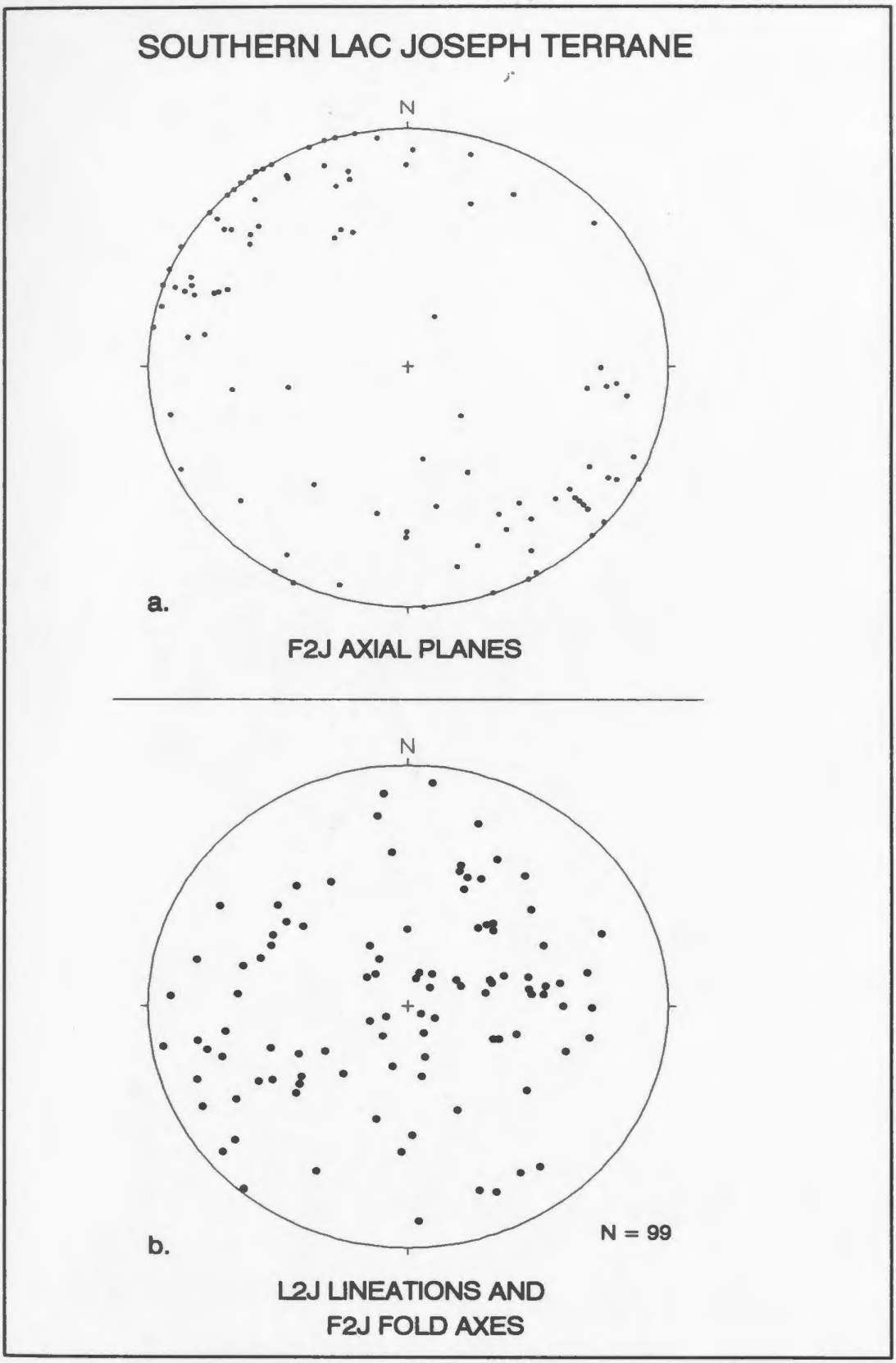

Figure 3-5: Orientations of F2J axial planes and L2J fold axis in the pelitic migmatites of the southern Lac Joseph Terrane.

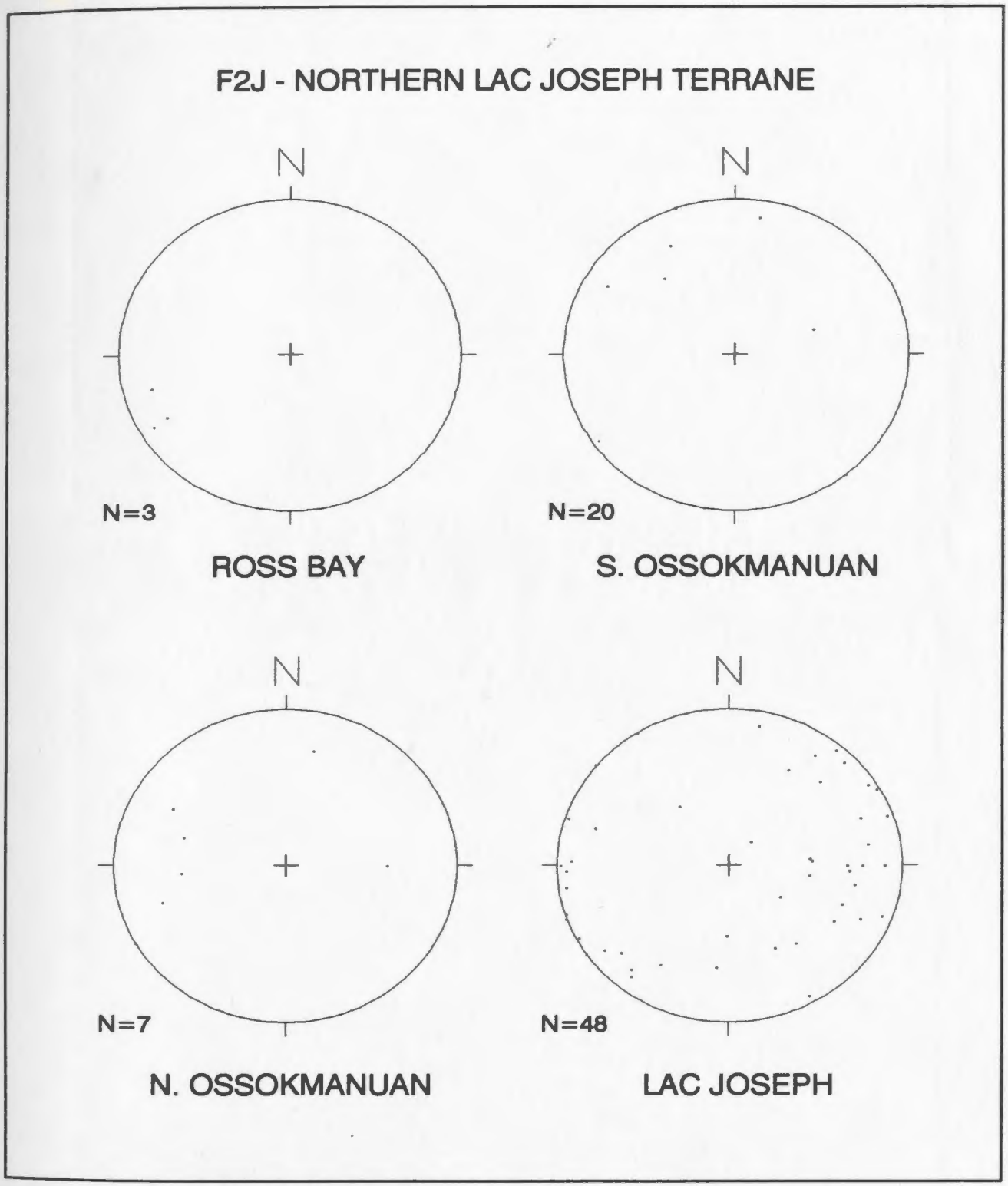

Figure 3-6: Orientations of F2J axial planes in the domains of the Lac Joseph Terrane as indicated.

Photo 3-5: Sillimanite and mineral rodding in both leucosomes define a lineation which is typically parallel to the F_{2} fold axes in the pelitic migmatites of the Lac Joseph Terrane.

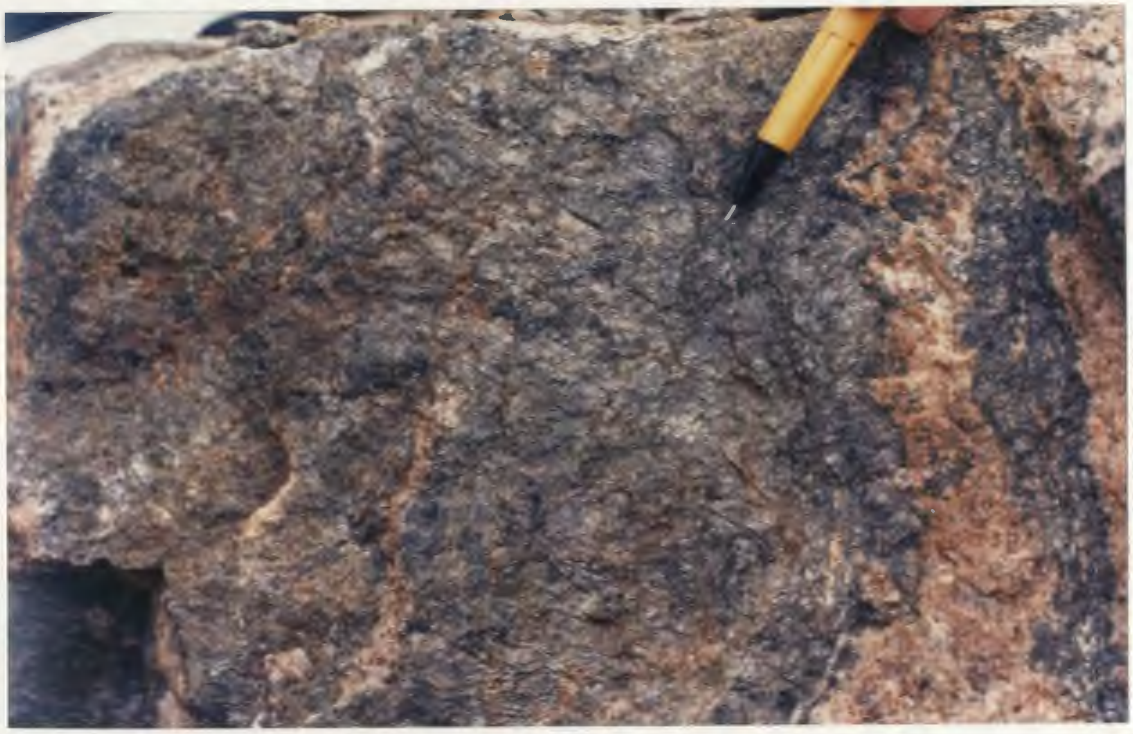

Photo 3-6: A-C fractures, infilled with magnetite, are oriented perpendicular to F_2 fold axes (here aligned perpendicular to the pencil and plane of the photograph)

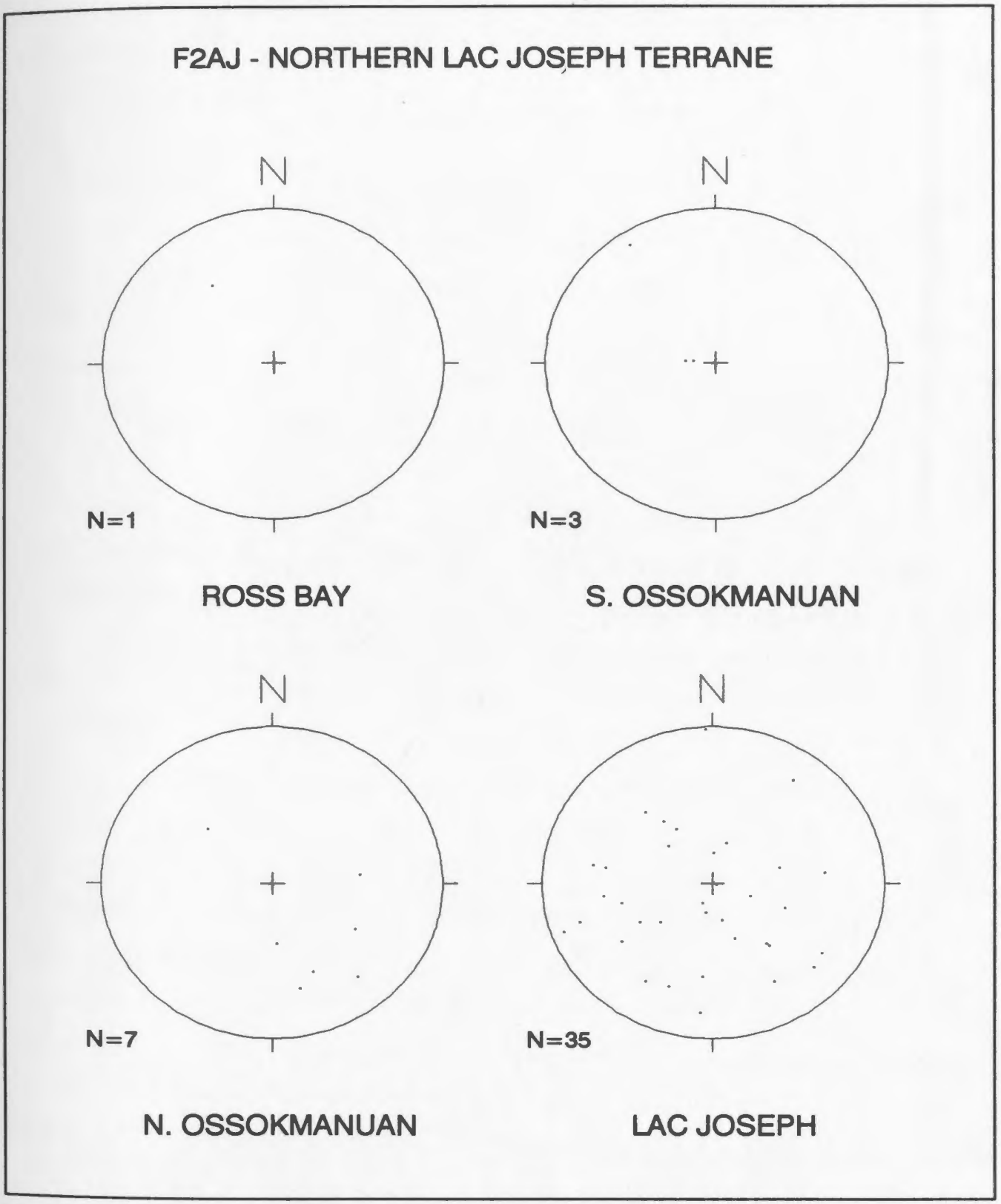

Figure 3-7: Orientations of F2AJ fold axis in the indicated domains of the Lac Joseph Terrane.

Small (less than 1 mm wide) brittle fractures in the restite layers of Unit 1 are oriented perpendicular to the F_{2J} fold axes (a-c fractures) suggesting the F_{2J} folding event may extended into more brittle conditions. Many of these fractures were subsequently infilled by magnetite (Photo 3-6).

3.2.1.5 F_{3J} Folding

The S_{1J} fabrics and F_{2J} axial planes in the pelitic supracrustal rocks are locally folded by northwest-trending tight to isoclinal folds which have upright axial planes. The fold axes are steep to vertically plunging to the northwest and the southeast. Since these folds affect the F_{2J} fold axial planes, they are termed F_{3J} (Photo 3-7). All earlier fabrics have been preserved in this refolding event and F_{3J} axial planar fabrics are absent.

3.2.2 Early Intrusive Rocks of the Lac Joseph Terrane

The state of strain in the intrusive rocks in the Lac Joseph Terrane is highly variable. These rocks range in appearance from massive and undeformed to strongly foliated and locally lineated. No evidence was observed to suggest that partial melting has occurred in any of the early intrusive units, suggesting that they were intruded after the main migmatite-generating event.

Unit 2 contains inclusions of gneissic fragments, wisps of sillimanite-bearing restite correlated with Unit 1 and its microstructure varies from massive to foliated; foliation trends are variable. Both the K-feldspar megacrystic and spatially related equigranular granites exhibit weak to well-developed foliations which generally trend between north and northeast and are steeply dipping, parallel to the main fabrics in the supracrustal rocks (especially in the southern domain as shown in Fig. 3-8a). Similarly, Units 3 and 4 exhibit foliations which are parallel to the northeast-trending regional fabric in the southern Lac Joseph Terrane (Fig. 3-8a).

The presence of fabrics in intrusive Units 2 to 4 with comparable orientations to the F_{2J} axial planes in host migmatites suggests that D_{2J} must have post-dated intrusion of these units.

Photo 3-7: F_{3J} folds in the pelitic migmatites of the Lac Joseph Terrane.

Photo 3-8: Mylonitic megacrystic granite wrapping around a losenge of gabbro of the Shabogamo Intrusive Suite which is internally foliated but was less ductile during mylonitization; from the north shore of Ossokmanuan Lake. Megacrysts indicate that the Lac Joseph Terrane moved northwestward over the Molson Lake Terrane.

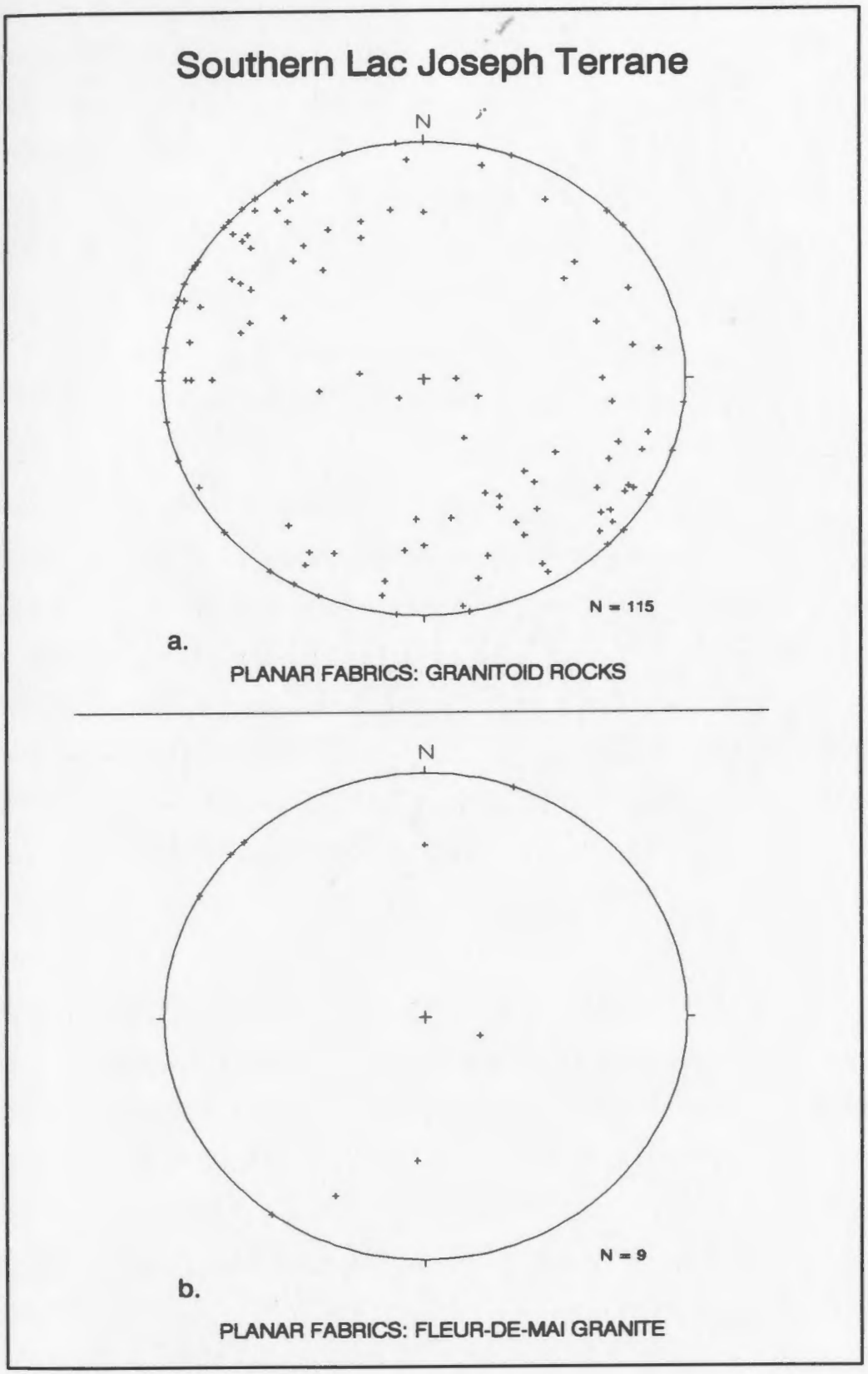

Figure 3-8: Orientations of the planar fabrics in the granitoid rocks of the southern Lac Joseph Terrane.

3.2.3 Late Intrusive Rocks of the Lac Joseph Terrane

Although the K-feldspar megacrystic Fleur-de-Mai granite (Unit 7) is predominantly massive, it exhibits a weak foliation in several localities. The fabrics in the Fleur-de-Mai granite are defined by aligned biotite and/or hornblende. There is no evidence of partial melting.

The foliation in the Fleur-de-Mai granite is correlated, on the basis of orientation (Fig. 3-8b) and intensity, with the F_{3J} folds locally observed in the supracrustal rocks. This correlation implies that the F_{3J} folding event must have post-dated the emplacement of the Fleur-de-Mai granite dated at 1133+10/-5 Ma (Emslie and Hunt, 1990) and is therefore most probably Grenvillian in age.

3.2.4 Topographic Lineaments in the Lac Joseph Terrane

Although few late brittle faults have been mapped, in the field a major lineament is apparent on both aeromagnetic and gravity maps. It can be traced from just south of the Labrador Trough in the Molson Lake Terrane, approximately 90 km into the interior of the Lac Joseph Terrane on a 070° trend. The aeromagnetic lineament terminates to the southeast of Lac Joseph (Fig. 2-1). The map pattern (Fig. 2.1) shows that there is a dextral offset of the boundary of Lac Joseph Terrane boundary along this trend, suggesting that it may be a fault. James et al. (1991) have interpreted two lineaments parallel to this major lineament, as late, brittle faults.

3.3 Structural Geology of the Molson Lake Terrane

Both the mafic and granitoid intrusive rocks of the Molson Lake Terrane exhibit a single planar and linear fabric. The similarities in style and orientation of this fabric in these two rock types suggest that they have experienced a similar deformation history and they will therefore be discussed together.

The planar and linear fabrics are well developed and commonly of equal intensity. Within the granitic rocks, the planar fabric (S_{1M}; subscript M denoting Molson Lake Terrane) is defined by aligned biotite, flattened mineral aggregates of quartz, plagioclase and feldspar and locally by an indistinct compositional layering. The comparable fabric in the Shabogamo Intrusive Suite is defined by flattened mineral aggregates and biotite alignment. Planar fabrics in the southern Molson Lake exhibit

dispersed trends, but dip mainly towards the northwest and southeast quadrants (Fig. 3-9a). Planar fabrics in the northern part of the Molson Lake Terrane show a wider range of orientations (Fig. 3-10).

Lineations in both rock types are typically defined by aligned hornblende and elongated mineral aggregates; they plunge down the dip of the foliation planes towards the north to southeast in the southern domain (Fig. 3-9b). In the northern part of the Molson Lake Terrane, L_{1M} plunges preferentially towards the southeast (Fig. 3-11).

Titanite, a stable phase of the fabric-forming mineral assemblage in the granitoid rocks of the Molson Lake Terrane, yields Grenvillian U-Pb ages suggesting that D_{1M} recrystallization and fabric development occurred during the Grenvillian Orogeny (see Section 6.4). This indicates that the D_{1M} fabrics in the Molson Lake Terrane are not related to the D_{1J} fabrics in the Lac Joseph Terrane.

Although the fabrics generated during the D_{1M} deformation event are typically not folded on the outcrop scale, the range of orientations of S_{1M} planar fabrics in the Molson Lake Terrane suggests that they were folded subsequent to D_{1M} fabric formation. This folding event, referred to as F_{2M}, resulted in tight, map scale fold patterns about northwest-trending axial surfaces which are well displayed by the outcrop pattern of the gabbro bodies (Fig. 2-1) and orientations of the pre-folding planar fabrics. The dominant southeast trend of the L_{1M} fabric suggests that F_{2M} folding may have been coaxial with D_{1M}. The F_{2M} folds do not have associated axial planar fabrics, suggesting that recrystallization during this event was minimal. The absence of small scale folds in the Molson Lake Terrane may be attributed to the lack of any significant compositional anisotropy on the outcrop scale. Although the abundance of hinge areas relative to the total outcrop coverage suggests that the fold patterns may be more complicated than interpreted, the sparse exposure in the Molson Lake Terrane precludes a more detailed interpretation. The similar orientation and position in the relative chronologies of deformation in the Molson Lake and Lac Joseph terranes of F_{2M} and F_{3J} folds, suggests that these folding events are correlative.

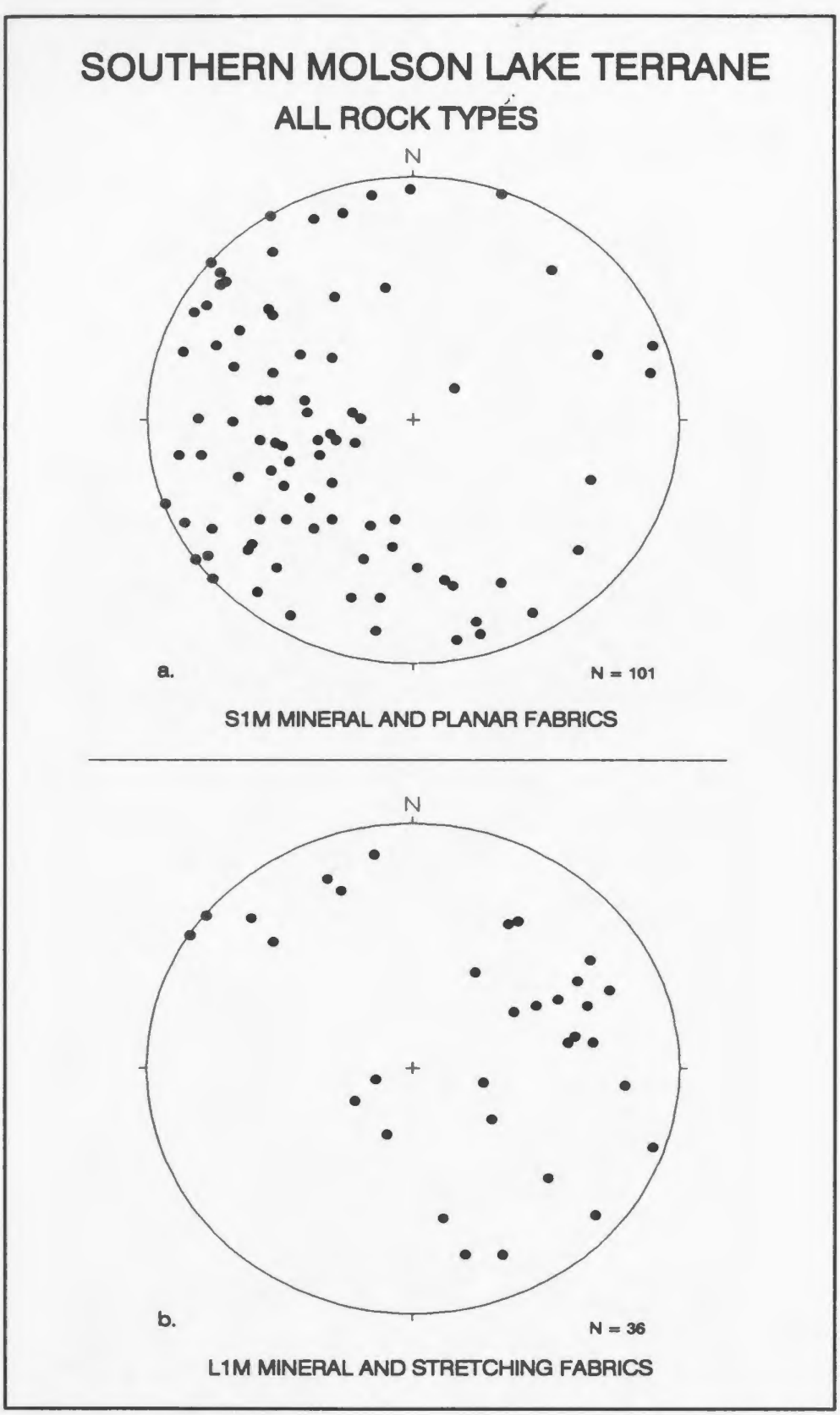

Figure 3-9: Orientations of the S1M planar and L1M linear fabrics in the southern Molson Lake Terrane.

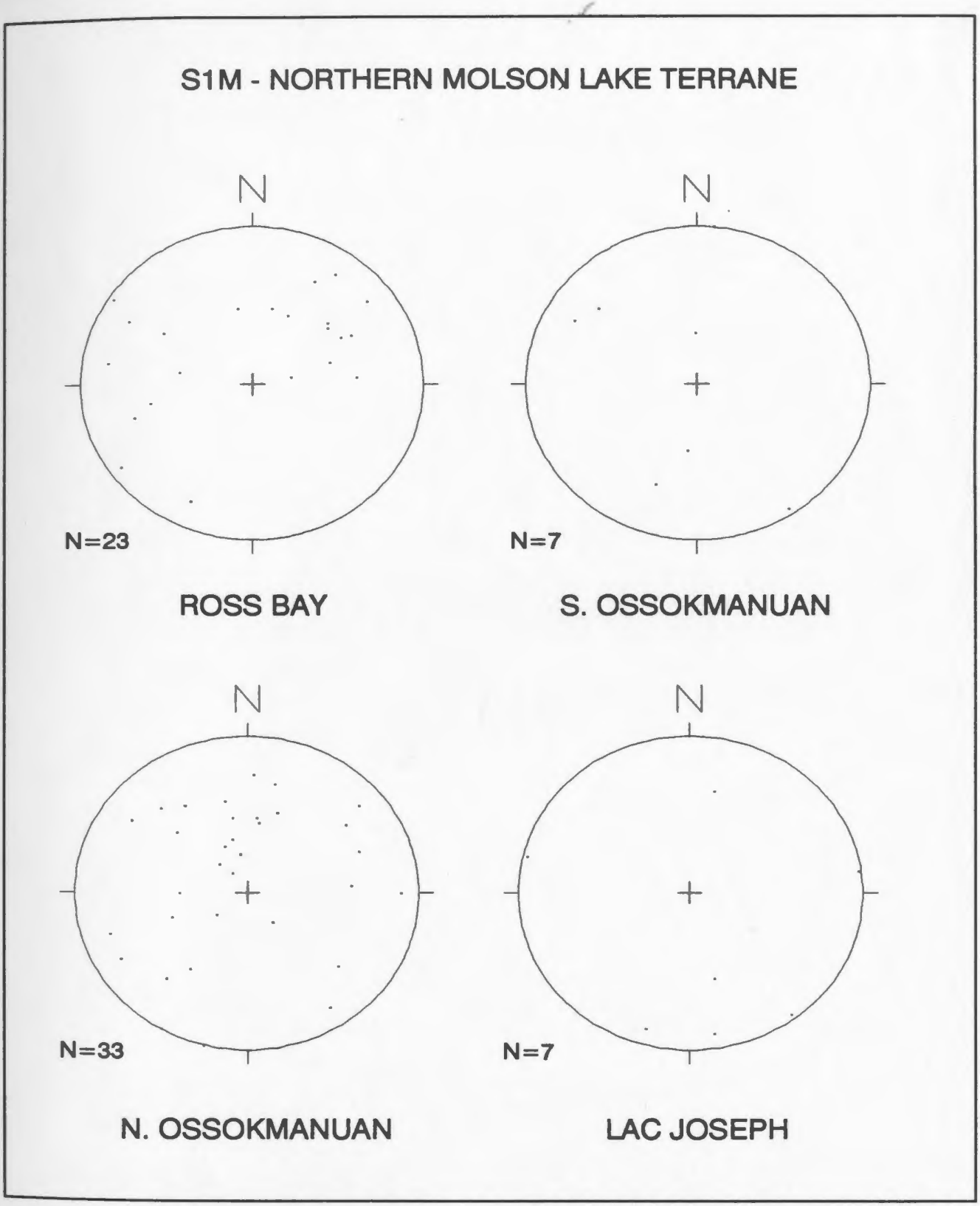

Figure 3-10: Orientations of planar fabrics in the northern domains of the Molson Lake Terrane.

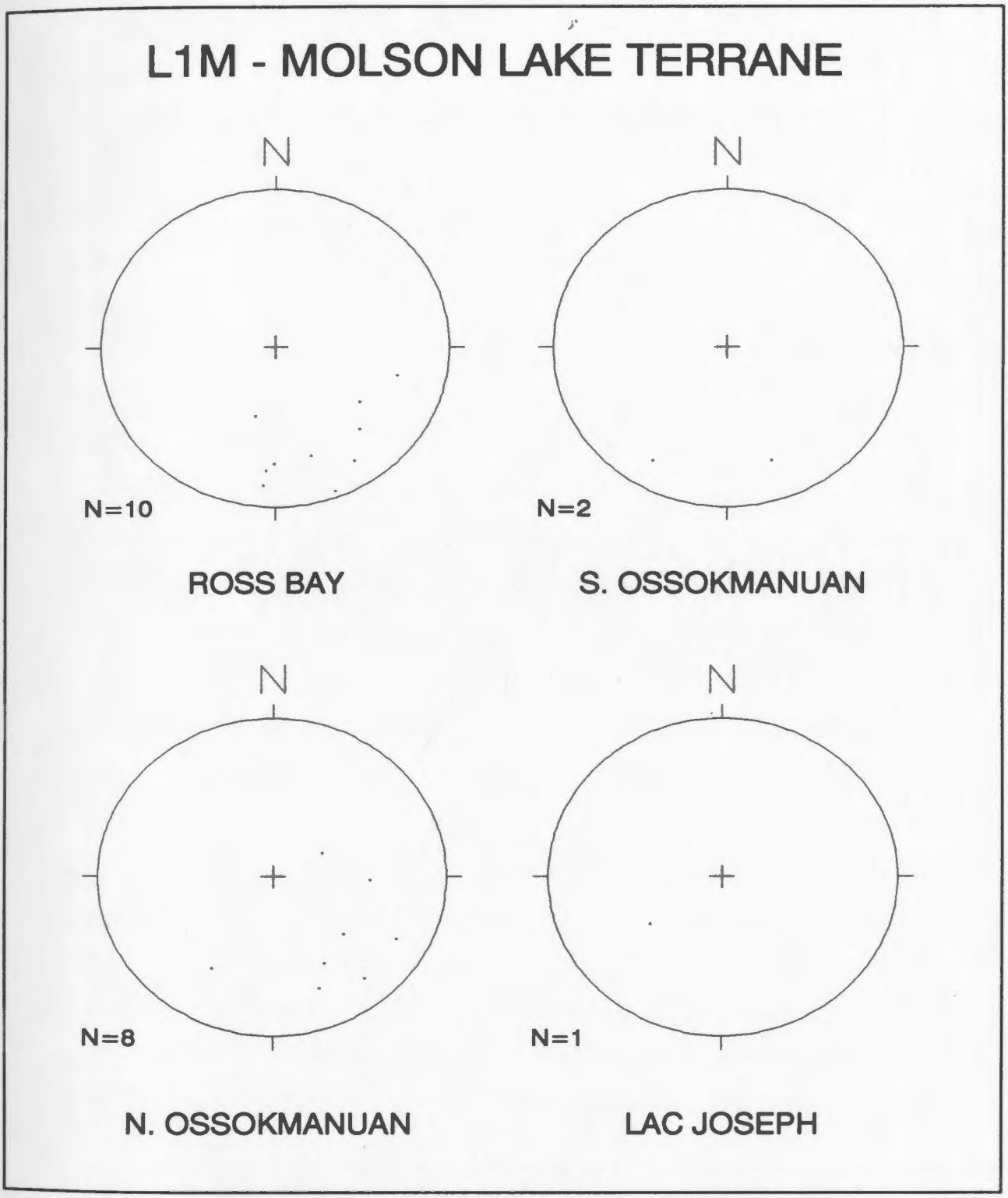

Figure 3-11: Linear fabrics in the northern domains of the Molson Lake Terrane.

3.3.1 Topographic Lineaments in the Molson Lake Terrane

In the southern part of the Molson Lake Terrane the straight, aligned southeast-trending shores of Lac Caopacho and Lac à la Marte (not shown on Figure 2-1) are interpreted to mark the location of a north-northeast trending brittle fault (shown in the southeast part of the Molson Lake Terrane in Figure 2-1). Rocks of the Shabogamo Intrusive Suite do not occur on the east side of this interpreted fault, suggesting that it may have significant relative displacement. Furthermore, the only known occurrences of supracrustal rocks in the Molson Lake Terrane lie to the east of this fault, and most probably represents a small klippe of Lac Joseph Terrane (too small to be represented on Figure 2-1).

3.4 Boundary Zone

The boundary of the Lac Joseph Terrane is well-exposed in only three areas, along the northern and southern shores of Ossokmanuan Lake and near Lac Emerillon (Fig 3-12). U-Pb data from the Lac Emerillon shear zone indicate that shearing occurred in the boundary zone at about 990±12 Ma, during the Grenvillian Orogeny (see Section 6.10).

3.4.1 North Ossokmanuan Shear Zone

The margin of Lac Joseph Terrane is well-exposed on the islands and shoreline in the northern part of Ossokmanuan Lake (Fig. 3-12). Rock types from both Lac Joseph and Molson Lake terranes are strongly deformed in an anastomosing system of ductile shear zones. Megacrystic granitoid rocks and the Shabogamo Intrusive Suite of the Churchill Falls Terrane occur as strongly foliated and lineated mylonites (Photos 3-8 and 3-9 respectively). The orientations of these shear zones vary from northeast to southeast trending, with an average east-west trend, and typically dip moderately towards the south (Fig. 3-13). Lineations are commonly down-dip towards the south to southeast. Kinematic indicators are rather rare in these mylonites in spite of the abundance of inclusions in the megacrystic granite. Where present, deflected foliations, shear bands, rotated megacrysts, sheath folds (Photos 3-10, 11 and 12) and C/S fabrics yield consistent kinematic information. To allow interpretation of a relative sense of displacement of the terranes, shear zones were restored to their presumed original south

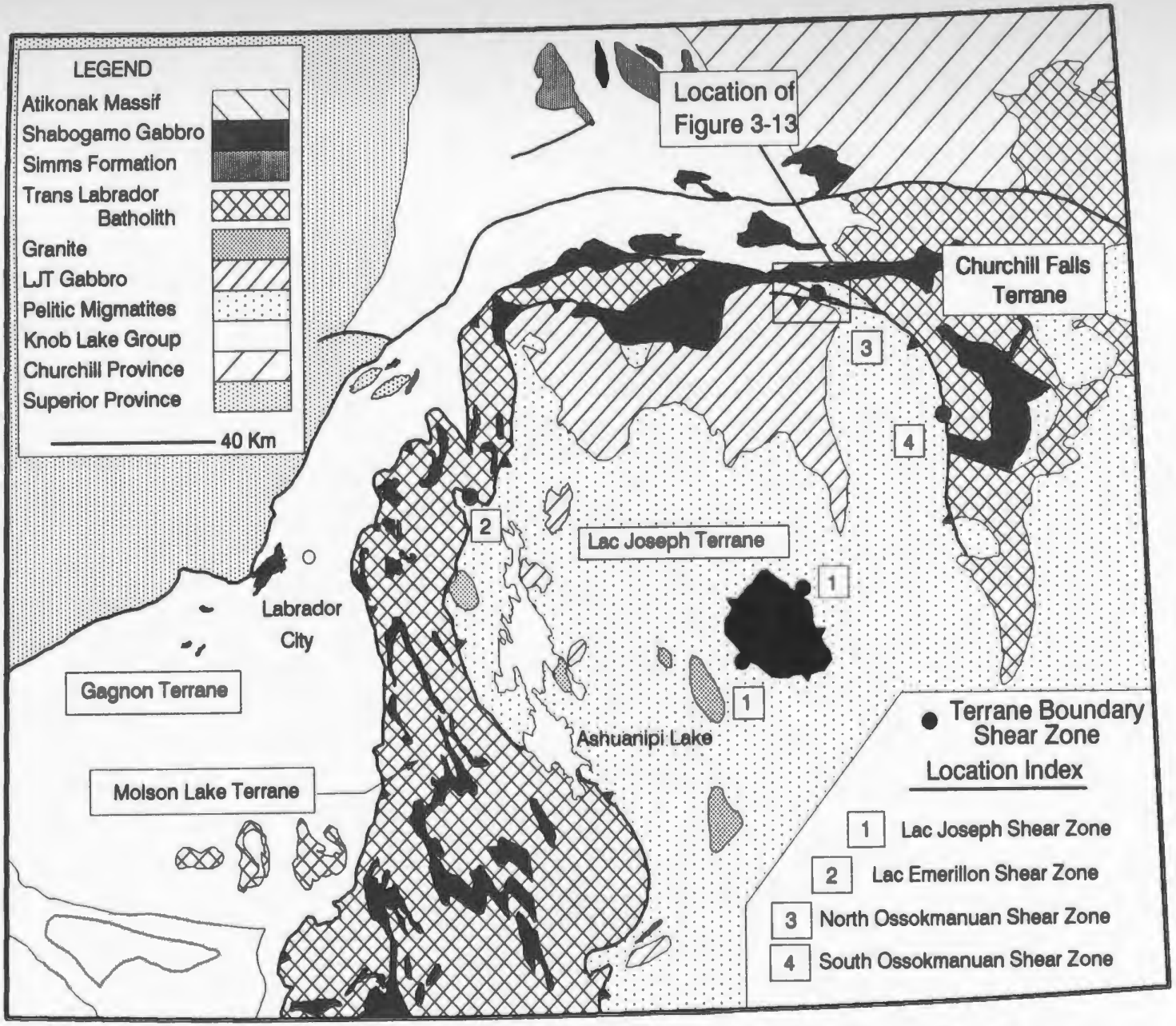

Figure 3-12: Location of shear zones marginal to the Lac Joseph Terrane which were studied in detailed.

Photo 3-9: Mylonitized gabbro of the Shabogamo Intrusive Suite in north Ossokmanuan Lake.

Photo 3-10: A narrow ductile shear zone in gabbro of the Shabogamo Intrusive Suite at the northern margin of the Lac Joseph Terrane (near Photo 3-11) indicates a dextral shear direction in this east-southeast dipping shear zone.

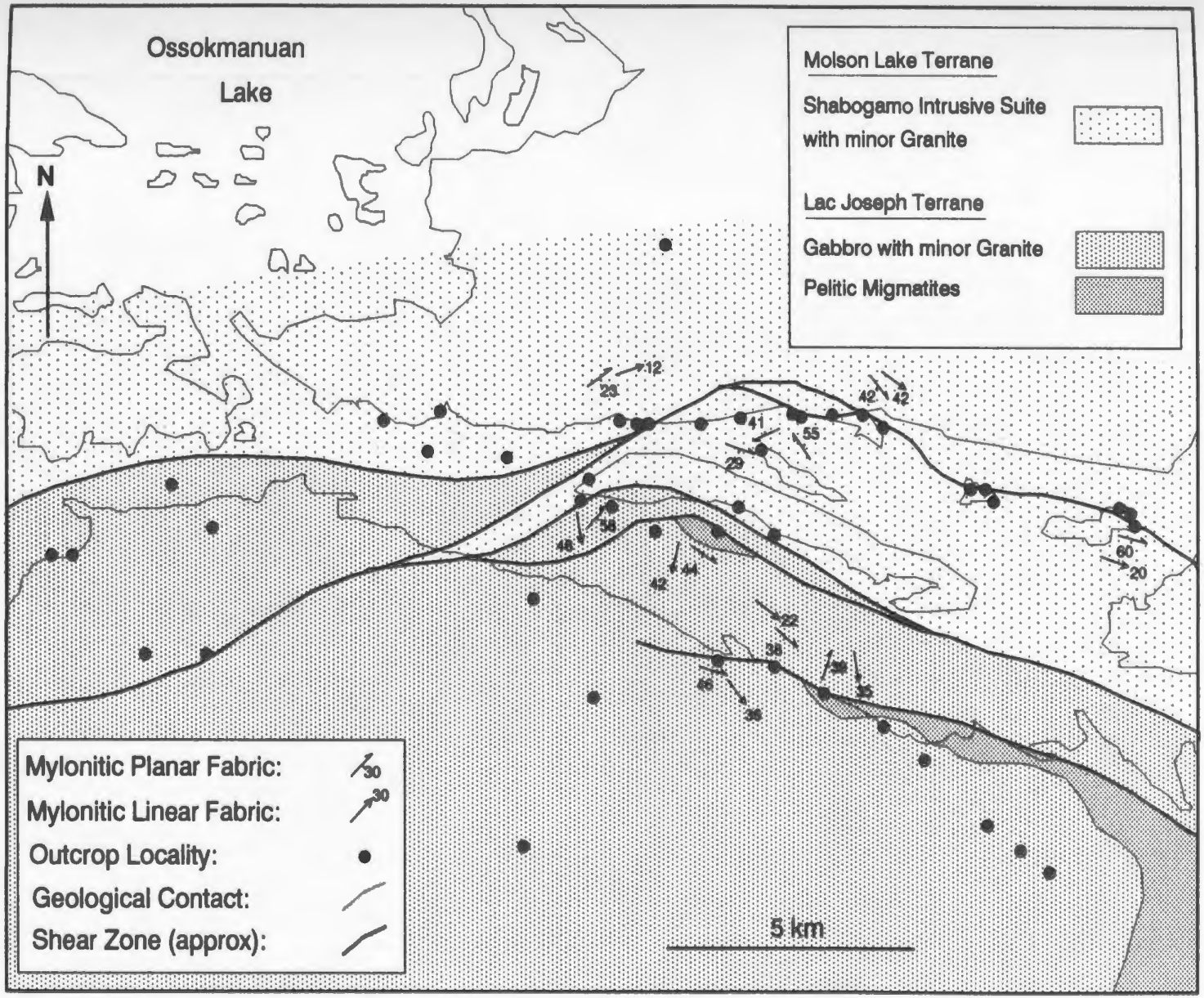

Figure 3-13: Detailed sketch map of the shear zone geometry at Ossokmanuan Lake. Location shown in Figure 3-12.

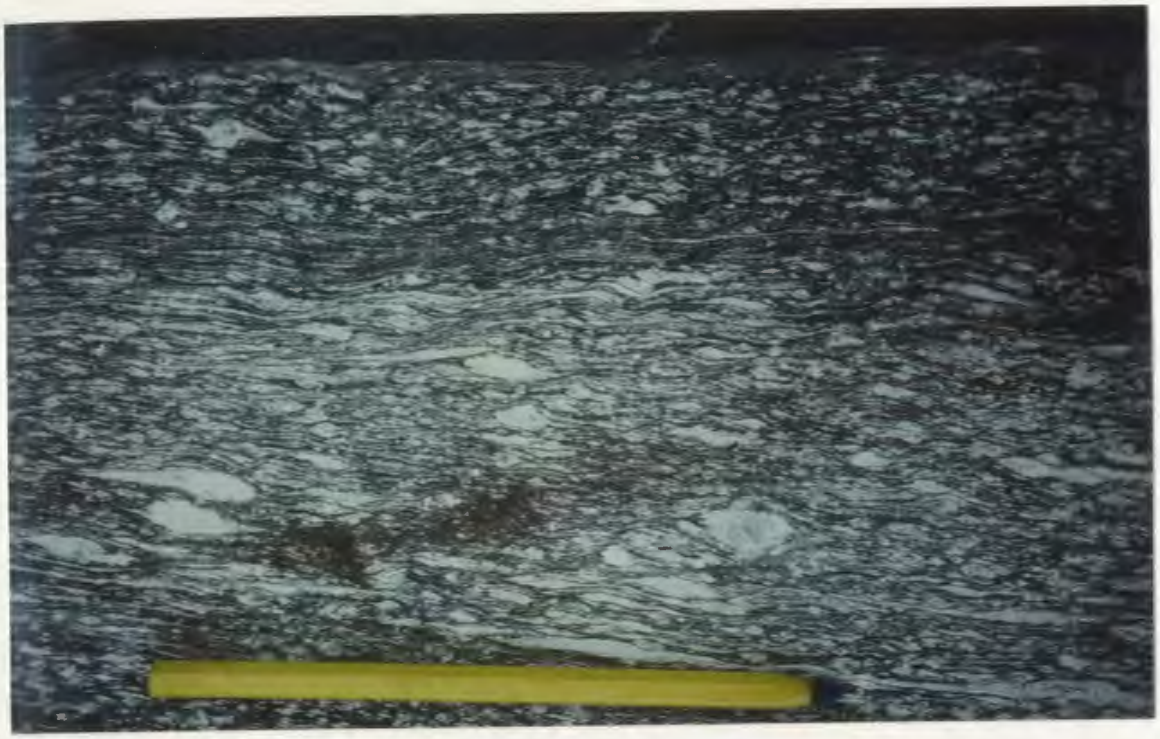

Photo 3-11: Shear bands (or extensional crenulation cleavage) and rotated feldspar inclusions indicate sinistral shear sense in this northeast dipping shear zone along the northern margin of the Lac Joseph Terrane.

Photo 3-12: A sheath fold protrudes from a narrow, flat-lying ductile mylonite zone along the northern margin of the Lac Joseph Terrane. With half the sheath fold preserved (beneath pencil), the foliation closes on itself behind the branch.

dipping orientation by rotation through the minimum angle. Following this method, multiple occurrences of the aforementioned kinematic indicators suggest that the Lac Joseph Terrane was displaced towards the north-northwest over the Molson Lake Terrane. This reconstruction method will not accommodate overturned shear zones, for which it will lead to a opposite sense of relative displacement (ie. normal vs. reversed). The total amount of displacement is an indeterminant function of the cumulative movements on all shear zones in the boundary fault system.

Mylonitized sillimanite-bearing migmatite of Unit 1, located along the southern shore of Ossokmanuan Lake, has not been correlated with the shear zone fabrics discussed above for several reasons. Although proximal to the margin and in an appropriate orientation, it is cross-cut by basic dykes of uncertain affinity (Photo 3-13), which render correlation equivocal for several reasons. Firstly, if the cross-cutting dykes are part of the Shabogamo Intrusive Suite, the shear zone must have formed prior to 1431$\pm$7 Ma, the U/Pb age of this suite; this contrasts with the anastomosing shear system described above which incorporates gabbro of the Shabogamo Intrusive Suite. Alternatively, however, this dyke may be part of a later, post-Grenvillian diabase suite. Secondly, the mineral assemblage in this shear zone is the same as that occurring throughout the Lac Joseph Terrane (ie. sillimanite - biotite - garnet - magnetite - leucosome). This observation constrains the shearing to have occurred at one of three possible times: 1) at the same time that the sillimanite-bearing assemblage was forming in the rest of the Lac Joseph Terrane; 2) subsequent to the formation of the sillimanite assemblage in the Lac Joseph Terrane, but under comparable conditions such that sillimanite remained stable; or 3) after the sillimanite-bearing assemblage formed throughout the Lac Joseph Terrane, but under anhydrous disequilibrium conditions so that sillimanite was preserved. Since a sillimanite-bearing shear zone elsewhere has been established to be Labradorian in age, (Section 6.5) it seems most probable that this shear zone may also be Labradorian and only coincidentally parallel to the marginal Grenvillian shear zone.

Photo 3-13: Mylonitic fabric in the sillimanite-bearing migmatites along the northern margin of the Lac Joseph Terrane, cross-cut by a diabasic dyke of unknown age.

Photo 3-14: Inhomogeneous shear strain in a shear zone exposed in south Ossokmanuan Lake at the eastern margin of the Lac Joseph Terrane.

3.4.2 South Ossokmanuan Shear Zone

The shear zone bounding the Lac Joseph Terrane is also exposed along the shore at the south end of Ossokmanuan Lake near the mouth of the Atikonak River. In this single outcrop, sillimanite-bearing migmatite is inhomogeneously mylonitized to a fine-grained strongly foliated matrix of quartz, feldspar, sillimanite, muscovite and biotite with K-feldspar porphyroclasts which are remnants of the coarse-grained leucosomes (Photo 3-14). This zone trends north-south with a steep westerly dip. Stretching lineations are horizontal to moderately plunging towards both the north and south. The orientation of F_{2M} fold axes is irregular within the outcrop, suggesting that reorientation of the axes occurred during shearing. Rare kinematic indicators (C/S fabrics and rotated inclusions) indicate that the west block (Lac Joseph Terrane) moved northward relative to the east block (Churchill Falls Terrane). These data are compatible with the interpretation that this shear zone was reoriented by later folding, and that the present erosion surface is an oblique section through what was originally a southeastward-dipping shear zone. The presence of synkinematic retrograde muscovite in the shear zone supports a Grenvillian age for the shearing determined by U-Pb geochronology (see Section 6.10).

3.4.3 Lac Emerillon Shear Zone

Although the Lac Emerillon Shear Zone (Fig. 3-12) is considered part of the boundary shear zone, it does not actually separate rocks that belong to the two terranes, but rather juxtaposes two slices of the Molson Lake Terrane. This is apparently typical of the anastomosing style of the boundary shear system as demonstrated in the better exposed outcrops of the north Ossokmanuan shear zone. The actual location of the boundary is restricted spatially by outcrops of rock types from both terranes within 5 km of each other.

The Lac Emerillon Shear Zone is a northwest-trending, southwest-dipping, annealed, ductile shear zone which has incorporated both granitoid and gabbroic rocks of the Molson Lake Terrane (Photo 3-15). Lineations plunge moderately towards the southeast. Scarce kinematic indicators (C/S fabrics, rotated feldspars) suggest that the southwest slice of Shabogamo Intrusive Suite moved northwestward over the lower

Photo 3-15: Interlayered mylonitic granite and gabbro in the annealed Lac Emerillon shear zone near Ross Bay.

slice of the same unit. Reorientation of the mylonite fabric back to an approximate pre-folding geometry by unfolding around the local F_{2M} fold axis direction yields a southeast-dipping mylonite zone with northwest-directed thrusting. U-Pb geochronology has established that this shear zone was operative during the Grenvillian Orogeny (see Section 6.10).

3.5 A Window in the Lac Joseph Terrane

A tectonic window is thought to be present in the centre of the Lac Joseph Terrane, based on two lines of evidence: 1) the area in the proposed window is underlain by coronitic metagabbro correlated with the distinctive Shabogamo Intrusive Suite, a unit which is known only to exist in the Parautochthonous Belt; 2) several outcrops of annealed mylonitic rocks have been found along the margin of the proposed window; and 3) no intrusive relationships (ie. dykes) were found in the surrounding migmatites. The bounding shear zones incorporate mafic gneiss and sillimanite-bearing migmatite of Unit 1. The mylonitized pelitic migmatites appear similar to those in the south Ossokmanuan shear zone, and consist of a fine- to medium-grained foliated and lineated matrix hosting porphyroclasts of K-feldspar, which are presumed to be remnants of coarse-grained leucosomes. No convincing kinematic indicators were observed in the sheared pelitic migmatite. The folded and agmatitic nature of the mafic gneiss around Lac Joseph (Photo 2-5) contrasts sharply with the straight layering of this same unit at the contact between the proposed tectonic window and the Lac Joseph Terrane. This interpretation of a tectonic window of Molson Lake or Churchill Falls terrane in the Lac Joseph Terrane places qualitative constraints on the maximum thickness of and minimum north-westward transport distance for the Lac Joseph Terrane.

3.6 The Scarcity of Kinematic Indicators in the Boundary Zone of the Lac Joseph Terrane

In contrast to some terrane boundaries in which there are abundant kinematic indicators of the sense of displacement during ductile shearing (eg. Hanmer, 1988;

1989) very few kinematic indicators have been observed along the boundary of the Lac Joseph Terrane. This observation has led the author to evaluate the criteria which lead to the formation of kinematic indicators in sheared rocks.

The efficiency with which an inclusion of constant aspect ratio is rotated in a ductile shear zone is, in part, a function of the ratio of pure to simple shear, with the maximum angular velocity achieved in ideal simple shear (Ghosh and Ramberg, 1976; Hanmer, 1984). Ideal simple shear, operative in a non-collapsing transcurrent shear zone, will give way to pure shear as a shear zone becomes transpressive. In a thrust zone, pure shear will similarly increase in importance relative to simple shear as the thickness of the over-riding plate, and therefore, the incumbent load, increases. If the Lac Joseph Terrane was thick enough to constitute a significant incumbent load on the basal thrust zone, the efficiency of inclusion rotation in the shear zone may have been considerably reduced, thereby resulting in a scarcity of kinematic indicators.

3.7 Structure of the Gagnon and Churchill Falls Terranes

3.7.1 Introduction

As previously mentioned, detailed mapping was not carried out in the Churchill Falls and Gagnon terranes. However, for future discussion of the regional tectonic framework, an overview of the structural styles in these terranes will be presented here. The tectonic evolution of the Gagnon Terrane was discussed by Rivers (1983) and has been the subject of two concurrent studies at Memorial University by J. van Gool, (in prep.) and D. Brown (1991); these sources have provided the following information about the Gagnon Terrane. The structural style of the Churchill Falls Terrane is described by Wardle (1982), Nunn and Christopher (1983) and Nunn et al. (1984).

3.7.2 Gagnon Terrane

The supracrustal rocks of the Gagnon Terrane extend across the Grenville Front into the tectonic foreland and have been interpreted to represent a passive margin sequence lying unconformably on the Superior Province (Wardle and Bailey, 1981; Rivers, 1983; van Gool, in prep.). Within the Grenville Orogen, these metasedimentary rocks comprise a narrow, arcuate, northwest-verging fold and thrust belt which drapes around, and is overlain by, the northwest margin of the Molson Lake Terrane (Fig.

2-1). Although the main penetrative fabrics, folding and thrusting are reported to be of Grenvillian age (van Gool, in prep.; Brown, 1991), Brown (1991) reported that local, relict early fabrics are cross-cut by a recrystallized mafic dyke which he correlated with the 1431 $\pm$7 Ma Shabogamo Intrusive Suite implying that there is local fabric of pre-Grenvillian in age. The presence of both in-sequence and out-of-sequence thrusts, reported by van Gool (in prep.) and Brown (1991), has been interpreted to suggest that Grenvillian thrusting occurred in two stages; initial thin-skinned in-sequence folding and thrusting at higher crustal levels (low metamorphic grade) which was followed by larger scale, fold-dominated, out-of-sequence thrusting and folding at deeper crustal levels (higher metamorphic grade). Slices of Archean basement gneisses up to several kilometres thick, bounded by Grenvillian thrusts, are correlated with the Ashuanipi Metamorphic Complex to the northwest in the Superior Province (van Gool, in prep.).

3.7.3 Structure of the Churchill Falls Terrane

Nunn and Christopher (1983) recognized migmatitic layering as the earliest structure in the northwest part of the Churchill Falls Terrane adjacent to the Lac Joseph Terrane. Nunn et al. (1985) reported geochronological evidence suggesting that this migmatization occurred during the Labradorian Orogeny between 1676 and 1666 Ma. Rare isoclinal folding of the migmatite layering predates the intrusion of a K-feldspar megacrystic granite which is reported to be mid-Labradorian in age, implying that this early folding episode must be early Labradorian. Although no supporting geochronological evidence was available, Nunn and Christopher (1983) suggested that a second phase of migmatization developed during the Grenvillian Orogeny. All previous tectonic fabrics were subsequently refolded, transposed and pervasively recrystallized at this time. In light of the results of the U/Pb data in this study, it would seem reasonable to suggest that, like the Lac Joseph Terrane, all migmatization in the supracrustal rocks of the Churchill Falls Terrane is Labradorian in age.

3.8 Conclusions

In the Lac Joseph Terrane, the Labradorian Orogeny resulted in partial melting and the development of gneissic layering during D_{1j}, at which time flattening and linear fabrics in the leucosomes, and planar and linear mineral fabrics in the restites (S_{1j} and

L_{1J}) were formed in the pelitic migmatites of the Lac Joseph and Churchill Falls Terranes. This D_{1J} event in the Lac Joseph Terrane was followed by widespread, penetrative F_{2J} refolding of the early fabrics and localized recrystallization of biotite. D_{1J} flattening fabrics and F_{2J} folding attest to the compressive nature of the Labradorian Orogeny in the Lac Joseph and Churchill Falls terranes. Although large volumes of granitoid rocks were intruded into the Molson Lake Terrane during the Labradorian Orogeny, no evidence was found to support the existence of Labradorian deformation in this terrane. Although Brown (1991) interpreted the pre-Grenvillian fabrics in the northern Gagnon Terrane to be Hudsonian in age, there is no evidence to preclude the possibility that they in fact are Labradorian, thereby raising the possibility that the effects of the Labradorian Orogeny may have extended into the Gagnon Terrane.

The intrusion of gabbros of the Shabogamo Intrusive Suite marks the first significant post-Labradorian event within the Grenville Orogen of western Labrador. No structural features are attributable to their emplacement.

The Grenvillian Orogeny resulted in the development of penetrative planar and linear fabrics (S_{1M} and L_{1M}) in the Molson Lake and Gagnon terranes of the Parautochthonous Belt. These early fabrics were subsequently folded later during the Grenvillian Orogeny, about northwest-trending F_{2M} axial planes which are correlated with the last folding event in the Lac Joseph Terrane (F_{3J}). Primarily on the basis of metamorphic evidence (Chapters 4 and 5), the Molson Lake Terrane is interpreted to have undergone major northwest-directed crustal shortening during the Grenvillian Orogeny. The structural pattern interpreted for the Molson Lake Terrane is in accord with that inferred for other Parautochthonous terranes. For instance, Rivers, (1983) and van Gool (in prep) have documented the progressive development of a large scale fold and thrust belt in the Gagnon Terrane at this time.

The parautochthonous and allochthonous terranes were juxtaposed into their present relative positions along ductile, locally anastomosing systems of shear zones. Kinematic indicators, which are scarce, are consistent with a northwest-directed, top-side-up sense of movement along the shear zones. The Lac Joseph Terrane is thus the highest structural level exposed; it overlies the Molson Lake and Churchill Falls

terranes, which in turn overlie the Gagnon Terrane all of which are parautochthonous with, and structurally overlie the foreland to the north of the Gagnon Terrane. The structural relationship between the Molson Lake and Churchill Falls terranes is not known at present.

CHAPTER 4
METAMORPHISM

4.1 Introduction

In the previous chapter, the relative chronology of mineral growth, as established from textural criteria and the relationships of mineral growth to structural fabrics, has been utilized to establish the relative timing of metamorphic and structural events in the Molson Lake and Lac Joseph terranes. In this chapter, mineral assemblages, mineral chemistry and reaction microstructures are linked to mineral equilibria in order to constrain the P-T conditions which prevailed in these terranes during the Labradorian and Grenvillian orogenies.

In general, P-T estimates may be based either on petrogenetic grids or on experimentally calibrated pressure and temperature sensitive continuous reactions. In this chapter the first approach is followed, such that the mineral assemblages, mineral chemistry and mineral reactions are discussed in terms of the constraints that they put on the P-T conditions of metamorphism during the Labradorian and Grenvillian orogenies. In Chapter 5, geothermometery and geobarometery are employed to more accurately quantify the P-T conditions during the two orogenic events.

4.2 Pelitic Migmatites of the Lac Joseph Terrane

The pelitic migmatites in the Lac Joseph Terrane comprise two distinct leucosomes (N_1 and N_2) interlayered with restite which contains aluminosilicate - biotite - garnet - magnetite or muscovite - biotite - garnet - hematite. The aluminosilicate may be sillimanite or, more rarely, kyanite; muscovite-bearing assemblages are subdivided according to whether the muscovite is aligned or randomly oriented. In the following sections, the petrography and petrogenetic implications of the leucosomes and the four types of restite assemblage are discussed.

4.2.1 Leucosomes in the Pelitic Migmatite

All metapelitic and semipelitic rocks are extensively migmatized throughout the map area, regardless of the assemblages in the restite. The early leucosomes (N_1), are dominated by plagioclase and quartz with lesser amounts of K-feldspar; these leucosomes are fine grained, foliated and lineated, and generally light grey in colour.

The N_2 leucosomes are subparallel to the earlier N_1 leucosomes, but can be distinguished from the latter by the greater abundance of K-feldspar. The N_2 leucosomes are also commonly foliated and lineated, but are coarser grained than N_1 leucosomes and are pinker in colour. In thin section, both N_1 and N_2 leucosomes exhibit a wide range of textures; granular textures dominate the lesser deformed leucosomes (Photo 4-1), but internally strained, elongated grains with extensive subgrain development and seriated grain boundaries are much more typical (Photo 4-2). The contacts between the restites and leucosomes are typically abrupt; restite minerals are rarely observed in the leucosomes except in the muscovite-bearing migmatites where muscovite is present in the leucosome. All phases are observed to be in mutual, stable contact except locally in areas dominated by the muscovite-bearing restite where muscovite preferentially rims K-feldspar.

No unequivocal evidence has been found to indicate the processes by which melt was generated and many questions therefore remain unanswered. The delicate interlayering of the leucosome and restite, the concentration of "residual phases" in the restite and the local presence of restite microrafts in the leucosomes suggest that the leucosomes were derived, at least partially, in situ. The presence of only quartz and feldspars, and the paucity of ferromagnesian residual phases in the leucosomes suggests that melting occurred primarily by the breakdown of plagioclase + K-feldspar + quartz + water, corresponding to the granite minimum melt reaction. However, it is also possible that dehydration melting of a muscovite-bearing assemblage generated a water undersaturated melt that crystallized K-feldspar upon cooling.

4.2.2 Aluminosilicate-Bearing Restites

Restites in the Lac Joseph Terrane typically contain the assemblage sillimanite-biotite-garnet-magnetite; kyanite locally occurs instead of, or with, sillimanite along the north and west margins of the terrane and adjacent to the western side of the tectonic window (Fig. 4-1). The relative timing of kyanite and sillimanite growth is uncertain, even in samples containing both minerals. The aluminosilicate and biotite are typically intergrown and subparallel, defining S_{1J} and L_{1J}. Biotite is locally recrystallized parallel to F_{2J} axial planes. Sillimanite and biotite both wrap around and terminate against garnet (Photos 4-3 and 4-4 respectively); aligned sillimanite inclusion

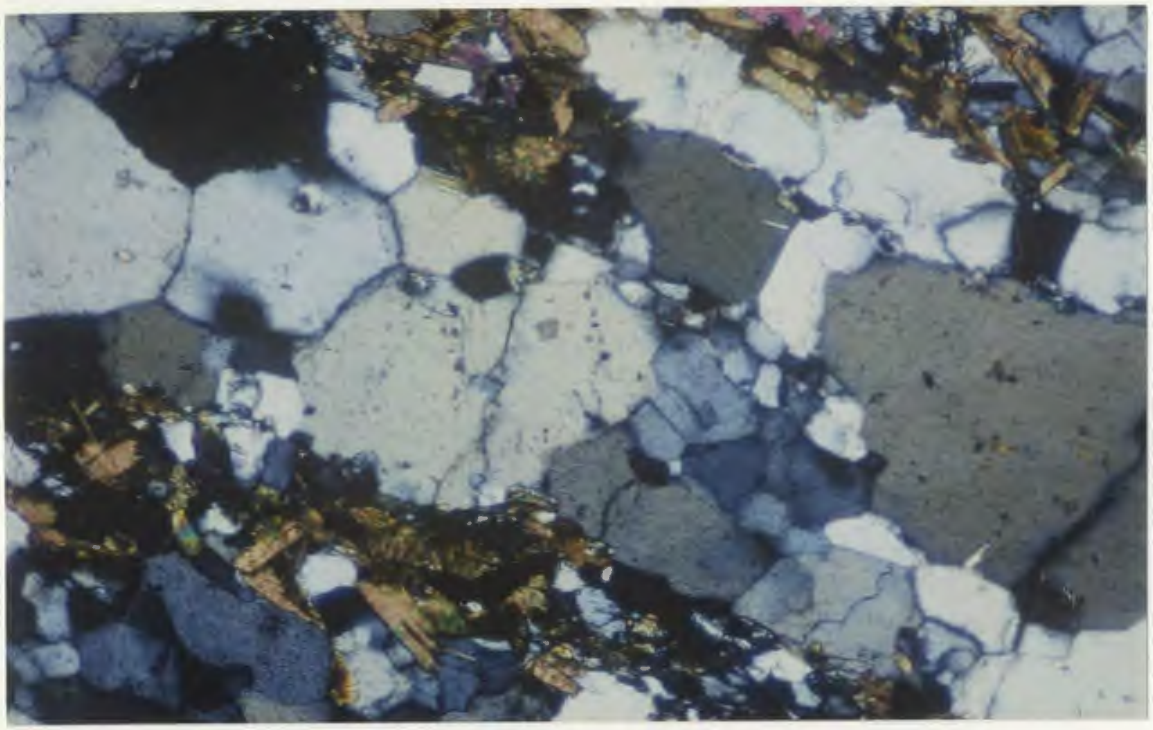

.2 mm

Photo 4-1: Unstrained leucosome within the pelitic migmatites of the Lac Joseph Terrane. Plane polarized light.

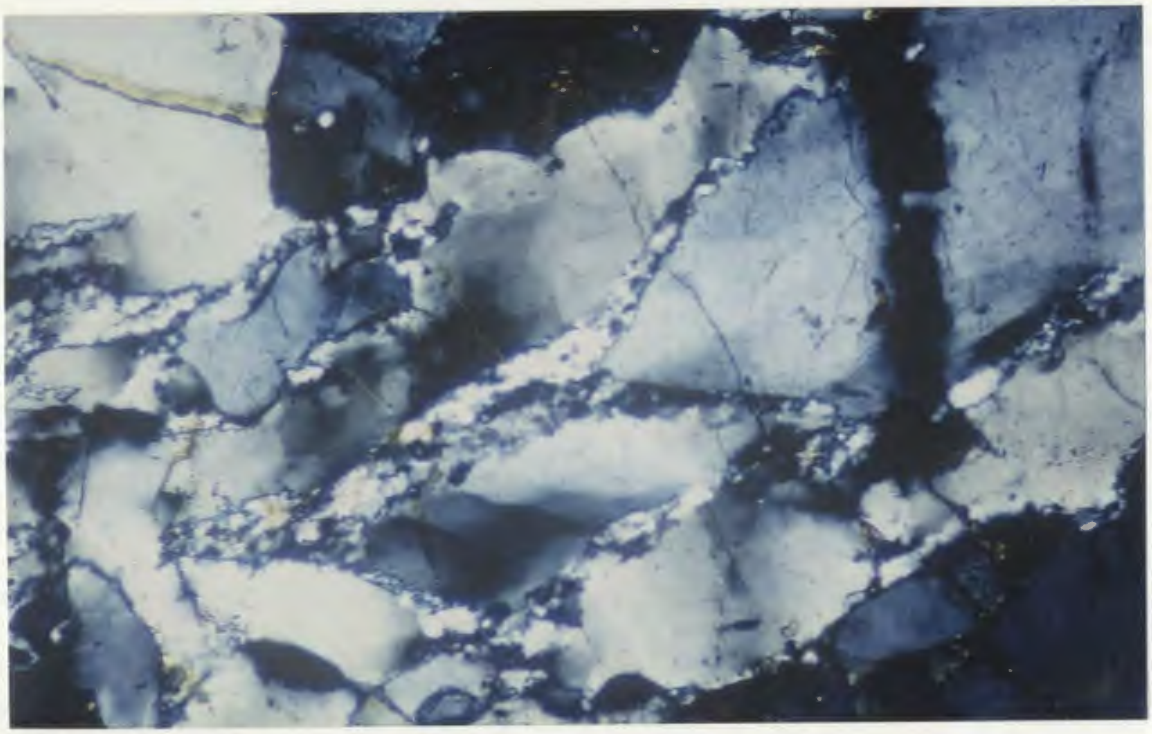

.2 mm

Photo 4-2: Subgrain development in quartz in the leucosome of the pelitic migmatites of the Lac Joseph Terrane. Plane polarized light.

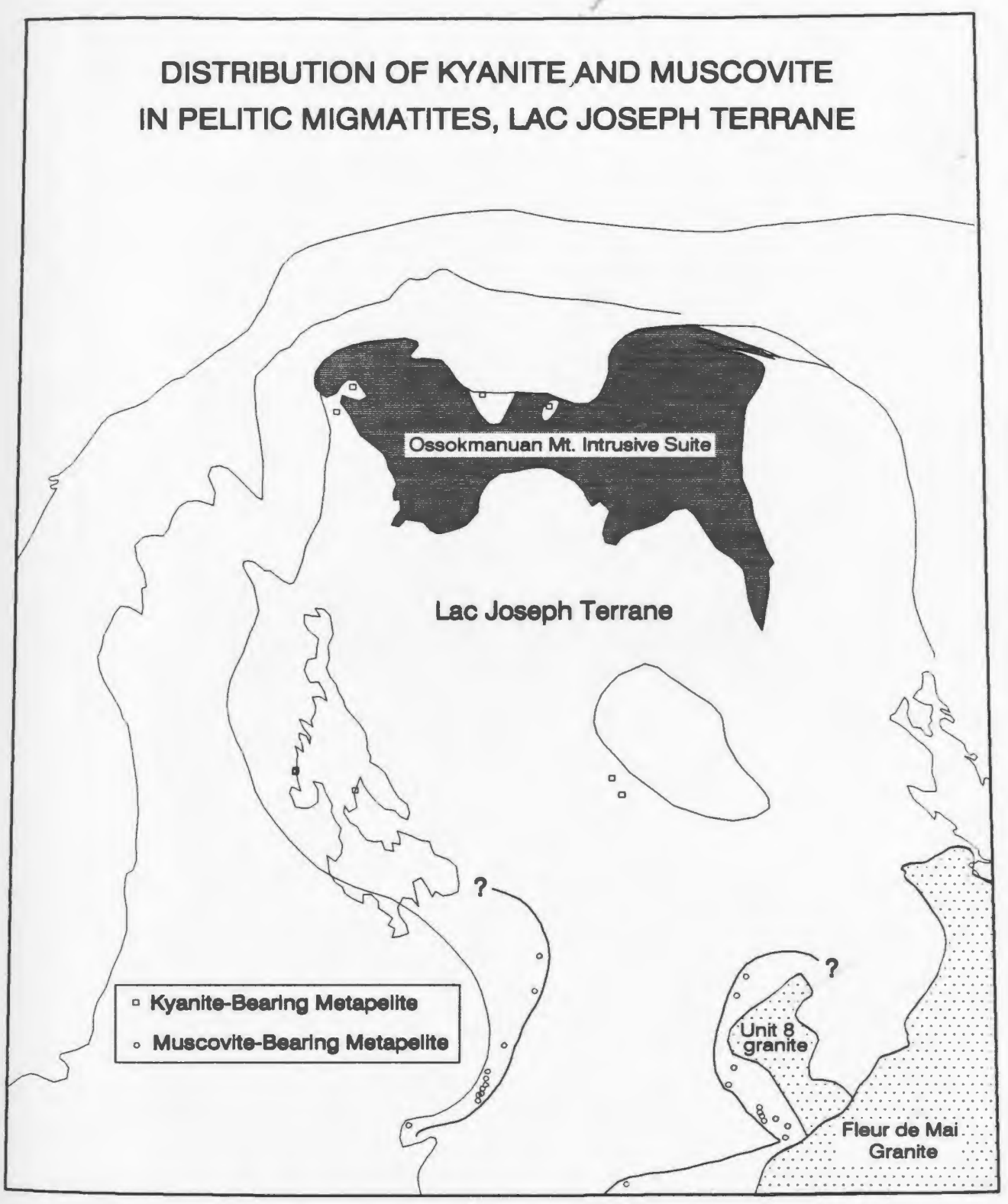

Figure 4-1: Distribution of kyanite- and muscovite-bearing assemblages in the restites of the pelitic migmatites in the Lac Joseph Terrane. Areas in the Lac Joseph Terrane without pattern contain the mineral assemblage sillimanite - biotite - garnet - magnetite in the restite.

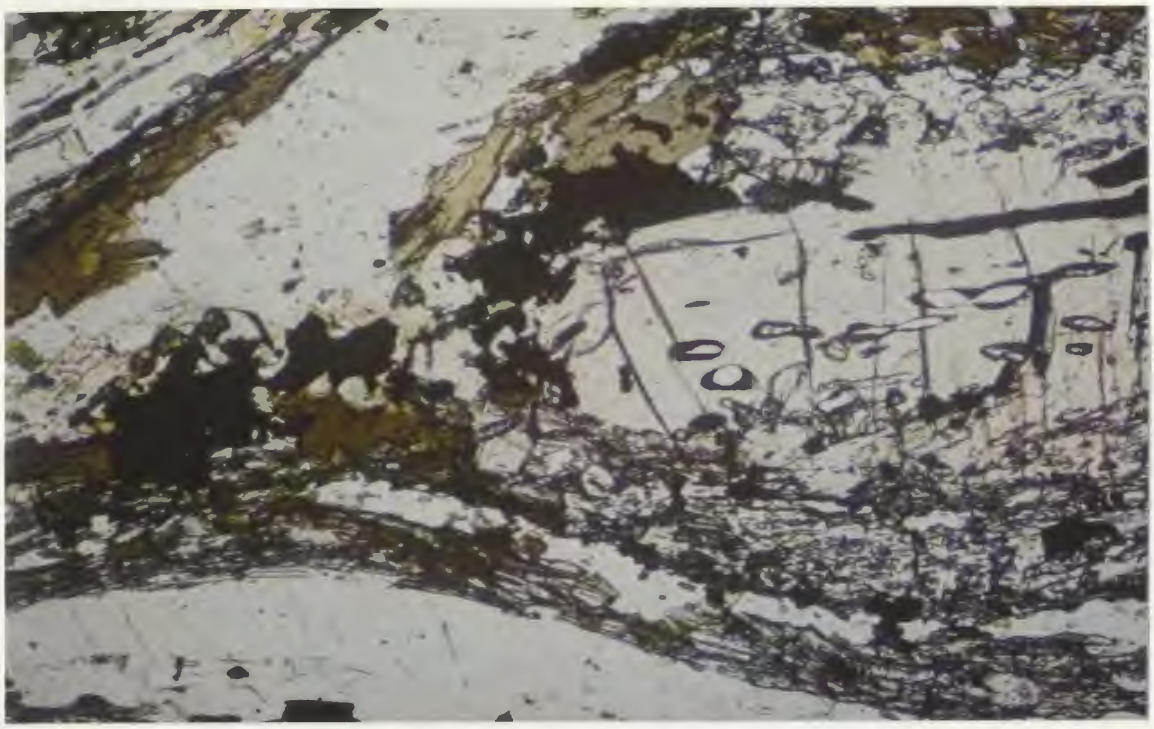

.2 mm

Photo 4-3: Garnet porphyroblast, containing relict internal fabric. The external fabric, S_{1J}, defined by biotite and sillimanite, wraps around the garnet indicating that garnet predated the end of the D_{1J} phase of deformation. Plane polarized light.

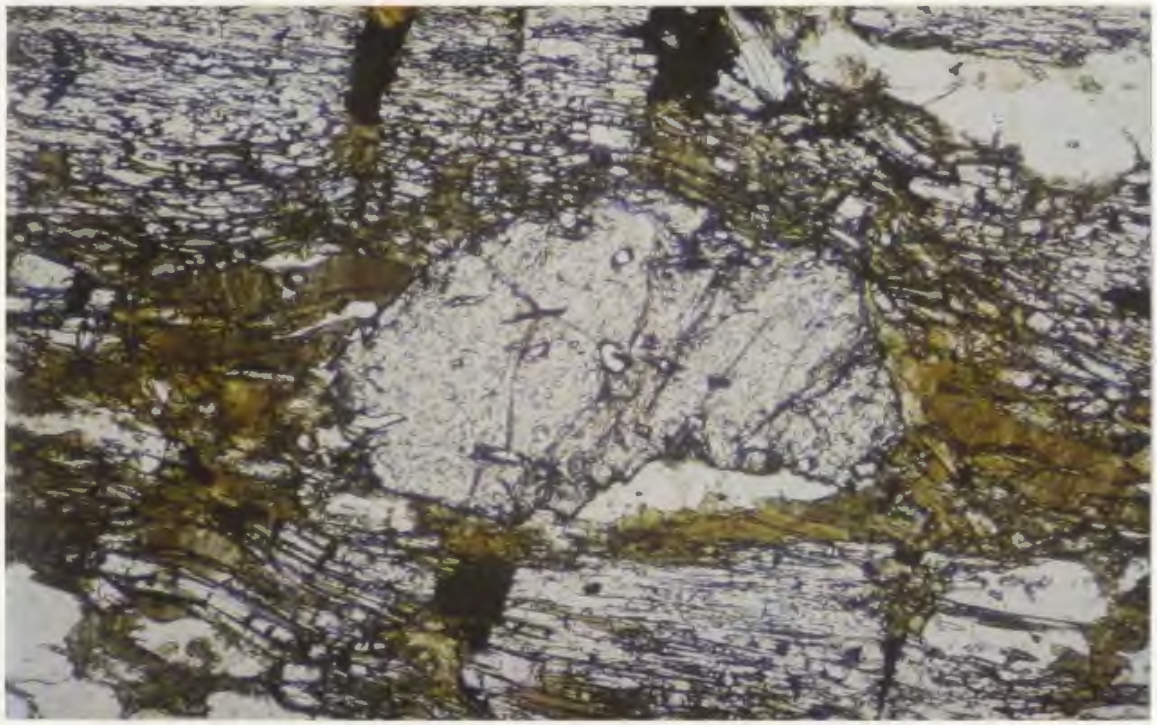

.2 mm

Photo 4-4: Biotite defining the S_{1J} fabric abutting garnet, which truncates the S_{1J} fabric. Plane polarized light.

trails in garnet are approximately parallel to the matrix fabric. Magnetite is present in two textural associations: 1) as small equant grains disseminated in the restite (Photo 4-5); and 2) infilling fractures perpendicular to the F_{2J} fold axes between boudinaged aggregates of restite phases (Photo 4-6). The aluminosilicate, biotite, garnet and magnetite are in mutual, sharp contact and appear to be stable together.

These microstructural relationships suggest that the aluminosilicate, biotite, garnet and the disseminated magnetite formed a stable assemblage and remained stable until the cessation of mineral reactions. The assemblage sillimanite - garnet - biotite - magnetite defines the principal fabric in the 1634+13/-4 Ma shear zones (see U-Pb data, Chapter 6) implying that it was generated during the Labradorian Orogeny. The local recrystallization of biotite into parallelism with F_{2J} axial planes apparently did not result in the penetrative recrystallization of biotite throughout the Lac Joseph Terrane. The consistent orientation of the magnetite-filled fractures perpendicular to F_{2J} fold axes is interpreted to indicate that the fractures are related to extension associated with the F_{2J} folding. This suggests that the magnetite in these fractures crystallized after the main restite mineral assemblage, and so it may not be in equilibrium with the other phases unless the earlier P-T conditions persisted during the F_{2J} folding. No textural evidence has been observed to indicate the origin of this late magnetite; it therefore remains uncertain whether it was precipitated from solutions, remobilized from the early disseminated magnetite and/or generated by the breakdown of ferromagnesian minerals in the restite. Within the aluminosilicate-bearing restite, there is no evidence for discontinuous reactions between any of the restite phases or between these phases and the minerals in the leucosome.

4.2.3 Bulk Chemistry of the Pelitic Migmatites

In order to quantify the chemical variability of the pelitic migmatites, nine representative samples of this unit were analyzed for major and minor elements at the laboratories of the Newfoundland Department of Mines; the analyses are tabulated in Appendix 1. As would be expected for a supracrustal unit, the major elements for the nine samples vary considerably. For example, SiO_2 and Al_2O_3 vary between about 68% and 79% and 10.5% to 17.5% respectively. The relative variation for the other elements is comparable in magnitude to that of Al_2O_3.

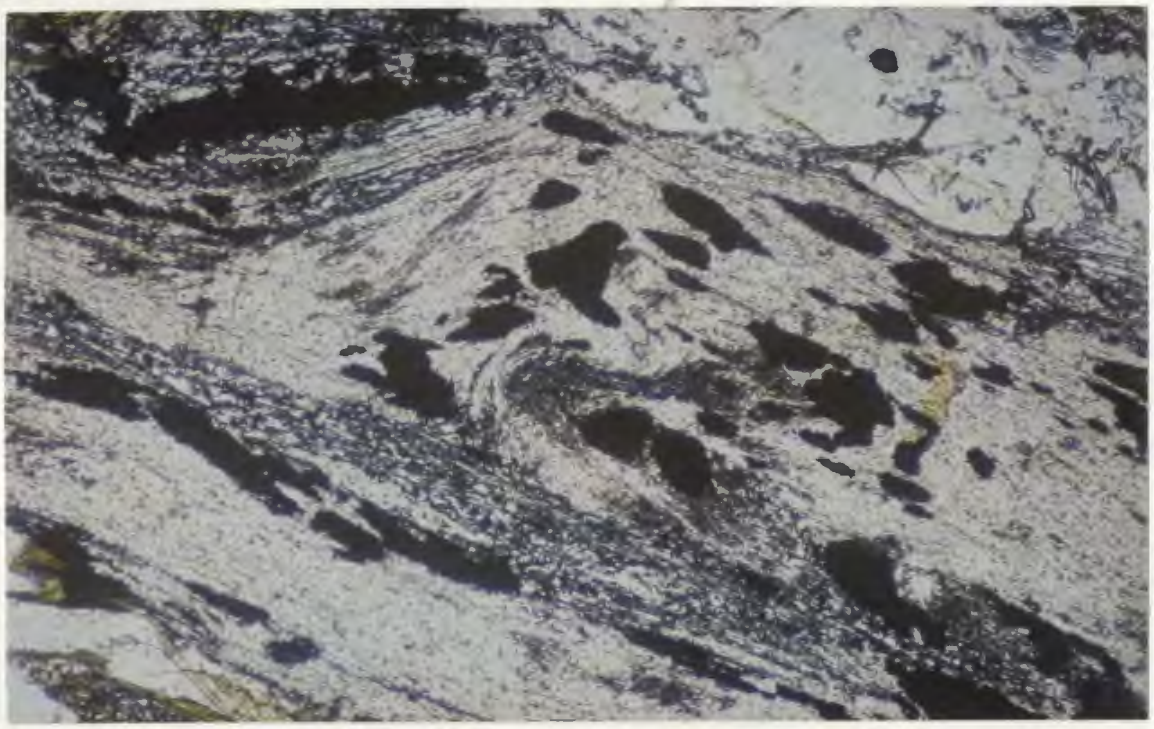

Photo 4-5: Magnetite (opaque phase) disseminated throughout the restite of the pelitic migmatites in the Lac Joseph Terrane. Plane polarized light.

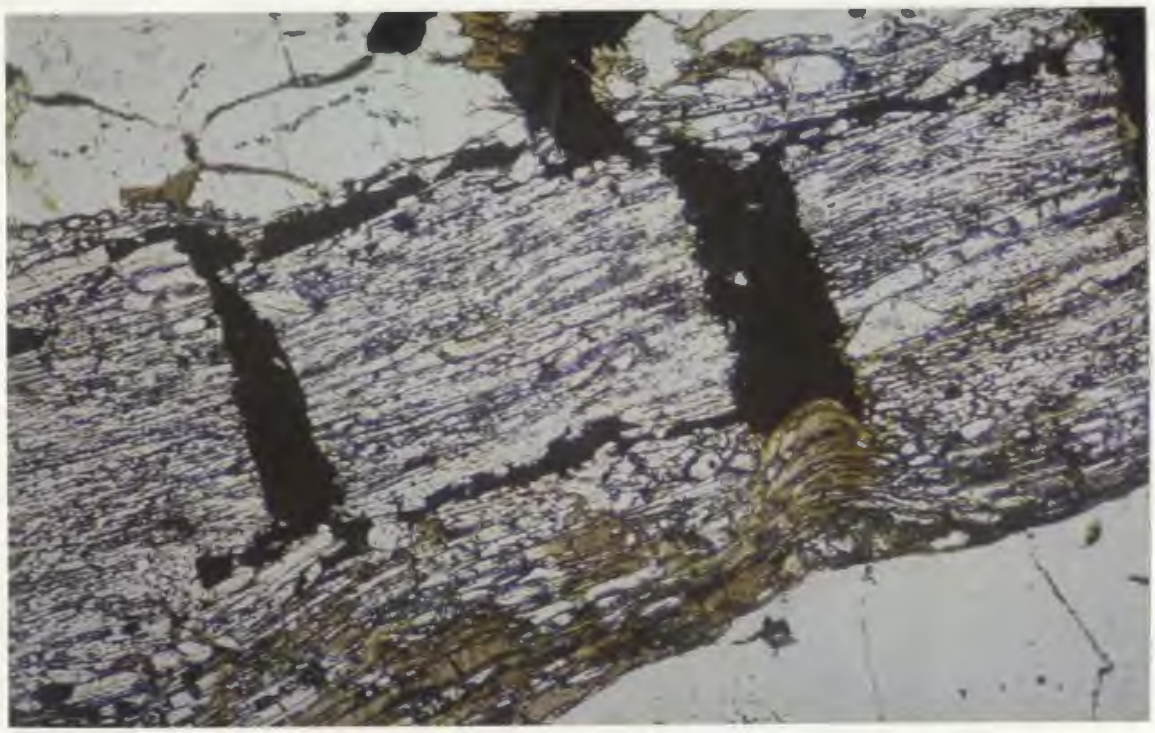

Photo 4-6: Secondary magnetite in a-c fractures in the restite of the pelitic migmatites in the Lac Joseph Terrane. Plane polarized light.

In order to assess the local variations in the Fe^{+2}:Mg ratio in ferromagnesian minerals, and to assess the amount of Fe^{+3} not held in magnetite, the relevant whole rock analyses of Fe and Mg have been plotted in Figure 4-2. Fe_2O_3 is more abundant than FeO in all but two samples, JNC-86-78 and JNC-86-96 (Fig. 4-2). The ratio of MgO/MgO+FeO(total) (where FeO(total) represents all FeO in the analyses) varies between about .15 and .31. In order to assess this ratio in the silicate phases in these rocks, the analyses have been recalculated assuming that all Fe_2O_3 occurs in magnetite; FeO is coupled with the Fe_2O_3 in magnetite assuming an FeO:Fe_2O_3 ratio of 31:69 by weight percent (Deer et al., 1966) and this amount is subtracted from FeO(total) to derive FeO(-mgt). MgO/MgO+FeO(-mgt) thus approximates the MgO/MgO+FeO ratio for ferromagnesian silicate minerals and has a restricted range of variation between .56 and .72.

4.2.4 Mineral Chemistry of the Aluminosilicate-bearing Pelitic Migmatites

4.2.4.1 Introduction

All mineral analyses discussed in this chapter were made with an electron microprobe, a technique which is not capable of distinguishing Fe^{+2} from Fe^{+3}. Several possible methods of calculating Fe^{+2} and Fe^{+3} from microprobe analyses have been proposed, but all suffer from certain shortcomings. In this study, all calculations of chemical formulae are based on the assumption that $Fe^{+2} = Fe^{TOTAL}$. A discussion of this assumption is presented in Appendix 2. Mineral analyses presented in this and the following chapter are tabulated in Appendix 3.

4.2.4.2 Garnet

Garnet compositions vary considerably in the pelitic migmatites of the Lac Joseph Terrane. The almandine-pyrope ratio exhibits the greatest variability with the Mg/(Mg+Fe) ranging from .148 to .571 (Fig. 4-3a). The negative correlation between Mg and Fe evident in Figure 4-3a implies that most garnets in the metapelites are predominantly mixtures of almandine and pyrope, although sample 7054 is an obvious exception. The northern and northwestern domains (5000-8000 numbers) are characterized by higher Mg/(Mg+Fe) ratios compared to the southern domain (0-2000 numbers). Spessartine varies between .025 and .1 cations per formula unit and

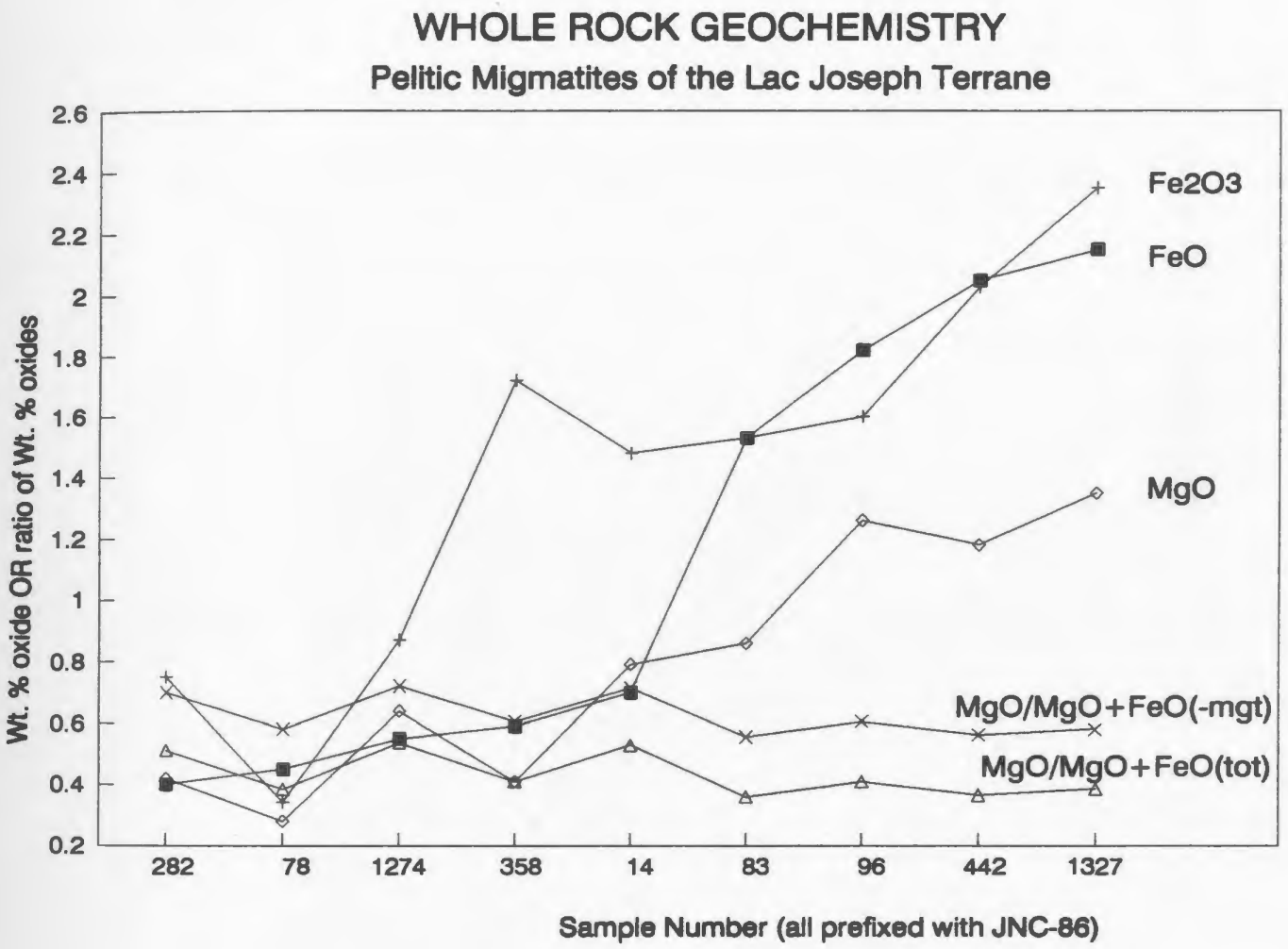

Figure 4.2: MgO, FeO and Fe2O3 weight percent oxides and ratios from whole rock geochemistry of the pelitic migmatites of the Lac Joseph Terrane plotted for each sample (x axis). Mg/Mg+Fe+2(tot) represents total Fe+2; Mg/Mg+Fe+2(-mgt) represents Fe+2 after removing Fe+2 in magnetite (assuming a ratio of 31:69 for FeO:Fe2O3 for magnetite (Deer et al., 1966) and all Fe2O3 is in magnetite).

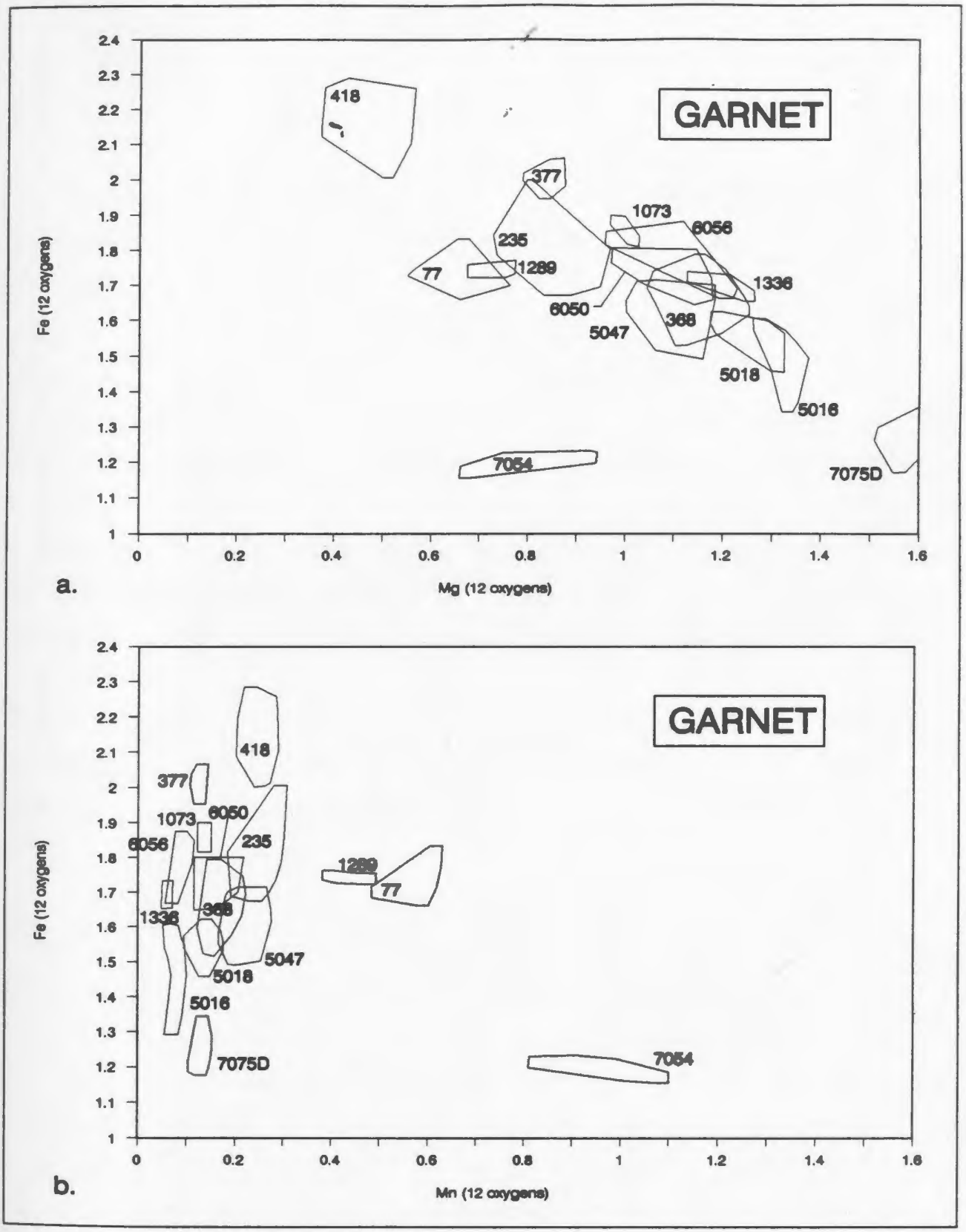

Figure 4-3: Chemical composition of garnets in migmatites of the in the Lac Joseph Terrane.

therefore forms only a minor component of the garnets (Fig. 4-3b). Ca varies between .05 and .2 cations per formula unit and shows a weak inverse relationship with Fe (Fig. 4-4).

Electron microprobe traverses were performed across garnets in most samples to test for the presence of chemical zonation in individual grains. A representative selection of garnet profiles is shown in Figure 4-5 in which it can be seen that there is a weak enrichment of Fe relative to Mg near the grain edges in two of the samples (235 and 418) while sample 368 exhibits no zonation. There is no perceptible systematic variation of Ca in the six traverses shown in Figure 4-5. Zonation patterns such as these are common in garnets of upper amphibolite- to granulite-facies rocks and imply that the garnets were homogenized during the peak of metamorphism (Tracy, 1982). The weak decrease in Mg/Mg+Fe ratio near the rims of some of the grains is interpreted to be a consequence of retrograde intergranular re-equilibration of Mg and Fe during cooling. In this case, it is likely that Fe and Mg were exchanged between garnet and biotite.

4.2.4.3 Biotite

Biotite aligned parallel to the $S_{1,}$ fabric was selected for electron microprobe analysis rather than that parallel to the F_2 axial surfaces for reasons noted above. The majority of Mg/(Mg+Fe) ratios from biotite in the pelitic migmatites fall between .6 and .8 with outliers around .5 and .85 (Fig. 4-6). These ratios indicate that a majority of analyses fall within the phlogopite field as defined by Deer et al. (1966) (Mg:Fe greater than 2:1). Mg/(Mg+Fe) ratios appear to show systematic spatial variation, with the north and northwestern parts of the Lac Joseph Terrane (5000-8000 numbers) having Mg/(Mg+Fe) ratios which are higher than those in the south (0-2000 numbers).

In order to assess the variability in the Mg/(Mg+Fe) ratios between coexisting garnet and biotite, the compositions of these phases have been plotted on AFM diagrams (Figs. 4-7 and 4-8). Figure 4-7 shows that coexisting garnets and biotites span a range of compositions in terms of their Fe:Mg ratios, but that the slope of the tie lines joining coexisting mineral pairs are rather constant in orientation suggests that chemical equilibrium was maintained on a gross scale during the metamorphism and over a limited range of temperature. Figure 4-8, in which the samples are grouped according

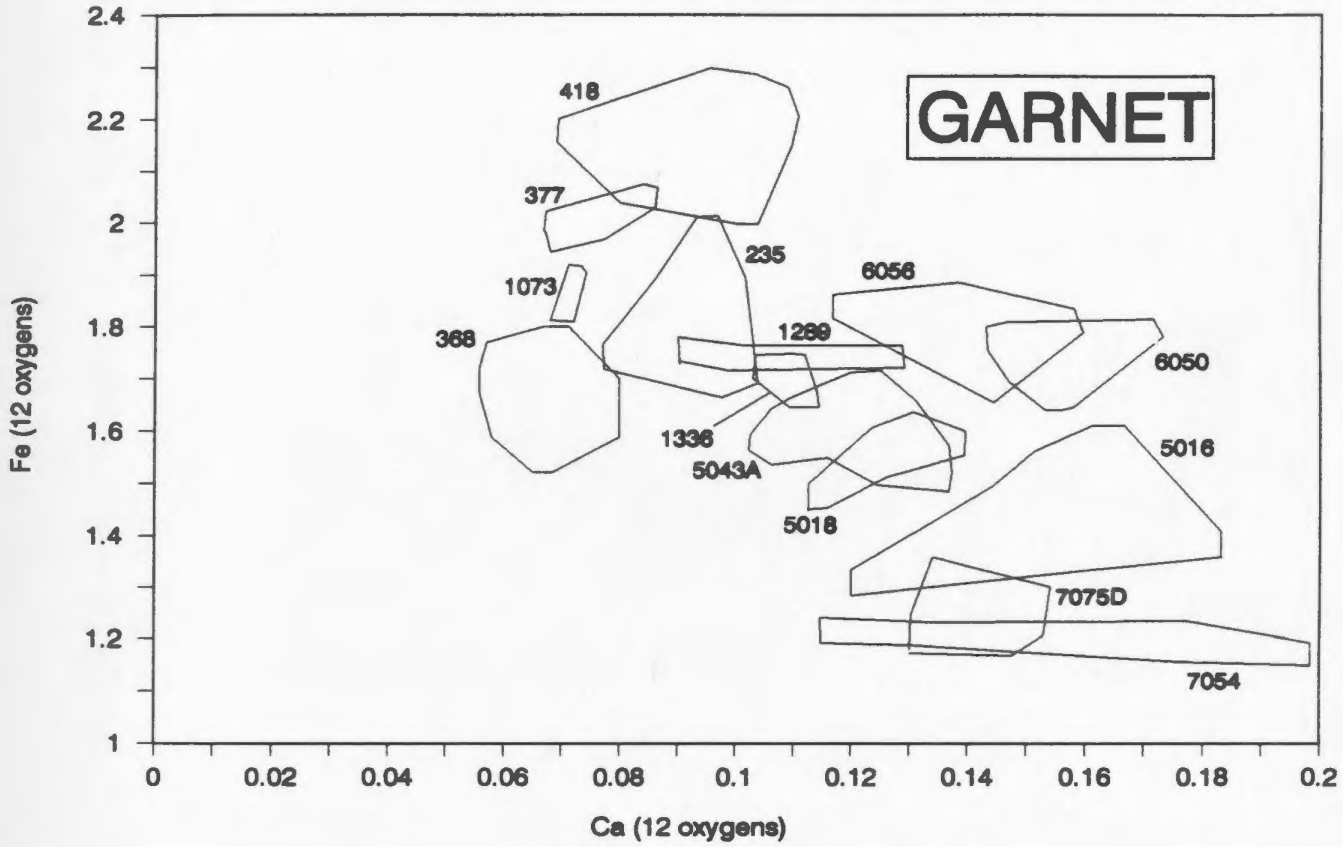

Figure 4-4: Chemical composition of garnets in pelitic migmatites in the Lac Joseph Terrane.

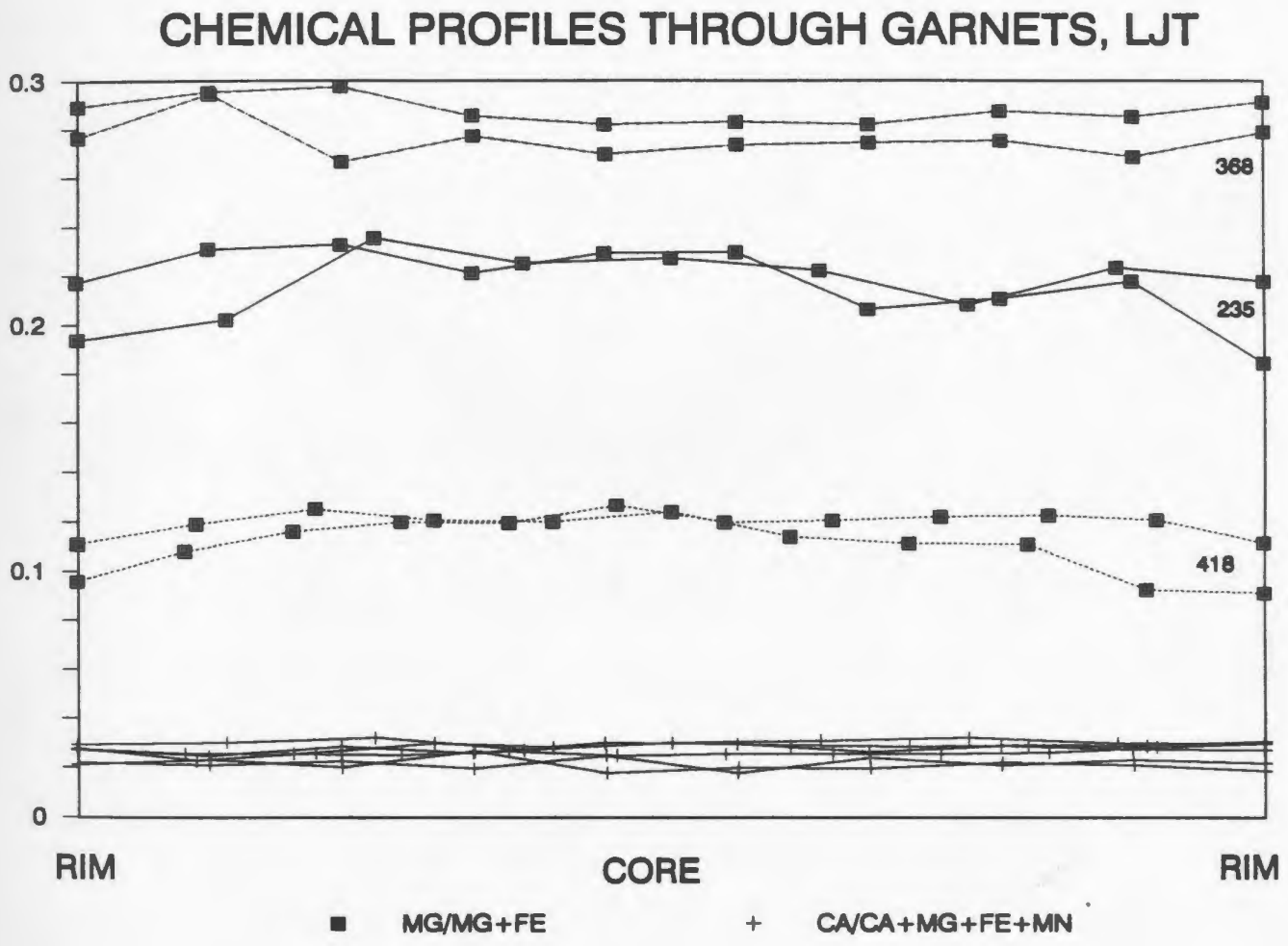

Figure 4-5: Chemical variations across garnets in the pelitic migmatites in the Lac Joseph Terrane.

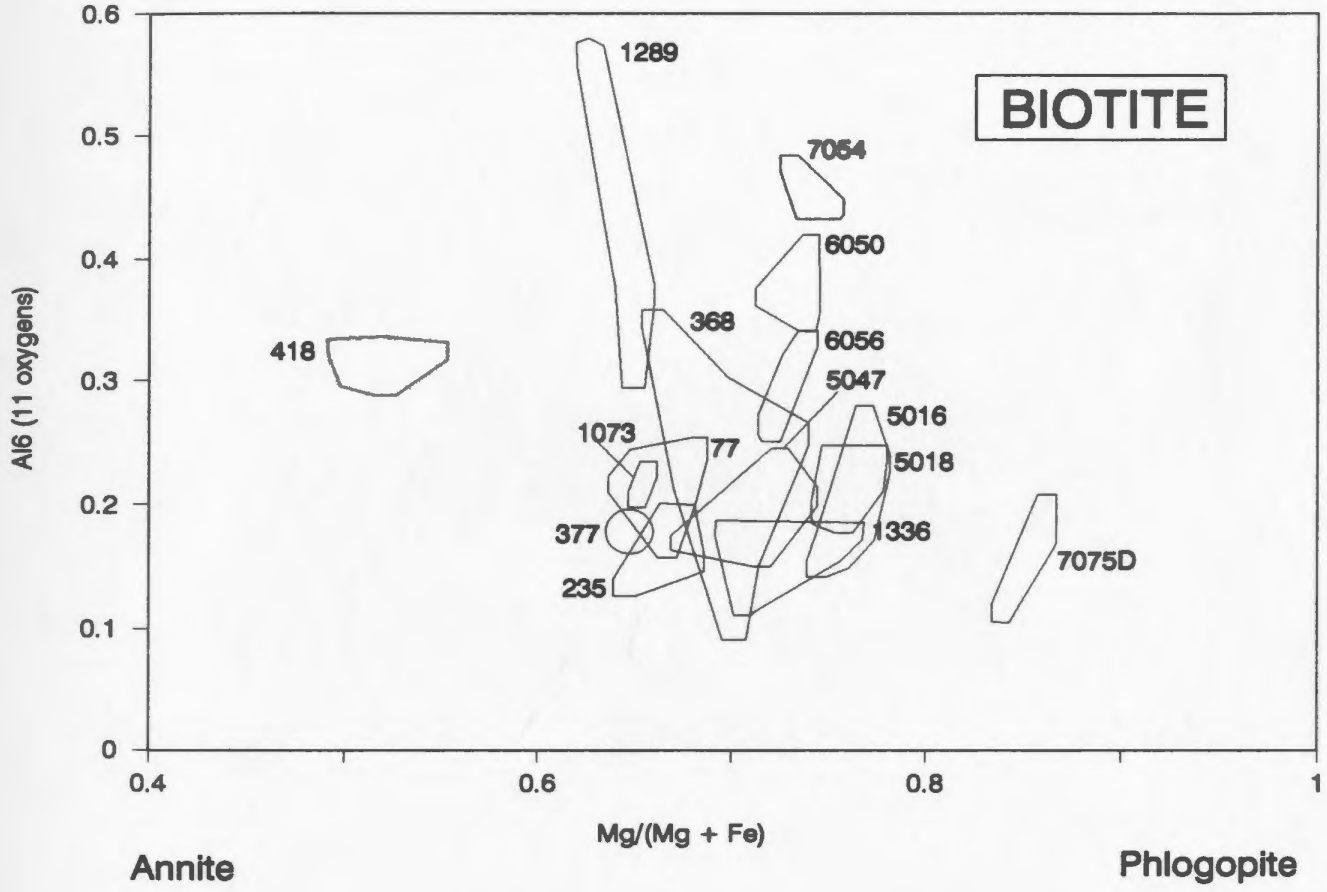

Figure 4-6: Chemical composition of biotite in the pelitic migmatites of the Lac Joseph Terrane.

COEXISTING GARNET - BIOTITE; ALL MIGMATITES OF THE LJT

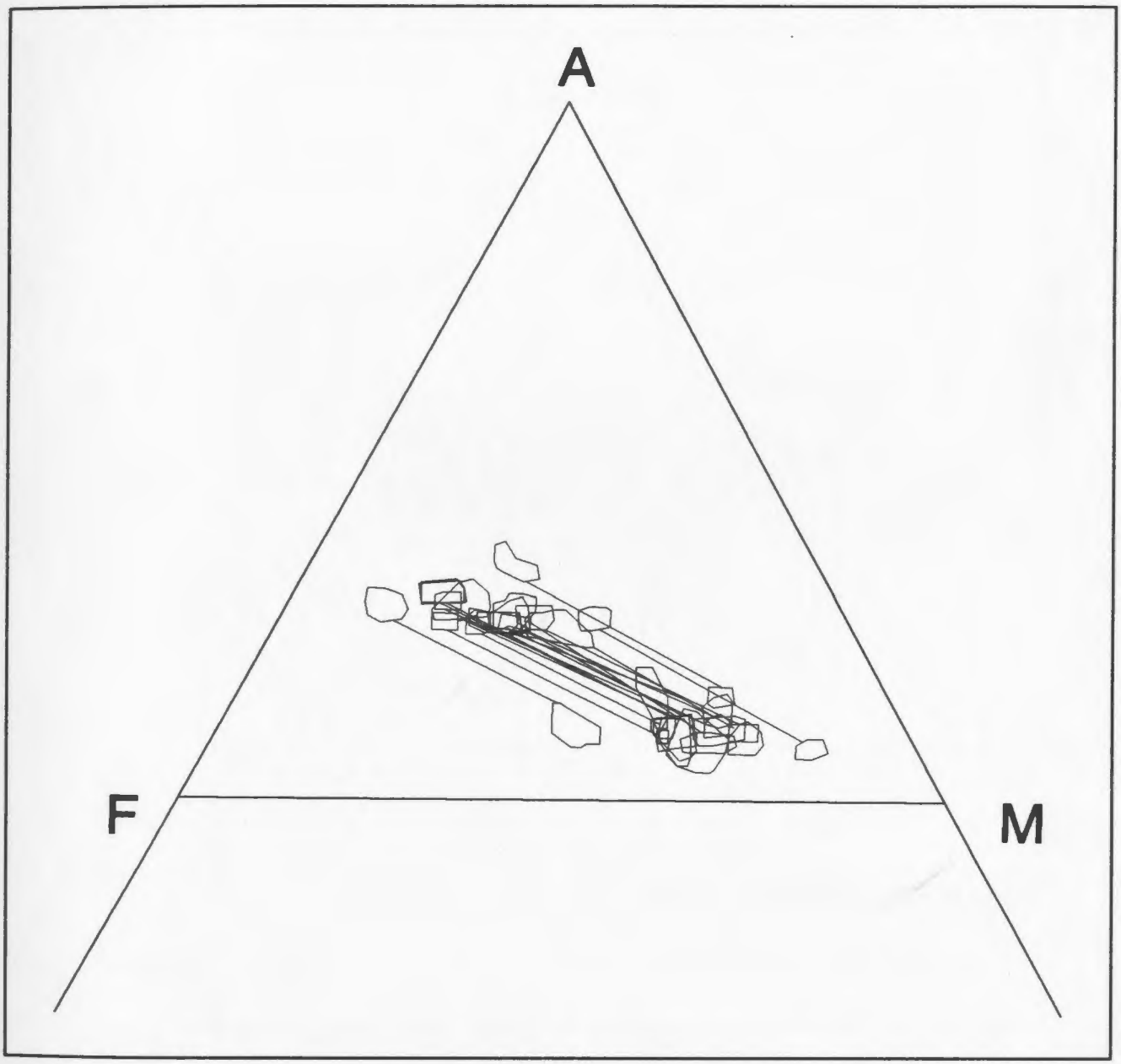

Figure 4-7: Composite plot of all co-existing garnet and biotite from pelitic migmatites in the Lac Joseph Terrane on an AFM diagram projected from K-Feldspar.

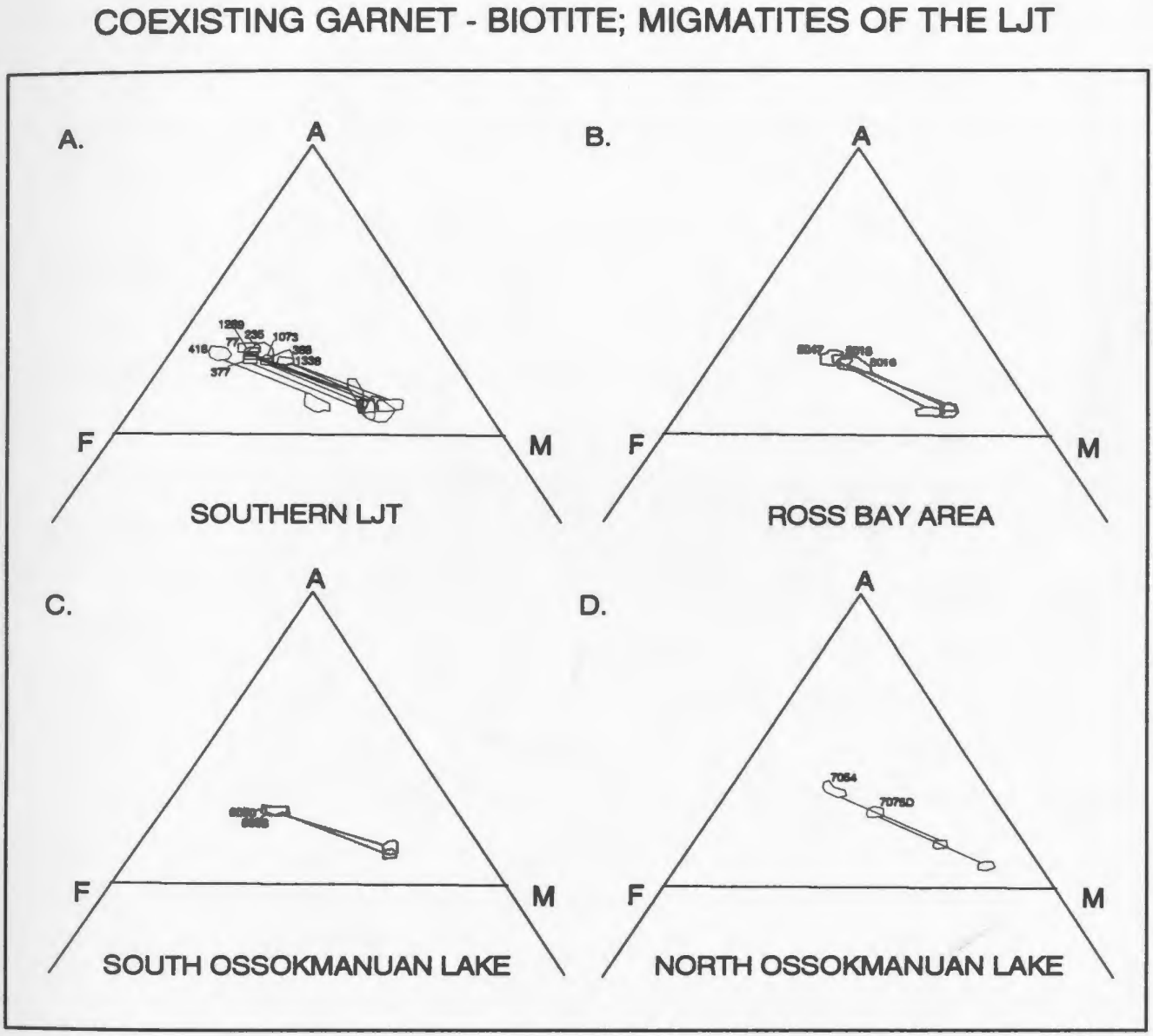

Figure 4-8: Compositional variations of co-existing garnet and biotite plotted on AFM diagrams projected from K-feldspar.

to their locations with respect to four domains in the Lac Joseph Terrane, suggests that there may be differences in Mg/Fe ratios in the ferromagnesian silicate minerals across the Lac Joseph Terrane. This may be due, in part, to differences in the modal abundance of magnetite between domains; a positive correlation is apparent between the modal abundance of magnetite and the Mg/Mg+Fe ratio in ferromagnesian minerals in most samples for which mineral chemistry data are available (see Section 4.2.5).

4.2.4.4 Plagioclase

Plagioclase in the aluminosilicate-bearing pelitic migmatites is albite rich, varying between about 20 and 40% An (oligoclase to andesine) (Fig. 4-9) and orthoclase contents are very low (generally <2% Or). Plagioclase in the northern and northwestern regions (5000-8000 numbers) tends to have a lower Ab content than those in the southern domain (0-2000 numbers). No exsolution textures were observed.

4.2.5 Relevant Reactions and Petrogenetic Constraints for the Aluminosilicate-bearing Migmatites.

The P-T conditions during the Labradorian Orogeny may be roughly constrained by three observations: 1) sillimanite - biotite - garnet - magnetite - K-feldspar are the stable phases in the Labradorian restite of the pelitic migmatites throughout most of the Lac Joseph Terrane; 2) kyanite - K-feldspar is the stable Labradorian subassemblage along the structural base of the Lac Joseph Terrane along the northern and western margins and around Lac Joseph; and 3) N_1 leucosome phases containing plagioclase - quartz - K-feldspar formed during the Labradorian Orogeny.

The assemblage kyanite - K-feldspar (bathozone 6, Carmichael, 1978) implies that the pressure exceeded about 7.5 kbar to 8 kbar in the kyanite-bearing samples. The apparent lack of a structural break between the sillimanite and kyanite-bearing samples suggests that the pressures were not significantly different for sillimanite-bearing samples proximal to those containing kyanite. Pressures may have been lower in areas containing the sillimanite - biotite - garnet - magnetite assemblage, distal from the kyanite-bearing samples.

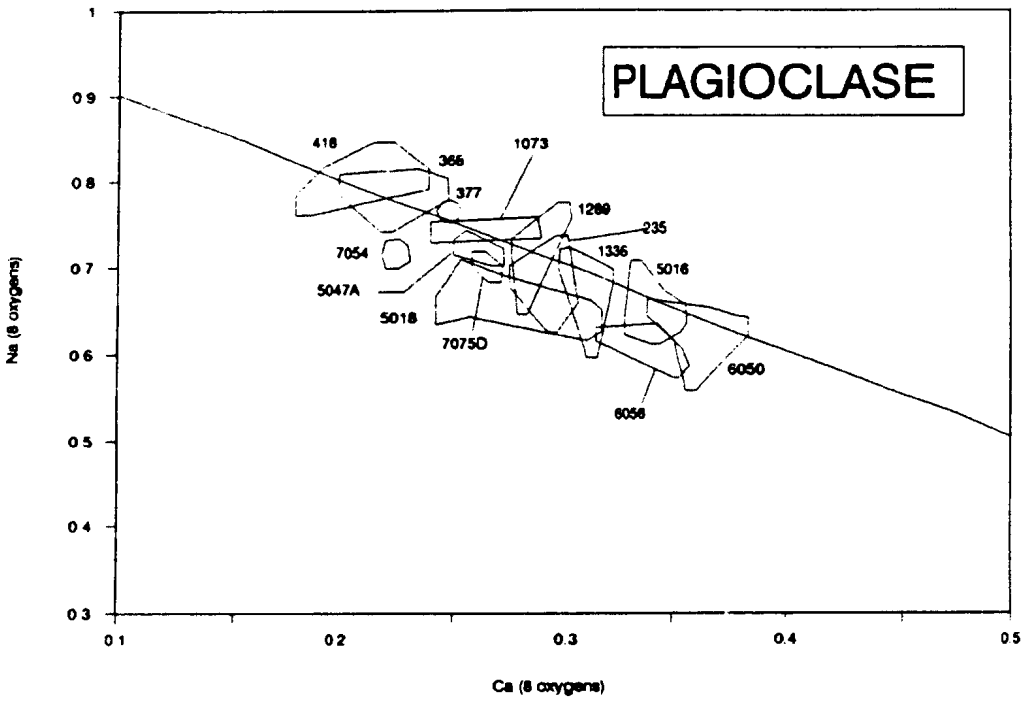

Figure 4-9: Chemical variation of plagioclase in pelitic migmatites in the Lac Joseph Terrane. Straight line represents Na+Ca=1.

The presence of sillimanite in the majority of samples of pelitic migmatites of the Lac Joseph Terrane requires that temperatures must have been in excess of 500°C, the invariant point in the aluminosilicate system (Fig. 4-10).

The presence of N_1 leucosomes containing plagioclase - quartz - K-feldspar, that are inferred to have formed by partial melting, implies that temperatures required for melting were exceeded throughout the Lac Joseph Terrane. The minimum melting temperatures for the system K_2O-Na_2O-Al_2O_3-SiO_2-H_2O is about 620°C for pressures between 5 and 10 kbar, where a_{H2O} is unity, for the reaction:

muscovite + K-feldspar + albite + quartz + H_2O = liquid (R4-1)

(Fig. 4-10). The absence of ferromagnesian phases in the N_1 leucosomes suggests that such phases were not involved in the melting reactions for which no adequate explanation can be given with the existing data base.

The assemblage sillimanite - biotite - garnet - magnetite - melt in the pelitic migmatites requires that temperatures must have been in excess of those required for the reaction:

muscovite + albite + quartz = sillimanite

K-feldspar + liquid (R4-2).

This indicates that temperatures were above approximately 700°C (Fig. 4-10).

The lack of prograde overprinting minerals, mineral zonation or significant spatial variability of assemblages in the Lac Joseph Terrane precludes a petrogenetic-based surmise of the prograde P-T-t particle paths which these rocks experienced during the Labradorian Orogeny.

Exchange and net transfer reactions in the stable aluminosilicate-bearing assemblage are thought to have operated to maintain chemical equilibrium between phases as the P-T conditions fluctuated. The dependence of the Fe^{+2} and Mg^{+2} distribution in co-existing garnet and biotite on temperature, and to a lesser degree, pressure in the reaction:

pyrope + annite = phlogopite + almandine (R4-3).

forms the basis for garnet - biotite geothermometry. However, the Fe^{+2} and Mg^{+2} distribution in these two minerals is also dependent on the reaction:

biotite + sillimanite + quartz = garnet + K-feldspar + H_2O (R4-4),

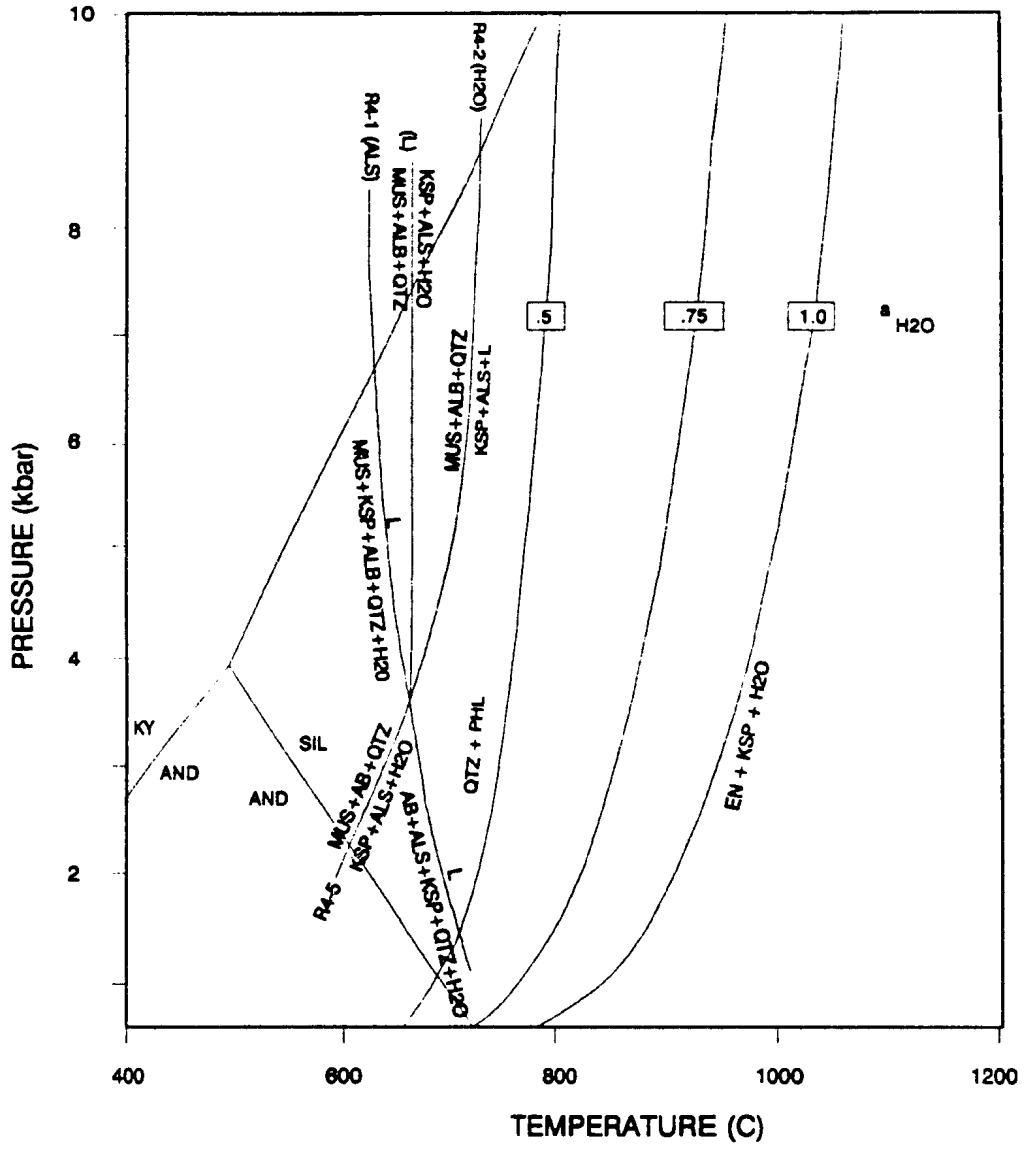

Figure 4-10: Reactions in P-T space relevant to the pelitic migmatites of the Lac Joseph Terrane. Aluminosilicate reactions: Holdaway, 1971; OPX reactions: Berman et al., 1987; remainder from Thompson and Algor, 1977.

in which the Fe/Mg ratio in biotite and garnet are dependent on both temperature and the activity of water. Kretz (1990) suggested that shifts in the distribution of Fe and Mg in coexisting garnet and biotite, which have traditionally been interpreted as an indication of changing temperature, may in fact be due to changes in the activity of water while reaction R4-4 is operative. However, in this case, the variation of the equilibrium constant (K) for garnet - biotite equilibria in reaction R4-3 changes very systematically over the Lac Joseph Terrane as a whole, suggesting that it is unlikely to have been caused by local differences in the activity of water. Thus the variation in K is interpreted to be due to P-T differences. Such an interpretation is consistent with independent constraints on P-T conditions in the Lac Joseph Terrane provided by variations in mineral assemblages.

The absolute amount of Fe^{+2}-bearing components in garnet and biotite is partially controlled by the oxidation reactions:

$$\text{almandine} + O_2 = \text{magnetite} + \text{aluminosilicate} + \text{quartz} \quad \text{(R4-5)}$$

and

$$\text{annite} + O_2 = \text{magnetite} + \text{K-feldspar} + \text{water} \quad \text{(R4-6)}$$

respectively. These reactions account for the positive correlation between the Mg/Fe ratios and the model percent of magnetite in the pelitic migmatites (discussed in Section 4.2.4.3). Although changes in the oxygen fugacity may have caused a shift in the Fe/Mg ratios in garnet and biotite, they would not have modified the equilibrium constants (K) for reactions R4-3 and R4-4. Changes in oxygen fugacity would, therefore, not have affected the biotite - garnet geothermometer.

The stability of anorthite in plagioclase is controlled by the pressure dependent net transfer reaction:

$$\text{anorthite} = \text{grossular} + \text{aluminosilicate} + \text{quartz} \quad \text{(R4-7)}.$$

The theoretical calibrated dependency of this reaction on pressure is utilized in Chapter 5 to estimate differences in pressure across the Lac Joseph Terrane.

4.2.6 Muscovite-bearing Restite of the Pelitic Migmatites

Two areas in southern Lac Joseph Terrane contain pelitic migmatites with muscovite-bearing restites (Fig. 4-1) consisting of muscovite, biotite, garnet and

hematite. The leucosomes are depleted in K-feldspar relative to the aluminosilicate-bearing migmatites, resulting in a bleached appearance on weathered surfaces.

4.2.6.1 Southwestern Margin of the Lac Joseph Terrane

Garnet and fine-grained biotite along the southwestern margin exhibit comparable microstructural relationships to those in the aluminosilicate-bearing migmatites discussed previously. Microstructures of hematite are similar to those exhibited by magnetite elsewhere. Muscovite in this area is typically aligned parallel to the main gneissic fabric, but is locally randomly oriented. Where preserved, sillimanite is overprinted and in reaction relationship with muscovite (Photo 4-7). Although muscovite may form small, radiating clusters at biotite grain boundaries (Photo 4-8), it is commonly observed in sharp contact with all phases in the restite. Randomly oriented chlorite is rare, and is interpreted to be a late phase and not in equilibrium with the rest of the assemblage.

Muscovite is interpreted to have replaced sillimanite by the reaction:

$$\text{sillimanite} + \text{K-feldspar} + H_2O = \text{muscovite} + \text{quartz} \quad \text{(R4-8)}$$

Microstructural relationships suggest that the reaction was initiated under deviatoric stress conditions, but subsequently continued under neutral stress conditions leading to the formation of randomly oriented muscovite. Biotite appears to have synchronously partially recrystallized under both stress environments. The common observation of sharp contacts between muscovite and biotite intergrowths suggests that the two phases were mutually stable. The radiating muscovite at biotite grain boundaries is interpreted to be a consequence of preferential nucleation of muscovite on biotite.

4.2.6.2 Aureole of the Fleur-de-Mai Granite

Within about 20 km of the Fleur-de-Mai granite in the southeastern Lac Joseph Terrane, muscovite randomly overprints aligned sillimanite (Photo 4-9) and is also disseminated in the leucosomes (Photo 4-10). Sillimanite gradually diminishes in modal abundance towards the contact with the intrusion and is absent in the immediate vicinity of the intrusive body. Randomly oriented biotite is much coarser grained (Photo 4-11) than in the aluminosilicate-bearing migmatites to the immediate northwest. Biotite in

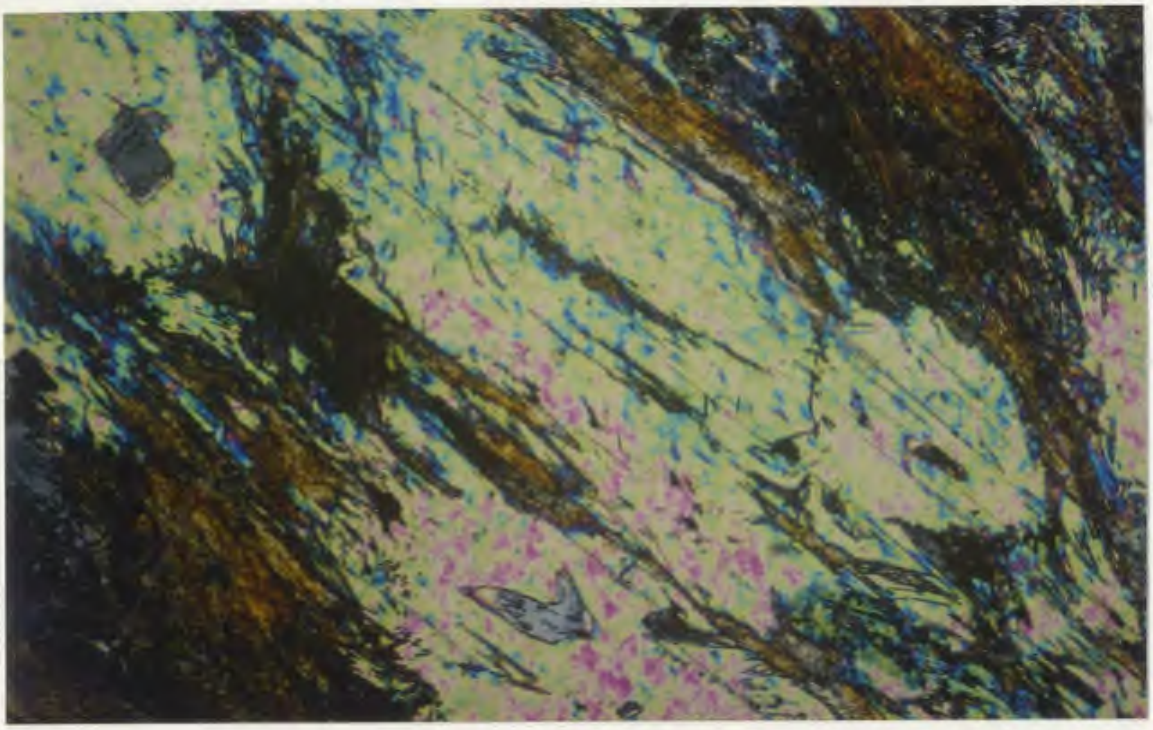

.2 mm

Photo 4-7: Aligned muscovite overprinting sillimanite in the pelitic migmatites of the Lac Joseph Terrane. Cross polarized light.

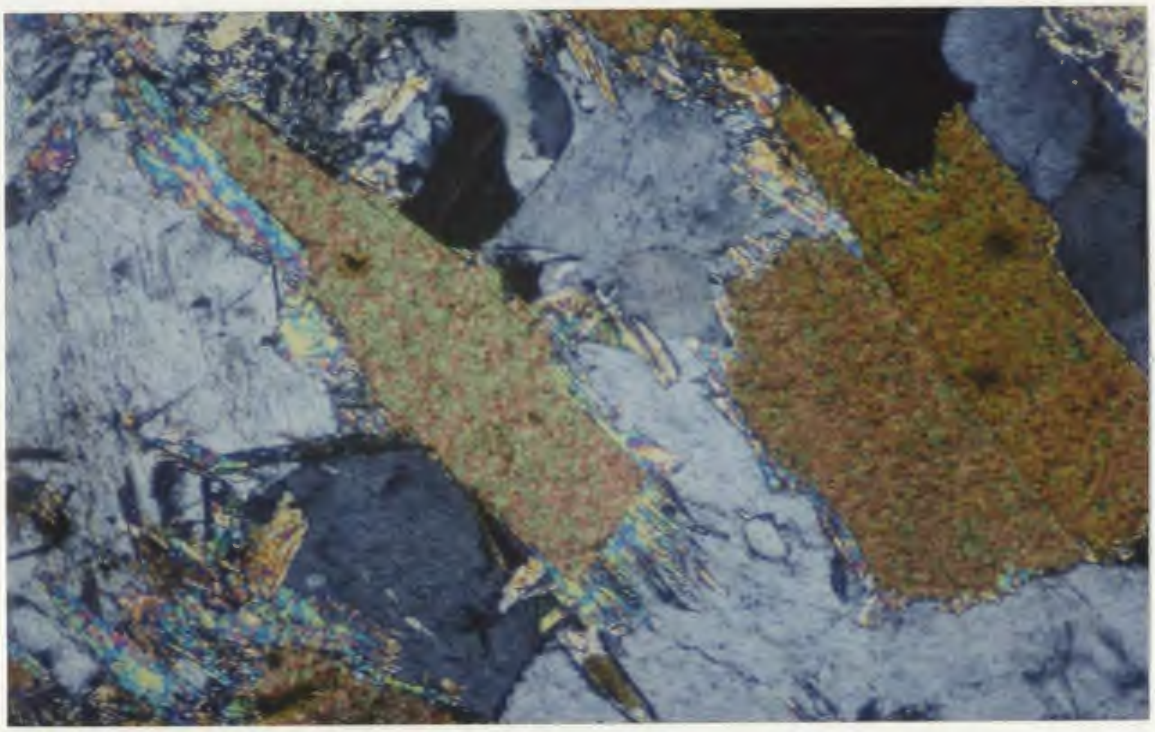

.2 mm

Photo 4-8: Muscovite growing preferentially around pre-existing biotite in pelitic migmatites along the southwestern margin of the Lac Joseph Terrane. Cross polarized light.

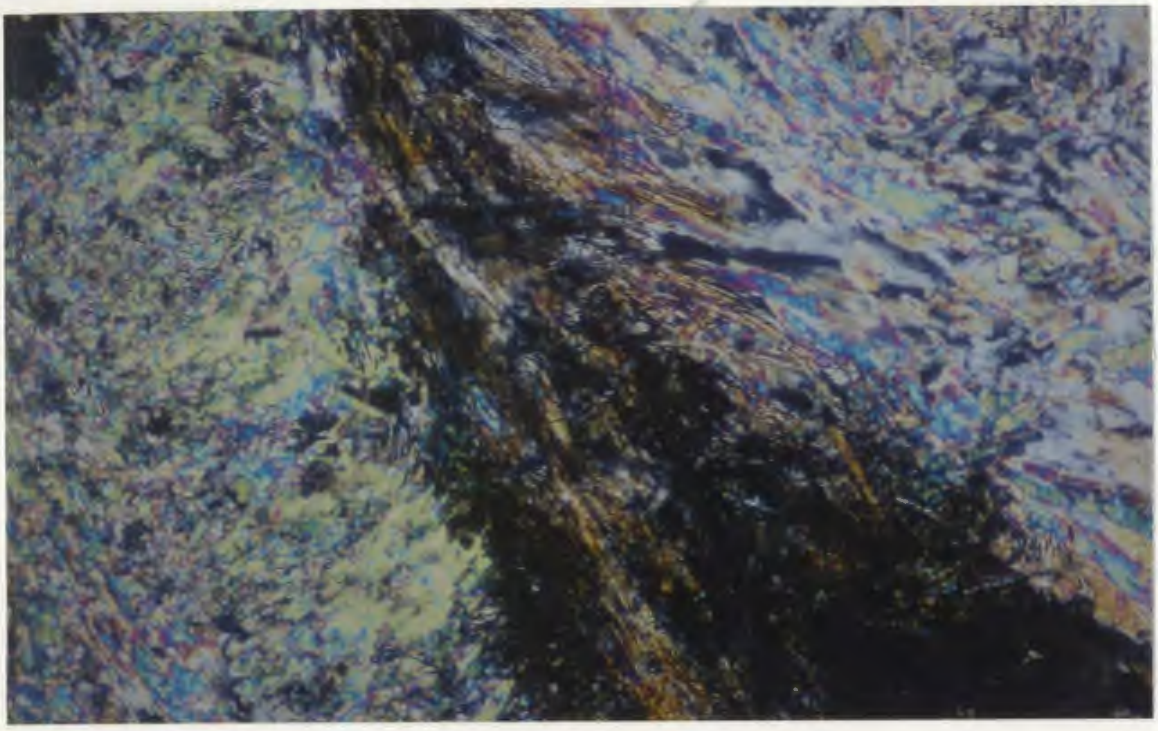

.2 mm

Photo 4-9: Randomly oriented muscovite overprinting sillimanite in the pelitic migmatites adjacent to the Fleur-de-Mai granite in southeastern Lac Joseph Terrane. Cross polarized light.

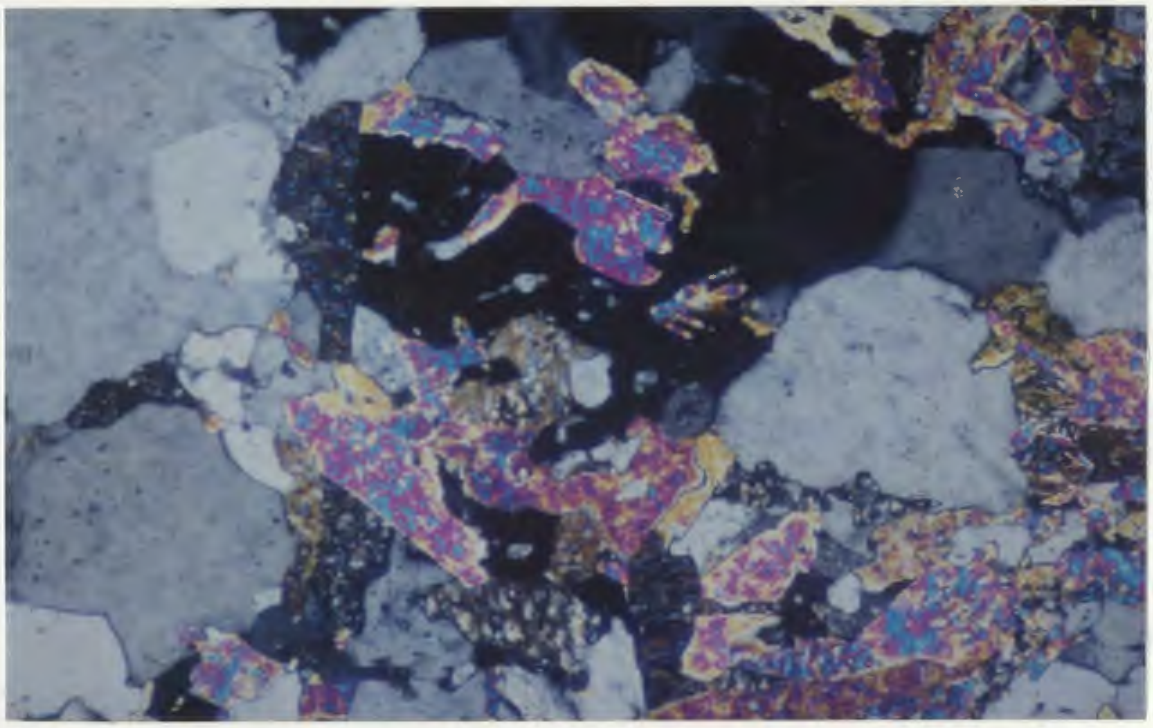

.2 mm

Photo 4-10: Random, coarse grained muscovite in the Fleur-de-Mai granite, southeastern Lac Joseph Terrane. Cross polarized light.

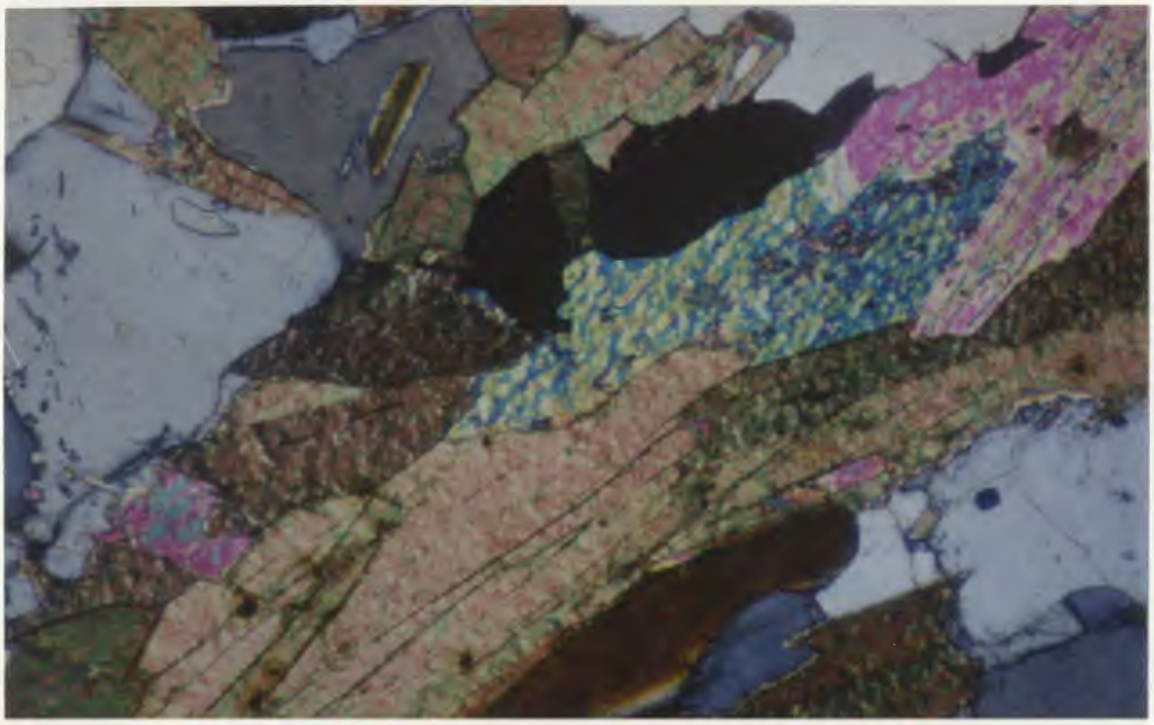

.2 mm

Photo 4-11: Coarse-grained biotite in the pelitic migmatites of the southeastern Lac Joseph Terrane. Cross polarized light.

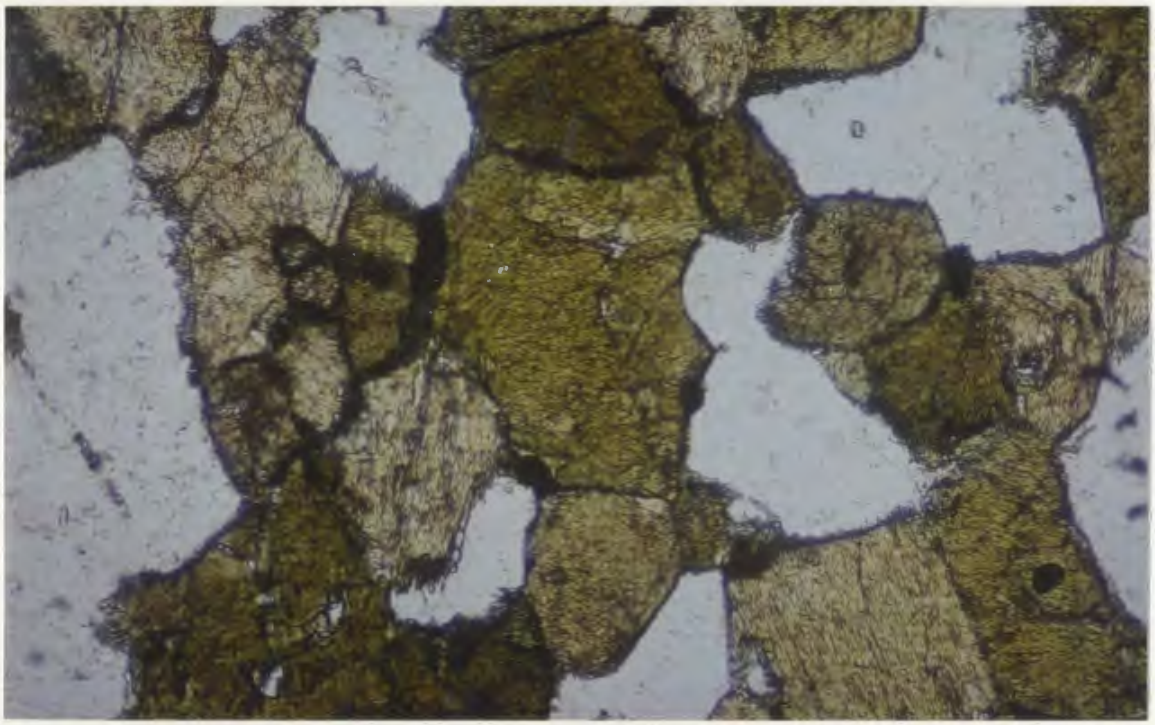

.2 mm

Photo 4-12: Coexisting hornblende and plagioclase in amphibolite facies mafic gneiss of the southwestern Lac Joseph Terrane. Plane polarized light.

this region is commonly overprinted by chlorite and epidote. Where sillimanite is absent, biotite and muscovite are in sharp contact with each other and with earlier phases in both the restites and leucosomes.

Muscovite is interpreted to have replaced sillimanite in the restites and K-feldspar in the leucosomes; muscovite, biotite, plagioclase, quartz, K-feldspar and hematite therefore comprise a stable retrograde metamorphic assemblage which replaced the original sillimanite-bearing assemblage. The random orientation of both muscovite and biotite implies that they were generated and/or recrystallized under approximately neutral stress conditions. The spatial association of this muscovite-bearing migmatite zone with the Fleur-de-Mai granite suggests that retrogression occurred as a consequence of contact metamorphism. This requires that the sillimanite-bearing assemblage that predated the formation of muscovite must have predated the intrusion of the Fleur-de-Mai granite (1133+10/-5 Ma; Emslie and Hunt, 1990). This reinforces the previous arguments that the sillimanite-bearing assemblage is Labradorian in age.

4.2.6.3 Relevant Mineral Reactions and Petrogenetic Constraints in the Muscovite-bearing Migmatites

The observations that muscovite overprints sillimanite and that K-feldspar is depleted in the muscovite-bearing migmatites suggests that muscovite was generated by the breakdown of sillimanite - K-feldspar - water (reaction R4-8) requiring that the temperature and pressure was within the muscovite + quartz stability field (Fig. 4-10). Assuming that significant dehydration occurred during the production of the aluminosilicate-bearing assemblages, the origin of the water necessary for this reaction must have been from outside the reaction site. Water availability may have been the rate-controlling step in preventing more widespread retrogression and muscovite formation. These waters are thought to have been responsible for the oxidizing conditions which prevailed during the retrogression, resulting in the conversion of magnetite to hematite in the muscovite-bearing migmatites. That the water was oxidizing, suggests that it may have been circulating meteoric fluids which, in turn, implies that the Fleur-de-Mai granite was emplaced into a shallow level.

Muscovite along the southwestern margin has yielded an $^{40}Ar/^{39}Ar$ date of ca. 1000 Ma (see Section 7.2.2), an age comparable to the age of the marginal Lac Emerillon shear zone to the north. Thus this muscovite was probably formed during the juxtapositioning of the Lac Joseph and Molson Lake terranes with water transferred from lower to upper plate during the Grenvillian emplacement.

4.3 Mafic Gneisses of the Lac Joseph Terrane

The mafic gneisses of the Lac Joseph Terrane exhibit both amphibolite and granulite facies mineral assemblages. The spatial distribution of the assemblages is shown in Figure 4-11.

4.3.1 Amphibolite Facies Mafic Gneisses in the Lac Joseph Terrane

Mafic gneisses in the amphibolite facies consist predominantly of plagioclase, hornblende, biotite and quartz with or without minor amounts of titanite, magnetite, epidote and/or clinopyroxene. Hornblende is typically equigranular, polygonal (Photo 4-12) and shows stable contacts with plagioclase and biotite (Photo 4-13). Actinolite locally replaces hornblende. Quartz is present as small rounded grains dispersed in coarser grained plagioclase. Titanite and magnetite are common as disseminated phases in stable contact with plagioclase, hornblende and biotite. Rare occurrences of clinopyroxene are small idioblastic grains which exhibit stable contacts with all other phases. Amphibole, titanite, clinopyroxene, biotite and plagioclase commonly preferentially define a weak planar fabric. Fine-grained epidote forms discontinuous rims around hornblende (Photo 4-14).

Hornblende - plagioclase - biotite - quartz $\pm$ clinopyroxene $\pm$ titanite $\pm$ magnetite comprise the stable assemblage in the amphibolite facies zone. Epidote appears to have been generated later and is therefore not included as part of the assemblage. The alignment of subequant minerals of this assemblage implies that crystallization occurred under deviatoric stress conditions. Titanite from southern Lac Joseph Terrane amphibolite facies has been dated at 1281 Ma (U-Pb, see Section 6.8) implying that syntectonic, amphibolite grade metamorphism occurred at this time (at least in the southern part of the Lac Joseph Terrane).

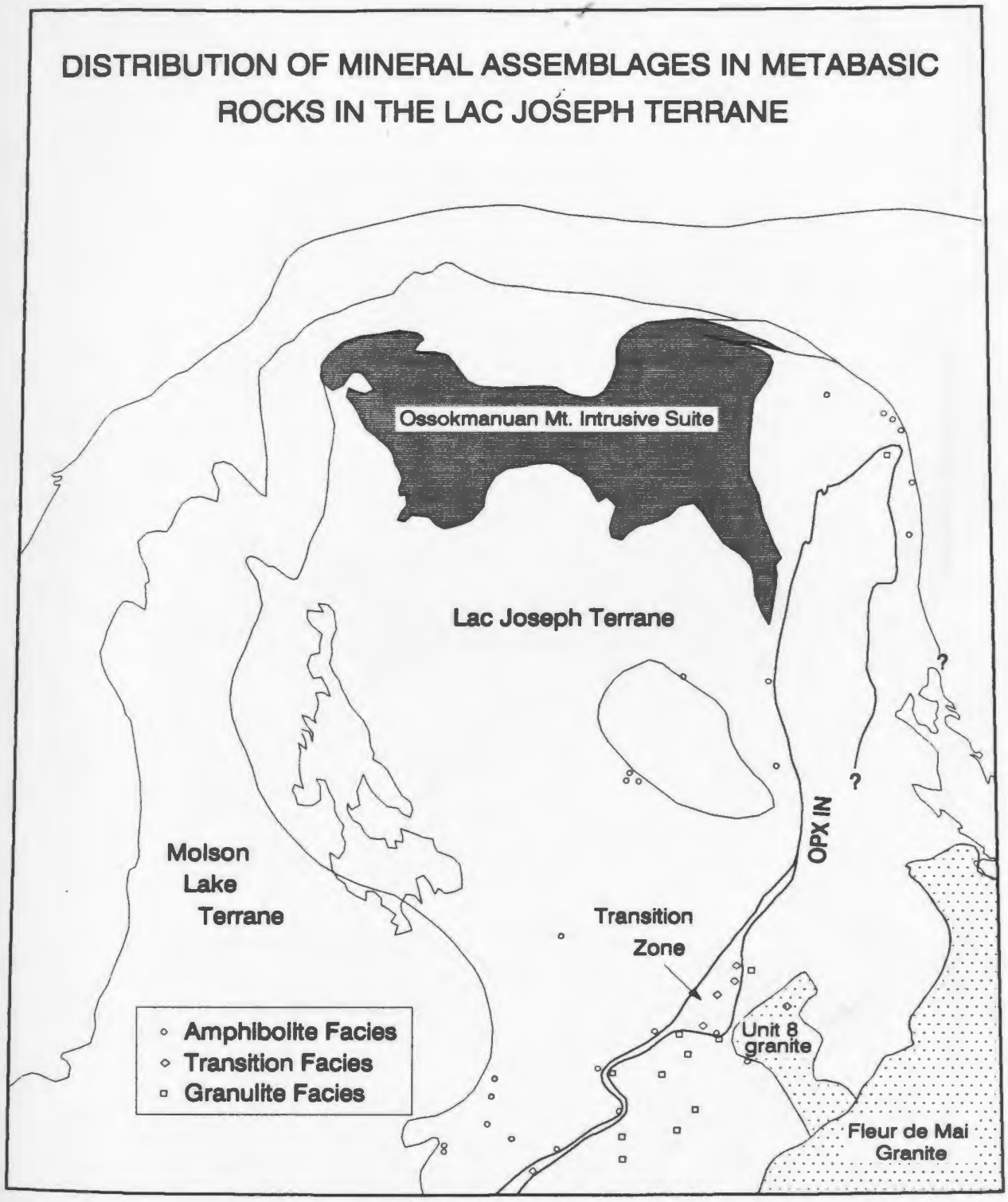

Figure 4-11: Distribution of mineral assemblages in the mafic gneisses of the Lac Joseph Terrane. Amphibole facies gneisses comprise the assemblage HBL - PLG - BIO - TTN; granulite facies assemblages comprise OPX - CPX - PLG - BIO; transition facies assemblages contain minerals from both the amphibolite and granulite facies. The northern part of the OPX IN isograd is from Nunn and Christopher (1983).

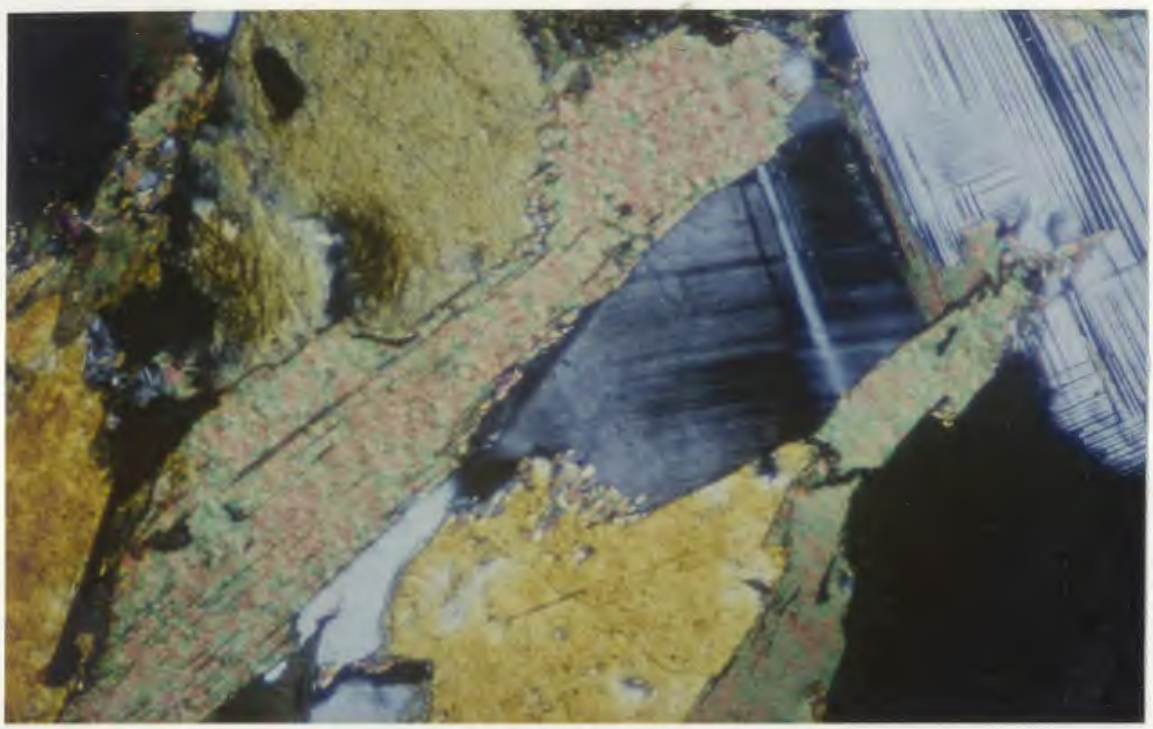

.2 mm

Photo 4-13: Coexisting hornblende, biotite, plagioclase and magnetite in amphibolite facies mafic gneiss of the southwestern Lac Joseph Terrane. Cross polarized light.

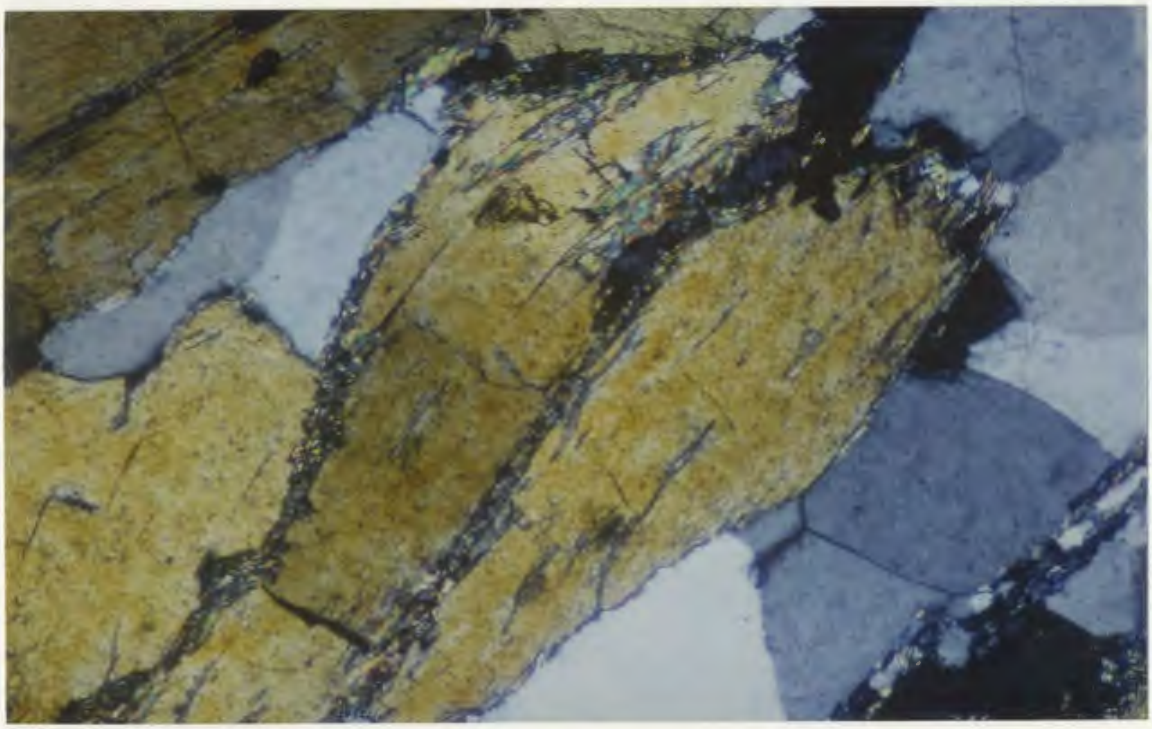

.2 mm

Photo 4-14: Hornblende rimmed by epidote in the amphibolite facies mafic gneiss of the southwestern Lac Joseph Terrane. Cross polarized light.

4.3.2 Granulite Facies Mafic Gneisses of the Lac Joseph Terrane

Granulite facies assemblages consist principally of plagioclase, orthopyroxene, clinopyroxene and biotite with or without quartz, hornblende and magnetite. These two-pyroxene-bearing rocks typically exhibit equigranular, granoblastic textures. Orthopyroxene, clinopyroxene, hornblende, plagioclase and biotite are typically in sharp mutual contact (Photos 4-15 and 16). Although hornblende is commonly part of the stable granulite assemblage, it also locally forms rims around orthopyroxene. Cummingtonite is locally present adjacent to or within orthopyroxene.

All phases in the granulite facies are thought to be in stable equilibrium, except where orthopyroxene shows incipient signs of alteration to hornblende and/or cummingtonite.

4.3.3 Granulite - Amphibolite Transition

Whereas evidence of instability of orthopyroxene is rare and localized in the granulite facies zone, it is pervasive in the transition zone in the southern Lac Joseph Terrane (Photo 4-17) which is dominated by the assemblage plagioclase - orthopyroxene - clinopyroxene - hornblende - biotite - quartz. Orthopyroxene is thought to break down by the reaction:

orthopyroxene + clinopyroxene + plagioclase = hornblende + quartz (R4.9).

Thus the amphibolite - granulite facies transition is interpreted to be due to retrograde rather than prograde metamorphic conditions. In the amphibolite facies proper, to the northwest of the transition zone, it appears that orthopyroxene was completely consumed in this reaction at approximately 1281 Ma, the age of titanite co-existing with amphibole. The presence of fine-grained, metamorphic orthopyroxene in rapakivi-textured granite (Photo 2-6) in the amphibolite facies zone as defined by metabasic rocks, is compatible with the interpretation that this area had previously experienced granulite facies conditions during the Labradorian Orogeny and that the amphibolite-granulite facies boundary is thus a retrograde rather than prograde transition. The preferential retrogression of orthopyroxene in the mafic gneiss as opposed to rapakivi granite suggests that the water activity in the former must have been greater than in the latter at the time of retrogression.

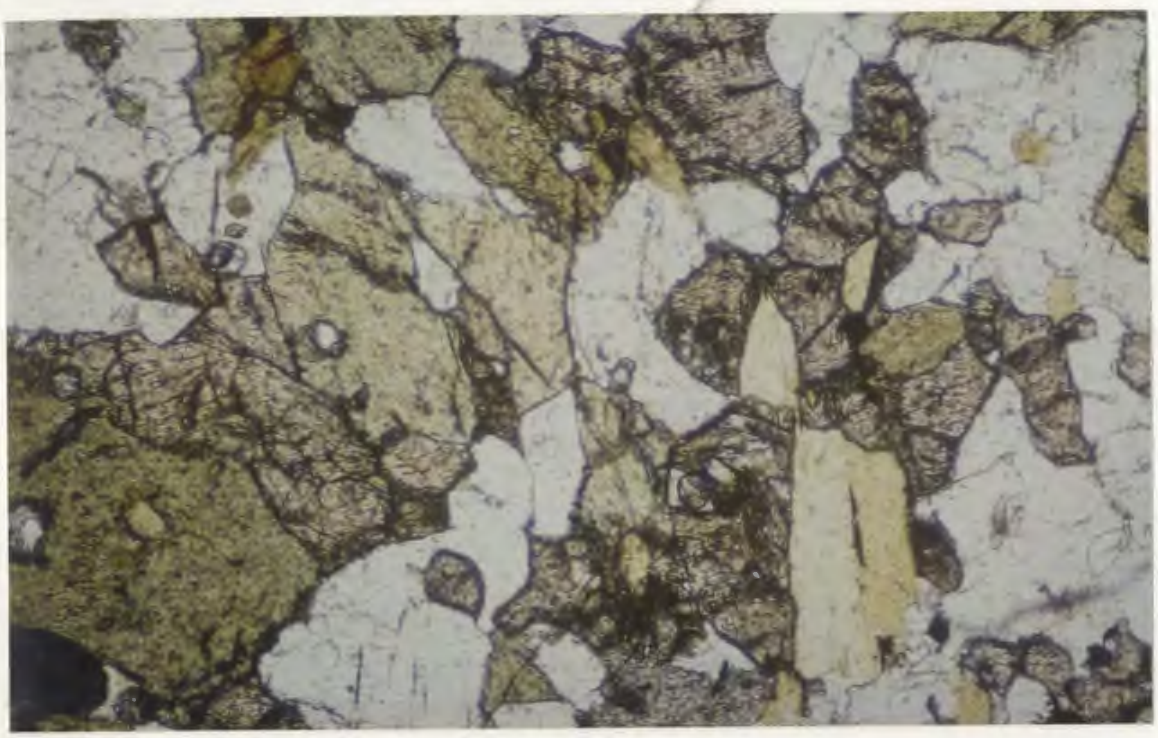

.2 mm

Photo 4-15: Coexisting orthopyroxene, hornblende, biotite and plagioclase in the granulite facies mafic gneiss of the southeastern Lac Joseph Terrane. Plane polarized light.

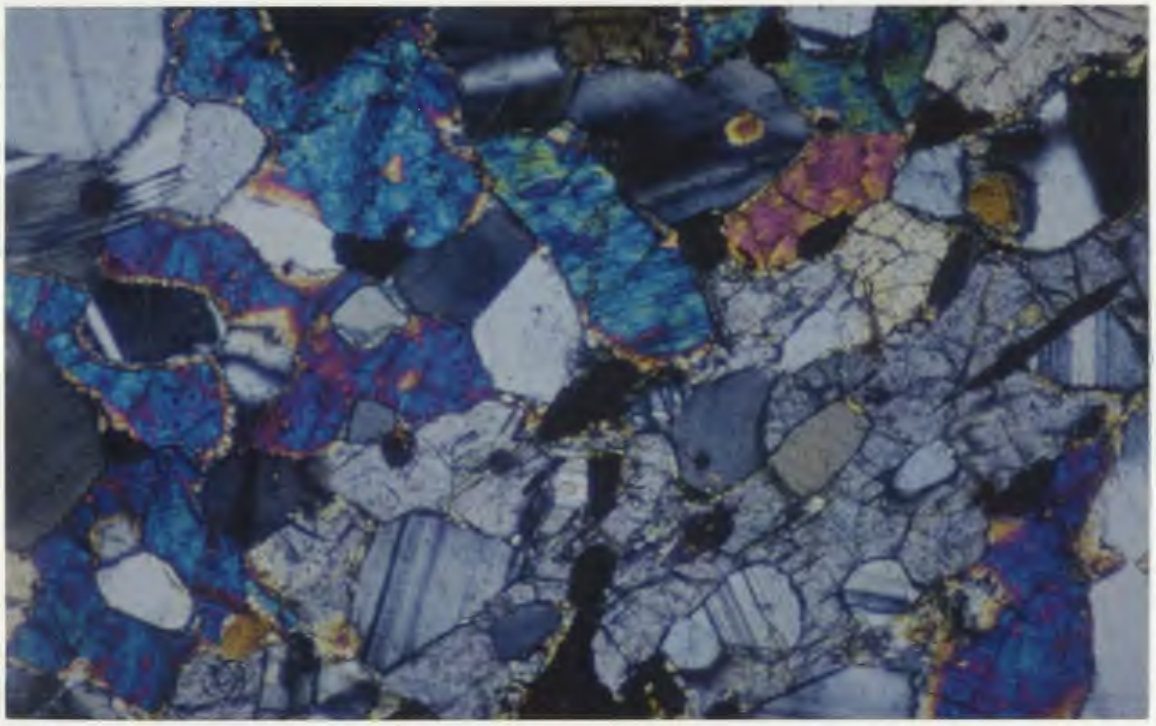

.2 mm

Photo 4-16: Coexisting orthopyroxene, clinopyroxene and plagioclase in the granulite facies mafic gneiss in the southeastern Lac Joseph Terrane. Cross polarized light.

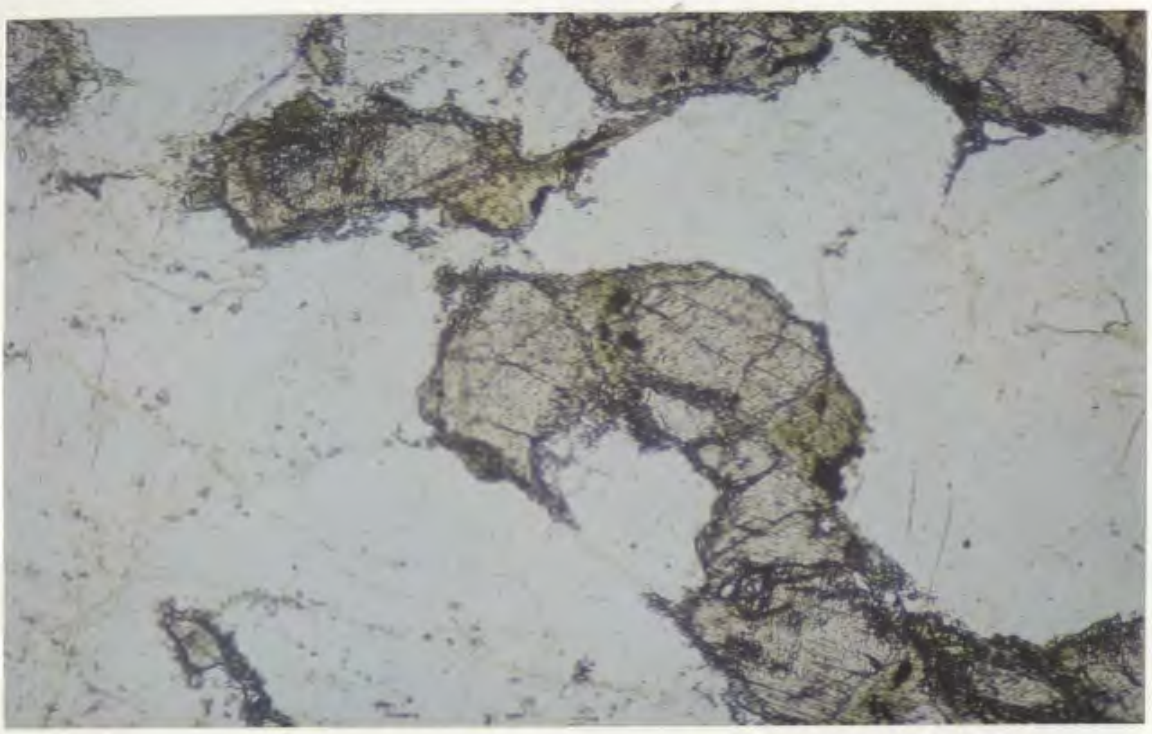

.2 mm

Photo 4-17: Orthopyroxene rimmed by hornblende in the transitional zone between amphibolite and granulite facies in the mafic gneiss of the southern Lac Joseph Terrane. Plane polarized light.

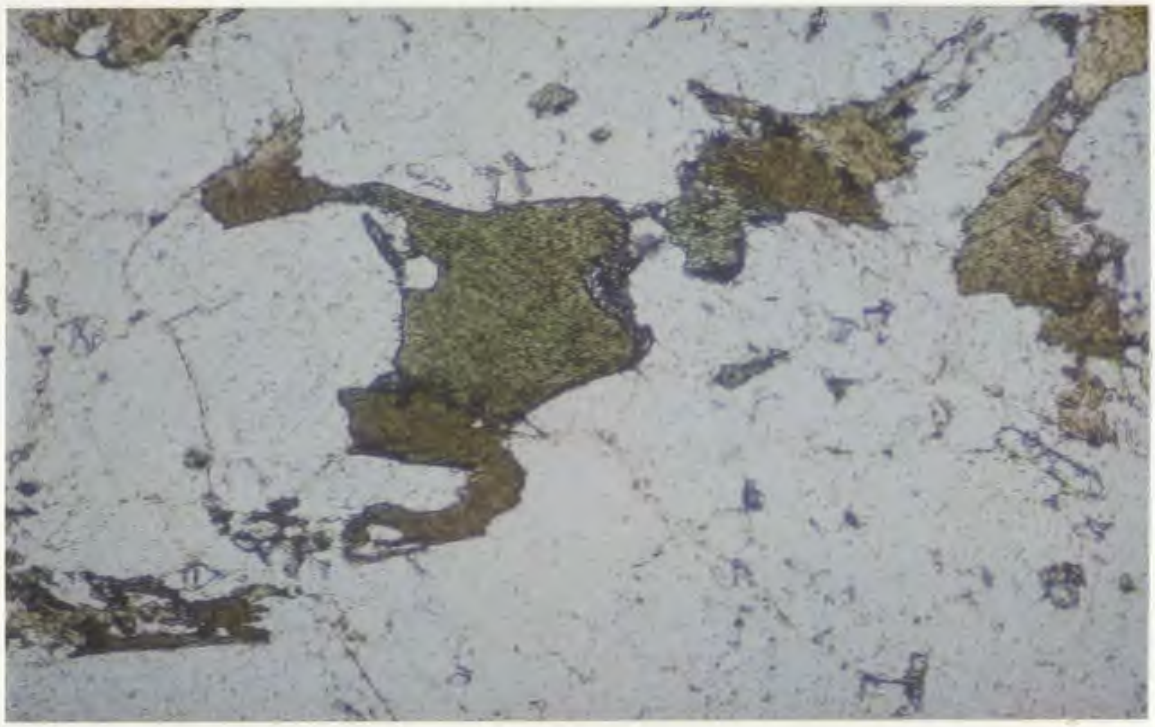

.2 mm

Photo 4-18: Coexisting hornblende, plagioclase, epidote and biotite in tonalitic rocks in Zone 1 of the southern Molson Lake Terrane. Plane polarized light.

The metamorphic and deformational styles in the granulite facies mafic gneiss and the pelitic migmatites are comparable and are therefore thought to have formed synchronously. It will be established by U-Pb geochronology (Chapter 6) that the main thermotectonic event in the pelitic migmatites occurred during the Labradorian Orogeny between approximately 1672 and 1611 Ma. It is therefore suggested that the granulite facies assemblages of the mafic gneiss were also generated during the Labradorian Orogeny and subsequently retrograded during a separate, spatially restricted amphibolite-facies event about 330 - 391 m.y. later. The granulite facies assemblages therefore provide information about P-T conditions during the Labradorian Orogeny whereas the amphibolite facies assemblages furnish information on the P-T signature of a cryptic retrograde event at 1281 Ma.

4.3.4 Relevant Reactions and Petrogenetic Grids for the Mafic Gneisses

Orthopyroxene is typically generated at the expense of amphibole in metabasites in a prograde metamorphic sequence. The dependence of amphibole stability on water activity, which is not well constrained in the metabasites in this study, precludes accurate estimation of quantitative minimum P-T estimates for the first appearance of orthopyroxene. The relevant orthopyroxene generating reaction:

hornblende + quartz = orthopyroxene + clinopyroxene + plagioclase + water

(R4.10)

has a steep slope in P-T space and is therefore relatively insensitive to pressure changes (Fig. 4-12), but its location is dependent on the activity of water. The hornblende - quartz stability field must have been exceeded during the Labradorian Orogeny.

4.3.5 Petrogenetic Grids for Pelitic Supracrustal Rocks and Mafic Gneiss, Lac Joseph Terrane

The mineral facies in the interlayered mafic and pelitic gneisses collectively constrain the P-T conditions of the Labradorian thermotectonic event. Temperatures must have reached the stability fields of: 1) sillimanite - K-feldspar - melt in the pelitic migmatites; and 2) orthopyroxene - clinopyroxene - plagioclase in the mafic gneiss. However, temperatures must have been below the water activity dependent orthopyroxene stability field for pelitic compositions (see Fig. 4-10). The presence of

P-T GRID SHOWING LOCATIONS OF RELEVANT REACTIONS IN METABASIC ROCKS

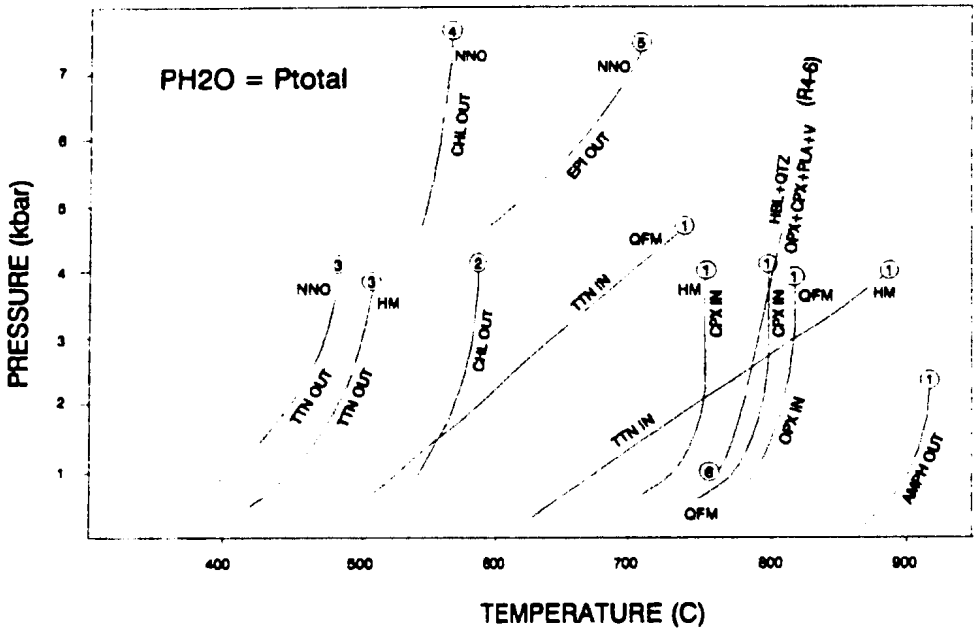

Figure 4-12: P-T grid of experimentally derived reaction curves at different oxygen fugacities; from (1) Spear (1981); (2) Liou et al. (1974); (3) Moody et al. (1983) (stability of titanite in the presence of epidote); (4) and (5) Apted and Liou (1983).

the bathozone 6 assemblage, kyanite - K-feldspar, (Carmichael, 1978) along the northern and northwestern margins and around the central tectonic window of the Lac Joseph Terrane indicates minimum pressures of about 8 kbar. However, pressures in areas away from the kyanite-bearing samples, although less than this, are not tightly constrained.

4.4 Granitoid Rocks of the Molson Lake Terrane

The granitoid rocks of the Molson Lake Terrane are diverse in composition and mineral assemblage. However, the poor exposure in most of this terrane, and in areas dominated by granitoid rocks in particular, has resulted in a small data set relative to the areal extent of the terrane. The greatest variability of mineral assemblages is recorded in the southern Molson Lake Terrane where the across-strike width is greatest. This region is divided into three metamorphic zones which are bound by northerly trending isograds subparallel to the eastern boundary of the terrane (Fig. 4-13); the easternmost isograd is apparently truncated by the Lac Joseph Terrane boundary.

Zone 1, along the eastern margin of the terrane, comprises the most diverse range of assemblages of the three zones and predominantly exhibits granoblastic textures with variable grain size. The assemblages comprise the following phases in various combinations: biotite - muscovite - epidote - plagioclase - quartz $\pm$ K-feldspar $\pm$ chlorite $\pm$ hornblende. Muscovite, biotite and locally chlorite typically contribute to the single planar S_{1M} fabric observed in this region. Sharp grain boundaries are observed between all of the phases present in this assemblage (Photos 4-18 to 4-21), except for randomly oriented fine-grained intergrowths of epidote and biotite which locally surround hornblende. Locally, randomly oriented chlorite is replacing biotite and is, therefore, not considered to be part of the equilibrium assemblage.

The textures indicate that the coarser grained phases in zone 1 assemblages were stable at the time of peak metamorphism. The pervasive granoblastic textures in this zone imply that temperatures were sufficient to facilitate pervasive recrystallization of quartz and feldspar after formation of the main fabric (S_{1M}). Late retrogression and local metasomatism in a neutral stress environment resulted in the conversion of amphibole to biotite and epidote and the chloritization of biotite.

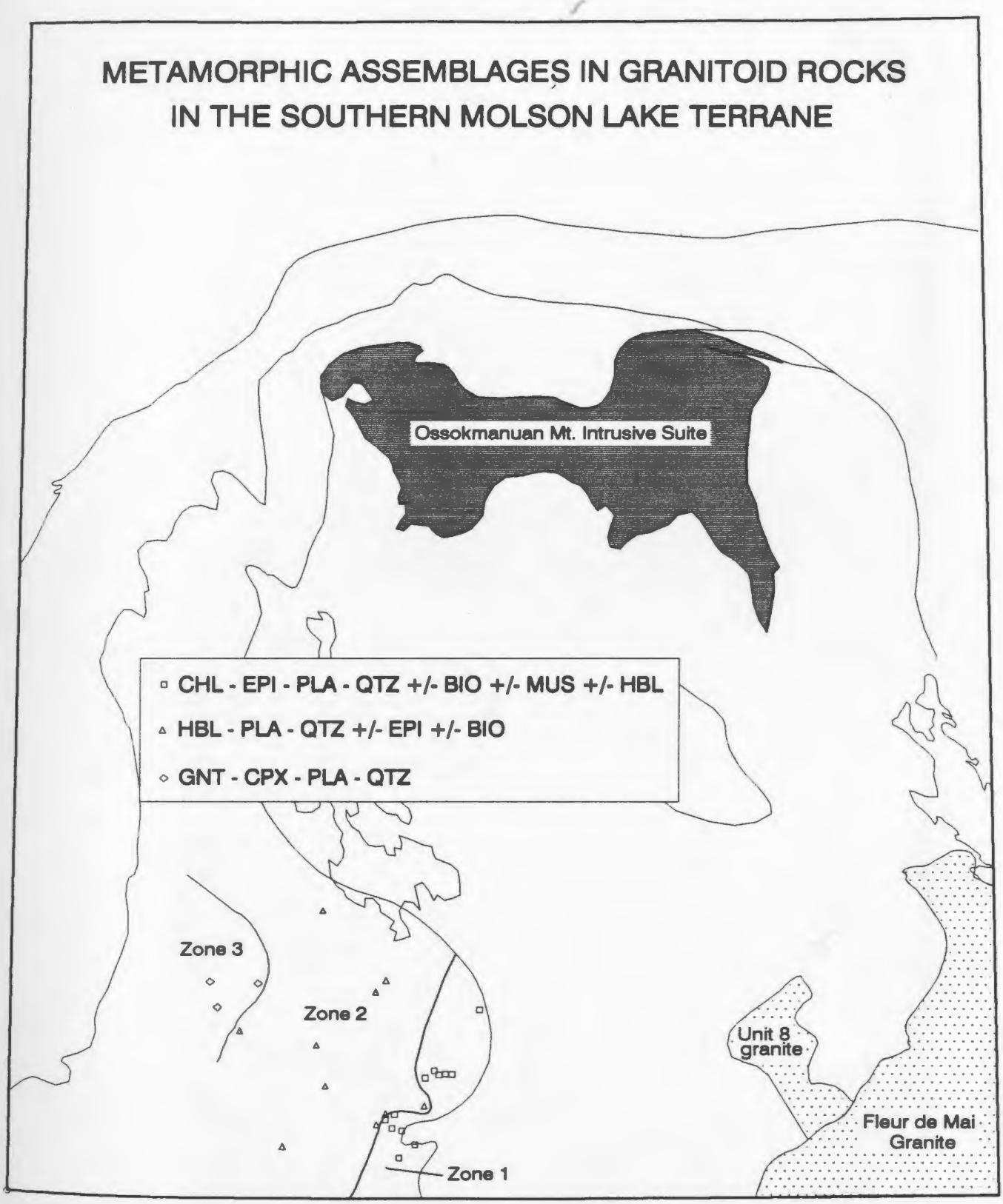

Figure 4-13: Distribution of mineral assemblages in the granitoid rocks of the southern Molson Lake Terrane.

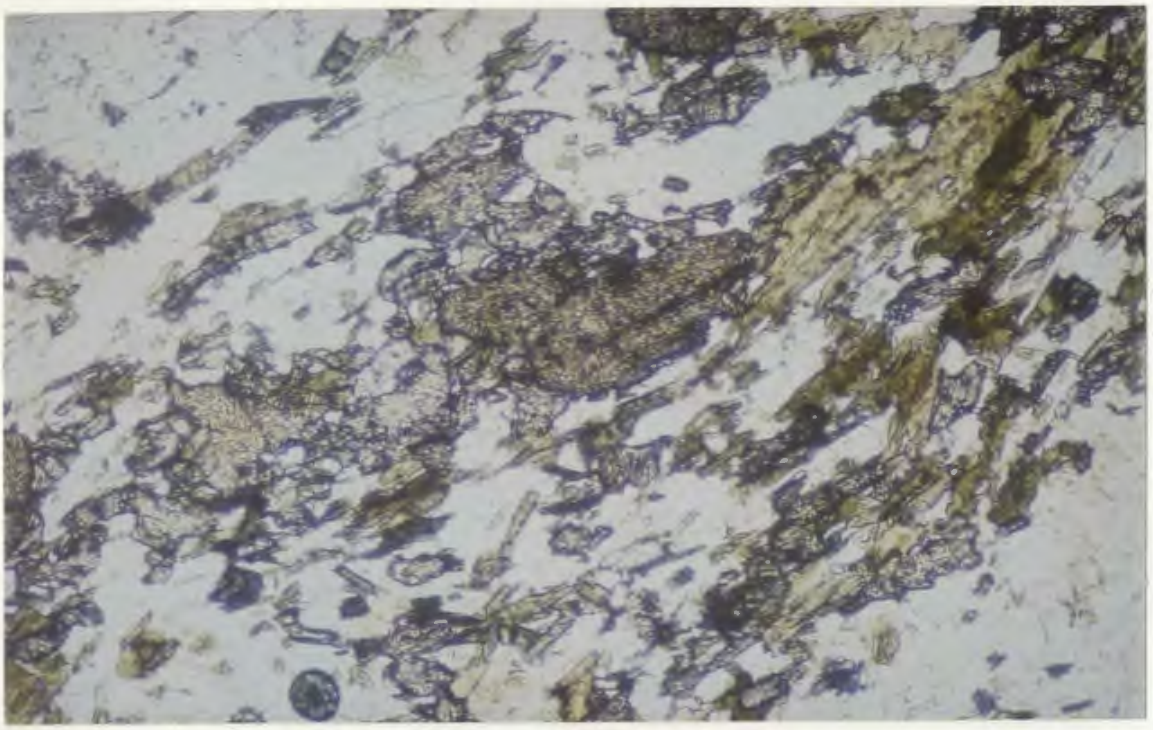

.2 mm

Photo 4-19: Coexisting biotite, epidote and titanite in tonalitic rocks of Zone 1 in the southern Molson Lake Terrane. Plane polarized light.

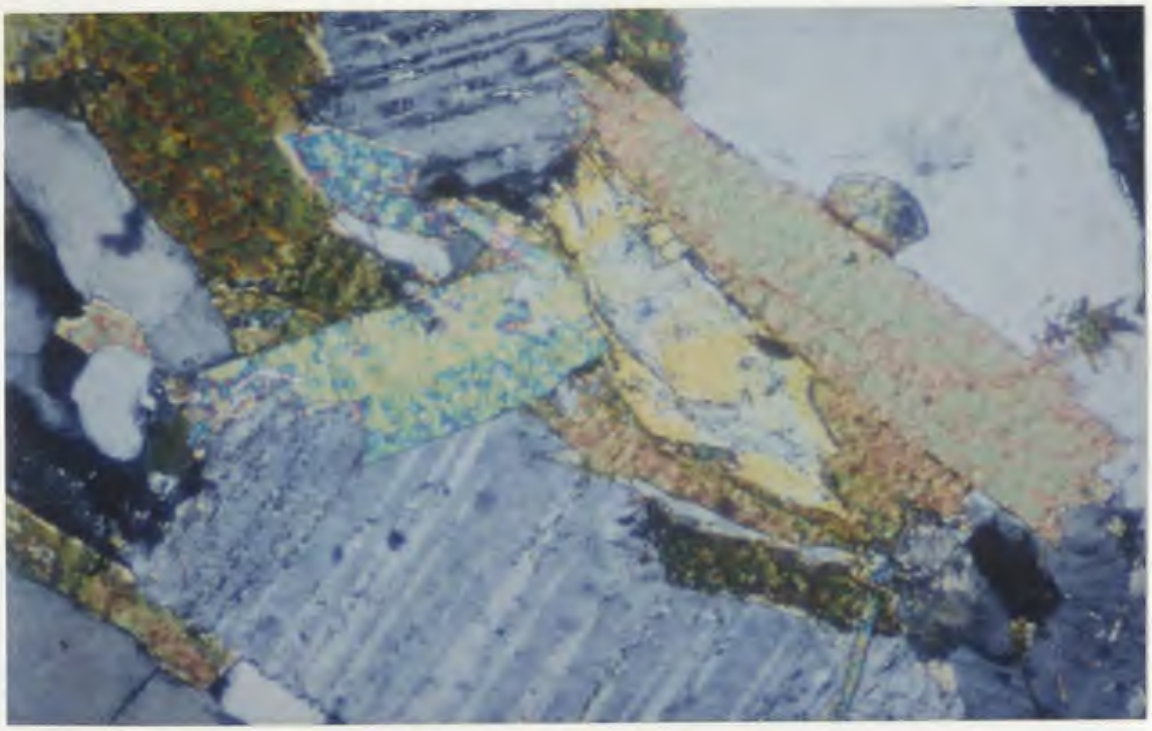

.2 mm

Photo 4-20: Coexisting biotite, muscovite and epidote in tonalitic rocks of Zone 1 in the southern Molson Lake Terrane. Cross polarized light.

.2 mm

Photo 4-21: Coexisting chlorite, epidote and muscovite in tonalitic rocks of Zone 1 in the southern Molson Lake Terrane. Cross polarized light.

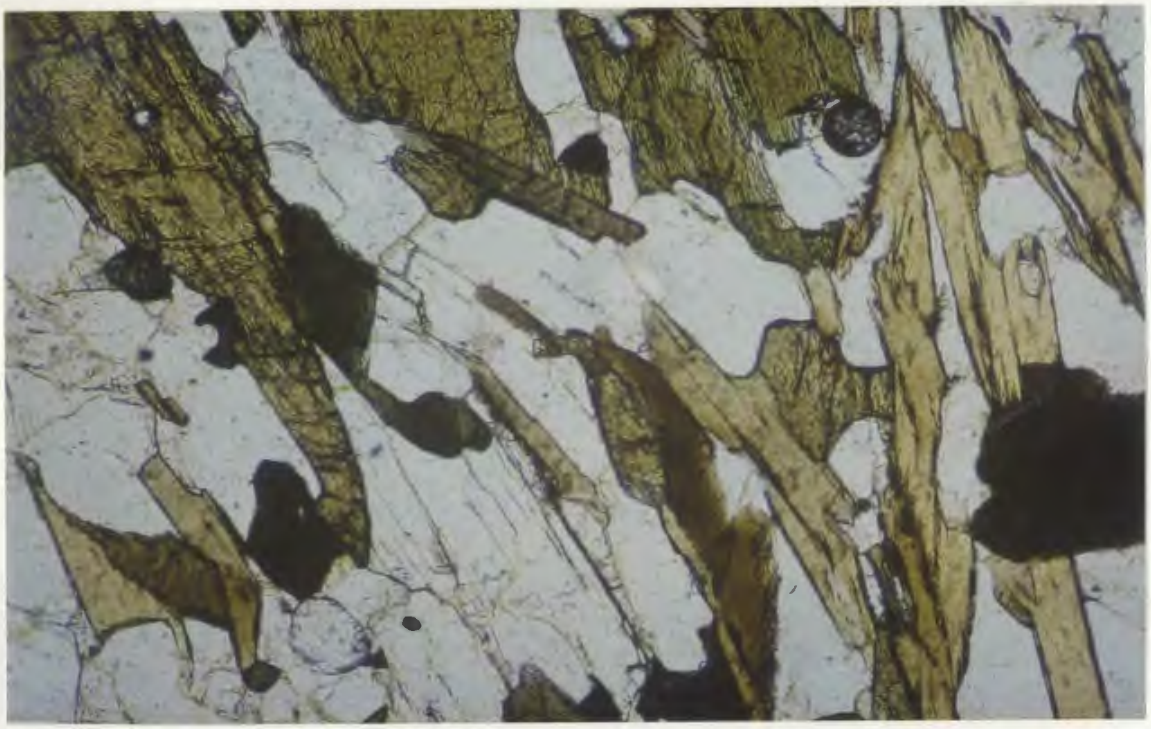

.2 mm

Photo 4-22: Coexisting hornblende and biotite in the tonalitic rocks of Zone 2 in the southern Molson Lake Terrane. Plane polarized light.

Zone 2 comprises the assemblage hornblende - biotite - epidote - plagioclase - quartz - titanite ± K-feldspar ± hornblende. This zone is characterized by equigranular, granoblastic textures and all phases in this zone have been observed in sharp, mutual contact with no signs of reactions (Photos 4-22 and 4-23). The prevalence of stable, aligned hornblende and the absence of muscovite and chlorite distinguish this zone from zone 1. There are no overprinting fabrics or mineral assemblages between zones 1 and 2 suggesting that they are both part of a single metamorphic field gradient, rather than zone 1 being a retrograde equivalent of zone 2. Assemblages in granitoid rocks in the northern Molson Lake Terrane are identical to those in zone 2 indicating that the isograds identified in the southern Molson Lake Terrane are truncated by the terrane boundaries at the present surface of erosion.

The microstructures in zone 2 indicate that all phases were stable at the time of metamorphism. The alignment of amphibole and biotite suggests that metamorphism occurred under deviatoric stress conditions; the comparable orientation and nature of these mineral fabrics with those in zone 1 suggests that metamorphism and deformation in these zones occurred approximately synchronously. Titanite in the zone 2 assemblage has yielded a U-Pb age of 995 Ma thereby establishing that the thermotectonic event in this terrane was part of the Grenvillian Orogeny (U-Pb data presented in Section 6.4.1).

The westernmost zone 3 is characterized by samples which contain the mineral assemblage garnet - clinopyroxene - biotite - plagioclase - quartz - magnetite ± K-feldspar. Microstructures are comparable to those in zone 2 but the assemblage garnet - clinopyroxene is stable in contrast to hornblende - plagioclase; titanite is absent. All phases of the zone 3 assemblage are in sharp, mutual contact (Photo 4-24). The single planar fabric S_{1M} is defined by biotite.

The pervasive granoblastic textures and sharp phase contacts in zone 3 attest to thorough recrystallization during the main metamorphic event. The alignment of biotite indicates that metamorphic recrystallization was accompanied by regional deformation, and the lack of overprinting assemblages across the isograds suggests that they were formed during a single thermotectonic event in response to different P-T conditions. However, due to the paucity of outcrops in the Molson Lake Terrane, there are few exposures close to the postulated locations of the isograds, and it is possible that each of

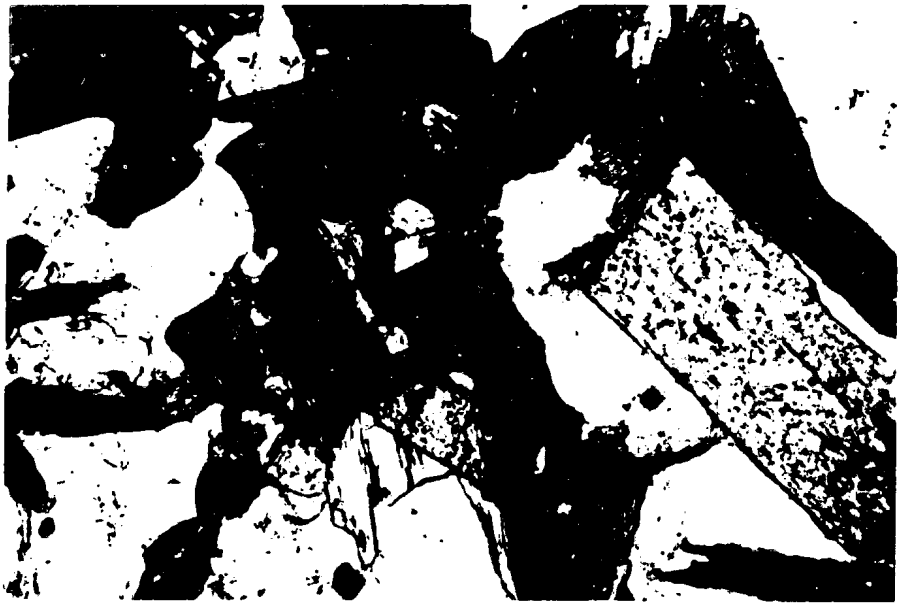

Photo 4-23: Coexisting hornblende, biotite and epidote in the tonalitic rocks of Zone 2 in the southern Molson Lake Terrane. Plane polarized light.

Photo 4-24: Coexisting garnet, clinopyroxene, plagioclase and biotite in the tonalitic rocks in Zone 3 in the southern Molson Lake Terrane. Plane polarized light.

the zones is in fault contact. No metamorphic minerals suitable for U-Pb geochronology were identified in zone 3, and so the age of the metamorphism has not been established unambiguously. Nevertheless, on the basis of microstructural evidence noted above, the single metamorphic episode in zone 3 is correlated with the single episode in zones 1 and 2, thus implying that the mineral assemblages of zone 3 are also of Grenvillian age.

4.4.1 Mineral Chemistry of the Molson Lake Terrane Granitoid Rocks

Microprobe analyses of minerals in granitoid rocks from the Molson Lake Terrane was focused on samples from zone 3, the only zone which contains phases suitable for both geothermometry and geobarometry. Garnets, biotite, clinopyroxene and plagioclase were analyzed.

4.4.1.1 Garnet

Garnets in zone 3 vary in Mg/(Mg+Fe) ratio from .17 to .52 (X_{ALM} from .36 to .63 and X_{PYR} from .13 to .43; Fig. 4-14a). Fe and Mg are negatively correlated whereas the spessartine and grossular contents are relatively low and are not correlated with X_{ALM} or X_{PYR} (X_{SPES} = .002 to .1 (Fig. 4-14b) and X_{GROS} = .13 to .23 (Fig. 4-15)).

4.4.1.2 Biotite

Mg/(Mg+Fe) ratios in biotite in this zone range between .52 and .66 (Fig. 4-16) and are positively correlated with the Mg/(Mg+Fe) ratios in coexisting garnet (Fig. 4-17) in the two samples which contain both phases. Al^{6} varies between 0.02 and .17, indicating locally significant substitution of Al^{6} for Mg and Fe.

4.4.1.3 Clinopyroxene

Compositions of clinopyroxenes in terms of the four quadrilateral components are shown in Fig. 4-18, a modified (opened up) quadrilateral diagram. Most clinopyroxenes are diopsides following the terminology of Deer et al. (1966). However, there are significant non-quadrilateral components in most of the analyses. These were calculated according to the following scheme: Na and Al were allocated equally to the M1 and M2 sites respectively to create jadeite until one was depleted. This method of preferentially calculating jadeite, rather than acmite as suggested by Lindsley (1983), is preferred in light of the positive correlation between Na and Al in pyroxene in the southern Molson

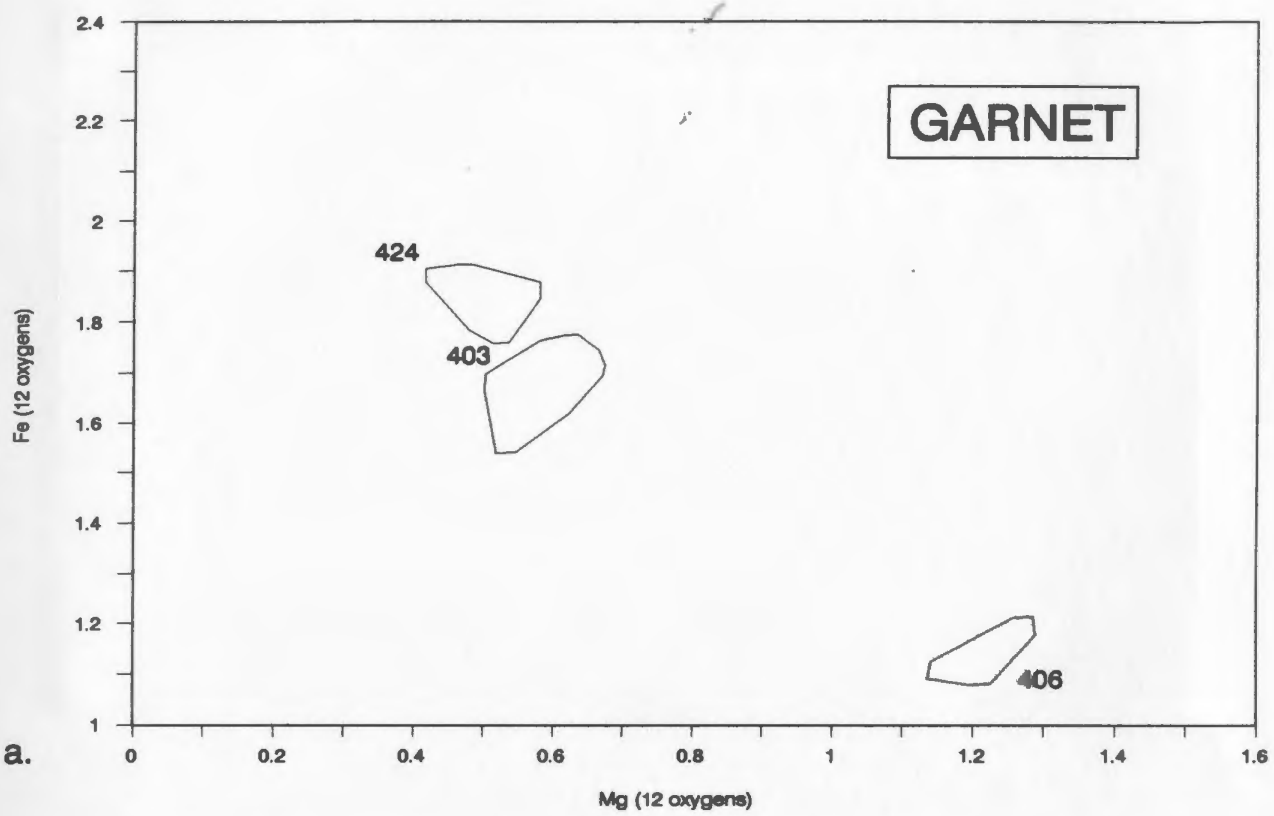

a.

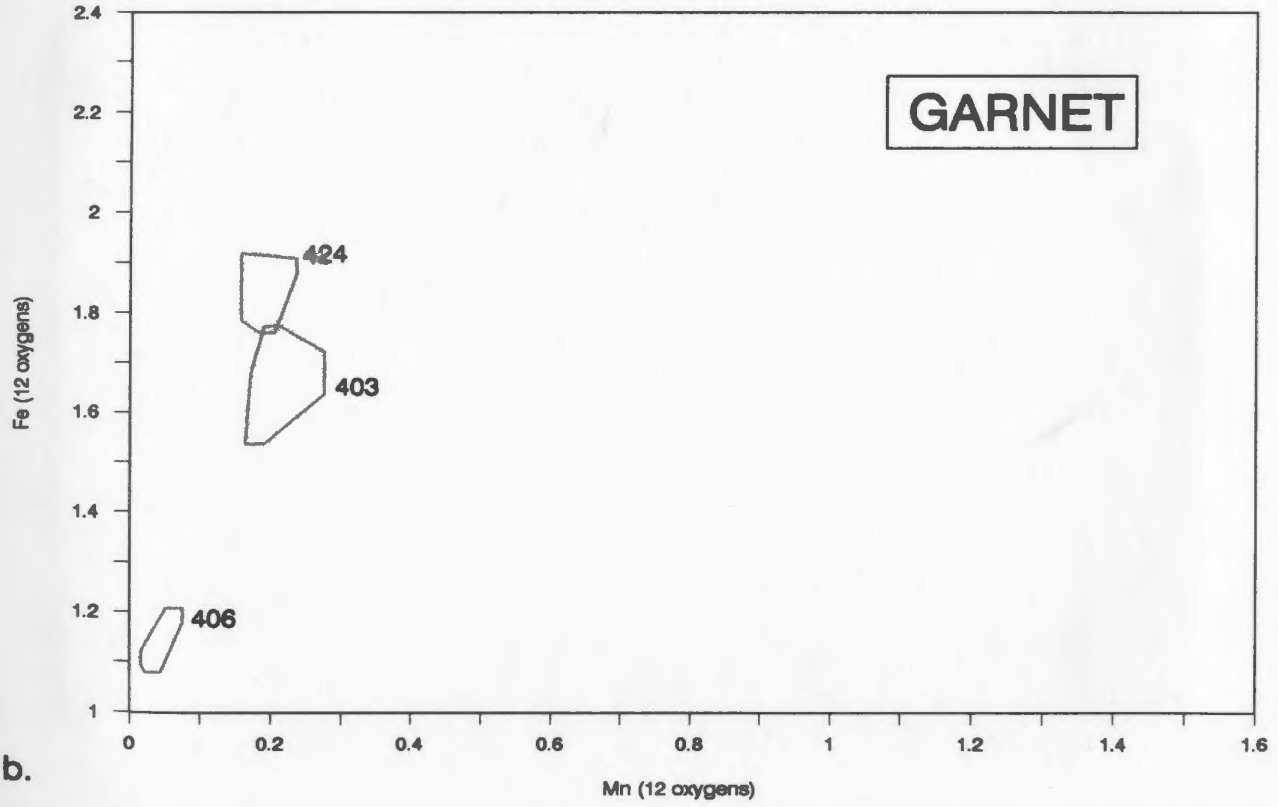

b.

Figure 4-14: Compositional variation of garnets in the clinopyroxene-bearing granitoid rocks in the southwest Molson Lake Terrane. Analyses for each sample in Appendix 2.

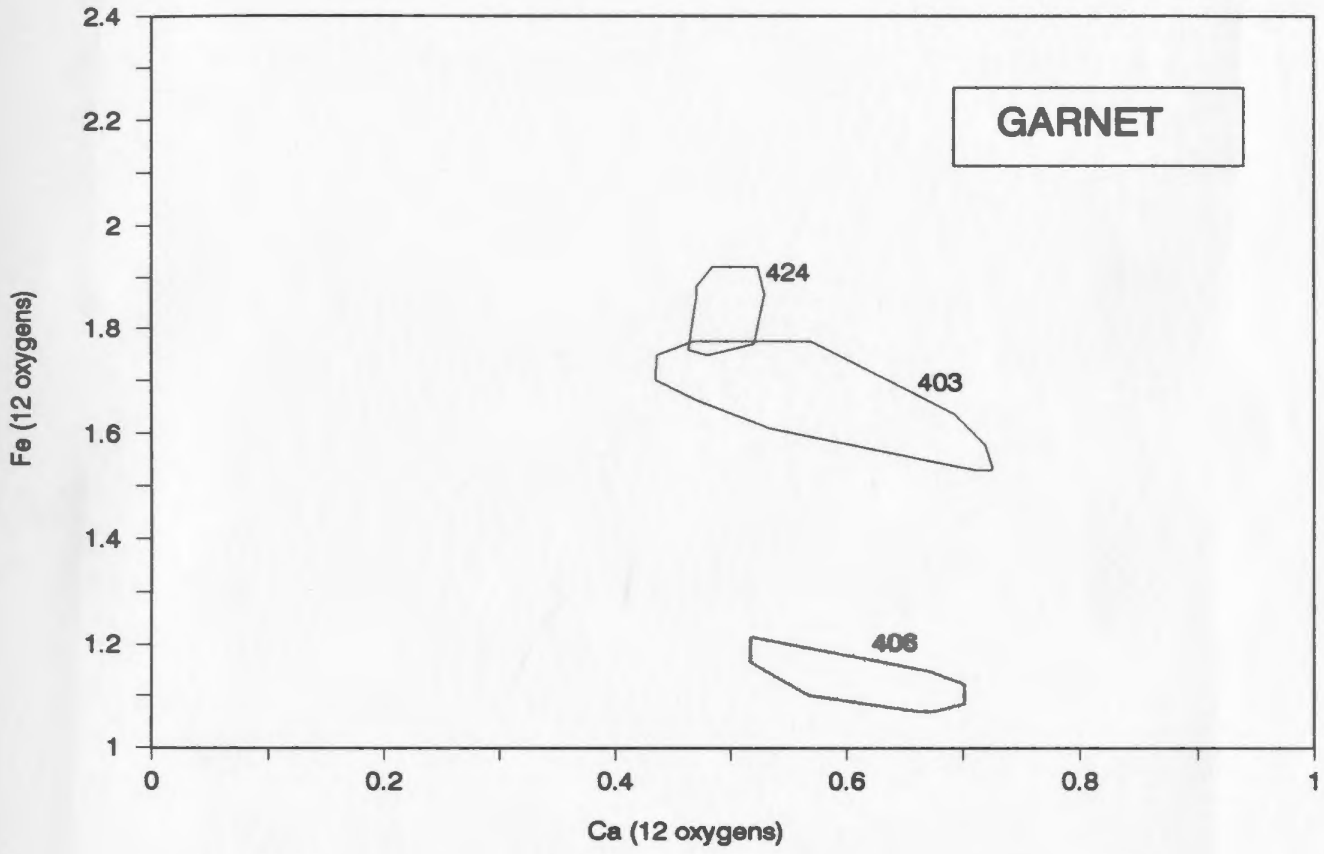

Figure 4-15: Compositional variation of garnet from the clinopyroxene-bearing granitoid rocks of the southwest Molson Lake Terrane. Analyses for each sample in Appendix 2.

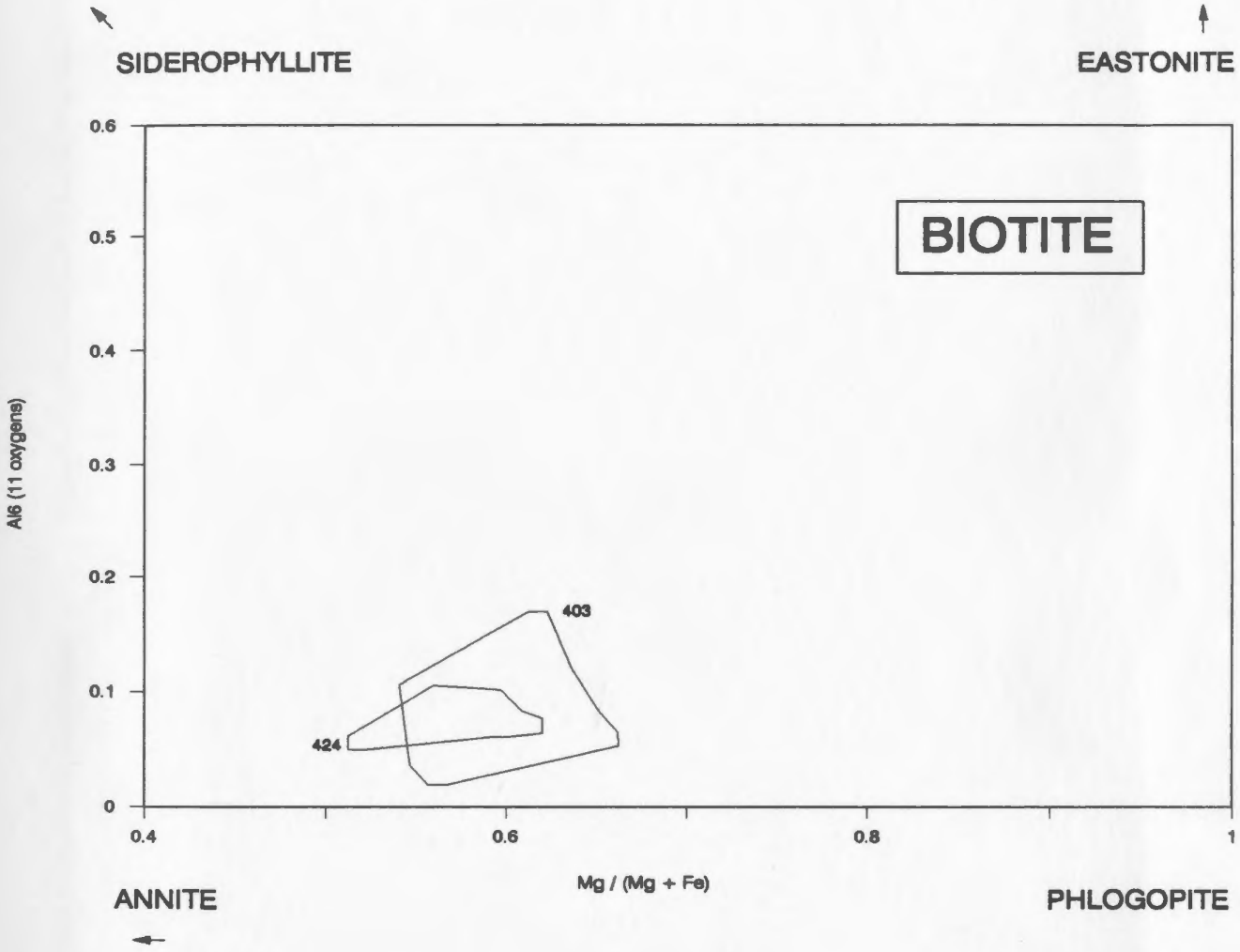

Figure 4-16: Compositional variation of biotite in the clinopyroxene-bearing granitoid rocks of the southwest Molson Lake Terrane. Analyses for each sample in Appendix 2.

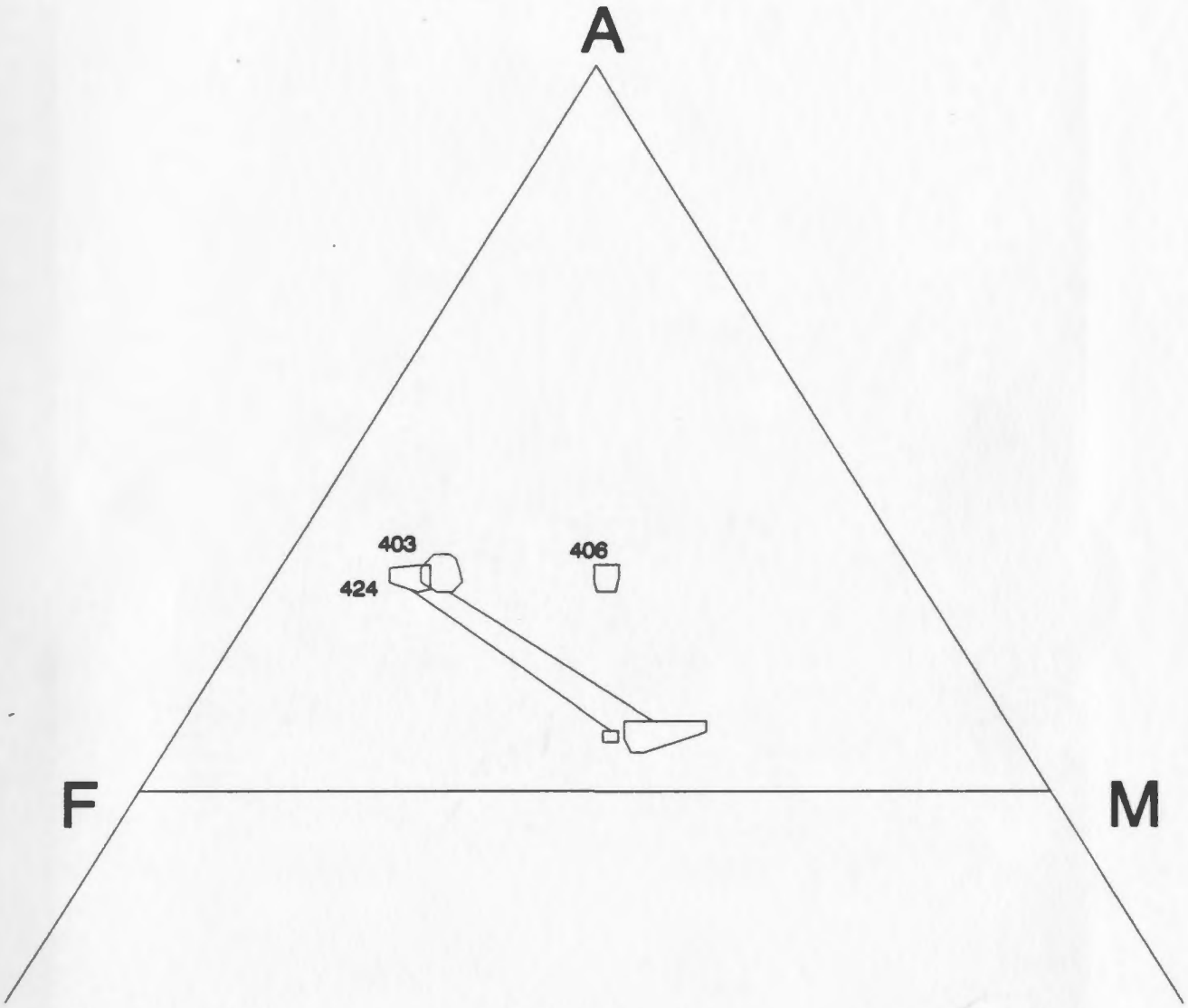

Figure 4-17: Compositional variation of co-existing garnet-biotite in the southwest Moison Lake Terrane.

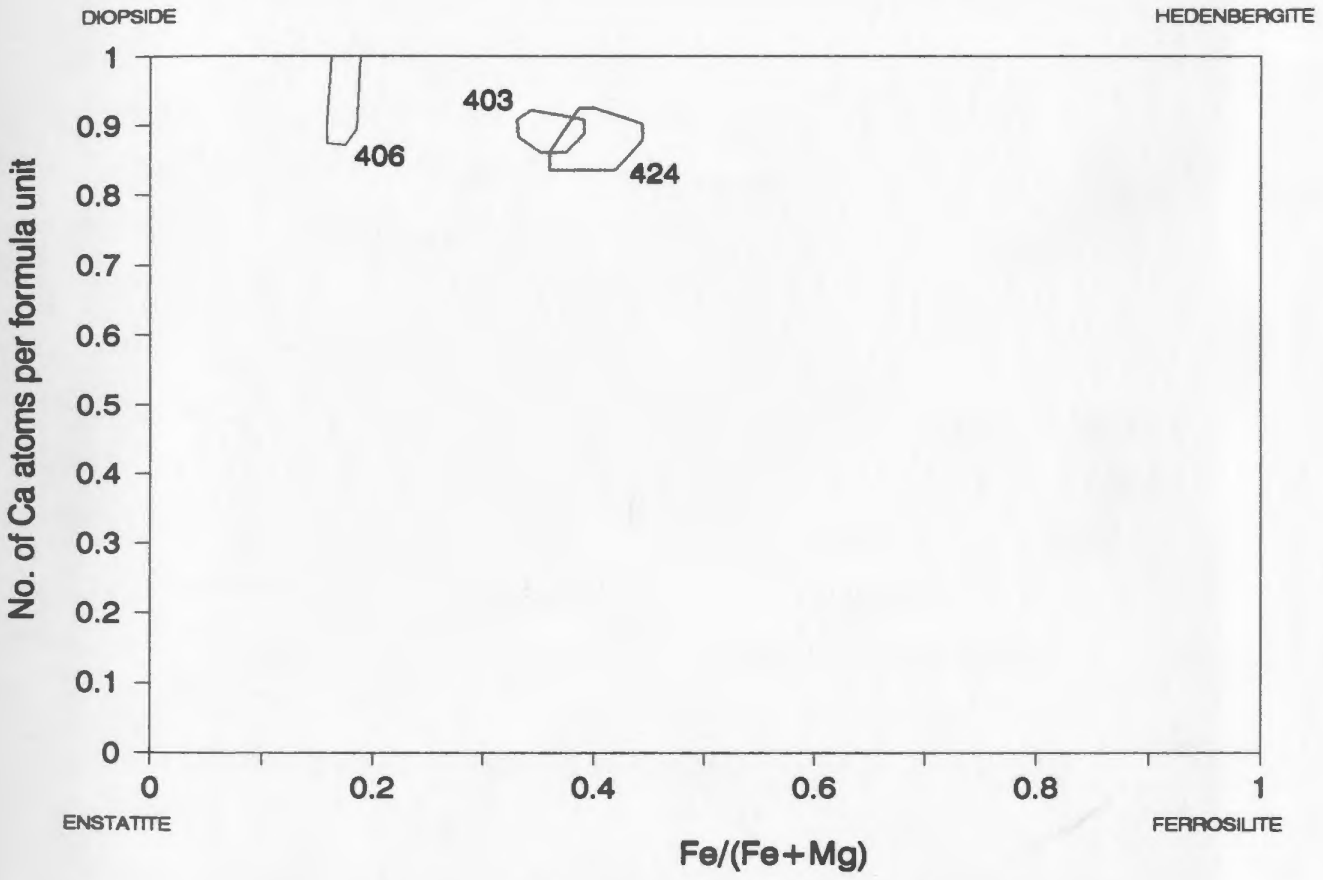

Figure 4-18: Composition of clinopyroxene in the granitoid rocks of the southwestern Molson Lake Terrane displayed on a modified pyroxene quadrilateral plot (the pyroxene quadrilateral has been opened up and plotted on a rectangular diagram). Analyses for each sample in Appendix 2.

Lake Terrane. Any remaining Na in M1 was coupled with Fe^{+3} in M2 to create acmite, any remaining Al in M2 was coupled with Ca to create Ca Tschermakite. The remaining Ca was then allocated to diopside-hedenbergite in proportion to the remaining Fe:Mg ratio for the mineral. Any excess Mg and Fe is assumed to occur as orthopyroxene with the enstatite-ferrosilite ratio equal to that of diopside:hedenbergite. Following this scheme, orthopyroxene comprises between 0 and .1 molecules per formula unit with the remaining clinopyroxene component comprising diopside (.46 to .68), hedenbergite (.13 to .33) and jadeite (.05 to .13). The mole fractions of acmite and Ca Tschermakite vary between 0 and .02. The very low amounts of acmite suggests that Fe^{+3} in clinopyroxene is not significant.

The range of Ca:Fe+Mg ratios for coexisting ferromagnesian minerals is shown on an ACF diagram in Figure 4-19.

4.4.1.4 Plagioclase

Plagioclase compositions in zone 3 of the southern Molson Lake Terrane vary between approximately An_{15} and An_{51} (Fig. 4-20). Orthoclase contents are typically less than 2%. Deviations from the condition XCa+XNa=1 required for charge balance are attributed principally to errors in Na_2O analyses. This is thought to be a consequence of significantly differing amounts of Na_2O between the calibrated microprobe standards and the unknowns and, therefore, a long extrapolation in the conversion of counts per second to weight percent. However, since XCa is the significant unknown in plagioclase for geobarometry, the potential error in Na_2O analyses is not critical for the present purposes.

4.4.2 Petrogenetic Grids and Implications for Metamorphism of the Granitoid Rocks of the Molson Lake Terrane

The assemblages observed in the granitoid rocks of the Molson Lake Terrane do not precisely constrain the P-T conditions during metamorphism. However, the interpretation that the changes in mineral assemblages across the Molson Lake Terrane are due to a single thermal event may broadly constrain the metamorphic field gradient. This interpretation does not exclude the possibility that the metamorphic zones of the southern Molson Lake Terrane are fault bounded.

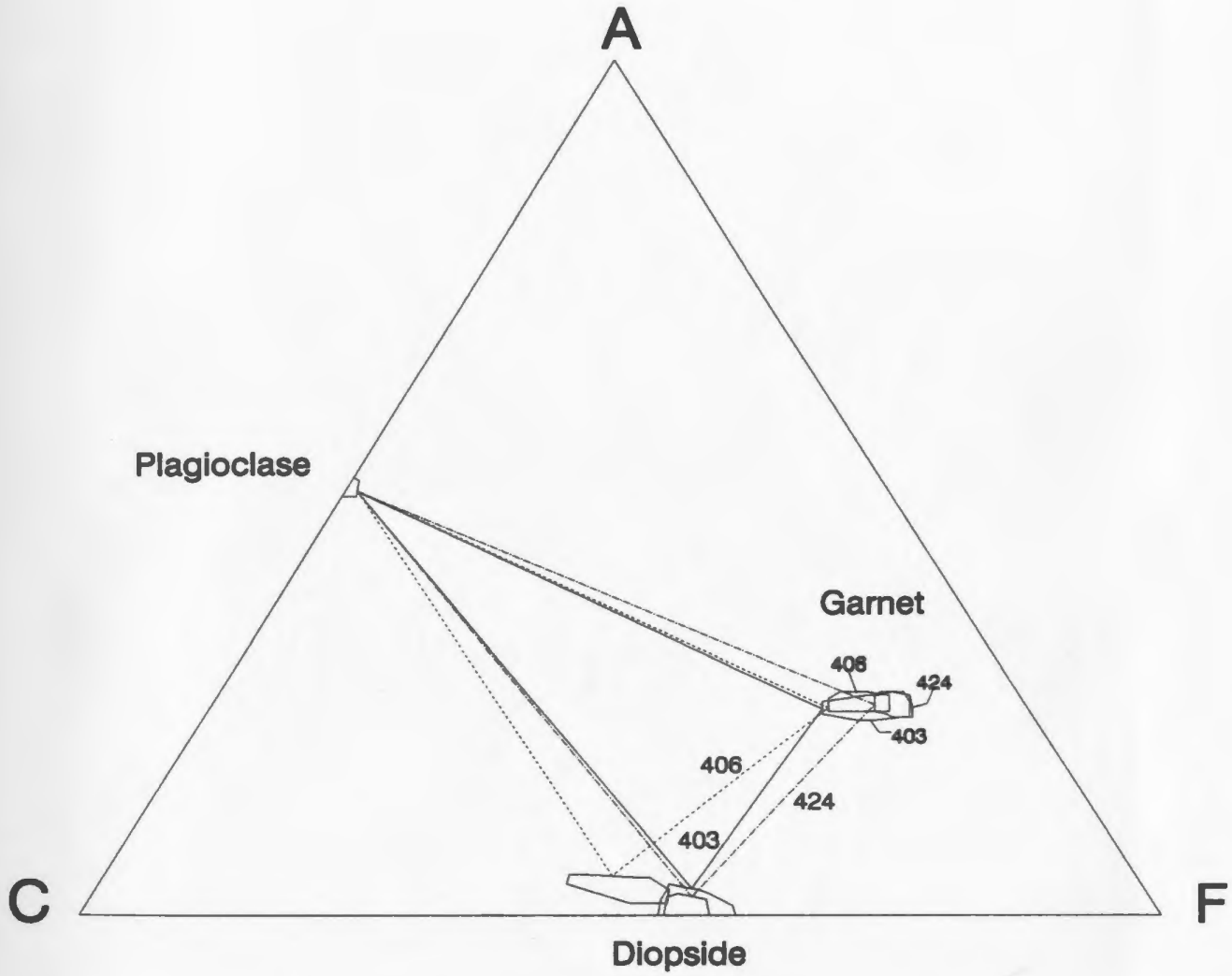

Figure 4-19: Compositional variations of co-existing PLG-CPX-GNT in the southwest Molson Lake Terrane plotted on an ACF diagram (note that pyroxenes contain up to 13% jadeite which cannot be plotted on this diagram; plagioclase is plotted as pure anorthite). Not corrected for jadeite in clinopyroxene.

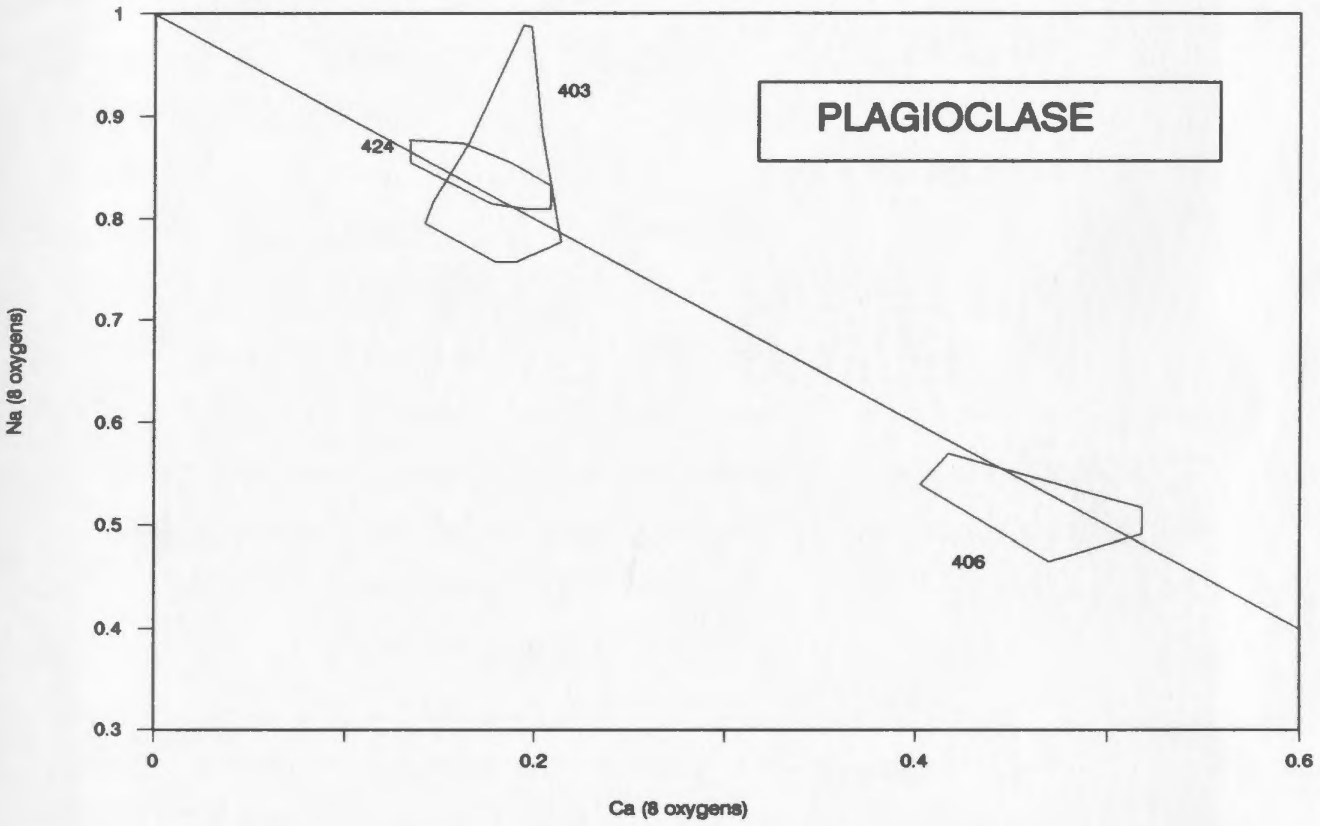

Figure 4-20: Compositional variation of plagioclase in clinopyroxene-bearing granitoid rocks of the southwestern Molson Lake Terrane. Analyses from each sample in Appendix 2.

The common occurrence of the assemblage plagioclase - epidote - muscovite - biotite and the local occurrence of syntectonic chlorite in zone 1 implies that P-T conditions in this zone must have predominantly been in greenschist facies. The local occurrence of hornblende in this zone implies that the temperature must have locally exceeded the lower limits of the hornblende stability field. Zone 2 in the southern Molson Lake Terrane and the assemblages in all of the northern Molson Lake Terrane are characterized by the presence of epidote, plagioclase (approximately An17) and hornblende in rocks of appropriate compositions, and therefore may be assigned to the epidote-amphibolite facies.

Mineral assemblages in zone 3 contain coexisting garnet, clinopyroxene and quartz. The model reaction in the CMAS system:

hornblende + plagioclase = clinopyroxene + garnet + quartz (R4.11)

occurs at elevated pressures and is relatively insensitive to temperature (Fig. 4-21, Wells, 1979), and so the assemblage clinopyroxene, garnet and quartz may be taken as a qualitative indicator of relatively high pressures during metamorphism. The presence of a significant amount of jadeite component in clinopyroxene provides independent confirmation of this interpretation (Holland, 1980). Using the GEOCALC software of Berman et al. (1987), the position of the equilibrium boundary for the reaction:

albite = jadeite + quartz (R4.12)

has been calculated for Jd_{10} and Ab_{85}, the approximate compositions of these two phases in samples JNC-86-403 and 424 from zone 3 of the southern Molson Lake Terrane, and are plotted in Figure 4-22. If the metamorphic field gradient is approximately continuous across the southern Molson Lake Terrane, the temperatures in zone 3 must have been about the same or higher than those in the adjacent epidote-amphibolite facies zone 2, shown on Figure 4-22. The position of reaction R4-12 for the specified composition in Figure 4-22, combined with this minimum temperature estimate, requires that pressures in the southern Molson Lake Terrane must have been in excess of 8 kbar during the recrystallization event. This indication of elevated pressures is in qualitative agreement with the evidence of high pressures indicated by the assemblage clinopyroxene - garnet - quartz (Wells, 1979).

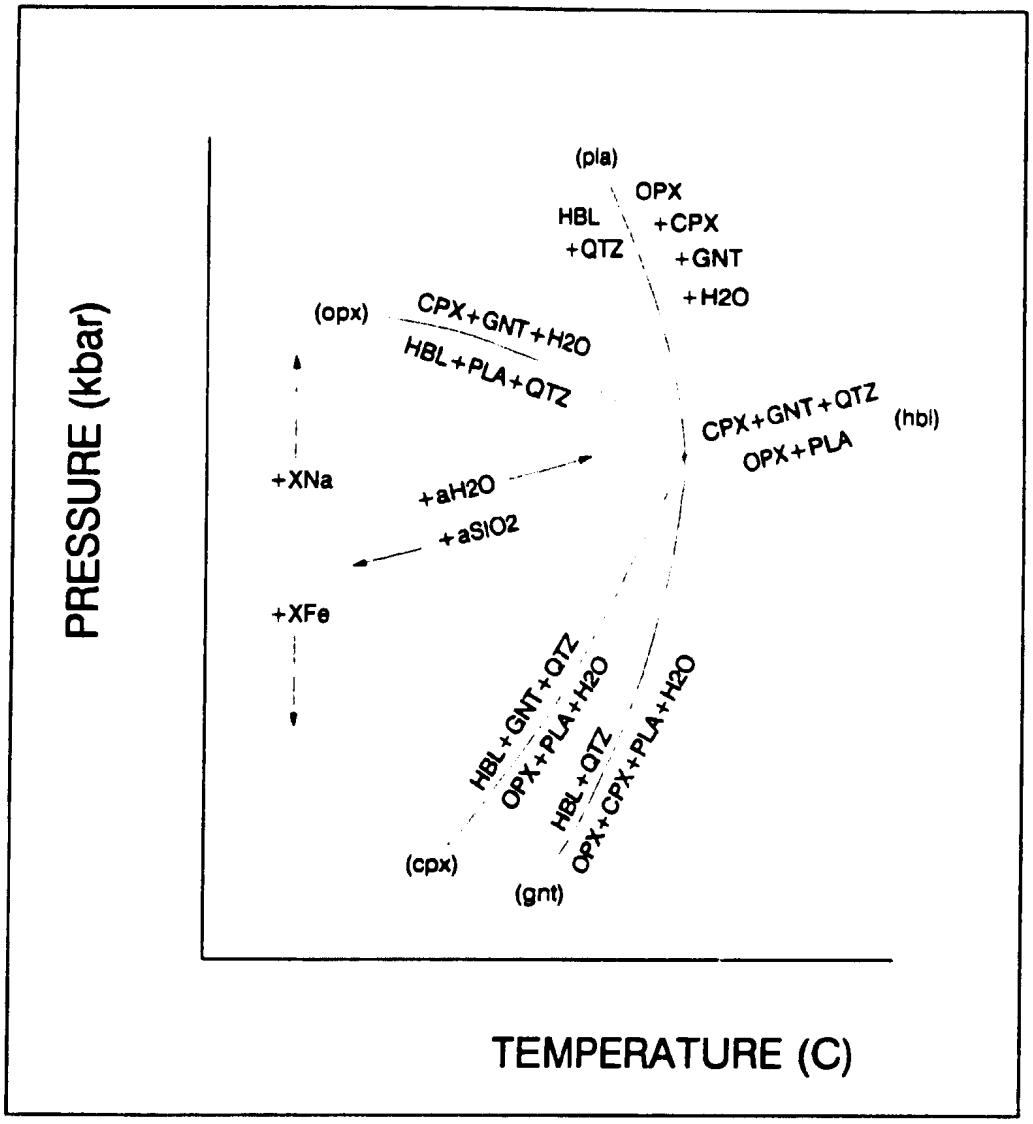

Figure 4-21: Model reactions in the Cao - Mgo - Al2O - SiO2 - H2O system, after Wells (1979).

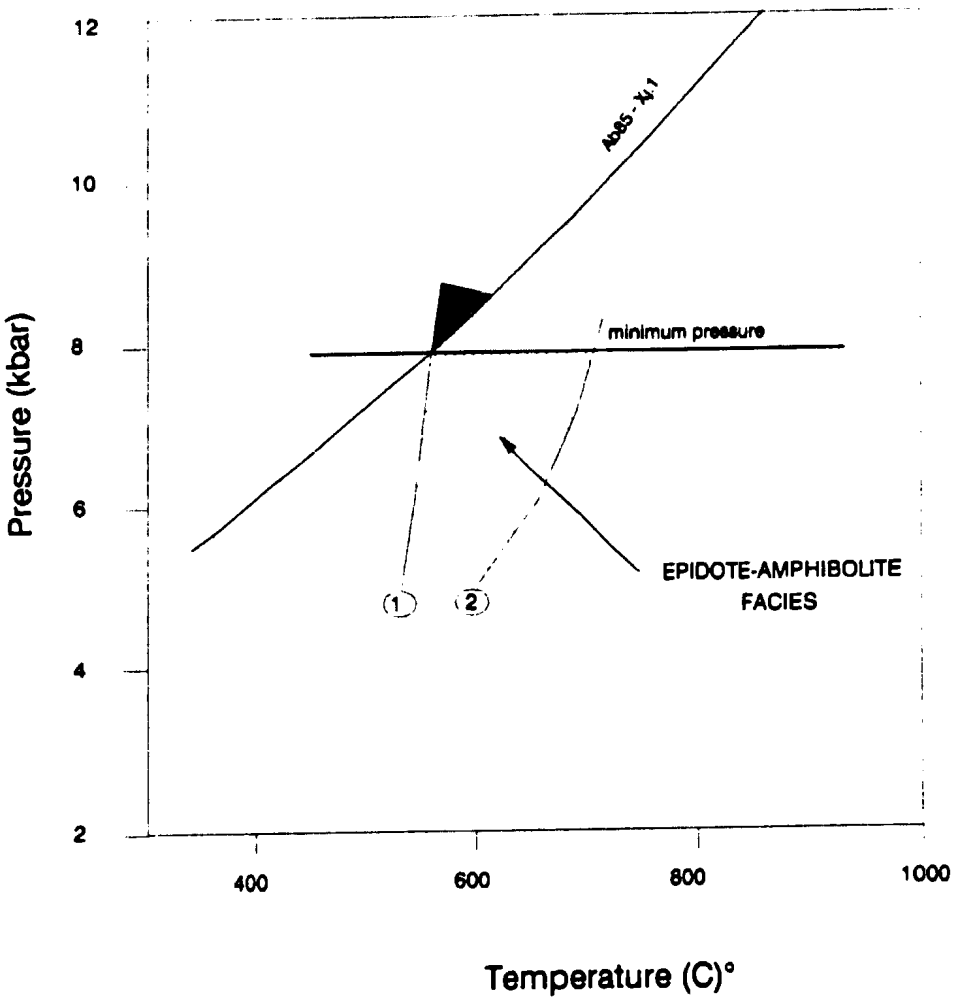

Figure 4-22: Minimum pressure estimate for the southwest Molson Lake Terrane as constrained by the reaction AB85 = JD15 + QTZ and the epidote - amphibolite facies stability field. (1) and (2) - Apted and Liou (1983).

The mineral assemblages in the three zones of the southern Molson Lake Terrane are interpreted to be a result of a single metamorphism during the Grenvillian Orogeny. The transition from greenschist facies along the eastern margin through epidote-amphibolite facies into garnet - clinopyroxene - quartz assemblages in the west reflects a temperature and pressure increase from east to west. The lack of detailed calibrated petrogenetic grids suitable for granodioritic-tonalitic compositions precludes the quantification of these P-T variations across the terrane on the basis of petrogenetic grids. The northern Molson Lake Terrane experienced epidote-amphibolite conditions, comparable to zone 2 of the southern Molson Lake Terrane.

4.5 The Shabogamo Intrusive Suite: Molson Lake Terrane

The gabbroic rocks of the Molson Lake Terrane are extensively recrystallized and most exhibit coronitic textures, which as noted previously, may be divided into three groups on the basis of the corona mineralogy. The areal distributions of these groups mutually overlap, suggesting that the coronas did not develop primarily as a function of the regional differences in P-T conditions. The corona mineralogies and possible reactions leading to their formation are discussed briefly below.

4.5.1 Group 1 - Amphibole Coronas on Clinopyroxene

Group 1 coronas are characterized by the presence of amphibole rims around clinopyroxene and biotite and by the absence of garnet and orthopyroxene in the coronas (Fig. 4-23a). This group does not contain orthopyroxene. The amphibole is commonly poikiloblastic, containing up to 10% by volume inclusions of quartz, especially where it rims clinopyroxene. Biotite is commonly rimmed by amphibole which displays darker green pleochroism than the blue-green pleochroism of amphibole that surrounds clinopyroxene. Biotite is spatially related to ilmenite and commonly defines a planar tectonic fabric suggesting syntectonic growth. Metamorphic garnet is present as a minor disseminated phase and is not spatially related to the coronas.

4.5.2 Group 2 - Amphibole - Garnet Coronas on Clinopyroxene

Group 2 coronas are characterized by a double corona on clinopyroxene consisting of an inner rim of amphibole and an outer rim of garnet (Figure 4-23b). Commonly there is a narrow moat ($<.1$ mm) of plagioclase between the amphibole and garnet

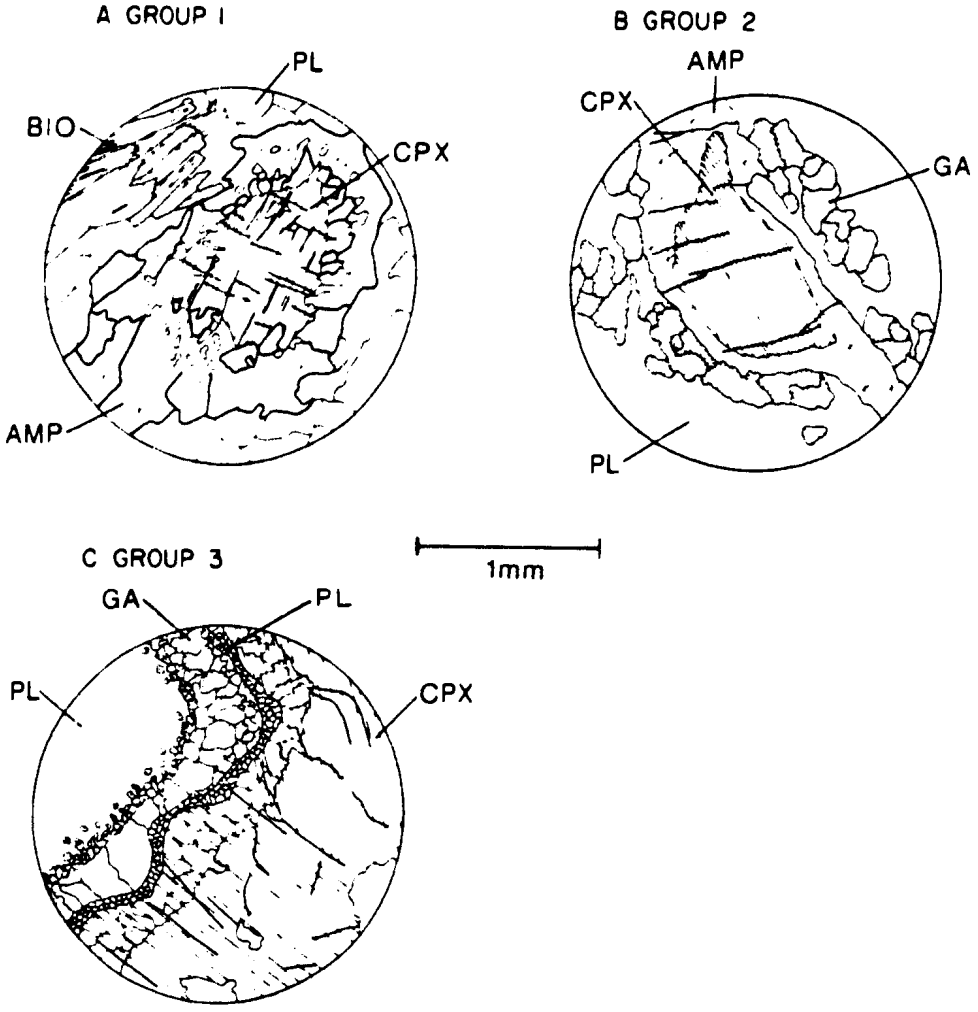

Figure 4-23: Corona textures in the Shabogamo Intrusive Suite in the Molson Lake Terrane.

rims. The garnet varies in texture from granular to a symplectic intergrowth with opaque phases and clinopyroxene inclusions. Locally amphibole is not present and clinopyroxene and garnet are separated only by a plagioclase moat which is wider than in samples where the amphibole is present. Biotite is commonly rimmed by amphibole. In spite of the high degree of recrystallization throughout much of this group, corona textures are well defined. Quartz is locally present as inclusions in poikiloblastic amphibole. As in the other two subgroups, ilmenite commonly cores clusters of biotite and associated amphibole.

4.5.3 Group 3 - Garnet Coronas on Clinopyroxene

Group 3 coronas are distinguished from the other groups by the absence of amphibole in the corona and by the garnet rim around clinopyroxene, with the two phases typically being separated by a narrow moat of plagioclase (Fig. 4-23c). Relict igneous olivine and orthopyroxene are still present, in proportions typically subordinate to clinopyroxene, such that this group ranges in composition from metagabbro to metagabbronorite. Olivines are locally rimmed by fibrous orthopyroxene. Recrystallized igneous plagioclase outside the garnet corona contains abundant corundum platelets. Amphibole is spatially associated with, and may locally rim, clinopyroxene, but is generally not part of the corona structure. Amphibole and associated biotite are spatially associated with igneous ilmenite.

4.5.4 Corona Reactions in the Shabogamo Intrusive Suite

4.5.4.1 Group 1 Reactions

The textures observed in Group 1 were probably formed by partial reaction between clinopyroxene and adjacent plagioclase in the presence of a fluid to form rims of amphibole. This may have been achieved by the hydration reaction proposed by Rivers and Mengel (1988) for coronas in gabbros of the Shabogamo Intrusive Suite in the northern part of the study area:

$$\text{clinopyroxene} + \text{plagioclase} + H_2O = \text{amphibole} + \text{quartz} \qquad \text{(R4.13)}.$$

A few samples in Group 1 experienced nearly complete recrystallization with the result that plagioclase, green-brown amphibole, garnet, quartz and relict clinopyroxene exhibit an equigranular, granoblastic texture. This assemblage is representative of the amphibolite facies.

4.5.4.2 Group 2 Reactions

The reaction(s) leading to the formation of double coronas in Group 2 is more enigmatic than that for the single corona of Group 1. The sequence of mineral growth can only be inferred through examination of phase relationships in individual thin sections and consideration of the transitional relationships between groups. The inner corona of amphibole appears to have developed at the expense of clinopyroxene and plagioclase, in a manner similar to the proposed reaction for the Group 1 coronas (see reaction R4.13). The development of the outer corona of garnet ±clinopyroxene has apparently been at the expense of the amphibole inner corona and matrix plagioclase in the reaction:

amphibole (pargasite) + anorthite + quartz =

garnet + diopside + albite + H_2O (R4-14).

The moat of plagioclase may have been produced from the breakdown of clinopyroxene - garnet - quartz upon decompression by reaction R4-11.

4.5.4.3 Group 3 Reactions

The presence of delicate rims of garnet between relict ophitic clinopyroxene and plagioclase laths in Group 3 coronas suggests that, in at least some samples, garnet formed as a product of the breakdown of igneous clinopyroxene. In other samples, the absence of amphibole may be attributed to the completion of amphibole consuming reactions which produced garnet (R4-14). The reaction leading to the production of garnet directly from clinopyroxene may be represented by:

clinopyroxene + anorthite + quartz = garnet + albite (R4.15)

(from Rivers and Mengel, 1988).

The presence of significant jadeite in clinopyroxene in the southern Molson Lake Terrane suggests that jadeite and quartz would replace albite in reaction R4-14 in areas of higher pressure.

4.5.5 Origin of the Coranitic Textures in the Shabogamo Intrusive Suite

The distribution of the aforementioned coronitic textures are not spatially correlated with the established metamorphic field gradient in the Molson Lake Terrane (this study, Rivers and Mengel, 1989). This strongly suggests that the development of the coronitic textures was a function of post-solidus cooling reactions rather than the metamorphic events responsible for the field gradient identified in the granitoid rocks of the Molson Lake Terrane.

4.6 Summary

The mineral facies in the supracrustal rocks of the Lac Joseph Terrane indicate that upper amphibolite to granulite facies metamorphism prevailed during the Labradorian Orogeny throughout this terrane. Kyanite-K-feldspar co-existing in rocks in the central region and along the northern margin of the Lac Joseph Terrane indicate that these areas experienced pressures above 8 kbar. Labradorian assemblages within the mafic gneisses are locally retrogressed during a cryptic event at 1281 Ma while pelitic migmatites near granitic intrusions and along the southwest margin were locally overprinted by muscovite.

Mineral facies in granitoid rocks in the southern Molson Lake Terrane are interpreted to have formed during the Grenvillian Orogeny and indicate increasing pressures and temperatures from east-southeast to west-northwest. Granitoid rocks in the northern region of the Molson Lake Terrane contains a single mineral facies, equivalent to the central zone of the southern Molson Lake Terrane. The presence of a garnet-clinopyroxene-quartz assemblage and a significant jadeite component in clinopyroxene indicate high pressures dominated during metamorphism in the southwestern part of the Molson Lake Terrane.

CHAPTER 5
GEOTHERMOBAROMETRY

5.1 Introduction

In order to quantify the metamorphic conditions of the Lac Joseph and Molson Lake terranes, P-T estimates were calculated utilizing several published geothermometric and geobarometric calibrations. Mineral analyses were performed on a Jeol JXA-50A wavelength dispersive electron microprobe at the Department of Earth Sciences, Memorial University, using the correction procedure outlined by Bence and Albee (1968). Natural standards were used for calibration and Fe^{+2} is assumed to equal Fe^{TOTAL} (see Appendix 4 for discussion of this assumption). Pressures and temperatures were calculated utilizing a computer program written by F.C. Mengel, which incorporates recent calibrations for a range of geothermometers and geobarometers. Appendix 3 contains sample calculations for mineral formulas, and for the geothermometers and geobarometers utilized in this study. Errors on the geothermobarometric estimates are discussed in Appendix 4. Discussions concerning thermobarometric techniques and their limitations are based on Mengel (1987, Appendix 4) and Essene (1989).

Samples for geothermobarometry were chosen on the basis of their mineral assemblages so that both pressure and temperature could be determined from a single outcrop. All minerals were analyzed at the core and near the rim to establish chemical variations within each phase. Activities (a) of components in solid substitution series were calculated from measured cation concentrations utilizing appropriate mixing models (see Appendix 3 for details and examples). Activities were combined in Vant Hoff expressions to determine the equilibrium constant (K) for the reactions of the type:

such that

$$K = \frac{[a_C^c][a_D^d]}{[a_A^a][a_B^b]} \quad \text{Eq.5.1.}$$

The equilibrium constant (K) is related to pressure (P) and temperature (T) by the generalized expression:

$$\Delta G = \Delta H - T\Delta S + P\Delta V + RT \ln K \quad \text{Eq.5.2}$$

where G=Gibbs free energy, H=enthalpy, S=entropy, V=molar volume and R=gas constant. At equilibrium, the condition that $\Delta G=0$ is satisfied and the equation may be rearranged to isolate either P or T. Since there is only one equation and two unknowns (P and T), a unique solution is not possible. However, by solving for different values of P or T, a line of constant K, or K isopleths, in P-T space can be obtained which represents the possible pressures and corresponding temperatures at which the mineral assemblage could have equilibrated.

Geothermometers are generally based on exchange reactions in which two elements of similar size and charge are partitioned between two mineral phases. Exchange reactions inherently have very small volume changes, so that K is predominantly controlled by temperature; lines of constant K therefore have a steep positive slope in P-T space.

Geobarometers are based on net transfer reactions where a phase or phases break down over a range of P-T conditions to form a new phase assemblage. Since these reactions typically involve substantial volume changes the lines of constant K are more pressure dependent than for exchange reactions and have a gently positive slope in P-T space.

For a sample containing both a geothermometric and geobarometric assemblage, a unique pressure and temperature may be estimated by the intersection of K isopleths for each reaction; this will be referred to as the "intersection pressure - temperature estimate". The data portrayed in figures displaying intersection pressure - temperature estimates are bounded by a rhombohedra in P-T space. The sides of the rhombohedra are parallel to the slopes of the K isopleth for the geothermometer and geobarometer utilized are bound all the data in that figure.

In order for the pressures and temperatures estimated by this method to be geologically significant, several conditions must be simultaneously satisfied. Firstly, there must have been chemical equilibrium between each phase at the time that they ceased to react. This requires that the sites in the phases analyzed for a particular calibration were in mutual chemical communication, and that they formed under the same P-T-X conditions. In this study, in order to maximize the probability that this condition was satisfied, compositions of cores of coexisting grains were utilized in some calculations and rim compositions were used in others.

The second condition is that the chemistry of phases utilized in a geothermometric or geobarometric calibration was not altered by subsequent reactions. Careful petrographic work has been employed in this study to identify reactions which occurred subsequent to the metamorphic peak, but it is acknowledged that textural arguments in general cannot prove the former existence of equilibrium, they can at best only provide permissive evidence that it may have occurred.

Since a P-T estimate is dependent on both the geothermometer and geobarometer, a third critical assumption requires that both the thermometric and barometric assemblages equilibrated at about the same time. It they did not, the P-T point will not lie on the real P-T path, and will, therefore, be an artifact of the computation. This assumption is particularly critical in the present study in which there is the possibility of two superposed metamorphic events of quite different age and P-T conditions. Independent arguments must be used to establish that the thermometric and barometric equilibria were operative at about the same time. In this study, this has been achieved by use of relative and absolute chronology.

5.2 Lac Joseph Terrane

Geothermobarometry of samples from the Lac Joseph Terrane concentrated on strategic areas with sufficient outcrop; this has resulted in an uneven distribution of samples across the terrane (Fig. 5-1). For the sake of presenting the P-T results, the Lac Joseph Terrane is divided into five domains; the southern, central, northeastern, northwestern and western domains (Fig. 5-1). Several of these domains exhibit

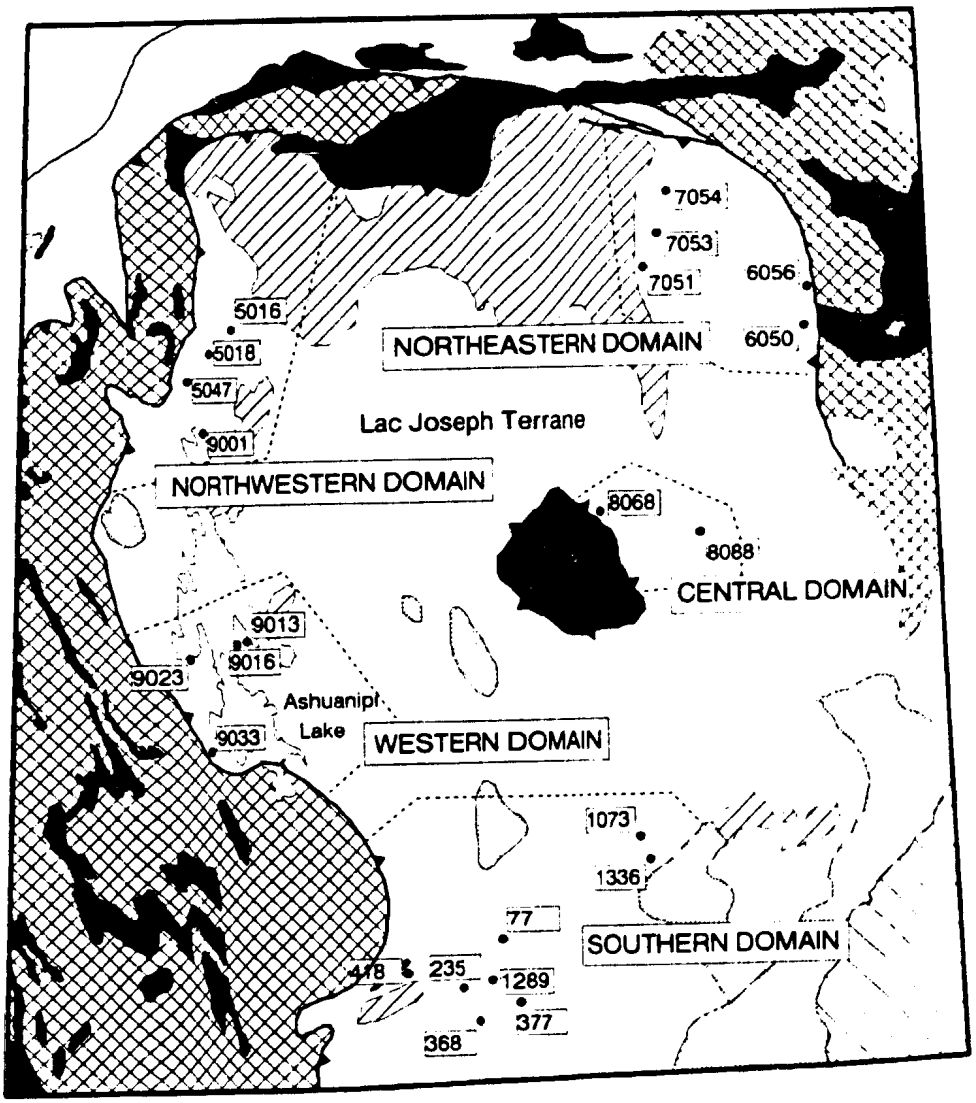

Figure 5-1: Locations of samples and domains utilized for geothermobarometry in the Lac Joseph Terrane.

evidence which suggests that chemical equilibrium was attained, and are discussed before the results from the central and western domains, in which there is considerable evidence for local disequilibria.

The sillimanite - garnet - biotite - quartz - K-feldspar - plagioclase - magnetite assemblage in pelitic migmatites of the Lac Joseph Terrane is suitable for the use of a garnet-biotite geothermometer, which is based on the exchange reaction:

almandine + phlogopite = pyrope + annite. R5.1

$Fe_3Al_2Si_3O_{12}$ $KMg_3AlSi_3O_{10}(OH)_2$ $Mg_3Al_2Si_3O_{12}$ $KFe_3AlSi_3O_{10}(OH)_2$

The calculations in this study utilized the calibration of Ferry and Spear (1978) which is expressed by the equation:

$$T = (2089 + 9.56P)/(\ln K + 0.00782) \quad \text{Eq.5.2}$$

where T is in °C and P is in bar. K is calculated assuming ideal mixing. Ferry and Spear (1978) suggested that this calibration is suitable for garnets with $Ca+Mn/Ca+Mn+Fe+Mg < .2$ and for biotites with $Al6+Ti/Al6+Ti+Fe+Mg < .2$, since non-ideal solid solution behavior is more pronounced outside these ranges. Since most of the garnets and biotites fall within these prescribed limits, Ferry and Spear's (1978) calibration is used throughout this study.

Temperature estimates from the garnet-biotite thermometer were combined with the garnet - anorthite - garnet - quartz (GASP) geobarometer, which is based on the net transfer reaction:

3 anorthite = garnet + 2 Al-silicate + quartz R5.5

$CaAl_2Si_2O_8$ $Ca_3Al_3Si_3O_{12}$ Al_2SiO_5 SiO_2.

Initially proposed by Ghent (1976) using simplified mixing models, subsequent formulations have involved more realistic mixing models for garnet and plagioclase (Ghent et al., 1979; Newton and Haselton, 1981; Hodges and Royden, 1984; Koziol and Newton, 1988). This study utilizes Newton and Haselton's (1981) calibration which assumes all Margules parameters are zero except for W_{CaMg} in garnet, which is calculated as 3300 - 1.5T°K joules (Haselton and Newton, 1980). The activity coefficient for grossular is calculated from Ganguly and Kennedy (1974). The partial

molar volume for grossular is calculated as a weighted average of Haselton and Newton's (1980) and Cressey et al.'s (1978) volume calibration of grossular diluted in pyrope and almandine respectively. The activity of anorthite in plagioclase is calculated from Newton et al. (1980), based on Kerrick and Darken's (1975) "Al-avoidance" model.

The garnets chosen for analysis in this study were those which exhibit syntectonic microstructures, having aligned sillimanite inclusions parallel to the fabric defined by sillimanite and biotite, which wraps around the garnets (e.g. Photo 4-3). The biotite grains lie in the main tectonic fabric; those showing signs of static recrystallization or alignment with the later F_2 fold axial plane were not analyzed. Plagioclase and quartz were present as granular aggregates of variable grain size.

5.2.1 Results: Lac Joseph Terrane

5.2.1.1 Southern Lac Joseph Terrane

Pressure estimates (39) from eight samples of pelitic migmatite in the southern part of the Lac Joseph Terrane lie in the range from 2 to 6 kbar (Fig. 5-2) with six outliers from two samples between 6 and 8 kbar. Temperatures typically range from 575 to 800°C with two estimates around 850°C. P-T determinations calculated from core analyses are typically higher than those from rim analyses suggesting, decompression and thermal relaxation with time. Utilizing the 500°C - 3.8 kbar aluminosilicate triple point and stability fields of Holdaway (1971), these P-T estimates are consistent with the presence of sillimanite, the aluminosilicate phase present in the migmatite restite. The estimates from this area represent the lowest pressure estimates from restite assemblages in migmatites of the Lac Joseph Terrane. The slopes of the lines connecting core and rim P-T estimates (P-T vectors, Mengel and Rivers, 1989) are variable but, in general, show a decompression-cooling path which is approximately parallel to the kyanite - sillimanite equilibrium boundary.

5.2.1.2 Northeastern Lac Joseph Terrane

Pressure estimates in the northeastern domain of the Lac Joseph Terrane are higher than those in the southern domain, but temperatures are comparable. Pressures

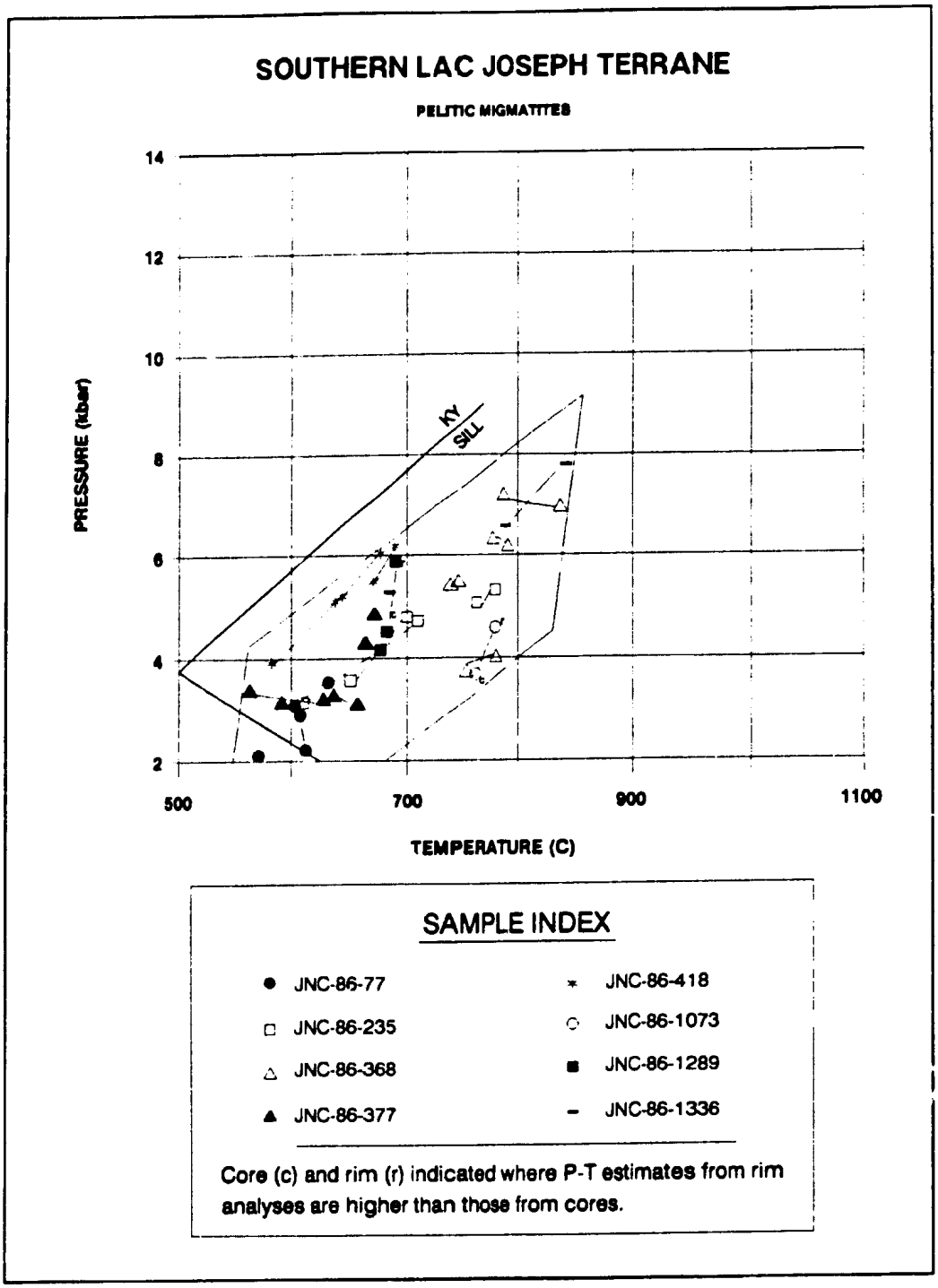

Figure 5-2: P-T estimates from the pelitic migmatites in the southern Lac Joseph Terrane. T: GNT-BIO; P: GNT-SILL-PLG-QTZ.

range from 4 to 8 kbar with one pair of core and rim analyses between 8.5 and 9.5 kbar (Fig. 5-3). The higher pressure estimates are within the kyanite stability field, compatible with the recent discovery of kyanite occurrences in pelitic migmatites along the northeastern margin of the Lac Joseph Terrane (James et al., 1991). Temperatures range between 600 and 775°C with the majority between 600 and 700°C. The slope of most of the P-T vectors connecting core-rim P-T estimates are comparable to those in the southern domain being approximately parallel to the kyanite-sillimanite equilibrium boundary. Two pairs of analyses show higher pressures for the rim analyses than for the cores, possibly due to localized disequilibrium considering the rather consistent decompression-cooling trends for the remainder of the samples. Two of the four samples are mylonitized sillimanite-bearing migmatite from the margin of the Lac Joseph Terrane. The mylonites yield similar P-T estimates to unmylonitized samples, compatible with the suggestion that mylonitization occurred synchronously with the regional metamorphic event which produced the sillimanite - garnet - biotite - magnetite assemblage throughout the Lac Joseph Terrane (see also Sections 3.2.1.3 and 6.5 for further discussions).

5.2.1.3 Northwestern Lac Joseph Terrane

Pressures in the northwestern part of the Lac Joseph Terrane are constrained between 6 and 10 kbar with temperatures ranging from 700 to 850°C (Fig. 5-4). Only one core-rim pair yielded P-T estimates which are higher from analyses of rims than those for cores. As in the northeastern part of the Lac Joseph Terrane, a mylonitized sample (JNC-87-5016) yielded similar P-T estimates to those for unmylonitized samples.

Comparisons with the northeastern domain show that although the intersection pressure estimates from samples in the northwestern region tend to be higher than in the northeastern area, values of K for the geobarometer overlap. The difference between intersection pressure estimates in the northwestern and northeastern domains are therefore a function of higher K values for the geothermometer. However, K values for the GASP geobarometer in the northwestern domain are typically larger than those from the southern domain. Although the samples utilized for geothermometers did not

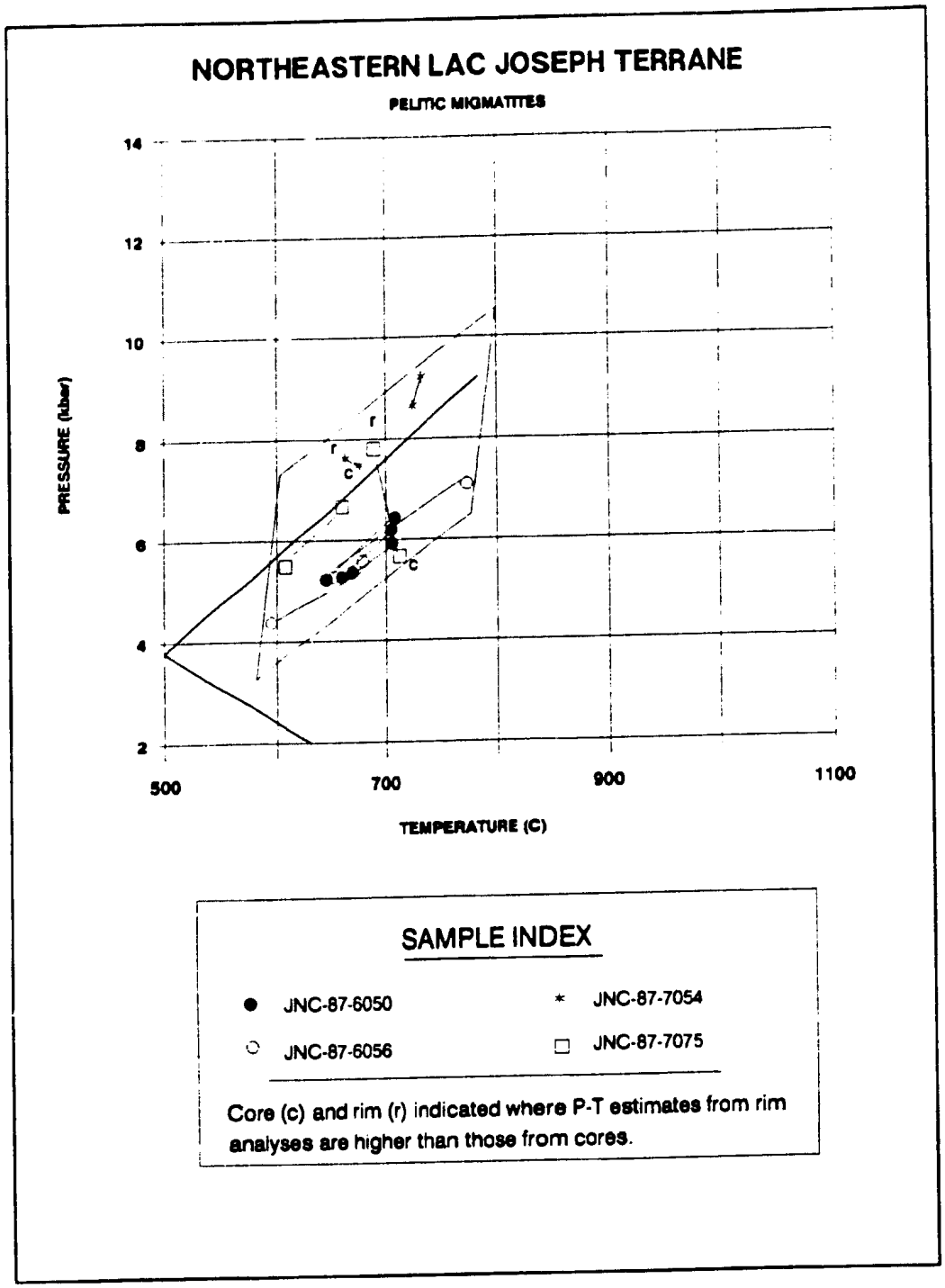

Figure 5-3: P-T estimates from the pelitic migmatites in the northeastern Lac Joseph Terrane. T: GNT-BIO; P: GNT-SILL-GNT-QTZ.

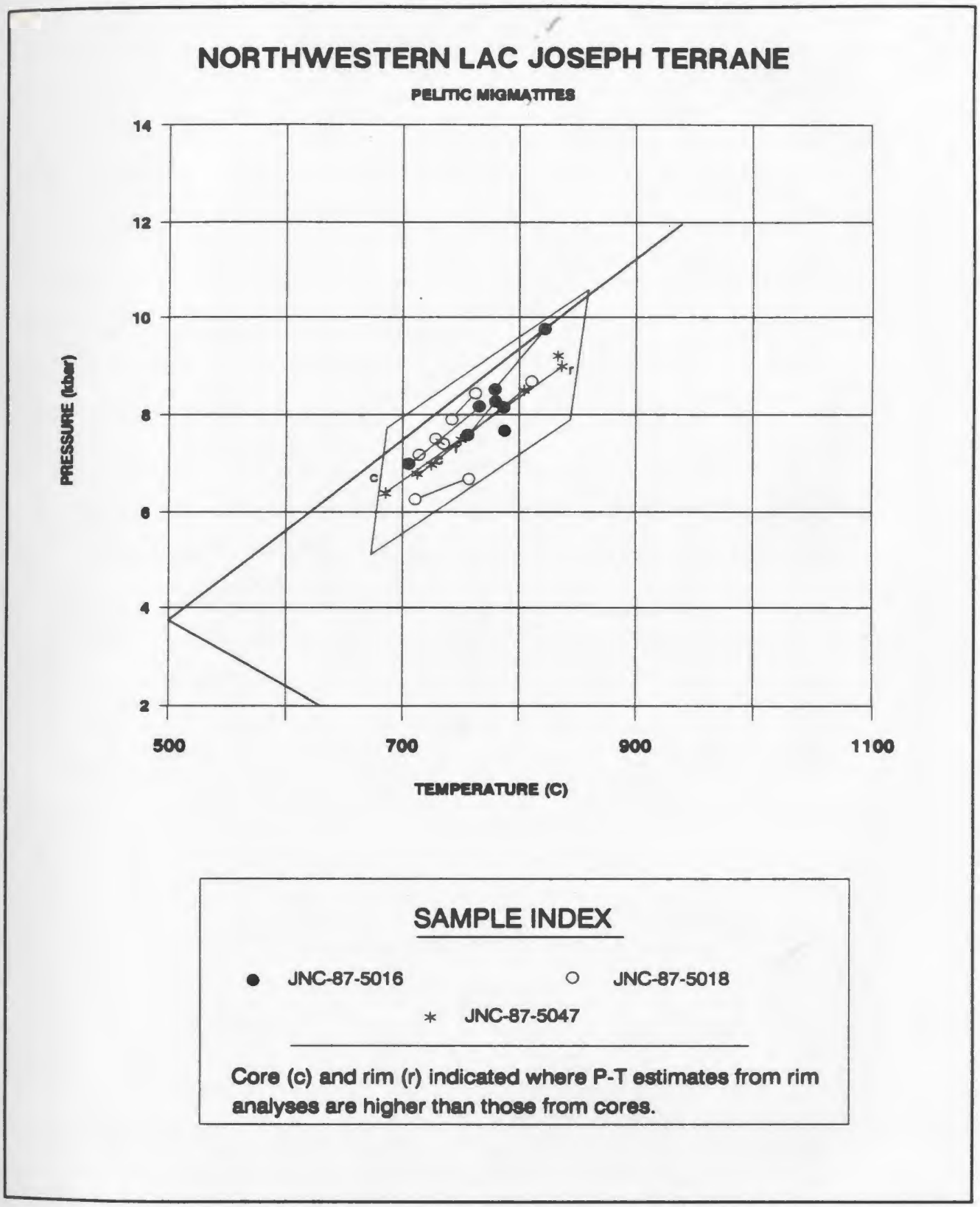

Figure 5-4: P-T estimates from the pelitic migmatites in the northwestern Lac Joseph Terrane. T: GNT-BIO; P: GNT-SIL-PLG-QTZ.

contain kyanite themselves, the higher pressure estimates in the northwestern domain are consistent with the observed presence of coexisting kyanite - K-feldspar in other samples collected from the northern and western margins (this study, James et al., 1991).

5.2.2 Significance of Equilibrium Thermobarometric Results

The utilization of a single geothermometer and geobarometer for all P-T estimates across the terrane results in an internally consistent data base. Thus, even if different calibrations had been chosen, the relative differences between the P-T estimates presented here would be unlikely to change significantly (although the absolute values of the estimates could change).

The clustering of the majority of the P-T estimates in each domain of the Lac Joseph Terrane, in conjunction with the equilibrium textures and mineral assemblages, suggests that the proposed exchange and net transfer reactions ceased in most samples while all phases were in or close to equilibrium. The geothermobarometric work thus provides information about the P-T history of an individual point or sample and shows differences in P-T conditions between domains.

The weak Fe-Mg zoning patterns in most garnets are typical of retrogression or diffusion that occurs during evolving metamorphic conditions after the peak metamorphic temperature; this zonation is evident in the different K values calculated using core and rim analyses. The typical lack of Ca zoning in the garnet and plagioclase, the two phases used for the GASP geobarometer, translates into K values which are similar for both core and rim analyses. The cooling - decompression paths established by P-T vectors from core and rim are therefore controlled primarily by the different isopleths of K from geothermometry. This indicates that cooling-decompression paths must have been approximately parallel to the isopleths of constant K for the GASP net transfer reaction.

Comparisons of P-T estimates between domains in the Lac Joseph Terrane indicate that although samples from the northeastern domain yield higher intersection pressure estimates than those from the northwestern region, the K isopleths from the

two domains overlap. The difference between intersection pressure estimates in the northwestern and northeastern domains are therefore a function of higher K values for the geothermometer. However, K values for the GASP geothermometer in both the northern domains are typically higher than those from the southern domain indicating that the higher pressure estimates are independent of the geothermometry results. Higher pressure estimates in the northwestern domain are consistent with the observed presence of coexisting kyanite - K-feldspar along the northern and western margins. Since the assemblages utilized for geothermobarometry equilibrated during the Labradorian Orogeny, the increase in pressure towards the northwest must therefore reflect an increase in the exposure of the Labradorian paleodepth towards the northwest. This is compatible with the interpretation of northwesterly directed thrusting of the Lac Joseph Terrane over the Molson Lake Terrane during the Grenvillian Orogeny (as discussed in Section 3.4) resulting in exhumation of deeper crustal levels at the leading edge of the Lac Joseph Terrane along frontal ramps. The pressure gradient in the Lac Joseph Terrane, although exhumed during the Grenvillian Orogeny, is, therefore, a feature of the Labradorian Orogeny.

5.2.3 Evidence of Disequilibrium in the Migmatites of the Lac Joseph Terrane

Although the majority of estimates from samples from the Lac Joseph Terrane yielded consistent pressures and temperatures, about 40% of them yielded highly erratic P-T estimates in a single sample, P-T vectors indicating increasing pressures and temperatures from core to rim and/or P-T estimates inconsistent with those from surrounding samples. For some samples this may be due to the presence of relict growth zoning in garnet. Samples which yield inconsistent P-T results are discussed below.

5.2.3.1 Northeastern Domain

Sample JNC-87-7053, collected in the northeastern domain of the Lac Joseph Terrane within 4 km of the Ossokmanuan Mountain Intrusive Suite, yielded results distinct from the other samples of this domain (Fig. 5-5). Two of three rim analyses yielded K isopleths which plotted at higher pressures in P-T space than the

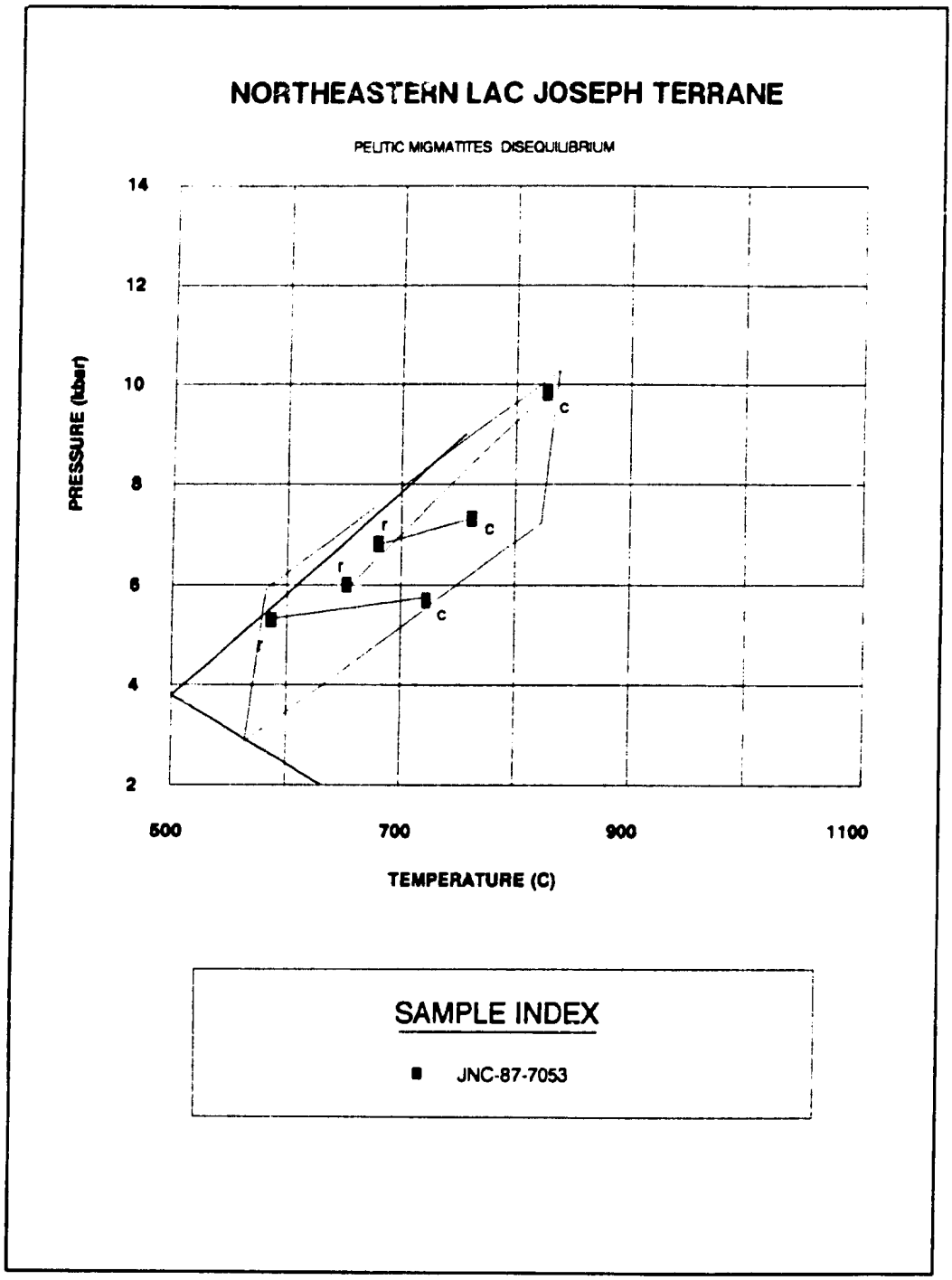

Figure 5-5: P-T estimates from sample JNC-87-7053, a pelitic migmatite from the the northeastern Lac Joseph Terrane. T: GNT-BIO; P: GNT-SIL-PLG-QTZ.

corresponding core analyses. All garnets show retrograde zoning of Mg and Fe, but yield a larger range of K isopleths than for any other single sample in this domain. This large variation of K isopleths results in intersection P-T estimates which range from 5.3 kbar to 9.9 kbar and between 575° and 825°C respectively. Rather than accepting these P-T estimates as reflecting anomalous temperature variations and cooling paths, it is suggested that mineral compositions may have been disturbed by heat transferred into the country rocks by the basic intrusion. Since the K isopleths for the GASP geobarometer have a significant slope in P-T space, the large variability of K for the thermometer in this sample controls the intersection P-T estimates. This is compatible with a disturbance of the mineral chemistries resulting from a thermal anomaly, after peak metamorphism, due to the adjacent basic intrusion.

5.2.3.2 Western Domain

All samples but one collected along the shores of Ashuanipi Lake yielded P-T estimates which were inconsistent, both between and within samples, and appeared unreasonable in comparison with those from the other domains in the Lac Joseph Terrane. Pressure estimates for samples within 10 km of each other ranged from 5 to 18 kbar, with temperatures between 700 and 940°C (Fig. 5-6). Several rim analyses yielded K isopleths which plotted at higher pressures than the corresponding core analyses. Fe-Mg zoning in garnet is retrograde in most cases, but much more pronounced than is typical for other samples of the Lac Joseph Terrane.

These erratic results are attributed to a thermal event, subsequent to the regional metamorphism, which affected the Fe-Mg distribution of garnet and biotite and Ca content of plagioclase and garnet but did not result in complete re-equilibration of the sample. As will be argued later, this event may have been related to the emplacement of the Lac Joseph Terrane over the Molson Lake Terrane during the Grenvillian Orogeny.

5.2.3.3 Central Domain

Two samples from locality 8088 and one sample from locality 8068 in the Lac Joseph area (Fig. 5-1) yield inconsistent results; P-T estimates varied between 530-950°

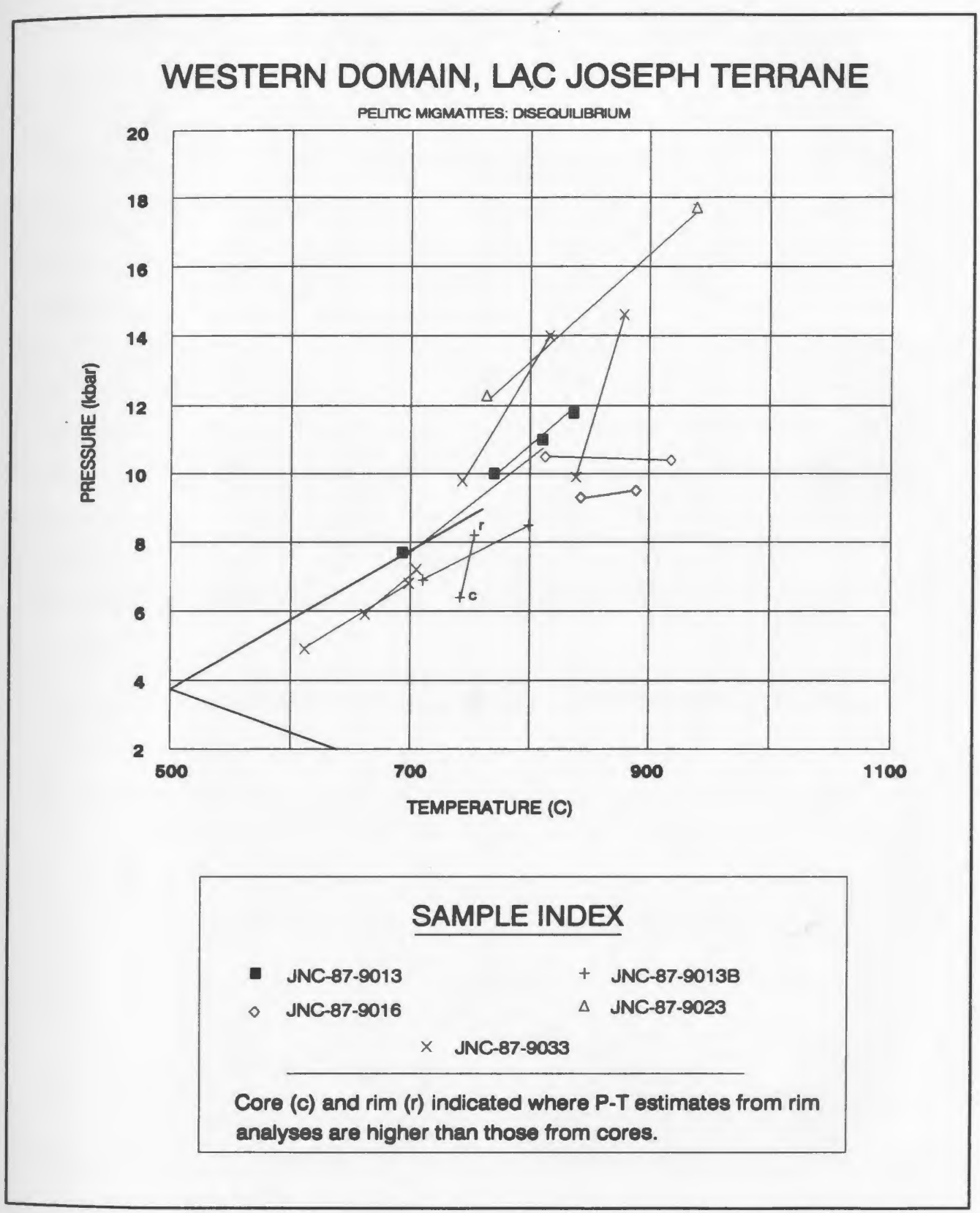

Figure 5-6: P-T estimates from pelitic migmatites in western Lac Joseph Terrane. T: GNT-BIO; P: GNT-SIL-PLG-QTZ.

and 2-14 kbar within a single sample (Fig. 5-7). As with the Ashuanipi Lake area of the Lac Joseph Terrane, this region is thought to have been affected by a thermal event after the Labradorian metamorphism during which the mineral assemblages formed.

5.2.3.4 Summary of Disequilibrium Assemblages in the Lac Joseph Terrane

Aside from a single sample which was collected next to a major basic intrusive complex, evidence of disequilibrium in pelitic migmatites in the Lac Joseph Terrane is attributed to a late thermal event which was restricted to the base of the terrane (recalling that there is interpreted to be a tectonic window in the Lac Joseph area of the central Lac Joseph Terrane). Disequilibrium is interpreted to be due to partial re-equilibrium which occurred as the Lac Joseph Terrane was emplaced over the Molson Lake Terrane in the Grenvillian Orogeny. There is evidence from a single sample of a thermal disturbance in the Lac Joseph Terrane during a cryptic event at ca. 1281 Ma (see Sections 6.9 and 7.2.1); this event may also have contributed to the disequilibrium presently observed in these samples.

5.3 Molson Lake Terrane

Both the granitoid and gabbroic rocks in the Molson Lake Terrane contain assemblages which are suitable for geothermometry and geobarometry. Although garnet and biotite are common in many of the granitoid rocks in the Molson Lake Terrane, only assemblages with clinopyroxene also permit pressure determinations to be made, and so these were the only ones utilized.

The temperature estimates for the granitoid rocks are based on the garnet-biotite geothermometer of Ferry and Spear (1978) and the Fe-Mg exchange reaction between garnet and clinopyroxene which is based on the reaction:

$$\text{almandine} + \text{diopside} = \text{pyrope} + \text{hedenbergite} \qquad \text{R5.3.}$$

In this study, the calibration of Ellis and Green (1979) was used; these authors demonstrated experimentally that the partitioning of Fe and Mg between garnet and clinopyroxene is influenced by the Ca content of garnet. This non-ideality in mixing is accounted for in the expression:

$$T = (3104X^{Ca} + 3030 + 10.86P)/\ln K + 1.9034) \qquad \text{Eq.5.4}$$

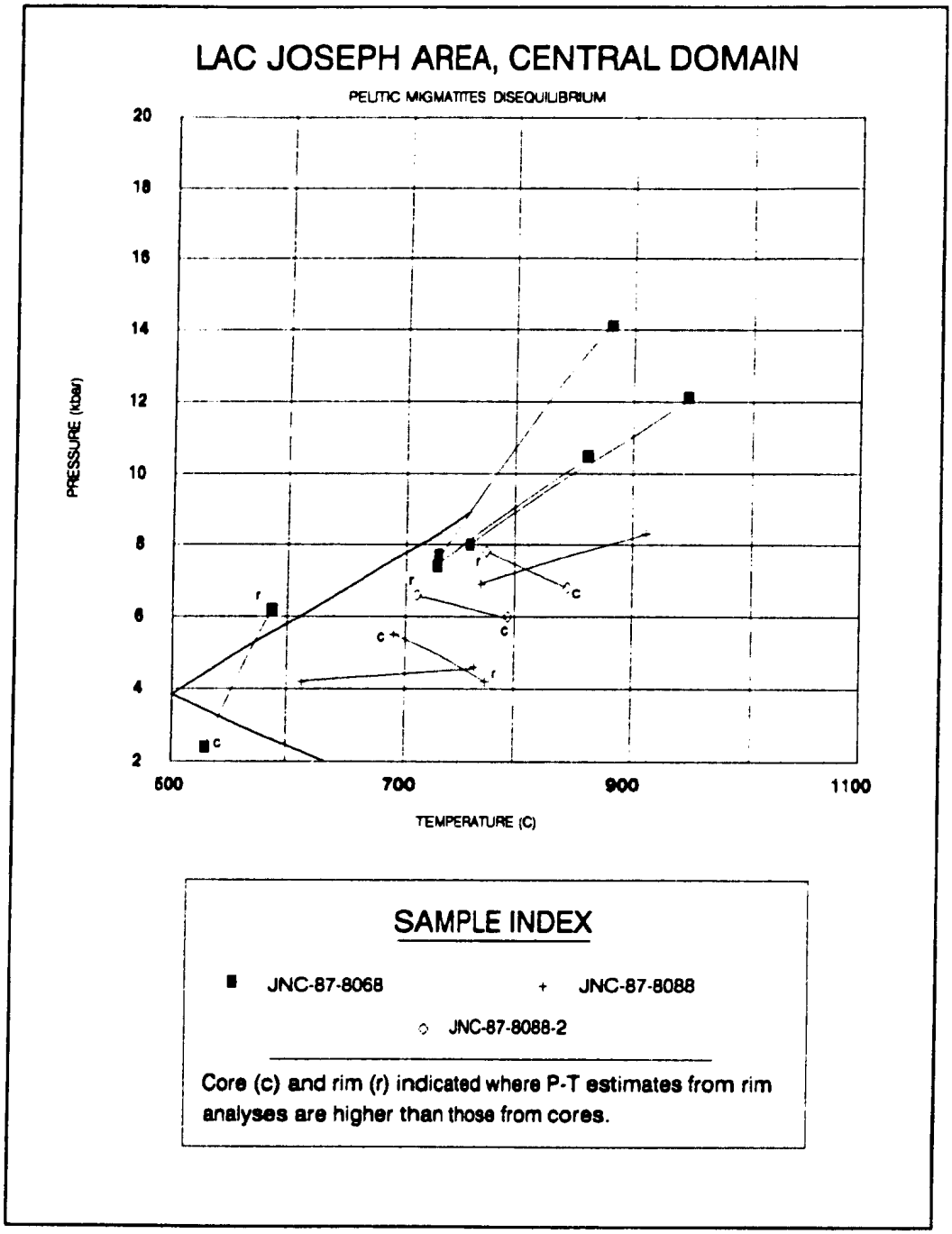

Figure 5-7: P-T estimates from pelitic migmatites in the Lac Joseph region in the Lac Joseph Terrane. T: GNT-BIO; P: GNT-SIL-PLG-QTZ.

where $X^{Ca} = Ca/Ca+Mg+Fe$ in garnet, $K = (X_{Fe}/X_{Mg})^{grt}/(X_{Fe}/X_{Mg})^{cpx}$, T is in °C and P is in bars.

The geobarometer used in this terrane is based on the net transfer reaction:

anorthite + diopside = 2/3 pyrope + 1/3 grossular + quartz R5.4.

The calibration of Newton and Perkins (1982) was employed in this study; the equilibrium expression is:

$$P = 675 + 17.179T + 3.5962\ln K \qquad \text{Eq.5.5}$$

where $K = [(a^{pyr})(a^{gro})^2]/[(a^{an})(a^{di})]$, T is in °C and P is in bars. The activity of diopside in clinopyroxene is calculated according to the ideal two-site mixing model of Wood and Banno (1973). The activity of anorthite in plagioclase is again calculated following the Al-avoidance model of Kerrick and Darken (1975) using the activity coefficient expression of Newton et al. (1980). Ca-Mg interaction in garnet is accounted for by Haselton and Newton's (1980) expression for the Margules interaction parameter, $W_{CaMg} = 3300 - 1.5°K$ joules, incorporated in Ganguly and Kennedy's (1974) expression for activity coefficients for three-component garnet.

5.3.1 Results: Molson Lake Terrane

Only two domains in the Molson Lake Terrane contain assemblages which are suitable for both geothermometry and geobarometry (Fig. 5-8). The southern domain contains garnet-clinopyroxene-biotite-bearing assemblages occurring in tonalitic protoliths. These rocks are strongly foliated and exhibit a granoblastic texture with no evidence of later retrogression. The second domain occurs further north between Wabush Lake and Ross Bay Junction where gabbroic rocks contain garnet, clinopyroxene, biotite, amphibole, plagioclase and quartz. Samples collected for geothermobarometry have undergone partial retrogression according to the reaction:

garnet + clinopyroxene = hornblende + plagioclase + quartz R5.5.

5.3.1.1 Southern Domain of the Molson Lake Terrane

As previously discussed in Section 4.4, the metamorphic grade in southern Molson Lake Terrane varies from upper-greenschist facies at the margin of the Lac Joseph Terrane, through plagioclase - hornblende - epidote assemblages to garnet -

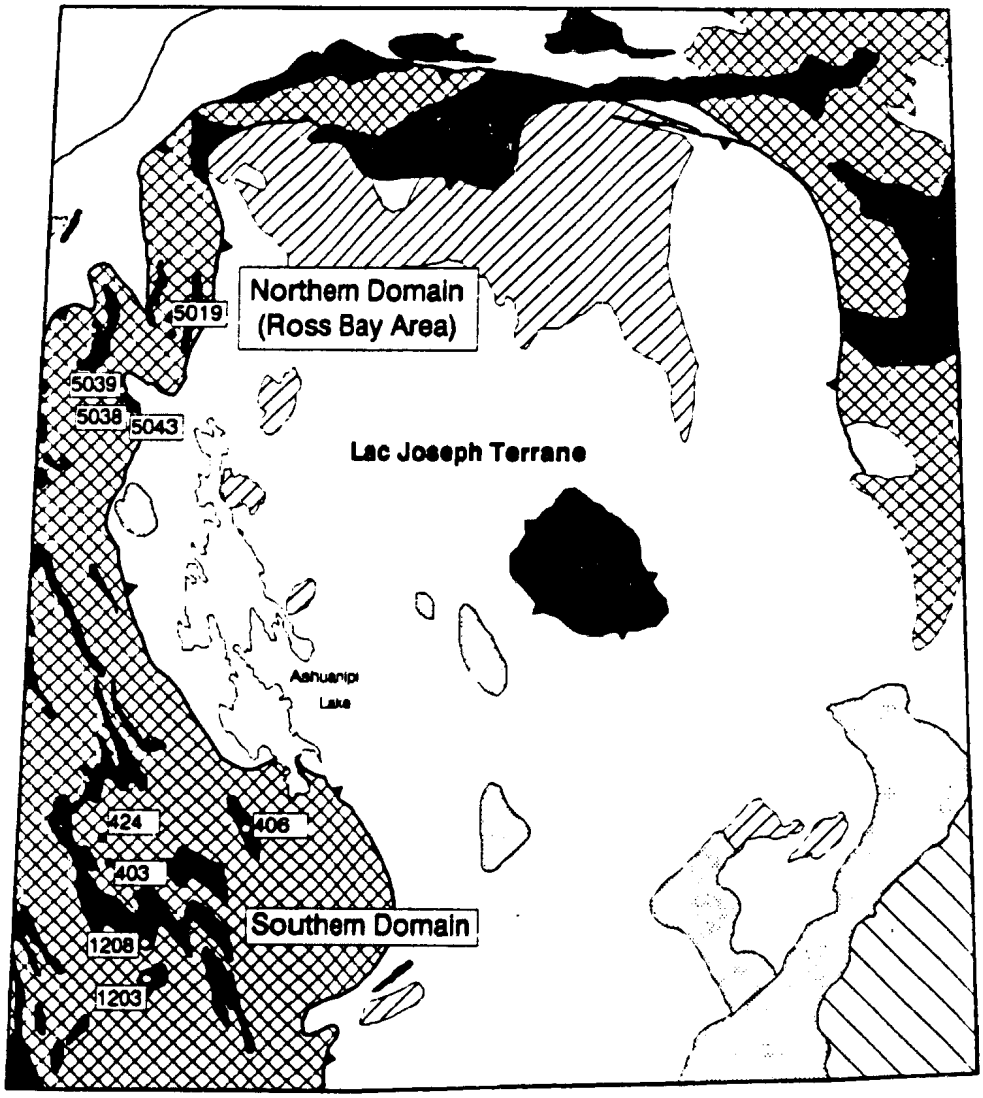

Figure 5-8: Location map of samples utilized for geothermobarometry in the Molson Lake Terrane.

clinopyroxene - quartz assemblages in the west, in which clinopyroxene contains a significant jadeite component. The garnet - clinopyroxene - plagioclase - quartz geobarometer of Newton and Perkins (1982), in conjunction with the garnet - clinopyroxene geothermometer of Ellis and Green (1979) yields intersection pressures between 8 and 12 kbar for the garnet - clinopyroxene - quartz zone (Fig. 5-9). Both garnet-biotite (Ferry and Spear, 1978) and garnet-clinopyroxene (Ellis and Green, 1979) geothermometers yield comparable intersection temperatures between 650 and 850°C. Core analyses consistently yield higher P-T estimates than rim analyses, suggesting that decompression accompanied cooling after the metamorphic peak. P-T estimates from granitoid rocks are thus in accord with the mineralogical evidence that the western part of the Molson Lake Terrane recrystallized under elevated pressures and moderate temperatures.

As described in Section 4.5, the gabbroic rocks in the Molson Lake Terrane typically exhibit coronitic textures with garnet and/or amphibole as the dominant corona minerals. Although coronitic textures inherently imply local disequilibrium conditions, several samples with excess quartz and containing garnet, clinopyroxene and plagioclase in mutual contact were analyzed for geothermobarometry. Employing the same geothermometer (Ellis and Green, 1979) and geobarometer (Newton and Perkins, 1982) as for the granitoid rocks, analyses of grain rims in three samples yielded P-T estimates which overlap with those from the granitoid rocks (Fig. 5-10) in spite of the textural complexity of the samples and partial retrogression of clinopyroxene to amphibole. Cores yielded slightly higher P-T estimates than the corona rims.

5.3.1.2 Evidence of Disequilibrium in the Molson Lake Terrane

In contrast to the favourable results in the southwestern domain of the Molson Lake Terrane, all attempts to calculate P-T conditions from samples collected from northern Molson Lake Terrane near Ross Bay Junction were unsuccessful. Although the same geothermometers and geobarometer were used as in the south, the intersection pressures range between 13 and 19 kbar and intersection temperatures between 750°C and 1050°C (Fig. 5-11) and are considered to be unrealistic.

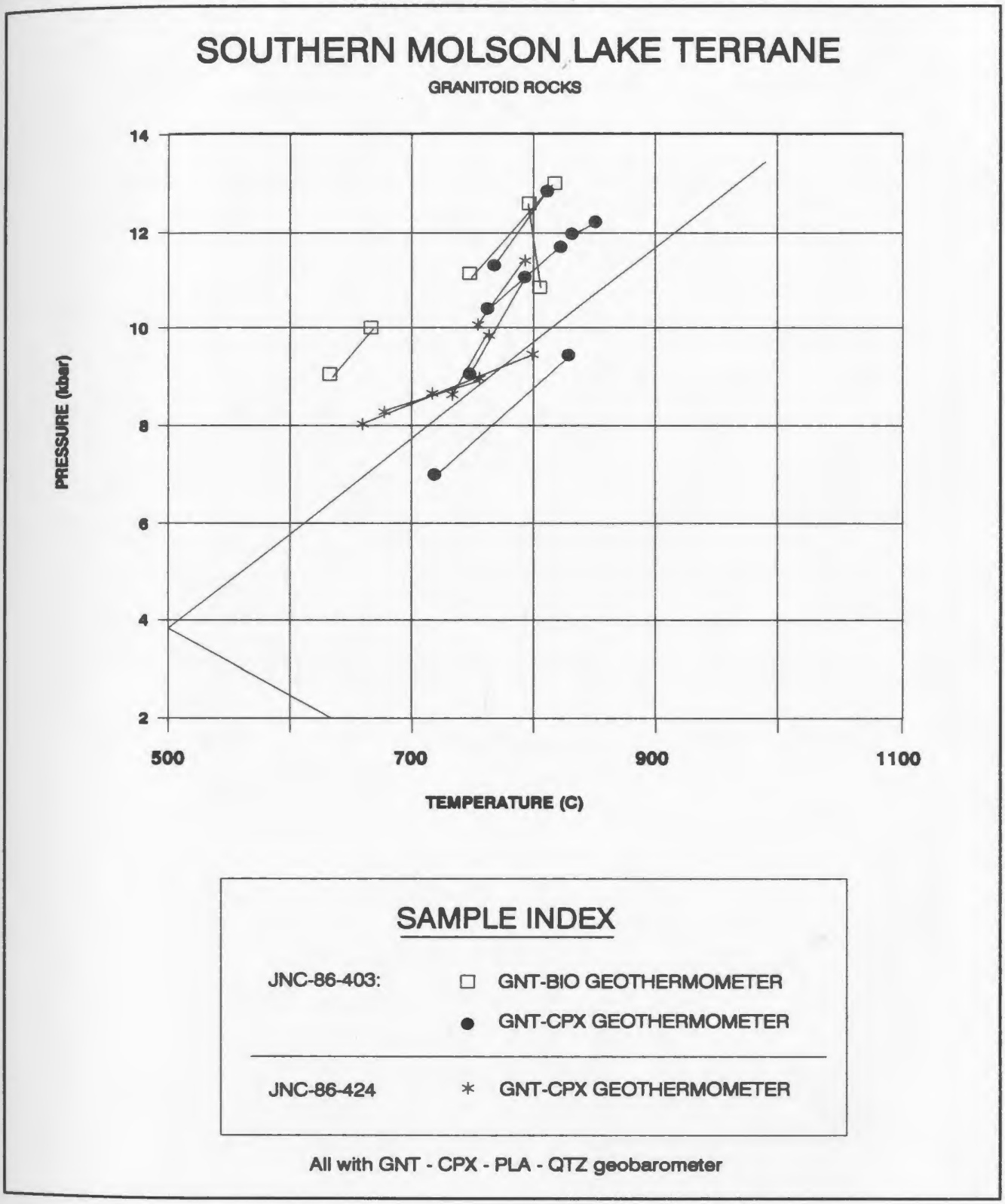

Figure 5-9: P-T estimates from tonalites in the southwestern Molson Lake Terrane.

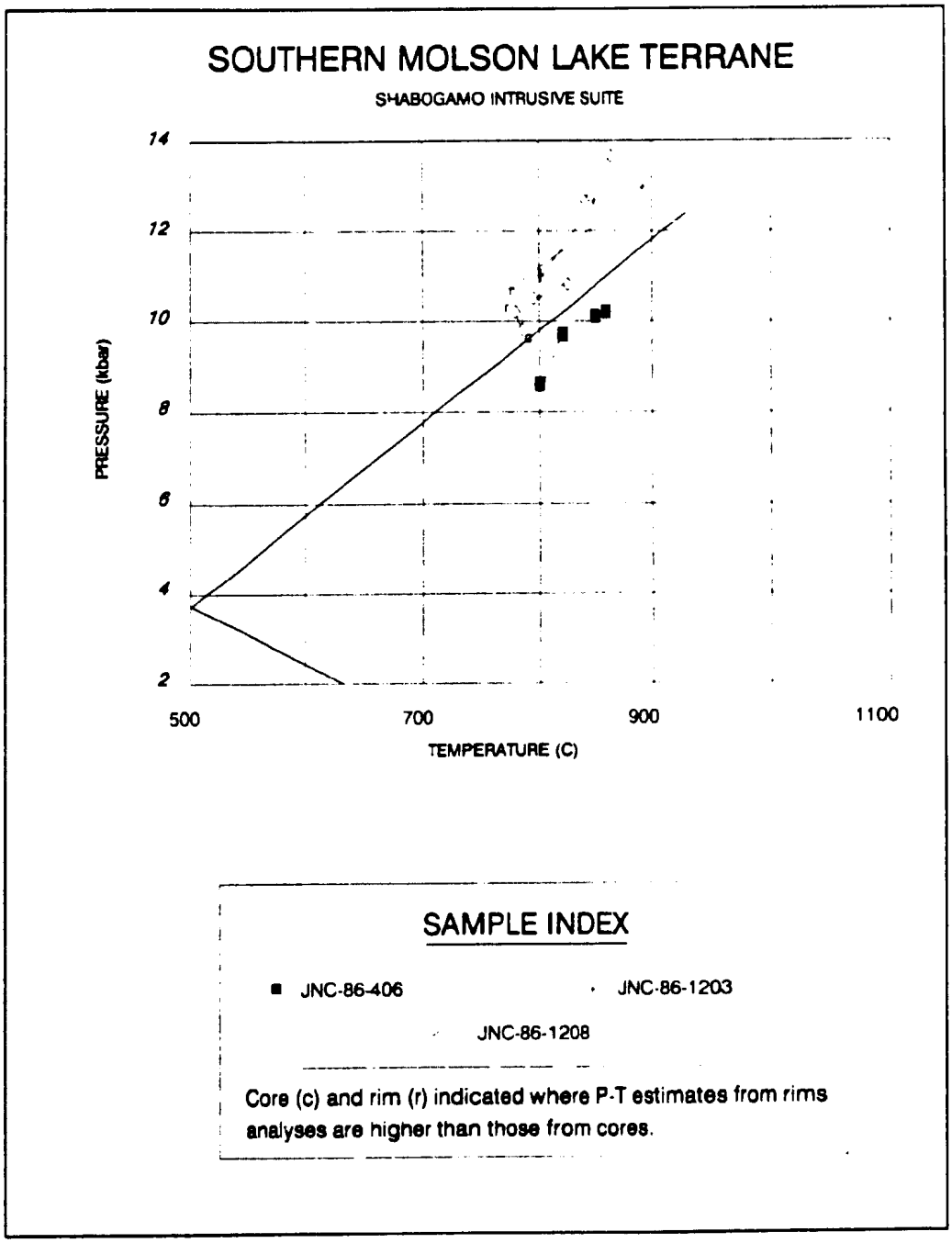

Figure 5-10: P-T estimates from the Shabogamo Intrusive Suite in the southwestern Molson Lake Terrane.T: GNT-CPX; P: GNT-CPX-PLA-QTZ.

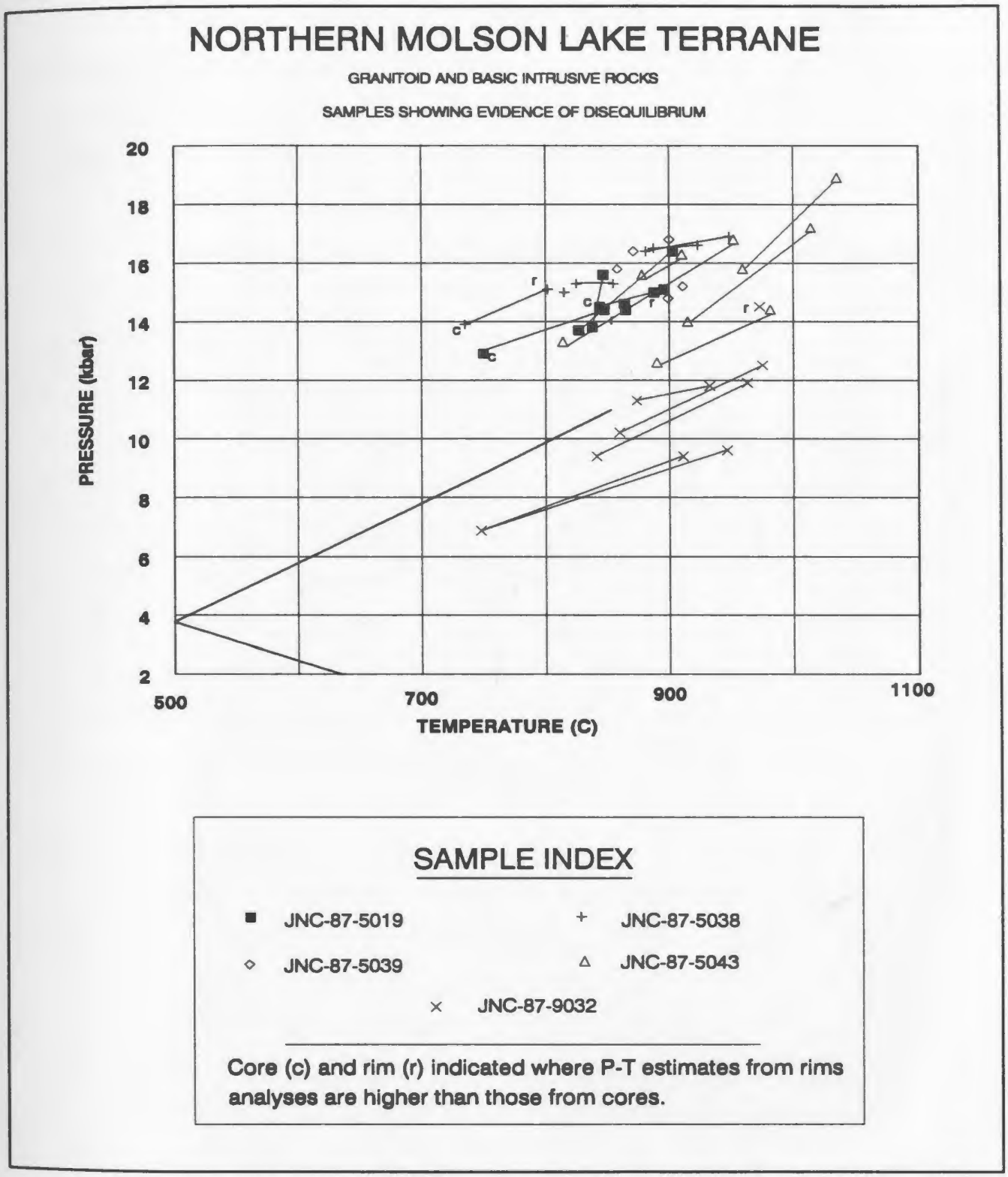

Figure 5-11: P-T estimates from samples in the northwestern Molson Lake Terrane which are thought to exhibit mineral disequilibrium. T: GNT-CPX; P: GNT-CPX-PLA-QTZ

All samples from the northern Molson Lake Terrane contained evidence (Photo 5-1) for incomplete operation of the decompression reaction R5-5.

The unrealistically high P-T results and the variability of P-T estimates over short distances (< 500 m) suggests that the northern Molson Lake Terrane experienced a more penetrative retrogression than the southern domain, perhaps reflecting slower uplift and cooling during the last thermal event. Nevertheless, it is proposed that the partial preservation of a garnet-clinopyroxene-quartz assemblage implies that this domain was also subjected to elevated pressures prior to disequilibrium conditions during decompression and cooling.

5.4 Summary of Geothermobarometric Results

Geothermobarometry applied to pelitic migmatites in the southwestern and northeastern domains of the Lac Joseph Terrane has established that pressures ranged from 3 to 6 kbar, and temperatures were between 575 and 800°C. Pressures and temperatures both increased towards the northwest, in the direction of thrusting, to between 6 to 10 kbar and 700 to 850°C respectively.

Pressure estimates from the southern Molson Lake Terrane, ranging between 8 and 13 kbar are distinctly higher than those in the adjacent Lac Joseph Terrane (3-6.5 kbar and 575 to 800°C). Even with uncertainties of ± 50°C and ± 1.6 kbar (recommended by Newton and Perkins, 1982; and see Appendix 4), there remains a distinct difference between the P-T estimates for the southern Molson Lake Terrane and adjacent southern Lac Joseph Terrane. Although P-T estimates cannot be made in the Ross Bay area, the mineral assemblage is consistent with the high pressure determinations and moderate temperatures from geothermobarometry in the southern domain, and a high pressure signature is thought to be characteristic of the terrane as a whole. However, the slopes of the P-T vectors, defined by lines joining core and rim intersection P-T estimates, are not distinct in their orientation in the two terranes. Whether this is a result of similar synmetamorphic uplift paths, or a function of the different calibrations used, cannot be evaluated with the available data base.

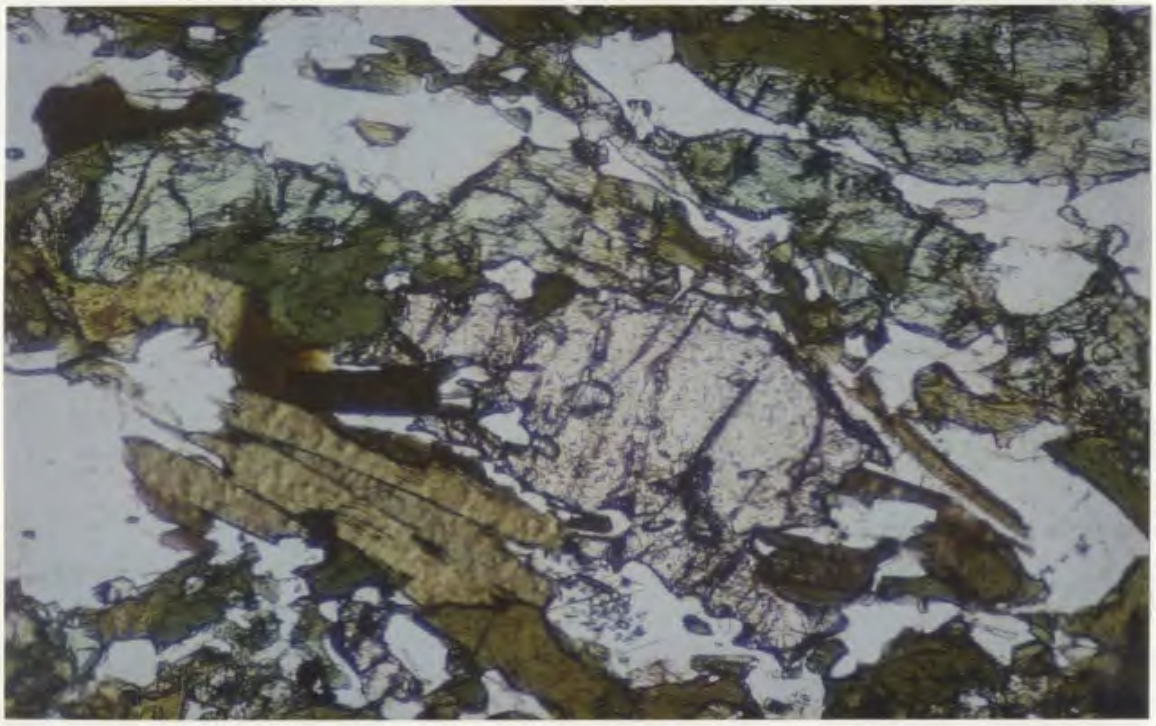

.2 mm

Photo 5-1: Garnet, clinopyroxene, biotite, hornblende, plagioclase and quartz in tonalitic rocks of the northern Molson Lake Terrane in the Lac Emerillon area near Ross Bay. Clinopyroxene is partially retrogressed to hornblende. Plane polarized light.

In summary, the results of geobarometry-geothermometry indicate that the two terranes developed under distinctly different pressure and temperature conditions. Furthermore, geochronological data (presented in the following chapters) suggest that the pelitic migmatites equilibrated during the Labradorian Orogeny in contrast to assemblages in the Molson Lake Terrane which penetratively equilibrated during the Grenvillian Orogeny.

CHAPTER 6
U-Pb GEOCHRONOLOGY

6.1 Introduction

Having discussed in previous chapters, the igneous, structural and metamorphic events in the study area in the context of a relative chronology, it now remains to establish their timing in an absolute sense. Knowledge of the absolute chronology of events is essential if this study is to contribute to the understanding of the regional tectonic history of the Grenville and Labrador orogens. For example, the interpretation of the tectonic processes is significantly dependent upon whether the pressure differences recorded by mineral assemblages in the two terranes were the result of a single orogenic event, or of two or more temporally unrelated events. Similarly, it is essential to know the age of the magmatic events, partial melting, the last thermal event, and so on, since they all provide constraints on the tectonic model. To this end, a program of U-Pb and $^{40}Ar/^{39}Ar$ geochronology was designed to answer specific questions which remained after completion of the field work. The U-Pb technique utilized zircon, monazite, titanite and rutile, depending on the rock type and motives for analyzing a particular sample. $^{40}Ar/^{39}Ar$ geochronology employed amphibole, muscovite and biotite. Results from the two geochronological techniques are presented in separate chapters.

6.2 Specific Objectives of U-Pb Geochronology

In the context of the discussions in the previous chapters, the U-Pb aspect of the study was designed to address the following unknowns: 1) the age of N_1 and N_2 leucosomes in the migmatites of the Lac Joseph Terrane; 2) the age of formation of the restite mineral assemblage in the migmatites of the Lac Joseph Terrane; 3) the age of the gabbroic rocks of the Ossokmanuan Mountain Intrusive Suite in the Lac Joseph Terrane; 4) the effects, if any, of the Grenvillian Orogeny in the Lac Joseph Terrane; 5) the age of the granitoid rocks in the Molson Lake Terrane; 6) the U-Pb age of the Shabogamo Intrusive Suite; 7) the age of metamorphism in the Molson Lake Terrane; and 8) the time of thrust emplacement of the Lac Joseph Terrane over the Molson Lake Terrane.

6.3 Analytical Techniques

All the U-Pb geochronology was carried out at the Jack Satterly Geochronology Laboratory at the Royal Ontario Museum (ROM) in Toronto, Ontario. Minerals analyzed in this study were isolated from 0.5 to 30 kg samples by standard crushing, heavy liquid and magnetic separation techniques and were hand-picked using a binocular microscope. While all zircon fractions were abraded, only those fractions of monazite, titanite and rutile noted in Table 6-1 were abraded. The U-Pb chemistry for zircons follows the procedure of Krogh (1973) and samples were spiked prior to dissolution using a mixed $^{205}Pb/^{235}U$ tracer solution (Krogh and Davis, 1975). U and Pb were loaded together onto outgassed, single Re-filaments using a silica gel - phosphoric acid mixture (Cameron et al. 1969). Zircon and some titanite fractions were run on a VG354 mass spectrometer; monazite and the remaining titanite fractions were run on a VG Micromass 30 mass spectrometer. Both mass spectrometers were operated in single collector mode. Conversion factors of 1.003 and 1.0015/atomic mass unit (amu) were applied to data collected on the Daly collector on the VG 354 and VG Micromass 30 respectively to normalize to data collected with a Faraday cup; a mass fractionation correction of 0.10 %/amu was applied to all data. Total procedure blanks were estimated at 10 pg Pb and 2 pg U for small column (2 cc reservoir) chemistry; for mini-columns (reservoir volume of 10% of the small columns) they were estimated at 5 pg for Pb and 1 pg for U. The initial common Pb composition was calculated using the two-stage model of Stacey and Kramers (1975).

Analytical data are presented in Table 6-1. Analytical uncertainties ($\pm 2\sigma$) on U/Pb and $^{207}Pb/^{206}Pb$ ratios in Table 6-1 were calculated using the unpublished error propagation program of L.M. Heaman. Errors are depicted on concordia plots by the size of the ellipses. Linear regression was carried out using the method of Davis (1982); errors on the calculated ages are quoted at the 95% confidence level. Samples in this chapter have been assigned numbers from one to ten; for cross-referencing these samples to those referred to in other chapters, the field sample number is included in

Table 6-1: U-Pb data.

FRACTIONS		CONCENTRATION				ATOMIC RATIOS								AGE (Ma)		
Fraction & Min. Code	Comments	Weight (ug)	U (ppm)	Pb Rad (ppm)	Tot Com Pb (pg)	206Pb/ 204Pb*	208Pb/ 206Pb#	206Pb/ 238U	+/-	207Pb/ 235U	+/-	207Pb/ 206Pb	+/-	206Pb/ 238U	207Pb/ 235U	207Pb/ 206Pb
1 - MLT GRANITE (JNC-86-1300)																
1-Z1	1 lg euh grn	8	126	42	16	876	0 2416	0 28652	116	3 9750	190	0 10062	40	1624	1629	1636
1-Z2	sm rnd	149	211	63	20	27112	0 1753	0 27140	118	3 6787	160	0.09831	4	1548	1567	1592
1-Z3	b sm rnd	163	221	67	14	45230	0 1876	0.27174	92	3 7274	98	0 09849	22	1550	1577	1614
1-T1	euh unabr	152	68	12	535	218	0 0868	0 17006	42	1 6906	58	0 07210	20	1012	1005	989
1-T2	gem unabr	201	75	12	685	248	0 0806	0 16696	150	1 6484	68	0 07161	4	995	989	975
2 - SHABOGAMO INTRUSIVE SUITE (LH-88-12)																
2-Z1	rnd facet	32	108	18	14	2752	0 0948	0 17056	44	1 7230	42	0 07327	8	1015	1017	1021
2-Z2	lg prisms	40	137	31	10	6641	0 2546	0 19611	54	2 1775	54	0 08053	12	1154	1174	1210
2-R3	frags	144	7	1	11	926	0 0054	0 16344	56	1 6121	86	0 07154	36	976	975	973
2-Z4	lg frags	80	137	32	48	2981	0 2497	0 20527	96	2 3774	128	0 08400	24	1204	1236	1293
2-Z5	med frags	92	149	35	3	60003	0.2408	0 20379	94	2 3148	74	0.08238	28	1196	1217	1255
3 - N1 LEUCOSOME: LJT (JNC-87-8113)																
3-Z1	sm rnd	28	211	74	63	1909	0 1679	0 31956	128	4 8468	180	0 11000	18	1788	1793	1799
3-Z2	sm rnd	66	220	75	12	34185	0 1650	0.31100	98	4 7299	148	0 11030	6	1746	1773	1804
3-Z3	needles	35	372	119	36	6917	0.1314	0 30057	116	4 5151	174	0.10895	6	1694	1734	1782
3-Z4!	9 lg grn	13	97	43	2	19884	0 1568	0.39309	176	8 0710	256	0 14892	48	2137	2239	2334
3-M2	frags unabr	23	1706	2403	60	11620	4 6299	0.28383	128	3 9341	176	0 10053	12	1611	1621	1634
3-M4	frags abr	11	4437	3590	38	23139	2 1419	0 28848	164	4 0245	222	0 10118	12	1634	1639	1646
3-M5	2 clr abr grn	7	1380	2064	44	3907	5 0059	0 28298	98	3 8393	120	0 09840	18	1606	1601	1594
4 - N2 LEUCOSOME: LJT (JNC-87-126)																
4-Z1	sm rnd	37	220	72	60	2600	0.1370	0.30506	120	4 6701	178	0.11103	14	1716	1762	1816
4-Z2	needles	15	267	82	32	2307	0.1296	0 28868	88	4 1353	102	0 10390	20	1635	1661	1695
4-Z3	sm rnd	19	192	63	6	12271	0 1379	0 30569	82	4 4719	110	0 10610	14	1719	1726	1733
4-M1	5 lg unabr frag	77	2104	2383	94	29956	3 5665	0 27786	150	3 7939	198	0 09903	14	1581	1591	1606
4-M2	2 gns abr	25	1138	2403	31	16157	7 4643	0 28455	80	3 9230	108	0 09999	10	1614	1618	1624
4-M3	8 gns rnd unabr	63	983	2488	106	10282	9 3095	0 28013	74	3 8735	90	0 10029	16	1594	1608	1627
4-M4	1 equant abr	23	681	2340	28	9954	12 6809	0 28749	72	3 9840	86	0 10051	14	1629	1631	1633

Table 6-1: U-Pb data.

FRACTIONS		CONCENTRATION				ATOMIC RATIOS								AGE (Ma)		
Fraction & Min Code	Comments	Weight (ug)	U (ppm)	Pb Rad (ppm)	Tot Com Pb (pg)	206Pb/ 204Pb*	208Pb/ 206Pb#	206Pb/ 238U		207Pb/ 235U		207Pb/ 206Pb		206Pb/ 238U	207Pb/ 235U	207Pb/ 206Pb
5 - MYLONITIZED MIGMATITE LJT (JNC-87-5016)																
5-Z1	needles	44	206	61	4	46080	0 0966	0 28601	94	3 9521	130	0 10022	6	1622	1624	1628
5-Z2	sm rnd	11	206	62	3	12550	0 1024	0 29011	96	4 0123	122	0 10031	16	1642	1637	1630
5-Z3	lg rnd	19	130	39	16	2910	0 0931	0 28972	110	4 0499	138	0 10138	20	1640	1644	1650
5-M1	unabr	69	801	2246	64	15320	10 2320	0 28550	178	3 9364	246	0 10000	6	1619	1621	1624
5-M2	abr	60	869	2952	42	22669	12 4703	0 28868	88	4 0013	118	0 10053	10	1635	1634	1634
6 - MUSCOVITE-BEARING MIGMATITE LJT MARGIN (JNC-86-14)																
6-Z1	sm needles	125	511	138	309	3532	0 0365	0 27740	148	3 7718	202	0 09862	6	1578	1587	1598
6-Z2	tips	12	399	106	5	16638	0 0300	0 27448	70	3 6976	86	0 09771	12	1563	1571	1581
6-Z3	sm rnd clr	19	520	139	6	26448	0 0302	0 27532	172	3 7281	230	0 09821	16	1568	1577	1590
6-Z4	sm needles	17	414	112	135	920	0 0355	0 27786	98	3 7733	136	0 09849	26	1581	1587	1596
6-M1	lustre unab	70	3930	8943	183	23082	8 0633	0 28660	180	3 9278	24	0 09939	12	1625	1619	1613
6-M2	frags unab	67	1424	2556	111	13064	7 4368	0 24295	72	2 9843	78	0 08909	14	1402	1404	1406
6-M3	frosted unab	35	1344	2313	63	11410	7 0756	0 24339	122	2 9787	76	0 08876	38	1404	1402	1399
6-M4	frags abr	26	1351	2841	64	8438	8 7991	0 24536	66	3 0412	78	0 08990	10	1415	1418	1423
7 - OSSOKMANUAN MT INTRUSIVE SUITE LJT (LH-88-23)																
7-Z1	v abr	38	109	45	8	9181	0 5912	0 28352	76	3 9332	94	0 10062	14	1609	1621	1635
7-Z2	2nd b alt abr	105	79	30	16	9322	0 4279	0 28663	88	3 9417	90	0 09974	22	1625	1622	1619
7-Z3	sm rnd	7	110	38	4	3666	0 3072	0 28700	138	3 9411	184	0 09959	18	1627	1622	1617
7-R1	frags	124	204	98	5	84582	0 8561	0 28391	932	3 9113	1284	0 09992	12	1611	1616	1623
8 - MAFIC GNEISS LJT (JNC-86-524)																
8-Z1	sm rnd	9	71	18	15	695	0 0816	0 25247	94	3 4669	126	0 09960	26	1451	1520	1617
8-Z2	17 med rnd	4	52	15	5	894	0 0810	0 28866	546	4 0505	764	0 10177	36	1635	1644	1657
8-Z3	sm rnd v abr	10	73	21	4	3086	0 1007	0 27620	76	3 7468	94	0 09831	14	1572	1581	1592
8-T1	facet abr	420	43	15	250	1017	0 7248	0 21889	108	2 5189	136	0 08346	22	1276	1278	1280
8-T2	clr brn abr	115	47	16	66	1133	0 7206	0 21906	68	2 5229	74	0 08353	12	1277	1279	1282
8-T3	lgt brn abr	66	31	11	31	915	0 7296	0 21684	206	2 5110	92	0 08398	76	1265	1275	1292

Table 6-1: U-Pb data.

FRACTIONS		CONCENTRATION				ATOMIC RATIOS								AGE (Ma)		
Fraction & Min Code	Comments	Weight (ug)	U (ppm)	Pb Rad (ppm)	Tot Com Pb (pg)	206Pb/ 204Pb*	208Pb/ 206Pb#	206Pb/ 238U		207Pb/ 235U		207Pb/ 206Pb		206Pb/ 238U	207Pb/ 235U	207Pb/ 206Pb
9 - PEGMATITIC DYKE BASE OF LJT (JNC-87-8126D)																
9-Z1	lg rnd	12	216	38	7	3692	0 1391	0 16750	72	1 6845	70	0 07294	14	998	1003	1012
9-Z2	needles	42	911	143	898	430	0 1034	0 15485	54	1 5423	70	0 07224	16	928	947	993
9-M1	unabr	18	1978	2869	60	6309	8 8758	0 16823	70	1 6775	70	0 07232	6	1002	1000	995
9-M2	abr	12	1864	2096	28	8433	6 6581	0 16786	116	1 6756	42	0 07240	48	1000	999	997
10 - MYLONITIZED GRANITE EAST MARGIN OF MLT (JNC-87-5043B)																
10-Z1	sm rnd	27	319	78	17	7336	0 1254	0 23501	122	2 9791	120	0 09194	30	1361	1402	1466
10-Z2	sm b	21	434	102	8	16433	0 1038	0 22783	84	2 8214	98	0 08981	12	1323	1361	1422
10-Z3	lg prisms	27	380	78	7	17531	0 0888	0 20465	52	2 3933	54	0 08482	12	1200	1241	1311
10-T1	lgt abr	65	680	126	695	684	0 2083	0 16781	138	1 6789	340	0 07257	124	1000	1001	1002
10-T2	dark abr	78	940	175	1089	734	0 2196	0 16692	154	1 6719	154	0 07264	10	995	998	1004

Mineral Code: Z Zircon, M Monazite, T Titanite, R Rutile

* Measured value

All other atomic ratios in table corrected for fractionation, laboratory blank, spike and initial common Pb

! Not plotted

Errors - 2 sigma

All zircon fractions were abraded

Pb Rad: Total radiogenic Pb after correction for blank, common Pb and spike

Tot Com Pb: Total common Pb, including laboratory blank

ABREVIATIONS: sm=small (<50 um), med=medium (50-100 um), lg=large (>100 um), frags=fragments, rnd=round, facet=faceted, euh=euhedral, clr=clear, grn=grain(s), abr=abraded, unabr=unabraded, b=best, aft=after, v=very, brn=brown, lgt=light, NM=non-magnetic

parenthesis at the beginning of each subsection. Zircon, titanite monazite and rutile fractions are referred to as Z, T, M and R respectively in the text and on diagrams such that fraction 1 from sample 1 is referred to as 1-Z1.

6.4 Results: Molson Lake Terrane

6.4.1 Molson Lake Terrane Granites: Sample 1 (JNC-86-1300)

A sample of foliated, biotite-hornblende-epidote-bearing granite, considered representative of the granitoid suite of zone 2 in the Molson Lake Terrane, was collected from the southern part of this terrane about 15 km west of the margin of the Lac Joseph Terrane (Fig. 6-1). This sample exhibited a northwest-trending fabric defined by biotite and hornblende. It yielded fractions of clear, colourless, equant, euhedral zircon and clear, yellow, flat, faceted titanite for U-Pb analysis.

A mixing line is interpreted by two zircon fractions which plot near the upper intercept with concordia at 1648±7 Ma and two titanite fractions which plot near the lower intercept with concordia at 995 Ma (Fig. 6-2). A third zircon fraction, 1-Z3 (see Table 6.1) is thought to have experienced secondary Pb loss and is not included in the linear regression. The titanite analyses fall slightly above concordia, suggesting that the common Pb correction calculated from Stacey and Kramers (1975) does not accurately represent the composition of the Pb incorporated into the titanite at the time of crystallization. Since radiogenic Pb^{206} is much more abundant than radiogenic Pb^{207} (the radiogenic Pb^{207}/Pb^{206} ratio is approximately .072 in a 1000 Ma sample), an error in the calculated common Pb composition will have a greater effect on the corrected Pb^{207}/U^{235} ratio than the corrected Pb^{206}/U^{238} ratio. For samples with significant amounts of common Pb and which plot above concordia, the Pb^{206}/U^{238} age is taken as being closer to the true age than the Pb^{207}/U^{235} age.

The upper intercept age of 1648±7 Ma is interpreted to be the crystallization age of the granite. The titanite which constrains the lower intercept is part of the recrystallized mineral assemblage and therefore establishes the age of metamorphism as Grenvillian at 995 Ma (Fig. 6-2). The partial resetting (approximately 10%) of Pb in zircon towards the lower intercept is attributed to increased temperatures during the Grenvillian Orogeny.

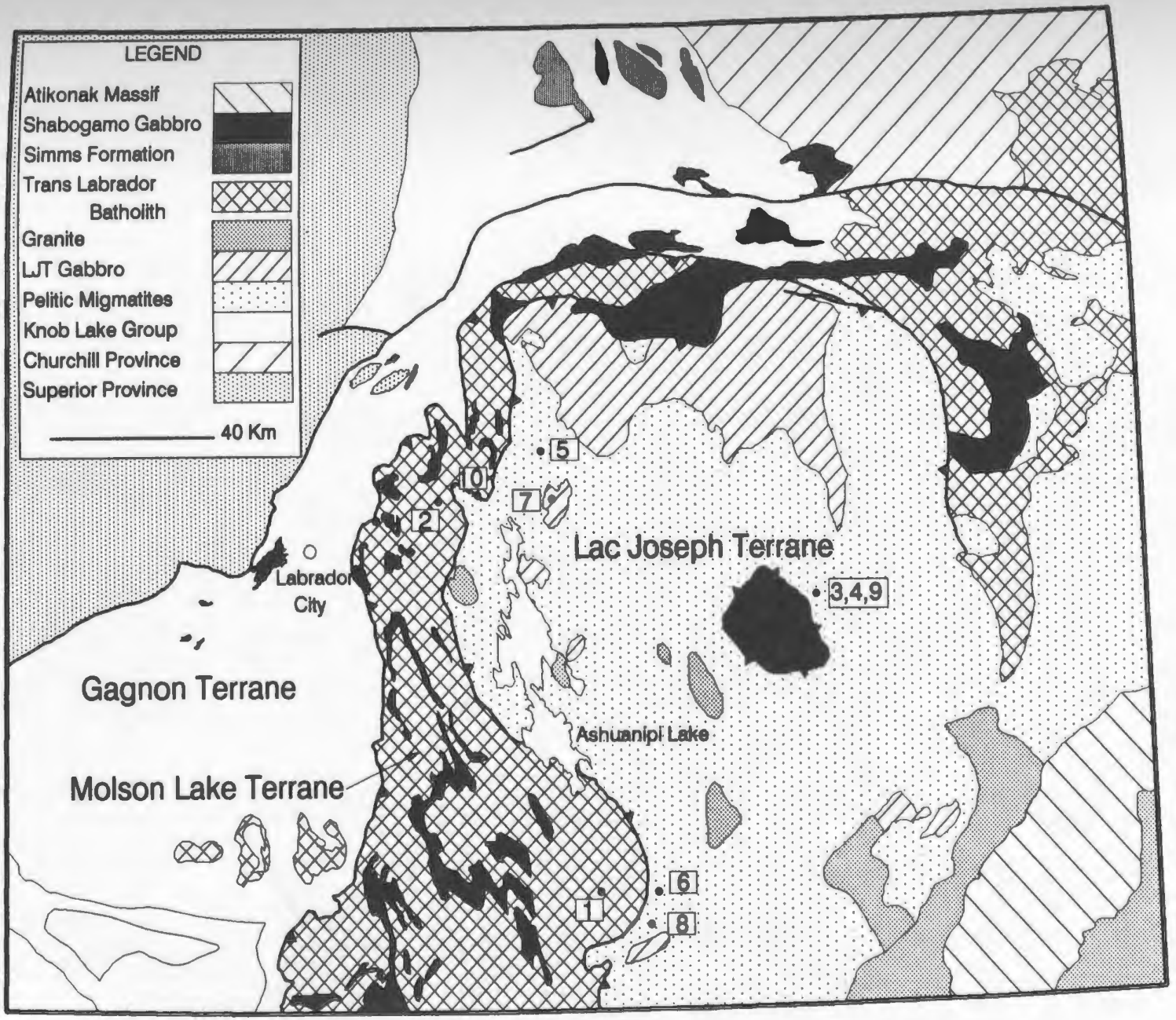

Figure 6-1: Location of samples utilized for U-Pb geochronology.

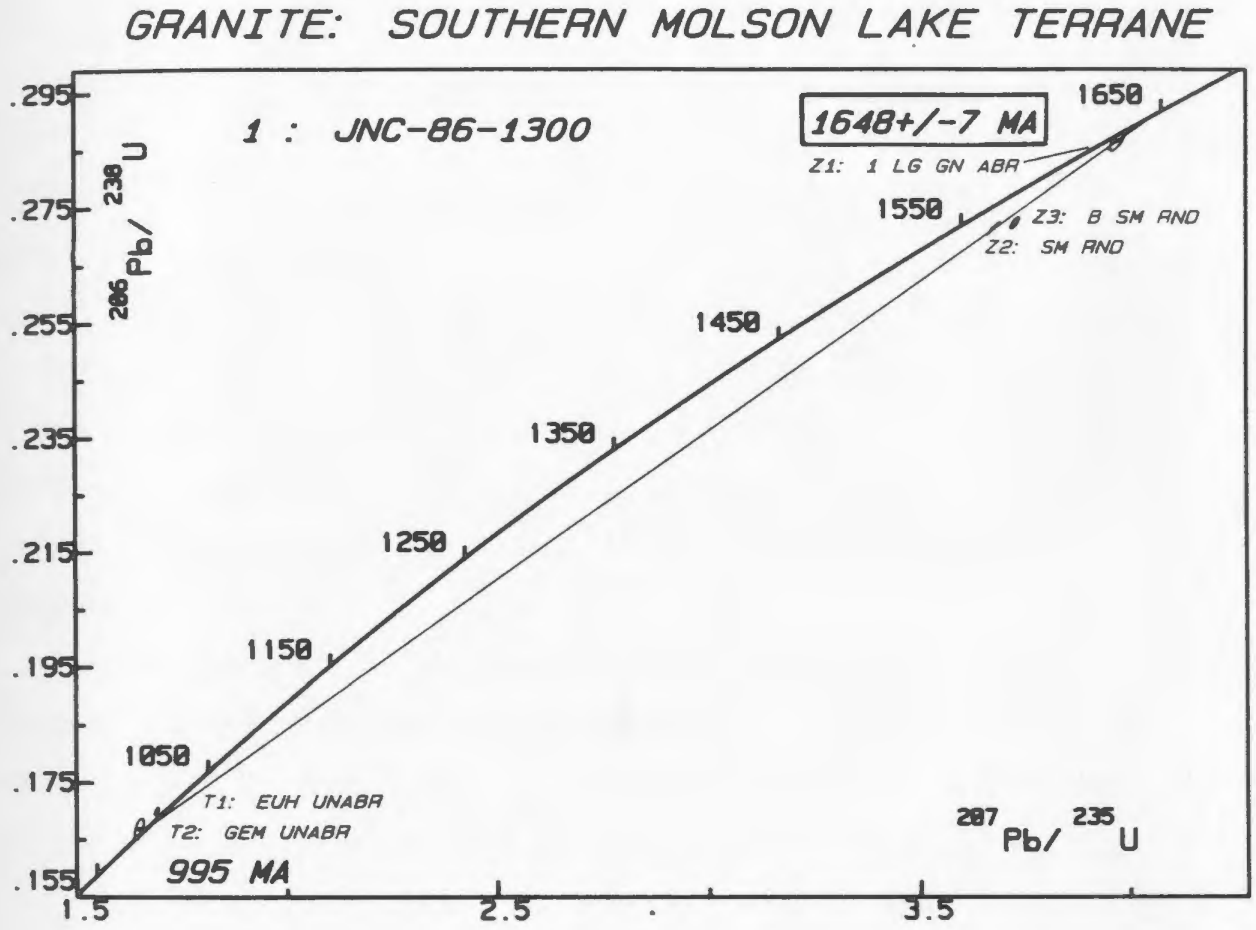

Figure 6-2: Concordia plot of zircon and titanite from a foliated granite in the southern Molson Lake Terrane; sample 1 (JNC-86-1300).

6.4.2 Shabogamo Intrusive Suite: Sample 2 (LH-88-12)

Previous $^{40}Ar/^{39}Ar$, Rb/Sr and Sm/Nd ages for the suite in western Labrador range between 1375 and 1400 Ma (Zindler et al., 1981; Brooks et al., 1981; Dallmeyer, 1982;). Furthermore, the Shabogamo Intrusive Suite has previously been correlated on geochemical grounds with the Michael Gabbro in eastern Labrador (Gower and Rivers, 1988; Gower et al., 1990) which has been dated by the U/Pb method at 1426±6 Ma (Schärer et al., 1986). In order to compare previous geochronological results for the Shabogamo Intrusive Suite with those by the U-Pb technique, and to further test the correlation with the Michael Gabbro, zircon and rutile fractions were analyzed from a sample of the Shabogamo Intrusive Suite. The sample chosen comes from the interior part of an intrusion in the northern part of the Molson Lake Terrane (Fig. 6-1). The sample was coarse-grained and displayed a primary igneous texture; the principal mineralogy included plagioclase, clinopyroxene, amphibole and biotite.

Most zircons in this sample were strongly discordant and the results for three fractions define a mixing line between 1431±7 Ma and 1001±10 Ma (Fig. 6-3). The upper intercept is interpreted to represent the age of igneous crystallization of this suite of gabbroic rocks. One fraction (2-Z4) lies off the mixing line, suggesting that it experienced secondary lead loss, and was not, therefore, included in the mixing line regression. A single fraction of rutile plots on concordia at 994 Ma, within error of the lower intercept of the mixing line defined by zircon.

The lower intercept of the mixing line at 1001±10 Ma, is interpreted to represent the age of a thermal event which affected these rocks and is within error of the age of metamorphism for the Molson Lake Terrane established from titanite in the granitoid sample. The high degree of resetting in zircon contrasts with zircon fractions from granites of the Molson Lake Terrane, perhaps reflecting new zircon growth, localized water availability and temperature differences during the Grenvillian Orogeny or differences in mineral size and/or radiation-induced crystal damage. Fraction 2-Z1 has a much lower $^{208}Pb/^{206}Pb$ ratio than the other three fractions implying a low Th content (the parent isotope of ^{208}Pb) which is common in metamorphic zircons.

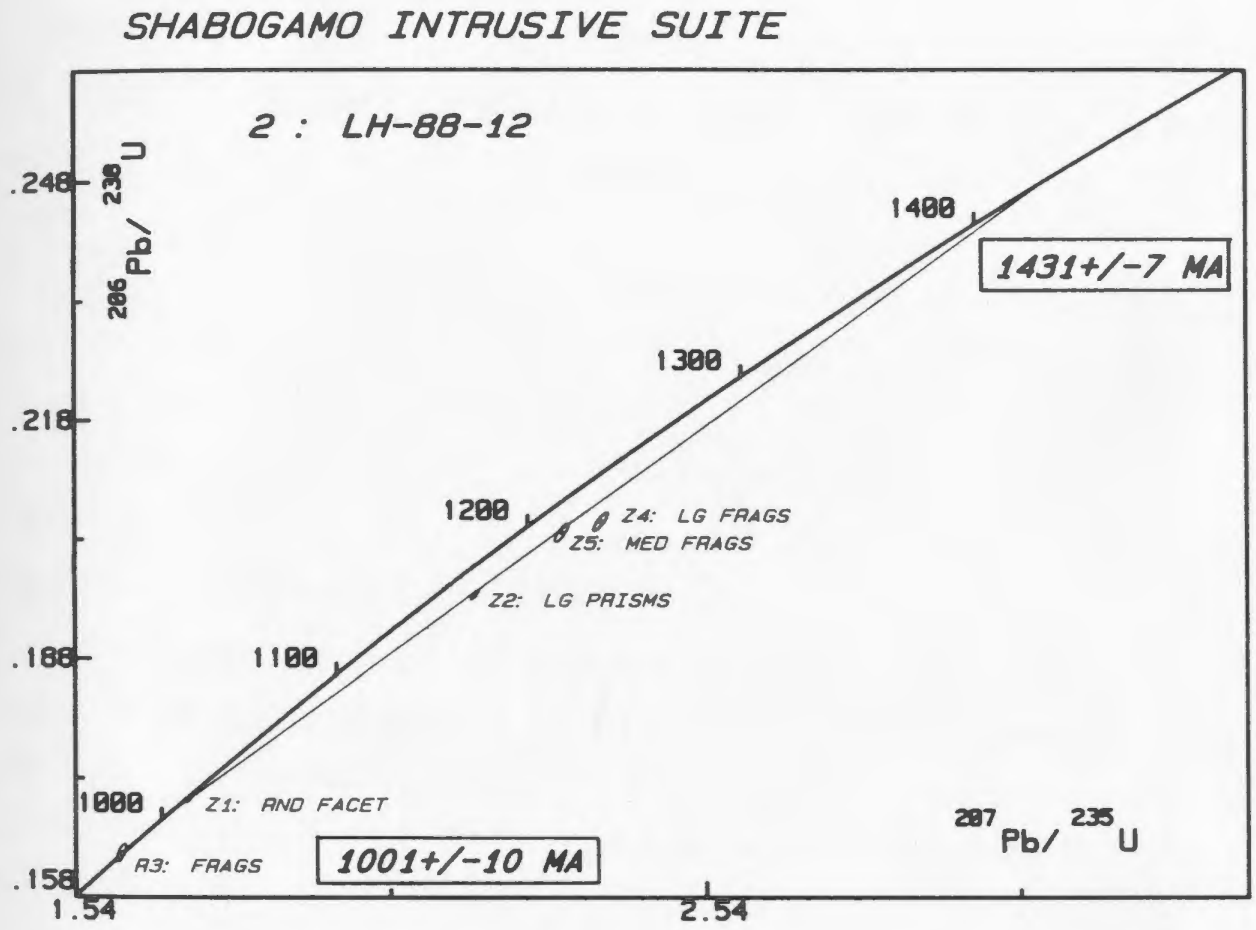

Figure 6-3: Concordia plot of zircon and rutile from gabbro of the Shabogamo Intrusive Suite in the northwestern Molson Lake Terrane, west of Ross Bay; sample 2 (LH-88-12).

The previously published U/Pb data from the Michael Gabbro of eastern Labrador (Schärer et al., 1986) plot on the 1431-1001 Ma mixing line defined by this work (Fig. 6-3) consistent with the previous correlation of the two suites noted above.

6.5 Results: Lac Joseph Terrane

6.5.1 Migmatites of the Lac Joseph Terrane - N_1 and N_2

Two samples chosen as representative of the N_1 and N_2 leucosomes (sample numbers 3 and 4 respectively) were collected at localities near the tectonic window at Lac Joseph in the interior of the Lac Joseph Terrane (Fig. 6-1). Both samples predominantly comprise the phases K-feldspar, plagioclase and quartz, but a minor restite component was unavoidably included. Fractions of anhedral monazite and zircons with crystal morphologies ranging from euhedral acicular to anhedral equant were separated from this sample. Some of the equant zircon grains contain cores with overgrowth rims.

6.5.2 N_1 Leucosome: Sample 3 (JNC-87-8113)

Two monazite analyses (3-M2 and 3-M4) define a short mixing line with an upper intercept of 1658+36/-10 Ma (Fig. 6-4) which is interpreted to be the crystallization age of the N_1 leucosome (ie. Labradorian in age). A long extrapolation from the closely spaced points near the top of the mixing line constrains the lower intercept rather imprecisely at about 1010 Ma. A third monazite (3-M5) fraction plots slightly above concordia, with a $^{208}Pb/^{238}U$ age of 1606 Ma. This fraction yielded a $^{206}Pb/^{204}Pb$ ratio approximately an order of magnitude lower than fractions 3-M2 and 3-M4 reflecting significantly higher amounts of common lead. The inconsistent result of fraction 3-M5 relative to the upper intercept age derived from fractions 3-M2 and 3-M4 is attributed to an inaccurate common Pb correction in the former.

All zircon populations are strongly discordant with $^{207}Pb/^{206}Pb$ ages ranging from 2330 to 1799 Ma indicating a significant component of pre-Labradorian inheritance. Only fraction 3-Z1 is near concordia with a $^{207}Pb/^{206}Pb$ age of 1799 Ma suggesting that a significant component of the zircon fraction formed or was reset at about this age. Interpretation is difficult, however, because the fraction is sufficiently discordant to allow a short mixing line from the 1658+36/-10 Ma melting event to an upper intercept

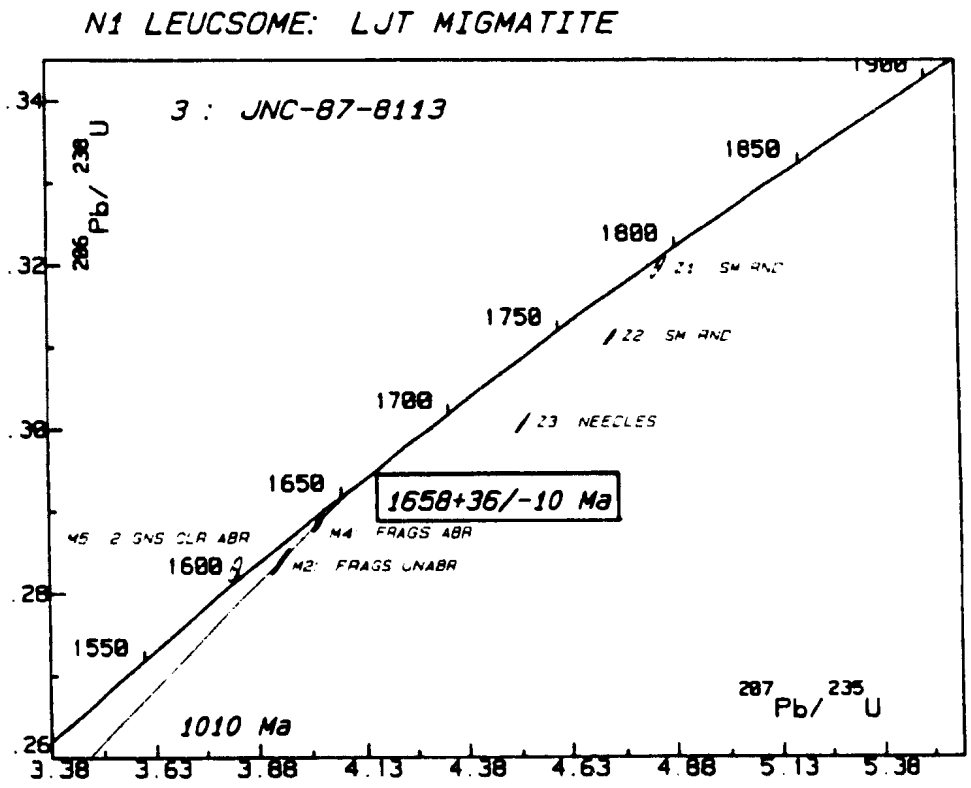

Figure 6-4: Concordia plot of zircon and monazite from an N_1 leucosome from a sample of pelitic migmatite from the Lac Joseph Terrane; sample 3 (JNC-87-8113).

around 1900 Ma. In either case however, this fraction is dominated by 1800 to 1900 Ma zircons implying an early Proterozoic provenance. The highly discordant nature of the other zircon fractions is attributed to new crystal growth around cores older than 1900 Ma and/or partial lead loss during or after generation of N1 leucosomes in the Labradorian Orogeny at 1658+36/-9 Ma (defined by the monazite discordia line).

6.5.3 N_2 Leucosome: Sample 4 (JNC-87-126)

Three euhedral monazite fractions consisting of 1, 2 and 5 grains respectively were analyzed from sample 4, and define a line with an upper intercept of 1639+12/-7 Ma and a poorly defined lower intercept of 1063 Ma (Fig. 6-5). The single grain was only 1.8% discordant from the upper intercept which is interpreted to represent the age of crystallization of this N_2 leucosome. This upper intercept age based on data from monazite establishes that the N_2 leucosomes formed during the Labradorian Orogeny and were thus not generated during the Grenvillian Orogeny. The zircon fractions show considerable scatter, suggesting that they have a significant component of inheritance, and they are therefore, not useful in determining the age of leucosome crystallization.

6.5.4 Mylonitic Migmatite of the Lac Joseph Terrane: Sample 5 (JNC-87-5016)

A mylonitic migmatite was collected about 8 km from the western margin of the southern Lac Joseph Terrane (Fig. 6-1) in order to determine the age of mylonitization and the synkinematic sillimanite - biotite - garnet - magnetite assemblage. Both leucosomes (N_1 and N_2) are flattened and attenuated and contain rotated K-feldspar inclusions. Biotite and sillimanite are aligned parallel to the shear plane and wrap around garnet.

One zircon and two monazite fractions define an upper intercept age of 1634+13/-4 Ma (Fig. 6-6). The limited discordance necessitates a long extrapolation to the lower intercept with a poorly defined age 1030 Ma. Zircon fraction 5-Z3, comprising large zircon grains, is slightly discordant with a $^{207}Pb/^{206}Pb$ age of 1650 Ma, whereas fraction 5-Z2 plots slightly above concordia with a $^{207}Pb/^{206}Pb$ age within error of the 1634+13/-4 Ma upper intercept. The near concordancy of all the zircon fractions contrasts strongly with those from samples 3 and 4 from the interior of the terrane,

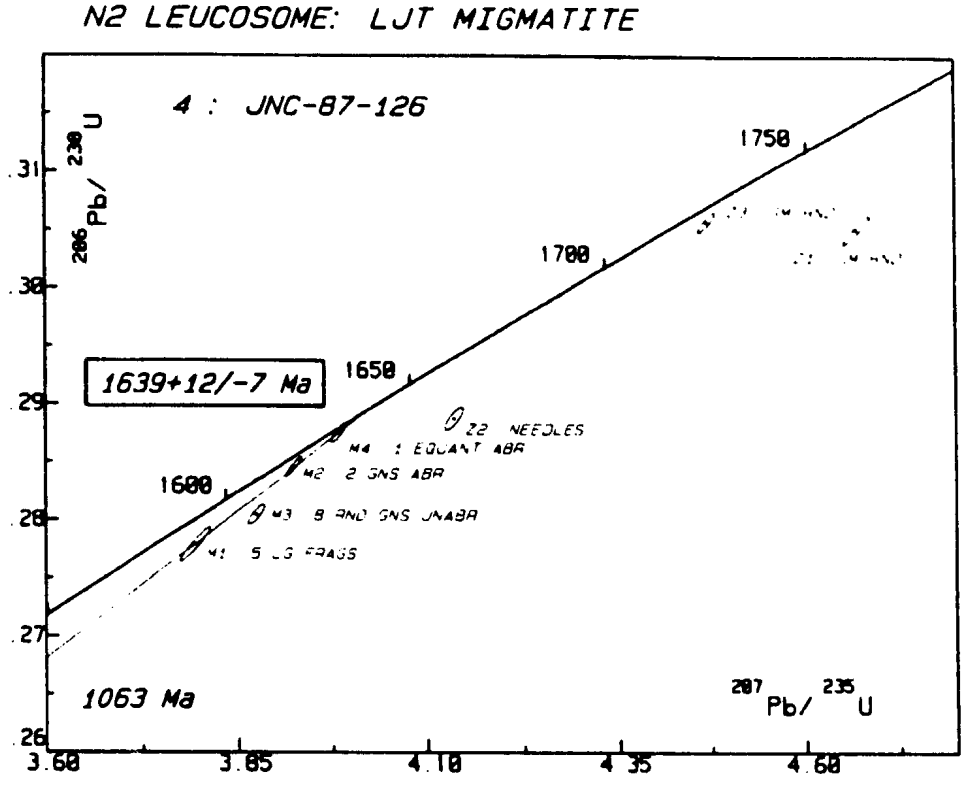

Figure 6-5: Concordia plot of zircon and monazite from an N_2 leucosome from a sample of pelitic migmatite from the Lac Joseph Terrane; sample 4 (JNC-87-126).

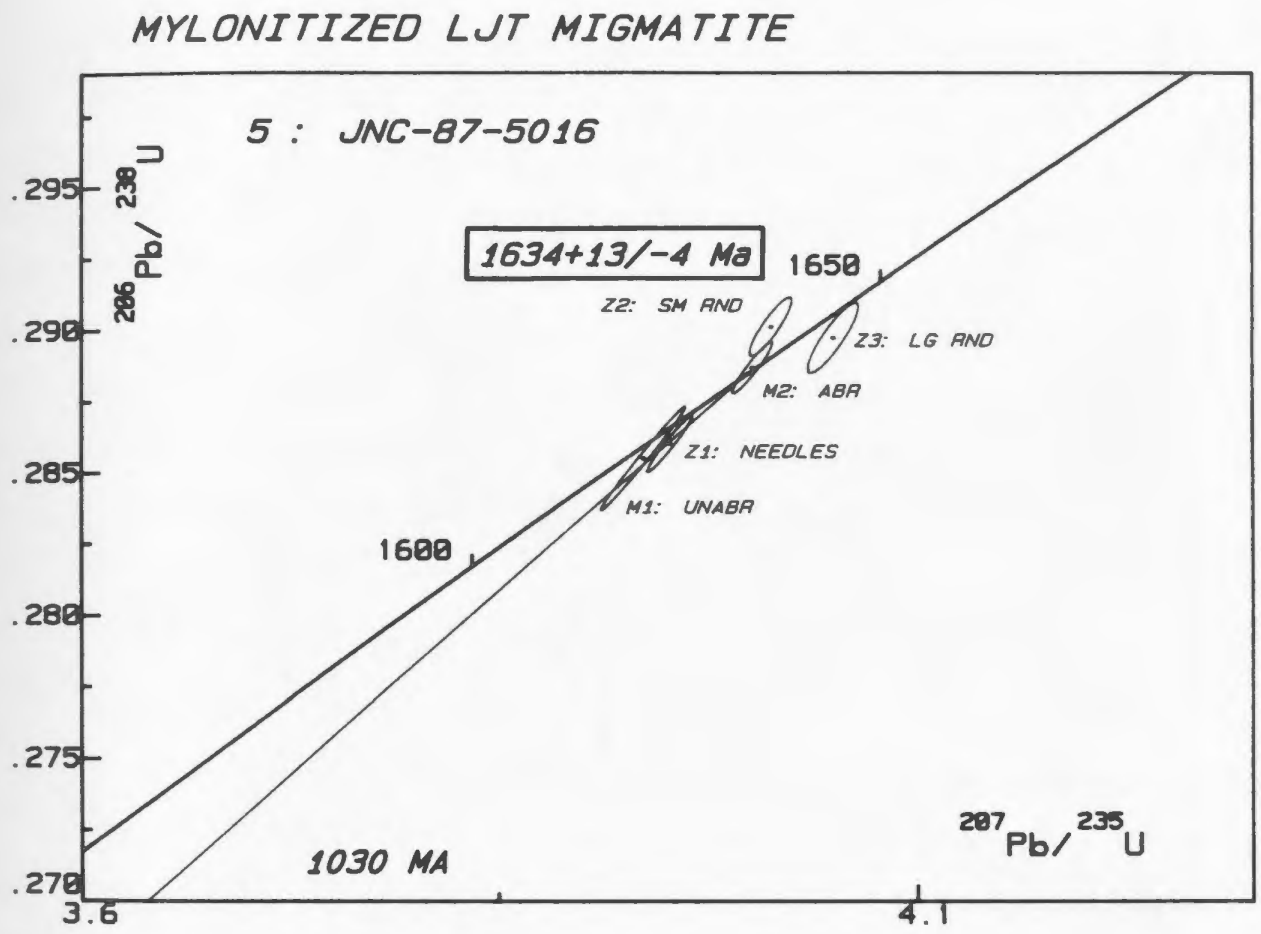

Figure 6-6: Concordia plot of zircon and monazite from a sample of mylonitized pelitic migmatite from the Lac Joseph Terrane; sample 5 (JNC-87-5016).

where a strong component of inheritance was found in all samples. It is interpreted that during the process of mylonitization, Pb was effectively reset in zircon in the shear zones. The U-Pb age from this sample therefore provides the age of mylonitization.

Since the restite assemblage is synkinematic, the U-Pb age from the shear zone also establishes that the sillimanite-biotite-garnet-magnetite assemblage formed at 1634+13/-4 Ma and must therefore be Labradorian in age. By extension, since this syn-kinematic mineral assemblage from within the shear zone is identical to the mineral assemblage in the migmatites outside the shear zone, and yields similar P-T results, it follows that the restite mineral assemblage throughout the Lac Joseph Terrane is of Labradorian age.

Since all fractions plot near the top of a discordia line between 1634 Ma - 1030 Ma it is apparent that the zircons were not strongly affected by the Grenvillian Orogeny, despite the proximity of the sample to the terrane boundary, a maximum distance of 8 km away.

6.6 Retrogressed Migmatite from the Margin of Lac Joseph Terrane: Sample 6 (JNC-86-14)

Sample 6 was collected near the southwestern margin of the Lac Joseph Terrane, where retrograde muscovite is pervasive (Fig. 6-1). This sample is an unmylonitized migmatite dominated by the younger melt phase (N_2). The leucosome primarily comprises plagioclase and quartz with minor K-feldspar, and the restite consists of muscovite, biotite, garnet and hematite. The object of dating this sample was to determine whether the presence of muscovite in the pelitic migmatites near the margin of the Lac Joseph Terrane could be correlated with Grenvillian growth of accessory minerals.

Four zircon fractions, all slightly discordant, and a monazite fraction which plots slightly above concordia, yield an upper intercept age of 1611+13/-6 Ma and a poorly defined lower intercept age of 1063 Ma (Fig. 6-7). The zircon fractions represent a diversity of morphologies which include needles (6-Z1 and 4), overgrowths (6-Z2) and small ($< 50\,\mu m$) round grains. The monazite fraction (6-M1) comprised large ($> 100\,\mu m$) rounded grains which were lustrous but not faceted. Two other monazite fractions

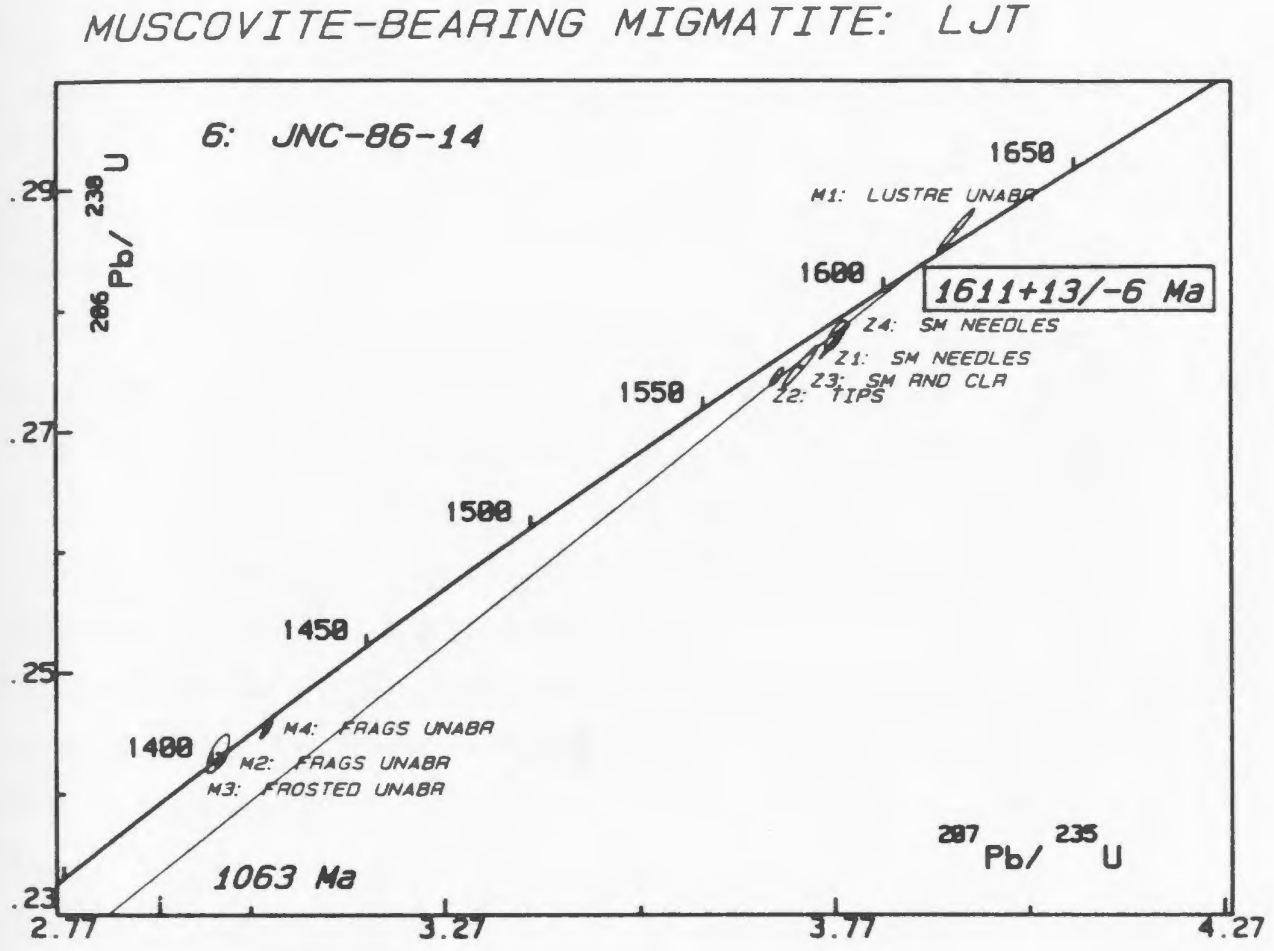

Figure 6-7: Concordia plot of zircon and monazite from an N_2 leucosome from a sample of pelitic migmatite from the Lac Joseph Terrane; sample 6 (JNC-86-14).

from this same migmatite yield $^{207}Pb/^{206}Pb$ ages of between 1423 to 1399 Ma, which are unique to the Allochthonous Polycyclic Belt of western Labrador (Fig. 6-7). Fractions 6-M2 and 6-M3 overlap within error with a $^{206}Pb/^{238}U$ age of 1403 Ma whereas fractions 6-M4 yields an older $^{206}Pb/^{238}U$ age of 1415 Ma and plots slightly below concordia. These fractions comprised large ($> 100\,\mu m$) fragments of monazite (6-M2 and 3) and one fraction of round, frosted grains, and therefore appeared distinct from the lustrous nature of fraction 6-M1.

Although there is some dispersion of the data among the 4 zircon fractions, there is no evidence of a pre-Labradorian inheritance (Fig. 6-7). In spite of the poor definition of the discordia caused by the clustering of the data points, three statements may be made; 1) the colinearity of analyses of zircon needles and overgrowths suggests that N_2 leucosomes in this sample crystallized during the Labradorian rather than Grenvillian Orogeny (reinforcing the conclusions from sample 4); 2) the lack of pre-Labradorian inheritance in this sample suggests that this part of the Lac Joseph Terrane must have been affected by a significant thermal event or resetting process during the Labradorian Orogeny which was absent in the interior; and 3) the U-Pb systematics of zircon and monazite at the margin were not significantly disturbed during the Grenvillian Orogeny.

The 1423 to 1399 Ma ages from the three monazite fractions are enigmatic for several reasons: 1) this age range has not been previously recorded in the Lac Joseph Terrane or any other allochthonous terrane in Labrador; 2) it is not known whether the monazites were located in the restite phase or the leucosomes; and 3) data at present are insufficient to determine whether the frosted monazite grains consistently yield ages in this range (the other fractions which yielded the same age may be fragments of the frosted population) in contrast to the lustrous grains which, so far, have a single Labradorian age. The $^{206}Pb/^{238}U$ age of 1403 Ma from the two concordant monazite fractions is thought to be the best estimate of this cryptic event; fraction 6-M4, which plots slightly below concordia and yields an older $^{207}Pb/^{206}Pb$ age, may have a small component of inheritance.

6.7 Ossokmanuan Mountain Intrusive Suite of the Lac Joseph Terrane: Sample 7 (LH-88-23)

A sample of medium-grained, massive gabbronorite exhibiting a primary igneous texture was collected from the site of the communication tower east of Ross Bay Junction (Fig. 6-1) and is thought to be representative of the gabbroic rocks of the Ossokmanuan Mountain Intrusive Suite along the northern margin of the Lac Joseph Terrane and many of the smaller bodies in the terrane. Two concordant fractions of anhedral zircon yielded an age of 1623+7/-5 Ma which is interpreted to be the age of crystallization (Fig. 6-8). Fragments of rutile grains from this sample yielded an identical age (within error) implying that it also crystallized at the time of intrusion. The lack of Pb-loss in zircon or rutile subsequent to their crystallization implies that this rock was not significantly affected during the Grenvillian Orogeny.

Whether this age is applicable to all the metabasic rocks in the Lac Joseph Terrane is unclear. However, the lithological diversity of the gabbroic rocks in the Lac Joseph Terrane requires that caution be exercised in correlations. In particular, the highly recrystallized, two pyroxene granulites appear to have undergone a different metamorphic history.

6.8 Mafic Migmatites of the Lac Joseph Terrane: Sample 8 (JNC-86-524)

An amphibolite facies retrogression locally overprints the granulite facies assemblage in the metabasic rocks in the Lac Joseph Terrane. To determine the timing of the amphibolite retrogression, a sample of foliated, fine-grained, partially melted metabasic gneiss containing plagioclase, hornblende, biotite, quartz, titanite and zircon was collected from the amphibolite facies zone near the southwestern margin of the terrane (Fig. 6-1). Since the U-Pb systematics in titanite are known to be sensitive to metamorphic/hydrothermal events, three fractions of euhedral titanite were analyzed in order to determine whether this overprinting was part of a protracted Labradorian Orogeny or a distinct younger event. Three fractions of small ($< 50\mu m$) round zircon were also analyzed.

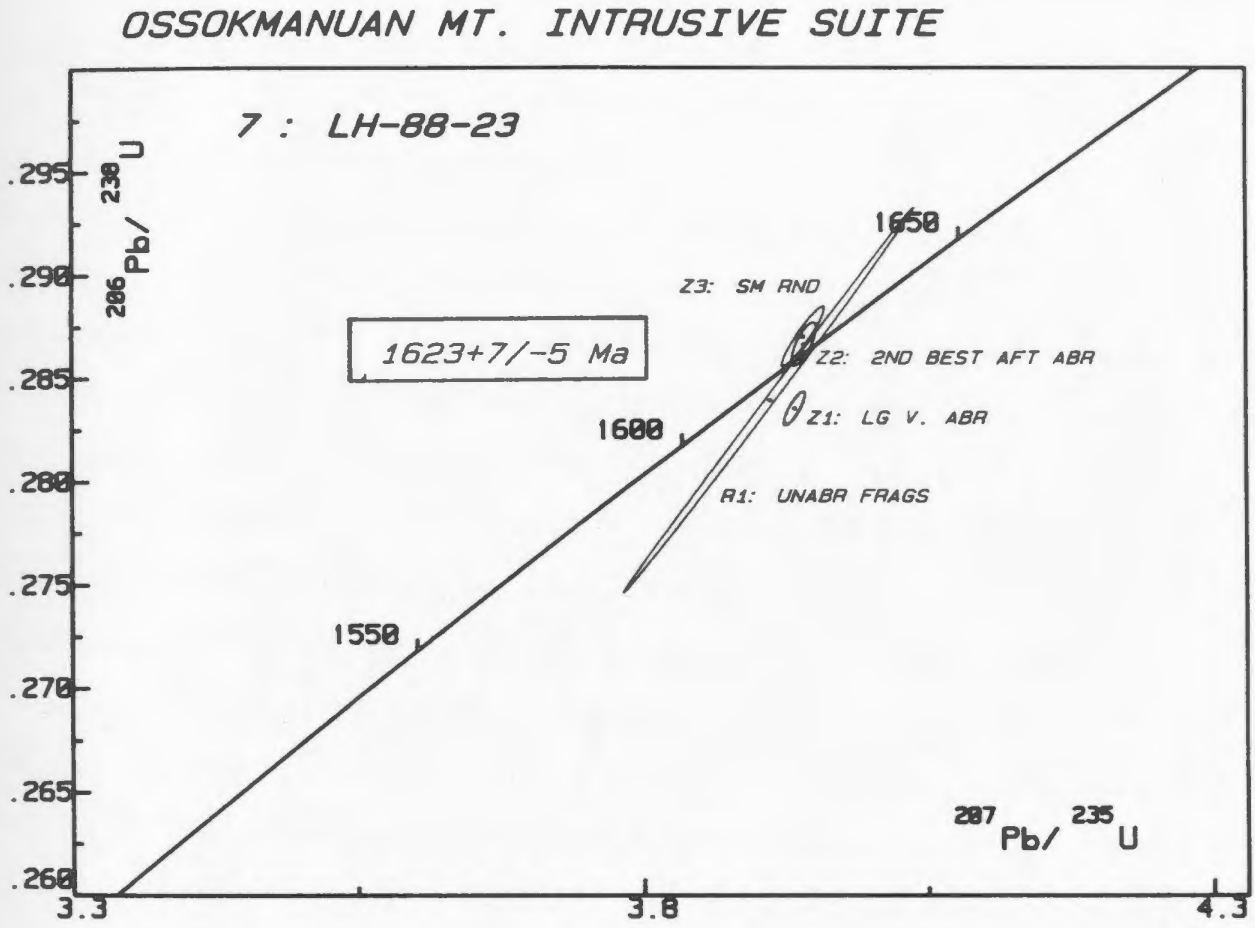

Figure 6-8: Concordia plot of zircon and rutile from a gabbronorite body of the Ossokmanuan Mountain Intrusive Suite of the Lac Joseph Terrane; sample 7 (LH-88-23).

Two titanite fractions fall on concordia at 1281 Ma with a third fraction being slightly discordant with a $^{207}Pb/^{206}Pb$ age of 1292 Ma (Fig. 6-9). Of the three zircon fractions analyzed from this sample, one (8-Z1) is highly discordant and was not utilized. Fraction 8-Z3 falls on a line between 1281 Ma (defined by the two concordant titanite fractions) and 1648 Ma, with fraction 8-Z2 plotting within error of the upper intercept with a $^{207}Pb/^{206}Pb$ age of 1657 Ma. Although the zircon analyses do not provide a precise upper intercept, the two zircon fractions fall on a line which suggests that this rock was originally metamorphosed at about 1650 Ma during the Labradorian Orogeny. Utilizing the two concordant titanite points it is interpreted that the Labradorian assemblage was affected by a hydrous amphibolite facies retrograde metamorphic event at 1281 Ma which resulted in titanite crystallization. The spatial extent of amphibolite facies assemblages of this age and the significance of the 1281 Ma age, previously unrecognized in western Labrador, is currently a matter of speculation.

6.9 Pegmatite Dyke in the Lac Joseph Terrane: Sample 9 (JNC-87-8126)

A weakly foliated, coarse-grained to pegmatitic, two mica granite dyke, which cross-cuts all fabrics in an outcrop of migmatite in the Lac Joseph Terrane, was collected to establish the maximum age of the last deformation event which affected the Lac Joseph Terrane (namely the event responsible for the fabric in the dyke).

Two concordant anhedral monazite fractions yielded an age of 999+5/-3 Ma (Fig. 6-10) which is interpreted to represent the age of crystallization of the pegmatite dyke. Zircon fractions from this sample are discordant and were therefore not utilized in the calculation of the age, although their Grenvillian $^{207}Pb/^{206}Pb$ ages of 1012 Ma and 993 Ma imply there is no component of Labradorian or older inheritance. This sample indicates that the fabric observed in the dyke must be of late Grenvillian age.

6.10 Shear Zone Boundary between the Lac Joseph and Molson Lake Terranes: Sample 10 (JNC-87-5043B)

Granites of the Molson Lake Terrane are deformed in ductile shear zones along the boundary between the Lac Joseph Terrane and Molson Lake Terrane. A sample of mylonitized granite was collected from the Lac Emerillon shear zone east of Labrador City on the Trans-Labrador highway (Fig. 6-1) in an effort to establish the age of

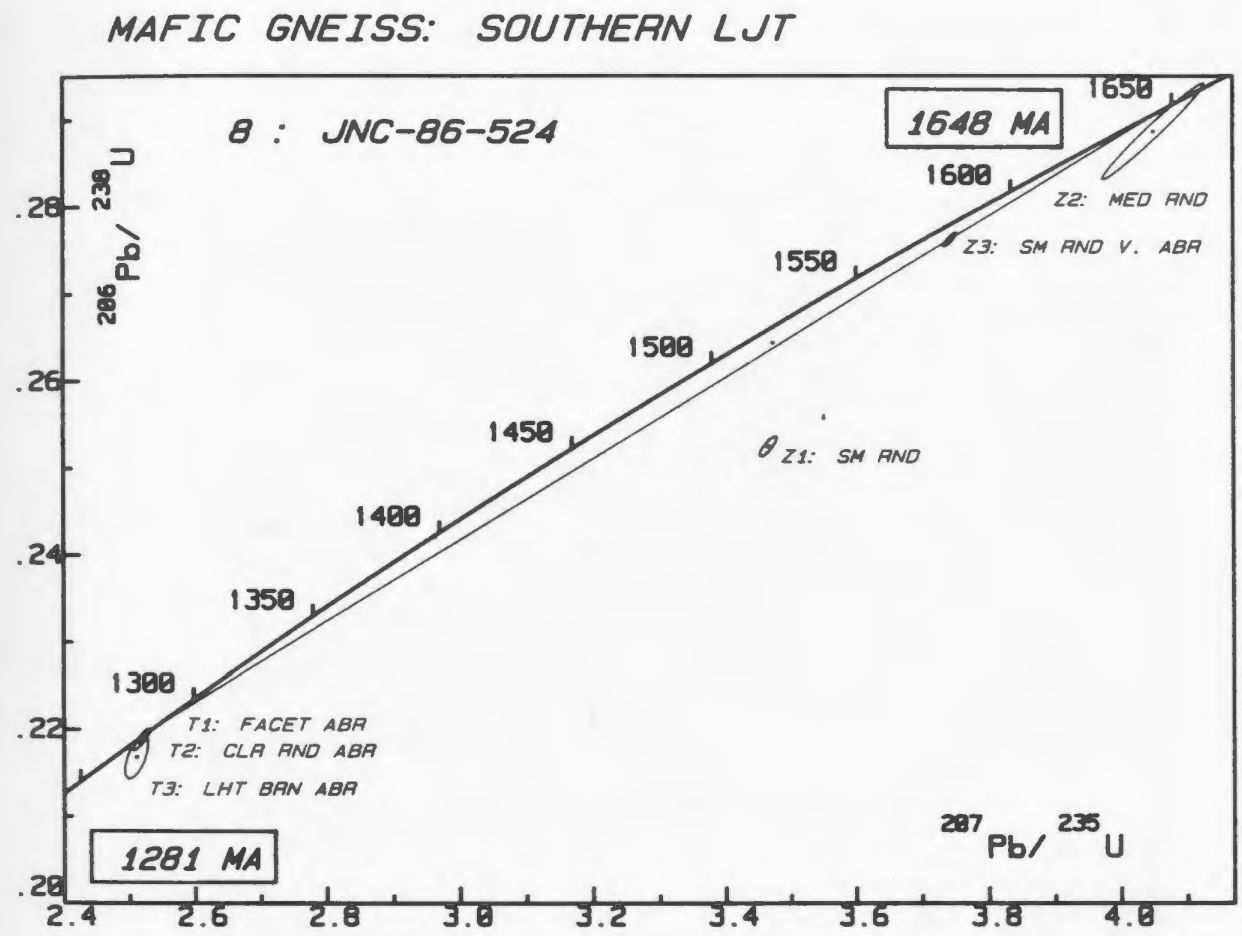

Figure 6-9: Concordia plot of zircon and titanite from amphibolite facies mafic gneiss in the southwestern Lac Joseph Terrane; sample 8 (JNC-86-524).

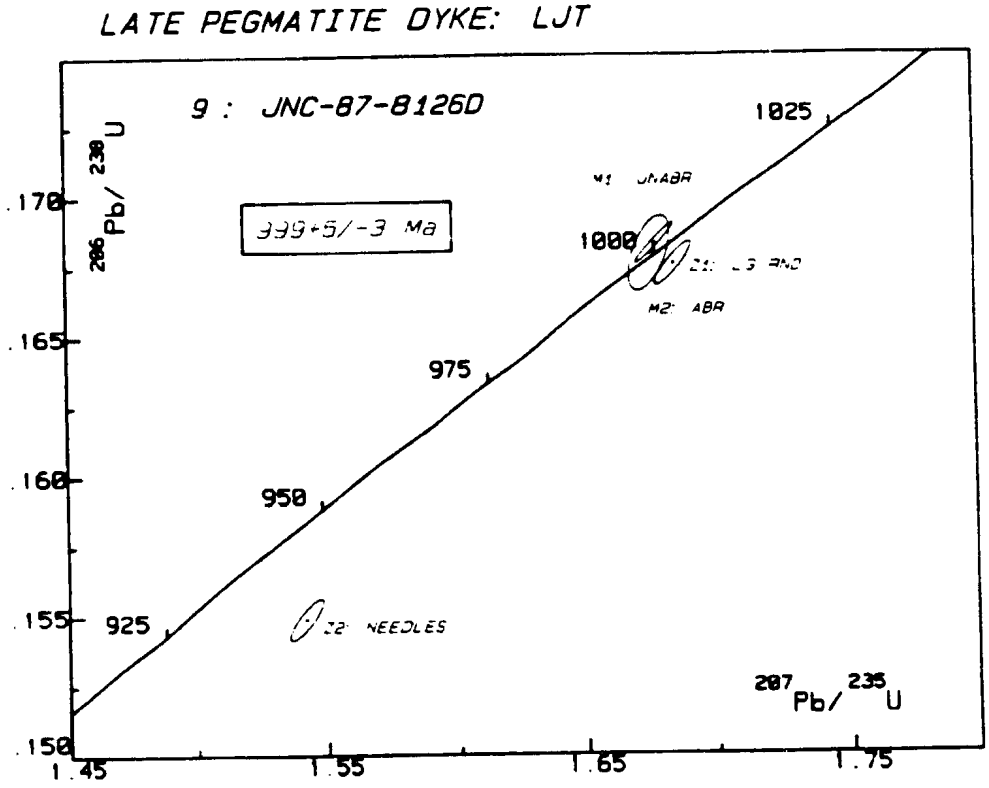

Figure 6-10: Concordia plot of zircon and monazite from a foliated, cross-cutting, pegmatite dyke at the base of the Lac Joseph Terrane; sample 9 (JNC-87-8126D).

shearing in this zone, and thus the approximate time of juxtapositioning of the Lac Joseph Terrane against the Molson Lake Terrane. The sample is of granitic composition, with accessory garnet, epidote, biotite, titanite and zircon. It exhibits a very strong fabric parallel to the shear plane; rotated inclusions were locally observed in the outcrop.

Three zircon fractions were analyzed and all fall on a mixing line between 1640±20 Ma and 990±12 Ma. These ages are within error of the previously defined mixing line for the unmylonitized granite in the Molson Lake Terrane to the south (Sample 1, Fig. 6-2). However, in contrast to the unmylonitized granites, the zircons within the shear zone have experienced significant Pb-loss and plot from 45% to 69% discordant along the mixing line towards the lower intercept at 990±12 Ma (Fig. 6-11). Two fractions of titanite, a phase which is part of the synmylonitic, stable mineral assemblage, plot on concordia at 995 and 1000 Ma.

It is interpreted that the significantly higher degree of resetting of zircon in this sample compared to the unmylonitized samples is due to the presence of fluids and/or mechanical deformation associated with ductile shearing. The lower intercept age of the discordia line of 990±12 Ma, defined by zircon, is therefore interpreted to represent the time of shearing. The age of the synmylonitic titanite is identical to the lower intercept of 990±12 Ma, and so the time of shearing is confidently estimated from two independent pieces of evidence.

It should be emphasized, however, that although sample 10 was collected from a shear zone at the margin of the Molson Lake Terrane, the terrane boundary is a complex zone of anastomosing shear zones, and movement along other parts of the zone could have pre- or post-dated the estimated age of 990±12 Ma. This age for shearing, therefore, provides an approximate age for the emplacement of the Lac Joseph Terrane, but does not require that the two terranes were assembled in their present configuration by 990±12 Ma.

6.11 Discussion

From the geochronological data presented above it is clear that, although the Molson Lake and Lac Joseph terranes experienced common igneous and metamorphic

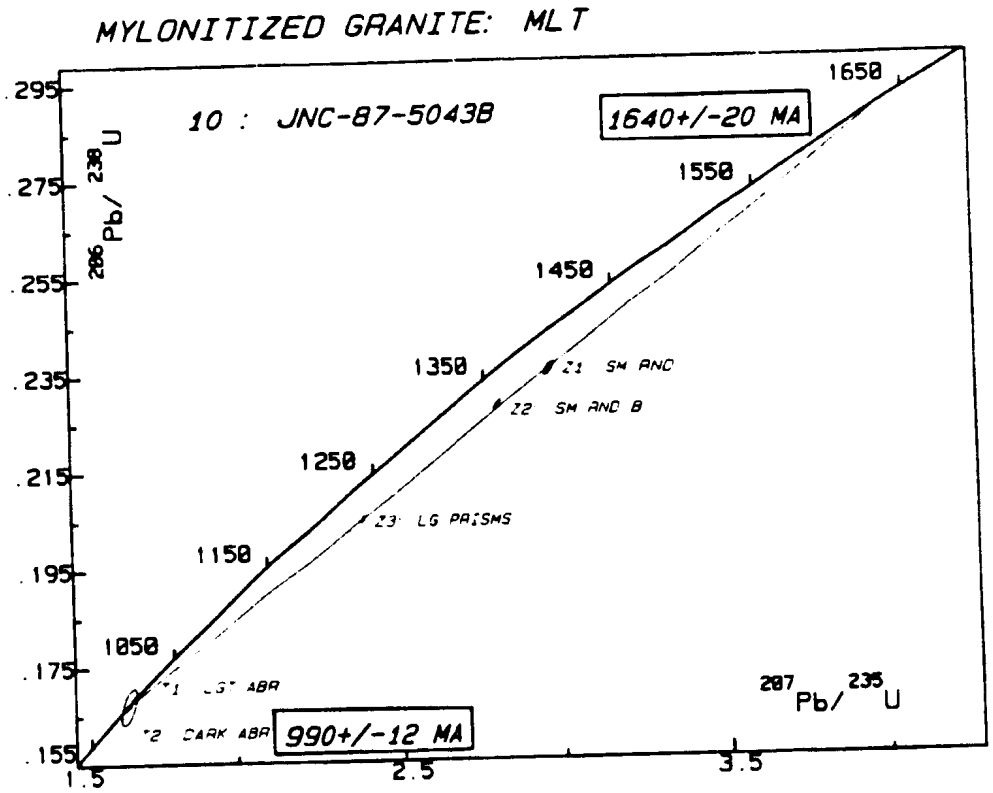

Figure 6-11: Concordia plot of zircon and titanite from mylonitized granite of the Molson Lake Terrane; sample 10 (JNC-87-5043B).

events, much of their histories are distinct (Fig. 6-12). For instance, although both terranes were affected by igneous events of Labradorian age, the Shabogamo Intrusive Suite appears to have been solely emplaced into the Molson Lake Terrane. On the other hand, events resulting in recrystallization of accessory phases in the interval between the Labradorian and Grenvillian orogenies in the Lac Joseph Terrane do not appear to be represented in the Molson Lake Terrane. The Grenvillian Orogeny resulted in penetrative recrystallization of rocks in the Molson Lake Terrane and thrusting of the Lac Joseph Terrane over the Molson Lake Terrane. Other implications of these data and their constraints on tectonic models, are discussed below.

6.12 Molson Lake Terrane

6.12.1 The Labradorian Orogeny

The granitoid rocks in the Molson Lake Terrane are thought to comprise an intrusive suite which was emplaced at about 1648±7 Ma. This age is comparable to the emplacement age of rocks in the Trans Labrador Batholith suite in eastern and central Labrador (Gower et al., 1984; Nunn et al., 1985; Thomas et al., 1985; Schärer et al,. 1986; Kerr, 1989). Since the compositions of the granitoid rocks of the Molson Lake Terrane are also apparently broadly comparable to those of the batholith to the east, it is suggested that they are a westerly continuation of the Trans Labrador Batholith, which is therefore interpreted to structurally underlie the Lac Joseph Terrane and extend on its western side.

6.12.2 Shabogamo Intrusive Suite

The 1431±7 Ma U-Pb age for the Shabogamo Intrusive Suite is in reasonable agreement with previously reported Rb/Sr, Sm/Nd and $^{40}Ar/^{39}Ar$ ages of between 1375-1400 Ma (Brooks et al., 1981, Zindler et al., 1981; Dallmeyer, 1982) and is identical within error to the 1426±6 Ma age previously reported for the Michael Gabbro of eastern Labrador (Schärer et al., 1986). The previous correlations between the Michael Gabbro and Shabogamo Intrusive Suite made by Gower et al. (in press) is thus supported by the new U/Pb data. There is no evidence to indicate that any metamorphic or compressional structural event accompanied the emplacement of this

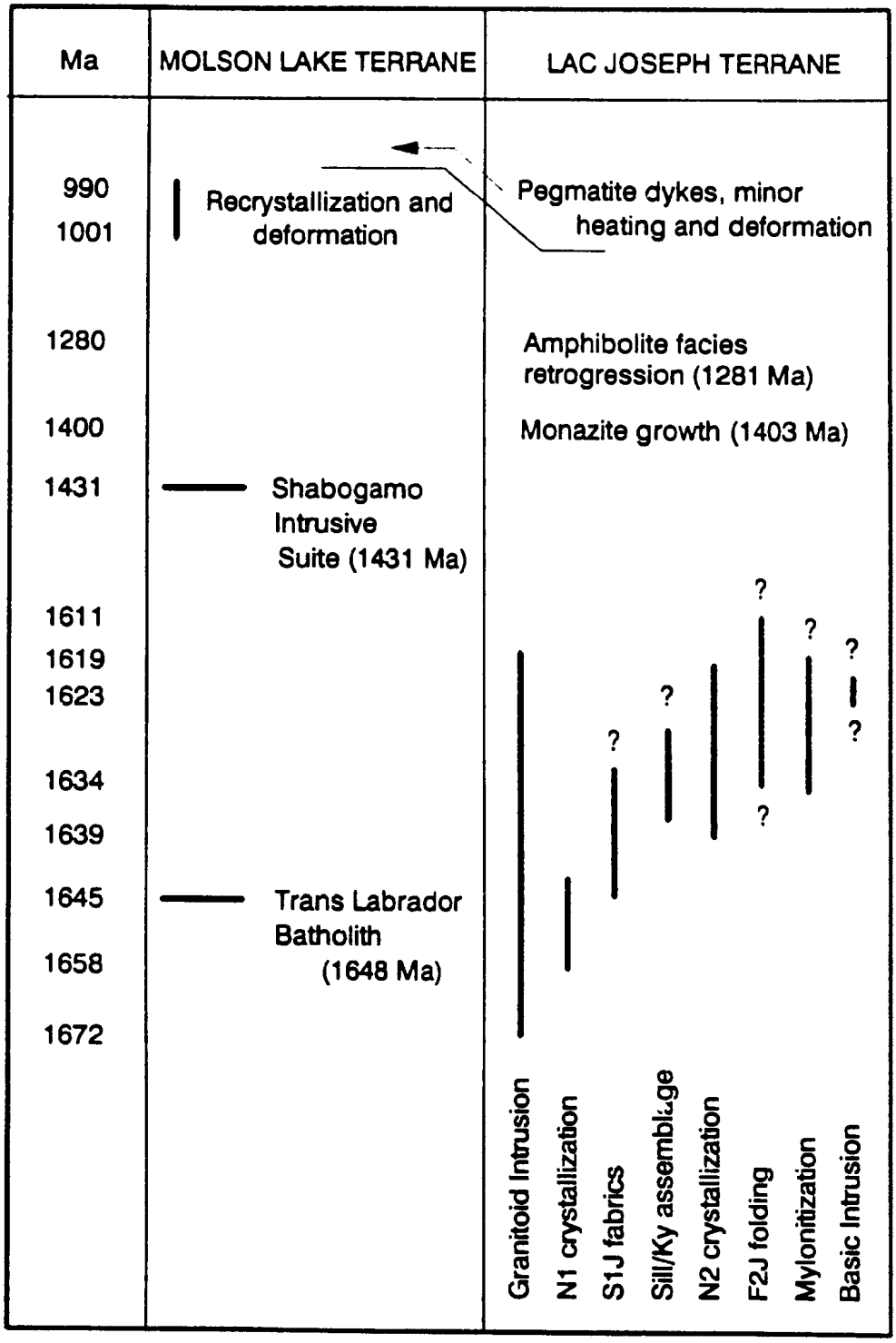

Figure 6-12: Summary of events in the Lac Joseph and Molson Lake terranes.

unit. These observations are compatible with the existence of a east-northeast oriented zone of extension at 1431 $\pm$7 Ma, subparallel to the future Grenville Front, into which the Shabogamo Intrusive Suite and Michael Gabbro were emplaced.

6.12.3 Grenvillian Orogeny

Titanite and rutile in the metagranitoid and metabasic rocks respectively in the Molson Lake Terrane crystallized or were reset during the Grenvillian Orogeny. Zircons from both rock types are partially to strongly discordant towards a lower intercept of 990 to 1001 Ma implying that this terrane was affected by an intense thermal event during this interval which resulted in extensive mineral recrystallization accompanied by penetrative fabric development.

6.13 Lac Joseph Terrane

6.13.1 Labradorian Orogeny

Both the N_1 and N_2 leucosomes in the migmatites in the Lac Joseph Terrane formed during the Labradorian Orogeny, the earlier dated at 1658+36/-10 Ma and the later at 1639+12/-7 Ma. A third migmatite sample, a retrogressed muscovite-bearing migmatite from the boundary of the Lac Joseph Terrane, has yielded an age of 1611+13/-6 Ma (upper intercept of a mixing line defined by zircon and a near concordant fraction of monazite). In this sample the N_1 and N_2 leucosomes cannot be distinguished, but the implication is that the leucosomes crystallized until this time, suggesting that the S_{1J} gneissosity is a composite feature which formed in the interval from 1658 Ma until about 1611 Ma. Sillimanite and biotite are in part aligned within this composite gneissosity and define D_{1J} fabrics, and must, therefore, have been forming at least during the formation of the N_2 leucosomes. These minerals are also coaxial and coplanar to F_{2J} folds which clearly postdate the younger leucosomes and the S_{1J} gneissosity, suggesting that the sillimanite - garnet - biotite - magnetite sub-assemblage continued to form, and perhaps locally recrystallized after melting had ceased. The age of 1634+13/-7 Ma from a shear zone which contains the stable synkinematic sillimanite - biotite - garnet - magnetite sub-assemblage implies that the latest movements on the shear zone occurred during the Labradorian Orogeny. Field

relationships indicate that the shear zone post-dated the F_2 folding, so the age of shearing is a minimum age for the F_{2J} folding and proves that F_{2J} folds are indeed Labradorian.

A metamorphic aureole around a granitoid body associated with the Atikonak Massif (Fig. 6-1) in the southern part of the Lac Joseph Terrane which has been dated at 1133+10/-5 Ma (U-Pb, Emslie and Hunt, 1990), overprints the sillimanite - garnet - biotite - magnetite assemblage and therefore independently attests to the pre-Grenvillian age of the latter.

6.13.2 Intrusive Rocks of the Lac Joseph Terrane

The medium- to coarse-grained basic intrusive rocks were emplaced during the latter part of the Labradorian Orogeny at 1623±7 Ma. The approximate coincidence of rutile and zircon ages implies that this rock type was not appreciably affected by any post-Labradorian thermal event.

Two previously reported ages for granitoid rocks in the Lac Joseph Terrane suggest that granitic intrusion occurred over an extended time interval in the Labradorian Orogeny. The earliest zircon age of 1672 Ma (Krogh, 1983) is apparently from a pre-tectonic body, as it predates the older leucosome phase determined here by about 14 m.y. The rapakivi-textured granitoid rocks dated by Brooks (1983) intruded at 1619 Ma (U-Pb), approximately coevally with the basic rocks dated in this study. The presence of metamorphic orthopyroxene in this unit supports the earlier suggestion that elevated temperatures persisted at least until this time.

6.13.3 Post-Labradorian to Pre-Grenvillian Mineral Growth

Two periods of mineral growth occurred between the Labradorian and Grenvillian orogenies which were previously unrecognized in western Labrador. Two monazite fractions from a migmatite sample collected near the margin of the Lac Joseph Terrane yielded ages of 1403 Ma (Fig 6-7). Although the recrystallization or diffusion of Pb must have been due to a thermal and/or hydrothermal event, no such event has yet been recognized and no structural signature has been identified. It is perhaps noteworthy, however, that this age determination comes from near the margin of the Lac Joseph Terrane, and may imply that movement along the boundary occurred sporadically in the

interval between Labradorian to Grenvillian times. Although speculative, this would imply that the formation of the Lac Joseph Terrane boundary was a pre-Grenvillian event.

In the southwestern part of the Lac Joseph Terrane, near the boundary with the Molson Lake Terrane, a titanite-bearing, amphibolite-facies assemblage has overprinted an earlier granulite-facies assemblage. Three titanite fractions from the amphibolite facies rocks yielded consistent ages of ca. 1281 Ma indicating that, at least locally, the Lac Joseph Terrane was affected by a retrograde amphibolite facies metamorphic event at this time. It is not known whether this 1281 Ma event only resulted in retrogression along the margins of the Lac Joseph Terrane, or whether it also affected the interior regions.

6.13.4 The Grenvillian Orogeny

A suite of 999+5/-3 Ma pegmatite dykes cross-cut Labradorian fabrics in the migmatites of the Lac Joseph Terrane. A single penetrative planar fabric within the dykes attests to the existence of at least local deformation of Grenvillian age in the Lac Joseph Terrane.

All four of the pelitic migmatites from the Lac Joseph Terrane that were dated by U-Pb methods show only slight discordance of both zircon and monazite fractions towards lower intercepts between 1000 and 1070 Ma. However, the clustering of data near the upper intercepts of the mixing lines precludes accurate determination of the lower intercepts. Examined independently, it would not be possible to determine whether the lower intercepts represent a significant geological event. However, since the lower intercepts in all four samples lie in the restricted range of 1000-1070 Ma, which is known to approximately coincide with the age of the Grenvillian Orogeny, it is likely that they reflect the latter event. Furthermore, when these results are considered in the context of other data from the Molson Lake Terrane which indicate the existence of a major metamorphic event between 990-1000 Ma, it appears reasonable to suggest that minor Pb-loss in accessory minerals in the migmatites also occurred as a result of the orogeny at this time. It is therefore suggested that much, if not all, of the Lac Joseph Terrane was heated sufficiently during the Grenvillian Orogeny to cause slight

Pb-loss in zircon and monazite. The preservation of Labradorian mineral assemblages and fabrics suggests that the thermal effects were not sufficient to cause widespread mineral recrystallization throughout the Lac Joseph Terrane.

6.14 Terrane Assembly

Shearing along the mutual boundary of the Lac Joseph and Molson Lake terranes occurred at about 990±12 Ma, coeval with recrystallization of the metagranitoid and metagabbroic rocks in the Molson Lake Terrane itself. This episode of shearing is interpreted to be associated with the emplacement of the Lac Joseph Terrane over the Molson Lake Terrane along southeast-dipping thrust faults. As noted above, the U-Pb isotopic systematics in minerals in the Lac Joseph Terrane were only slightly reset during the Grenvillian Orogeny, implying that the Lac Joseph Terrane was not heated sufficiently at this time to cause penetrative mineral recrystallization. The Grenvillian imprint is therefore limited to the emplacement of sparse granitic pegmatites and the development of a localized fabric.

CHAPTER 7
$^{40}Ar/^{39}Ar$ GEOCHRONOLOGY

7.1 Introduction

The results of U-Pb geochronology have established the timing of crystallization of major intrusive units, and of the leucosomes in the pelitic migmatites, and have elucidated the chronology of fabric-forming recrystallization and mylonitization events. $^{40}Ar/^{39}Ar$ geochronology was employed as a complementary geochronological tool to investigate the post-peak metamorphic history in both the Molson Lake and Lac Joseph terranes. Hand-picked mineral fractions were separated from some of the samples that were used for U-Pb geochronology (as previously outlined in Section 6.2) and from other samples chosen specifically for $^{40}Ar/^{39}Ar$ dating and sent to Dr. John Hanes at Queen's University at Kingston. These fractions were further "cleaned up" by Hanes prior to shipment to McMaster University in Hamilton, Ontario for irradiation to convert ^{40}K to ^{40}Ar. Fractions were analyzed at Queen's University by J. Hanes. In the age spectra, the vertical height of the bars for each fraction represent $\pm$ 2 sigma, suitable for comparing within-spectrum dates (ie. error in J=0). A conservative 0.5% error in J estimates can be used for between-spectra age comparisons of samples irradiated together; this corresponds to an additional ca. $\pm$ 2 Ma (2 sigma) error in step dates. The sample sites and mineral fractions selected for analysis are shown on Figure 7-1. Since some samples analyzed for $^{40}Ar/^{39}Ar$ were also analyzed for U-Pb geochronology, only descriptions of samples not discussed in the Chapter 6 will be presented here.

7.2 The Lac Joseph Terrane

Samples from the Lac Joseph Terrane were specifically chosen to: 1) test the U-Pb results which suggest that amphibolite facies retrograde metamorphism occurred at about 1281 Ma; 2) determine the age of the fabric defined by aligned muscovite that occurs along the southwest margin of the Lac Joseph Terrane; 3) investigate more fully the thermal effects of the Grenvillian Orogeny; and 4) compare qualitatively, post-metamorphic cooling rates at the margin and interior of the terrane.

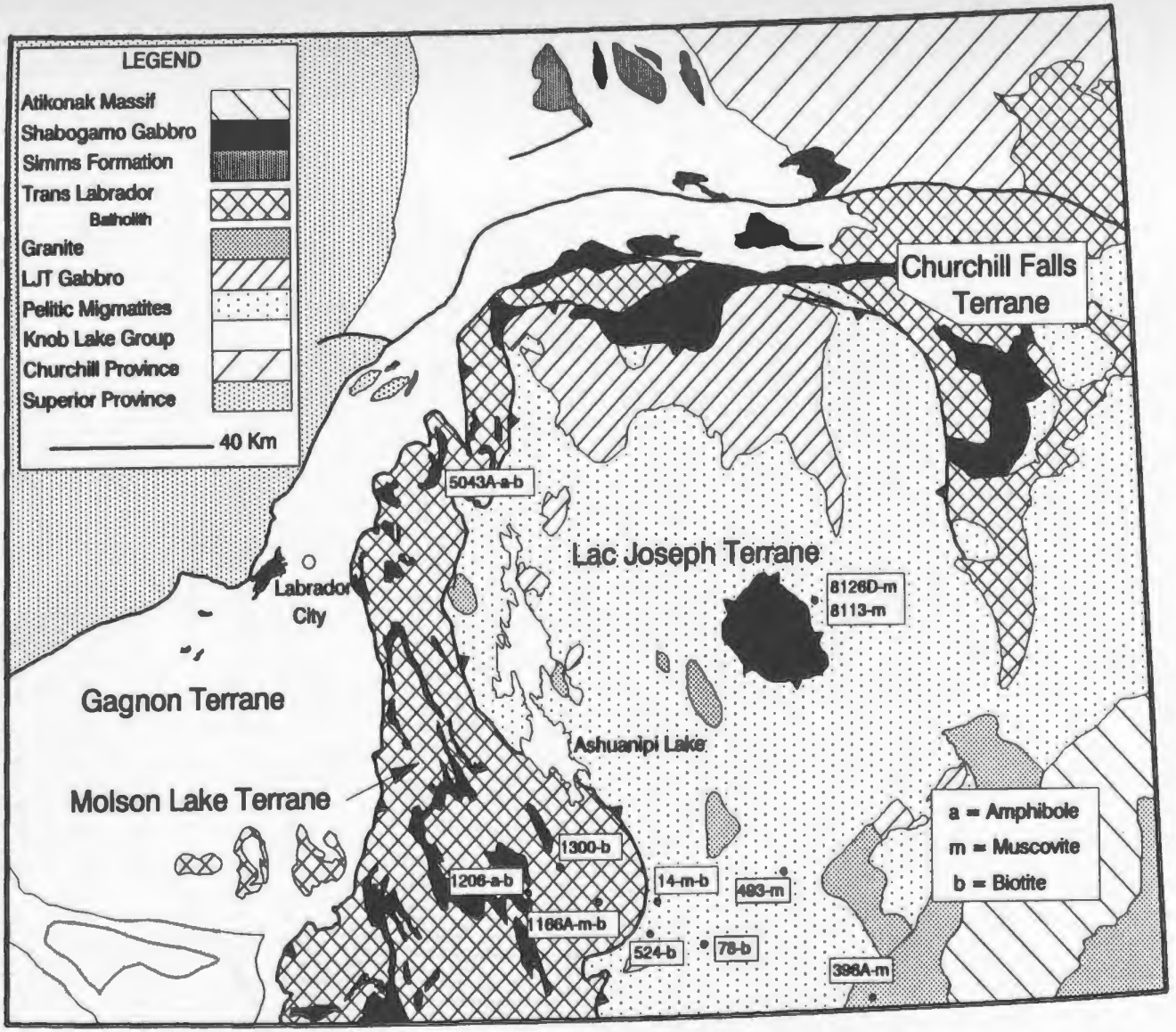

Figure 7-1: Location of samples utilized for 40Ar/39Ar geochronology. Sample numbers are prefixed by JNC-86 or JNC-87. The suffixes a, m and b refer to the amphibole, muscovite and biotite phases used for 40Ar/39Ar analyses.

7.2.1 Amphibolite Facies Retrogression: JNC-86-524

Hornblende from the same sample (JNC-86-524) which yielded titanite for U-Pb analysis (Fig. 7-1) was analyzed in order to obtain independent confirmation of the 1281 Ma age for amphibolite facies retrogression, and also to constrain the maximum Grenvillian temperatures in the Lac Joseph Terrane. Apart from a small amount of "excess" Ar in the first two heating steps, hornblende from this sample yielded a well-defined plateau age of 1263±4 Ma (Fig. 7-2).

This 1263±4 Ma age is 18 Ma younger than the U-Pb age from coexisting titanite. The near coincidence of the amphibole and titanite ages, both stable phases in the amphibolite facies assemblage, confirms that retrogression occurred at about 1281 Ma. The absence of any Grenvillian effects on argon systematics in the hornblende implies that temperatures during the Grenvillian Orogeny did not exceed ca. 530°C (the closure temperature for Ar in hornblende) in the southern Lac Joseph Terrane (Harrison and McDougall, 1980)

7.2.2 Muscovite and Biotite from the Retrogressed Margin of the Lac Joseph Terrane: JNC-86-14.

The spatial relationship between the zone of foliated, retrogressed muscovite-bearing metapelites and the southwest margin of the Lac Joseph Terrane raised the question as to whether the retrogression was related to the emplacement of the Lac Joseph Terrane over the Molson Lake Terrane during the Grenvillian Orogeny (see Section 4.2.6.1). Muscovite was extracted from sample JNC-86-14, from which zircon and monazite were also analyzed for U-Pb geochronology (Fig. 6.7). Muscovite shows slight excess argon in the first two steps, with the steps 3 and 4 defining a plateau age of about 991±6 Ma (Fig. 7-3). Coexisting biotite also shows a reasonable plateau with a slightly disturbed spectrum, but the plateau age of 1165±4 Ma (Fig. 7-3; steps 4 and 5), older than that of coexisting muscovite, is interpreted to be a consequence of excess argon and is therefore regarded as geologically meaningless.

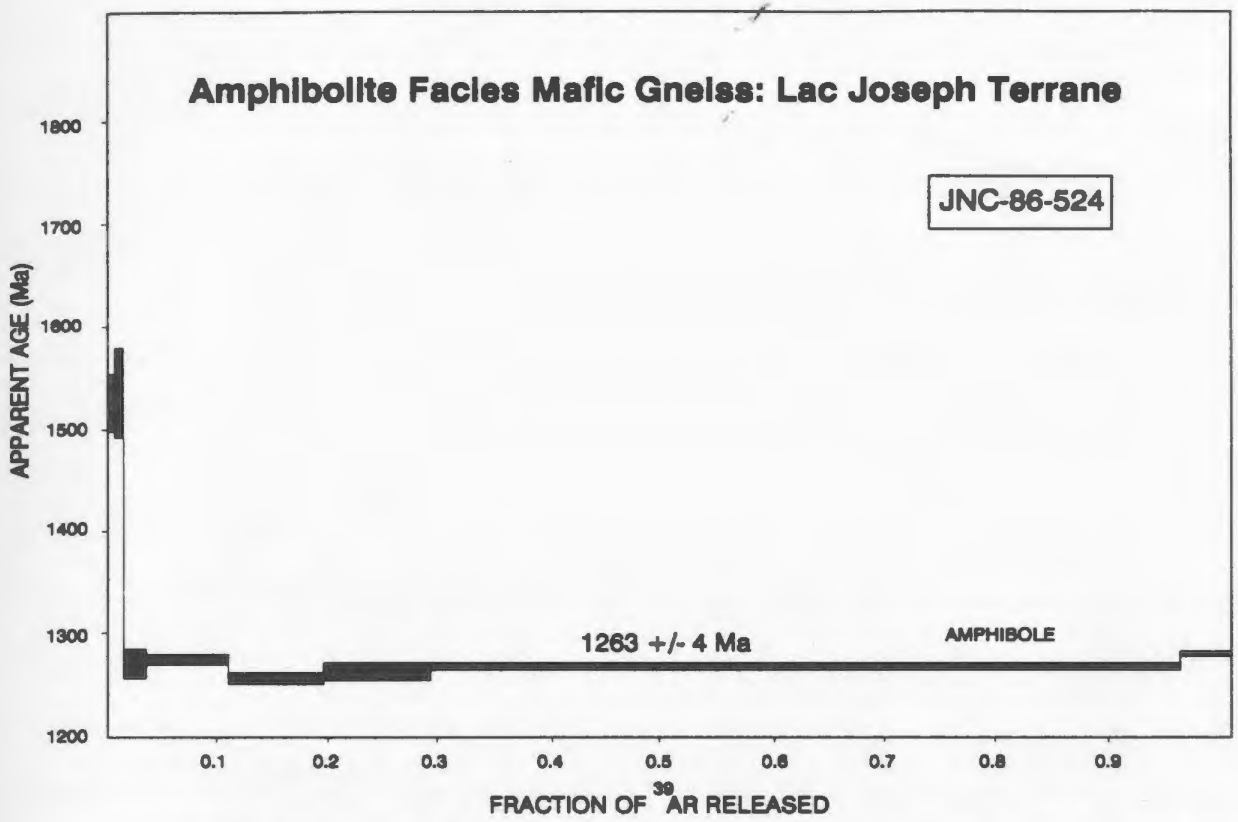

Figure 7-2: Incremental Ar release spectrum for amphibole from sample JNC-86-524

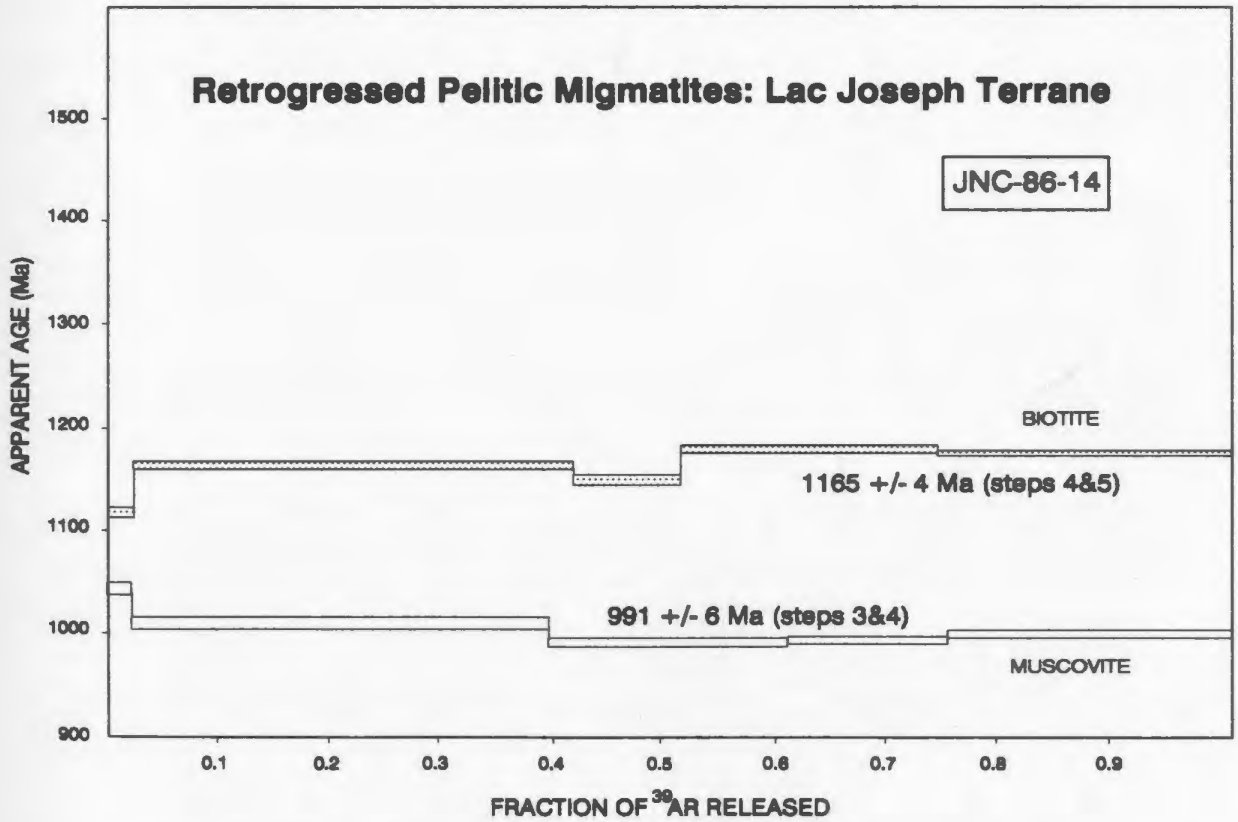

Figure 7-3: Incremental Ar release spectra for biotite and muscovite in sample JNC-86-14.

The 991 ± 6 Ma plateau age for muscovite implies that it either formed at this time or the ambient temperature fell below the Ar closure temperature for muscovite at this time, either interpretation requiring that temperatures were elevated in this zone during the Grenvillian Orogeny. Considering the location of the sample at the structural base of the Lac Joseph Terrane, the preferred interpretation is that the aligned muscovite formed syntectonically at this time and that heat and fluids required for the retrograde reaction were transferred from the underlying Molson Lake Terrane. This interpretation is consistent with the 995 Ma U-Pb age for the mylonitization in the Lac Emerillon boundary shear zone.

7.2.3 Muscovite from a Grenvillian Dyke from the boundary of the Terrane Boundary: JNC-86-8126D

A foliated granitic dyke which cuts across the gneissic layering near the structural base of the Lac Joseph Terrane has been dated at 999 + 5/-3 Ma by U-Pb methods. Muscovite from this dyke was analyzed in order to assess post-Grenvillian cooling rates along the base of the Lac Joseph Terrane by comparing $^{40}Ar/^{39}Ar$ and U-Pb ages. Muscovite yields an $^{40}Ar/^{39}Ar$ plateau age of about 963 ± 6 Ma (Fig. 7-4), implying that Ar closure occurred about 36 m.y. after crystallization.

7.2.4 Muscovite and Biotite from the Interior of the Lac Joseph Terrane: JNC-86-78, JNC-86-493 and JNC-86-396A.

Several mica fractions from the interior of the Lac Joseph Terrane were analyzed for $^{40}Ar/^{39}Ar$ to determine whether the Grenvillian thermal overprint recorded at the terrane margin was also present in the interior of the terrane. Muscovite and/or biotite were separated from three samples, none of which were analyzed for U-Pb geochronology. Sample JNC-86-78 is a sillimanite - biotite - garnet - magnetite-bearing pelitic migmatite, typical of the interior of the Lac Joseph Terrane. Sample JNC-86-493 is a muscovite-bearing pelitic migmatite from the southeastern Lac Joseph Terrane in which muscovite is randomly oriented; on the basis of field relationships, the muscovite was interpreted to have formed in a contact metamorphic aureole around the

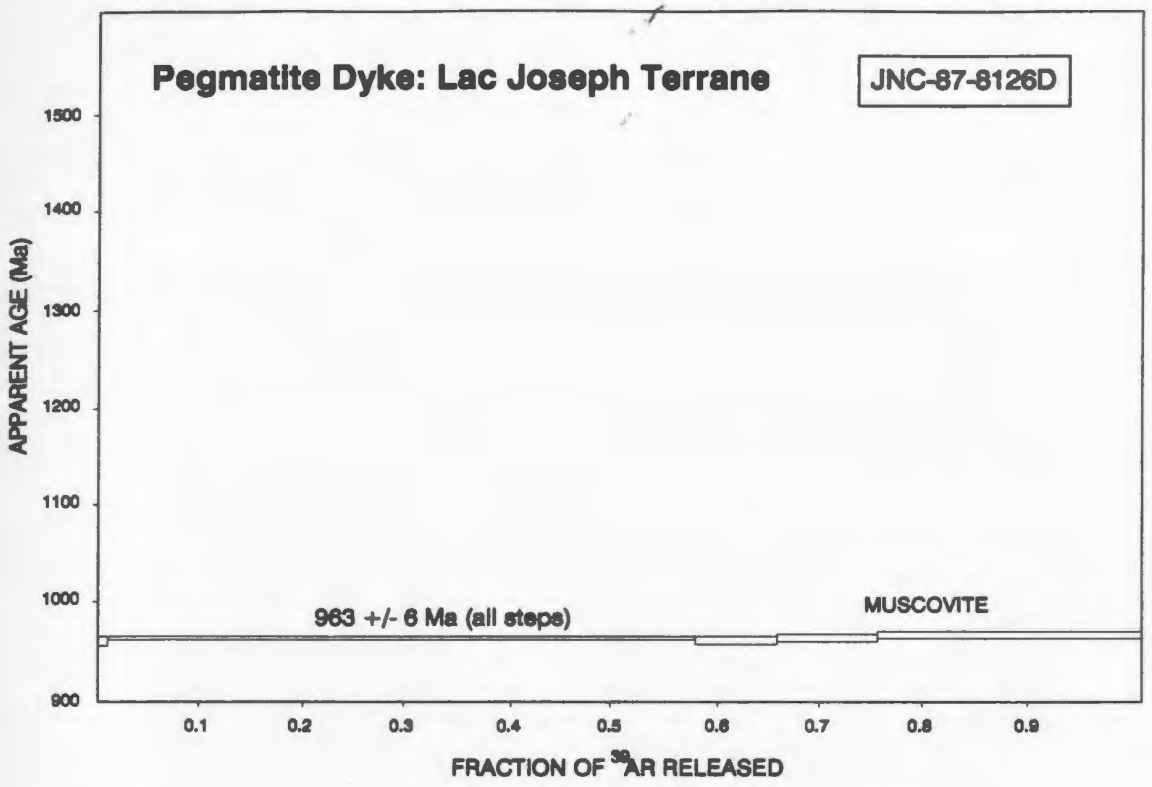

Figure 7-4: Incremental Ar release spectrum for muscovite for sample JNC-87-8126D.

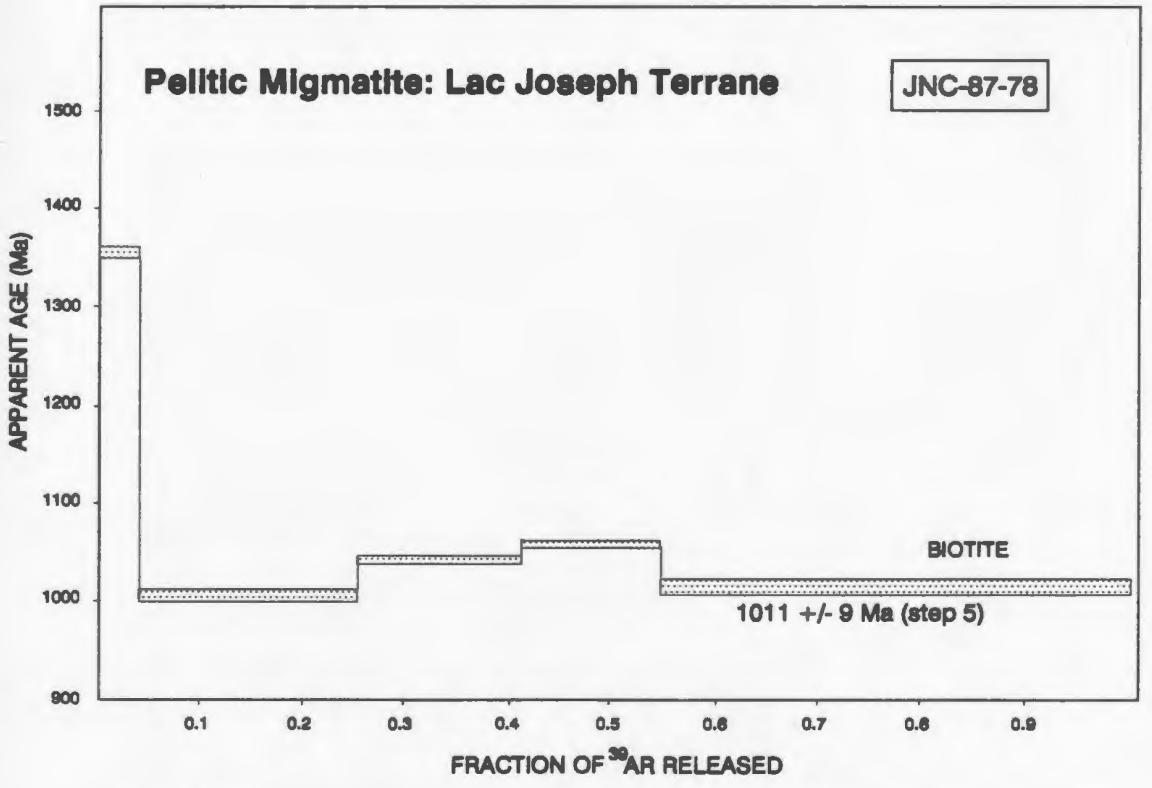

Figure 7-5: Incremental Ar release spectrum for biotite from sample JNC-87-78

1133+10/-5 Ma Fleur-de-Mai granite around the Atikonak Massif (Emslie and Hunt, 1990). Sample JNC-86-396A is a late, muscovite-bearing pegmatite which cross-cuts the gneissic layering in the migmatites.

Biotite from the Labradorian restite assemblage in sample JNC-86-78 yielded a disturbed spectrum step and five yielding a plateau age of 1011±9 Ma (Fig. 7-5). This disturbed spectrum may be due to excess Ar in the biotite or the biotite may have formed earlier, possibly during the Labradorian Orogeny, but lost Ar during the Grenvillian Orogeny. Muscovite fractions from samples JNC-86-396 and JNC-86-493 give very good plateau ages of 937±6 and 974±4 Ma respectively (Fig. 7-6), with only a small proportion of excess argon in the first step of the latter sample.

The muscovite ages from the interior of the Lac Joseph Terrane thus imply that ambient temperatures had fallen below about 350°C, the closure temperature of Ar in muscovite (Harrison and McDougall, 1982), by 937-974 Ma. The 37 m.y. range suggests that cooling through the closure temperature was rather slow. The older age for biotite than for muscovite, even though the two minerals were not from the same samples, again raises the possibility of excess Ar in biotite. Another implication is that cooling was heterogeneous throughout the Lac Joseph Terrane.

7.3 The Molson Lake Terrane

Biotite, muscovite and amphibole fractions from the Molson Lake Terrane were analyzed in order to constrain the timing and rate of post-Grenvillian uplift. $^{40}Ar/^{39}Ar$ spectra from the southern Molson Lake Terrane are typically concordant and contrast with disturbed spectra from the northern domain; the two areas will be presented separately.

7.3.1 Southern Molson Lake Terrane

Muscovite, amphibole and/or biotite fractions from three samples from the southern Molson Lake Terrane have been analyzed for $^{40}Ar/^{39}Ar$. Samples JNC-86-1206 and JNC-86-1300 were collected in the amphibolite facies zone 2, and contain the accessory minerals biotite, hornblende and epidote; JNC-86-1300 is the only

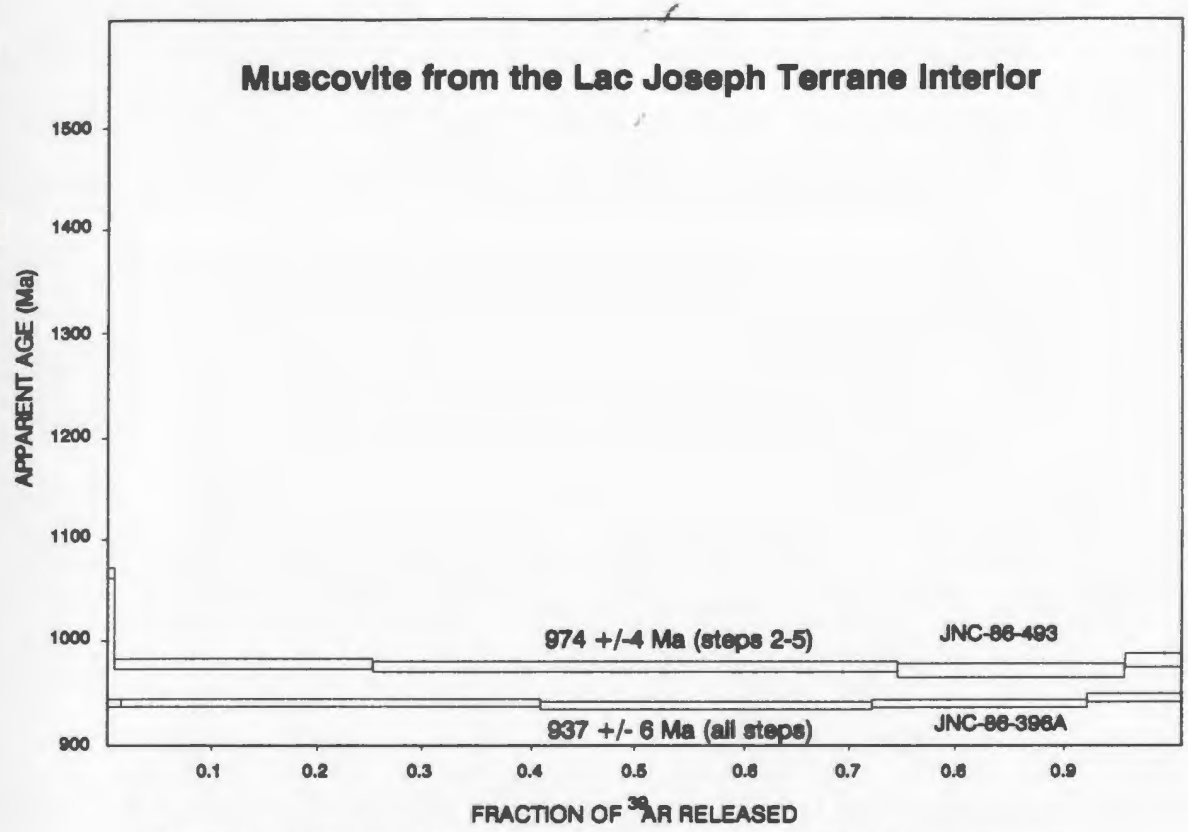

Figure 7-6: Incremental Ar release spectra for muscovite from samples JNC-86-493 and 396A.

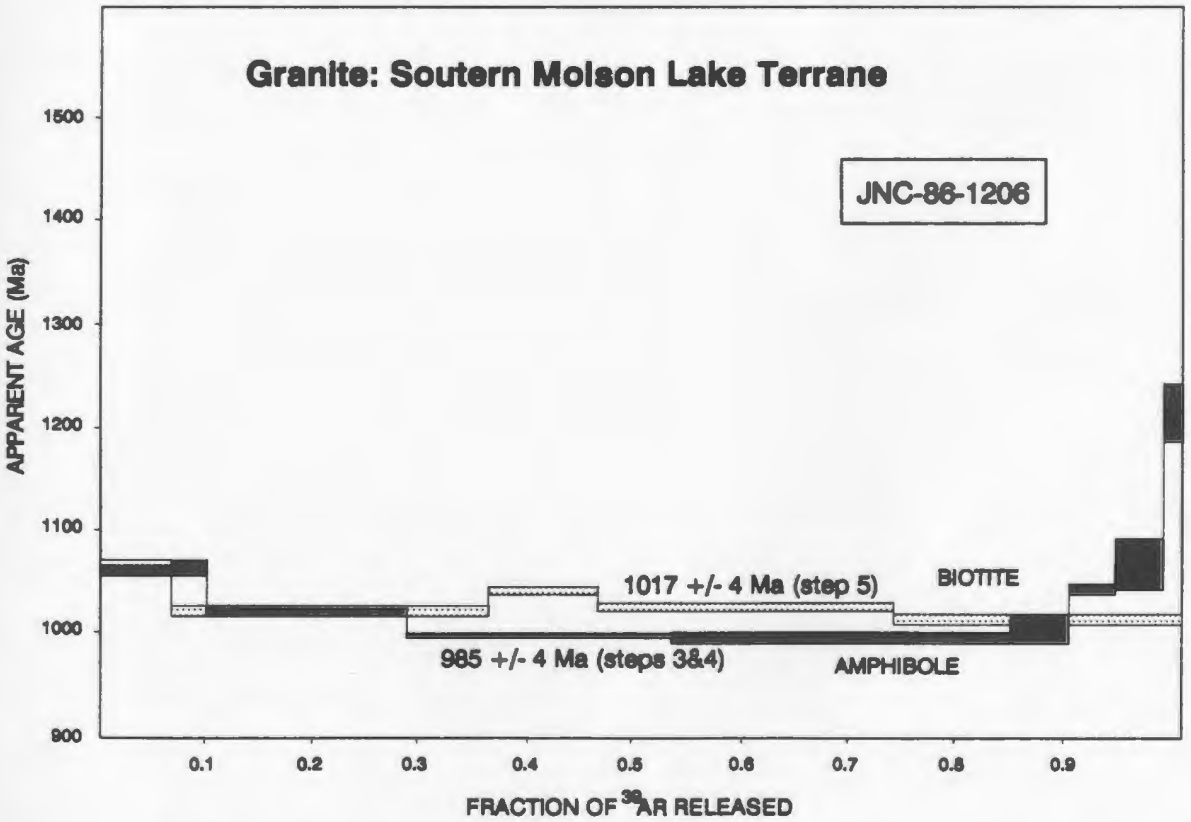

Figure 7-7: Incremental Ar release spectra for hornblende and biotite from sample JNC-86-1206.

sample from the southern Molson Lake Terrane which was also analyzed for U-Pb geochronology. Sample JNC-86-1166A comes from the upper greenschist facies zone 1 and contains biotite, muscovite and epidote, as accessory minerals.

$^{40}Ar/^{39}Ar$ ages from muscovite and amphibole in the southern Molson Lake Terrane are in agreement at 985±4 and 989±6 Ma respectively (samples JNC-86-1206 (amphibole), Fig. 7-7; and JNC-86-1166A (muscovite), Fig. 7-8). Two of three biotite fractions (JNC-86-1206 and 1166A) from the southern Molson Lake Terrane yield spectra exhibiting slight inverse discordance with respect to the coexisting amphibole and muscovite (Figs. 7-7 and 7-8). A third biotite fraction from this area (JNC-86-1300) yields a well-defined plateau age of 997±6 Ma (Fig. 7-9).

Fractions yielding biotite ages older than those of muscovite and amphibole are interpreted to indicate the presence of excess argon; biotite ages from these samples are therefore geologically meaningless. The 997±6 Ma age for biotite from sample JNC-86-1300 from the southern Molson Lake Terrane may be a reasonable estimate of the time of closure of the biotite lattice to Ar. However, since the common tendency of biotite to incorporate excess argon during metamorphism in high grade terranes is well established (eg. Dallmeyer and Rivers, 1983), it is clear that caution is warranted when interpreting spectra for this mineral.

The muscovite and amphibole fractions yielded age estimates that are within error of the U-Pb ages for mineral recrystallization in the Molson Lake Terrane, implying that cooling through the closure temperatures of Pb in titanite and Ar in amphibole and muscovite occurred in less than 10 to 15 m.y.

7.3.2 Northern Molson Lake Terrane: JNC-87-5043B

Biotite and amphibole fractions separated from sample JNC-87-5043B from the Lac Emerillon shear zone were analyzed to determine the time interval between the closure of U-Pb and $^{40}Ar/^{39}Ar$ isotopic systems.

The amphibole spectrum is saddle shaped with an plateau age of 1083±6 Ma for the lowest step, whereas biotite yielded a very good plateau at 1158±4 Ma (Fig. 7-10). The shape of the amphibole spectrum and comparison with the U-Pb age from

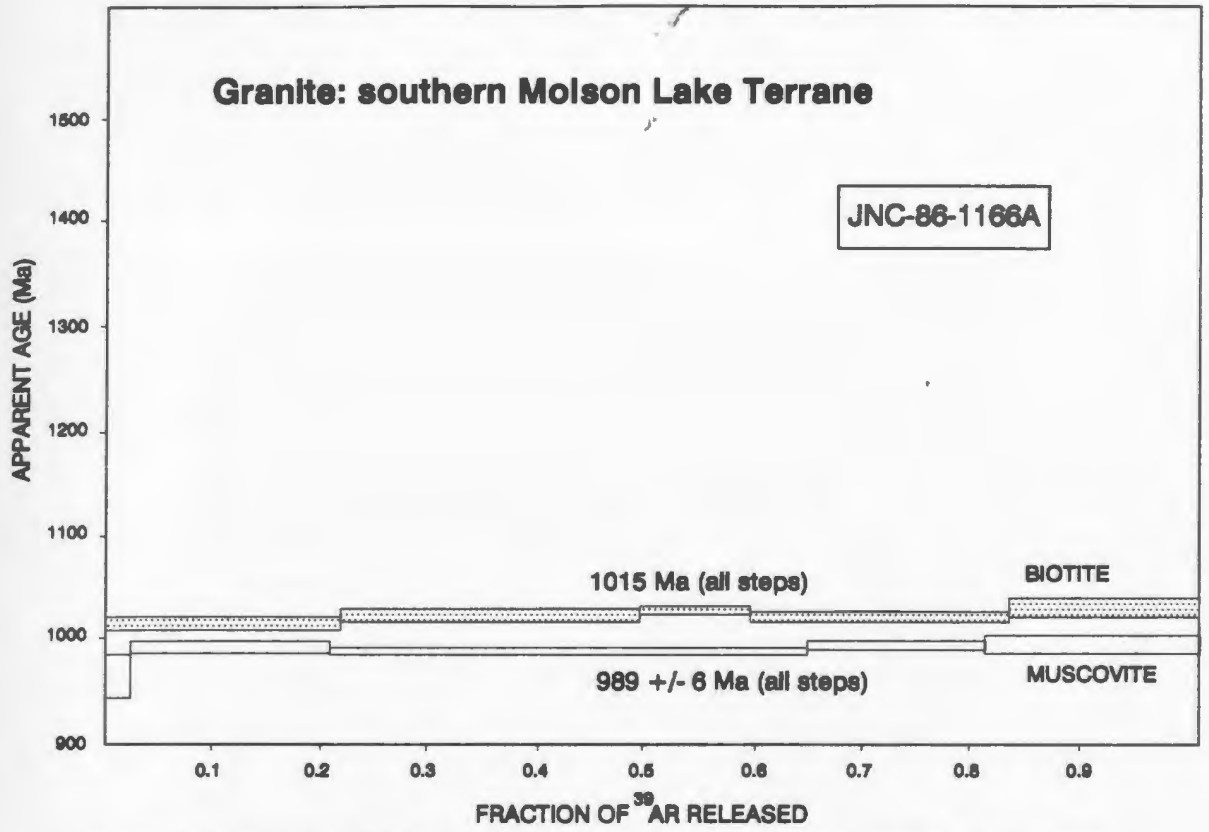

Figure 7-8: Incremental Ar release spectrum for biotite and muscovite for sample JNC-86-1166A.

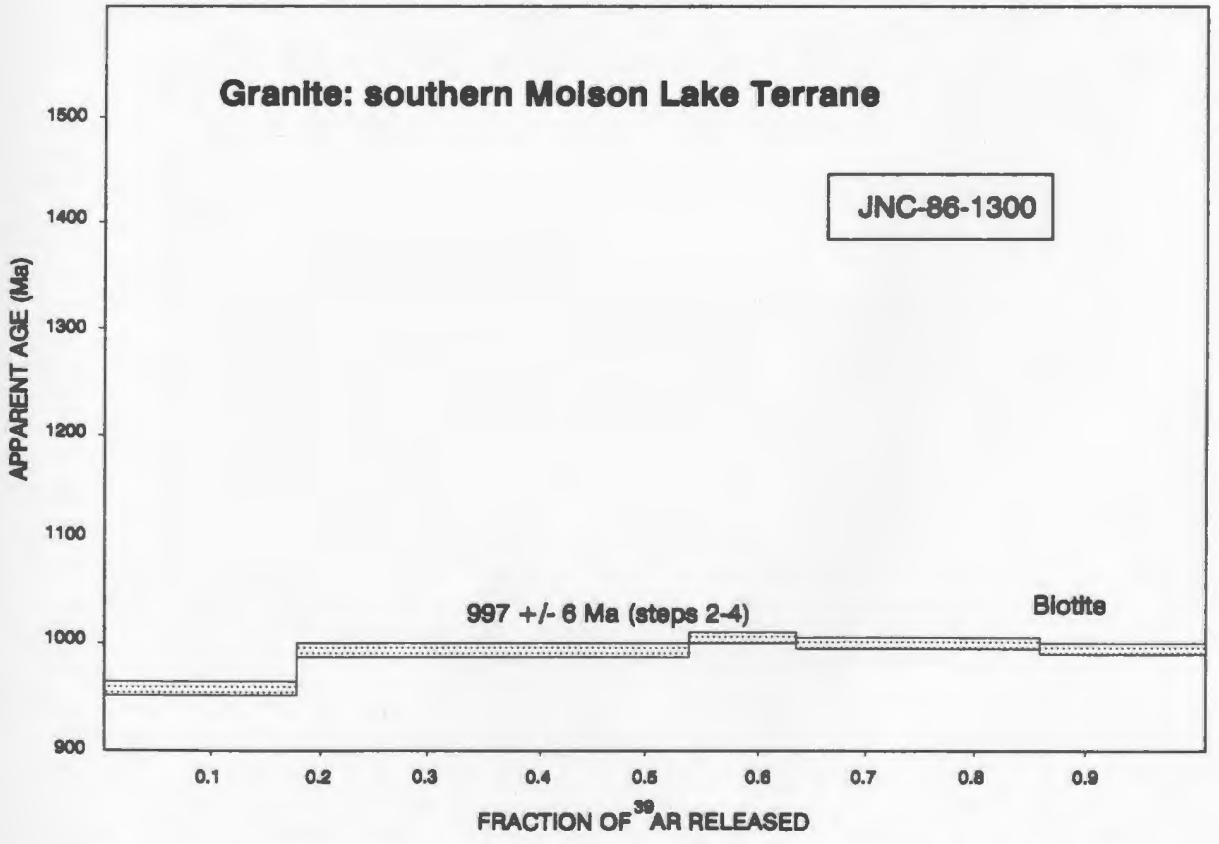

Figure 7-9: Incremental Ar release spectrum for biotite for sample JNC-86-1300.

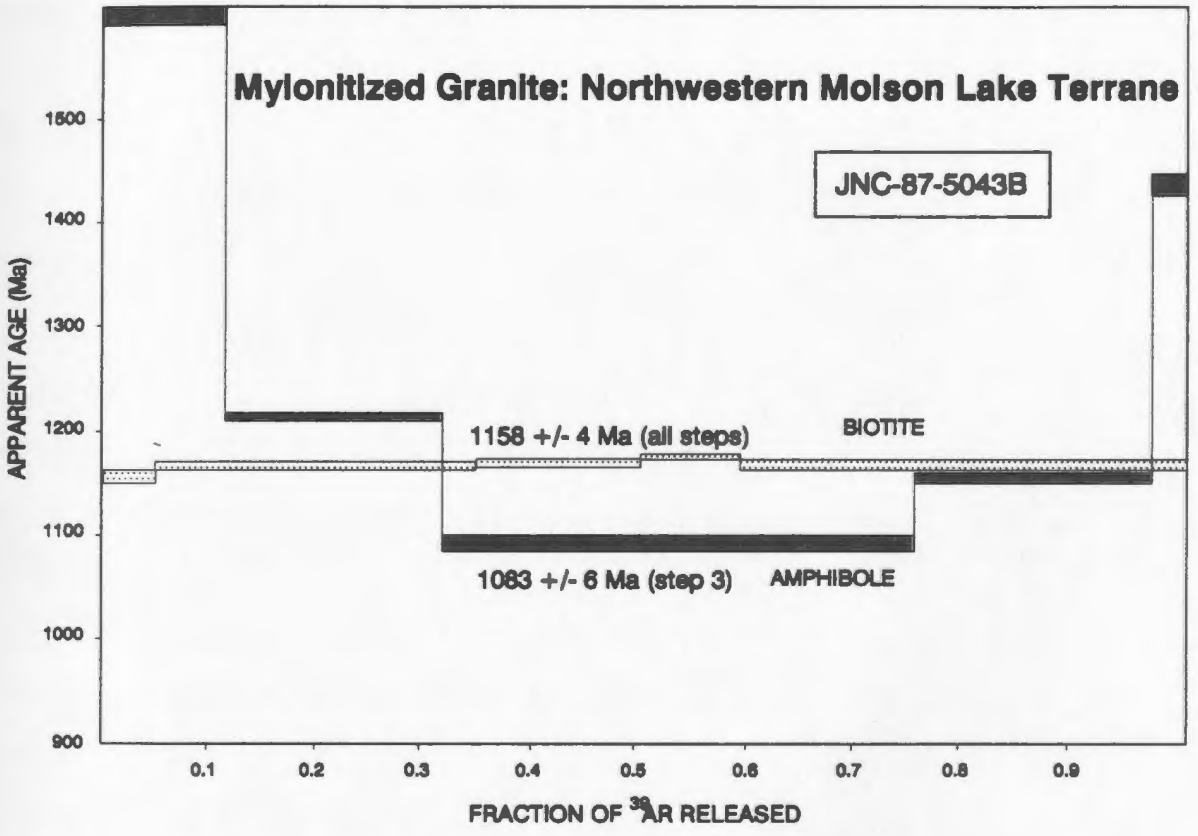

Figure 7-10: Incremental Ar release spectra for amphibole and biotite from sample JNC-87-5043B.

coexisting titanite (990±12 Ma, Fig. 6-11), indicates that the amphibole fraction contained excess argon. It is interesting to note however, that the highest temperature step in the amphibole spectrum yielded an age of 1440 Ma, an age comparable to the crystallization of the Shabogamo Intrusive Suite at 1431±7 Ma (from U/Pb data). It is therefore, not clear whether amphibole contains a small component of inheritance, in addition to the excess Ar which is obvious in the lower temperature steps of the spectrum. Although the biotite spectrum shows no independent evidence of excess argon, its comparison with the amphibole spectrum and U/Pb titanite data points to an interpretation of excess Ar. The excess Ar in this sample therefore, precludes useful interpretations of these $^{40}Ar/^{39}Ar$ ages and so they will not be utilized further.

7.3.3 Previous $^{40}Ar/^{39}Ar$ Data from the Gagnon Terrane

The work of Dallmeyer and Rivers (1983) in western Labrador, principally in what is now known as the Gagnon Terrane, yielded results comparable to this study. Biotite typically exhibited excess argon and therefore yielded inversely discordant ages relative to co-existing amphibole. The amphibole plateau ages ranged between 968 Ma and 905 Ma, consistently younger than amphibole and muscovite ages in the adjacent Molson Lake Terrane. This implies that cooling must have been diachronous across the parautochthonous terranes late in the Grenvillian Orogeny, with temperatures in the Molson Lake Terrane reduced below the closure temperature for Ar in amphibole before those in the Gagnon Terrane.

7.4 Summary of $^{40}Ar/^{39}Ar$ Ages: Molson Lake and Lac Joseph Terranes

The $^{40}Ar/^{39}Ar$ data presented above complement the U-Pb data by confirming ages of some of the metamorphic events and yielding information about other lower temperature events that are not recorded by the U-Pb systematics. They thus contribute several critical pieces of information towards the tectonic model for the Grenville Province in western Labrador.

The $^{40}Ar/^{39}Ar$ data confirm the U-Pb results that the southwestern part of the Lac Joseph Terrane was subjected to an amphibolite facies retrogression event at about 1281 Ma. However, as noted previously, the areal extent of this event and its tectonic

significance are both presently unknown. $^{40}Ar/^{39}Ar$ data from the Lac Joseph Terrane imply that the peak ambient Grenvillian temperatures must have been between about 350°C and 530°C in the interior of the terrane that is, they were above the closure temperature of Ar in muscovite but below that of Ar in amphibole.

Those $^{40}Ar/^{39}Ar$ ages from muscovite, biotite and amphibole separates from granitoid rocks of the Molson Lake Terrane which do not contain excess argon, confirm the conclusions drawn from the U-Pb results that this terrane was metamorphosed and penetratively deformed during the Grenvillian Orogeny. The similarity between U/Pb ages of 1001 Ma to 990 Ma (defined by the lower intercept with concordia of mixing lines defined by zircon, and by the ages of titanite and rutile) and the $^{40}Ar/^{39}Ar$ ages for biotite and muscovite of about 995 Ma to 985 Ma, imply that the Molson Lake Terrane must have cooled rapidly after peak Grenvillian metamorphism.

The presence of syntectonic muscovite dated at 991 ± 6 Ma along the margin of the Lac Joseph Terrane is independent evidence supporting the U-Pb results which suggests that the Lac Joseph Terrane was emplaced over the Molson Lake Terrane at about this time.

The similarity of $^{40}Ar/^{39}Ar$ ages of muscovite from the Molson Lake Terrane and the southwestern margin of the Lac Joseph Terrane suggests that the two areas cooled through the closure temperature of Ar in muscovite at about the same time and may therefore have experienced a comparable cooling history during the late Grenvillian Orogeny. This contrasts with the results from the interior of the Lac Joseph Terrane, which apparently experienced elevated temperatures until as late as 937 ± 6 Ma (the youngest muscovite age), suggesting either that cooling rates were slower or that cooling began later in that area.

Upward heat transfer from the Molson Lake Terrane to the Lac Joseph Terrane during the Grenvillian Orogeny is interpreted to have caused sufficient increase in temperature such that Ar isotopic ratios in biotite and muscovite were reset, whereas those in amphibole were apparently not affected. Superficially, this interpretation is not easy to reconcile with the inference that the structural base of the Lac Joseph Terrane

cooled through the closure temperature of Ar in mica earlier than the interior of the terrane. Two explanations, which are supported by independent structural and petrological data, are possible: 1) given the evidence of thrust emplacement of the Lac Joseph Terrane over the Molson Lake Terrane, it is reasonable to suggest that cooling after the attainment of maximum temperature in the Lac Joseph Terrane was principally a result of exhumation of the leading edge along the frontal thrusts rather than being a result of isostatic uplift as probably occurred in the interior of the Lac Joseph Terrane; and/or 2) the widespread presence of retrograde muscovite along the base of the Lac Joseph Terrane attests to the presence of H_2O rich fluids, which may have resulted in the cooling of the base of the terrane before the anhydrous interior. The occurrence of hematite with muscovite in the retrograde assemblages is consistent with a meteoric source for the water, and with relatively low initial temperatures.

CHAPTER 8
TECTONIC MODELS

8.1 Introduction

Data presented in this thesis constrain the timing and conditions of thermotectonic events in the Grenville Province of western Labrador; this chapter begins with a review and summary of these constraints, discusses their implications, and follows with descriptions of a tectonic model for western Labrador which accommodates most of the available data.

8.2 Labradorian Orogeny

8.2.1 Lac Joseph Terrane: Labradorian Orogeny

Geochronological data from this and previous studies (for review of previous work, see Nunn et al. 1985) indicate that the terranes of the Polycyclic Allochthonous Belt in Labrador, including the Lac Joseph Terrane, experienced regional metamorphism, widespread mafic and granitic intrusive activity and penetrative, polyphase deformation during the Labradorian Orogeny.

8.2.1.1 Intrusive Rocks of the Lac Joseph Terrane

U-Pb ages of 1672 and 1619 Ma for granitoid rocks in the Lac Joseph Terrane (Krogh, 1983; Brooks, 1983) imply that granite emplacement took place over approximately 50 m.y. during the Labradorian Orogeny. Although only two granite bodies have been dated, the contact relationships with the Labradorian migmatites, the high state of strain and the similar fabric orientations to those in the host rocks suggests that much of the granitic plutonism in the Lac Joseph Terrane was Labradorian in age. On the basis of U/Pb data collected in this study, it can be stated that the Labradorian Orogeny extended from 1658 Ma to 1611 Ma.

A gabbronorite intrusion dated at 1623 ± 7 Ma (U-Pb, zircon and rutile; this study) has established that basic plutonism also occurred during the Labradorian Orogeny, but the extent of the time interval over which this suite was emplaced has yet to be established. The 1623 ± 7 Ma age is thought to be representative of the medium-grained, relatively undeformed, post-peak metamorphism, mafic intrusive

bodies which have not been extensively recrystallized. The occurrence of extensively recrystallized metabasites which have only relict igneous textures suggests that mafic magmas were also intruded before and/or during the thermal peak of the Labradorian Orogeny. Future refinements to the tectonic model of the Labradorian Orogeny in western Labrador will depend on resolving the age range of the early basic intrusions, their genetic links, if any, with the granitoid rocks and their contribution to the thermal budget during Labradorian metamorphism.

8.2.1.2 Metamorphism and Deformation of the Supracrustal Rocks of the Lac Joseph Terrane.

The intrusion of the earliest granitoid bodies was followed by regional partial melting of the host pelitic and basic supracrustal rocks; the oldest U/Pb date from the N_1 leucosomes in the metapelites is 1658+38/-10 Ma, which overlaps within error with a poorly constrained age of 1648 Ma for the metamorphism and partial melting of the basic gneisses. The N_1 leucosomes in the metapelites were folded prior to the formation of N_2 leucosomes (probably by injection), an example of which has been dated at 1639+12/-7 Ma.

F_2 folds typically deform the N_2 leucosomes implying that F_2 folding postdated the formation of N_2 leucosomes in the supracrustal rocks. Ductile mylonite zones in the supracrustal rocks, dated at 1634+13/-4 Ma, cut across both the N_2 leucosomes and F_2 folds, indicating that F_2 folding must have commenced by this time. The area continued to be subjected to thermal effects of the Labradorian Orogeny as late as 1611+13/-6 Ma, the youngest age determination for zircon and monazite from leucosomes of the pelitic migmatites from the southwest margin of the Lac Joseph Terrane. Although it is not possible to rule out the possibility that periods of crustal extension prevailed intermittently, the pre- and post-N_2 folding and mylonitization at 1634+13/-4 Ma suggests that the Labradorian Orogeny was principally compressional in character.

8.2.1.3 Development of Mineral Assemblages in the Supracrustal Rocks of the Lac Joseph Terrane.

In order to correlate P-T estimates from the restite assemblage in the migmatites of the Lac Joseph Terrane with a specific thermotectonic event, the age of crystallization and equilibration of the restite assemblage is required. Sillimanite and biotite are folded around F_{2J} folds and oriented parallel to the F_{2J} axial surfaces. This indicates that the sillimanite - biotite - garnet - magnetite assemblage in the restites crystallized both before and during the F_{2J} folding event. The syn-kinematic nature of this restite assemblage in the 1634+13/-4 Ma shear zone indicates that these minerals are Labradorian. Randomly oriented muscovite overprints sillimanite in a metamorphic aureole around the 1133+5/-5 Ma old Fleur-de-Mai granite (Emslie and Hunt, 1990) providing independent evidence that the sillimanite-bearing subassemblage is pre-Grenvillian.

Geothermobarometry, combined with U-Pb data which constrain the ages of the mineral assemblages, indicates that the southwest and northeast regions of the Lac Joseph Terrane were metamorphosed under pressures between 3 and 8 kbar and temperatures from 575 to 800°C during the Labradorian Orogeny. Pressure estimates in the northwestern domain of the Lac Joseph Terrane are between 6 and 10 kbar, with temperature estimates from 700 to 850°C. This indicates that pressure, and to a lesser extent temperature, increased along the present erosion surface from southeast towards the northwest in the Lac Joseph Terrane during the Labradorian Orogeny.

8.2.2 Molson Lake Terrane: Labradorian Orogeny

The Molson Lake Terrane comprises some Labradorian lithotectonic elements which are both similar to and distinct from those in the Lac Joseph Terrane. Although only a single U-Pb age of 1648±7 Ma is presently available from the granitic rocks of this terrane, it is proposed that the majority of granitoid rocks were formed during the Labradorian Orogeny, and were therefore emplaced synchronously with Labradorian migmatization and deformation in the Lac Joseph Terrane. These granites were not partially melted, recrystallized or penetratively deformed during the Labradorian

Orogeny and therefore lack Labradorian metamorphic assemblages, thus precluding determination of the P-T conditions in the Molson Lake Terrane at this time. The granites in the Molson Lake Terrane are interpreted to be a westerly continuation of the Trans Labrador Batholith, which has been dated by zircons between 1654 ± 11 Ma and 1635 Ma farther east (Krogh, 1983).

8.2.3 Churchill Falls Terrane: Labradorian Orogeny

The Churchill Falls Terrane contains tectonic and lithologic elements which are comparable to those in both the Molson Lake and Lac Joseph terranes. The southeastern part of the terrane is dominated by supracrustal, pelitic migmatites identical to those in the Lac Joseph Terrane, whereas the northern part of the Churchill Falls Terrane contains granite and gabbro comparable to rock units in the Molson Lake Terrane.

8.2.4 Gagnon Terrane: Labradorian Orogeny

The Gagnon Terrane comprises a pre-Labradorian continental margin sequence of supracrustal rocks which were deposited unconformably on the eastern edge of the Archean Superior Province. Labradorian fabrics have not been identified in rocks of the Gagnon Terrane.

8.2.5 Lithotectonic Links Between the Terranes of Western Labrador During The Labradorian Orogeny

The similarity of the age of granite emplacement in the Molson Lake Terrane and the age of migmatization and igneous activity in the Lac Joseph Terrane suggests that these two terranes were both affected by the Labradorian Orogeny and, by extension, may have been proximal to each other at this time. The occurrence in the Churchill Falls Terrane of lithologies characteristic of the Molson Lake and Lac Joseph terranes (Nunn et al., 1984; Nunn and Christopher, 1983), and the lack of evidence for Grenvillian shear zones between these lithologies implies that the Molson Lake and Lac Joseph terranes were proximal, if not juxtaposed, by the end of the Labradorian Orogeny.

The unconformable contact between the supracrustal rocks of the Gagnon Terrane with the Superior Province provides an unequivocal link to the pre-Labradorian, stable North American craton. The presence of satellite plutons of the Trans Labrador Batholith in the southwestern Churchill Province (Nunn et al., 1985), also part of the stable pre-Labradorian North American craton, indirectly establishes terrane linkage between the Gagnon Terrane and the Labradorian rocks in the Molson Lake, Churchill Falls and Lac Joseph terranes by the end of the Labradorian Orogeny.

The establishment of a link between the Gagnon and other terranes of western Labrador during the Labradorian Orogeny leads to two possible conclusions: 1) as the foreland to the Labradorian Orogeny, the Gagnon Terrane was northwest of the Labradorian thermotectonic front; or 2) although not yet recognized, the Gagnon Terrane was deformed during the Labradorian Orogeny. Although this study has no new information to further address this question, it seems probable, given the scale and intensity of the Labradorian Orogeny in adjacent terranes, the Gagnon Terrane may have been at least locally affected by the Labradorian Orogeny. Brown (1991) reported the existence of fabrics in the Gagnon Terrane, north of Ossokmanuan Lake, which are cross-cut by dykes of the Shabogamo Intrusive Suite, thus establishing the existence of at least one generation of pre-1431 $\pm$7 Ma fabrics. However, he interpreted this fabric to have been generated during the Hudsonian Orogeny rather than the Labradorian Orogeny.

8.3 The Interval Between the Labradorian and Grenvillian Orogenies

8.3.1 Lac Joseph Terrane

It has been determined by U-Pb and $^{40}Ar/^{39}Ar$ geochronology that the Lac Joseph Terrane was affected by two recrystallization events, both of unknown areal extent, in the time interval between the Labradorian and Grenvillian orogenies.

Although the cause of the recrystallization of monazite at 1403 Ma is presently not understood, this age indicates that there must have been at least a localized thermal event at this time. The lack of any established relationship between the monazites which were analyzed and any other features (i.e. structural, metamorphic or mineralogical)

precludes a detailed interpretation of the tectonic significance of this age. The spatial association of this sample to the margin of the Lac Joseph Terrane may indicate that the southeastern margin of the Lac Joseph Terrane was active as early as 1403 Ma. That this monazite recrystallization age is close to the intrusion age of the Shabogamo Intrusive Suite invites speculation that the event responsible for the intrusion of this basic suite in the presently adjacent terrane may have affected the Lac Joseph Terrane. This would imply that the Lac Joseph and Molson Lake terranes were proximal at about this time.

Mafic granulites in the southwestern domain of the Lac Joseph Terrane experienced penetrative amphibolite facies retrogression producing titanite, which has yielded concordant U-Pb ages of ca. 1281 Ma. This is in good agreement with the $^{40}Ar/^{39}Ar$ 1260 Ma age for one fraction of amphibole from the same sample. Since both minerals can be related to the stable metamorphic assemblage, the age of the retrogression is confirmed to be ca. 1281 Ma. This age is similar to 1260 ± 5 and 1241 ± 3 Ma $^{40}Ar/^{39}Ar$ ages determined for amphibole in the Groswater Bay and Lake Melville terranes of the eastern Grenville Province (van Nostrand, 1988). Although further work is required to determine the spatial extent of the amphibolite facies retrogression in western Labrador, it would appear that this event may have had regional significance. On the other hand, if the retrogression is restricted to the margin of the Lac Joseph Terrane, it would provide additional evidence to indicate that the terrane boundary has experienced a long history of tectonothermal activity.

8.3.2 Parautochthonous Terranes: Molson Lake, Churchill Falls and Gagnon Terranes

Gabbroic rocks of the Shabogamo Intrusive Suite were emplaced as dykes and irregular bodies into the Molson Lake, Churchill Falls and Gagnon terranes at 1431 ± 7 Ma. These rocks are equivalent in age and chemistry to the Michael Gabbro which intruded the terranes of the Parautochthonous Belt in eastern Labrador (Shärer, 1986; Gower et al., 1990). This unit thus provides the first direct lithological linkage between the Gagnon, Molson Lake and Churchill Falls terranes. The apparent anorogenic style of intrusion of the Shabogamo Intrusive Suite and correlative Michael Gabbro along a

linear belt which extends across Labrador, is compatible with the interpretation that the gabbros were intruded in a rifting environment. The absence of gabbros of the Shabogamo Intrusive Suite and correlative Michael Gabbro in the terranes of the Allochthonous Belt in Labrador, including the Lac Joseph Terrane, suggests that these terranes were distal to the rifting zone at this time.

8.4 The Grenvillian Orogeny

8.4.1 Lac Joseph Terrane: Grenvillian Orogeny

Although the lower intercepts of the discordia lines are poorly defined, U-Pb analyses of four migmatite samples from the Lac Joseph Terrane indicate that Pb was lost from zircon and monazite in the period between 1000 and 1070 Ma. The similarities of these lower intercept ages with the generally recognized age of the Grenvillian Orogeny suggests that Pb was lost in response to increased temperatures during Grenvillian metamorphism in the Lac Joseph Terrane at this time. The lack of significant resetting of the fractions analyzed indicates that the temperature increase during the Grenvillian Orogeny was either moderate or very brief.

A granitic dyke, dated by U/Pb methods at 999+5/-3 Ma, cuts across all structures and melt phases at the base of the Lac Joseph Terrane at Lac Joseph. The weak, single foliation in the dyke attests to the style of Grenvillian deformation in the Lac Joseph Terrane. This fabric is presumed to be correlative with the northwest-trending F_{3j} folds which are documented very locally in the Lac Joseph Terrane. The general lack of mineral recrystallization associated with this late folding event further attests to the low temperatures which prevailed in the Lac Joseph Terrane during the Grenvillian Orogeny.

The $^{40}Ar/^{39}Ar$ data provide the greatest constraints on the temperature conditions in the Lac Joseph Terrane during the Grenvillian Orogeny. The resetting of muscovite in the Lac Joseph Terrane between 980 Ma and 940 Ma suggests that temperatures reached a minimum of about 350°C throughout the terrane during the Grenvillian

Orogeny. However, the preservation of the 1281 Ma age from an amphibole fraction in the southwestern part of the Lac Joseph Terrane indicates that temperatures did not exceed about 530°C at that locality after 1281 Ma.

This study has determined, therefore, that the Lac Joseph Terrane was essentially assembled by the end of the Labradorian Orogeny. Although mineral recrystallization has been documented to have occurred sporadically during the period between the Labradorian and Grenvillian orogenies, there is no evidence to suggest that these post-Labradorian events created new crust or significantly altered the geometry of the Labradorian structures. Although there is no evidence of penetrative Grenvillian mineral recrystallization in the Lac Joseph Terrane, the results of geothermobarometry, U-Pb and $^{40}Ar/^{39}Ar$ analyses all independently indicate that this terrane was at least locally heated during the Grenvillian Orogeny. Upward heat transfer apparently occurred along the base where consistent evidence of phase disequilibrium was noted and contrasts with equilibrium phase relations in the interior of the terrane.

8.4.2 Molson Lake Terrane: Grenvillian Orogeny

Although only a minor amount of juvenile crust is known to have formed in western Labrador during the Grenvillian Orogeny (Connelly, unpub. U-Pb data), the Molson Lake Terrane was penetratively recrystallized and deformed during this event. Titanite and rutile crystallized between 990 - 1001 Ma, while Pb in zircons was partially to completely reset towards a lower intercept of similar age. $^{40}Ar/^{39}Ar$ ages from those samples of biotite and amphibole not containing excess Ar suggest that these minerals were closed to Ar between about 1020 and 995 Ma.

P-T conditions in the highest grade zone of the Molson Lake Terrane are estimated to have varied between 8-12 kbar with temperatures between 650 and 850°C. These estimates, from the southwestern part of the Molson Lake Terrane, are considered to represent the upper limits for the P-T conditions for this terrane in the study area. Lower grade assemblages towards the north and east suggest that, at least in the southern region, the crust is tilted towards the southeast. This is compatible with northwesterly-directed thrusting which would have resulted in tectonic transport of the

terrane over southeast-dipping ramps. F_{2M} folding of the mineral fabrics, and the development of ductile shear zones in the Molson Lake Terrane at this time, attest to the compressional nature of the Grenvillian Orogeny.

Construction of quantitative P-T-t paths requires that P-T estimates be constrained by independent estimates of the time at which the continuous reactions ceased. Only isotopic age determinations from minerals with closure temperatures known to correspond with a temperature estimated from geothermometry adequately defines an absolute age for that temperature estimate. The lower intercept age of 1001 ± 10 Ma defined by discordant zircon, with an estimated closure temperature of $> 800°C$ (Heaman and Parrish, 1991), indicates that temperatures were in excess of 800°C until this time. Since the temperature estimates in the southern Molson Lake Terrane range from 850 to 650°C, the rocks in this area are interpreted to have experienced the conditions defined by the upper segment of the cooling path at about 1001 ± 10 Ma. Since there are no isotopic age determination from minerals in the lower temperature estimates of the P-T path, no other absolute ages can be defined along the P-T path.

$^{40}Ar/^{39}Ar$ geochronology provides some constraints on the latter parts of the P-T-t paths. The coincidence of the $^{40}Ar/^{39}Ar$ muscovite and amphibole ages and the lower intercepts of the U-Pb discordia lines suggests that the Molson Lake Terrane experienced rapid cooling after the closure of Pb in zircon.

8.4.3 Timing of Assembly of the Lac Joseph and Molson Lake Terranes

An upper amphibolite facies shear zone in the Molson Lake - Lac Joseph terrane boundary fault system at Lac Emerillon has been dated by U-Pb methods at 995 ± 8 Ma, thereby establishing that amalgamation of the Molson Lake and Lac Joseph terranes took place during the Grenvillian Orogeny. It should be noted, however, that this age comes from a single locality in an anastomosing system of ductile shear zones, and that the cessation of movement across the system and the final emplacement of the Lac Joseph Terrane may have occurred at different times in different localities along and across the shear zone.

Additional evidence concerning the timing of juxtaposition of the Lac Joseph and Molson Lake terranes comes from the dating of syntectonic muscovite from the retrogressed pelitic gneisses in the southwestern margin of the Lac Joseph Terrane, which has yielded an $^{40}Ar/^{39}Ar$ age of 998 Ma. This independent line of evidence is consistent with the U-Pb age from the Lac Emerillon shear zone, and thereby supports the interpretation that the juxtaposition of the two terranes occurred during the Grenvillian Orogeny. The similarity of the U-Pb and $^{40}Ar/^{39}Ar$ ages from widely separated localities on the terrane boundary suggests, but does not prove, that cooling following tectonic emplacement of Lac Joseph Terrane on the Molson Lake Terrane was rapid.

8.4.4 Heat and/or Fluid Transfer During Grenvillian Terrane Amalgamation

The preservation of pre-Grenvillian phase equilibria, hornblende $^{40}Ar/^{39}Ar$ ages, U-Pb zircon and monazite ages, together with the lack of penetrative deformation in the Lac Joseph Terrane during the Grenvillian Orogeny, attest to the modest temperatures that were achieved in this terrane during this event. There is no evidence to suggest that the Lac Joseph Terrane underwent regional recrystallization during the Grenvillian Orogeny. The preferential distribution of Grenvillian muscovite along the structural base of the Lac Joseph Terrane, together with the observation that most of the Labradorian mineral assemblages which show evidence of disequilibrium in their mineral chemistry also come from near the structural base of the terrane, suggests that heat, and probably fluids, were transferred to the Lac Joseph Terrane from the underlying Molson Lake Terrane. The coincidence of the estimated age of shearing along the marginal Lac Emerillon shear zone with the $^{40}Ar/^{39}Ar$ age of syntectonic muscovite, retrogressed from sillimanite, at the base of the Lac Joseph Terrane, indicates that heat/fluid transfer occurred as the Lac Joseph Terrane was emplaced over the Molson Lake Terrane during the Grenvillian Orogeny.

The limited extent of recrystallization in the Lac Joseph Terrane during the Grenvillian Orogeny must be explained. Two possible explanations are given here, both involving the late tectonic emplacement of the Lac Joseph Terrane on the Molson Lake Terrane: (a) emplacement of the Lac Joseph Terrane continued after the peak

metamorphic conditions in the Molson Lake Terrane, such that the leading edge of the Lac Joseph Terrane acted as a major heat sink as it moved over the Molson Lake Terrane; or (b) the emplacement of the Lac Joseph Terrane was late, occurring after the Molson Lake Terrane had been partially uplifted and cooled. Although each of these models is superficially attractive, neither satisfactorily accounts for all the data. Model (a) would require that there was extensive Grenvillian recrystallization of the leading edge of Lac Joseph Terrane, evidence of which is lacking (although it may have existed above the present erosion surface). Model (b) necessitates the existence of significantly younger ages for the terrane boundary shear zone than for the regionally metamorphism of the Molson Lake Terrane. Available data indicate the terrane boundary shear zone was active at 990 ± 12 Ma and became closed to Ar at about this time, and that metamorphism of the Molson Lake Terrane took place between 1001-990 Ma, essentially synchronous within the limits of resolution of the data. However, the similarity between the U-Pb and $^{40}Ar/^{39}Ar$ ages in the Molson Lake Terrane does indicate that exhumation and cooling were rather rapid such that the time interval between peak metamorphism in the Molson Lake Terrane and the final emplacement of the Lac Joseph Terrane may have been minimal. This observation is consistent with model (b) but does not prove it.

8.4.5 Summary of the Grenvillian Orogeny in Western Labrador

The thermal peak of the Grenvillian Orogeny in western Labrador took place prior to 1001 ± 10 Ma (the oldest Grenvillian lower intercept of a discordia line defined by zircon from the Shabogamo Intrusive Suite in the Molson Lake Terrane) approximately coeval with large-scale crustal shortening of all the terranes in the Parautochthonous Belt. The manifestations of this orogeny vary considerably across the preserved remnants of the Parautochthonous Belt: i.e. fold and thrust tectonics in the supracrustal rocks of the Gagnon Terrane; penetrative deformation, recrystallization and associated folding in the Molson Lake and Churchill Falls terranes; and major shear zones along terrane boundaries. The Molson Lake Terrane was rapidly exhumed and cooled after peak metamorphism.

The Lac Joseph Terrane was apparently emplaced over the Molson Lake and Churchill Falls terranes late in the Grenvillian Orogeny as a pre-assembled package and experienced heating to 350°C to 530°C and mild internal folding, with penetrative recrystallization and hydration only along its structural base. Labradorian phase equilibria and thermally robust isotopic systems were not significantly disturbed in the interior of the Lac Joseph Terrane at this time. A minimum transport distance of approximately 120 km for the Lac Joseph Terrane relative to the underlying Molson Lake and Churhill Falls terranes would account for the distance between the southeast margin of the central tectonic window and its present northwestern leading edge.

8.5 Tectonic Models

8.5.1 Pre-Labradorian Geometry

The spatial superposition of two major thermotectonic events, the Labradorian and Grenvillian Orogenies, along the southeastern margin of the North American craton renders an accurate account of the tectonic configuration prior to the onset of the Labradorian Orogeny difficult. However, it is clear that in Labrador, dramatic lithological, structural and metamorphic differences are preserved in the pre-Labradorian margin of North America. Western Labrador, dominated by an Early Proterozoic shelf sequence which originally rested unconformably on the margin of the Archean Superior Province, underwent crustal shortening and metamorphism during the Early Proterozoic Hudsonian Orogeny. Subdivisions of the southern Churchill Province trend north-south into the presumed former location of the Labradorian orogenic front. Further east the reworked Archean and juvenile Early Proterozoic supracrustal and plutonic rocks of the Makkovik Province, all with northeast-trending tectonic fabrics, are intruded by the Trans Labrador Batholith. This diverse structural and lithological character of the pre-Labradorian stable craton contrasts strongly with the continuity of the pelitic supracrustal and associated plutonic rocks which exist in a 700 km long belt in the present Grenville Province of Labrador. The lack of any known lithological link between the high grade Labradorian terranes and the craton prior to 1670 Ma strongly implies that the supracrustal rocks in the Labradorian terranes were exotic with respect to North America prior to the Labradorian Orogeny.

8.5.2 Labradorian Orogeny

The Labrador Orogen in western Labrador is characterized by the presence of large volumes of granitoid and gabbroic intrusive rocks, and so the Labradorian Orogeny was clearly a major crust forming event. Tectonic modelling of the orogenic process is constrained by two first order observations: 1) Labradorian magmatism extended from the North American craton in the north (southeastern Churchill Province) at least as far south as, and into, the Labradorian pelitic migmatite belt; and 2) the pelitic migmatite belt appears to have been exotic with respect to North America prior to the Labradorian Orogeny. Point 1 implies that the granitoid rocks of the Molson Lake Terrane and other parautochthonous terranes are part of a continental magmatic arc founded on the edge of the North American craton; point 2 implies that a suture must have existed between the pelitic migmatite terranes and the Molson Lake Terrane (which, as previously discussed, was linked to North America during the Labradorian Orogeny). Since there are granitoid intrusive rocks of comparable age on both sides of the proposed suture, it is suggested that subduction zones existed beneath both the margin of the North American craton and the approaching pelitic migmatite terranes during the Labradorian Orogeny. This implies that oceanic crust was consumed along both margins, culminating with the collision of the two continents (Fig. 8-1a-c). The subduction zones under each margin gave rise to distinct intrusive suites; those in the Molson Lake Terrane comprises a two-mica to hornblende-bearing granitic to granodioritic suite, whereas Labradorian intrusive rocks in the Lac Joseph Terrane range from gabbronorite to charnockitic rapakivi granites. This does not implicitly require that subduction was coeval along both margins or that it was continuous for the entire duration of the Labradorian Orogeny. Instead, active subduction, and magma generation, may have switched from one margin to the other during the prolonged Labradorian Orogeny (minimum 50 m.y.). The geochronological data base is presently insufficient to identify separate pulses of magmatic activity during this event.

The approximately synchronous emplacement of granitic and mafic magmas into the Lac Joseph Terrane suggests a causal link between the two rock types. It is proposed that basic magma, generated in a subduction environment beneath the Lac

a. Oceanic crust is subducted beneath the NA craton and Lac Joseph Terrane (LJT). Subduction beneath the LJT leads to the generation of mafic magmas which pond in the lower crust, causing granitoid partial melts. Granitoid melts are emplaced into the mid-crustal levels of the LJT, lowering the density of the lower crust, thus encouraging basic magma ascent. A granitoid magmatic arc is established on the margin of the NA craton above the NW dipping subduction zone; no Labradorian mafic intrusive rocks have been identified in the MLT.

b. Granitic and mafic magmas are emplaced at different levels in the Lac Joseph Terrane while grainitoid rocks continue to intrude into the Molson Lake Terrane. Plutonism leads to increased T and partial melting in the Lac Joseph Terrane.

c. Plutonism ceases with the collision of Lac Joseph Terrane with the arc. Partial melting in the Lac Joseph Terrane ceases as temperatures decrease.

d. Extension and separation of the Lac Joseph and Molson Lake terranes. Shabogamo Intrusive Suite emplaced at 1431 Ma in tensional environment.

Figure 8-1: Tectonic models for the Labradorian Orogeny and the emplacement of the Shabogamo Intrusive Suite at 1431 Ma.

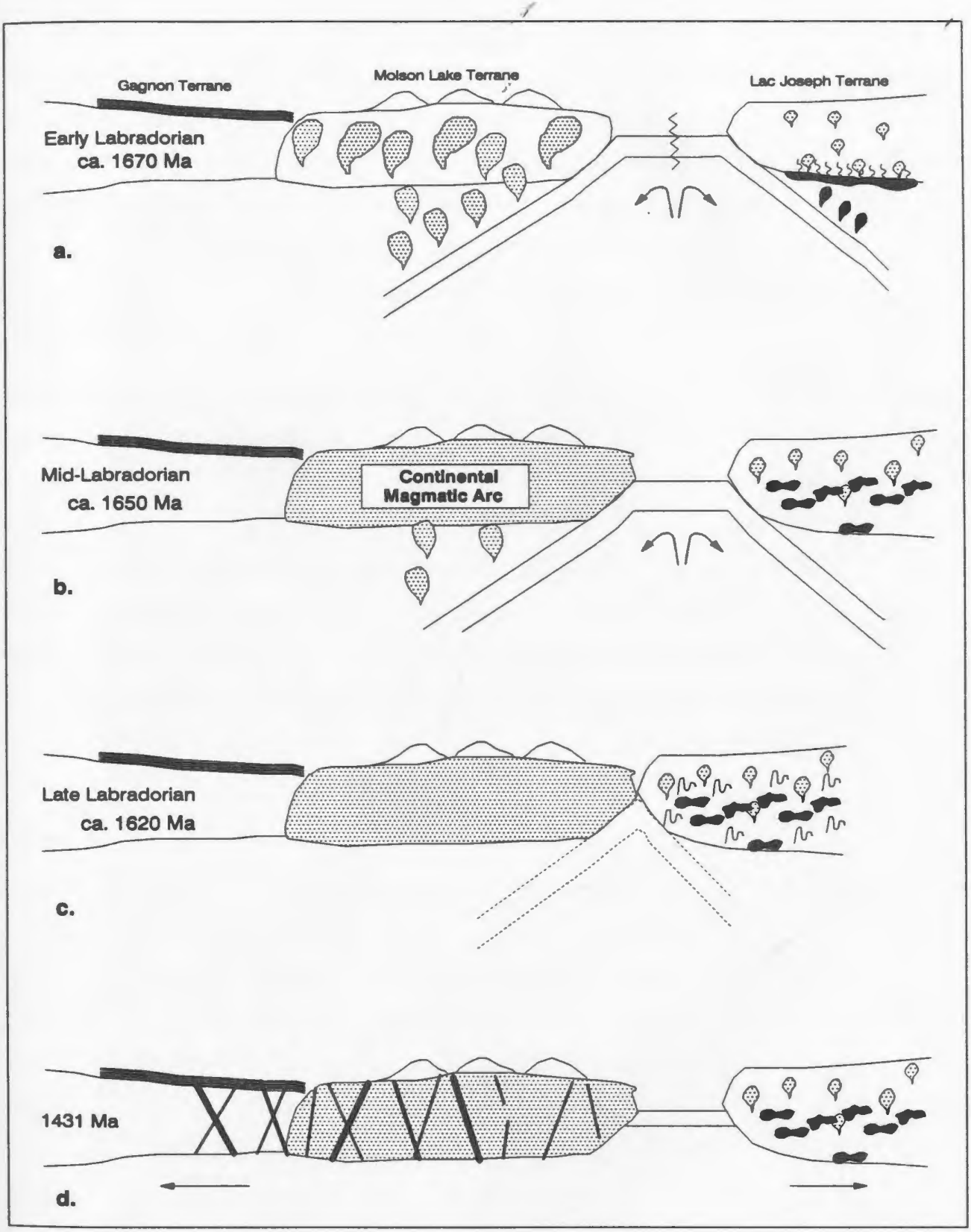
Gagnon Terrane
Molson Lake Terrane
Lac Joseph Terrane
Early Labradorian
ca. 1670 Ma
a.
Mid-Labradorian
ca. 1650 Ma
Continental
Magmatic Arc
b.
Late Labradorian
ca. 1620 Ma
c.
1431 Ma
d.

Joseph Terrane, ponded in the lower crustal levels due to inadequate buoyancy (Fig. 8-1a), and caused heating of the surrounding rocks, leading to partial melting of the lower crust and the generation of granitic magmas. These magmas rose through the crust and crystallized in the mid-crustal levels between about 1672 and 1619 Ma, the range of U-Pb ages for this suite (Fig. 8-1b). The emplacement of granitoid rocks resulted in elevated temperatures in the mid to upper crust which led to upper amphibolite to granulite facies metamorphism and extensive in-situ partial melting of the host supracrustal rocks.

Although this model suggests that mafic magmas were generated in a subduction environment early in the Labradorian, U-Pb data indicate that the final emplacement and crystallization of mafic magma actually post-dates early Labradorian granitic rocks and initial partial melting of the supracrustal rocks. The final ascent of the mafic magmas may have been facilitated by more ductile conditions in the lower and mid-crustal levels after heating and rise of the granitic magmas and/or an increased density of the host rocks after the departure of the granitic magmas. It is predicted, therefore, that future geochronology will reveal that basic magmas crystallized earlier in the Labradorian Orogeny than is presently known; the recrystallized, two-pyroxene granulite metabasites are considered the most likely candidates for such early basic magmas.

The Molson Lake Terrane represents part of the main Labradorian magmatic arc in western Labrador. The lack of geochemistry from the suite in this area precludes detailed speculation on the origin and petrogenesis of these rocks beyond the interpretation that granitoid magmas were generated in response to northwestward directed subduction extending beneath the margin of the pre-Labradorian North American craton.

On the basis of work in eastern Labrador, Kerr (1989) concluded that northwestward subduction of oceanic crust beneath the North American margin was responsible for the generation of the Labradorian granitoid suite in the Trans Labrador Batholith, of which the Molson Lake Terrane is believed to be the westerly extension. Based on detailed geochemical analyses of Sm/Nd, Rb/Sr and rare earth elements, he

concluded that subducted oceanic crust and sediments were partially melted to form slab-derived granitic magmas. He envisaged the upward transport of volatiles and granitic melts from the subducting slab which resulted in the generation of mafic magmas in the overlying mantle wedge. Kerr (1989) suggested that the granitic magmas were emplaced in the mid to upper crust as intrusive and extrusive rocks, whereas the mafic magmas were emplaced at greater depth. Detailed geochemical work is required in western Labrador to determine whether Kerr's (1989) petrogenetic model for eastern Labrador is applicable.

8.5.3 Labradorian - Grenvillian Events

The linear belt of "anorogenic" mafic intrusions of the Shabogamo Intrusive Suite and Michael Gabbro extending across Labrador attests to a period of crustal-scale extension after the collisional Labradorian Orogeny (Fig. 8-1d). Although the age of emplacement of these intrusions has been established at 1431 ± 7 Ma, there are no data available to determine the beginning or end of this extensional period. Utilizing the observation that there are no dykes correlated with the Shabogamo Intrusive Suite or Michael Gabbro in any of the allochthonous terranes, it is inferred that the Lac Joseph Terrane was distal to the North American margin at this time.

The presence of 1403 Ma monazite in a leucosome of pelitic migmatite along the southwest margin of the Lac Joseph Terrane suggests that this area was affected by elevated temperatures at this time. Unfortunately, this monazite has not yet been correlated with any metamorphic or structural elements in this area and so the significance of this age is enigmatic. The proximity of this sample to the margin of the Lac Joseph Terrane may indicate that temperature increased along the terrane margin as it interacted with another terrane to the west. This would imply that the present margin existed as early as 1403 Ma.

The southern Lac Joseph Terrane was affected by a penetrative amphibolite facies retrogression at approximately 1281 Ma to 1260 Ma, the extent of which is presently

unknown. Further geochronology from other areas of amphibolite-facies rocks will be required to determine whether the mafic rocks in the Lac Joseph Terrane were extensively affected by this event.

8.5.4 Grenvillian Orogeny

The pre-Grenvillian period of crustal extension and mafic dyke injection was followed by a major period of shortening during the Grenvillian Orogeny which is interpreted to be due to the convergence of the Lac Joseph Terrane and the terranes marginal to the pre-Grenvillian North American craton to the northwest. Although the consequences and tectonic styles of the Grenvillian Orogeny vary considerably in western Labrador, it essentially resulted in the re-assembly and telescoping of Labradorian terranes in a northwest-directed collisional event. The general lack of volumetrically significant Grenvillian magmatism in the study area suggests that a significant magmatic arc was not established in the Grenville Orogen of western Labrador during this compressional event and probably precludes the earlier presence of a significant pre-Grenvillian oceanic crust between the Lac Joseph and Molson Lake Terranes. This would imply that the Lac Joseph Terrane was not far-travelled during the extensional period during the emplacement of the Shabogamo Intrusive Suite. The Gagnon, Molson Lake and Churchill Falls Terranes were extensively deformed and penetratively recrystallized during the Grenvillian Orogeny.

The tectonic models for the re-assembly of the Molson Lake and Lac Joseph terranes during the Grenvillian Orogeny must account for the following constraints: 1) the exposure of high pressure - moderate temperature metamorphic assemblages in southwest Molson Lake Terrane; 2) rapid cooling, probably implying rapid uplift, after metamorphism at about 1001 ± 10 Ma in the Molson Lake Terrane; and 3) an absence of penetrative metamorphism in the Lac Joseph Terrane during the Grenvillian Orogeny.

Two models are proposed to for the Grenvillian Orogeny in western Labrador: 1) internal imbrication and thrusting of the Molson Lake Terrane (Fig. 8-2); and 2)

a. Pre-Grenvillian configuration prior to thrusting. Dashed line represents position of future thrusts; dash-dotted line represents 30 km (10 kbar) depth.

b. Internal imbrication and thrusting commences in the Molson Lake Terrane as the Lac Joseph Terrane impinges.

c. The thrusting of hot crustal sheets over cool results in elevated pressures and temperatures, which in turn leads to regional metamorphism and deformation in the Molson Lake Terrane.

d. Rapid uplift and erosion leads to rapid cooling of the Molson Lake Terrane.

e. The Lac Joseph Terrane is emplaced late in the Grenvillian Orogeny after peak metamorphism in the Molson Lake Terrane.

Figure 8-2: Model 1 for the tectonic evolution of western Labrador during the Grenvillian Orogeny.

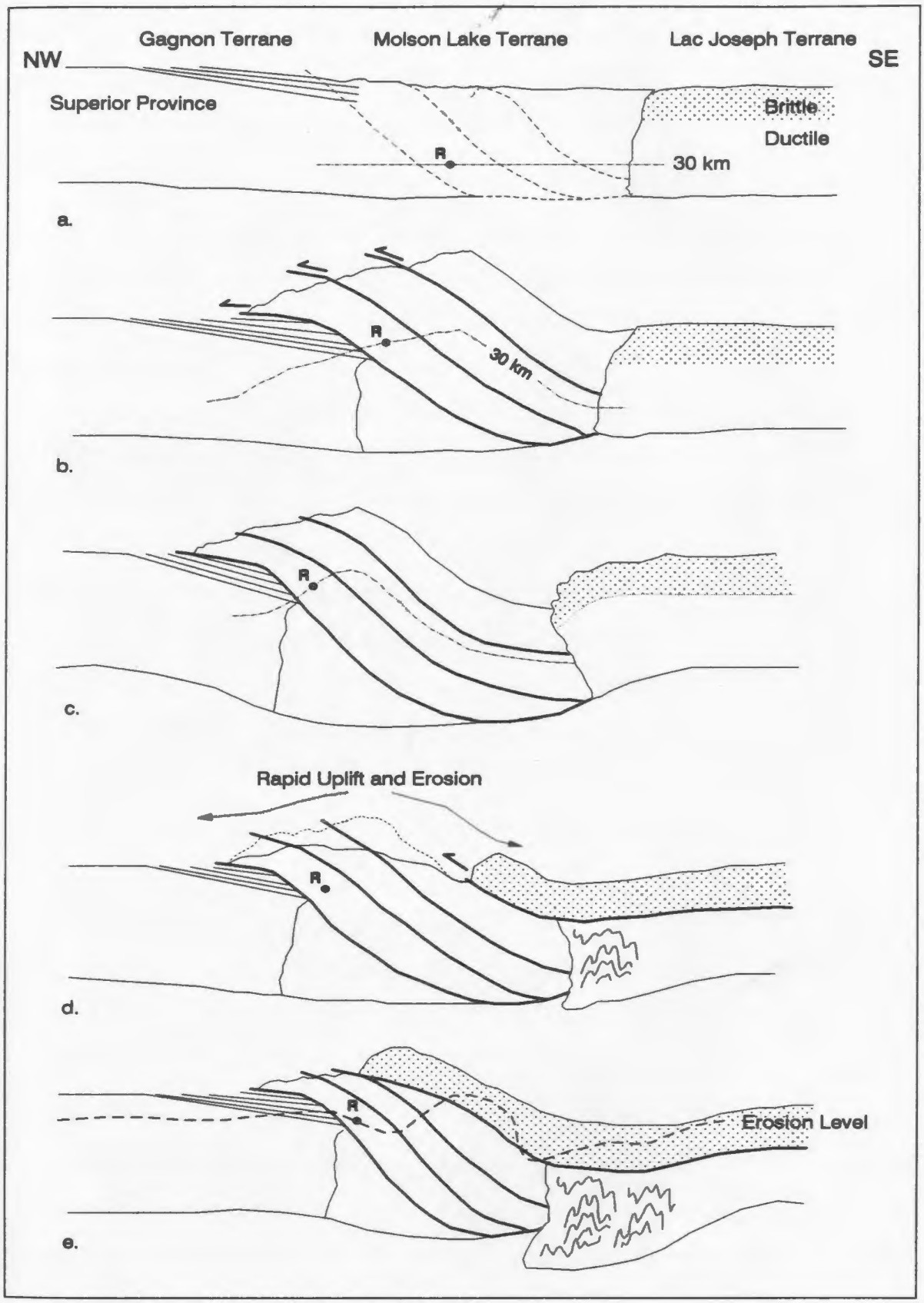
Gagnon Terrane
Molson Lake Terrane
Lac Joseph Terrane
NW
SE
Superior Province
Brittle
Ductile
R
30 km
a.
R
30 km
b.
R
c.
Rapid Uplift and Erosion
R
d.
R
Erosion Level
e.

exposure of lower levels of the Molson Lake Terrane through deformation and exhumation of the leading edge along a crustal scale detachment zone (Fig. 8-3). For reasons outlined in the discussion of these models below, model 2 is favoured.

8.5.4.1 Model 1: Internal Imbrication of the Molson Lake Terrane

In this model, the Molson Lake Terrane was thickened by a series of southeast-dipping, crustal-scale thrusts which led to depression of the crust (Fig. 8-2b and c). Initial uplift and erosion rates must have been slow enough to permit temperature increases at mid-structural levels, a consequence of thrusting hot rocks over cool. These elevated P-T conditions resulted in the crystallization of high P - moderate T assemblages in the western portion of the Molson Lake Terrane, represented by Point R on Figure 8.2c. These assemblages must have been brought towards the surface by isostatic crustal rebound and/or continued thrusting coupled with rapid erosion. Late in the Grenvillian Orogeny, it became mechanically more favourable for the shortening strain to be accommodated in the Lac Joseph Terrane. The subsequent formation of a detachment zone at the brittle-ductile transition (Fig 8.2d) resulted in ductile deformation in the lower crust of the Lac Joseph Terrane while the upper crust moved along the detachment zone and over the Molson Lake Terrane, further cooling the underlying rocks. The present erosion surface is shown in Figure 8.2e.

This model requires initial slow uplift rates, followed by rapid uplift and erosion to facilitate preservation of high pressure assemblages in the Molson Lake Terrane, but does not provide an adequate explanation for why these contrasting conditions should have occurred.

8.5.4.2 Model 2: Exhumation Along a Frontal, Crustal-Scale Thrust Fault

In this model, shortening by ductile deformation and exhumation of the leading, northwestern margin of the Molson Lake Terrane along a crustal-scale, southeast-dipping thrust fault, is comparable to the orogenic models of Jamieson and Beaumont (1989). The rapid exhumation of the Molson Lake Terrane over the Gagnon Terrane accounts for the sustained elevated temperatures in the Gagnon Terrane, as

a. Pre-Grenvillian configuration prior to thrusting.

b. Rapid exhumation of leading edge of Molson Lake Terrane along a major detachment zone. Rapid erosion allows continued exhumation.

c. A second major detachment occurs at the brittle-ductile transition such that the upper Lac Joseph Terrane moves northwestward over the Molson Lake Terrane. Ductile deformation occurs in the lower Lac Joseph Terrane.

d. Shortening continues to move the Lac Joseph Terrane over the Molson Lake Terrane. Labradorian assemblages preserved in the Lac Joseph Terrane.

Figure 8-3: Model 2 for the tectonic evolution of western Labrador during the Grenvillian Orogeny.

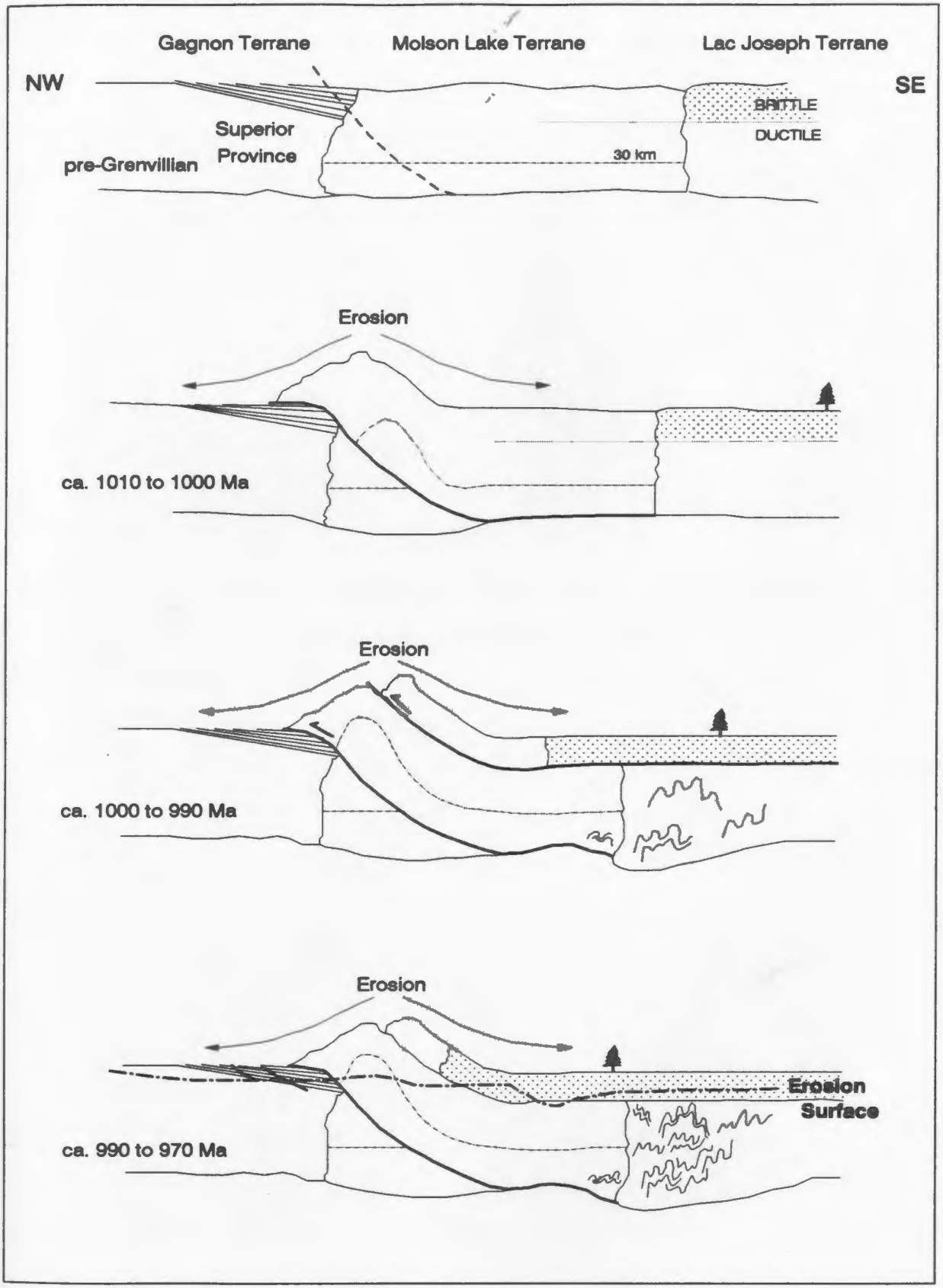
Gagnon Terrane
Molson Lake Terrane
Lac Joseph Terrane
NW
SE
BRITTLE
DUCTILE
Superior
Province
pre-Grenvillian
30 km
Erosion
ca. 1010 to 1000 Ma
Erosion
ca. 1000 to 990 Ma
Erosion
Erosion
Surface
ca. 990 to 970 Ma

evidenced by the younger $^{40}Ar/^{39}Ar$ amphibole ages (up to 90 m.y.) in the latter terrane. As the elevation along the western margin of the Molson Lake Terrane increased, it became mechanically favourable to accommodate shortening in the Lac Joseph Terrane, at which time the crust below the brittle-ductile transition deformed in a ductile manner, while the upper crust detached and moved northwestward over the Molson Lake Terrane (Fig. 8-3c). Although not shown in Figure 8.3c, ductile deformation in the lower crust and detachment of the upper crust most probably occurred in the southeast Molson Lake Terrane at this time. The base of the Lac Joseph Terrane was heated as it moved over the Molson Lake Terrane thereby further cooling the underlying rocks. With low temperatures and, therefore, slow reaction kinetics, the pressure increase in the Molson Lake Terrane resulting from the emplacement of the Lac Joseph Terrane is not recorded by mineral equilibria.

In this model, the orogenic process provided the means by which rocks that were experiencing high P - moderate T conditions deep in a "stable" crust were rapidly exhumed and exposed at the surface. This contrasts with the model 1, in which the orogenic event caused elevated temperatures and pressures at higher crustal levels through internal imbrication of the Molson Lake Terrane (placing hot thrust sheets over cold), which led to high P - moderate T assemblages and their eventually exposure by isostatic uplift and erosion.

8.5.5 Late Grenvillian

Northeast-southwest oriented cross folds (F_{3J} and F_{2M}) overprint the Grenvillian thrust faults, and reflects a change in the principal shortening direction after thrusting. This late cross-folding is responsible for the presently preserved lobate shape of the Lac Joseph Terrane and reorienting the marginal shear zones into their present orientation. Late brittle faults are also thought to have formed late in the Grenvillian Orogeny and may be responsible for the close proximity of high and low pressure assemblages in the southwestern Molson Lake Terrane.

CHAPTER 9
CONCLUSIONS

9.1 Summary

As the Lac Joseph Terrane was intruded by granitic and mafic magmas and regionally metamorphosed and deformed during the Labradorian Orogeny between 1672 Ma and 1611 Ma, large volumes of granitoid rocks were emplaced into the Molson Lake Terrane. Subduction of pre-Labradorian oceanic crust beneath both terranes is thought to be responsible, either directly or indirectly, for the granitic and mafic magmas emplaced in the overlying terranes, such that a suture is proposed to exist between the Molson Lake and Lac Joseph terranes. The details of the subduction-related processes which led to the distinct intrusive suites in each terrane remain unresolved.

The coincidence of Labradorian events in the Molson Lake and Lac Joseph terranes suggests that they were proximal during the Labradorian Orogeny. The collision of the two terranes by late-Labradorian is though to have arrested subduction and, secondarily, magmatism, while deformation continued. It is proposed that the Molson Lake and Lac Joseph terranes, and indeed the Allochthonous Polycyclic and Parautochthonous terranes across Labrador, were juxtaposed by the end of the Labradorian Orogeny.

The spatial distribution, orientation and anorogenic style of emplacement of intrusions of the Shabogamo Intrusive Suite suggests that north-northwest - south-southeast extension was extant at ca. 1431 Ma. The apparent absence of the Shabogamo Intrusive Suite in the Lac Joseph Terrane suggests that post-Labradorian rifting resulted in the Lac Joseph Terrane being distal to the site of basic magma intrusion.

Grenvillian metamorphism in western Labrador, which peaked prior to 1001 Ma (the oldest Grenvillian U/Pb age), resulted in extensive recrystallization and deformation in the Molson Lake Terrane but did not penetratively affect the Lac Joseph Terrane. This study suggests that the western Molson Lake Terrane was rapidly exhumed towards the northwest along a crustal scale frontal thrust zone during the

Grenvillian Orogeny. It subsequently became mechanically more favourable to accommodate shortening within the orogen by detachment and northwestward transport of the upper brittle crust while the lower crust deformed in a ductile manner. This change in the deformation style led to the emplacement of the Lac Joseph Terrane over the Molson Lake Terrane late in the Grenvillian Orogeny, after temperatures in the latter had diminished.

9.2 Future Work

In an attempt to advance the understanding of the tectonic processes which shaped the Grenville Province of western Labrador, new uncertainties are raised which set the stage for future research. The proposal of opposed Labradorian subduction zones beneath the Molson Lake and Lac Joseph terranes must be tested by future geochemical work on the intrusive suites in both terranes. Trace element geochemistry and Sm/Nd isotopic studies would place constraints on parental materials for these magmas, thereby elucidating the geometry and processes in the proposed subduction zones. Two cryptic events at 1403 Ma and 1281 Ma have been identified by U/Pb and $^{40}Ar/^{39}Ar$ geochronology. A combination of detailed petrographic and geochronologic work will be required to establish the extent and significance of these events which lead to the recrystallization of monazite, titanite and hornblende at these times.

The majority of work in the Grenville Province to date, including this study, has necessarily concentrated on documenting the structural and metamorphic histories of a specific area. Tectonic models for the Grenville Orogen which rise from such studies are typically based upon models which are either theoretically founded (ie. Jamieson and Beaumont, 1989) or extrapolated from the more abundant information from higher level orogens. As the timing and conditions of the events which affected the Grenville Orogen become more accurately quantified, future work will undoubtedly reverse this trend and utilize studies of the Grenville Orogen as a data base to understand, and test theoretical models of, deep orogenic processes.

REFERENCES

Apted, M.J. & Liou, J.G. (1983) Phase relations among greenschist, epidote amphibolite and amphibolite facies in a basaltic system. Am. J. Sci. 283A: 328-358.

Bence, A.E. & Albee, A.L. (1968) Empirical correction factors for the electron microanalysis of silicates and oxides. J. Geol. 76: 382-403.

Berman, R.G., Brown, T.H. & Greenwood, H.J. (1985) An internally consistent thermodynamic data base for minerals in the system Na_2O - K_2O - CaO - MgO - FeO - Fe_2O_3 - Al_2O_3 - SiO_2 - TiO_2 - H_2O - CO_2. Atomic Energy of Canada Ltd. Technical Report 377, 62p.

Berman, R.G., Brown, T.H. & Perkins, E.H. (1987) GeOcalc: Software for calculation and display of pressure-temperature-composition phase diagrams. The University of British Colombia, 1-25.

Brooks, C., Wardle, R.J. & Rivers, T. (1981) Geology and geochronology of Helikian magmatism, western Labrador. Can. J. Earth Sci. 18: 1211-1227.

Brooks, C. (1983) U-Pb zircon geochronological ages. Newfoundland Department of Mines and Energy, Mineral Development Division, Unpublished report, 32p.

Brown, D., van Gool, J., Calon, T., & Rivers, T. (1991) The geometric and kinematic development of the Emma Lake thrust stack. Can. J. Earth Sci. 28: 136-144.

Brown, D. (1991) A structural analysis of the Grenville Front Zone, northwest Gagnon Terrane, Labrador. Unpublished M.Sc. thesis, Memorial University of Newfoundland.

Cameron, A.E., Smith, D.H., & Walker, R.K. (1969) Mass spectrometry of nanogram-size samples of lead. Analytical Chem. 41: 525-526.

Carmichael, D.M. (1978) Metamorphic bathozones and bathograds: a measure of the depth of post-metamorphic uplift and erosion on the regional scale. Amer. J. Sci. 278: 769-797.

Connelly, J.N. & Scowen, P. (1987) Geology of the Lac Caopacho - Lac Fleur-de-May area southwestern Labrador. In: Current Research. Newfoundland Department of Mines and Energy, Mineral Development Division, Report 87-1: 225-235.

Connelly, J.N. (1988) An investigation of the margin of the Lac Joseph Allochthon, Grenville Province, southwestern Labrador. In: Current Research. Newfoundland Department of Mines, Mineral Development Division, Report 88-1: 37-48.

Connelly, J.N. & Nunn, G.A.G. (1988) Relationships between the Lac Joseph Allochthon and underlying Terranes, southwestern Labrador. In: Geol. Assoc. Can., Annual Meeting, Program with Abstracts, 13: A24.

Connelly, J.N., van Gool, J & Rivers, T. (1989a) Molson Lake Terrane, a new terrane in the parautochthonous belt of the Grenville Province in southwestern Labrador. In: Geol. Assoc. Can., Annual Meeting, Program with Abstracts, 14: A23.

Connelly J.N., Heaman, L., Krogh, T. & Rivers, T. (1989b) U-Pb geochronology within the Molson Lake and Lac Joseph Terranes, Grenville Province, southwestern Labrador. In: Geol. Assoc. Can., Annual Meeting, Program with Abstracts, 14: A84.

Cressey, G., Schmid, R., & Wood, B.J. (1978) Thermodynamic properties of almandine - grossular garnet solid solutions. Contrib. Mineral. Petrol. 67: 397-404.

Dallmeyer, R.D. (1982) $^{40}Ar/^{39}Ar$ incremental-release age of biotite from a gabbro of the Shabogamo Intrusive Suite, southwestern Labrador. Can. J. Earth Sci. 19: 1877-1881.

Dallmeyer, R.D. & Rivers, T. (1983) Recognition of extraneous argon components through incremental-release $^{40}Ar/^{39}Ar$ analysis of biotite and hornblende across the Grenvillian metamorphic gradient in southwestern Labrador. Geochimica et Cosmochim. Acta 47: 413-428.

Davis, D.W. (1982) Optimum linear regression and error estimation applied to U-Pb data. Can. J. Earth Sci. 23: 2141-2149.

Deer, W.A., Howie, R.A. & Zussman, J. (1966) An Introduction to the Rock-Forming Minerals, Longman, 528p.

Ellis, D.J. & Green, D.H. (1979) An experimental study of the effect of Ca upon garnet - clinopyroxene Fe-Mg exchange equilibria. Contrib. Mineral. Petrol. 71: 13-22.

Emslie R. & Hunt, P. (1990) Ages and petrogenetic significance of igneous mangerite-charnockite suites associated with massif anorthosites, Grenville Province. J. of Geol. 98: 213-231.

Essene, E.J. (1989) The current status of thermobarometry in metamorphic rocks. In: Daly, J.S., Cliff, R.A., & Yardley, B.W.D. (eds.), Evolution of metamorphic belts., Geol. Soc. Special Publication, No. 43: 1-44.

Ferry, J.M. & Spear, F.S. (1978) Experimental calibration of the partitioning of Fe and Mg between biotite and garnet. Contrib. Mineral. and Petrol. 66: 113-117

Ganguly, J., & Kennedy, G.C. (1974) The energetics of natural garnet solid solution: I. Mixing of the aluminosilicate end-members. Contrib. Mineral. Petrol. 48: 137-148.

Geological Survey of Canada, (1977a) Map 5953G, Riviere Embarrassee, Newfoundland, Geophysical Series (Aeromagnetic).

Geological Survey of Canada, (1977b) Map 5911G, Seahorse Lake, Newfoundland - Quebec, Geophysical Series (Aeromagnetic).

Geological Survey of Canada, (1977c) Map 5912G, Lac Assigny, Newfoundland - Quebec, Geophysical Series (Aeromagnetic).

Ghent, E.D. (1976) Plagioclase - garnet - Al_2SiO_5: a potential geobarometer - geothermometer. Amer. Mineral. 61: 710-714.

Ghosh, S.K. & Ramberg, H. (1976) Reorientation of inclusions by combination of pure and simple shear. Tectonophysics, 34: 1-70.

Ghent, E.D., Robbins, D.B. & Stout, M.Z. (1979) Geothermometry, geobarometry, and fluid compositions of metamorphosed calcsilicates and pelites, Mica Creek, British Columbia. Am. Mineral. 64: 874-885.

Gower, C.F. (1984) Geology of the Double Mer White Hills and surrounding region, Grenville Province, eastern Labrador. In: Current Research, Newfoundland Department of Mines and Energy, Mineral Development Division, Report 84-1: 68-79.

Gower, C.F., Rivers, T. & Brewer, T.S. (in press) Mid-Proterozoic mafic magmatism in Labrador, eastern Canada. In: Gower, C.F., Rivers, T. & Ryan, B., Middle Proterozoic Laurentia-Baltica. Geol. Assoc. Can. Sp. Paper 38.

Hanmer, S. (1984) The potential use of planar and elliptical structures as indicators of strain regime and kinematics of tectonic flow. In: Current Research, Part B, Geol. Surv. Can. Paper 84-1B: 133-142.

Hanmer, S. (1988) Ductile thrusting at mid-crustal level, southwestern Grenville Province. Can. J. Earth Sci. 25: 1049-1059.

Hanmer, S. (1989) Great Slave Lake shear zone, Canadian Shield: reconstructed vertical profile of a crustal-scale fault zone. Tectonophysics 149: 245-264.

Harrison, T.M. and McDougall, 1. (1980) Investigations of an intrusive contact, northwest Nelson, New Zealand - II Diffusion of radiogenic and excess ^{40}Ar in hornblende revealed by $^{40}Ar/^{39}Ar$ age spectrum analysis. Geochim. Cosmochim. Acta. 4: 2005-2020.

Harrison, T.M., Duncan, I. and McDougall, I. (1985) Diffusion of ^{40}Ar in biotite: temperature, pressure and compositional effects. Geochim. Cosmochim. Acta. 49: 2461-2468.

Heaman, L. and Parrish, R. (1991) U-Pb geochronolgy of accessory minerals. In: L. Heaman and J.N. Ludden (eds.), Short Course Handbook On Application of Radiogenic Isotope Systems To Problems In Geology, Mineral. Assoc. Can. Vol. 19: 59-102.

Hodges, K.V. & Royden, L. (1984) Geologic thermobarometry of retrograded metamorphic rocks: an indication of the uplift trajectory of a portion of the northern Scandinavian Calidonides. J. Geophys. Res. 89: 7077-7090.

Hoffman, P.J. (1989) Precambrian geology and tectonic history of North America: an overview. Geological Society of America, Decade of North American Geology A: 447-512.

Holdaway, M.J. (1971) Stability of andalusite and the alumino-silicate phase diagram. Am. J. Sci. 271: 97-131.

Holland, T.J.B. (1980) The reaction albite = jadite + quartz determined experimentally in the range 600-1200°C. Am. Mineral. 65: 129-134.

Jackson, G.D. (1976) Opocopa Lake map sheet (east half), Quebec - Newfoundland. Geological Survey of Canada, Map 1417A.

James, D.T., Dunphy, D.G., & Stephenson, D.M. (1991) The Lac Joseph Terrane and the Churchill Falls Terrane: structural and metamorphic relations, Ossokmanuan Lake (NTS 23H/SW) map areas, Grenville Province, Western Labrador. In: Current Research, Newfoundland Department of Mines and Energy, Mineral Development Division, Report 91-1: 217-227.

Jamieson, R.A. & Beaumont, C. (1989) Deformation and metamorphism in convergent orogens: a model for uplift and exhumation of metamorphic terrains. In: Daly, J.S., Cliff, R.A., & Yardley, B.W.D. (eds.), Evolution of Metamorphic Belts, Geol. Soc. Spec. Pub. No. 43: 117-129.

Kerr, A. (1989) Early Proterozoic granitoid magmatism and crustal evolution in the Makkovik Province of Labrador: a geochemical and isotopic study. Unpublished Ph.D. thesis, Memorial University of Newfoundland, 528p.

Kerrick, D.M. & Darken, L.S. (1975) Statistical thermodynamic models for ideal oxide and silicate solid solution, with application to plagioclase. Geochim. Cosmochim. Acta 39: 1431-1442.

Koziol, A.M. & Newton, R.C. (1988) Redetermination of the garnet breakdown reaction and improvement of the plagioclase - garnet - Al_2SiO_5-quartz geobarometer. Amer. Mineral. 73: 216-223.

Kretz, Ralph (1990) Biotite and garnet compositional variation and mineral equilibria in Grenville gneisses of the Otter Lake area, Quebec. J. Meta. Geol. 8: 493-506.

Krogh, T.E. (1973) A low contamination method for hydrothermal decomposition of zircon and extraction of U and Pb for isotopic age determination. Geochim. Cosmochim. Acta 37: 488-494.

Krogh, T.E. (1983) U-Pb zircon and sphene determinations, Newfoundland and Labrador. Newfoundland Department of Mines and Energy, Mineral Development Division, Unpublished report, 79p.

Krogh,T.E. & Davis, G.L. (1975) The production and preparation of ^{205}Pb for use as a tracer for isotope dilution analysis. Carnegie Inst. Washington Yearbook 74: 416-417.

Lindsley, D.H. (1983) Pyroxene thermometry. Amer. Mineral. 68: 477-493.

Liou, J.G., Kuniyoshi, S. & Ito, K. (1974) Experimental studies of the phase relations between greenschist and amphibolite in a basalitic system. Am. J. Sci. 274: 613-632.

Mengel, F.C. (1987) Thermotectonic evolution of the Proterozoic-Archaean boundary in the Saglak area, northern Labrador. Unpublished Ph.D. thesis, Memorial University of Newfoundland, 350p.

Mengel, F.C. & Rivers, T. (1989) Thermotectonic evolution of Proterozoic and reworked Archaean terranes along the Nain - Churchill boundary in the Saglek area, northern Labrador. In: Daly, J.S., Cliff, R.A., & Yardley, B.W.D. eds., Evolution of Metamorphic Belts, Geol. Soc. Spec. Pub. No. 43: 319-324.

Moody, J.B., Meyer, D. & Jenkins, J.E. (1983) Experimental characterization of the greenschist/amphibolite boundary in mafic systems. Am. J. Sci. 283: 48-92.

Newton, R.C., Charlu, T.V. & Kleppa, O.J. (1980) Thermochemistry of the high structural state plagioclase. Geochim. Cosmochim. Acta 44: 933-941.

Newton, R.C. & Haselton, H.T. (1981) Thermodynamics of the garnet-plagioclase-Al_2SiO_5 geobarometer. In: Newton, R.C., A Navrotsky and B.J. Wood (eds.) Thermodynamics of Minerals and Melts, Springer-Verlag, 129-145.

Newton, R.C. & Perkins, D. (1982) Thermodynamic calibration of geobarometers based on the assemblages garnet - plagioclase - orthopyroxene - clinopyroxene - quartz. Am. Mineral. 67: 203-222.

Nunn, G.A.G. & Christopher, A. (1983) Geology of the Atikonak River area, Grenville Province, western Labrador. In: Current Research, Newfoundland Department of Mines and Energy, Mineral Development Division, Report 83-1: 107-114.

Nunn, G.A.G., Noel, N. & Culshaw, N.G. (1984) Geology of the Atikonak Lake Area, Grenville Province, western Labrador. In: Current Research, Newfoundland Department of Mines and Energy, Mineral Development Division, Report 84-1: 30-41.

Nunn, G.A.G., Thomas, A. & Krogh, T.E. (1985) The Labradorian Orogeny: geochronological database. In: Current Research, Newfoundland Department of Mines and Energy, Mineral Development Division, Report 85-1: 43-54.

Nunn, G.A.G, Emslie, R.F., Lefebvre, C.E., Noel, N. & Wells, S. (1986) The Atikonak River Massif and surrounding area, western Labrador and Quebec. In: Current Research, Newfoundland Department of Mines and Energy, Mineral Development Division, Report 86-1: 125-145.

Parrish, R. & Roddick, J.C. (1985) Geochronology and isotope geology for the geologist and explorationist. Geological Association of Canada, Cordilleran Section, Short course no. 4.

Perkins, E.H., Brown, T.H. & Bergman, R.G. (1986) PTX-System: three programs for calculation of pressure-temperature-composition phase diagrams. Computers & Geosciences, 12: 749-755.

Prudy, J.W. and Jäger, E. (1976) K-Ar ages on rock-forming minerals from the Central Alps. Memoirs, Institute of Geology and Mineralogy, University of Padova, 30: 1-31.

Rivers, T. (1980) Revised stratigraphic nomenclature for Aphebian and other rock units, southern Labrador Trough, Grenville Province. Can. J. Earth Sci., 17: 668-670.

Rivers, T. (1983) The northern margin of the Grenville Province in western Labrador - anatomy of an ancient orogenic front. Precambrian Research, 22: 41-73.

Rivers, T. (1985) Geology of the Opocopa Lake area, Labrador-Quebec. Newfoundland Department of Mines and Energy, Mineral Development Division, Map 85-24.

Rivers, T. & Nunn, G.A.G. (1985) A reassessment of the Grenvillian Orogeny in western Labrador. In: A.C. Tobi and J.L.R. Touret, (eds.), The Deep Proterozoic Crust in the North Atlantic Provinces. NATO Advanced Study Institute, Series C, 158: 163-174.

Rivers, T. & Chown, E.H. (1986) The Grenville Orogen in eastern Quebec and western Labrador - definition, identification and tectonometamorphic relationships of autochthonous, parautochthonous and allochthonous terranes. In J.M. Moore, A. Davidson and A. Baer. (eds.), The Grenville Province. Geol. Assoc. Can. Paper 31: 31-50.

Rivers, T. & Mengel, F.C. (1988) Contrasting assemblages in corona and non-corona gabbros in the Grenville Province of western Labrador. Can. J. Earth Sci. 25: 1629-1648.

Rivers, T., Martingnole J., Gower, C.F. & Davidson, A. (1989) New tectonic subdivisions of the Grenville Province, southeast Canadian Shield. Tectonics 8: 63-84.

Schärer, U., Krogh, T.E., & Gower, C.F. (1986) Age and evolution of the Grenville Province in eastern Labrador from U-Pb systematics in accessory minerals. Contrib. Mineral. and Petrol. 94: 438-451.

Spear, F.S. (1981) An experimental study of hornblende stability and compositional variability in amphibole. Am. J. Sci. 281: 697-734.

Stevenson, I.M. (1968) Geology of the Lac Joseph map area (23A), Newfoundland and Quebec. Geological Suvey of Canada, Paper 67-62, 4p.

Thomas, A., Culshaw, N., Mannard, G., & Whalen,J.G. (1984) Geology of the Lac Ghyvelde-Lac Long area, Grenville Province, Labrador and Quebec. Current Research, Report 84-1: 42-52.

Thomas, A., Nunn, G.A.G. & Wardle, R.J. (1985) A 1650 Ma orogenic belt within the Grenville Province of northeastern Canada. In: A.C. Tobi and J.L.R. Touret (eds), The Deep Proterozoic Crust in the North Atlantic Provinces. NATO Advanced Study Institute, Series C, 158: 151-161.

Tracey, R.J. (1982) Compositional zoning and inclusions in metamorphic minerals. In: Ferry, J.M. (ed) Characterization of Metamorphism through Mineral Equilibria. Mineral. Soc. Am. 10: 355-397.

van Gool, J. (in prep) The thermotectonic development of the Grenville Front fold-and-thrust belt in southwestern Labrador. Ph.D. thesis, Memorial University of Newfoundland.

van Nostrand, T.S. (1987) Geothermometry - geobarometry and $^{40}Ar/^{39}Ar$ incremental release dating in the Sandwich Bay Area, Grenville Province, eastern Labrador. Unpub. M.Sc. thesis, Memorial University of Newfoundland, 203p.

Wardle, R.J. (1979) Geology of the Sandgirt-Gabbro Lake area. Newfoundland Department of Mines and Energy, Mineral Developement Division, Map 79-17 with marginal notes.

Wardle, R.J. & Britton, J.M. (1981) The geology of the Churchill Falls area, Labrador. In: Current Research, Newfoundland Department of Mines and Energy, Mineral Development Division, Report 81-1: 130-137.

Wardle, R.J. & Bailey, D.G. (1981) Early Proterozoic sequences in Labrador. In: Campbell F.H.A. (ed), Proterozoic Basins of Canada, Geol. Surv. Can., Paper 81-10: 331-359.

Wardle, R. J. (1982) The Geology of the Churchill Falls Region. In: Current Research, Newfoundland Department of Mines and Energy, Mineral Development Division, Report 82-1: 131-148.

Wardle, R.J., Rivers, T., Gower, C.F., Nunn, G.A.G. & Thomas, A. (1986) The northeastern Grenville Province: new insights. In: J.M. Moore, A. Davidson and A. Baer (eds), The Grenville Province, Geol. Assoc. Can. Special Paper 31: 13-29.

Wells, P.R.A. (1979) Chemical and Thermal Evolution of Archaean Sialic Crust, Southern West Greenland. J. Petrol. 20: 187-226.

Wood, B.J. & Banno, S. (1973) Garnet-orthopyroxene and orthopyroxene-clinopyroxene relationships in simple and complex systems. Contrib. Mineral. Petrol. 42: 109-124.

Wynne-Edwards, H.R. (1972) Tectonic overprinting in the Grenville Province, southwestern Quebec. In: Price, R.A and Douglas, R.J.W., (eds.), Variations in Tectonic Styles in Canada, Geol. Assoc. Can. Special Paper 5: 193-205.

Zindler, A., Hart, S.B. & Brooks, C. (1981) The Shabogamo Intrusive Suite: Sr and Nd isotopic evidence for contaminated mafic magmas in the Proterozoic. Earth and Planet. Sci. Lett. 54: 217-235.

APPENDIX 1

MAJOR AND TRACE ELEMENT WHOLE ROCK ANALYSES

A representative suite of the major rock units within the map area were submitted to the geochemical laboratories of the Newfoundland Department of Mines and Energy. The analyses are presented in Table A1-1. Unit codes are explained in Chapter 2 and Figure 2-1.

Table A1-1: Whole rock geochemisty of samples representative of the major rock units in the map area.

Sample	78	83	96	358	1274	1327	14	282	442	81	1159
Unit	1A	1A	1A	1A	1A	1A	1A-M	1A-M	1A-M	1D	1D
SiO2	74 35	70 30	70 05	78 90	73 65	67 70	68.20	74.10	70.15	51.45	48.70
TiO2	0 05	0 52	0 48	0 44	0.19	0 58	0 28	0.17	0.52	2.45	2.15
Al2O3	14.50	14 34	14.76	10 44	14.63	16.74	17.51	13.48	15.72	13.54	13 18
FeO	0 45	1 53	1.82	0 59	0.55	2.15	0.70	0.40	2.05	4.43	10 18
Fe2O3	0 34	1 53	1.60	1.72	0.87	2.35	1.48	0.75	2.03	8.12	6.13
MnO	0 03	0 04	0.07	0.03	0 04	0 08	0.05	0.04	0.08	0.31	0 27
MgO	0 28	0.86	1.26	0.41	0 64	1.35	0 79	0.42	1.18	3.87	5.60
CaO	1 56	1 35	1.08	1.10	1.51	1.70	3.71	0.89	0 61	11.28	12 92
Na2O	2.83	2.48	1.94	2.14	3.10	2.46	4.64	2.28	1.49	0.84	0.77
K2O	4.73	6 38	4 77	3.19	4.03	3.31	1.47	6.40	3.39	0.42	0 31
P2O5	0 05	0.10	0 05	0.04	0.07	0.05	0.12	0.10	0.04	0 82	0.19
LOI	0.74	0.65	0 66	0.49	0.63	1.53	1.20	0.87	2.37	1.05	0.35
SUM	99.90	100.08	98 54	99.49	99 91	100.00	100 15	99.70	99 63	98.58	98 75
Ba	827	1080	1110	653	956	865	360	725	637	621	103
Sr	239	161	183	226	246	253	464	151	133	222	181
Rb	100	148	106	49	85	86	40	124	111	20	14
Ga	3	6	6	6	4	9	8	3	9	24	26
Nb	1	9	7	1	1	11	9	1	14	63	2
Zr	60	115	82	105	53	128	103	96	121	143	46
Th	1	73	3	16	2	4	78	34	5	6	1
Y	6	39	7	17	7	11	53	25	10	41	44
La	9	138	41	69	24	45	309	72	34	63	9
Ce	12	302	64	132	42	84	585	152	70	126	27

Sample	1149	1023	55	1066	226	229	426	436	310	1326
Unit	3A	4B	4C	4C	7B	7B	7B	7B	8	8
SiO2	70 60	47.30	47.10	48.35	48.15	45.40	47 15	47 65	69.60	67 50
TiO2	0.58	0.68	1.53	2.74	0 51	1.08	0 13	2 97	0.57	1.10
Al2O3	13 94	22.65	16.52	13.05	17.24	20.07	18.32	14 93	14 56	13.17
FeO	2.28	5.71	9.79	10.75	4.85	5.78	4.66	8.43	2.10	2.88
Fe2O3	1 01	1.04	2.31	3 67	3.39	7.09	3.08	5.33	1 36	2.78
MnO	0 08	0.11	0.19	0.24	0.14	0.14	0.13	0.20	0.06	0.12
MgO	0 98	7.73	8.12	6.20	10.66	5.24	14.47	5.58	0.61	1.15
CaO	1.89	11.07	9.89	10.41	9.96	11.81	9.71	8.84	1.99	2.41
Na2O	3.06	2.74	2.44	2.56	2.14	2.37	2.08	3.12	3.75	2.58
K2O	4 36	0 16	0.52	0.64	0.94	0.19	0.23	1.10	4.52	5 26
P2O5	0.12	0 12	0.18	0.25	0.20	0.04	0.05	0.35	0.18	0.39
LOI	0.51	0.61	0.27	0.61	0.97	0.32	0.44	0.50	0.58	0.52
SUM	99.41	99.92	98.86	99.47	99.15	99.53	100.45	99.00	99.88	99.86
Ba	717	61	154	439	572	178	174	424	1030	1360
Sr	149	383	231	164	1020	1190	797	314	282	160
Rb	142	11	19	136	27	11	12	26	144	99
Ga	6	13	25	25	14	25	7	25	8	8
Nb	17	1	6	9	1	1	54	3	30	35
Zr	186	79	127	85	53	29	151	61	123	31
Th	16	1	2	1	1	1	65	2	14	8
Y	20	10	21	39	9	5	156	31	58	70
La	56	3	11	15	16	6	14	22	57	121
Ce	102	13	31	37	35	17	41	48	114	248

APPENDIX 2

MINERAL ANALYSES AND FORMULAS

Mineral analyses, determined by electron microprobe, were utilized to calculated mineral formulas and site distributions for phases used in geothermometry and geobarometry. The mole fractions of components in minerals were calculated following the schemes described by authors of the geothermometers and geobarometers in which each phase is utilized (except for clinopyroxene in Chapter 4, where the calculation scheme is outlined). All mineral formula calculations were based on the assumption that $Fe^{TOTAL} = Fe^{+2}$ (see Appendix 4 for discussion of this assumption).

GARNET

The general formula for garnet, calculated on the basis of 12 oxygens, may be represented by:

$A_3B_2[TO_4]_3$ where

$T = Si^{+4}$ or Ti^{+3} (Deer et al. 1966),

$B = Al^{+3}, Fe^{+3}$ and Cr^{+3} and

$A = Ca^{+2}, Mg^{+2}, Mn^{+2}$ and Fe^{+2}.

Since Al^{+3} in the B site is typically close to the maximum of two cations per formula unit, there is no requirement for significant Fe^{+3} to fill this site such that the andradite component of garnet is small to insignificant. X_{Mg} for garnet is calculated by:

$$X_{Mg} = \frac{Mg}{Mg + Fe + Ca + Mn}.$$

BIOTITE

Biotite, when calculated on the basis of 11 oxygens may be represented by the general formula:

$AX_3T_4O_{10}(OH, Cl, F)_2$ where:

$T = Si^{+4}$ and Al^{+3},

$X = Fe^{+2}, Fe^{+3}, Al^{+3}, Mg^{+2}, Mn^{+2}$ and Ti^{+4} and

$A = K^{+1}$ with minor substitution of $Na^{+1}, Ca^{+2}, Ba^{+2}, Rb^{+1}$ and Cs^{+1}. F, Cl and OH concentrations were not determined. The X^{Mg} ratio for biotite is calculated by:

$$X_{Mg} = \frac{Mg}{Mg + Fe^{*}}$$

CLINOPYROXENE

The general formula for clinopyroxene, calculated on the basis of 6 oxygens, may be represented as:

XYT_2O_6 where

$T = Si^{+4}$ and Al^{+3},

$X = Na^{+1}, Ca^{+2}, Mn^{+2}, Fe^{+2}$ and Mg^{+2} and

$Y = Mn^{+2}, Fe^{+2}, Mg^{+2}, Fe^{+3}, Al^{+3}, Cr^{+3}$ and Ti^{+4} where Fe - Mg proportions are the same in the X and Y sites.

Newton and Perkins (1982) followed site allocation which differs from the general scheme above. They suggested that Si and Al fill the T site to a total of 2 cations; the X site incorporates Ca, Na, Mn and enough Fe to total 1 cation, with the remaining Al and Fe joining Mg and Ti in the Y site. This scheme, which does not allow for an enstatite component, is used in their GADS geobarometer. When calculating mole fractions for the geobarometer of Newton and Perkins (1982), X^{Mg} for clinopyroxene is calculated by:

$$X_{Mg}^{CPX} = \frac{Mg}{Mg + Fe^{Y\,sub}}$$

while the X_{Ca} for clinopyroxene is calculated:

$$X_{Ca}^{CPX} = \frac{Ca}{Ca + Na + Mn + Fe^{X\,sub}}$$

The mole fraction of diopside for the geobarometer of Newton and Perkins (1982) is subsequently calculated by:

$$X_{Dio}^{CPX} = X_{Ca}^{X\,site} X_{Mg}^{Y\,site}.$$

In the experimentally calibrated geothermometer of Ellis and Green (1979) X_{Mg} is calculated as Mg/Mg+Fe based on total Mg and Fe without considering element site distribution.

PLAGIOCLASE

Plagioclase forms a solid solution between albite and anorthite: $NaAlSi_3O_8$ and $CaAl_2Si_2O_8$. Mole fractions of anorthite utilized in the geobarometers of Newton and Haselton (1981) and Newton and Perkins (1982) are based on the Al-avoidence model of Kerrick and Darken (1975) and expressed by:

$$X_{AN}^{PLG} = X_{Ca}^{PLG}\left[\frac{(1 + X_{Ca}^{PLG})}{1}\right]$$

where X_{Ca}^{PLG} represents the ratio Ca/Ca+Na.

MINERAL ANALYSES

In the following tables, mineral analyses and mineral formula calculations for garnet (GNT), biotite (BIO), plagioclase (PLG) and clinopyroxene (CPX) are grouped according to sample number and location of point (core / rim / intermediate / traverse).

Despite considerable time and effort spent in repeated calibration of the electron microprobe, some analyses have weight percent totals that are not correct. For instance, total weight percent for some analyses of garnet and plagioclase are in excess of 102% and some biotite analyses sum to approximately 94% rather than an expected value of about 97%. The source of these errors is not always clear, but in at least some of the analyses, it can be traced to Si values, which are stoichiometrically in excess of the

required amounts. Analyses of analytical errors with respect to standards is discussed in Appendix 4. Table A2-1 includes only analyses utilized in this study for geothermobarometric estimates or evaluation of elemental zonation in minerals.

Table A2-1: Electron microprobe mineral analyses.

Sample:	77	77	77	77	77	77	77	77	77	77	77	77	77	77	77
Min:	GNT	GNT	PLG	PLG	BIO	BIO	GNT	GNT	PLG	PLG	BIO	BIO	GNT	GNT	PLG
Type:	CORE	RIM	CORE	RIM	RIM	CORE	CORE	RIM	CORE	RIM	CORE	RIM	CORE	RIM	CORE
Code:	A01	A02	A35	A36	A43	A44	B01	B03	B37	B38	B44	B45	C01	C03	C3
SiO2	39 32	39 47	62 99	61.72	36.60	37.55	38.97	34 29	61 14	63.14	37.57	36 17	37.70	36 72	62.84
TiO2	0.00	0 02	0.01	0.02	3 63	3.58	0 02	0.03	0 00	0 01	3 80	3.77	0 00	0 00	0.01
Al2O3	21.07	21 74	24 20	24.20	17 67	17.15	22 01	22 27	24 03	24 40	17.04	17.89	22 02	21.51	22.79
Cr2O3	0.02	0 03	0 02	0 00	0 02	0 02	0 03	0 02	0 00	0.00	0 02	0 00	0.00	0.00	0.00
FeO	26.71	26 09	0.00	0.06	13.01	13 99	26 82	26 68	0 04	0 08	14.27	13.67	25.35	24 83	0 00
MnO	9 14	8 88	0 00	0 04	0 07	0.14	8 27	8 91	0 02	0 00	0 14	0 11	7.48	8 60	0 18
MgO	4 96	4 89	0 00	0 00	14 94	14 45	5.43	5 47	0 00	0 00	14 39	14.28	6 39	5 49	0 00
CaO	1 00	0 91	6 04	5 98	0.00	0.00	0 88	1 14	5 94	5.78	0.00	0 00	1.01	0 89	5 65
Na2O	0 09	0 04	8 89	8.77	0 03	0.05	0 04	0 00	8 36	8 10	0.15	0.16	0.05	0 01	8 61
K2O	0.00	0 00	0.15	0.13	9.27	9 54	0 00	0.01	0 11	0.09	9.11	9 56	0 07	0 02	0.15
Sum	102 31	102 67	102 30	100 92	95 24	96 47	102 47	98 82	99 64	102.60	96.49	95 61	100 65	98.07	100 23
Si	3 053	3 044	2 739	2.723	2.701	2.748	3 009	2.794	2 727	2 737	2 747	2 676	2 956	2 964	2 783
Ti	0 000	0 001	0 000	0 001	0 201	0 197	0 001	0 002	0 000	0 000	0 209	0 210	0 000	0 000	0 000
Al	1.928	1 976	1 240	1 258	1 537	1.479	2 003	2 139	1 263	1 247	1.468	1.560	2 035	2 046	1.190
Cr	0 001	0 002	0 001	0 000	0 001	0 001	0 002	0 001	0 000	0 000	0.001	0 000	0 000	0 000	0 000
Fe	1 734	1 722	0 000	0 002	0 803	0 856	1 732	1 818	0 001	0 003	0 872	0 846	1 701	1 676	0 000
Mn	0 601	0 580	0 000	0 001	0 004	0 009	0 541	0 615	0 001	0 000	0 009	0 007	0 495	0 588	0 007
Mg	0 574	0 562	0 000	0 000	1 643	1 576	0 625	0 664	0 000	0 000	1.568	1.574	0 747	0 660	0 000
Ca	0 083	0 075	0 281	0 283	0 000	0 000	0 073	0 100	0 284	0 268	0 000	0 000	0 085	0 077	0 268
Na	0 014	0 006	0 749	0 750	0 004	0 007	0 006	0 000	0 723	0 765	0 021	0 023	0 008	0 002	0 739
K	0 000	0 000	0 008	0 007	0 873	0 691	0 000	0 001	0 006	0 005	0 850	0 902	0 007	0 002	0 008
Sum	7 989	7 968	5 019	5 026	7 767	7 764	7 991	8 134	5 006	5 024	7 745	7 797	8 034	8 015	4 996
XMg	0 249	0 246	0 000	0 000	0 672	0 648	0 265	0 268	0 000	0 000	0 642	0 651	0 305	0 283	0 000
Al4	0 000	0 000	0 261	0 277	1 299	1 252	0 000	0 206	0 273	0 263	1 253	1 324	0 044	0 036	0 217
Al6	1 928	1 976	0 979	0 981	0 238	0 227	2 003	1 933	0 990	0 983	0 215	0 235	1 991	2 010	0 973

Table A2-1: Electron microprobe mineral analyses.

Sample	77	77	77
Min.	PLG	BIO	BIO
Type	RIM	CORE	RIM
Code	C32	C42	C43
SiO2	63.66	36.66	36.96
TiO2	0.00	2.81	2.73
Al2O3	22.63	16.78	16.51
Cr2O3	0.00	0.00	0.00
FeO	0.02	12.71	13.11
MnO	0.25	0.11	0.13
MgO	0.00	14.97	14.95
CaO	4.56	0.00	0.00
Na2O	8.21	0.12	0.08
K2O	0.28	11.19	11.10
Sum	99.61	95.35	95.59
Si	2.820	2.734	2.753
Ti	0.000	0.158	0.153
Al	1.182	1.475	1.449
Cr	0.000	0.000	0.000
Fe	0.001	0.793	0.816
Mn	0.009	0.007	0.008
Mg	0.000	1.664	1.658
Ca	0.216	0.000	0.000
Na	0.705	0.017	0.012
K	0.016	1.065	1.054
Sum	4.949	7.912	7.903
XMg	0.000	0.677	0.670
AI4	0.180	1.266	1.247
AI6	1.002	0.209	0.201

Table A2-1: Electron microprobe mineral analyses.

Sample:	235	235	235	235	235	235	235	235	235	235	235	235	235	235	235
Min:	PLG	PLG	BIO	BIO	GNT	GNT	GNT	GNT	GNT	GNT	GNT	GNT	GNT	PLG	BIO
Type:	CORE	RIM	CORE	RIM	TRAV	TRAV	TRAV	TRAV	TRAV	TRAV	TRAV	TRAV	TRAV	RIM	CORE
Code:	A31	A32	A41	A42	A51	A52	A54	A55	A56	A57	A58	A59	A60	C32	C41
SiO2	61.46	62.00	37.59	37.84	37.12	37.42	36.21	38.06	37.94	37.53	35.16	36.91	37.10	62.01	37.84
TiO2	0.00	0.02	4.07	4.45	0.06	0.00	0.01	0.00	0.04	0.05	0.00	0.02	0.01	0.00	4.18
Al2O3	23.49	23.30	15.97	15.59	22.26	21.98	21.90	22.21	22.17	21.92	23.39	22.68	22.35	23.13	16.07
Cr2O3	0.01	0.01	0.02	0.00	0.00	0.00	0.00	0.00	0.00	0.00	0.00	0.00	0.00	0.00	0.00
FeO	0.07	0.10	14.57	14.21	28.68	26.43	25.02	26.30	26.12	25.20	25.21	27.15	26.38	0.09	12.90
MnO	0.03	0.00	0.03	0.17	4.26	4.05	2.93	3.96	3.73	3.57	3.50	3.96	3.71	0.05	0.03
MgO	0.01	0.00	14.80	14.52	6.88	6.68	7.69	7.63	7.67	7.19	6.62	7.81	7.34	0.00	15.42
CaO	6.29	6.24	0.00	0.00	1.19	1.14	1.17	1.04	1.15	1.14	1.16	1.18	1.14	6.18	0.00
Na2O	7.75	8.07	0.07	0.07	0.12	0.00	0.00	0.13	0.02	0.00	0.01	0.09	0.04	8.26	0.10
K2O	0.09	0.09	9.80	9.39	0.16	0.00	0.04	0.03	0.00	0.00	0.05	0.05	0.03	0.07	9.55
Sum	99.20	99.83	96.92	96.24	100.73	97.70	94.97	99.36	98.84	96.60	95.10	99.85	98.10	99.79	96.09
Si	2.749	2.757	2.754	2.781	2.911	2.985	2.950	2.978	2.979	3.004	2.873	2.894	2.945	2.760	2.768
Ti	0.000	0.001	0.224	0.246	0.004	0.000	0.001	0.000	0.002	0.003	0.000	0.001	0.001	0.000	0.230
Al	1.238	1.221	1.379	1.351	2.058	2.067	2.103	2.048	2.052	2.068	2.253	2.096	2.092	1.214	1.386
Cr	0.000	0.000	0.001	0.000	0.000	0.000	0.000	0.000	0.000	0.000	0.000	0.000	0.000	0.000	0.000
Fe	0.003	0.004	0.893	0.873	1.881	1.763	1.705	1.721	1.715	1.687	1.723	1.780	1.751	0.003	0.789
Mn	0.001	0.000	0.002	0.011	0.283	0.274	0.202	0.262	0.248	0.242	0.242	0.263	0.249	0.002	0.002
Mg	0.001	0.000	1.616	1.590	0.804	0.794	0.934	0.890	0.898	0.858	0.806	0.913	0.868	0.000	1.681
Ca	0.301	0.297	0.000	0.000	0.100	0.097	0.102	0.087	0.097	0.098	0.102	0.099	0.097	0.295	0.000
Na	0.672	0.696	0.010	0.010	0.018	0.000	0.000	0.020	0.003	0.000	0.002	0.014	0.008	0.713	0.014
K	0.005	0.005	0.916	0.880	0.016	0.000	0.004	0.003	0.000	0.000	0.005	0.005	0.003	0.004	0.891
Sum	4.970	4.982	7.795	7.743	8.074	7.981	8.000	8.009	7.994	7.959	8.004	8.066	8.013	4.991	7.762
XMg	0.203	0.000	0.644	0.645	0.299	0.311	0.354	0.341	0.344	0.337	0.319	0.339	0.331	0.000	0.681
AlIV	0.251	0.243	1.246	1.219	0.089	0.015	0.050	0.022	0.021	0.000	0.127	0.106	0.055	0.240	1.232
AlVI	0.987	0.979	0.133	0.132	1.968	2.052	2.053	2.026	2.031	2.068	2.125	1.990	2.037	0.974	0.154

Table A2-1: Electron microprobe mineral analyses.

Sample:	235	235	235	235	235	235	235	235	235	235	235	235	235	235	235
Min:	BIO	GNT	GNT	GNT	GNT	GNT	GNT	GNT	GNT	GNT	GNT	GNT	GNT	PLG	BIO
Type:	RIM	TRAV	TRAV	TRAV	TRAV	TRAV	TRAV	TRAV	TRAV	TRAV	TRAV	CORE	RIM	CORE	CORE
Code:	C42	C51	C52	C53	C54	C55	C56	C57	C58	C59	C60	D01	D02	D31	D44
SiO2	37.90	38.41	38.39	37.77	37.91	37.63	37.10	38.04	39.96	37.90	37.33	38.50	39.68	61.46	37.66
TiO2	4.17	0.03	0.06	0.06	0.05	0.06	0.04	0.07	0.02	0.04	0.04	0.04	0.03	0.00	4.43
Al2O3	16.34	23.08	22.48	22.71	22.91	22.67	22.14	23.23	22.57	22.63	22.37	21.80	21.40	23.49	16.00
Cr2O3	0.00	0.00	0.00	0.00	0.00	0.00	0.00	0.00	0.00	0.00	0.00	0.03	0.00	0.02	0.03
FeO	13.29	28.52	26.96	27.10	27.36	27.87	26.50	28.38	27.58	27.63	30.76	27.34	28.40	0.06	13.40
MnO	0.07	3.48	3.84	3.93	3.44	3.92	3.81	3.66	3.83	2.98	4.46	4.21	4.11	0.01	0.06
MgO	15.56	7.89	8.07	8.20	7.75	8.27	7.88	7.36	7.35	7.66	6.94	7.41	6.41	0.00	14.57
CaO	0.00	1.09	0.96	1.13	1.01	1.22	1.14	1.04	1.12	1.06	1.15	1.07	1.19	6.23	0.00
Na2O	0.10	0.03	0.07	0.08	0.11	0.06	0.13	0.00	0.00	0.00	0.10	0.01	0.01	8.37	0.18
K2O	9.48	0.04	0.04	0.00	0.07	0.00	0.03	0.04	0.02	0.03	0.08	0.01	0.00	0.09	9.26
Sum	96.91	102.57	100.87	100.98	100.61	101.70	98.77	99.82	102.45	99.95	103.23	100.42	101.23	99.73	95.59
Si	2.752	2.927	2.961	2.919	2.935	2.899	2.931	2.841	3.028	2.951	2.881	2.994	3.066	2.741	2.773
Ti	0.228	0.002	0.003	0.003	0.003	0.003	0.002	0.004	0.001	0.002	0.002	0.002	0.002	0.000	0.245
Al	1.399	2.073	2.044	2.069	2.091	2.059	2.062	2.159	2.016	2.077	2.035	1.999	1.949	1.235	1.389
Cr	0.000	0.000	0.000	0.000	0.000	0.000	0.000	0.000	0.000	0.000	0.000	0.002	0.000	0.001	0.002
Fe	0.807	1.818	1.739	1.751	1.772	1.796	1.751	1.871	1.748	1.799	1.985	1.778	1.835	0.002	0.825
Mn	0.004	0.225	0.251	0.257	0.226	0.256	0.255	0.244	0.246	0.197	0.292	0.277	0.269	0.000	0.004
Mg	1.684	0.896	0.928	0.944	0.894	0.950	0.928	0.865	0.830	0.891	0.798	0.859	0.738	0.000	1.599
Ca	0.000	0.089	0.079	0.094	0.084	0.101	0.096	0.088	0.091	0.088	0.095	0.089	0.099	0.298	0.000
Na	0.014	0.004	0.010	0.012	0.017	0.009	0.020	0.000	0.000	0.000	0.015	0.002	0.001	0.724	0.028
K	0.878	0.004	0.004	0.000	0.007	0.000	0.003	0.004	0.002	0.003	0.008	0.001	0.000	0.005	0.870
Sum	7.767	8.038	8.020	8.049	8.028	8.072	8.047	8.077	7.963	8.009	8.111	8.004	7.959	5.006	7.733
XMg	0.676	0.330	0.348	0.350	0.335	0.346	0.346	0.316	0.322	0.331	0.287	0.326	0.287	0.000	0.660
Al4	1.248	0.073	0.039	0.081	0.065	0.101	0.069	0.159	0.000	0.049	0.119	0.006	0.000	0.259	1.227
Al6	0.151	2.001	2.005	1.987	2.026	1.958	1.992	2.000	2.016	2.028	1.916	1.993	1.949	0.976	0.162

Table A2-1: Electron microprobe mineral analyses.

Sample:	368	368	368	368	368	368	368	368	368	368	368	368	368	368	368
Min:	GNT	GNT	PLG	PLG	BIO	GNT	GNT	PLG	PLG	BIO	BIO	GNT	GNT	GNT	GNT
Type:	CORE	RIM	CORE	RIM	RIM	CORE	RIM	CORE	RIM	RIM	CORE	TRAV	TRAV	TRAV	TRAV
Code:	A01	A02	A33	A34	A46	B01	B02	B35	B36	B43	B44	B51	B52	B53	B54
SiO2	39.29	39.41	62.47	61.38	37.39	40.42	40.26	65.20	64.42	36.45	38.54	38.88	38.82	38.47	38.37
TiO2	0.02	0.00	0.00	0.04	3.22	0.00	0.02	0.01	0.01	2.98	3.45	0.02	0.05	0.02	0.02
Al2O3	22.05	22.15	23.46	23.73	16.82	22.01	21.91	24.59	23.81	18.35	17.78	23.32	23.23	23.09	22.73
Cr2O3	0.02	0.02	0.00	0.02	0.05	0.00	0.02	0.02	0.00	0.05	0.00	0.00	0.00	0.00	0.00
FeO	27.23	26.79	0.04	0.00	12.72	26.27	26.91	0.04	0.03	12.10	12.48	27.05	25.31	28.23	26.96
MnO	3.12	2.82	0.02	0.02	0.08	3.16	2.56	0.00	0.00	0.05	0.04	2.44	2.18	2.40	2.50
MgO	9.43	9.37	0.00	0.00	15.64	9.57	9.37	0.01	0.00	15.31	15.74	10.34	10.56	10.26	10.34
CaO	0.86	0.86	5.18	4.88	0.00	0.86	0.70	5.45	4.96	0.00	0.00	0.86	0.90	0.84	1.08
Na2O	0.09	0.04	9.21	9.22	0.06	0.02	0.10	5.54	9.47	0.10	0.11	0.01	0.11	0.09	0.02
K2O	0.01	0.02	0.16	0.17	9.16	0.00	0.00	0.20	0.10	9.09	9.07	0.00	0.00	0.00	0.00
Sum	102.12	101.48	100.54	99.46	95.14	102.31	101.85	101.06	102.80	94.48	97.21	102.92	101.16	103.40	102.02
Si	2.982	2.998	2.760	2.742	2.754	3.039	3.042	2.815	2.778	2.695	2.761	2.917	2.937	2.890	2.910
Ti	0.001	0.000	0.000	0.001	0.178	0.000	0.001	0.000	0.000	0.166	0.186	0.001	0.003	0.001	0.001
Al	1.973	1.986	1.222	1.249	1.460	1.951	1.952	1.251	1.210	1.599	1.502	2.059	2.072	2.045	2.032
Cr	0.001	0.001	0.000	0.001	0.003	0.000	0.001	0.001	0.000	0.003	0.000	0.000	0.000	0.000	0.000
Fe	1.728	1.704	0.001	0.000	0.784	1.652	1.701	0.001	0.001	0.748	0.748	1.695	1.601	1.774	1.710
Mn	0.201	0.182	0.001	0.001	0.005	0.201	0.184	0.000	0.000	0.003	0.002	0.155	0.140	0.153	0.161
Mg	1.067	1.062	0.000	0.000	1.717	1.072	1.055	0.001	0.000	1.687	1.681	1.155	1.191	1.149	1.169
Ca	0.070	0.070	0.245	0.234	0.000	0.069	0.057	0.252	0.229	0.000	0.000	0.069	0.073	0.068	0.088
Na	0.013	0.006	0.789	0.799	0.009	0.003	0.015	0.464	0.792	0.014	0.015	0.001	0.016	0.013	0.003
K	0.001	0.002	0.009	0.010	0.861	0.000	0.000	0.011	0.006	0.858	0.829	0.000	0.000	0.000	0.000
Sum	8.037	8.012	5.028	5.036	7.770	7.987	7.987	4.796	5.015	7.774	7.724	8.052	8.032	8.092	8.074
XMg	0.382	0.384	0.000	0.000	0.687	0.394	0.383	0.308	0.000	0.693	0.692	0.405	0.426	0.393	0.406
Al4	0.018	0.002	0.240	0.258	1.246	0.000	0.000	0.185	0.222	1.305	1.239	0.197	0.063	0.110	0.090
Al6	1.955	1.984	0.982	0.991	0.214	1.951	1.952	1.066	0.988	0.295	0.263	1.785	2.009	1.935	1.942

Table A2-1: Electron microprobe mineral analyses.

Sample:	368	368	368	368	368	368	368	368	368	368	368	368	368	368	368
Min:	GNT	GNT	GNT	GNT	GNT	GNT	GNT	GNT	GNT	PLG	PLG	BIO	BIO	GNT	GNT
Type:	TRAV	TRAV	TRAV	TRAV	TRAV	TRAV	CORE	INT	RIM	CORE	RIM	CORE	RIM	TRAV	TRAV
Code:	B55	B56	B57	B58	B59	B60	C01	C02	C03	C31	C32	C41	C43	C51	C52
SiO2	38.16	38.24	39.20	38.82	39.21	38.31	37.57	37.91	38.41	62.41	63.42	37.88	37.16	38.77	36.89
TiO2	0.04	0.02	0.00	0.00	0.00	0.01	0.00	0.00	0.05	0.07	0.02	2.05	2.68	0.02	0.02
Al2O3	23.22	22.06	23.48	23.53	23.13	23.52	22.65	21.51	22.83	21.32	21.98	17.63	16.48	23.35	22.80
Cr2O3	0.00	0.00	0.00	0.00	0.00	0.00	0.00	0.00	0.00	0.00	0.00	0.00	0.00	0.00	0.00
FeO	27.54	27.27	27.36	27.29	26.96	27.64	25.43	24.46	25.55	0.00	0.01	10.98	10.97	23.96	25.30
MnO	2.52	2.53	2.53	2.52	2.59	2.66	2.88	2.83	2.41	0.00	0.06	0.01	0.05	2.33	2.23
MgO	10.17	10.27	10.35	10.36	9.90	10.69	10.37	10.34	10.95	0.00	0.00	16.96	15.11	9.75	10.59
CaO	0.73	0.81	0.81	0.80	0.84	0.77	0.78	0.70	0.80	4.79	4.65	0.00	0.00	0.81	0.81
Na2O	0.00	0.01	0.07	0.00	0.13	0.01	0.06	0.07	0.01	9.07	8.66	0.03	0.09	0.04	0.05
K2O	0.04	0.02	0.01	0.00	0.04	0.03	0.02	0.06	0.04	0.11	0.12	11.03	11.16	0.11	0.02
Sum	102.42	101.23	103.81	103.42	102.80	103.64	99.76	97.88	101.05	97.77	98.94	96.57	93.70	99.14	98.71
Si	2.888	2.929	2.916	2.900	2.943	2.866	2.904	2.974	2.919	2.827	2.830	2.749	2.791	2.975	2.877
Ti	0.002	0.001	0.000	0.000	0.000	0.001	0.000	0.000	0.003	0.002	0.001	0.112	0.151	0.001	0.001
Al	2.071	1.992	2.059	2.072	2.047	2.074	2.064	1.989	2.045	1.138	1.156	1.508	1.459	2.112	2.096
Cr	0.000	0.000	0.000	0.000	0.000	0.000	0.000	0.000	0.000	0.000	0.000	0.000	0.000	0.000	0.000
Fe	1.743	1.747	1.702	1.705	1.692	1.730	1.644	1.605	1.624	0.000	0.000	0.667	0.689	1.538	1.650
Mn	0.162	0.164	0.159	0.159	0.165	0.169	0.189	0.188	0.155	0.000	0.002	0.001	0.003	0.151	0.147
Mg	1.147	1.172	1.147	1.154	1.107	1.192	1.194	1.209	1.240	0.000	0.000	1.835	1.692	1.115	1.231
Ca	0.059	0.066	0.065	0.072	0.068	0.062	0.065	0.059	0.065	0.232	0.222	0.000	0.000	0.067	0.068
Na	0.000	0.001	0.010	0.000	0.019	0.001	0.009	0.011	0.001	0.797	0.751	0.004	0.013	0.008	0.008
K	0.004	0.002	0.001	0.000	0.004	0.003	0.002	0.006	0.004	0.006	0.007	1.021	1.070	0.011	0.002
Sum	8.076	8.075	8.060	8.063	8.045	8.098	8.070	8.040	8.058	5.003	4.970	7.897	7.869	7.976	8.079
XMg	0.397	0.402	0.403	0.404	0.396	0.408	0.421	0.430	0.433	0.000	0.000	0.734	0.711	0.420	0.427
AlⅣ	0.112	0.071	0.084	0.100	0.057	0.134	0.096	0.026	0.081	0.173	0.170	1.251	1.209	0.025	0.123
AlⅥ	1.959	1.921	1.975	1.973	1.990	1.941	1.967	1.963	1.965	0.965	0.986	0.258	0.251	2.087	1.972

Table A2-1: Electron microprobe mineral analyses.

Sample:	368	368	368	368	368	368	368	368	368	368	368	368	368	368	368
Min:	GNT	GNT	GNT	GNT	GNT	GNT	GNT	GNT	GNT	GNT	GNT	PLG	PLG	BIO	BIO
Type	TRAV	TRAV	TRAV	TRAV	TRAV	TRAV	TRAV	TRAV	CORE	RIM	RIM	CORE	RIM	CORE	RIM
Code:	C53	C54	C55	C56	C57	C58	C59	C60	D01	D02	D03	D31	D32	D41	D42
SiO2	38 73	39.07	38.93	39.23	38.24	38 84	38.24	38 82	39 47	38 13	37.83	63.43	63 45	36.16	37.52
TiO2	0 00	0 02	0 02	0 02	0.00	0 00	0.00	0 06	0.02	0.03	0.00	0 03	0.05	3 36	2 96
Al2O3	23 06	22 83	22 82	23.16	22 22	23 06	22 40	22.79	22 87	22 64	22 77	21 95	21 41	15 15	16 23
Cr2O3	0 00	0 00	0.00	0.00	0 00	0 01	0 00	0 00	0.00	0 00	0 00	0 00	0 00	0 00	0 00
FeO	24.72	26.15	25.33	27.13	26 05	25 54	25 23	25.19	24.77	24.49	25.34	0.02	0 04	12 12	12.05
MnO	2 41	2 38	2.68	2 56	2 70	2.45	2 71	2 58	2 46	2.09	2 23	0 09	0.12	0 05	0 04
MgO	10 46	10 44	9 94	10.70	10 22	10.30	10 06	10 34	10 22	9 64	9 86	0 00	0 00	15 92	16.43
CaO	0 86	0 77	0 96	0.73	0 95	0 81	0 89	0 84	0 77	0.78	0 83	4 87	4 22	0 00	0 00
Na2O	0 05	0 03	0 08	0 00	0 04	0 00	0 02	0 06	0.00	0 00	0 02	9 08	9 18	0 04	0.08
K2O	0 04	0 04	0 00	0 00	0 00	0 00	0 09	0 03	0 01	0 00	0 04	0 09	0 05	10 64	10 94
Sum	100 33	101 73	100 76	103 53	100 42	101 01	99 64	100 71	100 59	97 80	98 92	99 56	98 52	93 44	96 25
Si	2 950	2 951	2 964	2 923	2 939	2 948	2 951	2 954	2 993	2 975	2 936	2 821	2 845	2 745	2 754
Ti	0 000	0 001	0 001	0 001	0 000	0 000	0 000	0 003	0 001	0 002	0 000	0 001	0 002	0 192	0 163
Al	2 071	2 033	2 048	2 034	2 013	2 063	2 038	2 045	2 044	2 082	2.083	1 151	1 132	1 356	1 404
Cr	0 000	0 000	0 000	0 000	0 000	0 001	0 000	0.000	0 000	0.000	0 000	0 000	0 000	0 000	0 000
Fe	1 575	1 652	1 613	1 691	1 674	1 621	1 628	1 603	1 571	1 598	1 645	0 001	0 001	0 770	0 740
Mn	0 155	0 152	0 173	0 162	0 176	0 157	0 177	0 166	0 158	0 138	0 147	0 003	0 005	0 003	0 002
Mg	1 187	1 175	1 128	1 188	1.171	1 165	1 157	1 173	1 155	1 121	1.140	0 000	0 000	1 801	1 797
Ca	0 070	0 062	0 078	0 058	0 078	0 066	0 074	0 069	0 063	0 065	0 069	0 232	0 203	0 000	0 000
Na	0 007	0 004	0 012	0 000	0 006	0 000	0 003	0 009	0 000	0 000	0 003	0 783	0 798	0 006	0 011
K	0 004	0 004	0 000	0 000	0 000	0 000	0 009	0 003	0 001	0 000	0 004	0 005	0 003	1 031	1 025
Sum	8 020	8 035	8 017	8 058	8 057	8 020	8 036	8 025	7 985	7 982	8 026	4 997	4 988	7 903	7 898
XMg	0 430	0 416	0 412	0 413	0 411	0 418	0 415	0 422	0 424	0 412	0 409	0 000	0 000	0 701	0 708
AlI4	0 050	0 049	0 036	0 077	0 061	0 052	0 049	0 046	0 007	0 025	0 064	0 179	0 155	1 255	1 246
AlI6	2 021	1 984	2 012	1 958	1 952	2 010	1 988	1 999	2 036	2 057	2 019	0 971	0 976	0 101	0 159

Table A2-1: Electron microprobe mineral analyses.

Sample	377	377	377	377	377	377	377	377	377	377	377	377	377	377	377
Min:	GNT	PLG	GNT	GNT	BIO	BIO	GNT	GNT	GNT	PLG	PLG	GNT	GNT	PLG	PLG
Type:	CORE	RIM	CORE	RIM	RIM	CPRE	CORE	INT	RIM	CORE	CORE	CORE	RIM	CORE	RIM
Code:	A01	A35	B01	B02	B43	B44	C01	C02	C03	C31	C32	D01	D03	D31	D32
SiO2	37.94	61.63	39.66	38.76	37.95	37.40	37.50	37.64	37.45	61.55	64.21	37.25	38.79	63.28	62.64
TiO2	0.00	0.03	0.02	0.02	3.25	3.21	0.00	0.02	0.01	0.03	0.06	0.02	0.02	0.03	0.00
Al2O3	21.71	23.41	21.61	20.96	16.71	17.04	22.39	22.00	21.89	22.25	22.54	22.41	21.81	22.04	22.63
Cr2O3	0.02	0.00	0.00	0.00	0.00	0.02	0.00	0.00	0.00	0.00	0.00	0.00	0.00	0.00	0.00
FeO	30.60	0.06	30.73	30.62	13.03	13.25	29.40	30.31	29.89	0.01	0.03	28.02	29.57	0.03	0.00
MnO	1.92	0.01	1.95	1.81	0.03	0.04	1.85	1.81	1.77	0.00	0.07	1.78	1.59	0.02	0.05
MgO	7.42	0.02	7.35	6.91	14.07	15.09	8.21	7.44	6.62	0.02	0.00	7.97	7.11	0.00	0.00
CaO	0.82	5.23	0.85	0.95	0.00	0.00	0.66	0.82	1.09	4.98	5.05	0.93	0.88	4.94	5.09
Na2O	0.00	8.81	0.04	0.00	0.16	0.13	0.12	0.04	0.00	8.80	8.48	0.00	0.00	8.73	8.83
K2O	0.01	0.11	0.03	0.00	8.84	8.75	0.01	0.04	0.03	0.14	0.17	0.02	0.03	0.13	0.10
Sum	100.44	99.31	102.24	100.03	94.04	94.93	100.14	100.12	98.75	97.78	100.61	98.40	97.80	99.20	99.34
Si	2.967	2.754	3.034	3.039	2.820	2.759	2.926	2.950	2.973	2.790	2.819	2.941	2.947	2.821	2.793
Ti	0.000	0.001	0.001	0.001	0.182	0.178	0.000	0.001	0.001	0.001	0.002	0.001	0.001	0.001	0.000
Al	2.001	1.233	1.949	1.937	1.464	1.482	2.059	2.032	2.048	1.189	1.167	2.086	2.059	1.158	1.189
Cr	0.001	0.000	0.000	0.000	0.000	0.001	0.000	0.000	0.000	0.000	0.000	0.000	0.000	0.000	0.000
Fe	2.001	0.002	1.966	2.008	0.810	0.818	1.918	1.986	1.984	0.000	0.001	1.850	1.961	0.001	0.000
Mn	0.127	0.000	0.126	0.120	0.002	0.002	0.122	0.120	0.119	0.000	0.003	0.119	0.108	0.001	0.002
Mg	0.865	0.001	0.838	0.807	1.558	1.659	0.955	0.869	0.783	0.001	0.000	0.938	0.849	0.000	0.000
Ca	0.069	0.250	0.070	0.080	0.000	0.000	0.055	0.069	0.093	0.242	0.238	0.079	0.078	0.236	0.243
Na	0.000	0.763	0.006	0.000	0.023	0.019	0.018	0.006	0.000	0.773	0.722	0.000	0.000	0.755	0.763
K	0.001	0.006	0.003	0.000	0.838	0.824	0.001	0.004	0.003	0.008	0.010	0.002	0.003	0.007	0.006
Sum	8.032	5.013	7.994	7.992	7.697	7.742	8.054	8.038	8.004	5.005	4.961	8.016	8.023	4.980	4.997
XMg	0.302	0.373	0.299	0.287	0.658	0.670	0.332	0.304	0.283	0.781	0.000	0.336	0.300	0.000	0.000
Al4	0.033	0.246	0.000	0.000	1.180	1.241	0.074	0.050	0.027	0.210	0.181	0.059	0.053	0.179	0.207
Al6	1.968	0.988	1.949	1.937	0.284	0.241	1.985	1.982	2.021	0.979	0.986	2.027	2.006	0.979	0.982

Table A2-1: Electron microprobe mineral analyses.

Sample:	377	377
Min:	BIO	BIO
Type:	CORE	RIM
Code:	D41	D42
SiO2	36.55	37.50
TiO2	2.50	2.25
Al2O3	16.39	16.43
Cr2O3	0.00	0.00
FeO	12.50	12.36
MnO	0.00	0.00
MgO	15.56	15.75
CaO	0.00	0.00
Na2O	0.03	0.12
K2O	10.96	11.05
Sum	94.49	95.46
Si	2.744	2.779
Ti	0.141	0.125
Al	1.451	1.435
Cr	0.000	0.000
Fe	0.785	0.766
Mn	0.000	0.000
Mg	1.741	1.740
Ca	0.000	0.000
Na	0.004	0.017
K	1.050	1.045
Sum	7.916	7.908
XMg	0.689	0.694
Al4	1.256	1.221
Al6	0.195	0.215

Table A2-1: Electron microprobe mineral analyses.

Sample	403	403	403	403	403	403	403	403	403	403	403	403	403	403	403
Min	GNT	GNT	BIO	GNT	GNT	CPX	CPX	PLA	PLA	BIO	BIO	GNT	GNT	CPX	CPX
Type	CORE	INT	RIM	CORE	RIM	CORE	RIM	CORE	RIM	RIM	CORE	CORE	RIM	CORE	RIM
Code	A01	A02	A45	B01	B02	B27	B28	B35	B36	B43	B44	C01	C03	C24	C25
SiO2	40 22	38 60	37 29	39 44	39.26	52 79	51.79	64 05	64 79	37 77	36.09	39 57	39 43	51 21	50 31
TiO2	0 00	0 01	4 65	0 06	0 03	0 18	0.20	0 00	0 01	4 67	4.77	0 00	0 00	0 05	0 02
Al2O3	21 04	20 72	13 79	21 55	20 46	2 59	3 24	22 00	22 20	14 33	14 27	20 70	21.10	2 80	2 39
Cr2O3	0 06	0 00	0 00	0 00	0 01	0 03	0 00	0 00	0 00	0 00	0 01	0 04	0 04	0 09	0 05
FeO	24 28	24 54	17 70	25 32	25 78	11 45	11.51	0 10	0 13	17 97	17 98	25.40	25 56	13 26	11 60
MnO	2 75	3 11	0 16	2 97	3 97	0 60	0 52	0 03	0 02	0 09	0.11	3 63	3 95	0 32	0 63
MgO	4 66	4 86	12 32	4 95	4 43	11 79	11 11	0 00	0 01	12 14	12 37	4 93	4 76	11 51	11 59
CaO	8 75	7 59	0 00	8 46	7.24	20 39	19 44	3 55	4 15	0 00	0.02	6 48	6 34	18 92	18 86
Na2O	0 04	0 06	0 04	0.01	0.01	1 35	0 82	9 84	9 47	0 02	0 04	0 00	0 00	1 16	0 82
K2O	0 00	0 00	9 15	0.00	0 00	0.01	0.02	0 32	0 32	8 66	9 04	0 01	0 00	0.00	0.00
Sum	101.80	99.49	95 10	102 76	101 19	101 18	98 65	99 89	101.10	95 65	94 70	100 76	101 18	99 32	96 27
Si	3 080	3.038	2 826	3.010	3 058	1 964	1 968	2 836	2 835	2 833	2 757	3 075	3 056	1 951	1 967
Ti	0.000	0.001	0 265	0.003	0.002	0 005	0 006	0.000	0 000	0 263	0 274	0 000	0 000	0 001	0 001
Al	1.899	1 923	1 232	1 939	1.879	0.114	0.145	1.148	1.145	1.267	1 285	1 896	1.928	0.126	0 110
Cr	0 004	0 000	0 000	0.000	0 001	0 001	0 000	0 000	0 000	0 000	0 001	0 002	0 002	0.003	0 002
Fe	1 555	1 616	1 122	1.616	1.679	0 356	0 366	0 004	0 005	1 127	1.149	1.651	1 657	0 423	0 379
Mn	0.178	0.207	0.010	0 192	0 262	0 019	0 017	0 001	0 001	0 006	0 007	0 239	0 259	0 010	0 021
Mg	0.532	0.570	1 392	0 563	0 514	0 654	0 629	0.000	0 001	1 357	1 408	0 571	0 550	0 654	0 675
Ca	0.718	0.640	0 000	0 692	0 604	0 813	0 792	0 168	0 195	0 000	0 002	0 540	0 527	0 772	0 790
Na	0 006	0 009	0 006	0.001	0 002	0 097	0 060	0 845	0 803	0 003	0 006	0 000	0 000	0 086	0 062
K	0 000	0 000	0 885	0 000	0 000	0 000	0 001	0 018	0 018	0 829	0 881	0 001	0 000	0 000	0 000
Sum	7 972	8 004	7 738	8 017	8 001	4 023	3 984	5 021	5 003	7 685	7 769	7 976	7 979	4 026	4 007
XMg	0 255	0 261	0 554	0 258	0 234	0 647	0 632	0 000	0 121	0 546	0 551	0 257	0 249	0 607	0 640
Al4	0 000	0 000	1 174	0 000	0 000	0 036	0 032	0 164	0 165	1 167	1 243	0 000	0 000	0 049	0 033
Al6	1 899	1 923	0 058	1 939	1 879	0 077	0 113	0 985	0 980	0 100	0 042	1 896	1 928	0 077	0 077

Table A2-1: Electron microprobe mineral analyses.

Sample:	403	403	403	403	403	403	403	403	403	403	403	403	403	403	403
Min:	CPX	PLA	PLA	PLA	BIO	BIO	GNT	GNT	GNT	CPX	CPX	PLG	PLG	GNT	GNT
Type:	CORE	CORE	CORE	RIM	CORE	RIM	CORE	INT	RIM	CORE	RIM	CORE	RIM	CORE	RIM
Code:	C26	C37	C38	C39	C41	C42	D01	D02	D03	D21	D22	D31	D32	E01	E03
SiO2	51.39	59.84	63.27	60.03	38.01	38.66	38.14	38.54	38.13	50.76	52.52	65.22	65.62	39.92	39.21
TiO2	0.04	0.00	0.00	0.00	4.08	3.95	0.02	0.03	0.01	0.25	0.16	0.03	0.02	0.01	0.00
Al2O3	2.67	22.29	21.84	21.81	15.32	15.33	21.64	21.69	21.71	2.86	2.25	21.47	21.47	21.00	20.92
Cr2O3	0.05	0.02	0.04	0.04	0.04	0.02	0.00	0.00	0.00	0.00	0.00	0.00	0.00	0.06	0.00
FeO	11.23	0.07	0.07	0.18	15.08	15.03	26.20	26.05	26.43	12.07	11.46	0.03	0.04	25.89	27.08
MnO	0.61	0.00	0.00	0.04	0.08	0.08	2.90	3.54	3.21	0.51	0.53	0.01	0.07	2.84	3.05
MgO	11.00	0.02	0.01	0.00	13.66	14.10	5.66	5.30	5.61	11.96	12.11	0.00	0.06	5.11	5.39
CaO	20.04	3.80	3.66	4.02	0.00	0.00	5.96	5.74	5.29	19.05	20.56	3.53	3.94	6.29	5.65
Na2O	1.23	9.84	9.86	10.00	0.02	2.03	0.00	0.09	0.00	1.26	1.25	10.13	9.04	0.00	0.12
K2O	0.00	0.26	0.22	0.22	9.15	8.86	0.07	0.04	0.01	0.02	0.00	0.26	0.15	0.01	0.00
Sum	98.26	96.14	98.97	96.34	95.44	98.06	100.59	101.02	100.40	98.74	100.84	100.68	100.41	101.13	101.42
Si	1.969	2.767	2.829	2.776	2.821	2.804	2.976	2.995	2.980	1.940	1.962	2.863	2.876	3.081	3.039
Ti	0.001	0.000	0.000	0.000	0.228	0.215	0.001	0.002	0.001	0.007	0.004	0.001	0.001	0.001	0.000
Al	0.121	1.215	1.151	1.189	1.341	1.311	1.990	1.987	2.000	0.129	0.099	1.111	1.109	1.911	1.911
Cr	0.002	0.001	0.001	0.001	0.002	0.001	0.000	0.000	0.000	0.000	0.000	0.000	0.000	0.004	0.000
Fe	0.360	0.003	0.003	0.007	0.936	0.912	1.709	1.693	1.728	0.386	0.358	0.001	0.001	1.671	1.755
Mn	0.020	0.000	0.000	0.002	0.005	0.005	0.192	0.233	0.213	0.017	0.017	0.000	0.003	0.186	0.200
Mg	0.628	0.001	0.001	0.000	1.511	1.524	0.658	0.614	0.654	0.681	0.674	0.000	0.004	0.588	0.623
Ca	0.823	0.188	0.175	0.199	0.000	0.000	0.498	0.478	0.443	0.780	0.823	0.166	0.185	0.520	0.469
Na	0.091	0.882	0.855	0.897	0.003	0.285	0.000	0.014	0.000	0.093	0.091	0.862	0.768	0.000	0.018
K	0.000	0.015	0.013	0.013	0.867	0.820	0.007	0.004	0.001	0.001	0.000	0.015	0.008	0.001	0.000
Sum	4.014	5.073	5.028	5.084	7.714	7.877	8.031	8.019	8.019	4.035	4.029	5.019	4.956	7.962	8.015
XMg	0.636	0.337	0.203	0.000	0.617	0.626	0.278	0.266	0.274	0.638	0.653	0.000	0.728	0.260	0.282
Al4	0.031	0.233	0.171	0.224	1.179	1.196	0.024	0.005	0.020	0.060	0.038	0.137	0.124	0.000	0.000
Al6	0.090	0.983	0.980	0.965	0.162	0.115	1.966	1.982	1.981	0.069	0.061	0.974	0.986	1.911	1.911

Table A2-1: Electron microprobe mineral analyses.

Sample	403	403	403	403	403	403	403	403
Min	CPX	PLA	GNT	GNT	CPX	CPX	PLG	PLG
Type	INT	INT	CORE	RIM	CORE	RIM	CORE	RIM
Code	E25	E38	F01	F02	F21	F22	F31	F32
SiO2	52 33	64 92	37.76	37.90	50.32	51.80	64 13	64 53
TiO2	0 04	0 00	0.00	0.02	0 27	0.16	0 00	0.04
Al2O3	2 32	21.58	21.99	21.85	2 81	2.07	20 84	21 50
Cr2O3	0 04	0 04	0 00	0.00	0.01	0.00	0 00	0 00
FeO	14 38	0.05	26.10	25.78	13.16	11 27	0.00	0 00
MnO	0 57	0 00	3.95	3.86	0 61	0 61	1.13	0.26
MgO	11 52	0.02	5.05	4.77	10.32	12 10	0 00	0.00
CaO	18 22	3.54	5.89	6.04	19.64	20 41	3 08	4 43
Na2O	1 29	9 80	0.07	0 04	1.43	0.83	9 30	9 22
K2O	0 02	0.19	0.03	0 03	0 01	0.00	0.25	0.21
Sum	100 73	100.14	100 84	100.29	98.58	99 25	98 73	100.19
Si	1 971	2.861	2.952	2.974	1 943	1 965	2 873	2 849
Ti	0 001	0.000	0.000	0.001	0.008	0.005	0.000	0.001
Al	0 103	1.121	2.026	2.021	0.128	0.093	1.101	1 119
Cr	0 001	0.001	0.000	0 000	0.000	0.000	0 000	0 000
Fe	0 453	0.002	1.706	1.692	0.425	0.358	0 000	0 000
Mn	0 018	0.000	0.262	0.257	0.020	0 020	0.043	0 010
Mg	0 647	0.001	0.588	0.558	0.594	0.684	0 000	0 000
Ca	0 735	0.167	0.493	0.508	0.813	0.830	0 148	0 210
Na	0 094	0 837	0.011	0.006	0.107	0.061	0 808	0 789
K	0 001	0.011	0.003	0 003	0.000	0 000	0.014	0.012
Sum	4 024	5.002	8.041	8.019	4 039	4.014	4 987	4 990
XMg	0 588	0.416	0 256	0 248	0.583	0 657	0 000	0 000
Al4	0 029	0.139	0.048	0 026	0.057	0 035	0.127	0 151
Al6	0 074	0 982	1 978	1 995	0.071	0.058	0 974	0 968

Table A2-1: Electron microprobe mineral analyses.

Sample	406	406	406	406	406	406	406	406	406	406	406
Min:	GNT	GNT	CPX	CPX	PLA	GNT	GNT	CPX	CPX	PLA	PLA
Type:	CORE	RIM	CORE	RIM	CORE	CORE	RIM	CORE	RIM	CORE	RIM
Code:	B01	B02	B23	B29	B38	D01	D02	D24	D25	D36	D37
SiO2	39 97	41.24	52 58	52.25	55 98	41 34	40 16	52 68	54 15	58 70	60.48
TiO2	0.00	0.00	0.02	0.02	0 00	0.00	0 00	0 00	0 01	0.00	0 00
Al2O3	22 42	22.47	4.33	6.72	27 37	22.79	22.40	3 31	3 34	26 18	24.08
Cr2O3	0 02	0 06	0.14	0.02	0 04	0.08	0 00	0.14	0 29	0.00	0 00
FeO	17 45	17 98	4 98	4 92	0.14	18 31	19 16	5 41	5 19	0.07	0.14
MnO	0.50	0 47	0.11	0.07	0.01	0 65	0 98	0 09	0 12	0 00	0.02
MgO	10 80	10 50	14.01	13.02	0 00	11 14	11 44	15 07	13 91	0 04	0.01
CaO	8 32	8 80	21 57	20 28	9.75	7 32	8 57	21 28	21 95	8 82	6 72
Na2O	0 12	0 00	1.11	1 96	5 57	0 01	0 00	1 03	1 10	6 45	4 09
K2O	0 00	0 00	0 00	0 00	0 25	0 00	0 01	0 02	0 00	0 32	0.32
Sum	99 60	101 52	98 85	105 26	99 11	101 64	100 72	99 03	100 06	100 58	96.86
Si	3 002	3 040	1 943	1 917	2 537	3 036	2 995	1 948	1 977	2 613	2.764
Ti	0 000	0 000	0 001	0 001	0 000	0 000	0 000	0 000	0 000	0 000	0 000
Al	1 985	1 952	0 189	0 290	1 462	1 973	1 970	0 144	0 144	1 374	1 297
Cr	0 001	0 003	0 004	0 001	0 001	0 005	0 000	0 004	0 008	0 000	0 000
Fe	1 096	1 108	0 154	0 151	0 005	1 125	1 195	0 167	0 158	0 003	0 005
Mn	0 032	0 029	0 003	0 002	0 000	0 040	0 062	0 003	0 004	0 000	0 001
Mg	1 209	1 153	0 772	0 711	0 000	1 219	1 272	0 831	0 757	0 003	0 001
Ca	0 670	0 695	0 854	0 796	0 473	0 576	0 525	0 843	0 859	0 421	0 329
Na	0 017	0 000	0 080	0 139	0 489	0 001	0 000	0 074	0 078	0 557	0 362
K	0 000	0 000	0 000	0 000	0 014	0 000	0 001	0 001	0 000	0 018	0 019
Sum	8 013	7 982	3 999	4 007	4 983	7 976	8 020	4 015	3 985	4 987	4 778
XMg	0 524	0 510	0 834	0 825	0 000	0 520	0 516	0 832	0 827	0 505	0 113
Al4	0 000	0 000	0 057	0 157	0 463	0 000	0 005	0 052	0 023	0 387	0 236
Al6	1 985	1 952	0 132	0 123	0 999	1 973	1 965	0 092	0 121	0 987	1 061

Table A2-1: Electron microprobe mineral analyses.

Sample:	418	418	418	418	418	418	418	418	418	418	418	418	418	418	418
Min:	GNT	GNT	BIO	BIO	GNT	GNT	PLA	PLA	BIO	BIO	GNT	GNT	GNT	GNT	GNT
Type:	CORE	RIM	CORE	RIM	CORE	RIM	CORE	RIM	CORE	RIM	TRAV	TRAV	TRAV	TRAV	TRAV
Code:	A01	A03	A04	A47	B01	B03	B36	B37	B44	B45	C51	C52	C53	C54	C55
SiO2	38.67	38.74	37.50	37.30	38.67	38.59	62.79	62.00	36.82	36.34	36.38	36.57	36.05	36.78	36.54
TiO2	0.00	0.00	3.52	2.95	0.02	0.00	0.01	0.00	3.28	3.21	0.00	0.01	0.02	0.01	0.02
Al2O3	21.18	20.97	17.64	17.32	21.51	21.43	23.39	22.93	17.35	17.95	22.24	21.51	21.65	21.71	21.62
Cr2O3	0.01	0.09	0.00	0.01	0.02	0.00	0.00	0.03	0.02	0.03	0.00	0.00	0.00	0.00	0.00
FeO	32.16	32.16	18.45	18.06	32.63	33.45	0.06	0.05	18.41	18.60	32.49	31.60	31.16	31.01	30.63
MnO	3.98	3.92	0.03	0.05	4.19	3.89	0.00	0.00	0.04	0.01	3.86	3.57	3.80	3.71	3.48
MgO	4.24	4.30	10.42	10.73	4.22	3.95	0.00	0.00	10.46	10.30	4.05	4.27	4.46	4.25	4.18
CaO	1.05	1.12	0.00	0.00	1.22	1.29	4.66	4.94	0.01	0.00	1.15	0.92	1.05	1.19	1.11
Na2O	0.03	0.10	0.04	0.07	0.04	0.01	9.75	9.24	0.07	0.10	0.06	0.09	0.00	0.00	0.02
K2O	0.00	0.00	9.22	9.07	0.01	0.00	0.18	0.20	9.44	9.14	0.10	0.06	0.03	0.00	0.01
Sum	101.32	101.42	96.82	95.56	102.53	102.61	100.84	99.39	95.90	95.68	100.33	98.60	98.22	98.66	97.61
Si	3.042	3.046	2.780	2.797	3.015	3.014	2.767	2.771	2.767	2.736	2.912	2.963	2.933	2.969	2.976
Ti	0.000	0.000	0.196	0.166	0.001	0.000	0.000	0.000	0.185	0.182	0.000	0.001	0.001	0.001	0.001
Al	1.964	1.944	1.541	1.531	1.977	1.973	1.215	1.208	1.537	1.593	2.098	2.054	2.077	2.066	2.076
Cr	0.001	0.006	0.000	0.001	0.001	0.000	0.000	0.001	0.001	0.002	0.000	0.000	0.000	0.000	0.000
Fe	2.116	2.116	1.144	1.133	2.128	2.185	0.002	0.002	1.157	1.171	2.175	2.141	2.120	2.094	2.086
Mn	0.265	0.261	0.002	0.003	0.277	0.257	0.000	0.000	0.003	0.001	0.262	0.245	0.262	0.254	0.240
Mg	0.497	0.504	1.151	1.199	0.490	0.460	0.000	0.000	1.171	1.156	0.483	0.516	0.541	0.511	0.507
Ca	0.089	0.094	0.000	0.000	0.102	0.108	0.220	0.237	0.001	0.000	0.099	0.080	0.092	0.103	0.097
Na	0.005	0.015	0.006	0.010	0.006	0.002	0.833	0.801	0.010	0.015	0.009	0.014	0.000	0.000	0.003
K	0.000	0.000	0.872	0.868	0.001	0.000	0.010	0.011	0.905	0.878	0.010	0.006	0.003	0.000	0.001
Sum	7.978	7.986	7.692	7.709	7.998	7.999	5.047	5.030	7.736	7.731	8.048	8.019	8.029	7.997	7.987
XMg	0.190	0.192	0.502	0.514	0.187	0.174	0.000	0.000	0.503	0.497	0.182	0.194	0.203	0.196	0.196
Al4	0.000	0.000	1.220	1.203	0.000	0.000	0.233	0.229	1.233	1.264	0.088	0.037	0.067	0.031	0.024
Al6	1.964	1.944	0.321	0.329	1.977	1.973	0.981	0.979	0.303	0.328	2.010	2.017	2.010	2.035	2.051

Table A2-1: Electron microprobe mineral analyses.

Sample:	418	418	418	418	418	418	418	418	418	418	418	418	418	418	418
Min:	GNT	GNT	GNT	GNT	GNT	GNT	GNT	GNT	PLG	PLG	BIO	BIO	GNT	GNT	GNT
Type:	TRAV	TRAV	TRAV	TRAV	TRAV	TRAV	CORE	RIM	CORE	RIM	CORE	RIM	TRAV	TRAV	TRAV
Code:	C55	C56	C57	C58	C59	C60	E01	E03	E31	E32	E41	E42	E51	E52	E53
SiO2	36.76	36.69	36.59	36.13	36.34	36.32	37.62	37.52	64.51	64.71	36.50	34.71	37.08	36.85	35.24
TiO2	0.02	0.00	0.02	0.00	0.02	0.00	0.03	0.00	0.02	0.01	2.45	2.53	0.05	0.02	0.00
Al2O3	21.22	21.88	21.12	21.40	21.76	21.85	21.93	22.14	20.93	21.81	17.36	17.12	22.00	21.41	21.73
Cr2O3	0.00	0.00	0.00	0.00	0.00	0.00	0.00	0.00	0.00	0.00	0.00	0.00	0.00	0.00	0.00
FeO	29.59	31.51	31.49	30.33	33.11	31.14	30.86	32.53	0.03	0.00	16.45	17.06	34.23	32.61	32.00
MnO	3.64	3.30	3.46	3.43	3.55	3.33	3.93	3.50	0.09	0.17	0.05	0.03	3.41	3.48	3.71
MgO	4.19	4.05	3.94	3.78	3.38	3.13	4.42	3.63	0.00	0.00	11.20	10.43	3.61	3.93	4.18
CaO	1.16	1.15	1.13	1.12	1.18	1.19	0.98	0.99	3.81	4.15	0.00	0.00	1.14	1.02	1.03
Na2O	0.14	0.10	0.00	0.01	0.07	0.14	0.09	0.08	8.92	9.41	0.11	0.10	0.12	0.12	0.00
K2O	0.08	0.01	0.00	0.00	0.03	0.08	0.00	0.05	0.07	0.17	10.80	11.16	0.04	0.00	0.00
Sum	96.80	96.69	97.75	96.20	99.44	97.18	99.86	100.44	98.38	100.43	94.92	93.14	101.68	99.44	97.89
Si	3.009	2.983	2.989	2.986	2.941	2.980	2.991	2.983	2.884	2.847	2.771	2.716	2.939	2.970	2.894
Ti	0.001	0.000	0.001	0.000	0.001	0.000	0.002	0.000	0.001	0.000	0.140	0.149	0.003	0.001	0.000
Al	2.048	2.083	2.034	2.085	2.076	2.113	2.055	2.075	1.103	1.131	1.554	1.579	2.056	2.034	2.103
Cr	0.000	0.000	0.000	0.000	0.000	0.000	0.000	0.000	0.000	0.000	0.000	0.000	0.000	0.000	0.000
Fe	2.026	2.128	2.151	2.096	2.241	2.137	2.052	2.163	0.001	0.000	1.045	1.117	2.269	2.198	2.197
Mn	0.252	0.226	0.239	0.240	0.243	0.231	0.265	0.236	0.003	0.006	0.003	0.002	0.229	0.238	0.258
Mg	0.511	0.487	0.480	0.466	0.408	0.383	0.524	0.430	0.000	0.000	1.267	1.217	0.426	0.472	0.512
Ca	0.102	0.100	0.099	0.099	0.102	0.105	0.083	0.084	0.183	0.196	0.000	0.000	0.097	0.088	0.091
Na	0.022	0.016	0.000	0.002	0.011	0.022	0.014	0.012	0.773	0.803	0.016	0.015	0.018	0.019	0.000
K	0.008	0.001	0.000	0.000	0.003	0.008	0.000	0.005	0.004	0.010	1.046	1.114	0.004	0.000	0.000
Sum	7.980	8.004	7.993	7.973	8.027	7.979	7.986	7.988	4.952	4.993	7.843	7.909	8.041	8.020	8.054
XMg	0.201	0.186	0.182	0.182	0.154	0.152	0.203	0.166	0.000	0.000	0.548	0.521	0.158	0.177	0.189
AI4	0.000	0.037	0.011	0.014	0.059	0.020	0.009	0.017	0.116	0.153	1.229	1.284	0.061	0.030	0.106
AI6	2.048	2.046	2.022	2.070	2.017	2.093	2.046	2.058	0.987	0.978	0.325	0.296	1.995	2.005	1.997

Table A2-1: Electron microprobe mineral analyses.

Sample:	418	418	418	418	418	418	418	418	418
Min:	GNT	GNT	GNT	GNT	GNT	GNT	GNT	GNT	GNT
Type	TRAV	TRAV	TRAV	TRAV	TRAV	TRAV	TRAV	TRAV	TRAV
Code:	E54	E55	E56	E57	E58	E59	E60	E61	E62
SiO2	37.24	36.35	36.78	36.43	36.96	35.49	36.28	36.54	36.75
TiO2	0.00	0.03	0.02	0.01	0.00	0.03	0.00	0.04	0.06
Al2O3	21.78	22.05	20.91	21.18	21.30	20.86	21.93	21.90	21.48
Cr2O3	0.00	0.00	0.01	0.00	0.00	0.00	0.00	0.00	0.00
FeO	31.49	32.34	31.13	32.16	31.02	32.62	33.17	32.29	31.19
MnO	3.84	3.93	3.76	3.95	3.16	3.47	3.58	3.24	3.21
MgO	4.27	4.36	4.50	4.35	4.23	4.52	4.61	4.42	3.89
CaO	1.00	1.08	0.98	1.03	0.96	1.04	1.09	1.14	1.15
Na2O	0.02	0.03	0.01	0.02	0.14	0.05	0.04	0.07	0.11
K2O	0.00	0.02	0.00	0.03	0.05	0.00	0.03	0.02	0.09
Sum	99.64	100.19	98.10	99.16	97.84	98.11	100.73	99.66	97.93
Si	2.978	2.912	2.991	2.950	3.002	2.915	2.898	2.933	2.988
Ti	0.000	0.002	0.001	0.001	0.000	0.002	0.000	0.002	0.004
Al	2.053	2.082	2.004	2.022	2.040	2.023	2.065	2.072	2.059
Cr	0.000	0.000	0.001	0.000	0.000	0.000	0.000	0.000	0.000
Fe	2.106	2.166	2.117	2.178	2.107	2.241	2.216	2.168	2.121
Mn	0.260	0.267	0.259	0.271	0.217	0.241	0.242	0.220	0.221
Mg	0.509	0.520	0.545	0.525	0.512	0.553	0.549	0.529	0.471
Ca	0.086	0.093	0.085	0.089	0.085	0.092	0.093	0.098	0.100
Na	0.003	0.005	0.002	0.003	0.022	0.008	0.006	0.011	0.017
K	0.000	0.002	0.000	0.003	0.005	0.000	0.003	0.002	0.009
Sum	7.996	8.049	8.006	8.042	7.991	8.075	8.073	8.035	7.992
XMg	0.195	0.194	0.205	0.194	0.195	0.198	0.199	0.196	0.182
Al4	0.022	0.088	0.009	0.050	0.000	0.085	0.102	0.067	0.012
Al6	2.032	1.994	1.995	1.972	2.040	1.938	1.964	2.005	2.047

Table A2-1: Electron microprobe mineral analyses.

Sample	424	424	424	424	424	424	424	424	424	424	424	424	424	424	424
Min	GNT	GNT	CPX	PLA	BIO	GNT	GNT	CPX	CPX	PLG	PLG	GNT	CPX	PLA	GNT
Type	CORE	RIM	CORE	CORE	RIM	CORE	RIM	CORE	RIM	CORE	RIM	CORE	CORE	CORE	CORE
Code	A01	A02	A24	A37	A43	C01	C02	C21	C22	C31	C32	E02	E23	E35	F02
SiO2	38 80	38 37	52 33	65 43	37 53	37 71	37 79	52 27	53 62	63 73	63 12	37 52	52.22	63 57	38 99
TiO2	0 03	0 00	0.19	0 00	4 41	0 05	0 03	0 21	0 11	0 05	0 02	0 00	0 04	0 00	0 00
Al2O3	21 20	21.16	2 25	22 02	13 77	20.85	21 17	2.52	1 68	21 00	21 44	20 95	2 30	22 00	21 09
Cr2O3	0 00	0 02	0 04	0 02	0 03	0 00	0 00	0 00	0 00	0 00	0 00	0 03	0 04	0 00	0 00
FeO	28 76	28 84	12 68	0 13	19 75	27 64	26 56	13.73	12 66	0 03	0 01	28 48	13 33	0 12	27 47
MnO	2 65	3 37	0 55	0 01	0 11	2 82	2 87	0 36	0 41	0 16	0 66	2 48	0 39	0 05	2 55
MgO	4 92	3 68	10 84	0 00	11 81	4 59	4 39	11 38	11 36	0 00	0 02	3 97	10 97	0 03	4 20
CaO	5 73	5 79	20 13	3 89	0 02	5 85	5 54	19 67	20 35	3 75	4 26	6 02	19 55	4 16	6 09
Na2O	0 01	0 11	1 09	9 78	0 04	0 00	0 01	1.26	1 07	9 49	9 45	0 01	1.28	9 53	0 02
K2O	0 00	0 02	0 01	0.36	8 53	0 03	0 02	0 01	0 00	0 44	0 36	0 01	0 01	0 27	0 00
Sum:	102 10	101 36	100 11	101 64	96 00	99 54	98 38	101 41	101 26	98 65	99 34	99 47	100 13	99 73	100 41
Si	3.006	3 010	1 977	2 848	2 832	2 997	3 019	1 956	1 997	2 859	2 825	2 993	1 975	2 824	3 054
Ti	0 002	0 000	0 005	0 000	0 250	0 003	0 002	0 006	0 003	0 002	0 001	0 000	0 001	0 000	0 000
Al	1 936	1 957	0 100	1 130	1 225	1 953	1 994	0 111	0 074	1 111	1 131	1 970	0 103	1 152	1 947
Cr	0 000	0 001	0 001	0 001	0 002	0 000	0 000	0 000	0 000	0 000	0 000	0 002	0 001	0 000	0 000
Fe	1 863	1 892	0 401	0 005	1 246	1 837	1 775	0 430	0 394	0 001	0 000	1 900	0 422	0 004	1 799
Mn	0 174	0 224	0 018	0 000	0 007	0 190	0 194	0 011	0 013	0 006	0 025	0 168	0 012	0 002	0 189
Mg	0 568	0 430	0 610	0 000	1 328	0 544	0 523	0 635	0 631	0 000	0 001	0 472	0 618	0 002	0 490
Ca	0 476	0 487	0 815	0 181	0 002	0 498	0 474	0 789	0 812	0 180	0 204	0 515	0 792	0 198	0 511
Na	0 002	0 017	0 080	0 825	0 006	0 000	0 002	0 091	0 077	0 825	0 820	0 002	0 094	0 821	0 003
K	0 000	0 002	0 000	0 020	0 821	0 003	0 002	0 000	0 000	0 025	0 021	0 001	0 000	0 015	0 000
Sum	8 025	8 020	4 007	5 010	7 718	8 025	7 984	4 029	4 001	5 009	5 029	8 022	4 019	5 018	7 974
XMg	0 234	0 185	0 604	0 000	0 516	0 228	0 228	0 596	0 615	0 000	0 781	0 199	0 595	0 308	0 214
AlIV	0 000	0 000	0 023	0 152	1 168	0 003	0 000	0 044	0 003	0 141	0 175	0 007	0 025	0 176	0 000
AlVI	1 936	1 957	0 077	0 977	0 056	1 950	1 994	0 067	0 071	0 969	0 956	1 963	0 078	0 976	1 947

Table A2-1: Electron microprobe mineral analyses.

Sample	424	424	424	424
Min	CPX	CPX	PLA	PLA
Type	CORE	INT	CORE	CORE
Code	F23	F24	F35	F36
SiO2	51 77	52 41	63 40	63 93
TiO2	0 04	0 03	0 00	0 00
Al2O3	3 07	2 33	22 06	21 49
Cr2O3	0 02	0 09	0 02	0 04
FeO	13 75	12 79	0 13	0 12
MnO	0 41	0 49	0 00	0 01
MgO	9 96	10 40	0 05	0 00
CaO	19 92	19 81	2 86	3 31
Na2O	1 25	1 03	10 00	9 99
K2O	0 00	0 00	0 32	0 30
Sum	100 19	99 38	98 84	99 19
Si	1 962	1 991	2 834	2 850
Ti	0 001	0 001	0 000	0 000
Al	0 137	0 104	1 162	1 129
Cr	0 001	0 003	0 001	0 001
Fe	0 436	0 406	0 005	0 004
Mn	0 013	0 016	0 000	0 000
Mg	0 563	0 589	0 003	0 000
Ca	0 809	0 806	0 137	0 158
Na	0 092	0 076	0 867	0 864
K	0 000	0 000	0 018	0 017
Sum	4 014	3 992	5 027	5 025
XMg	0 563	0 592	0 407	0 000
Al4	0 038	0 009	0 166	0 150
Al6	0 099	0 096	0 996	0 980

Table A2-1: Electron microprobe mineral analyses.

Sample	1073	1073	1073	1073	1073	1073
Min	GNT	GNT	PLG	PLG	BIO	BIO
Type	CORE	RIM	CORE	RIM	CORE	CORE
Code	A01	A02	A35	A36	A43	A44
SiO2	40 00	39 48	60 70	61 49	35.77	36 55
TiO2	0 00	0 00	0 00	0 01	3 80	3 79
Al2O3	21 47	22 27	24 28	23 47	16 60	17 16
Cr2O3	0 01	0 03	0 00	0 00	0 03	0 02
FeO	29 73	28 95	0 03	0 06	13 48	13 38
MnO	2 04	2 09	0 00	0 00	0 01	0 03
MgO	8 68	8 94	0 00	0 00	14 12	14 38
CaO	0 89	0 88	5 97	5 09	0 00	0 02
Na2O	0 02	0 00	8 63	8 52	0 06	0 14
K2O	0 00	0 00	0 14	0 07	9 06	8 97
Sum	102 84	102 64	99 75	98 71	92 93	94 44
Si	3 029	2 987	2 710	2 759	2 717	2 722
Ti	0 000	0 000	0 000	0 000	0 217	0 212
Al	1 916	1 986	1 278	1 241	1 486	1 507
Cr	0 001	0 002	0 000	0 000	0 002	0 001
Fe	1 883	1 832	0 001	0 002	0 856	0 833
Mn	0 131	0 134	0 000	0 000	0 001	0 002
Mg	0 980	1 008	0 000	0 000	1 598	1 596
Ca	0 072	0 071	0 286	0 245	0 000	0 002
Na	0 003	0 000	0 747	0 741	0 009	0 020
K	0 000	0 000	0 008	0 004	0 878	0 852
Sum	8 014	8 019	5 029	4 993	7 765	7 748
XMg	0 342	0 355	0 000	0 000	0 651	0 657
Al4	0 000	0 013	0 290	0 241	1 283	1 278
Al6	1 916	1 973	0 987	1 000	0 204	0 229

Table A2-1: Electron microprobe mineral analyses.

Sample	1098	1098	1098	1098	1098	1098	1098	1098	1098	1098
Min	GNT	GNT	BIO	BIO	GNT	GNT	BIO	BIO	PLG	PLG
Type	CORE	RIM	CORE	RIM	CORE	RIM	CORE	RIM	CORE	RIM
Code:	A01	A03	A41	A42	B01	B02	B41	B42	Z01	Z02
SiO2	39 09	38 42	36 10	37 55	38 37	38 64	37 90	38 39	62 68	63 18
TiO2	0 00	0 01	2 15	2 08	0 02	0 05	1 66	1 80	0 04	0 04
Al2O3	23 10	23 05	15 78	17 09	23 26	22 89	17 62	18 09	23 16	22 44
Cr2O3	0 00	0 00	0 00	0 00	0.00	0 00	0 00	0 00	0 00	0 01
FeO	27 56	29 08	12.86	12.57	26 45	28 88	11 70	11 54	0 00	0 00
MnO	1 50	1 73	0 03	0 04	2 69	2 04	0 00	0 00	0 02	0 04
MgO	10 33	9 83	15 44	15 45	9 02	8 38	16 65	15 71	0 00	0 02
CaO	0 27	0 30	0 00	0 00	0 43	0 46	0 00	0 03	5.30	5 00
Na2O	0 06	0 06	0 09	0 07	0 00	0 07	0 10	0 00	8 38	8 85
K2O	0 03	0 00	10 86	10 71	0 04	0.10	10 81	10 00	0 21	0 11
Sum	101 94	102 48	93 31	95 56	100 28	101 51	96.44	95 56	99 79	99 69
Si	2 948	2 910	2 755	2 774	2 947	2 957	2 760	2 797	2 781	2 805
Ti	0.000	0 001	0 123	0 116	0 001	0.003	0 091	0 099	0 001	0 001
Al	2.054	2 058	1.420	1 488	2.106	2 065	1 513	1 554	1 211	1 174
Cr	0 000	0 000	0 000	0 000	0 000	0 000	0 000	0 000	0 000	0 000
Fe	1 738	1 842	0 821	0 777	1 699	1 848	0 713	0.703	0 000	0 000
Mn	0 096	0 111	0 002	0 003	0 175	0 132	0 000	0 000	0 001	0 002
Mg	1 161	1 110	1 756	1 701	1 033	0 956	1 807	1 706	0 000	0 001
Ca	0 022	0 024	0 000	0 000	0.035	0 038	0 000	0 002	0 252	0 238
Na	0 009	0 009	0 013	0 010	0 000	0 010	0 014	0 000	0 721	0 762
K	0 003	0 000	1 057	1 009	0 004	0 010	1 004	0 930	0 012	0 006
Sum	8 031	8 064	7 947	7 876	8 000	8 018	7 902	7 791	4 979	4 990
XMg	0 400	0 376	0 681	0 687	0 378	0 341	0 717	0 708	0 000	1 000
Al4	0 052	0 090	1 245	1 226	0 053	0 043	1 240	1 203	0 219	0 195
Al6	2 002	1 968	0 174	0 262	2 053	2 021	0 273	0 351	0 992	0 980

Table A2-1: Electron microprobe mineral analyses.

Sample	1203	1203	1203	1203	1203	1203	1203	1203	1203	1203	1203	1203	1203
Min	GNT	GNT	GNT	CPX	CPX	PLG	GNT	GNT	GNT	CPX	CPX	PLG	PLG
Type	CORE	RIM	INT	CORE	CORE	CORE	CORE	RIM	INT	CORE	RIM	CORE	CORE
Code	A01	A02	A03	A25	A26	A37	B01	B02	B03	B24	B25	A36	A37
SiO2	39 73	40 59	40 79	49 61	52 07	61 34	38 71	37 79	39 73	49 96	50 80	59 67	55 84
TiO2	0 00	0 00	0 01	0 04	0 03	0 00	0 01	0 00	0 00	0 07	0 09	0 00	0 00
Al2O3	22 00	21 82	21 89	5 72	3 40	24 14	22 23	21 77	22 17	4 88	4 50	24 75	24 92
Cr2O3	0 02	0 03	0 03	0 56	0 49	0 00	0 03	0 02	0 08	0 60	0 63	0 04	0 02
FeO	20 13	21 67	19 93	6 62	6 37	0 07	19 51	21 60	19 52	6 80	6 39	0 12	0 04
MnO	0 39	0 46	0 38	0 02	0 09	0 00	0 43	0 59	0 52	0 09	0 07	0 01	0 00
MgO	9 12	8 21	8 95	13 18	13 86	0 03	8 81	7 96	8 76	13 73	14 30	0 00	0 02
CaO	8 76	8 04	9 53	21 96	22 21	6 14	9 54	8 89	9 54	22 15	20 66	6 80	7 23
Na2O	0 01	0 00	0 07	0 92	0 66	8 56	0 04	0 01	0 01	0 01	0 69	8 09	7 98
K2O	0 01	0 01	0 01	0 00	0 00	0 34	0 00	0 01	0 00	0 05	0 09	0 33	0 31
Sum	100 17	100 83	101 59	98 63	99 18	100 62	97 31	98 64	100 33	98 34	98 42	99 81	96 36
Si	3 007	3 060	3 041	1 864	1 937	2 718	2 882	2 943	3 002	1 881	1 902	2 673	2 605
Ti	0 000	0 000	0 001	0 001	0 001	0 000	0 001	0 000	0 000	0 002	0 003	0 000	0 000
Al	1 963	1 939	1 924	0 253	0 149	1 261	2 057	1 999	1 975	0 217	0 199	1 307	1 370
Cr	0 001	0 002	0 002	0 017	0 014	0 000	0 002	0 001	0 005	0 018	0 019	0 001	0 001
Fe	1 274	1 366	1 243	0 208	0 198	0 003	1 281	1 407	1 234	0 214	0 200	0 004	0 002
Mn	0 025	0 029	0 024	0 001	0 003	0 000	0 029	0 039	0 033	0 003	0 002	0 000	0 000
Mg	1 029	0 922	0 994	0 738	0 768	0 002	1 031	0 924	0 986	0 770	0 798	0 000	0 001
Ca	0 710	0 649	0 761	0 884	0 885	0 291	0 803	0 742	0 772	0 894	0 837	0 326	0 361
Na	0 001	0 000	0 010	0 067	0 048	0 735	0 006	0 002	0 001	0 001	0 050	0 703	0 722
K	0 001	0 001	0 001	0 000	0 000	0 019	0 000	0 001	0 000	0 002	0 004	0 019	0 018
Sum	8 012	7 970	8 001	4 033	4 004	5 029	8 091	8 058	8 009	4 001	4 014	5 034	5 080
XMg	0 447	0 403	0 445	0 780	0 795	0 433	0 446	0 396	0 444	0 783	0 800	0 000	0 471
AlIV	0 000	0 000	0 000	0 136	0 063	0 282	0 118	0 057	0 000	0 119	0 098	0 327	0 395
AlVI	1 963	1 939	1 924	0 117	0 086	0 978	1 939	1 942	1 975	0 098	0 101	0 980	0 975

Table A2-1: Electron microprobe mineral analyses.

Sample	1208	1208	1208	1208	1208	1208	1208	1208	1208	1208	1208	1208	1208	1208	1208
Min	GNT	GNT	CPX	CPX	PLG	PLG	GNT	GNT	CPX	CPX	PLG	PLG	GNT	GNT	CPX
Type	CORE	RIM	CORE	CORE	CORE	RIM	CORE	RIM	RIM	CORE	CORE	RIM	CORE	RIM	RIM
Code:	B01	B02	B23	B24	B35	B36	D01	D02	D23	D24	D35	D36	E01	E02	E23
SiO2	40 59	37 66	51 89	50 96	65 49	60 68	38 48	40 82	50 48	51 82	64 09	64 50	40 37	39 65	51 97
TiO2	0 00	0 00	0 07	0 06	0 00	0 00	0 00	0 00	0 07	0 06	0 00	0 00	0 00	0 00	0 08
Al2O3	21 75	21 91	5 05	3 39	22 27	22 91	21 00	21 81	4 04	3 80	22 40	22 45	21 29	21 66	4 41
Cr2O3	0 08	0 00	0 11	0 07	0 04	0 00	0 02	0 03	0 07	0 00	0 00	0 00	0 03	0 03	0 04
FeO	26 00	26 15	9 79	9 23	0 12	0 13	26 53	26 27	0 00	11 44	0 04	0 15	24 87	24 19	10 20
MnO	0 55	0 44	0 07	0 04	0 03	0 00	0 59	0 59	9 38	0 06	0 00	0 00	0 55	0 50	0 02
MgO	6 75	5 76	11 31	12 24	0 02	0 00	7 11	7 64	12 23	12 65	0 00	0 05	6 16	5 98	12 14
CaO	6 91	7 36	20 89	21 03	4 23	4 93	5 88	5 96	21 13	19 34	4 67	4 04	8 22	9 43	20 52
Na2O	0 03	0 05	1 14	0 90	9 17	9 10	0 00	0 08	0 72	0 88	8 25	8 92	0 11	0 03	1 32
K2O	0 01	0 02	0 02	0 02	0 61	0 50	0 00	0 00	0 01	0 01	1 17	0 54	0 00	0 01	0 00
Sum	102 67	99 35	100 34	97 94	101 98	98 25	99 61	103 20	98 13	100 06	100 82	100 65	101 60	101 48	100 70
Si	3 055	2 957	1 927	1 941	2 842	2 752	3 004	3 051	1 919	1 937	2 824	2 832	3 070	3 024	1 927
Ti	0 000	0 000	0 002	0 002	0 000	0 000	0 000	0 000	0 002	0 002	0 000	0 000	0 000	0 000	0 002
Al	1 930	2 028	0 221	0 152	1 139	1 225	1 933	1 921	0 181	0 167	1 163	1 162	1 909	1 947	0 193
Cr	0 005	0 000	0 003	0 002	0 001	0 000	0 001	0 002	0 002	0 000	0 000	0 000	0 002	0 002	0 001
Fe	1 636	1 717	0 304	0 294	0 004	0 005	1 732	1 642	0 000	0 358	0 001	0 006	1 582	1 543	0 316
Mn	0 035	0 029	0 002	0 001	0 001	0 000	0 039	0 037	0 302	0 002	0 000	0 000	0 035	0 032	0 001
Mg	0 757	0 674	0 626	0 695	0 001	0 000	0 827	0 851	0 693	0 705	0 000	0 003	0 698	0 680	0 671
Ca	0 557	0 619	0 831	0 858	0 197	0 240	0 492	0 477	0 861	0 775	0 220	0 190	0 670	0 771	0 815
Na	0 004	0 008	0 082	0 066	0 771	0 800	0 000	0 012	0 053	0 064	0 705	0 759	0 016	0 004	0 095
K	0 001	0 002	0 001	0 001	0 034	0 029	0 000	0 000	0 000	0 000	0 066	0 030	0 000	0 001	0 000
Sum	7 980	8 034	4 000	4 014	4 991	5 050	8 029	7 993	4 014	4 010	4 980	4 982	7 982	8 004	4 021
XMg	0 316	0 282	0 673	0 703	0 229	0 000	0 323	0 341	1 000	0 663	0 000	0 373	0 306	0 306	0 680
Al4	0 000	0 043	0 073	0 059	0 158	0 248	0 000	0 000	0 081	0 063	0 176	0 168	0 000	0 000	0 073
Al6	1 930	1 985	0 148	0 094	0 981	0 977	1 933	1 921	0 100	0 105	0 987	0 994	1 909	1 947	0 120

Table A2-1: Electron microprobe mineral analyses.

Sample	1208	1208	1208
Min.	CPX	PLG	PLG
Type	RIM	CORE	RIM
Code	E24	E36	E37
SiO2	50 34	63 99	62 84
TiO2	0 05	0 00	0 00
Al2O3	3 84	21 14	22 08
Cr2O3	0 04	0 00	0 04
FeO	10 67	0 07	0 06
MnO	0 07	0 00	0 00
MgO	12 91	0 02	0 00
CaO	19 71	4 55	4 46
Na2O	1 02	8 14	9 49
K2O	0 02	0 93	0 56
Sum	98 67	98 84	99 53
Si	1 912	2 863	2 806
Ti	0 001	0 000	0 000
Al	0 172	1 115	1 162
Cr	0 001	0 000	0 001
Fe	0 339	0 003	0 002
Mn	0 002	0 000	0 000
Mg	0 731	0 001	0 000
Ca	0 802	0 218	0 213
Na	0 075	0 706	0 822
K	0 001	0 053	0 032
Sum	4 038	4 959	5 039
xMg	0 683	0 337	0 000
Al4	0 088	0 137	0 194
Al6	0 084	0 978	0 968

Table A2-1: Electron microprobe mineral analyses.

Sample	1289	1289	1289	1289	1289	1289	1289	1289	1289
Min	GNT	GNT	PLG	PLG	BIO	BIO	GNT	PLG	BIO
Type	CORE	RIM	CORE	RIM	CORE	RIM	CORE	CORE	RIM
Code	A01	A02	A35	A36	A43	A44	B01	B36	B43
SiO2	37 95	39 84	62 03	61 75	38 09	38 68	39 50	60 57	36 70
TiO2	0 04	0.00	0 03	0 00	2.24	1 98	0 04	0 00	2 09
Al2O3	21 93	21 63	24 97	24 63	18.89	20 02	21 96	24 32	18.29
Cr2O3	0 00	0 01	0 00	0.01	0 02	0 02	0 00	0 00	0 02
FeO	26 68	27 21	0 01	0 05	13 77	12 80	27 38	0 04	14 16
MnO	7 24	6 51	0 00	0 03	0 08	0 04	6 08	0 01	0 07
MgO	6 37	6 00	0 00	0 00	14.11	12 00	6 66	0 00	14 70
CaO	1 19	1 55	5 99	5 91	0 00	0 00	1 13	6 27	0 00
Na2O	0.00	0 02	7 72	8 46	0 04	0 11	0 01	8 86	0 14
K2O	0.02	0 01	0.16	0 13	9.03	8.71	0 01	0 11	9 49
Sum	101 42	102 78	100 91	100 97	96 27	94 36	102 77	100 18	95 66
Si	2.958	3 048	2 722	2.718	2 768	2 836	3 017	2 698	2.711
Ti	0.002	0 000	0 001	0 000	0 122	0 109	0 002	0 000	0 116
Al	2 015	1 951	1 292	1.278	1.618	1 730	1.977	1 277	1 593
Cr	0 000	0.001	0 000	0.000	0 001	0 001	0 000	0 000	0 001
Fe	1.739	1 741	0 000	0.002	0 837	0 785	1 749	0 001	0 875
Mn	0.478	0 422	0 000	0 001	0 005	0.002	0 393	0 000	0 004
Mg	0 740	0 684	0 000	0.000	1 528	1.311	0 758	0 000	1 618
Ca	0 099	0 127	0 282	0.279	0 000	0 000	0 092	0 299	0 000
Na	0.000	0 003	0 657	0.722	0 006	0 016	0 001	0 765	0 020
K	0 002	0 001	0 009	0 007	0 837	0 815	0 001	0 006	0 894
Sum	8 033	7 978	4 963	5 007	7 722	7 605	7 993	5 049	7 833
XMg	0 298	0 282	0 000	0 000	0 646	0 626	0 302	0 000	0 649
Al4	0 042	0 000	0 278	0 282	1 232	1 164	0 000	0 302	1 289
Al6	1 973	1 951	1 014	0 996	0 386	0 566	1 977	0 976	0 304

Table A2-1: Electron microprobe mineral analyses.

Sample	1336	1336	1336	1336	1336	1336	1336	1336	1336
Mineral	GNT	GNT	PLG	PLG	BIO	BIO	GNT	BIO	PLG
Type	CORE	RIM	CORE	RIM	CORE	RIM	RIM	RIM	RIM
Code	A01	A02	A35	A36	A43	A47	B02	B44	B37
SiO2	39 37	39 77	60 50	61 75	37 01	37 60	39 81	36 23	59 85
TiO2	0 02	0 02	0 01	0 01	4 55	4 50	0 01	3 85	0 01
Al2O3	21 81	21 99	24 04	25 26	15 99	16 49	22 06	17 34	24 27
Cr2O3	0 03	0 03	0 01	0 00	0 07	0 09	0 02	0 05	0 00
FeO	26 26	27 17	0 04	0 05	12 05	12 02	27 23	9 75	0 04
MnO	0 88	0 92	0 00	0 03	0 00	0 04	0 91	0 01	0 01
MgO	11 04	10 07	0 04	0 00	16 15	15 48	10 70	17 52	0 02
CaO	1 38	1 36	6 61	6 61	0 00	0 00	1 30	0 04	6 20
Na2O	0 01	0 00	7 88	7 11	0 07	0 04	0 06	0 15	8 11
K2O	0 01	0 01	0 10	0 13	9 09	9 05	0 01	9 06	0 07
Sum	100 81	101 34	99 23	100 95	94 98	95 31	102 11	94 00	98 58
Si	2 990	3 012	2 713	2 710	2 728	2 754	2 993	2 671	2 701
Ti	0 001	0 001	0 000	0 000	0 252	0 248	0 001	0 213	0 000
Al	1 952	1 963	1 271	1 307	1 389	1 424	1 955	1 507	1 291
Cr	0 002	0 002	0 000	0 000	0 004	0 005	0 001	0 003	0 000
Fe	1 668	1 721	0 001	0 002	0 743	0 736	1 712	0 601	0 002
Mn	0 057	0 059	0 000	0 001	0 000	0 002	0 058	0 001	0 000
Mg	1 249	1 136	0 003	0 000	1 774	1 690	1 199	1 925	0 001
Ca	0 112	0 110	0 318	0 311	0 000	0 000	0 105	0 003	0 300
Na	0 001	0 000	0 685	0 605	0 010	0 008	0 009	0 021	0 710
K	0 001	0 001	0 006	0 007	0 855	0 846	0 001	0 852	0 004
Sum	8 033	8 005	4 997	4 943	7 755	7 710	8 033	7 797	5 010
XMg	0 428	0 398	0 641	0 000	0 705	0 697	0 412	0 762	0 471
AlI4	0 010	0 000	0 267	0 290	1 272	1 246	0 007	1 329	0 299
AlI6	1 942	1 963	0 983	1 016	0 117	0 177	1 948	0 178	0 992

Table A2-1: Electron microprobe mineral analyses.

Sample:	5016	5016	5016	5016	5016	5016	5016	5016	5016	5016	5016	5016	5016	5016	5016
Min:	GNT	GNT	PLG	BIO	GNT	GNT	BIO	BIO	PLG	PLG	GNT	PLG	BIO	GNT	GNT
Type:	RIM	CORE	CORE	CORE	RIM	CORE	CORE	RIM	RIM	CORE	RIM	CORE	RIM	CORE	RIM
Code:	A01	A07	A36	A44	B02	B08	B44	B45	B32	B33	C03	C32	C44	D01	D03
SiO2	41.62	41.71	60.36	38.32	41.16	41.66	39.09	39.99	61.56	61.36	41.39	61.18	40.41	40.71	40.30
TiO2	0.00	0.00	0.00	2.82	0.01	0.01	2.56	2.52	0.03	0.00	0.00	0.00	2.77	0.02	0.01
Al2O3	21.79	21.70	24.71	16.01	22.44	21.81	16.16	16.47	23.92	23.94	21.88	24.23	17.40	21.44	21.55
Cr2O3	0.05	0.03	0.00	0.05	0.05	0.02	0.03	0.01	0.00	0.04	0.03	0.01	0.05	0.08	0.02
FeO	21.82	23.97	0.05	10.06	23.78	22.43	10.26	9.36	0.04	0.08	23.82	0.13	9.64	24.92	25.27
MnO	1.23	1.38	0.03	0.12	0.13	1.27	0.00	0.00	0.01	0.05	0.00	0.02	0.04	1.09	1.07
MgO	12.02	11.94	0.00	18.09	12.19	12.13	18.67	18.32	0.00	0.00	12.34	0.00	17.98	11.82	11.39
CaO	1.98	1.96	6.98	0.02	1.84	2.29	0.02	0.00	7.11	7.18	1.98	7.41	0.00	2.01	2.03
Na2O	0.05	0.02	8.06	0.11	0.11	0.00	0.04	0.15	7.25	7.21	0.01	7.41	0.09	0.00	0.05
K2O	0.01	0.01	0.26	9.75	0.01	0.01	9.54	9.83	0.40	0.38	0.02	0.22	9.49	0.02	0.00
Sum	100.57	102.72	100.45	95.35	101.72	101.63	96.37	96.65	100.32	100.24	101.47	100.61	97.87	102.11	101.69
Si	3.098	3.071	2.684	2.790	3.043	3.080	2.807	2.848	2.730	2.725	3.067	2.710	2.834	3.034	3.023
Ti	0.000	0.000	0.000	0.154	0.001	0.001	0.138	0.135	0.001	0.000	0.000	0.000	0.146	0.001	0.001
Al	1.912	1.884	1.295	1.374	1.956	1.901	1.368	1.383	1.250	1.253	1.911	1.265	1.438	1.884	1.905
Cr	0.003	0.002	0.000	0.003	0.003	0.001	0.002	0.001	0.000	0.001	0.002	0.000	0.003	0.005	0.001
Fe	1.358	1.476	0.002	0.613	1.470	1.387	0.616	0.557	0.001	0.003	1.476	0.005	0.565	1.553	1.585
Mn	0.078	0.086	0.001	0.007	0.008	0.080	0.000	0.000	0.000	0.002	0.000	0.001	0.002	0.069	0.068
Mg	1.333	1.310	0.000	1.963	1.343	1.337	1.998	1.944	0.000	0.000	1.363	0.000	1.879	1.313	1.273
Ca	0.158	0.155	0.333	0.002	0.146	0.181	0.002	0.000	0.338	0.342	0.157	0.352	0.000	0.161	0.163
Na	0.007	0.003	0.695	0.016	0.016	0.000	0.006	0.021	0.623	0.621	0.001	0.636	0.012	0.000	0.007
K	0.001	0.001	0.015	0.906	0.001	0.001	0.874	0.893	0.023	0.022	0.002	0.012	0.849	0.002	0.000
Sum	7.948	7.988	5.024	7.827	7.986	7.968	7.810	7.782	4.967	4.969	7.978	4.982	7.730	8.021	8.027
XMg	0.495	0.470	0.000	0.762	0.477	0.491	0.764	0.777	0.000	0.000	0.480	0.000	0.769	0.458	0.445
Al4	0.000	0.000	0.316	1.210	0.000	0.000	1.193	1.152	0.270	0.275	0.000	0.290	1.166	0.000	0.000
Al6	1.912	1.884	0.979	0.164	1.956	1.901	0.175	0.231	0.980	0.978	1.911	0.975	0.272	1.884	1.905

Table A2-1: Electron microprobe mineral analyses.

Sample:	5016	5016	5016	5016
Min:	PLG	PLG	BIO	BIO
Type:	CORE	RIM	CORE	RIM
Code:	D36	D37	D44	D45
SiO2	59 80	59 73	38.06	38 72
TiO2	0.04	0.04	2.94	2 80
Al2O3	23 86	24 25	15 97	16.12
Cr2O3	0.00	0 04	0 05	0 05
FeO	0 19	0 30	10.42	9.74
MnO	0 01	0 30	0.02	0 00
MgO	0 01	0 00	17 54	18 22
CaO	7.32	7 11	0 00	0 02
Na2O	7 34	7 32	0 04	0 09
K2O	0 27	0 31	9 91	10 02
Sum	98 84	99 40	94 95	95 78
Si	2 700	2 686	2 790	2 802
Ti	0 001	0 001	0 162	0 152
Al	1 270	1 286	1 380	1 375
Cr	0 000	0 001	0 003	0 003
Fe	0 007	0 011	0 639	0 589
Mn	0 000	0 011	0 001	0 000
Mg	0 001	0 000	1 916	1 965
Ca	0 354	0 343	0 000	0 002
Na	0 643	0 638	0 006	0 013
K	0 016	0 018	0 927	0 925
Sum	4 992	4 996	7 823	7 826
XMg	0 086	0 000	0 750	0 769
Al4	0 300	0 314	1 210	1 198
Al6	0 970	0 972	0 170	0 177

Table A2-1: Electron microprobe mineral analyses.

Sample	5018	5018	5018	5018	5018	5018	5018	5018	5018	5018	5018	5018	5018	5018	5018
Min:	GNT	GNT	PLG	PLG	BIO	BIO	GNT	GNT	BIO	BIO	GNT	GNT	PLG	PLG	BIO
Type:	CORE	RIM	CORE	RIM	CORE	RIM	CORE	RIM	CORE	RIM	CORE	RIM	CORE	RIM	CORE
Code:	A01	A03	A31	A33	A41	A42	B01	B02	B41	B42	C01	C03	C31	C33	C41
SiO2	39 16	39.27	61.48	62 91	37.46	37.52	39 24	39.00	37 96	37.76	39.12	39.28	61 47	61 68	37.19
TiO2	0.00	0.00	0.07	0.05	2 39	2.46	0 00	0.00	2.01	2.00	0 00	0.00	0.02	0 00	2 29
Al2O3	22 09	21.93	24.16	23.90	16 86	17.02	22 27	22.20	17 08	17.36	21.23	22.16	23 70	23 68	16 80
Cr2O3	0 05	0.03	0 00	0.02	0 07	0 05	0.02	0.02	0 03	0.00	0 04	0 02	0 02	0.00	0 03
FeO	24 53	24.44	0.03	0.21	9.81	10.49	23 19	24 51	10.53	9.54	24.68	25.34	0 09	0 04	10 37
MnO	2.56	2.46	0.00	0 03	0 01	0 04	2 14	2.18	0.00	0 03	2 07	2 20	0 01	0 00	0 05
MgO	11.50	10.86	0.00	0 00	17 95	18.46	11.54	11 64	17.80	18.50	11 21	10 48	0 01	0 03	17 43
CaO	1.52	1.56	5.11	5.38	0 05	0.04	1 40	1.57	0.00	0.00	1.48	1 60	6 44	6.52	0 00
Na2O	0.00	0.04	7.50	8 16	0.13	0.08	0.02	0 07	0.03	0.07	0.09	0.04	7.26	7.57	0 09
K2O	0.01	0.01	0.59	0.44	9.30	9.52	0 01	0.00	9.63	9.65	0.00	0 02	0 37	0 39	9.54
Sum	101 42	100.60	98 94	101 10	94.03	95.68	99 83	101.19	95.07	94 91	99.92	101.14	99 39	100 11	93 79
Si	2 957	2.987	2.749	2.760	2 756	2.726	2.984	2.949	2.771	2.750	2.998	2.979	2.745	2.738	2.756
Ti	0.000	0.000	0.002	0.002	0.132	0.134	0.000	0.000	0 110	0.110	0.000	0.000	0.001	0.000	0.128
Al	1.967	1.966	1.273	1.236	1.462	1 458	1 996	1.978	1 470	1 491	1 918	1.981	1 247	1 249	1 468
Cr	0.003	0.002	0.000	0 001	0 004	0.003	0.001	0 001	0.002	0.000	0.002	0.001	0 001	0 000	0.002
Fe	1.549	1.555	0.001	0.008	0 604	0 637	1 475	1 550	0.643	0.581	1 582	1.607	0.003	0 001	0 643
Mn	0.164	0 158	0 000	0.001	0.001	0.002	0.138	0.140	0.000	0 002	0.134	0 141	0.000	0.000	0.003
Mg	1 294	1.231	0.000	0 000	1 968	1.999	1.308	1.312	1.936	2.008	1.280	1.185	0.001	0 002	1 925
Ca	0.123	0.127	0.245	0.253	0 004	0.003	0.114	0.127	0.000	0.000	0.122	0 130	0.308	0.310	0.000
Na	0.000	0.006	0 650	0.694	0 019	0 011	0.003	0 010	0 004	0.010	0.013	0.006	0 629	0 651	0.013
K	0.001	0.001	0.034	0.025	0 873	0.882	0.001	0 000	0.897	0.897	0.000	0.002	0.021	0 022	0.902
Sum	8 058	8.033	4 954	4 979	7.824	7 856	8 019	8.066	7.833	7 848	8 049	8 033	4.955	4 974	7.839
XMg	0.455	0.442	0.000	0 000	0 765	0.758	0.470	0.458	0 751	0.776	0 447	0.424	0.165	0 572	0.750
Al4	0 043	0.013	0.251	0 240	1 244	1.274	0.016	0.051	1.229	1.250	0.002	0.021	0 255	0 262	1.244
Al6	1 924	1.953	1 022	0 996	0 219	0 183	1 980	1.927	0 241	0.241	1 915	1 961	0 992	0 987	0 224

Table A2-1: Electron microprobe mineral analyses.

Sample:	5018	5018	5018	5018	5018	5018	5018
Min:	BIO	GNT	GNT	PLG	PLG	BIO	BIO
Type:	RIM	CORE	RIM	CORE	RIM	CORE	RIM
Code:	C42	D01	D03	D31	D33	D41	D42
SiO2	37.80	38.90	39.66	62.61	61.42	37.33	37.93
TiO2	2.29	0.00	0.00	0.00	0.00	2.58	2.45
Al2O3	16.98	21.85	21.83	23.72	23.69	17.03	16.83
Cr2O3	0.08	0.02	0.02	0.02	0.00	0.04	0.05
FeO	9.59	24.62	24.63	0.04	0.00	10.81	10.94
MnO	0.06	1.96	2.32	0.00	0.00	0.08	0.01
MgO	18.39	10.96	10.57	0.00	0.00	17.90	17.99
CaO	0.00	1.65	1.70	5.16	5.38	0.00	0.00
Na2O	0.00	0.03	0.00	7.71	7.53	0.07	0.11
K2O	9.67	0.00	0.00	0.52	0.56	9.60	9.40
Sum	94.86	99.99	100.93	99.78	98.58	95.44	95.71
Si	2.757	2.976	3.007	2.774	2.758	2.725	2.755
Ti	0.126	0.000	0.000	0.000	0.000	0.142	0.134
Al	1.460	1.971	1.951	1.239	1.254	1.466	1.441
Cr	0.005	0.001	0.001	0.001	0.000	0.002	0.003
Fe	0.585	1.575	1.575	0.001	0.000	0.660	0.665
Mn	0.004	0.127	0.149	0.000	0.000	0.005	0.001
Mg	1.999	1.250	1.194	0.000	0.000	1.947	1.947
Ca	0.000	0.135	0.138	0.245	0.259	0.000	0.000
Na	0.000	0.004	0.000	0.662	0.656	0.010	0.015
K	0.900	0.000	0.000	0.029	0.032	0.894	0.871
Sum	7.835	8.040	8.016	4.952	4.959	7.851	7.832
XMg	0.774	0.442	0.431	0.000	0.000	0.747	0.746
Al4	1.243	0.024	0.000	0.226	0.242	1.275	1.245
Al6	0.217	1.947	1.951	1.013	1.012	0.191	0.196

Table A2-1: Electron microprobe mineral analyses.

Sample	5019-A2	5019-A2	5019-A2	5019-A2	5019-A2	5019-A2	5019-A2	5019-A2	5019-A2	5019-A2	5019-A2	5019-A2	5019-A2	5019-A2	5019-A2
Min	GNT	GNT	GNT	CPX	CPX	PLG	PLG	BIO	BIO	GNT	PLG	CPX	BIO	BIO	GNT
Type	CORE	RIM	CORE	CORE	RIM	RIM	CORE	CORE	RIM	CORE	CORE	CORE	CORE	RIM	CORE
Code	A01	A02	A03	A24	A25	A32	A33	A42	A45	B01	B31	B21	B41	B42	E01
SiO2	40 02	40 08	39 87	53 39	53 15	64 45	65 11	38 55	38 89	40 27	64 21	52 92	38 84	37 65	39 82
TiO2	0 00	0 00	0 01	0 03	0 04	0 00	0 00	3 88	4 08	0 00	0 00	0 37	4 03	3 73	0 09
Al2O3	21 22	21 11	21.21	5 93	6 45	20 91	20 70	13 96	13 98	21 14	21 14	6 83	13 81	14 99	20 68
Cr2O3	0 05	0 07	0 02	0 05	0 02	0 00	0 02	0 06	0 02	0 00	0 02	0 04	0 05	0 00	0 02
FeO	24 16	25.52	23 98	7 87	8 67	0 12	0 15	14 88	14 10	23 27	0 15	8 56	14 54	15 88	24 16
MnO	1 09	1 01	0 89	0 06	0 08	0 03	0 00	0 04	0 00	0 85	0 01	0 06	0 00	0 05	0 59
MgO	7 30	6 99	7 00	10 42	10 46	0 02	0 00	15 00	15 32	7 28	0 00	11 07	15 28	15 56	6 80
CaO	8 31	8 34	8 45	18 05	17 82	3 45	3 59	0 02	0 00	8 25	3 50	18 44	0 02	0 02	8 35
Na2O	0.03	0 00	0.00	4 49	3 42	9 62	9 66	0 07	0 05	0 01	9 51	3 38	0 11	0 07	0 00
K2O	0.00	0.03	0.03	0 01	0 00	0 25	0 36	9 67	9 68	0.01	0 20	0 00	9 45	9 22	0 00
Sum	102 18	103 15	101 46	100 30	100 11	98 85	99 59	96 13	96 12	101 08	98 74	101.67	96 13	97 17	100 51
Si	3 029	3 022	3 036	1 962	1 955	2 877	2 887	2 850	2 861	3 062	2 869	1 921	2 861	2.763	3 060
Ti	0 000	0 000	0 001	0 001	0 001	0 000	0 000	0 216	0 226	0 000	0 000	0 010	0 223	0 206	0 005
Al	1 893	1.876	1 904	0 257	0 280	1 100	1 082	1 217	1 212	1 895	1 113	0 292	1 199	1 297	1 873
Cr	0 003	0 004	0 001	0 001	0 001	0 000	0 001	0 004	0 001	0 000	0 001	0 001	0 003	0 000	0 001
Fe	1 529	1 609	1 527	0 242	0 267	0 004	0 008	0 920	0 868	1 480	0 006	0 260	0 896	0 975	1 553
Mn	0 070	0 065	0.057	0 002	0 002	0 001	0 000	0 003	0 000	0 055	0.000	0 002	0 000	0 003	0 038
Mg	0 823	0 786	0 794	0 571	0 573	0 001	0 000	1 653	1 680	0 825	0 000	0 599	1 678	1 702	0 779
Ca	0 674	0 674	0 689	0 711	0 702	0 165	0 171	0 002	0 000	0 672	0 168	0 717	0 002	0 002	0 688
Na	0 004	0 000	0 000	0 320	0 244	0 833	0 831	0 010	0 007	0 001	0 824	0 238	0 016	0 010	0 000
K	0 000	0 003	0 003	0 000	0 000	0 014	0 020	0 912	0 909	0 001	0 011	0 000	0 888	0 863	0 000
Sum	8 025	8 039	8 012	4 068	4 026	4 996	4 997	7 785	7 764	7 991	4 992	4 041	7 766	7 819	7 997
XMg	0 350	0 328	0 342	0 702	0 683	0 229	0 000	0 642	0 659	0 358	0 000	0 697	0 652	0 636	0 334
AlIV	0 000	0 000	0 000	0 038	0 045	0 123	0 113	1 150	1 139	0 000	0 131	0 079	1 139	1 237	0 000
AlVI	1 893	1 876	1 904	0 219	0 235	0 977	0 969	0 067	0 074	1 895	0 982	0 214	0 061	0 059	1 873

Table A2-1: Electron microprobe mineral analyses.

Sample:	5019-A2	5019-A2	5019-A2	5019-A2	5019-A2
Min:	GNT	CPX	CPX	PLG	PLG
Type:	RIM	CORE	RIM	CORE	RIM
Code:	E02	E23	E25	E36	E37
SiO2	39.40	53 05	52 81	65 52	64.28
TiO2	0 07	0 29	0 29	0 01	0 02
Al2O3	20.92	6 69	5 45	21 75	21 63
Cr2O3	0 02	0 02	0 00	0 03	0 00
FeO	25 74	8.86	9 13	0 16	0 25
MnO	0 71	0 07	0 09	0 02	0 03
MgO	6 44	10 23	11 32	0 03	0 00
CaO	8 20	17 84	19 21	3 59	3 77
Na2O	0 04	3 41	2 63	9 52	9 36
K2O	0 00	0 00	0 01	0 36	0 34
Sum	101 54	100 46	100 94	100 99	99 68
Si	3 022	1 946	1 939	2 863	2 850
Ti	0 004	0 008	0 008	0 000	0 001
Al	1 891	0 289	0 236	1 121	1 131
Cr	0 001	0 001	0 000	0 001	0 000
Fe	1 651	0 272	0 280	0 006	0 009
Mn	0 046	0 002	0 003	0 001	0 001
Mg	0 736	0 559	0 619	0 002	0 000
Ca	0 674	0 701	0 756	0 168	0 179
Na	0 006	0 243	0 187	0 807	0 805
K	0 000	0 000	0 000	0 020	0 019
Sum	8 031	4 022	4 029	4 989	4 995
XMg	0 308	0 673	0 688	0 250	0 000
Al4	0 000	0 054	0 061	0 137	0 150
Al6	1 891	0 236	0 175	0 984	0 981

Table A2-1: Electron microprobe mineral analyses.

Sample	5038B	5038B	5038B	5038B	5038B	5038B	5038B	5038B	5038B	5038B	5038B	5038B	5038B	5038B	5038B
Min	GNT	CPX	CPX	PLG	PLG	GNT	GNT	CPX	PLG	BIO	BIO	GNT	GNT	CPX	CPX
Type	CORE	CORE	RIM	RIM	CORE	CORE	RIM	CORE	CORE	CORE	CORE	CORE	CORE	CORE	RIM
Code	A01	A23	A24	A35	A36	B01	B02	B23	B35	B41	B42	C01	C02	C21	C22
SiO2	39.59	51.57	52.49	65.36	66.34	39.60	38.02	50.75	67.18	37.25	37.75	39.38	40.07	52.46	50.93
TiO2	0.05	0.25	0.32	0.00	0.00	0.09	0.06	0.41	0.00	5.03	5.21	0.12	0.06	0.50	0.30
Al2O3	19.86	4.11	5.48	20.79	20.59	20.04	20.36	4.88	20.53	13.48	13.02	19.73	20.27	6.24	5.07
Cr2O3	0.03	0.05	0.04	0.03	0.00	0.03	0.02	0.05	0.00	0.04	0.00	0.05	0.01	0.01	0.00
FeO	27.10	12.45	12.13	0.12	0.12	26.36	26.15	12.72	0.07	19.81	19.50	25.42	26.54	11.77	12.57
MnO	0.88	0.13	0.06	0.04	0.01	1.15	1.17	0.12	0.00	0.00	0.03	1.02	0.85	0.12	0.15
MgO	4.43	10.14	9.21	0.00	0.00	3.86	4.23	9.34	0.02	12.04	11.71	4.34	4.38	8.34	9.75
CaO	9.28	18.54	17.81	2.90	2.85	9.17	9.06	18.98	2.73	0.00	0.00	10.09	9.16	18.37	19.25
Na2O	0.02	1.92	2.98	8.91	9.61	0.07	0.13	2.28	10.00	0.02	0.04	0.02	0.02	3.87	2.44
K2O	0.02	0.00	0.02	0.55	0.52	0.01	0.00	0.00	0.38	9.25	9.39	0.00	0.02	0.01	0.00
Sum	101.26	99.16	100.54	98.70	100.04	100.38	99.20	99.53	100.91	96.92	96.65	100.17	101.38	99.69	100.46
Si	3.077	1.956	1.955	2.909	2.918	3.096	3.018	1.927	2.927	2.799	2.841	3.082	3.095	1.962	1.917
Ti	0.003	0.007	0.009	0.000	0.000	0.005	0.004	0.012	0.000	0.284	0.295	0.007	0.003	0.014	0.008
Al	1.820	0.184	0.241	1.091	1.067	1.847	1.905	0.218	1.054	1.194	1.155	1.820	1.845	0.275	0.225
Cr	0.002	0.001	0.001	0.001	0.000	0.002	0.001	0.002	0.000	0.002	0.000	0.003	0.001	0.000	0.000
Fe	1.761	0.395	0.378	0.004	0.004	1.724	1.736	0.404	0.003	1.245	1.227	1.664	1.714	0.369	0.396
Mn	0.058	0.004	0.002	0.002	0.000	0.076	0.079	0.004	0.000	0.000	0.002	0.068	0.058	0.004	0.005
Mg	0.513	0.573	0.511	0.000	0.000	0.450	0.500	0.529	0.001	1.348	1.313	0.506	0.504	0.465	0.547
Ca	0.773	0.753	0.711	0.138	0.134	0.768	0.771	0.772	0.127	0.000	0.000	0.846	0.758	0.656	0.776
Na	0.003	0.141	0.215	0.769	0.819	0.011	0.020	0.168	0.845	0.003	0.006	0.003	0.003	0.281	0.178
K	0.002	0.000	0.001	0.031	0.029	0.001	0.000	0.000	0.021	0.887	0.902	0.000	0.002	0.000	0.000
Sum	8.012	4.015	4.023	4.945	4.973	7.980	8.035	4.035	4.979	7.763	7.740	8.000	7.981	4.026	4.051
XMg	0.226	0.592	0.575	0.000	0.000	0.207	0.224	0.567	0.337	0.520	0.517	0.233	0.227	0.558	0.580
Al4	0.000	0.044	0.045	0.091	0.082	0.000	0.000	0.073	0.073	1.201	1.159	0.000	0.000	0.038	0.083
Al6	1.820	0.140	0.195	1.000	0.985	1.847	1.905	0.145	0.981	0.000	0.000	1.820	1.845	0.238	0.142

Table A2-1: Electron microprobe mineral analyses.

Sample:	5038B	5038B	5038B	5038B	5038B
Min:	GNT	GNT	CPX	CPX	PLA
Type:	CORE	RIM	CORE	RIM	CORE
Code:	D05	D09	D21	D22	D31
SiO2	39 75	40 20	51 84	51 39	65 82
TiO2	0 12	0 07	0 49	0 36	0 00
Al2O3	20 13	20 76	6 29	4 68	21 16
Cr2O3	0 03	0 02	0 02	0 07	0 00
FeO	27 23	27 52	12 93	13 68	0 12
MnO	0 61	1 16	0 07	0 12	0 00
MgO	4 15	3 76	8 35	8 48	0 00
CaO	9 45	8 89	16 66	16 64	3 45
Na2O	0 00	0 10	3 90	2 64	9 84
K2O	0 00	0 01	0 01	0 00	0 21
Sum	101 47	102 49	100 58	100 06	100 60
Si	3 079	3 083	1 938	1 947	2 885
Ti	0 007	0 004	0 014	0 010	0 000
Al	1 838	1 877	0 277	0 209	1 093
Cr	0 002	0 001	0 001	0 002	0 000
Fe	1 764	1 765	0 404	0 433	0 004
Mn	0 040	0 075	0 002	0 004	0 000
Mg	0 479	0 430	0 465	0 479	0 000
Ca	0 784	0 731	0 667	0 757	0 182
Na	0 000	0 015	0 283	0 194	0 836
K	0 000	0 001	0 000	0 000	0 012
Sum	7 994	7 982	4 051	4 034	4 992
XMg	0 214	0 196	0 535	0 525	0 000
AlI4	0 000	0 000	0 062	0 053	0 115
AlI6	1 838	1 877	0 215	0 156	0 978

Table A2-1: Electron microprobe mineral analyses.

Sample	5039C	5039C	5039C	5039C	5039C	5039C	5039C	5039C	5039C	5039C	5039C	5039C
Min	GNT	CPX	PLG	GNT	GNT	CPX	PLG	GNT	CPX	CPX	PLA	PLA
Type	CORE	CORE	CORE	RIM	CORE	CORE	CORE	RIM	CORE	RIM	CORE	RIM
Code	A01	A23	A37	B01	B02	B23	B34	C03	C21	C22	C31	C32
SiO2	40 59	53 33	64 52	40 33	40 79	52 86	66 86	40 60	52 32	52 62	65 98	65 14
TiO2	0.02	0 42	0 02	0 05	0 06	0 34	0 02	0 08	0.40	0 34	0 00	0 00
Al2O3	20 73	6 24	21 25	20.75	20 58	6 54	21 02	20 46	5 59	5 41	21 14	20 96
Cr2O3	0.07	0 02	0 01	0 03	0 05	0 05	0 02	0 02	0 04	0 02	0 00	0 00
FeO	26 91	10 58	0 12	26 84	26 72	10.71	0 09	26 05	11 44	11 69	0 12	0 12
MnO	0 27	0 09	0 00	0 00	0 65	0 03	0 05	0 67	0 05	0 14	0 00	0 01
MgO	5 05	9 46	0 04	5 48	5 53	9 10	0.00	5 64	9 89	10 39	0 00	0 00
CaO	8 40	17 74	3 09	8 10	8 15	16 83	3 11	8 33	18 58	18 61	3 24	3 39
Na2O	0 07	3 49	10 11	0 03	0 03	3 59	9 9'	0 00	2 52	2 09	9 47	9 13
K2O	0.00	0 00	0 49	0.00	0 01	0 01	0 58	0 02	0.00	0 00	0 52	0 62
Sum	102.11	101.37	99 65	101 61	102 57	100 06	101 64	101 87	100 83	101 31	100 47	99 37
Si	3.097	1 954	2.864	3 087	3 097	1 959	2 901	3 099	1 939	1 941	2 893	2 890
Ti	0.001	0 012	0 001	0 003	0 003	0 009	0 001	0 005	0 011	0 009	0 000	0 000
Al	1.864	0.269	1.112	1.872	1 842	0 286	1 075	1 841	0 244	0 235	1 093	1 096
Cr	0 004	0 001	0 000	0.002	0 003	0 001	0 001	0 001	0 001	0 001	0 000	0 000
Fe	1 717	0 324	0 004	1 718	1 697	0 332	0 003	1 663	0 355	0 361	0 004	0 004
Mn	0 017	0 003	0 000	0 000	0 042	0 001	0 002	0 043	0 002	0 004	0 000	0 000
Mg	0 574	0.517	0 003	0 625	0 626	0 503	0 000	0 642	0 546	0 571	0 000	0 000
Ca	0.687	0 696	0 147	0 664	0 663	0 668	0 145	0 681	0.738	0 735	0 152	0 161
Na	0 010	0 248	0 870	0 004	0 004	0 258	0 834	0 000	0 181	0 149	0 805	0 785
K	0 000	0 000	0 028	0 000	0 001	0 000	0 031	0 002	0 000	0 000	0 029	0 035
Sum	7 973	4 023	5 028	7 975	7 979	4 017	4 992	7 976	4 017	4 007	4 977	4 972
XMg	0 251	0 614	0 373	0 267	0 269	0 602	0 000	0 278	0 606	0 613	0 000	0 000
Al4	0 000	0 046	0 136	0 000	0 000	0 041	0 099	0 000	0 061	0 059	0 107	0 110
Al6	1.864	0 223	0 975	1 872	1 842	0 244	0 977	1 841	0 184	0 176	0 986	0 986

Table A2-1: Electron microprobe mineral analyses.

Sample:	5043A	5043A	5043A	5043A	5043A	5043A	5043A	5043A	5043A	5043A	5043A	5043A	5043A	5043A	5043A
Min:	GNT	GNT	CPX	CPX	PLG	GNT	CPX	PLG	CPX	GNT	GNT	GNT	CPX	CPX	PLG
Type	CORE	RIM	RIM	CORE	CORE	CORE	CORE	CORE	RIM	RIM	RIM	CORE	CORE	RIM	CORE
Code.	A01	A02	A03	A04	A05	B01	B02	B03	B04	B05	B07	B08	B28	B29	B32
SiO2	39 51	40.01	51 85	49.52	65 63	38 33	50 66	66 59	52 30	39 80	40 11	39 66	51 80	51 29	64 76
TiO2	0 09	0 08	0 35	0 41	0 01	0 06	0 45	0 01	0 29	0 07	0 09	0 07	0 44	0 44	0 00
Al2O3	20 00	19 96	5 06	6 28	20 96	20 27	6 07	21 17	5 11	20 71	20 54	20 71	6 41	5 66	21 66
Cr2O3	0 00	0 00	0 02	0 04	0 00	0 01	0 03	0 02	0 05	0 01	0 04	0 00	0 00	0 02	0 04
FeO	26 38	26 80	11 43	11 83	0 08	26 03	12 35	0 10	12 08	26 98	26 95	26 25	12 70	12 57	0 12
MnO	0 74	0 86	0 14	0 09	0 01	2 23	0 08	0 00	0 09	1 23	0 89	0 69	0 15	0 14	0 00
MgO	4 68	4 81	9 88	8 89	0 04	5 01	8 90	0 00	9 57	3 89	4 12	4 54	8 77	9 57	0 02
CaO	8 74	8 85	18 99	17 38	3 39	9 21	17 90	3 11	19 58	8 91	9 30	9 73	18 12	18 89	3 68
Na2O	0 01	0 12	2 07	3 23	9 64	0 09	3 00	10 00	2 20	0 00	0 04	0 01	2 77	2 59	9 50
K2O	0 00	0 00	0 01	0 02	0 32	0 01	0 02	0 18	0 00	0 00	0 02	0 00	0 03	0 01	0 24
Sum	100 15	101 49	99 80	97 69	100 08	101 25	99 46	101 18	101 27	101 60	102 10	101 68	101 19	101 18	100 02
Si	3 087	3 091	1 945	1 907	2 890	2 993	1 917	2 897	1 941	3 076	3 082	3 056	1 924	1 912	2 857
Ti	0 005	0 005	0 010	0 012	0 000	0 004	0 013	0 000	0 008	0 004	0 005	0 004	0 012	0 012	0 000
Al	1 842	1 818	0 224	0 285	1 088	1 866	0 271	1 084	0 224	1 887	1 860	1 880	0 281	0 249	1 127
Cr	0 000	0 000	0 001	0 001	0 000	0 001	0 001	0 001	0 001	0 001	0 002	0 000	0 000	0 001	0 001
Fe	1 724	1 731	0 359	0 381	0 003	1 700	0 391	0 004	0 375	1 744	1 732	1 691	0 395	0 392	0 004
Mn	0 049	0 056	0 004	0 003	0 000	0 147	0 003	0 000	0 003	0 081	0 058	0 045	0 005	0 004	0 000
Mg	0 545	0 554	0 552	0 510	0 003	0 583	0 502	0 000	0 529	0 448	0 472	0 521	0 485	0 532	0 001
Ca	0 732	0 733	0 763	0 717	0 160	0 771	0 726	0 145	0 779	0 738	0 766	0 803	0 721	0 755	0 174
Na	0 002	0 018	0 151	0 241	0 823	0 014	0 220	0 845	0 158	0 000	0 006	0 001	0 199	0 187	0 813
K	0 000	0 000	0 000	0 001	0 018	0 001	0 001	0 017	0 000	0 000	0 002	0 000	0 001	0 000	0 014
Sum	7 987	8 005	4 009	4 059	4 986	8 078	4 044	4 993	4 018	7 977	7 985	8 001	4 024	4 045	4 991
XMg	0 240	0 242	0 608	0 572	0 471	0 255	0 562	0 000	0 585	0 204	0 214	0 236	0 552	0 576	0 229
Al4	0 000	0 000	0 055	0 093	0 110	0 007	0 083	0 000	0 059	0 000	0 000	0 000	0 076	0 088	0 143
Al6	1 842	1 818	0 169	0 192	0 978	1 858	0 188	0 683	0 164	1 887	1 860	1 880	0 205	0 161	0 984

Table A2-1: Electron microprobe mineral analyses.

Sample:	5043A	5043A	5043A	5043A	5043A	5043A	5043A	5043A	5043A	5043A	5043A	5043A	5043A	5043A	5043A
Min	PLG	GNT	GNT	CPX	CPX	PLG	PLG	GNT	GNT	CPX	CPX	PLG	PLG	GNT	GNT
Type:	CORE	CORE	RIM	CORE	RIM	CORE	RIM	CORE	RIM	CORE	RIM	CORE	RIM	CORE	RIM
Code:	B33	C01	C06	C23	C24	C31	C32	D01	D03	D23	D24	D31	D32	E02	E03
SiO2	65 12	38 56	38 24	49 50	50 96	65 04	64 39	38 26	37 50	50 33	52 02	63 46	64 11	37 50	37 70
TiO2	0 02	0 11	0 09	0 45	0 34	0 04	0 00	0 09	0 11	0 41	0 26	0 01	0 03	0 11	0 06
Al2O3	21 80	21 41	21 56	6 47	5 50	21 06	22 27	21 49	21 39	5 86	4 77	22 58	21 43	21 33	21 61
Cr2O3	0 00	0 00	0 04	0 03	0 04	0 01	0 01	0 00	0 05	0 04	0 09	0 02	0 02	0 05	0 06
FeO	0 09	25 00	24 75	12 47	12 66	0 06	0 13	25 25	25 66	12 93	12 13	0 09	0 09	24 29	26 01
MnO	0 08	0 69	2 80	0 00	0.12	0 02	0 03	0 75	0 79	0 13	0 14	0 01	0 00	0 68	0 76
MgO	0 00	5 44	4 78	8 78	9 72	0 00	0 02	5 16	4 96	9 09	10 12	0 00	0 00	5 25	5 09
CaO	3 93	8 75	8 50	18 09	19 46	3 33	4 07	8 75	8 73	19 30	20 46	4 45	4 49	9 44	8 77
Na2O	9 45	0 06	0 02	3 52	2 06	9 60	9 34	0 02	0 00	2 52	1 30	8 44	8 76	0 03	0 02
K2O	0 18	0 00	0 04	0.01	0 00	0 21	0 25	0 01	0 02	0 00	0 01	0 24	0 21	0 00	0 00
Sum	100 67	100 02	100 82	99 32	100 86	99 37	100 51	99 78	99 23	100 61	101 30	99 30	99 14	98 68	100 08
Si	2 855	3 001	2 977	1 886	1 908	2 883	2 832	2 991	2 961	1 896	1 933	2 819	2 854	2 964	2 953
Ti	0 001	0 006	0 005	0 013	0 010	0 001	0 000	0 005	0 007	0 012	0 007	0 000	0 001	0 007	0 004
Al	1 127	1 964	1 979	0 291	0 243	1 100	1 154	1 980	1 991	0 260	0 209	1 182	1 125	1 988	1 996
Cr	0 000	0 000	0 002	0 001	0 001	0 000	0 000	0 000	0 003	0 001	0 003	0 001	0 001	0 003	0 004
Fe	0 003	1 627	1 611	0 397	0 396	0 002	0 005	1 651	1 695	0 407	0 377	0 003	0 003	1 606	1 704
Mn	0 003	0 045	0 185	0 000	0 004	0 001	0 001	0 050	0 053	0 004	0 004	0 000	0 000	0 046	0 050
Mg	0 000	0 631	0 555	0 499	0 542	0 000	0 001	0 601	0 586	0 510	0 560	0 000	0 000	0 619	0 594
Ca	0 185	0 730	0 709	0 739	0 781	0 158	0 192	0 733	0 739	0 779	0 814	0 212	0 214	0 800	0 736
Na	0 803	0 009	0 003	0 260	0 150	0 825	0 798	0 003	0 000	0 184	0 094	0 727	0 756	0 005	0 003
K	0 010	0 000	0 004	0 000	0 000	0 012	0 014	0 001	0 002	0 000	0 000	0 014	0 012	0 000	0 000
Sum	4 987	8 014	8 030	4 086	4 035	4 983	4 996	8 015	8 036	4 054	4 001	4 959	4 966	8 036	8 045
XMg	0 000	0 279	0 256	0 558	0 578	0 000	0 215	0 267	0 257	0 556	0 598	0 000	0 000	0 278	0 259
Al4	0 145	0 000	0 023	0 114	0 092	0 117	0 168	0 009	0 039	0 104	0 067	0 181	0 146	0 036	0 047
Al6	0 982	1 964	1 956	0 177	0 151	0 984	0 986	1 971	1 952	0 156	0 141	1 002	0 979	1 952	1 949

Table A2-1: Electron microprobe mineral analyses.

Sample	5043A	5043A	5043A	5043A	5043A
Min:	CPX	CPX	PLG	PLG	BIO
Type:	CORE	RIM	CORE	RIM	RIM
Code:	E21	E22	E31	E32	E41
SiO2	51 70	50 97	65 63	64 37	36 92
TiO2	0 46	0.39	0 01	0 03	4 80
Al2O3	6 50	6 07	20 60	20 87	13 82
Cr2O3	0 05	0 05	0 00	0 02	0 03
FeO	12 59	12 47	0 02	0 05	21 34
MnO	0 05	0 11	0 00	0 03	0 27
MgO	8 91	8 91	0 00	0 00	11 44
CaO	16 92	18 17	3 06	3 41	0 00
Na2O	3 61	2 98	9 49	9 21	0 06
K2O	0 01	0 01	0 30	0 25	9 43
Sum	100 80	100 13	99 11	98 24	98 11
Si	1 925	1 918	2 911	2 885	2 768
Ti	0 013	0 011	0 000	0 001	0 271
Al	0 285	0 269	1 077	1 102	1 221
Cr	0 001	0 001	0 000	0 001	0 002
Fe	0 392	0 392	0 001	0 002	1 338
Mn	0 002	0 004	0 000	0 001	0 017
Mg	0 494	0 500	0 000	0 000	1 278
Ca	0 675	0 732	0 145	0 164	0 000
Na	0 261	0 217	0 816	0 800	0 009
K	0 000	0 000	0 017	0 014	0 902
Sum	4 049	4 045	4 967	4 970	7 805
XMg	0 558	0 560	0 000	0 000	0 489
AlI4	0 075	0 082	0 089	0 115	1 232
AlI6	0 210	0 187	0 987	0 987	0 000

Table A2-1: Electron microprobe mineral analyses.

Sample	5047A	5047A	5047A	5047A	5047A	5047A	5047A	5047A	5047A	5047A	5047A	5047A	5047A	5047A	5047A
Min	GNT	PLG	BIO	GNT	GNT	GNT	GNT	GNT	GNT	GNT	GNT	GNT	GNT	GNT	GNT
Type	CORE	CORE	CORE	TRAV	TRAV	TRAV	TRAV	TRAV	TRAV	TRAV	TRAV	TRAV	TRAV	TRAV	CORE
Code	A03	A31	A41	A51	A52	A54	A55	A56	A57	A58	A59	A60	A61	A62	B01
SiO2	40 70	62 81	38 32	38 60	38 23	38 57	39 07	38 67	38 45	38 57	38 77	39 15	37.24	38 48	39 64
TiO2	0 02	0 00	2 61	0 02	0 00	0 05	0 00	0 03	0 04	0 00	0 05	0 05	0 02	0 00	0 00
Al2O3	21 00	22 93	16 23	22.77	22 74	22 69	23 54	23 19	22 99	23 14	23 36	23 40	22 74	22 83	21 09
Cr2O3	0 02	0 02	0 00	0 00	0 00	0 00	0 00	0 00	0 00	0 01	0 00	0 00	0 00	0 01	0 00
FeO	25 00	0 04	13 12	23 44	23 48	25 23	25 04	25 77	26 37	26 09	25 93	25 86	26 12	25 39	26 58
MnO	3 56	0 01	0 08	3 01	3 32	2 96	3 22	3 37	2 97	3 22	3 20	3 09	3 03	3 27	3 88
MgO	9 67	0 05	16 57	10 05	9 32	9 44	9 78	9 95	9 97	10 31	10 32	9 92	10 20	9 68	9 28
CaO	1 55	5 32	0 00	1 65	1 59	1 50	1 53	1 50	1 57	1 42	1 32	1 55	1 42	1 53	1 26
Na2O	0 00	8 41	0 06	0 00	0 02	0 11	0 06	0 06	0 01	0 07	0 12	0 00	0 00	0 04	0 00
K2O	0 00	0 31	9 45	0 03	0 02	0 00	0 03	0 00	0 00	0 05	0 03	0 03	0 00	0 03	0 00
Sum	101 52	99 90	96 44	99 57	98 72	100 55	102 27	102 54	102 37	102 88	103.10	103 05	100 77	101 26	101 73
Si	3 080	2 786	2 790	2 961	2 965	2 953	2 935	2 913	2 907	2 900	2 903	2 928	2 867	2 932	3 025
Ti	0 001	0 000	0 143	0 001	0 000	0 003	0 000	0 002	0 002	0 000	0 003	0 003	0 001	0 000	0 000
Al	1 873	1.199	1 393	2 059	2 079	2 048	2 085	2 059	2 049	2 051	2.062	2 063	2.064	2 051	1 897
Cr	0 001	0 001	0 000	0 000	0 000	0 000	0 000	0 000	0 000	0 001	0 000	0 000	0 000	0 001	0 000
Fe	1 582	0 001	0 799	1 504	1 523	1 616	1 573	1 624	1 667	1 641	1 624	1 617	1 682	1 618	1 696
Mn	0 228	0 000	0 005	0 196	0 218	0 192	0 205	0 215	0 190	0 205	0 203	0 196	0 198	0 211	0 251
Mg	1 090	0.003	1 798	1 149	1 077	1 077	1 095	1 117	1 123	1 155	1 152	1.106	1 170	1 099	1 055
Ca	0 126	0 253	0 000	0 136	0 132	0 123	0 123	0 121	0 127	0 114	0 106	0 124	0 117	0 125	0 103
Na	0 000	0 723	0 008	0 000	0 003	0 016	0 009	0 009	0 001	0 010	0 017	0 000	0 000	0 006	0 000
K	0 000	0.018	0 878	0 003	0 002	0 000	0 003	0 000	0 000	0 005	0 003	0 003	0 000	0 003	0 000
Sum	7 982	4 984	7 814	8 009	7 998	8 028	8 028	8 060	8 067	8 082	8 073	8 039	8 099	8 046	8 027
XMg	0 408	0 690	0 692	0 433	0 414	0 400	0 410	0 408	0 403	0 413	0 415	0 406	0	0 405	0 384
Al4	0 000	0 214	1 210	0 039	0 035	0 047	0 065	0 087	0 093	0 100	0 097	0 072	,3	0 068	0 000
Al6	1 873	0 985	0 183	2 021	2 043	2 001	2 020	1 972	1 955	1 951	1 965	1 991	1 931	1 983	1 897

Table A2-1: Electron microprobe mineral analyses.

Sample:	5047A	5047A	5047A	5047A	5047A	5047A	5047A	5047A	5047A	5047A	5047A	5047A	5047A	5047A	5047A
Min:	GNT	BIO	BIO	GNT	GNT	BIO	PLG	GNT	GNT	GNT	GNT	GNT	GNT	GNT	GNT
Type:	RIM	CORE	RIM	CORE	RIM	RIM	CORE	TRAV	TRAV	TRAV	TRAV	TRAV	TRAV	TRAV	TRAV
Code:	B02	B41	B42	C01	C02	C03	C31	C51	C52	C53	C54	C55	C56	C57	C58
SiO2	38 42	38 52	38 39	40.01	39 60	38 91	65 62	38 74	39 75	38 63	37 96	39 21	38 95	38.73	37 64
TiO2	0 02	2 97	2.88	0.02	0 00	2 41	0 07	0 03	0 02	0 02	0 05	0 03	0 06	0 02	0 02
Al2O3	22.31	16 66	15 86	20.80	21 05	16 49	18.02	23 02	23.10	23 11	23 16	23 49	22 19	23 18	22 96
Cr2O3	0.03	0 00	0 02	0.00	0 04	0 03	0 00	0 00	0 00	0 00	0 00	0 00	0 00	0 00	0 00
FeO	24 23	12 10	12 11	25 61	25 35	11 39	0 11	24 91	25 25	26 37	24 76	24 86	25 30	26 64	26 42
MnO	3 69	0 06	0 08	3 92	3 97	0 09	0 00	3 39	3 45	3 42	3 15	3 43	3 25	3 52	3 43
MgO	10 00	17 22	17 08	9 57	9 32	16 73	0 00	9 62	9 62	10 14	9 59	9 89	10 15	10 00	9 68
CaO	1 64	0.00	0 00	1 33	1 45	0 02	0 04	1 27	1 46	1 49	1 35	1 33	1 50	1 48	1 51
Na2O	0 01	0 07	0 09	0 01	0 02	0 04	1 93	0 06	0 04	0 12	0 01	0 00	0 02	0 00	0 09
K2O	0.00	9 86	9 70	0 02	0 02	9 73	13.22	0 00	0 01	0 00	0 01	0 08	0 04	0.04	0 00
Sum	100 35	97 46	96 21	101 29	100 82	95 84	99 01	101 04	102 70	103 30	100 04	102 32	101 46	103 61	101 75
Si	2 947	2 767	2 795	3 053	3 036	2 826	3 023	2 948	2 974	2 898	2 918	2 942	2 960	2 900	2 876
Ti	0 001	0 160	0 158	0 001	0 000	0 132	0 002	0 002	0 001	0 001	0 003	0 002	0 003	0 001	0 001
Al	2 018	1 410	1 361	1 871	1 903	1 412	0 979	2 065	2 038	2 044	2 099	2 078	1 988	2 046	2 068
Cr	0 002	0 000	0 001	0 000	0 002	0 002	0 000	0 000	0 000	0 000	0 000	0 000	0 000	0 000	0 000
Fe	1 555	0 727	0 737	1 634	1 626	0 692	0 004	1 585	1 580	1 655	1 592	1 560	1 608	1 668	1 688
Mn	0 240	0 004	0 005	0 253	0 258	0 006	0 000	0 219	0 219	0 217	0 205	0 218	0 209	0 223	0 222
Mg	1 143	1 843	1 853	1 088	1 065	1 811	0 000	1 091	1 073	1 134	1 099	1 106	1 149	1 116	1 102
Ca	0 135	0 000	0 000	0 109	0 119	0 002	0 002	0 104	0 117	0 120	0 111	0 107	0 122	0 119	0 124
Na	0 001	0 010	0 013	0 001	0 003	0 006	0 172	0 009	0 006	0 017	0 001	0 000	0 003	0 000	0 013
K	0 000	0 903	0 901	0 002	0 002	0 902	0 777	0 000	0 001	0 000	0 001	0 008	0 004	0 004	0 000
Sum	8 042	7 824	7 823	8 012	8 014	7 789	4 960	8 022	8 009	8 087	8 030	8 021	8 046	8 077	8 095
XMg	0 424	0 717	0 715	0 400	0 396	0 724	0 000	0 408	0 404	0 407	0 408	0 415	0 417	0 401	0 395
AI4	0 053	1 233	1 205	0 000	0 000	1 174	0 000	0 052	0 026	0 102	0 082	0 058	0 040	0 100	0 124
AI6	1 965	0 177	0 156	1 871	1 903	0 238	0 979	2 013	2 012	1 942	2 017	2 020	1 947	1 946	1 944

Table A2-1: Electron microprobe mineral analyses.

Sample	5047A	5047A	5047A	5047A	5047A	5047A	5047A	5047A	5047A	5047A
Min:	GNT	GNT	GNT	GNT	GNT	GNT	PLG	PLG	BIO	BIO
Type:	TRAV	TRAV	TRAV	TRAV	TRAV	CORE	CORE	RIM	CORE	RIM
Code:	C59	C60	C61	C62	C63	D01	D31	D32	D42	D43
SiO2	39 24	37 26	37 84	37 94	38 64	39.90	61 97	97 57	38 35	37 80
TiO2	0.00	0 00	0 00	0 02	0 03	0 01	0 03	0.00	2 65	2 93
Al2O3	23 02	23 22	23 23	23 42	23 04	21 07	23 12	0 05	16 39	16 34
Cr2O3	0.00	0 00	0.00	0 00	0 00	0 03	0 00	0 02	0 02	0 03
FeO	24.78	25 44	25 79	26.43	26 72	25 55	0 16	0 16	11 04	12 76
MnO	2.78	3 12	3.51	3 08	3 38	3 98	0 00	0 04	0 09	0 08
MgO	9 97	9 87	9 79	9 54	9.20	8 89	0 02	0 00	16 51	16 50
CaO	1 44	1 46	1 48	1 54	1.47	1.57	5 66	0.00	0 00	0.00
Na2O	0 04	0 06	0 00	0 00	0 04	0 04	8 23	0 00	0 09	0 08
K2O	0.04	0 03	0 09	0 10	0 03	0 01	0.21	0 01	9 74	9 38
Sum	101 31	100 46	101.73	102.07	102.55	101 05	99 40	97 85	94 88	95 90
Si	2 966	2 869	2 882	2 882	2 923	3 053	2.766	3 994	2 814	2 766
Ti	0 000	0 000	0 000	0 001	0.002	0 001	0.001	0 000	0 146	0 161
Al	2.051	2.108	2 086	2 097	2.055	1 901	1.217	0 002	1.418	1 409
Cr	0.000	0 000	0.000	0.000	0 000	0 002	0.000	0 001	0 001	0 002
Fe	1.567	1 638	1.643	1.679	1.691	1.635	0 006	0 005	0 678	0 781
Mn	0 178	0 203	0.226	0 198	0.217	0 258	0 000	0 001	0 006	0 005
Mg	1.123	1 133	1 111	1 080	1 037	1 014	0 001	0 000	1 805	1.799
Ca	0.117	0 120	0.121	0 125	0 119	0 129	0 271	0 000	0 000	0 000
Na	0 006	0 009	0 000	0 000	0 006	0 006	0 712	0 000	0 013	0 011
K	0 004	0 003	0 009	0 010	0 003	0 001	0 012	0 001	0 912	0 876
Sum	8.012	8 083	8 079	8 073	8.052	7 998	4.986	4 005	7 792	7 811
XMg	0 418	0 409	0 404	0 391	0 380	0 383	0 182	0 000	0 727	0 697
AlI4	0 034	0 131	0 118	0 118	0 077	0 000	0 234	0 000	1 186	1 234
AlI6	2 018	1 976	1 968	1 979	1 978	1 901	0 983	0 002	0 232	0 175

Table A2-1: Electron microprobe mineral analyses.

Sample:	6050	6050	6050	6050	6050	6050	6050	6050	6050	6050	6050	6050	6050	6050	6050
Min:	GNT	GNT	PLG	PLG	BIO	BIO	GNT	GNT	PLG	PLG	BIO	BIO	GNT	GNT	PLG
Type:	CORE	RIM	CORE	RIM	CORE	RIM	CORE	RIM	CORE	RIM	CORE	RIM	CORE	RIM	CORE
Code:	A01	A03	A31	A33	A41	A42	B01	B03	B31	B32	B41	B42	D01	D03	D31
SiO2	38 20	38.46	61.21	60 12	37 76	38 26	39 29	38 32	61 24	61 33	38 39	38.00	39 54	39 25	61 29
TiO2	0 00	0.00	0 00	0.05	0.99	0 98	0.00	0.00	0.00	0.05	0.33	0.33	0 00	0 00	0 05
Al2O3	21 07	21.14	24 92	24.91	19 11	19 29	21 98	21 29	24 86	24.96	19 15	19 37	21 78	21 96	24 98
Cr2O3	0.02	0.03	0 04	0 00	0 06	0 01	0 00	0.02	0 02	0.00	0 00	0 07	0 02	0 03	0 00
FeO	26 61	27 59	0 05	0.12	11 81	11 60	26 97	26 43	0 07	0.04	11.50	11.36	26 27	28 04	0 07
MnO	2 97	3.10	0 00	0 01	0 05	0 04	1.98	2 34	0 02	0 00	0 06	0 06	1 93	2 20	0 00
MgO	9 16	8 53	0 00	0 00	16 71	16 95	10.34	9 48	0.00	0 00	18 26	18 21	10 13	9 47	0 00
CaO	1 88	2.05	7 63	7.46	0 01	0 00	1 90	1 85	7 78	7 64	0 00	0 02	1 91	1 79	7 54
Na2O	0 00	0 04	6 84	6 77	0 00	0 09	0 05	0 01	7 55	6 93	0 10	0 16	0 04	0 04	7 15
K2O	0 00	0 01	0 33	0 28	9 61	9 77	0 00	0 00	0 20	0 28	9 70	9 01	0.01	0 00	0 24
Sum	99 91	100 95	101 02	99 72	96 11	96 99	102 51	99 74	101 74	101 23	97 49	96 59	101 63	102 78	101 32
Si	2 974	2.978	2.697	2.684	2 736	2 743	2 962	2 976	2 687	2.696	2 737	2 724	2 995	2 967	2 693
Ti	0 000	0 000	0 000	0 002	0 054	0 053	0 000	0 000	0 000	0 002	0 018	0 018	0 000	0 000	0 002
Al	1 934	1 929	1 294	1 311	1 632	1 630	1 953	1 949	1 286	1 293	1 609	1.637	1 945	1 957	1 294
Cr	0 001	0 002	0 001	0 000	0.003	0 001	0 000	0 001	0 001	0 000	0.000	0 004	0 001	0 002	0 000
Fe	1 733	1 786	0 002	0 004	0 716	0 696	1 700	1 717	0 003	0 001	0 686	0 681	1 664	1 773	0 003
Mn	0 196	0 203	0 000	0 000	0 003	0 002	0 126	0 154	0 001	0 000	0 004	0 004	0 124	0 141	0 000
Mg	1 063	0 984	0 000	0 000	1 804	1 811	1 162	1 097	0 000	0 000	1 940	1 945	1 144	1 067	0 000
Ca	0 157	0 170	0 360	0 357	0 001	0 000	0 153	0 154	0 366	0 360	0 000	0 002	0 155	0 145	0 355
Na	0 000	0 006	0 584	0 585	0 000	0 013	0 007	0 002	0 642	0 591	0 014	0 022	0 006	0 006	0 609
K	0 000	0 001	0 019	0 016	0 888	0 894	0 000	0 000	0 011	0 016	0 882	0 824	0 001	0 000	0 013
Sum	8 058	8 060	4 957	4 960	7 837	7 842	8 065	8 049	4 996	4 959	7 889	7 861	8 035	8 057	4 969
xMg	0 380	0 355	0 000	0 000	0 716	0 723	0 406	0 390	0 000	0 000	0 739	0 741	0 407	0 376	0 000
AlI4	0 026	0 022	0 303	0 316	1 264	1 257	0 038	0 024	0 313	0 304	1 263	1 276	0 005	0 033	0 307
AlI6	1 908	1 907	0 991	0 995	0 368	0 373	1 915	1 925	0 973	0 989	0 346	0 361	1 940	1 924	0 987

Table A2-1: Electron microprobe mineral analyses.

Sample:	6050	6050	6050
Min:	PLG	BIO	BIO
Type:	RIM	CORE	RIM
Code:	D33	D41	D42
SiO2	60.17	37.50	37.66
TiO2	0.00	0.08	0.06
Al2O3	25.38	19.07	18.90
Cr2O3	0.04	0.04	0.00
FeO	0.04	10.81	11.29
MnO	0.03	0.07	0.03
MgO	0.00	17.25	17.49
CaO	8.07	0.04	0.01
Na2O	7.37	0.20	0.13
K2O	0.19	8.84	9.13
Sum	101.29	93.90	94.70
Si	2.656	2.758	2.756
Ti	0.000	0.004	0.003
Al	1.321	1.653	1.630
Cr	0.001	0.002	0.000
Fe	0.001	0.665	0.691
Mn	0.001	0.004	0.002
Mg	0.000	1.891	1.907
Ca	0.382	0.003	0.001
Na	0.631	0.029	0.018
K	0.011	0.829	0.852
Sum	5.004	7.839	7.861
XMg	0.000	0.740	0.734
Al4	0.344	1.242	1.244
Al6	0.976	0.411	0.386

Table A2-1: Electron microprobe mineral analyses.

Sample:	6056	6056	6056	6056	6056	6056	6056	6056	6056	6056
Min:	GNT	GNT	BIO	BIO	GNT	GNT	PLG	PLG	BIO	BIO
Type:	CORE	RIM	CORE	RIM	CORE	RIM	CORE	RIM	CORE	RIM
Code:	A01	A02	A41	A42	B01	B02	B31	B32	B41	B42
SiO2	37.10	38.71	36.93	41.18	39.00	38.46	60.19	60.68	37.15	37.26
TiO2	0.00	0.00	2.85	2.95	0.00	0.00	0.00	0.05	2.75	2.68
Al2O3	22.01	21.93	17.24	16.99	22.34	21.86	24.09	24.45	17.87	18.08
Cr2O3	0.03	0.05	0.04	0.04	0.00	0.03	0.00	0.02	0.00	0.03
FeO	28.54	28.48	11.04	10.09	26.59	28.11	0.15	0.23	11.29	10.48
MnO	1.31	1.55	0.00	0.00	1.06	1.52	0.01	0.03	0.09	0.04
MgO	9.50	8.49	16.02	16.00	10.66	9.18	0.00	0.03	16.30	15.86
CaO	1.67	1.43	0.00	0.00	1.78	1.92	7.31	7.47	0.00	0.00
Na2O	0.00	0.22	0.07	0.09	0.00	0.04	6.70	6.90	0.12	0.15
K2O	0.01	0.02	9.54	9.56	0.01	0.01	0.44	0.34	9.94	10.02
Sum	100.17	100.88	93.73	96.90	101.44	101.13	98.89	100.20	95.51	94.60
Si	2.889	2.981	2.746	2.916	2.954	2.955	2.709	2.699	2.719	2.741
Ti	0.000	0.000	0.159	0.157	0.000	0.000	0.000	0.002	0.151	0.148
Al	2.021	1.991	1.511	1.418	1.995	1.980	1.278	1.282	1.542	1.568
Cr	0.002	0.003	0.002	0.002	0.000	0.002	0.000	0.001	0.000	0.002
Fe	1.859	1.835	0.687	0.597	1.684	1.806	0.006	0.009	0.691	0.645
Mn	0.086	0.101	0.000	0.000	0.068	0.099	0.000	0.001	0.006	0.002
Mg	1.103	0.975	1.775	1.688	1.203	1.051	0.000	0.002	1.778	1.739
Ca	0.139	0.118	0.000	0.000	0.144	0.158	0.353	0.356	0.000	0.000
Na	0.000	0.033	0.010	0.012	0.000	0.006	0.585	0.595	0.017	0.021
K	0.001	0.002	0.905	0.864	0.001	0.001	0.025	0.019	0.928	0.940
Sum	8.100	8.039	7.795	7.655	8.049	8.058	4.956	4.965	7.831	7.807
XMg	0.372	0.347	0.721	0.739	0.417	0.368	0.000	0.189	0.720	0.729
Al4	0.111	0.019	1.254	1.084	0.046	0.045	0.291	0.301	1.281	1.259
Al6	1.910	1.973	0.257	0.334	1.948	1.935	0.988	0.981	0.260	0.309

Table A2-1: Electron microprobe mineral analyses.

Sample:	7051	7051	7051	7051	7051	7051	7051	7051	7051	7051	7051	7051	7051	7051	7051
Min:	GNT	GNT	PLG	PLG	BIO	BIO	GNT	GNT	PLG	PLG	BIO	BIO	GNT	GNT	PLG
Type:	CORE	RIM	CORE	RIM	CORE	RIM	CORE	RIM	CORE	RIM	CORE	RIM	CORE	RIM	CORE
Code:	A01	A03	A31	A32	A41	A42	B01	B03	B31	B32	B41	B42	C01	C03	C31
SiO2	39.03	38.32	61.95	62.57	38.26	37.35	39.17	39.20	62.42	63.54	36.99	37.15	39.30	38.94	62.45
TiO2	0.02	0.04	0.03	0.02	1.81	1.85	0.00	0.00	0.02	0.05	2.04	1.84	0.03	0.02	0.04
Al2O3	22.00	21.94	23.38	22.76	17.79	17.63	22.88	22.51	23.02	23.38	17.26	17.01	22.96	22.00	22.77
Cr2O3	0.00	0.00	0.00	0.00	0.00	0.00	0.00	0.00	0.00	0.00	0.00	0.00	0.00	0.00	0.00
FeO	25.05	24.78	0.05	0.01	11.47	11.68	25.56	24.64	0.00	0.00	10.68	11.07	25.75	24.84	0.00
MnO	1.49	1.69	0.12	0.09	0.02	0.09	2.07	3.00	0.05	0.14	0.09	0.03	2.35	2.85	0.22
MgO	11.04	10.30	0.02	0.00	16.10	16.03	10.27	9.97	0.00	0.13	14.86	15.38	10.64	9.75	0.00
CaO	2.09	2.04	5.46	5.51	0.00	0.00	1.50	1.95	5.49	5.20	0.00	0.00	1.44	1.52	5.13
Na2O	0.04	0.09	7.22	8.43	0.16	0.16	0.00	0.02	9.10	8.21	0.31	0.10	0.11	0.01	8.53
K2O	0.00	0.11	0.17	0.12	8.92	9.02	0.02	0.05	0.16	0.13	11.20	10.93	0.07	0.04	0.22
Sum	100.76	99.31	98.40	99.51	94.53	93.81	101.47	101.34	100.26	100.78	93.43	93.61	102.65	99.97	99.36
Si	2.965	2.960	2.778	2.786	2.803	2.770	2.959	2.971	2.768	2.786	2.784	2.788	2.942	2.992	2.786
Ti	0.001	0.002	0.001	0.001	0.100	0.103	0.000	0.000	0.001	0.002	0.115	0.109	0.002	0.001	0.001
Al	1.970	1.998	1.236	1.195	1.536	1.541	2.037	2.011	1.203	1.209	1.531	1.505	2.026	1.992	1.197
Cr	0.000	0.000	0.000	0.000	0.000	0.000	0.000	0.000	0.000	0.000	0.000	0.000	0.000	0.000	0.000
Fe	1.592	1.601	0.002	0.000	0.703	0.725	1.615	1.562	0.000	0.000	0.672	0.695	1.612	1.596	0.000
Mn	0.096	0.111	0.005	0.003	0.001	0.006	0.132	0.193	0.002	0.005	0.006	0.002	0.149	0.185	0.008
Mg	1.250	1.186	0.001	0.000	1.758	1.772	1.156	1.126	0.000	0.008	1.667	1.720	1.187	1.116	0.000
Ca	0.170	0.169	0.262	0.263	0.000	0.000	0.121	0.158	0.261	0.244	0.000	0.000	0.115	0.125	0.245
Na	0.006	0.013	0.628	0.728	0.023	0.023	0.000	0.003	0.782	0.698	0.045	0.015	0.016	0.001	0.738
K	0.000	0.011	0.010	0.007	0.834	0.854	0.002	0.005	0.009	0.007	1.075	1.047	0.007	0.004	0.013
Sum	8.051	8.051	4.922	4.983	7.757	7.794	8.023	8.028	5.026	4.960	7.895	7.880	8.055	8.013	4.989
XMg	0.440	0.426	0.416	0.000	0.714	0.710	0.417	0.419	0.000	1.000	0.713	0.712	0.424	0.412	0.000
Al4	0.035	0.040	0.222	0.214	1.197	1.230	0.041	0.029	0.232	0.214	1.216	1.212	0.058	0.008	0.214
Al6	1.936	1.958	1.013	0.981	0.339	0.312	1.996	1.981	0.971	0.995	0.315	0.293	1.967	1.984	0.984

Table A2-1: Electron microprobe mineral analyses.

Sample:	7051	7051	7051
Min:	PLG	BIO	BIO
Type:	RIM	CORE	RIM
Code:	C32	C41	C42
SiO2	63.20	36.85	38.06
TiO2	0.03	2.05	2.01
Al2O3	22.61	17.86	18.19
Cr2O3	0.00	0.00	0.00
FeO	0.00	10.82	11.38
MnO	0.41	0.02	0.05
MgO	0.00	15.94	15.63
CaO	5.02	0.00	0.00
Na2O	8.52	0.09	0.14
K2O	0.17	9.26	9.25
Sum	99.96	92.89	94.71
Si	2.801	2.754	2.787
Ti	0.001	0.115	0.111
Al	1.181	1.573	1.570
Cr	0.000	0.000	0.000
Fe	0.000	0.676	0.697
Mn	0.015	0.001	0.003
Mg	0.000	1.775	1.706
Ca	0.238	0.000	0.000
Na	0.732	0.013	0.020
K	0.010	0.883	0.864
Sum	4.978	7.792	7.759
XMg	0.000	0.724	0.710
Al4	0.199	1.246	1.213
Al6	0.982	0.328	0.358

Table A2-1: Electron microprobe mineral analyses.

Sample:	7053	7053	7053	7053	7053	7053	7053	7053	7053	7053	7053	7053	7053	7054	7053
Min:	GNT	GNT	PLG	PLG	BIO	BIO	GNT	GNT	PLG	PLG	BIO	BIO	GNT	GNT	GNT
Type:	CORE	RIM	CORE	RIM	CORE	RIM	CORE	RIM	CORE	RIM	CORE	RIM	TRAV	TRAV	TRAV
Code:	A01	A03	A31	A32	A41	A42	B01	B03	B31	B34	B41	B42	B51	B52	B53
SiO2	38.45	38.77	60.34	59.84	39.22	37.74	38.23	38.15	59.27	60.98	37.01	36.64	38.39	38.55	38.18
TiO2	0.00	0.00	0.03	0.00	1.54	2.01	0.00	0.00	0.03	0.00	2.13	2.32	0.00	0.00	0.00
Al2O3	21.41	21.39	23.30	23.74	21.87	17.74	21.72	21.18	23.77	23.07	17.52	17.48	21.32	21.15	21.81
Cr2O3	0.00	0.04	0.00	0.03	0.06	0.04	0.02	0.02	0.00	0.02	0.03	0.04	0.04	0.04	0.01
FeO	23.54	25.76	0.07	0.04	10.64	11.52	23.39	24.47	0.04	0.19	10.77	10.97	24.20	23.79	24.01
MnO	4.67	5.70	0.01	0.02	0.05	0.06	4.85	6.02	0.02	0.00	0.12	0.13	5.50	5.23	5.69
MgO	9.49	7.95	0.02	0.00	14.27	16.55	9.54	8.18	0.00	0.00	16.13	16.08	8.85	9.20	9.68
CaO	2.34	2.12	6.82	6.63	0.00	0.05	1.72	2.28	6.95	6.73	0.00	0.00	2.00	1.66	1.64
Na2O	0.02	0.00	7.09	7.71	0.04	0.09	0.01	0.02	7.45	7.28	0.10	0.13	0.01	0.00	0.00
K2O	0.00	0.00	0.62	0.50	9.70	9.89	0.00	0.00	0.59	0.47	9.58	9.97	0.00	0.00	0.00
Sum	99.92	101.73	98.30	98.51	97.39	95.69	99.48	100.32	98.12	98.74	93.39	93.76	100.31	99.62	101.02
Si	2.975	2.984	2.733	2.710	2.767	2.754	2.967	2.973	2.698	2.748	2.758	2.733	2.977	2.997	2.936
Ti	0.000	0.000	0.001	0.000	0.082	0.110	0.000	0.000	0.001	0.000	0.119	0.130	0.000	0.000	0.000
Al	1.953	1.941	1.244	1.267	1.819	1.526	1.987	1.946	1.276	1.226	1.539	1.537	1.949	1.932	1.977
Cr	0.000	0.002	0.000	0.001	0.003	0.002	0.001	0.001	0.000	0.001	0.002	0.002	0.002	0.002	0.001
Fe	1.523	1.658	0.003	0.002	0.628	0.703	1.518	1.595	0.002	0.007	0.671	0.684	1.569	1.547	1.544
Mn	0.306	0.372	0.000	0.001	0.003	0.004	0.319	0.397	0.001	0.000	0.008	0.008	0.361	0.344	0.371
Mg	1.094	0.912	0.001	0.000	1.500	1.800	1.103	0.950	0.000	0.000	1.792	1.788	1.023	1.066	1.110
Ca	0.194	0.175	0.331	0.322	0.000	0.004	0.143	0.190	0.339	0.325	0.000	0.000	0.166	0.138	0.135
Na	0.003	0.000	0.623	0.677	0.005	0.013	0.002	0.003	0.658	0.636	0.014	0.019	0.002	0.000	0.000
K	0.000	0.000	0.036	0.029	0.873	0.921	0.000	0.000	0.034	0.027	0.911	0.949	0.000	0.000	0.000
Sum	8.049	8.044	4.973	5.008	7.680	7.838	8.040	8.055	5.008	4.970	7.814	7.851	8.048	8.033	8.074
XMg	0.418	0.355	0.337	0.000	0.705	0.719	0.421	0.373	0.000	0.000	0.727	0.723	0.395	0.408	0.418
Al4	0.025	0.016	0.267	0.290	1.233	1.246	0.033	0.027	0.302	0.252	1.242	1.267	0.023	0.003	0.064
Al6	1.928	1.925	0.978	0.977	0.585	0.281	1.954	1.918	0.974	0.974	0.297	0.270	1.925	1.935	1.914

Table A2-1: Electron microprobe mineral analyses.

Sample:	7053	7053	7053	7053	7053	7053	7053	7053	7053	7053
Min:	GNT	GNT	GNT	GNT	GNT	GNT	PLG	PLG	BIO	BIO
Type:	TRAV	TRAV	TRAV	TRAV	CORE	RIM	CORE	RIM	CORE	RIM
Code:	B54	B55	B56	B57	C01	C03	C31	C32	C41	C42
SiO2	38.22	38.69	38.10	37.96	38.58	37.93	59.68	60.73	36.62	37.29
TiO2	0.00	0.00	0.00	0.00	0.00	0.00	0.03	0.07	2.63	2.14
Al2O3	20.94	21.25	21.34	21.37	21.81	21.40	23.71	23.16	17.68	17.75
Cr2O3	0.00	0.04	0.03	0.00	0.00	0.00	0.00	0.00	0.06	0.09
FeO	24.28	24.13	23.57	23.24	24.36	26.12	0.08	0.06	10.33	10.84
MnO	5.68	5.77	5.68	5.48	4.95	6.64	0.00	0.04	0.02	0.09
MgO	9.41	9.41	9.09	9.17	9.55	7.27	0.00	0.00	15.94	16.65
CaO	1.58	1.73	1.70	2.34	1.64	2.29	7.21	6.13	0.01	0.02
Na2O	0.00	0.04	0.00	0.00	0.02	0.11	7.27	7.02	0.06	0.00
K2O	0.00	0.00	0.00	0.02	0.01	0.00	0.57	0.64	9.83	9.87
Sum	100.11	101.06	99.51	99.58	100.92	101.76	98.83	97.85	93.18	94.74
Si	2.972	2.976	2.971	2.958	2.982	2.945	2.709	2.754	2.735	2.742
Ti	0.000	0.000	0.000	0.000	0.000	0.000	0.001	0.002	0.148	0.118
Al	1.920	1.927	1.962	1.963	1.974	1.958	1.262	1.238	1.557	1.539
Cr	0.000	0.002	0.002	0.000	0.000	0.000	0.000	0.000	0.004	0.005
Fe	1.579	1.552	1.537	1.515	1.564	1.696	0.002	0.002	0.645	0.667
Mn	0.374	0.376	0.375	0.362	0.322	0.437	0.000	0.002	0.001	0.006
Mg	1.091	1.079	1.057	1.065	1.093	0.841	0.000	0.000	1.774	1.825
Ca	0.132	0.143	0.142	0.195	0.135	0.190	0.349	0.298	0.001	0.002
Na	0.000	0.006	0.000	0.000	0.003	0.017	0.637	0.617	0.009	0.000
K	0.000	0.000	0.000	0.002	0.001	0.000	0.033	0.037	0.937	0.926
Sum	8.068	8.062	8.046	8.061	8.053	8.084	4.993	4.951	7.810	7.830
XMg	0.409	0.410	0.407	0.413	0.411	0.332	0.000	0.000	0.733	0.732
Al4	0.028	0.024	0.029	0.042	0.038	0.055	0.291	0.246	1.265	1.258
Al6	1.892	1.903	1.933	1.922	1.936	1.903	0.972	0.993	0.292	0.281

Table A2-1: Electron microprobe mineral analyses.

Sample:	7075D	7075D	7075D	7075D	7075D	7075D	7075D	7075D	7075D	7075D	7075D
Min:	GNT	GNT	PLG	PLG	BIO	BIO	GNT	GNT	PLG	PLG	BIO
Type:	CORE	RIM	CORE	RIM	CORE	RIM	CORE	RIM	CORE	RIM	RIM
Code:	B01	B03	B31	B32	B41	B42	C01	C03	C31	C32	C41
SiO2	40.14	39.17	63.70	61.29	38.77	38.82	39.54	39.21	65.98	63.26	38.34
TiO2	0.00	0.00	0.04	0.05	1.61	1.50	0.00	0.00	0.04	0.02	2.84
Al2O3	22.48	22.87	23.37	22.96	16.44	16.73	22.61	22.57	23.92	23.30	15.99
Cr2O3	0.02	0.03	0.04	0.04	0.03	0.00	0.02	0.02	0.04	0.01	0.04
FeO	19.37	21.49	0.07	0.05	6.24	6.15	19.74	20.30	0.08	0.09	7.18
MnO	1.84	2.10	0.00	0.00	0.00	0.01	2.18	2.21	0.00	0.01	0.01
MgO	14.66	14.47	0.00	0.00	21.82	21.66	14.24	13.59	0.00	0.00	21.00
CaO	1.66	1.71	5.75	5.78	0.00	0.00	1.89	1.89	5.88	5.56	0.00
Na2O	0.01	0.01	8.20	7.89	0.01	0.05	0.05	0.01	3.17	8.30	0.06
K2O	0.02	0.00	0.25	0.39	9.91	9.84	0.01	0.00	0.29	0.52	9.80
Sum	100.20	101.85	101.42	98.45	94.83	94.76	100.28	99.80	99.40	101.07	95.26
Si	2.983	2.902	2.782	2.763	2.785	2.787	2.952	2.950	2.869	2.778	2.758
Ti	0.000	0.000	0.001	0.002	0.087	0.081	0.000	0.000	0.001	0.001	0.154
Al	1.969	1.997	1.203	1.220	1.392	1.416	1.990	2.002	1.226	1.206	1.356
Cr	0.001	0.002	0.001	0.001	0.002	0.000	0.001	0.001	0.001	0.000	0.002
Fe	1.204	1.331	0.003	0.002	0.375	0.369	1.232	1.277	0.003	0.003	0.432
Mn	0.116	0.132	0.000	0.000	0.000	0.001	0.138	0.141	0.000	0.000	0.001
Mg	1.624	1.598	0.000	0.000	2.336	2.317	1.584	1.524	0.000	0.000	2.252
Ca	0.132	0.136	0.269	0.279	0.000	0.000	0.151	0.152	0.274	0.262	0.000
Na	0.001	0.001	0.694	0.690	0.001	0.007	0.007	0.001	0.267	0.707	0.008
K	0.002	0.000	0.014	0.022	0.908	0.901	0.001	0.000	0.016	0.029	0.900
Sum	8.033	8.099	4.968	4.980	7.886	7.878	8.057	8.049	4.658	4.986	7.863
XMg	0.574	0.545	0.000	0.000	0.862	0.863	0.562	0.544	0.000	0.000	0.839
AlⅣ	0.017	0.098	0.218	0.237	1.215	1.213	0.048	0.050	0.131	0.222	1.242
AlⅥ	1.953	1.899	0.985	0.984	0.177	0.202	1.941	1.952	1.095	0.984	0.114

Table A2-1: Electron microprobe mineral analyses.

Sample:	7054	7054	7054	7054	7054	7054	7054	7054	7054	7054
Min:	GNT	GNT	PLG	PLG	BIO	BIO	GNT	GNT	BIO	BIO
Type:	CORE	RIM	CORE	RIM	CORE	RIM	CORE	RIM	CORE	RIM
Code:	A01	A02	A31	A32	A41	A42	B01	B02	B41	B42
SiO2	37.68	37.23	63.46	64.16	37.18	38.21	37.94	38.35	38.02	38.91
TiO2	0.01	0.00	0.00	0.00	1.07	1.09	0.02	0.02	1.43	1.27
Al2O3	22.18	22.46	24.58	24.68	19.66	20.23	22.55	22.91	19.48	19.64
Cr2O3	0.00	0.00	0.00	0.00	0.02	0.04	0.00	0.00	0.08	0.04
FeO	18.57	17.99	0.12	0.02	10.25	10.38	18.98	19.09	9.58	9.69
MnO	14.85	16.49	0.01	0.02	0.27	0.44	13.78	12.79	0.20	0.35
MgO	6.52	5.82	0.00	0.00	16.09	15.63	8.03	8.20	16.31	16.61
CaO	2.11	2.36	4.89	4.89	0.00	0.00	1.43	1.62	0.00	0.00
Na2O	0.00	0.04	8.49	8.56	0.09	0.06	0.00	0.01	0.16	0.09
K2O	0.04	0.00	0.23	0.13	9.27	9.66	0.00	0.01	8.88	9.23
Sum	101.96	102.39	101.78	102.46	93.90	95.74	102.73	103.00	94.14	95.83
Si	2.923	2.893	2.757	2.765	2.735	2.757	2.903	2.912	2.769	2.786
Ti	0.001	0.000	0.000	0.000	0.059	0.059	0.001	0.001	0.078	0.068
Al	2.028	2.057	1.259	1.254	1.705	1.721	2.034	2.051	1.672	1.658
Cr	0.000	0.000	0.000	0.000	0.001	0.002	0.000	0.000	0.005	0.002
Fe	1.205	1.169	0.004	0.001	0.631	0.626	1.215	1.212	0.583	0.580
Mn	0.976	1.085	0.000	0.001	0.017	0.027	0.893	0.823	0.012	0.021
Mg	0.754	0.674	0.000	0.000	1.764	1.681	0.916	0.928	1.770	1.772
Ca	0.175	0.196	0.228	0.226	0.000	0.000	0.117	0.132	0.000	0.000
Na	0.000	0.006	0.715	0.715	0.013	0.008	0.000	0.001	0.023	0.012
K	0.004	0.000	0.013	0.007	0.870	0.889	0.000	0.001	0.825	0.843
Sum	8.064	8.081	4.977	4.969	7.794	7.771	8.079	8.062	7.738	7.743
XMg	0.385	0.366	0.000	0.000	0.737	0.729	0.430	0.434	0.752	0.753
AlI4	0.077	0.107	0.243	0.235	1.265	1.243	0.097	0.088	1.231	1.214
AlI6	1.951	1.950	1.016	1.019	0.440	0.478	1.937	1.963	0.441	0.443

Table A2-1: Electron microprobe mineral analyses.

Sample	7132	7132	7132	7132	7132	7132	7132	7132	7132	7132	7132	7132
Min	GNT	GNT	PLG	PLG	BIO	BIO	GNT	GNT	PLG	PLG	BIO	BIO
Type	CORE	RIM	CORE	RIM	CORE	RIM	CORE	RIM	CORE	RIM	CORE	RIM
Code:	A01	A03	A31	A32	A41	A42	B01	B03	B31	B32	B41	B42
SiO2	40 07	39.48	62.74	62 85	38 62	38.53	39 85	39.67	61.89	62.38	38.26	39 93
TiO2	0 00	0.02	0.05	0.01	2 39	2.16	0 02	0.03	0 00	0 02	1 99	1 63
Al2O3	23 40	22 92	22 69	23 21	15 32	16.75	23 05	23.09	23 96	22 98	15.95	18 01
Cr2O3	0 00	0 00	0 00	0 00	0 00	0.00	0 00	0 00	0 00	0 00	0 00	0 00
FeO	18 71	19 05	0 05	0 00	13 05	13 02	19 25	20 65	0 01	0 03	12 96	11 27
MnO	1 65	1 68	0 04	0 10	0 14	0 12	1 52	1 61	0 04	0 06	0 11	0 04
MgO	15 14	13 80	0 00	0 00	14 84	15 50	14 98	13 32	0 00	0 00	15 30	16 14
CaO	1.49	2 27	5 86	5 43	0 01	0.00	1 49	2 41	6 26	5 90	0 04	0 00
Na2O	0 04	0 01	8 25	8 43	0 07	0 00	0 12	0 01	7 79	8 29	4 57	0 18
K2O	0 00	0 06	0 14	0 10	9 31	9 24	0 00	0 06	0 12	0 14	7.10	9 12
Sum	100 50	99 29	99 82	100 13	93 75	95 32	100 28	100 85	100 07	99 80	96 28	96 32
Si	2 954	2 962	2 787	2 779	2 888	2 827	2 953	2 951	2 743	2 773	2 797	2 858
Ti	0 000	0 001	0 002	0 000	0 134	0 119	0 001	0 002	0 000	0 001	0 109	0 088
Al	2 034	2 027	1 188	1 210	1 351	1 449	2 014	2 025	1 252	1 204	1 375	1 520
Cr	0 000	0 000	0 000	0 000	0 000	0 000	0 000	0 000	0 000	0 000	0 000	0 000
Fe	1 154	1 195	0 002	0 000	0 816	0 799	1 193	1 285	0 000	0 001	0 792	0 675
Mn	0 103	0 107	0 002	0 004	0 009	0 007	0 095	0 101	0 002	0 002	0 007	0 002
Mg	1 664	1 543	0 000	0 000	1 654	1 695	1 655	1 477	0 000	0 000	1 667	1 722
Ca	0 118	0 183	0 279	0 257	0 001	0 000	0 118	0 192	0 297	0 281	0 003	0 000
Na	0 006	0 001	0 710	0 723	0 010	0 000	0 017	0 001	0 669	0 715	0 648	0 025
K	0 000	0 006	0 008	0 006	0 888	0 865	0 000	0 006	0 007	0 008	0 662	0 833
Sum	8 032	8 026	4 977	4 979	7 751	7 762	8 047	8 039	4 969	4 985	8 061	7 723
XMg	0 590	0 563	0 000	0 000	0 670	0 680	0 581	0 535	0 000	0 000	0 678	0 718
Al4	0 046	0 038	0 213	0 221	1 112	1 173	0 047	0 049	0 257	0 227	1 203	1 142
Al6	1 988	1 990	0 975	0 989	0 239	0 276	1 967	1 975	0 994	0 977	0 172	0 378

Table A2-1: Electron microprobe mineral analyses.

Sample	8068	8068	8068	8068	8068	8068	8068	8068	8068	8068	8068	8068	8068	8068	8068
Min.	GNT	GNT	PLG	PLG	BIO	BIO	GNT	GNT	PLG	PLG	BIO	BIO	GNT	GNT	PLG
Type	CORE	RIM	CORE	RIM	CORE	RIM	CORE	RIM	CORE	RIM	CORE	RIM	CORE	RIM	CORE
Code	A01	A02	A31	A32	A41	A42	B01	B02	B31	B32	B41	B42	C01	C02	C31
SiO2	39 23	37 82	61 61	61 23	38 01	37 95	38 38	34 66	61 34	60 46	37 70	37 75	37 10	36 48	60 16
TiO2	0 03	0 02	0 00	0 00	1 53	1 45	0 01	0 00	0 00	0 00	1 34	1 50	0 03	0 03	0 00
Al2O3	22 20	22 41	25 66	25 77	17 85	17 61	22 93	22 65	25 59	25 38	17 85	18 06	21 44	21 63	24 21
Cr2O3	0 00	0 00	0 00	0 00	0 05	0 03	0 00	0 00	0 00	0 00	0 01	0 01	0 00	0 00	0 00
FeO	20 93	22 09	0 04	0 09	12 32	12 12	21 27	21 88	0 11	0 16	12 06	12 08	25 78	24 06	0 08
MnO	7 42	8 12	0 01	0 00	0 14	0 17	8 06	8 85	0 02	0 03	0 16	0 19	10 44	9 69	0 00
MgO	9 50	7 81	0 00	0 00	15 59	16 02	9 00	7 20	0 00	0 02	16 03	15 81	5 16	5 40	0 05
CaO	2 32	2 11	6 58	6 40	0 00	0 02	2 21	2 20	6 55	6 48	0 00	0 00	1 58	2 85	6 02
Na2O	0 00	0 00	7 46	7 13	0 00	0 00	0 00	0 00	7 48	7 73	0 05	0 10	0 00	0 07	8 10
K2O	0 04	0 02	0 29	0 20	9 31	8 91	0 01	0 05	0 22	0 15	9 44	9 86	0 01	0 00	0 21
Sum	101 67	100.40	101 65	100.82	94 80	94 28	101 87	97 49	101 31	100.41	94 64	95 36	101 54	100 21	98 83
Si	2 975	2 936	2 692	2 691	2 796	2 799	2 920	2 805	2 690	2 679	2 780	2 770	2 930	2 904	2 708
Ti	0 002	0 001	0 000	0 000	0 085	0 080	0 001	0 000	0 000	0 000	0 074	0 083	0 002	0 002	0 000
Al	1 985	2 051	1 322	1 335	1 548	1 531	2 056	2 161	1 323	1 326	1 552	1 562	1 996	2 030	1 285
Cr	0 000	0 000	0 000	0 000	0 003	0 002	0 000	0 000	0 000	0 000	0 001	0 001	0 000	0 000	0 000
Fe	1 328	1 434	0 001	0 003	0 758	0 748	1 353	1 481	0 004	0 006	0 744	0 741	1 703	1 602	0 003
Mn	0 477	0 534	0 000	0 000	0 009	0 011	0 519	0 607	0 001	0 001	0 010	0 012	0 698	0 653	0 000
Mg	1 074	0 904	0 000	0 000	1 709	1 761	1 020	0 868	0 000	0 001	1 782	1 729	0 607	0 641	0 003
Ca	0 189	0 176	0 308	0 301	0 000	0 002	0 180	0 191	0 308	0 308	0 000	0 000	0 134	0 243	0 290
Na	0 000	0 000	0 632	0 608	0 000	0 000	0 000	0 000	0 636	0 664	0 007	0 014	0 000	0 011	0 707
K	0 004	0 002	0 016	0 011	0 874	0 839	0 001	0 005	0 012	0 008	0 888	0 923	0 001	0 000	0 012
Sum	8 032	8 038	4 971	4 950	7 781	7 773	8 051	8 117	4 973	4 994	7 817	7 834	8 071	8 085	5 009
XMg	0 447	0 387	0 000	0 000	0 693	0 702	0 430	0 370	0 000	0 182	0 703	0 700	0 263	0 286	0 527
Al4	0 025	0 064	0 308	0 309	1 204	1 201	0 080	0 195	0 310	0 321	1 220	1 230	0 070	0 096	0 292
Al6	1 960	1 987	1 013	1 027	0 344	0 331	1 976	1 965	1 012	1 005	0 332	0 332	1 926	1 933	0 993

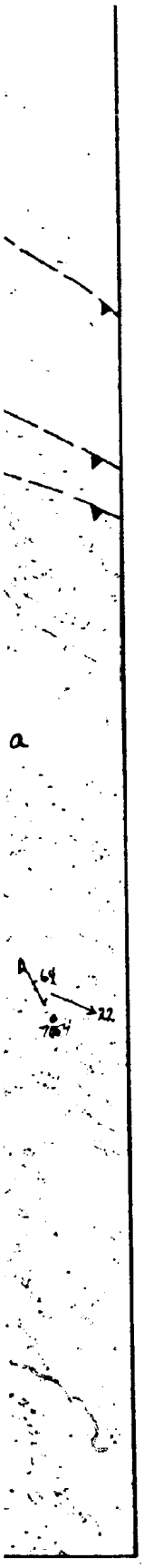
a
64
22

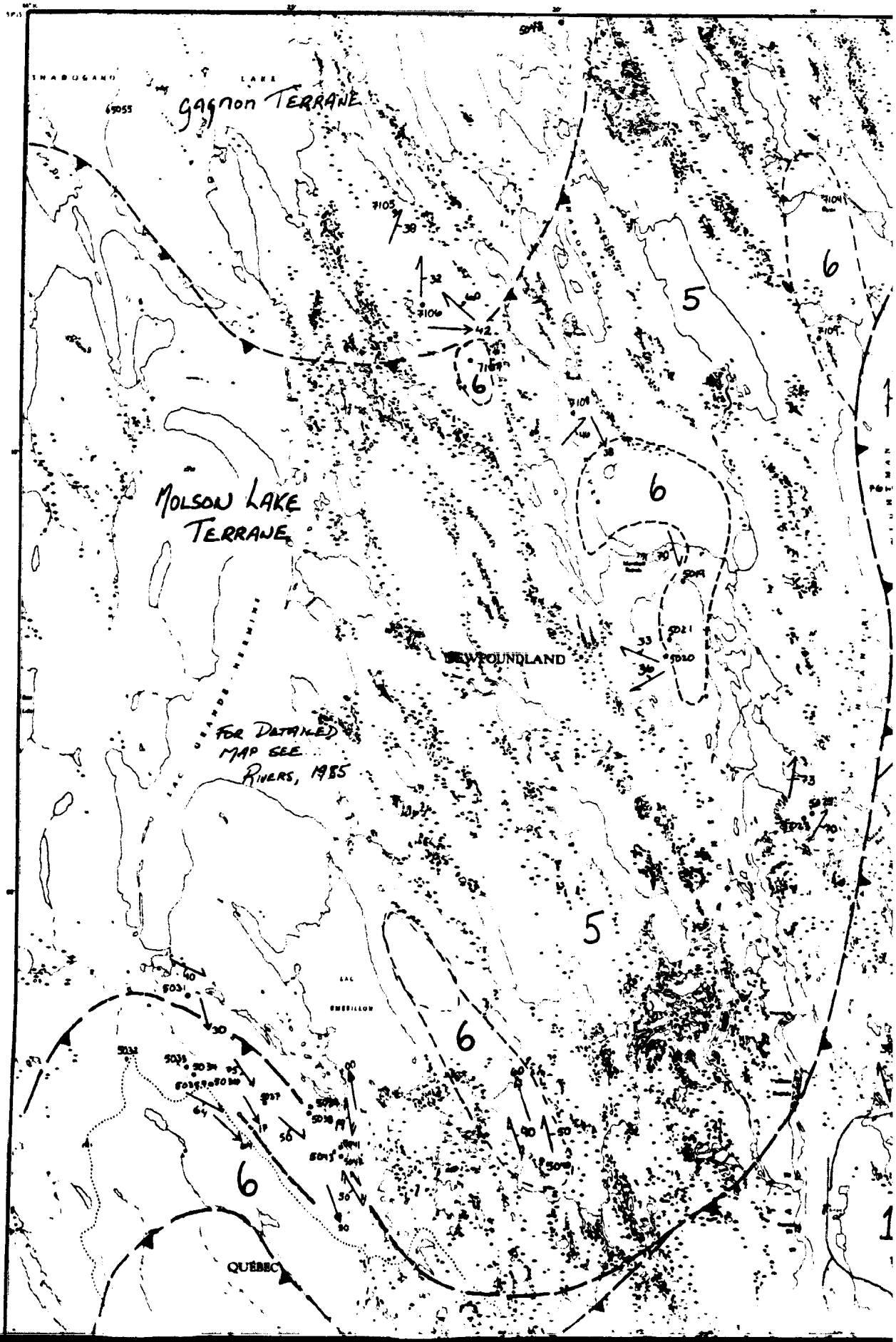
Gagnon TERRANE
MOLSON LAKE TERRANE
FOR DETAILED MAP SEE RIVERS, 1985
NEWFOUNDLAND
QUÉBEC
LAC RIBEILLON
5
6

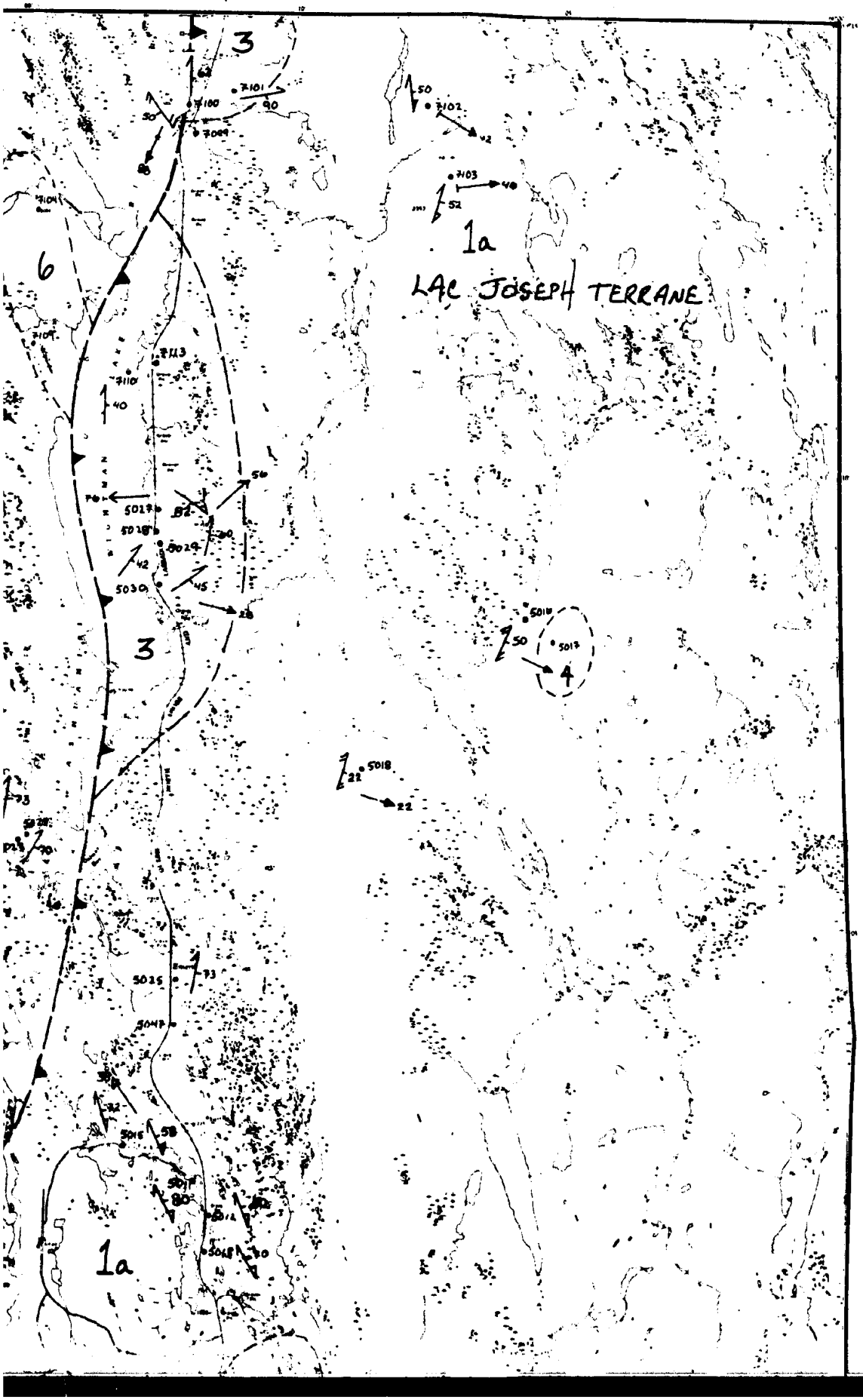
3
6
1a
LAC JOSEPH TERRANE
3
1a
4

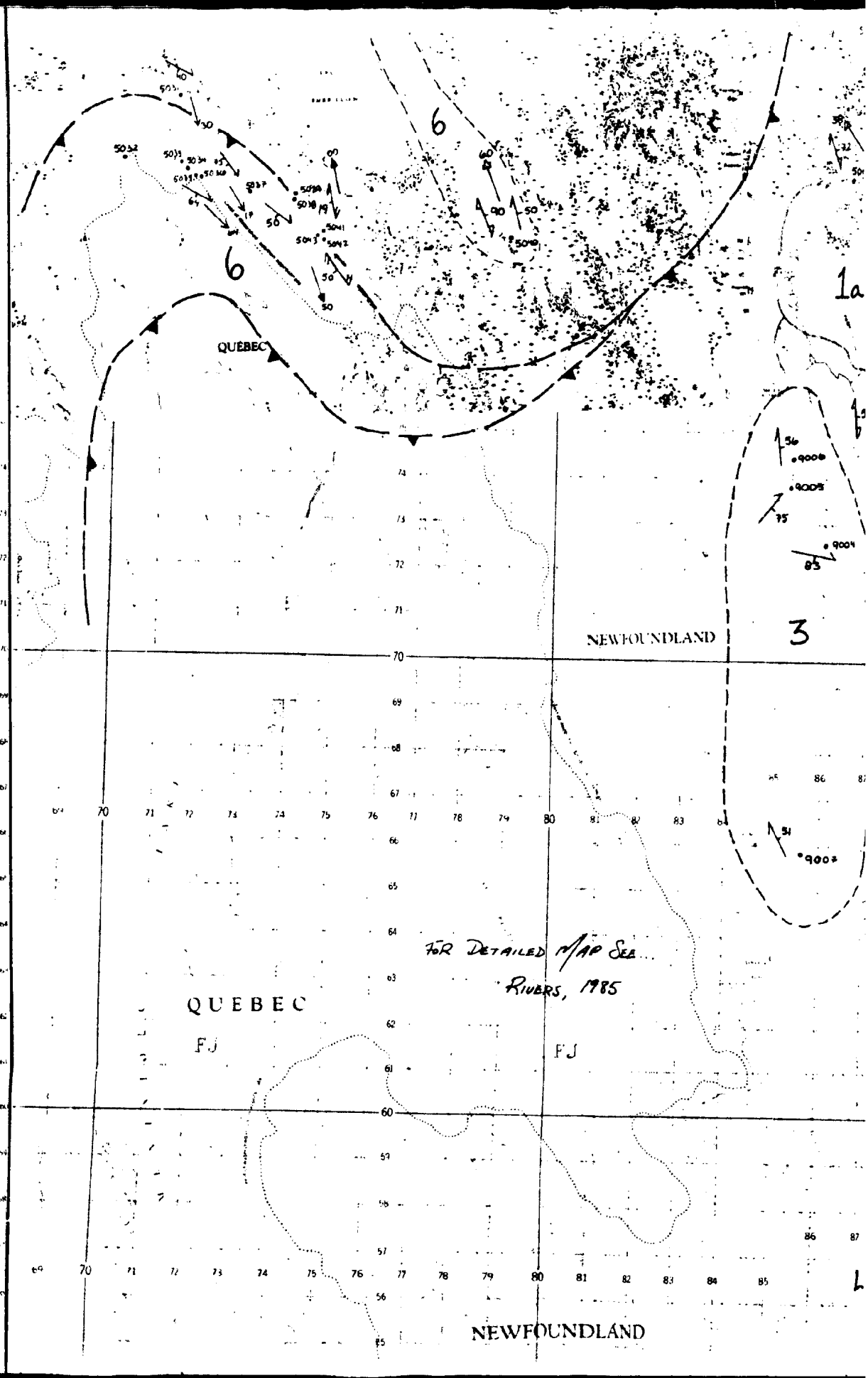
QUEBEC
NEWFOUNDLAND
1a
3
FOR DETAILED MAP SEE...
RIVERS, 1985
QUEBEC
FJ
FJ
NEWFOUNDLAND

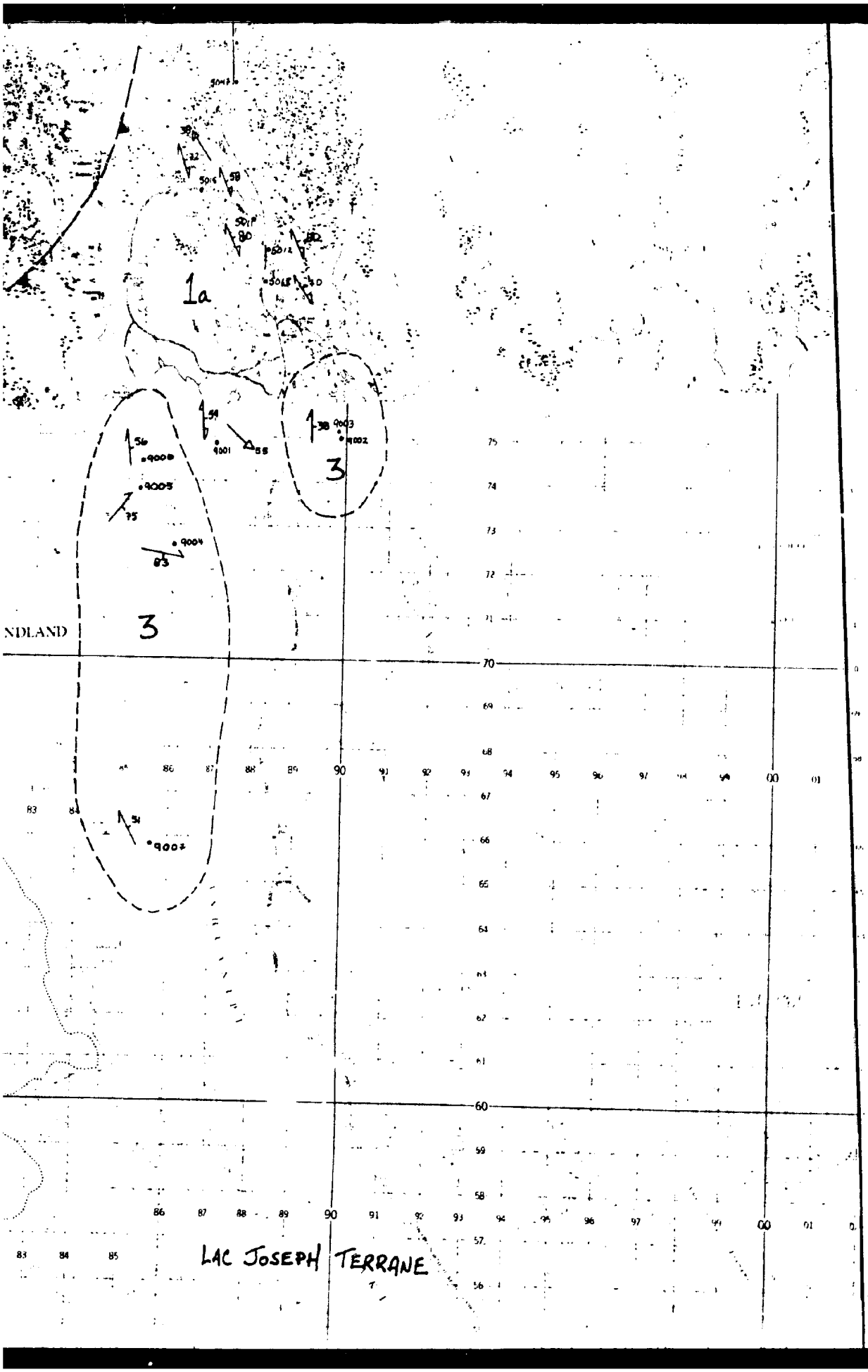
1a
3
3
NDLAND
LAC JOSEPH TERRANE

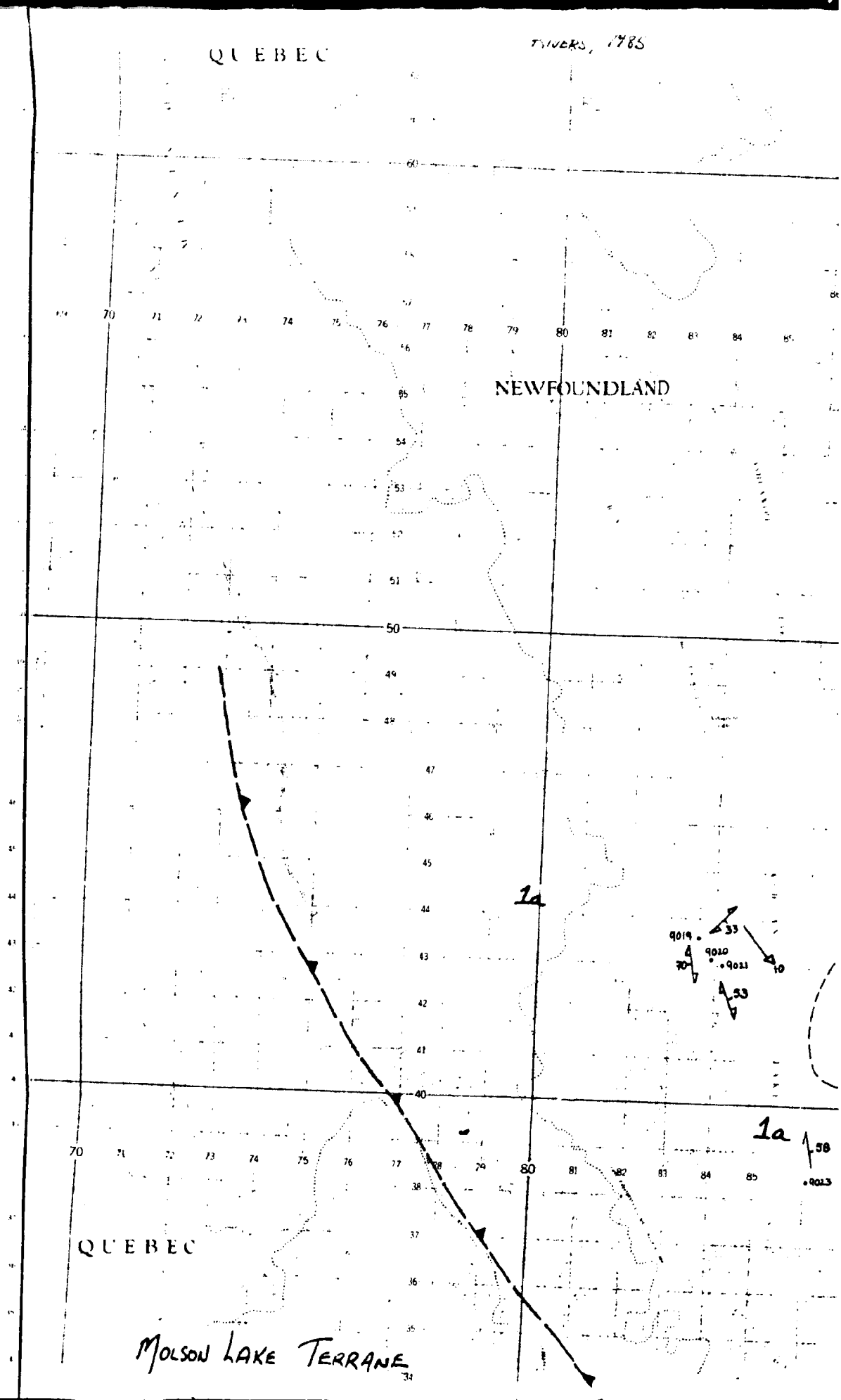
QUEBEC
NEWFOUNDLAND
QUEBEC
1a
1a
9019
9020
9021
9023
Molson Lake Terrane

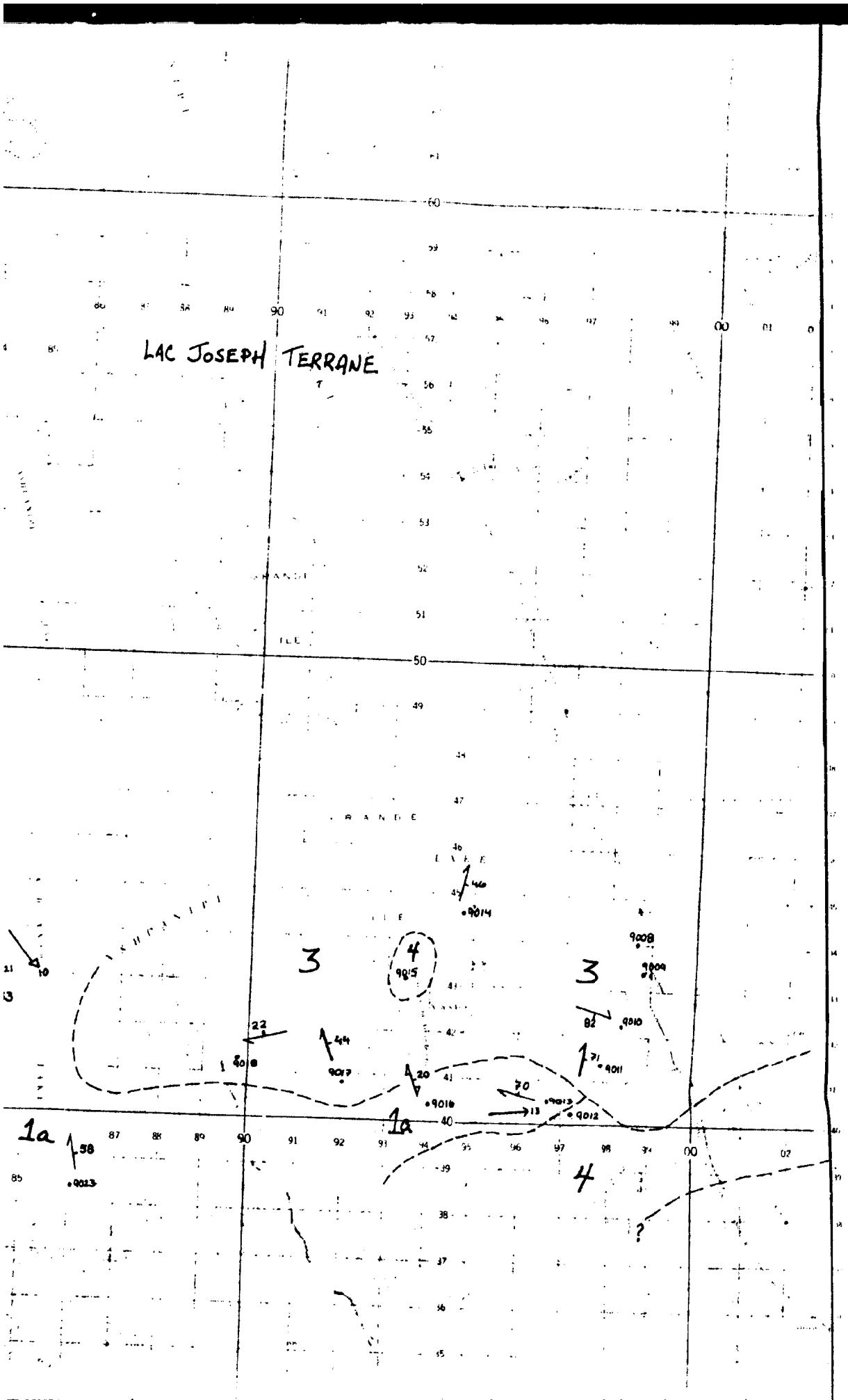
LAC JOSEPH TERRANE
3
4
9015
3
1a
1a
4
?
9008
9009
9010
9011
9012
9013
9014
9016
9017
9018
9023

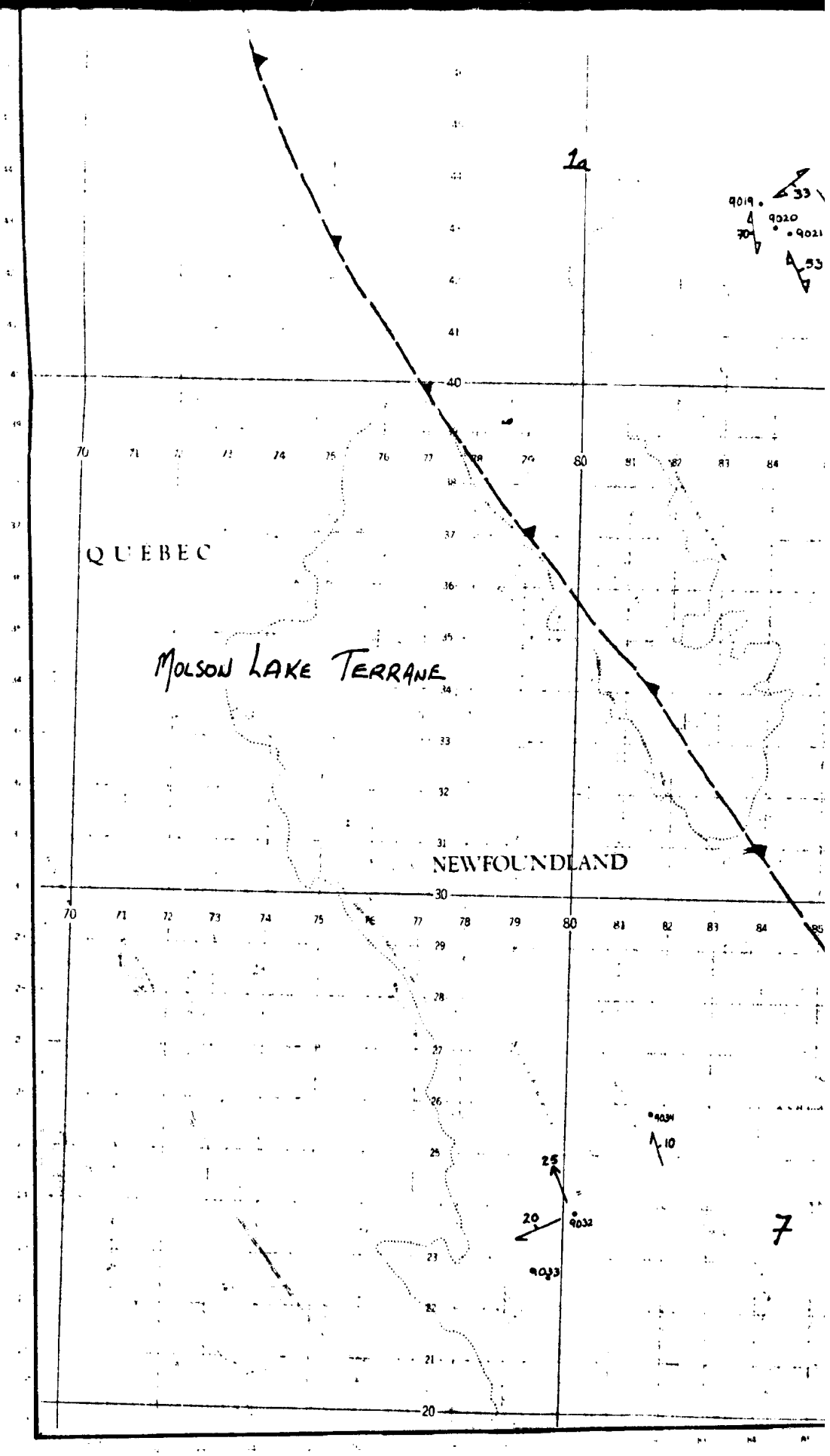
1a
QUEBEC
MOLSON LAKE TERRANE
NEWFOUNDLAND
9019
9020
9021
9032
9033
9034
7

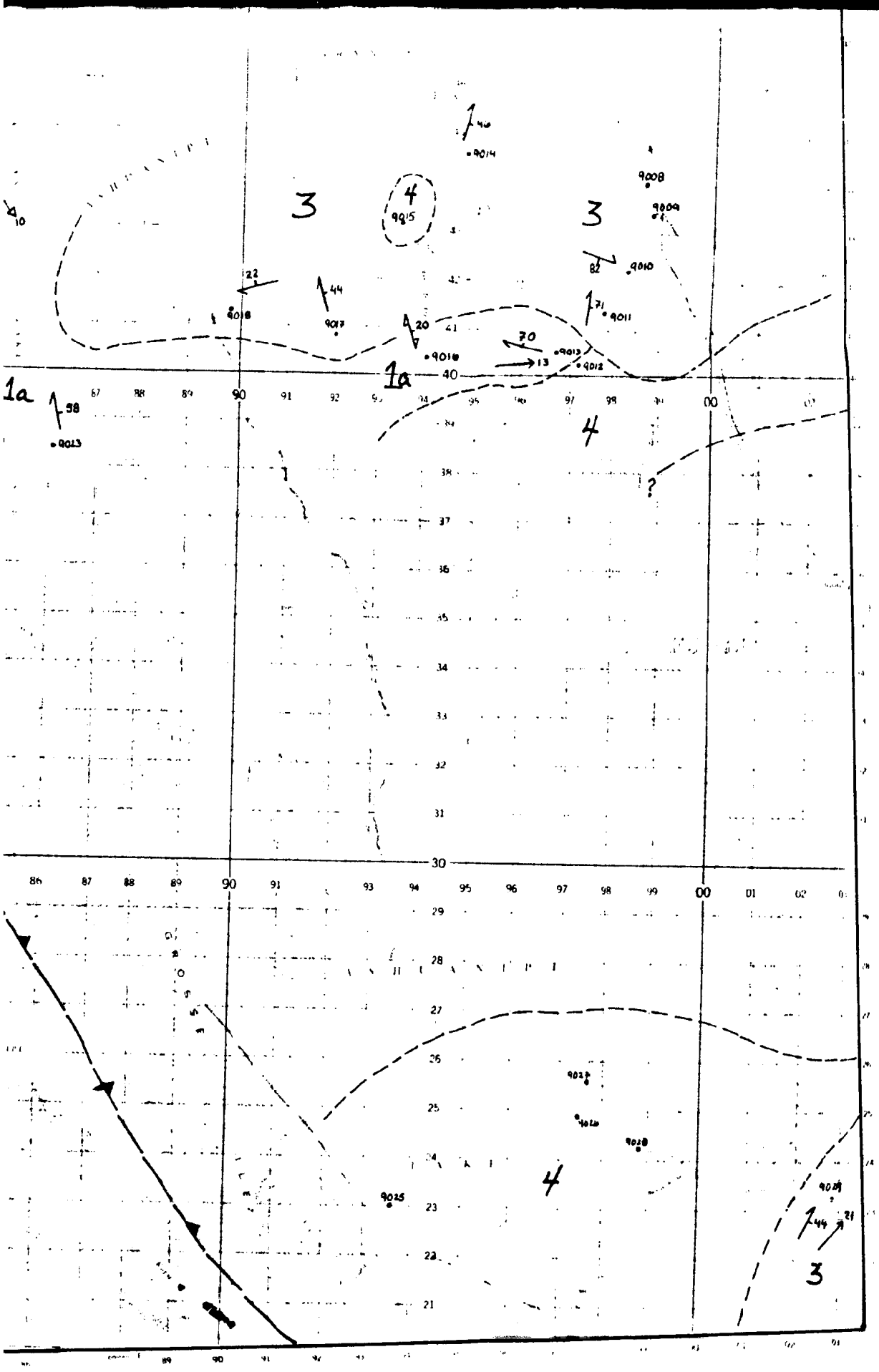
1a
1a
3
4
9015
3
9008
9009
9010
9011
9012
9013
9014
9016
9017
9018
4
?
4
4
3
9023
9024
9025
9026
9027
9028
9029
30
40
86
87
88
89
90
91
93
94
95
96
97
98
99
00
01
02

Table A2-1: Electron microprobe mineral analyses.

Sample	8038	8068	8068
Min	PLG	BIO	BIO
Type	RIM	CORE	RIM
Code	C32	C41	C42
SiO2	62 17	36 58	37 68
TiO2	0 00	1.53	1 58
Al2O3	25 20	18 59	18 20
Cr2O3	0 00	0 04	0 03
FeO	0 26	12 09	11 94
MnO	0 05	0 16	0 11
MgO	0 00	15 32	14 86
CaO	6 06	0 00	0 00
Na2O	7 92	0 01	0 00
K2O	0.18	9 79	9 65
Sum	101 84	94 11	94 05
Si	2 711	2 724	2 794
Ti	0 000	0 086	0 088
Al	1 295	1 632	1 591
Cr	0 000	0 002	0 002
Fe	0 009	0 753	0 740
Mn	0 002	0 010	0 007
Mg	0 000	1 700	1 642
Ca	0 283	0 000	0 000
Na	0 670	0 001	0 000
K	0 010	0 930	0 913
Sum	4 981	7 839	7 778
XMg	0 000	0 693	0 689
AlIV	0 289	1 276	1 206
AlVI	1 007	0 356	0 385

Table A2-1: Electron microprobe mineral analyses.

Sample:	8088-1	8088-1	8088-1	8088-1	8088-1	8088-1	8088-1	8088-1	8088-1	8088-1	8088-1	8088-1	8088-1	8089-1	8088-1
Min:	GNT	GNT	PLG	PLG	BIO	BIO	GNT	GNT	PLG	PLG	BIO	BIO	GNT	GNT	PLG
Type:	CORE	RIM	CORE	RIM	CORE	RIM	CORE	RIM	CORE	RIM	CORE	RIM	CORE	RIM	CORE
Code:	A01	A03	A31	A32	A41	A42	B01	B03	B31	B32	B41	B42	C01	C03	C31
SiO2	38 87	37 97	67 27	62 59	37 98	37 35	40 11	39 28	64 89	64 72	38 15	38 39	39 28	38 92	60 38
TiO2	0 00	0 00	0 03	0 02	1 68	1 79	0 00	0 00	0 03	0 03	2 05	2 02	0 00	0 00	0 03
Al2O3	22 51	22 72	23 34	22 79	17 29	17 61	22 29	22 28	22 71	22 42	17.14	17 01	22 49	22 23	23 42
Cr2O3	0 00	0 00	0 00	0 01	0 01	0 07	0 00	0 01	0 02	0 04	0 01	0 06	0 02	0 02	0 05
FeO	19 23	19 48	0 04	0.18	8 36	7 87	18 64	19 68	0 11	0 12	9 13	8 60	19 11	20 78	0 04
MnO	6.61	8 14	0 00	0 02	0 09	0 15	5 60	7 10	0 01	0 03	0 12	0 12	6 23	8 90	0 03
MgO	12 99	11 90	0 00	0 05	19 77	20 32	13 41	12 26	0 00	0 00	18 75	19 41	12 62	9 78	0 00
CaO	1 03	1 02	4 85	4 70	0 00	0 00	0 95	1 02	5 35	4 74	0 00	0 00	0 94	0 95	6 44
Na2O	0.03	0 04	4 00	8.75	0 08	0 14	0 05	0 14	8 58	8 82	0 07	0 11	0 01	0 02	7.16
K2O	0.00	0 01	0 23	0 27	9 21	9 57	0 01	0.02	0 23	0 20	10 02	9 40	0 00	0 01	0 41
Sum	101 27	101 28	99 76	99 38	94 47	94 87	101 06	101 79	101 93	101 12	95 44	95 12	100 70	101 61	97 96
Si	2 920	2 881	2 907	2 790	2 757	2 706	2 989	2 947	2 817	2 828	2 764	2 773	2 956	2 961	2 738
Ti	0 000	0 000	0 001	0 001	0 092	0 098	0 000	0 000	0 001	0 001	0 112	0 110	0 000	0 000	0 001
Al	1 994	2 032	1 189	1.198	1 479	1 504	1 958	1 970	1 162	1 155	1 464	1.448	1 995	1 994	1 252
Cr	0.000	0.000	0 000	0 000	0 001	0 004	0 000	0 001	0 001	0 001	0 001	0 003	0 001	0 001	0 002
Fe	1.208	1 236	0 001	0 007	0 507	0 477	1 162	1 235	0 004	0 004	0 563	0 519	1 203	1 322	0 002
Mn	0 421	0.523	0 000	0 001	0 006	0 009	0 353	0 451	0 000	0 001	0 007	0 007	0 397	0 574	0 001
Mg	1 454	1 345	0 000	0 003	2 138	2 194	1 485	1 371	0 000	0 000	2 024	2 089	1 416	1 109	0 000
Ca	0 083	0 083	0 225	0 225	0 000	0 000	0 076	0 082	0 249	0 222	0 000	0 000	0 078	0 077	0 313
Na	0 004	0 006	0 335	0 756	0 011	0 020	0 007	0 020	0 722	0 747	0 010	0 015	0 001	0 003	0 629
K	0.000	0.001	0 013	0 015	0 853	0 884	0 001	0 002	0 013	0 011	0 926	0 866	0 000	0 001	0 024
Sum	8 085	8 107	4 671	4 996	7 844	7 895	8 038	8 079	4 968	4 972	7 860	7 832	8 046	8 043	4 961
XMg	0 546	0 521	0 000	0 331	0 808	0 821	0 562	0 526	0 000	0 000	0 785	0 801	0 541	0 456	0 000
Al4	0 080	0 119	0 093	0 210	1 243	1 294	0 011	0 053	0 183	0 172	1 236	1 227	0 044	0 039	0 262
Al6	1 914	1 912	1 096	0 988	0 236	0 209	1 947	1 917	0 979	0 983	0 227	0 221	1 952	1 955	0 989

Table A2-1: Electron microprobe mineral analyses.

Sample:	8088-1	8088-1	8088-1
Min:	PLG	BIO	BIO
Type:	RIM	CORE	RIM
Code:	C32	C41	C42
SiO2	61.79	38 11	37.97
TiO2	0 01	1 84	1 81
Al2O3	24 76	17 06	16 9!
Cr2O3	0 00	0.06	0 05
FeO	0 07	8 45	8.32
MnO	0 04	0 05	0 12
MgO	0 00	20 04	19 86
CaO	3 89	0 00	0 0[illegible]
Na2O	7 83	0 15	0 17
K2O	0 60	9 73	9.78
Sum	98 79	95 49	94 99
Si	2 755	2 748	2 754
Ti	0 000	0 100	0 099
Al	1 301	1 450	1 446
Cr	0 000	0 003	0 003
Fe	0 003	0 510	0 505
Mn	0 002	0 003	0 007
Mg	0 000	2 154	2 146
Ca	0 186	0 000	0 000
Na	0 660	0 021	0 024
K	0 034	0 895	0 905
Sum	4 941	7 883	7 888
XMg	0 000	0 809	0 810
AlIV	0 245	1 252	1 246
AlVI	1 056	0 198	0 199

Table A2-1: Electron microprobe mineral analyses.

Sample:	8088-2	8088-2	8088-2	8088-2	8088-2	8088-2	8088-2	8088-2	8088-2	8088-2
Min:	GNT	GNT	PLG	PLG	BIO	BIO	GNT	GNT	BIO	BIO
Type:	CORE	RIM	CORE	RIM	CORE	RIM	CORE	RIM	CORE	RIM
Code:	A01	A03	A31	A32	A41	A42	B01	B03	B41	B42
SiO2	40.18	39.31	63.07	63.41	38.99	39.25	39.67	39.06	39.06	39.41
TiO2	0.02	0.05	0.00	0.03	1.36	1.32	0.02	0.00	1.65	1.60
Al2O3	23.14	22.65	23.43	22.39	16.67	16.88	22.18	21.77	17.45	16.79
Cr2O3	0.00	0.00	0.00	0.00	0.00	0.00	0.00	0.00	0.00	0.00
FeO	18.37	18.96	0.03	0.00	8.70	8.93	19.18	19.39	7.96	7.84
MnO	4.94	6.59	0.07	0.19	0.09	0.09	4.45	6.88	0.04	0.12
MgO	13.66	11.47	0.00	0.00	20.21	19.54	14.35	11.77	20.36	19.54
CaO	0.95	1.08	5.86	4.59	0.00	0.01	0.80	0.78	0.00	0.00
Na2O	0.01	0.04	8.08	9.21	0.00	0.20	0.00	0.11	0.21	0.06
K2O	0.00	0.03	0.17	0.14	9.30	9.05	0.00	0.00	9.50	9.10
Sum	101.27	100.18	100.71	99.96	95.32	95.27	100.65	99.76	96.23	94.46
Si	2.972	2.976	2.774	2.810	2.805	2.822	2.963	2.983	2.776	2.842
Ti	0.001	0.003	0.000	0.001	0.074	0.071	0.001	0.000	0.088	0.087
Al	2.018	2.021	1.215	1.169	1.414	1.431	1.953	1.960	1.462	1.427
Cr	0.000	0.000	0.000	0.000	0.000	0.000	0.000	0.000	0.000	0.000
Fe	1.136	1.201	0.001	0.000	0.523	0.537	1.198	1.238	0.473	0.473
Mn	0.309	0.423	0.003	0.007	0.005	0.005	0.282	0.445	0.002	0.007
Mg	1.506	1.294	0.000	0.000	2.167	2.094	1.598	1.339	2.157	2.100
Ca	0.075	0.088	0.276	0.218	0.000	0.001	0.064	0.064	0.000	0.000
Na	0.001	0.006	0.689	0.791	0.000	0.028	0.000	0.016	0.029	0.008
K	0.000	0.003	0.010	0.008	0.854	0.830	0.000	0.000	0.861	0.837
Sum	8.019	8.014	4.968	5.004	7.841	7.820	8.059	8.045	7.849	7.781
XMg	0.570	0.519	0.000	0.000	0.805	0.796	0.571	0.520	0.820	0.816
AlI4	0.028	0.024	0.226	0.190	1.195	1.178	0.037	0.017	1.224	1.158
AlI6	1.989	1.998	0.989	0.979	0.219	0.253	1.916	1.942	0.238	0.269

Table A2-1: Electron microprobe mineral analyses.

Sample:	9001A	9001A	9001A	9001A	9001A	9001A	9001A	9001A	9001A
Mir.:	GNT	GNT	PLG	PLG	BIO	BIO	GNT	GNT	BIO
Type:	CORE	RIM	CORE	RIM	CORE	RIM	CORE	RIM	CORE
Code:	A01	A02	A32	A33	A41	A42	B01	B04	B41
SiO2	37 12	36.55	63.09	62.77	39 13	38 72	39 47	37.65	38 43
TiO2	0.00	0.03	0.00	0.02	2.36	2 38	0.02	0.06	2 33
Al2O3	23.09	22 65	22.74	22.51	16 88	17.29	22.50	22.53	16.80
Cr2O3	0 03	0.03	0.02	0.03	0 02	0 04	0.04	0.04	0.05
FeO	22 56	23 83	0 11	0.10	11.16	10.91	21.96	24.76	12.16
MnO	5 14	5 09	0 00	0.00	0 06	0 08	5.95	3 36	0.07
MgO	9.95	9 51	0.03	0.00	17.67	17 82	10.21	9.49	17.83
CaO	1.21	1 18	5.57	5 32	0.00	0 00	1 19	1.36	0 00
Na2O	0 01	0 01	8 53	8.34	0.11	0.09	0.03	0 01	0 07
K2O	0.00	0.01	0.21	0.11	9 56	9.49	0.00	0.01	9 57
Sum	99 11	100 89	100 30	99 20	96 95	96 82	101 37	99.27	97 31
Si	2.884	2.948	2.790	2.800	2.802	2 774	2 984	2 925	2.761
Ti	0 000	0 002	0 000	0.001	0.127	0 128	0 001	0 004	0 126
Al	2 115	2 042	1.185	1 184	1 425	1.460	2.005	2 063	1 423
Cr	0 002	0 002	0 001	0 001	0 001	0 002	0 002	0 002	0 003
Fe	1 466	1 524	0 004	0 004	0 668	0 654	1 388	1 609	0 731
Mn	0 338	0 330	0 000	0 000	0 004	0 005	0 381	0 221	0 004
Mg	1 152	1 084	0 002	0 000	1 886	1 903	1 150	1 099	1 909
Ca	0 101	0.097	0 264	0 254	0 000	0 000	0 096	0.113	0 000
Na	0 002	0 001	0.731	0 721	0 015	0 013	0 004	0 002	0 010
K	0 000	001	0 012	0 006	0 873	0 867	0 000	0 001	0 877
Sum	8 058	8 030	4 989	4 971	7 802	7 806	8 013	8 039	7 844
XMg	0 440	0 416	0 327	0 000	0 738	0 744	0 453	0 408	0 723
AlⅣ	0 116	0 052	0 210	0 200	1 198	1 226	0 016	0 075	1 239
AlⅥ	1 998	1 99	0 975	0 983	0 227	0 234	1 989	1 989	0 184

Table A2-1: Electron microprobe mineral analyses.

Sample	9013A	9013A	9013A	9013A	9013A	9013A	9013A	9013A	9013A	9013A
Min	GNT	GNT	GNT	GNT	PLG	PLG	BIO	BIO	BIO	BIO
Type	CORE	RIM	CORE	RIM	CORE	RIM	CORE	RIM	CORE	RIM
Code:	A01	A02	A03	A04	A31	A32	A41	A42	A43	A44
SiO2	37 42	37.56	38 23	38.12	61 09	61.64	36 50	37 14	36 82	37 19
TiO2	0 02	0 00	0 04	0 01	0 00	0 00	2 40	2 09	2 27	2 18
Al2O3	22 21	22.46	22.55	21.99	25.07	24 49	18 02	18 55	18 11	17.99
Cr2O3	0 00	0 00	0 01	0 00	0.00	0.00	0 02	0.03	0.03	0 04
FeO	26 48	26.82	27 57	27 37	0.07	0 12	14 04	14.29	14 61	14.63
MnO	4 79	5 38	4 39	5 41	0 00	0 01	0 06	0 16	0 13	0.11
MgO	7.20	6 84	7.34	6 09	0 00	0.00	12 96	13 84	13 23	13 46
CaO	2.61	2 58	2.54	2.23	5.52	5.61	0 00	0.00	0 00	0 00
Na2O	0.03	0 00	0.06	0 00	8 43	8 04	0 08	0 07	0.14	0.00
K2O	0 00	0.01	0.01	0.03	0 12	0.10	9 97	9 31	9 09	9 11
Sum	100 76	101 48	102 74	101 25	100.30	100 01	94 05	95 28	94 43	94 71
Si	2 918	2 917	2.924	2 968	2 704	2 731	2 749	2.748	2 753	2.769
Ti	0 001	0.000	0.002	0.001	0 000	0.000	0.136	0.116	0 128	0.122
Al	2 041	2.056	2.033	2.019	1.308	1.279	1.600	1.618	1.598	1.579
Cr	0.000	0 000	0.001	0 000	0.000	0.000	0.001	0 002	0 002	0.002
Fe	1.727	1.742	1.763	1.783	0.003	0 004	0 884	0.884	0 914	0.911
Mn	0 316	0 354	0 284	0 357	0 000	0 000	0 004	0 010	0 008	0 007
Mg	0 837	0.769	0.837	0 707	0 000	0.000	1 455	1 504	1 474	1.494
Ca	0 218	0 215	0 208	0 186	0.262	0.266	0 000	0 000	0 000	0.000
Na	0 005	0 000	0 009	0 000	0.724	0 691	0 012	0 010	0 020	0 000
K	0 000	0.004	0 001	0 003	0.007	0 006	0 958	0 879	0.867	0 865
Sum	8 062	8 056	8.062	8 023	5.007	4 977	7 799	7.770	7 763	7.750
XMg	0.326	0 306	0.322	0 284	0 000	0 000	0.622	0.630	0 617	0.621
Al4	0 082	0 083	0 076	0 032	0.296	0 269	1 251	1 252	1.247	1.231
Al6	1 959	1 973	1 957	1 987	1.012	1 010	0 349	0 365	0 350	0 349

Table A2-1: Electron microprobe mineral analyses.

Sample:	9013B	9013B	9013B	9013B	9013B	9013B	9013B	9013B	9013B	9013B	9013B	9013B
Min:	GNT	GNT	PLG	PLG	BIO	BIO	GNT	GNT	PLG	PLG	BIO	BIO
Type.	CORE	RIM	CORE	RIM	CORE	RIM	CORE	RIM	CORE	RIM	CORE	RIM
Code.	A01	A03	A31	A32	A41	A42	B01	B03	B31	B32	B41	B42
SiO2	37.65	37.80	60.78	57.72	38.40	35.46	37.93	37.58	60.72	61.59	36.59	36.93
TiO2	0.00	0.03	0.02	0.00	2.22	2.36	0.01	0.02	0.00	0.00	2.43	2.26
Al2O3	22.25	21.67	24.06	21.60	19.39	17.59	21.76	22.32	24.92	23.57	18.28	18.36
Cr2O3	0.01	0.00	0.00	0.00	0.00	0.00	0.01	0.01	0.00	0.00	0.00	0.00
FeO	26.78	26.45	0.07	0.05	12.96	12.79	26.60	26.30	0.00	0.01	13.41	13.36
MnO	4.33	3.77	0.07	0.18	0.04	0.06	4.65	4.32	0.06	0.03	0.10	0.08
MgO	6.72	6.42	0.00	0.00	11.28	12.72	6.78	6.75	0.00	0.00	13.02	12.96
CaO	1.97	2.50	6.88	11.15	0.00	0.00	1.70	2.01	6.96	6.32	0.00	0.00
Na2O	0.07	0.07	7.85	7.74	0.02	0.07	0.00	0.00	7.71	7.93	0.13	0.00
K2O	0.03	0.02	0.16	0.15	9.00	9.23	0.04	0.02	0.21	0.12	8.82	9.36
Sum	99.81	98.73	99.89	98.59	93.31	90.28	99.48	99.33	100.60	99.57	92.78	93.31
Si	2.954	2.992	2.711	2.663	2.857	2.762	2.985	2.956	2.689	2.746	2.764	2.778
Ti	0.000	0.002	0.001	0.000	0.124	0.138	0.001	0.001	0.000	0.000	0.138	0.128
Al	2.058	2.022	1.265	1.175	1.700	1.615	2.018	2.070	1.301	1.239	1.628	1.628
Cr	0.001	0.000	0.000	0.000	0.000	0.000	0.001	0.001	0.000	0.000	0.000	0.000
Fe	1.757	1.751	0.003	0.002	0.806	0.833	1.750	1.730	0.000	0.000	0.847	0.840
Mn	0.288	0.253	0.003	0.007	0.003	0.004	0.310	0.288	0.002	0.001	0.006	0.005
Mg	0.786	0.757	0.000	0.000	1.251	1.476	0.795	0.791	0.000	0.000	1.466	1.453
Ca	0.166	0.212	0.329	0.551	0.000	0.000	0.143	0.169	0.331	0.302	0.000	0.000
Na	0.011	0.011	0.679	0.692	0.003	0.011	0.000	0.000	0.662	0.686	0.019	0.000
K	0.003	0.002	0.009	0.009	0.854	0.917	0.004	0.002	0.012	0.007	0.850	0.898
Sum	8.023	8.001	4.999	5.100	7.597	7.756	8.007	8.008	4.997	4.981	7.718	7.730
xMg	0.309	0.302	0.000	0.000	0.608	0.639	0.312	0.314	0.000	0.000	0.634	0.634
AlI	0.046	0.008	0.289	0.337	1.143	1.238	0.015	0.044	0.311	0.254	1.236	1.222
AlII	2.012	2.014	0.976	0.838	0.557	0.377	2.003	2.026	0.990	0.985	0.392	0.405

Table A2-1: Electron microprobe mineral analyses.

Sample:	9016	9016	9016	9016	9016	9016	9016	9016	9016	9016	9016	9016	9016	9016
Min:	GNT	GNT	BIO	BIO	GNT	GNT	PLG	PLG	GNT	GNT	PLG	PLG	BIO	BIO
Type:	CORE	RIM	CORE	RIM	CORE	RIM	CORE	RIM	CORE	RIM	CORE	RIM	RIM	CORE
Code:	A06	A07	A41	A43	B01	B02	B05	B06	C01	C05	C35	C37	C43	C44
SiO2	38.01	38.30	36.89	38.10	39.94	40.49	64.05	63.26	37.97	38.09	63.05	63.91	38.20	38.35
TiO2	0.00	0.00	2.22	2.14	0.02	0.00	0.00	0.02	0.00	0.02	0.01	0.02	2.23	2.12
Al2O3	22.55	21.98	18.03	18.79	20.30	20.98	22.82	21.73	22.96	22.00	23.15	23.44	17.89	18.11
Cr2O3	0.00	0.02	0.02	0.02	0.00	0.00	0.02	0.00	0.03	0.00	0.00	0.00	0.02	0.01
FeO	23.70	22.91	14.64	13.61	24.42	24.15	0.09	0.14	23.11	22.64	0.09	0.07	13.71	13.61
MnO	6.79	7.98	0.15	0.15	8.40	8.62	0.03	0.03	7.02	7.41	0.01	0.03	0.14	0.15
MgO	3.13	7.07	14.44	14.44	7.30	7.07	0.02	0.00	7.94	7.21	0.00	0.00	14.07	13.98
CaO	0.78	1.72	0.00	0.00	1.29	1.54	4.71	3.88	1.38	1.40	5.44	5.16	0.00	0.00
Na2O	0.04	0.10	0.06	0.09	0.05	0.00	8.93	7.71	0.06	0.00	8.55	8.76	0.13	0.12
K2O	0.00	0.01	9.14	9.36	0.00	0.00	0.11	2.68	0.01	0.02	0.09	0.14	9.71	9.80
Sum	100.00	100.09	95.59	96.70	101.72	102.85	100.78	99.45	100.48	98.79	100.39	101.53	96.10	96.25
Si	2.953	2.986	2.727	2.762	3.079	3.030	2.809	2.836	2.935	2.996	2.782	2.786	2.796	2.800
Ti	0.000	0.000	0.123	0.117	0.001	0.000	0.000	0.001	0.000	0.001	0.000	0.001	0.123	0.116
Al	2.065	2.020	1.571	1.606	1.845	1.881	1.180	1.148	2.092	2.040	1.204	1.205	1.544	1.559
Cr	0.000	0.001	0.001	0.001	0.000	0.000	0.001	0.000	0.002	0.000	0.000	0.000	0.001	0.001
Fe	1.540	1.494	0.905	0.825	1.574	1.536	0.003	0.005	1.494	1.489	0.003	0.003	0.839	0.831
Mn	0.447	0.527	0.009	0.009	0.549	0.555	0.001	0.001	0.460	0.494	0.000	0.001	0.009	0.009
Mg	0.941	0.822	1.591	1.560	0.839	0.801	0.001	0.000	0.915	0.845	0.000	0.000	1.535	1.521
Ca	0.065	0.144	0.000	0.000	0.107	0.126	0.221	0.186	0.114	0.118	0.257	0.241	0.000	0.000
Na	0.006	0.015	0.009	0.013	0.007	0.000	0.759	0.670	0.009	0.000	0.731	0.741	0.018	0.017
K	0.000	0.001	0.862	0.866	0.000	0.000	0.008	0.153	0.001	0.002	0.005	0.008	0.907	0.913
Sum	8.017	8.011	7.799	7.757	8.001	7.979	4.983	5.001	8.022	7.984	4.984	4.985	7.771	7.768
XMg	0.379	0.355	0.637	0.654	0.348	0.343	0.284	0.000	0.380	0.362	0.000	0.000	0.646	0.647
Al4	0.047	0.014	1.273	1.238	0.000	0.000	0.191	0.164	0.065	0.004	0.218	0.214	1.204	1.200
Al6	2.018	2.007	0.298	0.367	1.845	1.881	0.989	0.984	2.028	2.035	0.986	0.991	0.340	0.359

Table A2-1: Electron microprobe mineral analyses.

Sample:	9032	9032	9032	9032	9032	9023	9032	9032	9032	9032	9032	9032	9032	9032	9032
Min:	GNT	PLG	CPX	GNT	GNT	CPX	PLG	GNT	GNT	CPX	CPX	PLG	PLG	GNT	GNT
Type:	RIM	RIM	RIM	CORE	RIM	CORE	CORE	CORE	RIM	CORE	RIM	RIM	CORE	TRAV	TRAV
Code:	A01	A33	A24	B01	B02	B23	B34	C01	C05	C21	C22	C32	C33	D02	D02
SiO2	40 41	58 19	51 93	41 66	41 78	52 27	61.59	39 64	39.36	52 55	52 57	60 21	60 27	41.77	41 57
TiO2	0 02	0.03	0 10	0.04	0.02	0.34	0 00	0 03	0 06	0.23	0 22	0 00	0 01	0.05	0 04
Al2O3	23 60	26.38	2.64	22.13	21.13	5.57	23.19	23 21	23 62	4 90	3.46	24.43	23 54	21.28	21 48
Cr2O3	0.01	0.00	0 02	0.02	0.02	0 07	0.02	0 00	0 00	0.05	0.04	0 01	0 02	0 00	0.00
FeO	17 36	0 09	6 19	18.12	19.97	6 34	0.09	17 57	18 86	6 53	5.77	0 21	0 10	17 86	20 11
MnO	0 45	0 01	0 01	0 43	0 58	0 11	0 01	0 41	0 51	0 14	0 09	0 00	0 01	0 53	0 64
MgO	13.39	0.02	14 98	12 25	11.84	13 20	0 00	12.96	12 55	14 14	14 99	0.00	0 00	12.69	11 77
CaO	6 18	8 91	22.30	6 43	6 29	20 57	6 54	6.98	7.13	21 57	22 11	7 68	6 41	7 06	6 61
Na2O	0.03	6.15	0 77	0 09	0 04	0 79	7 82	0 02	0 01	0 96	0 68	6 92	7 43	0 00	0 00
K2O	0 00	0 23	0 05	0 00	0 02	0 00	0 43	0 00	0 02	0 00	0 00	0 39	0 47	0 00	0 01
Sum	101.45	100 01	98 99	101 17	101 67	99 26	99 69	100 82	102 12	101.07	99.93	99 85	98 26	101 24	102 23
Si	2 955	2 603	1 937	3 062	3 082	1 926	2 750	2 932	2 895	1 912	1.932	2 691	2 729	3 073	3 057
Ti	0 001	0 001	0 003	0 002	0 001	0 009	0 000	0 002	0 003	0 006	0 006	0 000	0 000	0 003	0 002
Al	2 034	1 391	0 116	1 917	1 839	0 242	1.221	2 024	2 048	0 210	0 150	1 287	1 257	1 846	1 862
Cr	0 001	0 000	0 001	0 001	0 001	0 002	0 001	0 000	0 000	0 001	0 001	0 000	0 001	0 000	0 000
Fe	1 062	0 003	0 193	1 114	1 233	0 195	0 003	1 087	1.160	0 199	0 177	0 008	0 004	1 099	1 237
Mn	0 028	0 000	0 000	0 027	0 036	0 003	0 000	0 026	0 032	0 004	0 003	0 000	0 000	0 033	0 040
Mg	1 459	0 001	0 833	1 342	1 302	0 725	0 000	1 429	1 376	0 767	0 821	0 000	0 000	1 391	1 290
Ca	0 484	0 427	0 891	0 506	0 497	0 812	0 313	0 553	0 562	0 841	0 871	0 368	0 311	0 557	0 521
Na	0 004	0 533	0 056	0 013	0 006	0 056	0 677	0 003	0 001	0 068	0 048	0 600	0 652	0 000	0 000
K	0 000	0 013	0 002	0 000	0 002	0 000	0 024	0 000	0 002	0 000	0 000	0 022	0 027	0 000	0 001
Sum	8 028	4 974	4 031	7 983	8 000	3 971	4 990	8 055	8 079	4 009	4 010	4 976	4 981	8 001	8 010
XMg	0 579	0 284	0 812	0 546	0 514	0 788	0 000	0 568	0 542	0 794	0 822	0 000	0 000	0 559	0 511
Al4	0 045	0 397	0 063	0 000	0 000	0 074	0 250	0 068	0 105	0 088	0 068	0 309	0 271	0 000	0 000
Al6	1 989	0 994	0 053	1 917	1 839	0 168	0 971	1 956	1 943	0 123	0 082	0 978	0 986	1 846	1 862

Table A2-1: Electron microprobe mineral analyses.

Sample	9023	9023	9023	9023	9023	9023
Min:	GNT	GNT	BIO	BIO	PLG	PLG
Type:	CORE	RIM	RIM	CORE	CORE	RIM
Code:	A01	A02	A43	A44	A31	A32
SiO2	40.55	40.93	38.38	38.55	65.17	65.88
TiO2	0.02	0.01	1.63	1.68	0.03	0.01
Al2O3	21.74	20.92	18.74	18.72	21.48	20.66
Cr2O3	0.02	0.00	0.02	0.02	0.00	0.00
FeO	20.69	21.27	11.21	11.37	0.19	0.15
MnO	6.86	8.64	0.17	0.11	0.07	0.04
MgO	9.91	8.05	16.33	16.06	0.00	0.02
CaO	2.14	2.15	0.00	0.01	2.54	2.37
Na2O	0.01	0.00	0.13	0.11	9.94	9.90
K2O	0.01	0.04	9.59	9.86	0.09	0.06
Sum	101.95	102.01	96.20	96.49	99.51	99.09
Si	3.045	3.103	2.769	2.777	2.880	2.917
Ti	0.001	0.001	0.088	0.091	0.001	0.000
Al	1.925	1.869	1.594	1.590	1.119	1.078
Cr	0.001	0.000	0.001	0.001	0.000	0.000
Fe	1.299	1.348	0.676	0.685	0.007	0.006
Mn	0.436	0.555	0.010	0.007	0.003	0.002
Mg	1.109	0.909	1.756	1.724	0.000	0.001
Ca	0.172	0.175	0.000	0.001	0.120	0.112
Na	0.001	0.000	0.018	0.015	0.852	0.850
K	0.001	0.004	0.883	0.906	0.005	0.003
Sum	7.992	7.964	7.795	7.797	4.987	4.970
XMg	0.460	0.403	0.722	0.716	0.000	0.192
Al4	0.000	0.000	1.231	1.223	0.120	0.083
Al6	1.925	1.869	0.363	0.367	1.000	0.995

Table A2-1: Electron microprobe mineral analyses.

Sample:	9032	9032	9032	9032	9032	9032	9032	9032	9032	9032	9032	9032	9032	9032	9032
Min:	GNT	GNT	GNT	GNT	GNT	GNT	GNT	GNT	CPX	CPX	PLG	PLG	GNT	GNT	CPX
Type:	TRAV	TRAV	TRAV	TRAV	TRAV	CORE	CORE	CORE	CORE	RIM	CORE	RIM	CORE	RIM	CORE
Code:	D03	D04	D05	D06	D07	E01	E02	E03	E24	E25	E36	E37	F02	F03	F25
SiO2	40 87	41.28	40 85	42.25	41.45	39 66	41 13	40 75	51 72	54.08	56 04	58 42	41.09	40 26	52 20
TiO2	0.02	0 04	0.02	0.03	0.03	0 05	0.03	0 02	0.31	0.12	0.03	0.03	0 02	0 05	0 28
Al2O3	21 98	21.41	21.72	21.71	21.32	20 86	21 82	21.71	5.94	2.03	26.51	24.55	21.84	21.75	5 83
Cr2O3	0 00	0 01	0 00	0.00	0.02	0.00	0.02	0 02	0.05	0.00	0 00	0.04	0.02	0 01	0 02
FeO	17.57	17.61	18 18	17 91	17.90	17 63	18 36	20 29	5 87	5 12	0.29	0.21	17 79	20.33	6 32
MnO	0 39	0 41	0 43	0 48	0 45	0 32	0 33	0 49	0 07	0 23	0 13	0 00	0 39	0 61	0 04
MgO	12 71	12 41	12 56	11 91	11 94	12 98	13 21	12.68	13 75	15.53	0.00	0 00	12.43	11 58	13 55
CaO	6 93	7 20	7 16	7.16	7.09	7 66	6.61	5 75	21 32	22 08	9 73	7 79	7 20	6 73	21 81
Na2O	0 00	0 07	0 08	0 09	0.10	0 01	0 03	0 01	1 11	0 65	5 68	6 64	0 01	0 02	0 99
K2O	0 01	0 01	0 01	0.00	0.01	0 01	0.00	0 01	0 02	0 01	0 28	0.37	0 04	0 00	0 00
Sum	100 48	100 45	101 01	101 54	100 31	99 20	101 54	101 73	100 16	99 85	98 69	98 05	100 83	101 34	101 04
Si	3 027	3 061	3 023	3 095	3 080	2 995	3 022	3 011	1 894	1 980	2 555	2 662	3 037	2 999	1 898
Ti	0 001	0 002	0 001	0 002	0 002	0 003	0 002	0 001	0 009	0 003	0 001	0 001	0 001	0 003	0 008
Al	1 919	1 871	1 894	1 875	1.867	1 857	1 890	1 891	0 256	0 088	1.425	1 319	1 903	1 910	0 250
Cr	0 000	0 001	0 000	0 000	0 001	0 000	0 001	0 001	0 001	0 000	0 000	0 001	0 001	0 001	0 001
Fe	1 088	1 092	1 125	1 097	1 112	1 114	1.128	1 254	0 180	0 157	0 011	0 008	1 100	1 267	0 192
Mn	0 024	0 026	0 027	0 030	0 028	0 020	0 021	0 031	0 002	0 007	0 005	0 000	0 024	0 038	0 001
Mg	1 403	1 371	1 385	1 300	1 322	1 461	1 446	1 396	0 750	0 848	0 000	0 000	1 369	1 286	0 734
Ca	0 550	0 572	0 568	0 562	0 564	0 622	0 520	0 455	0 836	0 866	0.475	0 380	0 570	0 537	0 850
Na	0 000	0 010	0 011	0 013	0 014	0 001	0 004	0 001	0 079	0 046	0 502	0 587	0 001	0 003	0 070
K	0 001	0 001	0 001	0 000	0 001	0 001	0 000	0 001	0 001	0 000	0 016	0 022	0 004	0 000	0 000
Sum	8 013	8 007	8 035	7 973	7 992	8 074	8 033	8 043	4 009	3 996	4 991	4 980	8 012	8 044	4 004
XMg	0 563	0 557	0 552	0 542	0 543	0 567	0 562	0 527	0 807	0 844	0 000	0 000	0 555	0 504	0 793
Al4	0 000	0 000	0 000	0 000	0 000	0 005	0 000	0 000	0 106	0 020	0 445	0 338	0 000	0 001	0 102
Al6	1 919	1 871	1 894	1 875	1 867	1 852	1 890	1 891	0 150	0 068	0 980	0 981	1 903	1 909	0 148

Table A2-1: Electron microprobe mineral analyses.

Sample:	9032	9032	9032
Min:	CPX	PLG	PLG
Type:	RIM	RIM	CORE
Code:	F26	F38	F39
SiO2	51.91	59.47	60.47
TiO2	0.22	0.01	0.02
Al2O3	5.27	24.84	24.07
Cr2O3	0.06	0.02	0.04
FeO	6.11	0.17	0.22
MnO	0.06	0.00	0.15
MgO	13.91	0.02	0.00
CaO	21.58	7.75	7.16
Na2O	1.17	6.81	7.09
K2O	0.02	0.36	0.39
Sum	100.31	99.45	99.81
Si	1.903	2.670	2.707
Ti	0.006	0.000	0.001
Al	0.228	1.314	1.270
Cr	0.002	0.001	0.001
Fe	0.187	0.006	0.008
Mn	0.002	0.000	0.006
Mg	0.760	0.001	0.000
Ca	0.848	0.373	0.343
Na	0.083	0.593	0.615
K	0.001	0.021	0.022
Sum	4.019	4.979	4.975
XMg	0.802	0.173	0.000
Al4	0.097	0.330	0.293
Al6	0.130	0.984	0.978

Table A2-1: Electron microprobe mineral analyses.

Sample:	9033B	9033B	9033B	9033B	9033B	9033B	9033B	9033B	9033B	9033B	9033B	9033B	9033B	9033B	9033B
Min:	GNT	GNT	PLG	PLG	BIO	BIO	GNT	BIO	GNT	BIO	PLG	GNT	GNT	GNT	BIO
Type:	CORE	RIM	RIM	CORE	RIM	CORE	CORE	CORE	RIM	RIM	CORE	CORE	CORE	RIM	RIM
Code:	A01	A02	A35	A36	A43	A44	C01	C42	C03	C44	C35	C06	E01	E05	E46
SiO2	39.95	39.40	61.13	59.89	36.65	38.00	39.16	37.84	39.32	37.21	60.11	39.00	39.54	39.06	37.34
TiO2	0.00	0.01	0.00	0.01	2.21	2.31	0.03	1.91	0.02	2.36	0.00	0.00	0.00	0.01	2.38
Al2O3	20.74	20.64	23.90	24.26	17.66	17.71	20.60	18.02	20.38	17.56	24.19	20.62	20.95	19.92	17.60
Cr2O3	0.02	0.01	0.00	0.01	0.02	0.01	0.01	0.04	0.01	0.04	0.01	0.02	0.02	0.04	0.07
FeO	26.71	27.52	0.17	0.18	14.37	13.93	25.30	13.58	24.00	13.92	0.10	23.85	28.89	27.15	14.23
MnO	6.25	7.04	0.00	0.00	0.11	0.14	4.90	0.03	4.94	0.07	0.05	4.55	5.67	5.76	0.08
MgO	6.18	5.21	0.00	0.00	13.95	13.59	7.10	13.46	6.04	13.76	0.00	6.61	6.29	6.38	13.96
CaO	2.07	2.38	6.87	7.09	0.00	0.00	3.04	0.01	5.38	0.09	6.47	5.14	2.02	2.22	0.00
Na2O	0.09	0.00	7.78	6.84	0.08	0.15	0.01	0.03	0.14	0.00	8.03	0.06	0.02	0.02	0.03
K2O	0.01	0.02	0.18	0.14	9.75	9.77	0.05	9.70	0.03	8.77	0.11	0.03	0.00	0.01	9.85
Sum	102.02	102.23	100.03	98.42	94.80	95.61	100.20	94.62	100.26	93.78	99.07	99.88	103.40	100.57	95.54
Si	3.078	3.058	2.722	2.704	2.741	2.802	3.052	2.810	3.066	2.785	2.703	3.044	3.028	3.065	2.765
Ti	0.000	0.001	0.000	0.000	0.124	0.128	0.002	0.107	0.001	0.133	0.000	0.000	0.000	0.001	0.133
Al	1.884	1.888	1.254	1.291	1.557	1.539	1.892	1.577	1.873	1.549	1.282	1.897	1.892	1.843	1.536
Cr	0.001	0.001	0.000	0.000	0.001	0.001	0.001	0.002	0.001	0.002	0.000	0.001	0.001	0.002	0.004
Fe	1.721	1.786	0.006	0.007	0.899	0.859	1.649	0.843	1.565	0.871	0.004	1.557	1.851	1.782	0.881
Mn	0.408	0.463	0.000	0.000	0.007	0.009	0.323	0.002	0.326	0.004	0.002	0.301	0.368	0.383	0.005
Mg	0.710	0.603	0.000	0.000	1.555	1.493	0.825	1.490	0.702	1.535	0.000	0.769	0.718	0.746	1.541
Ca	0.171	0.198	0.328	0.343	0.000	0.000	0.254	0.001	0.449	0.007	0.312	0.430	0.166	0.187	0.000
Na	0.013	0.000	0.672	0.599	0.012	0.021	0.002	0.004	0.021	0.000	0.700	0.009	0.003	0.003	0.004
K	0.001	0.002	0.010	0.008	0.930	0.919	0.005	0.919	0.003	0.837	0.006	0.003	0.000	0.001	0.931
Sum	7.987	7.998	4.992	4.953	7.826	7.771	8.003	7.755	8.008	7.725	5.009	8.012	8.026	8.013	7.800
XMg	0.292	0.252	0.000	0.000	0.634	0.635	0.333	0.638	0.310	0.638	0.000	0.331	0.280	0.295	0.636
Al4	0.000	0.000	0.278	0.296	1.259	1.198	0.000	1.190	0.000	1.215	0.297	0.000	0.000	0.000	1.235
Al6	1.884	1.888	0.976	0.995	0.298	0.341	1.892	0.387	1.873	0.334	0.985	1.897	1.892	1.843	0.301

Table A2-1: Electron microprobe mineral analyses.

Sample	9033B	9033B	9033B
Min	BIO	PLG	PLG
Type	CORE	CORE	RIM
Code	E48	E31	E33
SiO2	37.89	60.43	60.42
TiO2	1.79	0.00	0.00
Al2O3	18.13	24.51	24.28
Cr2O3	0.02	0.00	0.00
FeO	14.07	0.16	0.20
MnO	0.09	0.02	0.02
MgO	13.95	0.00	0.00
CaO	0.00	7.09	6.85
Na2O	0.03	7.79	7.59
K2O	9.90	0.11	0.17
Sum	95.87	100.11	99.53
Si	2.787	2.692	2.704
Ti	0.099	0.000	0.000
Al	1.572	1.287	1.281
Cr	0.001	0.000	0.000
Fe	0.866	0.006	0.007
Mn	0.006	0.001	0.001
Mg	1.529	0.000	0.000
Ca	0.000	0.338	0.328
Na	0.004	0.673	0.659
K	0.929	0.006	0.010
Sum	7.794	5.004	4.990
XMg	0.639	0.000	0.000
Al4	1.213	0.308	0.296
Al6	0.359	0.979	0.985

APPENDIX 3

P-T CALCULATIONS AND TABLES

This appendix provides sample calculations for the geothermometers and geobarometers utilized in this study. Table A3-1 contains P-T estimates calculated by these methods.

Garnet - Biotite Geothermometer of Ferry and Spear (1978)

Ferry and Spear's (1978) experimentally based garnet-biotite thermometer exploits the continuous Fe-Mg exchange reaction:

$$Fe_3Al_2Si_3O_{12} + KMg_3AlSi_3O_{10}(OH)_2 \Leftrightarrow Mg_3Al_2Si_3O_{12} + KFe_3AlSi_3O_{10}(OH)_2$$

$$almandine + phlogopite \Leftrightarrow pyrope + annite.$$

The energy balance for this reaction is expressed by:

$$12454 - 4.662T + .057P + 3RT\ln K = 0 \qquad Eq.A1-1.$$

where the equilibrium constant is defined by:

$$K = \left[\frac{a_{Mg}^{GNT} / a_{Fe}^{GNT}}{a_{Mg}^{BIO} / a_{Fe}^{BIO}} \right].$$

This calibration is based on analyses of experimental charges and ideal mixing is assumed. Ferry and Spear (1978) noted that this should not introduce problems when used with phases of comparable compositions to those in the experimental work. The activities are therefore calculated by:

$$a_i^{GNT} = X_i^{GNT}$$

and

$$a_i^{BIO} = X_i^{BIO}$$

Using microprobe data and the mineral formula scheme of Appendix 1 for analyses of garnet and biotite, the temperature is calculated as follows:

$X_{Mg}^{GNT} = .1798$

$X_{Fe}^{GNT} = .7021$

$X_{Mg}^{BIO} = .548$

$X_{Fe}^{GNT} = .452$

$$K = \left[\frac{.1798/.7021}{.548/.452} \right] = .2112.$$

The temperature at 8 kbar is calculated by rearranging and substituting K into equation Eq. A1-1:

$$T_{8kbar}(K) = \left[\frac{-12454 - .057 \times 8000}{3R \ln .2112 - 4.662} \right]$$

$$T_{8kbar} = 926.7°K = 653.7°C$$

Grossular-Almandine-Anorthite-Quartz (GASP) Geobarometer of Newton and Haselton (1981)

The geobarometer of Newton and Haselton (1981) is based on the continuous net transfer reaction:

$$3CaAl_2Si_2O_8 \Leftrightarrow Ca_3Al_2Si_3O_{12} + 2Al_2SiO_5 + SiO_2$$

$$anorthite \Leftrightarrow grossular + aluminosilicate + quartz.$$

This calibration requires calculation of the activities of anorthite in plagioclase and grossular in garnet and the volume change for the reaction. Calibration of the activity of grossular in garnet utilizes the expression of Newton and Haselton (1981) where:

$$a_{Ca}^{GNT} = \gamma_{Ca}^{GNT} X_{Ca}^{GNT}$$

and

$$\gamma_{Ca}^{GNT} = \exp\left[\frac{W_{CaMg}(X_{Fe}^{GNT\,2} + X_{Fe}^{GNT} X_{Mg}^{GNT})}{RT} \right]$$

and

$W_{Ca}^{GNT} = (3300 - 1.5T(K))$.

Utilizing the mole fraction of Ca in garnet (X_{Ca} = Ca/Ca+Mg+Fe+Mn) for the same garnet analysis utilized in the geothermometric calibration of Ferry and Spear (1978) above, and assuming a temperature of 873°K:

$$\gamma_{Ca(873)}^{GNT} = \exp\left[\frac{(3300 - 1.5(873))(.1798^2 + .702(.1798))}{1.987 \times 873}\right] = 1.1995.$$

The activity is calculated by the general relationship:

$$a_i^{GNT} = \gamma_i^{GNT} X_i^{GNT}$$

such that for this example:

$$a_{Ca(873)}^{GNT} = (1.1772)(.0277) = .0332$$

The activity coefficient for the mixing of anorthite in plagioclase is calculated following Newton et al. (1980) by the expression:

$$\gamma_{An}^{PLG} = \exp\left[\frac{(1 - X_{Ca}^{PLG})^2 (2050 + 9392(X_{Ca}^{PLG}))}{RT}\right].$$

The mole fraction of anorthite in plagioclase is based on the Al-avoidance model of Kerrick and Darken (1975) and calculated by:

$$X_{An}^{PLG} = \frac{X_{Ca}^{PLG}(1 + X_{Ca}^{PLG})^2}{4}.$$

The activity of anorthite in plagioclase is therefore represented by:

$$a_{An}^{PLG} = \gamma_{An}^{PLG} X_{An}^{PLG}.$$

Combining expressions for the activity coefficient and mole fraction yields:

$$a_{An}^{PLG} = \frac{X_{Ca}^{PLG}(1 + X_{Ca}^{PLG})^2}{4} \exp\left[\frac{(1 - X_{Ca}^{PLG})^2 (2050 + 9392(X_{Ca}^{PLG}))}{RT}\right] \qquad Eq. A1 - 2.$$

For the plagioclase coexisting with garnet in this sample:

$X_{Ca}^{PLG} = .19$, where $X_{Ca}^{PLG} = \frac{Ca}{Ca+Na}$.

The activity can therefore be calculated by substituting X_{Ca}^{PLG} into Eq. A1-2:

$$a_{An}^{PLG} = \frac{.19(1+.19)^2}{4}\exp\left[\frac{(1-.19)^2(2050+9392(.19))}{(1.987)(873)}\right] = .2868$$

Calculation of the volume change for the reaction requires the determination of the molar volume of grossular in garnet. This is determined by independent calculation of the partial molar volume of grossular in both pyrope and almandine and subsequently determining the weighted average of these two values. The molar volume of grossular in pyrope and almandine is calculated by substituting the mole fraction of grossular (.0277) into the following equations of Haselton and Newton (1980):

$$V_{CaFe}^{GNT} = 125.24 + 1.482(1-X_{Ca}^{GNT})^3 - .480\left[1+\frac{(1-X_{Ca}^{GNT}-.914)(1-X_{Ca}^{GNT})}{.066^2}\right]\exp\left[-\frac{(1-X_{Ca}^{GNT}-.914)^2}{2(.066)^2}\right] = 122.08$$

and

$$V_{CaMg}^{GNT} = 125.24 + .512(1-X_{Ca}^{GNT})^3 - .418\left[1+\frac{(1-X_{Ca}^{GNT}-.94)(1-X_{Ca}^{GNT})}{.083^2}\right]\exp\left[-\frac{(1-X_{Ca}^{GNT}-.94)^2}{2(.083)^2}\right] = 123.56$$

with the weighted average of the two partial molar volumes calculated by:

$$V_{Ca}^{GNT}(cm^3) = \frac{(X_{Mg}^{GNT} x V_{CaMg}^{GNT}) + (X_{Fe}^{GNT} x V_{CaFe}^{GNT})}{X_{Mg}^{GNT} + X_{Fe}^{GNT}}$$

$$V_{Ca}^{GNT}(cm^3) = \frac{(X_{Mg}^{GNT} x 123.56)) + (X_{Fe}^{GNT} x 122.08)}{X_{Mg}^{GNT} + X_{Fe}^{GNT}} = 122.38$$

where the mole fractions of almandine and pyrope are the same as those made in the Ferry and Spear (1978) geothermometer calculation above. The volume change for the reaction is calculated by:

$$\delta V_{reaction} = V_{prod} - V_{react}$$

$$\delta V_{reaction} = (V_{qtz} + V_{Ca}^{GNT} + 2V_{sill}) - 3V_{An}^{PLG}$$

$$\delta V_{reaction} = 22.688 + 122.38 + 2(49.90) - 3(100.79) = -57.502 cm^3$$

$$\delta V_{reaction} = -5.7502 J^{-1}$$

With the volume change for the reaction and the activity of both grossular and plagioclase calculated, a pressure for the reaction at a given temperature (873°) can be calculated from the equation:

$$P_{873} = \frac{P^{\circ}_{Als}\delta V^{\circ}_{Als} - RT\ln K_D}{\delta V} \qquad \text{Eq. A1-3}$$

where

$$P^{\circ}_{Sil} = -1180 + 23.8T(C)$$

or

$$P^{\circ}_{Ky} = -2100 + 23.2T(C)$$

(original sillmanite calibration of Newton and Haselton (1981), as corrected by Ganguly and Saxena (1984)) and

$$\delta V^{\circ}_{Sil} = -5.4582$$

or

$$\delta V^{\circ}_{Ky} = -6.6202$$

for sillimanite and kyanite respectively. The values of the equilibrium constant (K) are calculated from the activities of grossular and anorthite by the relationship:

$$K = \left[\frac{a_{Ca}^{GNT\,3}}{a_{An}^{PLG\,3}}\right] = \frac{.0326^3}{.2868^3} = .00147$$

For a temperature of 873°K (600°C) the pressure is estimated by substituting the value for K into Eq. A1-3:

$$P_{873}(bars) = \frac{(-1180 + 23.8(600))(-5.4582) - (8.3144)(873)\ln[.00147]}{-5.7502}$$

$$P_{873} = 4273 bars = 4.3 kbar$$

Garnet-Clinopyroxene Geothermometer of Ellis and Green (1979)

The geothermometer of Ellis and Green (1979) is based on the continuous Fe-Mg exchange reaction:

$$\frac{1}{3}Mg_3Al_2Si_3O_{12} + CaFeSi_2O_6 \Leftrightarrow \frac{1}{3}Fe_3Al_2Si_3O_{12} + CaMgSi_2O_6$$

$$pyrope + hedenbergite \Leftrightarrow almandine + diopside$$

The experimentally derived calibration of Ellis and Green (1979) is based on the equation:

$$T(K) = \frac{3104X_{Ca}^{GNT} + 3030 + P(kbar)x10.86}{\ln K_D + 1.9034}$$

where

$$K_D = \frac{X_{Fe}^{GNT} / X_{Mg}^{GNT}}{X_{Fe}^{CPX} / X_{Mg}^{CPX}}.$$

Mole fractions for garnet and clinopyroxene are calculated by:

$$X_{Fe}^{GNT} = \frac{Fe}{Fe + Mg + Ca + Mn}$$

and

$$X_{Fe}^{CPX} = \frac{Fe}{Fe + Mg}$$

respectively such that:

$X_{Fe}^{GNT} = .528$, $X_{Mg}^{GNT} = .184$, $X_{Ca}^{GNT} = .226$, $X_{Fe}^{CPX} = .352$ and $X_{Mg}^{CPX} = .647$ for sample JNC-86-403. The K is calculated by:

$$K = \left[\frac{.528 + 184}{.352 + 647} \right]$$

For a pressure of 6 Kbar, the corresponding temperature for this K is calculated by:

$$T_{6Kbar}(K) = \frac{3104(.266) + 3030 + 6(Kbar) \times 10.86}{\ln 5.274 + 1.903 - 4} = 1099.4°K$$

$$T_{6Kbar} = 826.4°C.$$

Garnet-Anorthite-Diopside-Quartz (GADS) Geobarometer of Newton and Perkins (1982)

The calibration of Newton and Perkins (1982) is based on the continuous net transfer reaction:

$$CaAl_2Si_2O_8 + CaMgSi_2O_8 \Leftrightarrow \frac{2}{3}Ca_3Al_2Si_3O_{12} + \frac{1}{3}Mg_3Al_2Si_3O_{12} + SiO_2$$

$$plagioclase + clinopyroxene \Leftrightarrow garnet + quartz.$$

This calibration requires calculation of the activity coefficients and activities of grossular in garnet, diopside in clinopyroxene and anorthite in plagioclase in order to calculate the equilibrium constant K. The activity coefficient of grossular in ternary garnet is based on Ganguly and Kennedy's (1974) mixing model described by:

$$\gamma_{Ca}^{GNT} = \exp\left[\frac{(W'_{CaMg})(X_{Mg}^{GNT\,2} + X_{Mg}^{GNT} X_{Fe}^{GNT})}{RT}\right]$$

and

$$\gamma_{Mg}^{GNT} = \exp\left[\frac{(W'_{CaMg})(X_{Ca}^{GNT\,2} + X_{Ca}^{GNT} X_{Fe}^{GNT})}{RT}\right]$$

where

$$X_{Ca}^{GNT} = \frac{Ca}{Ca+Fe+Mg}, X_{Mg}^{GNT} = \frac{Mg}{Ca+Fe+Mg} \text{ and } X_{Fe}^{GNT} = \frac{Fe}{Ca+Fe+Mg}.$$

Substituting mole fractions of grossular and pyrope in garnet (from sample JNC-86-403, the same sample utilized in the Ellis and Green (1975) geothermometer calculation above) into the appropriate equations yields:

$$\gamma_{Ca}^{GNT} = \exp\left[\frac{(3300 - 1.5(873))(.196^2 + (.196)(.563))}{(1.9872)(873)}\right] = 1.186$$

and

$$\gamma_{Mg}^{GNT} = \exp\left[\frac{(3300 - 1.5(873))(.240^2 + (.240)(.563))}{(1.9872)(873)}\right] = 1.247.$$

The activities are calculated by:

$$a_{Ca}^{GNT} = \gamma_{Ca}^{GNT} X_{Ca}^{GNT} = (1.186)(.240) = .284$$

and

$$a_{Mg}^{GNT} = \gamma_{Mg}^{GNT} X_{Mg}^{GNT} = (1.247)(.196) = .244$$

The activity of diopside in clinopyroxene follows the scheme described in Appendix 2 for this calibration. The resulting expression for diopside activity is:

$$a_{Dio}^{CPX} = X_{Ca}^{CPX-X\,site} X_{Mg}^{CPX-Y\,site} = (.657)(.813) = .534.$$

For the calculation of the activity coefficient of anorthite in plagioclase, the expression of Newton et al. (1980) is used:

$$\alpha_{An}^{PLG} = \exp\left[\frac{X_{Na}^{PLG\,2}(W_{Ca} + 2(X_{An}^{PLG})(W_{Ab} - W_{an}))}{RT}\right]$$

where

$W_{An}^{PLG} = 2025 cal$

$W_{Ab}^{PLG} = 6746 cal$

such that

$$\gamma_{An}^{PLG} = \exp\left[\frac{X_{Na}^{PLG\,2}(2025 + 2(X_{Ca}^{PLG})(6746 - 2025))}{RT}\right] \qquad Eq.\,A1-4.$$

Plagioclase coexisting with garnet in Sample JNC-86-403 has the composition:

$X_{Na}^{PLG} = .834$ and $X_{Ca}^{PLG} = .166$.

Substituting these mole fractions into Eq. A1-4 yields an activity coefficient:

$$\gamma_{An-873}^{PLG} = \exp\left[\frac{.834^2(2050 + 2(.166)(6746 - 2050))}{(1.987)(873)}\right] = 4.255$$

The activity is calculated by:

$$a_{An-873}^{PLG} = \gamma_{An}^{PLG}\left[\frac{X_{Ca}^{PLG}(1 - X_{Ca}^{PLG})^2}{4}\right]$$

$$a_{An}^{PLG} = (4.251)\left[\frac{(.163)(1 + .166)^2}{4}\right] = .240.$$

The pressure is calculated by substituting the component activities into the calibration of Newton and Perkins (1982):

$$P(bars) = 675 + 17.179T + 3.5962T \ln K_D$$

where

$$K_D = \left[\frac{(a_{Ca}^{GNT\,2} a_{Mg}^{GNT})}{(a_{An}^{PLG} a_{Dio}^{CPX})}\right] = \left[\frac{(.284^2)(.244)}{(.240)(.534)}\right] = .1652$$

For a temperature of 873°K (600°C) the pressure estimate is calculated:

$$P_{873}(bars) = 675 + 17.179(873) + 3.5962(873)\ln .1652 = 10019 bars$$

$$P_{873} = 10.0 kbar$$

RESULTS

Table A3-1 contains the P-T estimates of all samples utilized in this study; all results are presented in graphical form in Chapter 5.

Table A3-1: P-T estimates.

Sample N	P	T	T Code	P Code	THERM	BAROM
77	2.1	571	CORE: A01-A44	CORE: A01-A36	GNT-BIO	GASP
77	1.1	529	RIM: A02-A43	RIM: A02-A35	GNT-BIO	GASP
77	2.2	611	CORE: B01-B44	CORE: B01-B37	GNT-BIO	GASP
77	2.9	605	RIM: B03-B45	RIM: B02-B38	GNT-BIO	GASP
77	3.4	631	CORE: C01-C42	CORE: C01-C31	GNT-BIO	GASP
77	3.1	601	RIM: C03-C43	RIM: C03-C32	GNT-BIO	GASP
235	5.1	760	CORE: A01-A41	CORE: A01-A31	GNT-BIO	GASP
235	5.3	778	RIM: A02-A42	CORE: C01-A32	GNT-BIO	GASP
235	3.6	652	CORE: C55-C41	CORE: C55-C31	GNT-BIO	GASP
235	4.8	701	RIM: C51-C42	RIM: C51-C32	GNT-BIO	GASP
235	4.7	710	CORE: D01-D44	CORE: D01-D31	GNT-BIO	GASP
368	6.2	790	CORE: A01-A46	CORE: A01-A33	GNT-BIO	GASP
368	6.3	776	INT: A02-A46	RIM: A02-A34	GNT-BIO	GASP
368	4.0	779	CORE: B01-B44	CORE: B01-B35	GNT-BIO	GASP
368	3.7	752	RIM: B02-B43	RIM: B02-B36	GNT-BIO	GASP
368	5.4	740	CORE: C01-C41	CORE: C01-C31	GNT-BIO	GASP
368	5.4	742	RIM: C04-C43	RIM: C04-C32	GNT-BIO	GASP
368	6.9	838	CORE: D01-D41	CORE: D01-D31	GNT-BIO	GASP
368	7.2	787	RIM: D03-D42	RIM: D03-D32	GNT-BIO	GASP
377	3.2	632	CORE: B01-B44	CORE: A01-B35	GNT-BIO	GASP
377	3.2	630	RIM: B02-B43	CORE: A01-B35	GNT-BIO	GASP
377	3.1	658	CORE: C01-D41	CORE: C01-C31	GNT-BIO	GASP
377	3.3	565	RIM: C03-D42	RIM: C03-C32	GNT-BIO	GASP
377	4.9	673	CORE: D01-D41	CORE: D01-D31	GNT-BIO	GASP
377	3.1	592	RIM: D03-D42	RIM: D03-D32	GNT-BIO	GASP
403	12.6	794	INT: A01-A45	CORE: B01-B27-B35	GNT-BIO	GADS
403	10.9	803	RIM: A02-A45	INT: B02-B28-B35	GNT-BIO	GADS
403	12.9	813	CORE: B01-B27	CORE: B01-B27-B35	GNT-CPX	GADS
403	11.3	765	RIM: B02-B28	INT: B02-B28-B35	GNT-CPX	GADS
403	12.8	812	CORE: B01-B44	CORE: B01-B27-B35	GNT-BIO	GADS
403	11.1	748	RIM: B02-B43	INT: B02-B28-B35	GNT-BIO	GADS
403	11.7	820	CORE: C01-C24	CORE: C01-C24-C37	GNT-CPX	GADS
403	11.7	820	RIM: C03-C26	RIM: C03-C24-C39	GNT-CPX	GADS
403	10.0	668	CORE: C01-C41	CORE: C01-C24-C37	GNT-BIO	GADS
403	9.0	634	RIM: C03-C42	RIM: C03-C24-C39	GNT-BIO	GADS
403	11.1	794	CORE: D01-D21	CORE: D01-D21-D31	GNT-CPX	GADS
403	9.1	747	RIM: D03-D22	RIM: D02-D22-D32	GNT-CPX	GADS
403	12.2	850	INT: E01-E25	INT: E01-E25-E38	GNT-CPX	GADS
403	12.0	831	INT: E03-E25	INT: E01-E25-E38	GNT-CPX	GADS
403	9.5	827	CORE: F01-F21	CORE: F01-F21-F31	GNT-CPX	GADS
403	7.0	718	INT: F02-F22	INT: F02-F22-F32	GNT-CPX	GADS
406	10.1	849	CORE: B01-B23	CORE: B01-B23-B38	GNT-CPX	GADS
406	10.2	859	RIM: B02-B29	CORE: B01-B23-B38	GNT-CPX	GADS
406	9.7	819	CORE: D01-D24	CORE: C01-D24-D36	GNT-CPX	GADS
406	8.6	801	RIM: D02-D25	RIM: D02-D25-D37	GNT-CPX	GADS
418	6.2	688	CORE: A01-A48	CORE: B01-B36	GNT-BIO	GASP
418	5.5	669	RIM: A03-A47	RIM: B03-B37	GNT-BIO	GASP
418	6.0	676	CORE: B01-B44	CORE: B01-B36	GNT-BIO	GASP
418	5.2	646	RIM: B03-B45	RIM: B03-B37	GNT-BIO	GASP
418	5.1	640	CORE: E01-E41	CORE: E01-E31	GNT-BIO	GASP
418	3.9	583	RIM: E03-E42	RIM: E03-E32	GNT-BIO	GASP

Table A3-1: P-T estimates.

Sample N	P	T	T Code	P Code	THERM	BAROM
424	9.0	754	CORE A01-A24	CORE A01-A24-A37	GNT-CPX	GADS
424	8.3	677	INT: A02-A24	INT A01-A24-A37	GNT-CPX	GADS
424	9.5	799	INT: A01-A43	CORE A01-A24-A37	GNT-BIO	GADS
424	8.1	658	RIM A02-A43	INT A01-A24-A37	GNT-BIO	GADS
424	9.9	764	CORE C01-C21	CORE C01-C21-C31	GNT-CPX	GADS
424	8.7	734	RIM C02-C22	RIM C02-C22-C32	GNT-CPX	GADS
424	8.7	718	CORE E02-E23	CORE E02-E23-E35	GNT-CPX	GADS
424	11.4	793	CORE F02-F23	CORE F02-F23-F35	GNT-CPX	GADS
424	10.1	754	INT: F02-F24	INT F02-F24-F36	GNT-CPX	GADS
1073	3.7	759	CORE A01-A43	CORE A01-A35	GNT-BIO	GASP
1073	4.6	779	RIM A02-A44	RIM: A02-A36	GNT-BIO	GASP
1098	0.7	804	CORE A01-A41	CORE A01-Z01	GNT-BIO	GASP
1098	0.8	738	RIM A03-A42	RIM: A03-Z02	GNT-BIO	GASP
1098	1.4	678	CORE B01-B41	CORE B01-Z01	GNT-BIO	GASP
1098	1.3	630	RIM B02-B42	RIM B02-Z02	GNT-BIO	GASP
1203	12.7	848	CORE A03-A25	CORE A01-A25-A37	GNT-CPX	GADS
1203	11.0	802	INT A02-A25	INT A02-A26-A37	GNT-CPX	GADS
1203	13.0	893	CORE B01-B24	CORE B01-B24-B36	GNT-CPX	GADS
1203	10.7	775	INT B02-B25	INT B02-B25-B37	GNT-CPX	GADS
1208	10.2	780	CORE B01-B24	CORE B01-B24-B36	GNT-CPX	GADS
1208	9.8	785	INT B02-B23	INT B02-B23-B35	GNT-CPX	GADS
1208	10.8	824	CORE D01-D24	CORE D01-D24-D35	GNT-CPX	GADS
1208	10.5	796	RIM D02-D23	RIM: D02-D23-D36	GNT-CPX	GADS
1208	12.7	839	CORE E01-E23	CORE E01-E23-E36	GNT-CPX	GADS
1208	13.7	864	RIM E02-E24	RIM: E02-E24-E37	GNT-CPX	GADS
1289	4.2	679	CORE: A01-A43	CORE: A01-A35	GNT-BIO	GASP
1289	5.9	690	RIM A02-A44	RIM. A02-A36	GNT-BIO	GASP
1289	4.4	681	CORE: B01-B43	CORE B01-B36	GNT-BIO	GASP
1336	7.8	841	CORE: A01-A43	CORE: A01-A35	GNT-BIO	GASP
1336	6.6	789	RIM: A02-A47	RIM. A02-A36	GNT-BIO	GASP
1336	5.3	684	RIM: B02-B44	RIM: B02-B37	GNT-BIO	GASP
5016	8.4	780	CORE: A07-A44	INT A07-A36	GNT-BIO	GASP
5016	7.7	787	INT: A01-A44	INT A03-A36	GNT-BIO	GASP
5016	9.8	823	CORE: B08-B44	CORE. B08-B33	GNT-BIO	GASP
5016	7.6	753	RIM: B02-B45	RIM: B06-B32	GNT-BIO	GASP
5016	8.3	780	RIM: C03-C44	INT. C03-C32	GNT-BIO	GASP
5016	8.2	784	CORE D01-D44	CORE. D01-D36	GNT-BIO	GASP
5016	7.0	704	RIM: D03-D45	RIM D03-D37	GNT-BIO	GASP
5018	7.4	734	CORE: A01-A41	CORE A01-A31	GNT-BIO	GASP
5018	7.5	728	RIM: A03-A42	RIM A03-A33	GNT-BIO	GASP
5018	8.7	811	CORE B01-B41	CORE: A01-A31	GNT-BIO	GASP
5018	7.2	713	RIM: B02-B42	RIM A03-A33	GNT-BIO	GASP
5018	6.7	757	CORE: C01-C41	CORE. C01-C31	GNT-BIO	GASP
5018	6.3	711	INT. C03-C41	RIM C03-C33	GNT-BIO	GASP
5018	8.4	763	CORE. D01-D41	CORE: D01-D31	GNT-BIO	GASP
5018	7.9	742	RIM: D03-D42	RIM D03-D33	GNT-BIO	GASP
5019	14.6	864	CORE: A03-A24	CORE. A03-A24-A33	GNT-CPX	GADS
5019	14.4	865	RIM: A02-A25	RIM A02-A25-A32	GNT-CPX	GADS
5019	14.4	848	CORE: A01-A42	CORE A03-A24-A33	GNT-BIO	GADS

Table A3-1: P-T estimates.

Sample N	P	T	T Code	P Code	THERM	BAROM
5019	12 9	750	RIM A02-A45	RIM A02-A25-A32	GNT-BIO	GADS
5019	15 1	896	CORE B01-B21	CORE B01-B21-B31	GNT-CPX	GADS
5019	14 5	844	CORE B01-B41	CORE B01-B21-B31	GNT-BIO	GADS
5019	15 0	888	INT B01-B42	CORE B01-B21-B31	GNT-BIO	GADS
5019	16 4	903	CORE E01-E23	CORE E01-E23-E36	GNT-CPX	GADS
5019	13.7	827	RIM E02-E25	RIM E03-E25-E37	GNT-CPX	GADS
5038	15 3	855	CORE A01-A23	CORE A01-A23-A36	GNT-CPX	GADS
5038	15 3	825	INT A01-A24	INT A01-A24-A35	GNT-CPX	GADS
5038	15 7	859	CORE B01-B23	CORE B01-B23-B35	GNT-CPX	GADS
5038	16 4	890	INT B02-B23	INT B02-B23-B35	GNT-CPX	GADS
5038	13 9	735	CORE B01-B41	CORE B01-B23-B35	GNT-BIO	GADS
5038	15 1	802	RIM B02-B42	INT B02-B23-B35	GNT-BIO	GADS
5038	16 9	948	CORE C01-C21	CORE D05-D21-D31	GNT-CPX	GADS
5038	16 4	881	RIM C02-C22	INT D09-D22-D31	GNT-CPX	GADS
5038	16 6	923	CORE D05-D21	CORE D05-D21-D31	GNT-CPX	GADS
5038	16 5	887	RIM D09-D22	INT D09-D22-D31	GNT-CPX	GADS
5039	15 8	858	CORE A01-A23	CORE A01-A23-A37	GNT-CPX	GADS
5039	16 8	900	CORE B02-B23	CORE B02-B23-B34	GNT-CPX	GADS
5039	16 7	894	INT B01-B23	CORE B02-B23-B34	GNT-CPX	GADS
5039	15 2	911	INT C03-C21	INT C03-C21-C31	GNT-CPX	GADS
5039	14 8	899	RIM C03-C22	RIM C03-C22-C32	GNT-CPX	GADS
5043	16 3	910	CORE A01-A24	CORE A01-A24-A35	GNT-CPX	GADS
5043	15 6	878	RIM A02-A23	RIM A02-A23-A35	GNT-CPX	GADS
5043	16 8	952	CORE B01-B22	CORE B08-B28-B32	GNT-CPX	GADS
5043	13 3	814	RIM B05-B24	RIM B07-B29-B33	GNT-CPX	GADS
5043	14 0	915	CORE C01-C23	CORE C01-C23-C31	GNT-CPX	GADS
5043	17 2	1014	RIM C06-C24	RIM C06-C24-C32	GNT-CPX	GADS
5043	12 6	890	CORE D01-D23	CORE D01-D23-D31	GNT-CPX	GADS
5043	14 4	981	RIM D03-D24	RIM D03-D24-D32	GNT-CPX	GADS
5043	18 9	1035	CORE E02-E21	CORE E02-E21-E31	GNT-CPX	GADS
5043	15 8	959	RIM E03-E22	RIM E03-E22-E32	GNT-CPX	GADS
5043	16 0	980	RIM E03-E41	RIM E03-E22-E32	GNT-BIO	GADS
5047	9 2	834	CORE A03-A41	CORE A03-A31	GNT-BIO	GASP
5047	8 5	805	CORE B01-B41	CORE D01-D31	GNT-BIO	GASP
5047	6 8	712	RIM B02-B42	CORE D01-D31	GNT-BIO	GASP
5047	7 5	750	INT C01-C43	CORE D01-D31	GNT-BIO	GASP
5047	7.0	724	RIM C02-C43	CORE D01-D31	GNT-BIO	GASP
5047	6 4	686	CORE D01-D42	CORE D01-D31	GNT-BIO	GASP
5047	9.0	835	RIM D03-D43	CORE D01-D31	GNT-BIO	GASP
6050	6 0	705	CORE A01-A41	CORE A01-A31	GNT-BIO	GASP
6050	5 2	643	RIM A03-A42	RIM A03-A33	GNT-BIO	GASP
6050	6 2	702	CORE B01-B41	CORE B01-B31	GNT-BIO	GASP
6050	5 4	666	RIM B03-B42	RIM B03-B32	GNT-BIO	GASP
6050	5.3	656	CORE D01-D41	CORE D01-D31	GNT-BIO	GASP
6050	6 3	703	RIM D03-D42	RIM D03-D33	GNT-BIO	GASP
6056	5 6	677	CORE A01-A41	CORE B01-B31	GNT-BIO	GASP
6056	4 4	595	RIM A02-A42	RIM B02-B32	GNT-BIO	GASP
6056	7 1	773	CORE B01-B41	CORE B01-B31	GNT-BIO	GASP
6056	5 3	652	RIM B02-B42	RIM B02-B32	GNT-BIO	GASP
7051	10 9	836	CORE A01-A41	CORE A01-A31	GNT-BIO	GASP
7051	10 6	856	RIM A03-A42	RIM A03-A32	GNT-BIO	GASP

Table A3-1: P-T estimates.

Sample N	P	T	T Code	P Code	THERM	BAROM
7051	8.9	801	CORE B01-B41	CORE B01-B31	GNT-BIO	GASP
7051	10.1	812	RIM B03-B42	RIM B03-B32	GNT-BIO	GASP
7051	8.3	783	CORE C01-C41	CORE C01-C31	GNT-BIO	GASP
7051	9.0	796	RIM C03-C42	RIM C03-C32	GNT-BIO	GASP
7053	9.8	827	CORE A01-A41	CORE A01-A31	GNT-BIO	GASP
7053	6.0	652	RIM A03-A42	RIM A03-A32	GNT-BIO	GASP
7053	7.3	763	CORE B01-B41	CORE B01-B31	GNT-BIO	GASP
7053	6.8	681	RIM B03-B42	RIM B03-B34	GNT-BIO	GASP
7053	5.7	723	CORE C01-C41	CORE C01-C31	GNT-BIO	GASP
7053	5.3	586	RIM C03-C42	RIM C03-C32	GNT-BIO	GASP
7054	7.5	675	CORE A01-A41	CORE A01-A31	GNT-BIO	GASP
7054	7.6	659	RIM A02-A42	RIM A02-A32	GNT-BIO	GASP
7054	8.6	726	CORE B01-B41	CORE A01-A31	GNT-BIO	GASP
7054	9.2	732	RIM B02-B42	RIM A02-A32	GNT-BIO	GASP
7075D	6.7	659	CORE B01-B41	CORE B01-B31	GNT-BIO	GASP
7075D	5.5	606	RIM B03-B42	RIM B03-B32	GNT-BIO	GASP
7075D	5.8	710	INT C01-C41	CORE C01-C31	GNT-BIO	GASP
7075D	7.9	686	RIM C03-C41	RIM C03-C32	GNT-BIO	GASP
7132	25.1	1803	CORE A01-A41	CORE A01-A31	GNT-BIO	GASP
7132	25.9	1552	RIM A03-A42	RIM A03-A32	GNT-BIO	GASP
7132	21.5	1635	CORE B01-B41	CORE B01-B31	GNT-BIO	GASP
7132	17.8	1157	RIM B03-B42	RIM B03-B32	GNT-BIO	GASP
8068	12.1	947	CORE A01-A41	CORE A01-A31	GNT-BIO	GASP
8068	8.0	758	RIM A02-A42	RIM A02-A32	GNT-BIO	GASP
8068	14.1	882	CORE B01-B41	CORE B01-B31	GNT-BIO	GASP
8068	7.7	727	RIM B02-B42	RIM B02-B32	GNT-BIO	GASP
8068	2.4	531	CORE C01-C41	CORE C01-C31	GNT-BIO	GASP
8068	6.2	588	RIM C02-C42	RIM C02-C32	GNT-BIO	GASP
8088-1	4.2	773	CORE A01-A41	CORE A01-A31	GNT-BIO	GASP
8088-1	5.5	690	RIM A03-A42	RIM A03-A32	GNT-BIO	GASP
8088-1	8.3	911	CORE B01-B41	CORE B01-B31	GNT-BIO	GASP
8088-1	6.9	769	RIM B03-B42	RIM B03-B32	GNT-BIO	GASP
8088-1	4.6	762	CORE C01-C41	CORE C01-C31	GNT-BIO	GASP
8088-1	4.2	612	RIM C03-C42	RIM C03-C32	GNT-BIO	GASP
8088-2	6.8	848	CORE A01-A41	CORE A01-A31	GNT-BIO	GASP
8088-2	7.8	774	RIM A03-A42	RIM A03-A32	GNT-BIO	GASP
8088-2	6.0	794	CORE B01-B41	CORE A01-A31	GNT-BIO	GASP
8088-2	6.6	708	RIM B03-B42	RIM A03-A32	GNT-BIO	GASP
9001	7.8	818	CORE A01-A41	CORE A01-A32	GNT-BIO	GASP
9001	5.8	706	RIM A02-A42	RIM A02-A33	GNT-BIO	GASP
9001	7.0	774	CORE B01-B41	CORE A01-A32	GNT-BIO	GASP
9001	7.7	816	INT B03-B41	RIM A02-A33	GNT-BIO	GASP
9013A	11.8	837	CORE A01-A43	CORE A01-A31	GNT-BIO	GASP
9013A	11.0	811	CORE A03-A41	CORE A03-A31	GNT-BIO	GASP
9013A	7.7	693	RIM A02-A44	RIM A02-A32	GNT-BIO	GASP
9013A	10.0	770	RIM A04-A42	RIM A04-A32	GNT-BIO	GASP
9013B	8.5	799	CORE A01-A41	CORE A01-A31	GNT-BIO	GASP
9013B	6.9	710	RIM A03-A42	RIM A03-A32	GNT-BIO	GASP

Table A3-1: P-T estimates.

Sample N	P	T	T Code	P Code	THERM.	BAROM.
9013B	6 4	742	CORE B01-B41	CORE: B01-B31	GNT-BIO	GASP
9013B	8 2	754	RIM: B03-B42	RIM: B03-B32	GNT-BIO	GASP
9016	10 4	918	CORE: A06-A41	CORE: B01-A35	GNT-BIO	GASP
9016	10 5	813	RIM: A07-A43	RIM: B02-B36	GNT-BIO	GASP
9016	9 5	889	CORE: C01-C44	CORE: C01-B35	GNT-BIO	GASP
9016	9 3	843	RIM: C05-C43	RIM: C05-C37	GNT-BIO	GASP
9023	17 7	939	CORE: A01-A44	CORE: A01-A31	GNT-BIO	GASP
9023	12 3	763	RIM: A02-A43	RIM: A02-A32	GNT-BIO	GASP
9032	14 5	972	RIM: A01-A24	RIM: A01-A24-A33	GNT-CPX	GADS
9032	11 8	932	CORE: B01-B23	CORE: B01-B23-B34	GNT-CPX	GADS
9032	11 3	874	INT: B02-B23	CORE: B01-B23-B34	GNT-CPX	GADS
9032	12 5	975	CORE: C01-C21	CORE: C01-C21-C33	GNT-CPX	GADS
9032	10 2	860	RIM: C05-C22	RIM: C05-C22-C32	GNT-CPX	GADS
9032	9 6	947	CORE: E01-E24	CORE: E02-E24-E36	GNT-CPX	GADS
9032	9 4	911	CORE: E02-E24	CORE: E02-E24-E36	GNT-CPX	GADS
9032	6 9	748	RIM: E03-E25	CORE: E03-E25-E37	GNT-CPX	GADS
9032	11 9	963	CORE: F02-F25	CORE: F02-F25-F39	GNT-CPX	GADS
9032	9 4	841	RIM: F03-E26	CORE: F03-F26-F38	GNT-CPX	GADS
9033	6 8	698	CORE: A01-A44	CORE: A01-A36	GNT-BIO	GASP
9033	4 9	612	RIM: A02-A43	RIM: A02-A35	GNT-BIO	GASP
9033	14 0	816	CORE: C06-C42	CORE: C06-C35	GNT-BIO	GASP
9033	9 8	743	RIM: C03-C44	INT: C01-C35	GNT-BIO	GASP
9033	5 9	662	CORE: E01-E48	CORE: E01-E31	GNT-BIO	GASP
9033	7 2	705	RIM: E05-E46	RIM: E05-E33	GNT-BIO	GASP

APPENDIX 4
P-T CALCULATION ERROR ASSESSMENT

Each geothermometric and geobarometric calibration has an inherent uncertainty in its ability to determine the correct P or T. This uncertainty is, in part, a function of the type of calibration. Uncertainties in estimates based on experimentally-based calibrations (ie. geothermometers used in this study) must account for errors in the analysis of the experimental phases, uncertainties in the calibration of P-T conditions during a run and deviations from the assumption of ideal mixing. Thermodynamically-based calibrations (ie. geobarometers used in this study) have errors on the thermodynamic variables (enthalpy, entropy and heat capacity) and volume change as a function of P-T as well as inaccuracies in the mixing models. The geothermometers of Ferry and Spear (1978) and Ellis and Green (1979) reported errors of $\pm 50°$. Newton and Haselton (1981) and Newton and Perkins (1982) suggested uncertainties of $\pm .8$ and ± 1.6 kbar for their respective geobarometers.

Another potential source of errors in P-T estimates lies in the uncertainties inherent in the electron microprobe data which are used to calculate P and T. These uncertainties control the reproducibility, or precision, of P or T estimates. In the following section, probe data errors are propagated through the various geothermometric and geobarometric calibrations to determine the precision of the P-T results.

Uncertainties in Electron Microprobe Analyses

A natural standard of garnet (H-GNT) was repeatedly measured over the period in which analytical work was performed in an attempt to determine the analytical precision (Table A4-1). One sigma relative errors of 3.9% and 2.5% for Mg and Fe respectively have been determined from 28 H-GNT analyses. The Mg/Fe ratio of this data set yields a one sigma relative error of 5.6%. The larger relative error for the Fe/Mg ratio than for the individual Fe and Mg analyses may indicate a negative correlation between the

Mg and Fe analyses, which would be consistent with Fe-Mg zonation within the H-GNT standard. If zonation is present within the standard, the estimated errors are probably higher than the actual errors.

Propagation of Errors Through Geothermometers and Geobarometers

The 1Σ errors estimated above were propagated through the geothermometers by two methods:

1. Modification of the analyzed Fe and Mg values in proportion to the relative errors in opposite directions (eg. increasing the Fe value while decreasing the Mg value by their respective 1 sigma errors) for each phase so that the K value is modified to the maximum extent allowed by the individual errors.

2. Calculation of the one sigma variance of the K value by:

$$\sigma_{K_d} = \sqrt{\sigma^{2GNT}_{Mg/Fe} + \sigma^{2BIO}_{Mg/Fe}} \qquad Eq.A4.4.$$

Errors for geobarometers have only been calculated by the first method.

Method 1

A data set has been fabricated based on analyses of samples 1073 and 403 (Table A4.2). The original analyses are coded AOR (site A, original) with the adjacent modified "analyses" coded APM (site A, plus/minus error). The shifts in the Fe and Mg are based on the one sigma relative error calculated for H-GNT; Ca was shifted 3.9%, the greater of the two errors.

This method yields an uncertainty of ±59° for Ferry and Spear's (1978) garnet-biotite calibration (Table A4.2). The GASP geobarometer (Newton and Haselton, 1981), which is used in conjunction with the garnet-biotite geothermometer, yields an error of ±.4 kbar. The geothermometer of Ellis and Green (1979) yields an uncertainty of ±45° while the GADS geobarometer of Newton and Perkins (1982) gives an error of ±.5 kbar (Table A4.1).

Method 2

While the above method provides the maximum errors on P-T estimates for the precision for the electron microprobe data, errors on geothermometers were also calculated by assessing the variabilility in the P-T estimates as a function of the changes in the Kd value where analytical error is assumed random. An error of 7.9% for the K value calculated by Eq. A4.1, where the one sigma relative Mg/Fe error is 5.6%. Changing the K by 7.9% results in a change of approximately $\pm 40°$ for the garnet-biotite calibration of Ferry and Spear (1978) and $\pm 33°$ for the garnet-clinopyroxene calibration of Ellis and Green (1989) (Table A4-4).

The first method results in the maximum deviation from the calculated temperature/pressure estimate for the stated errors. This is presented as a worst case scenario and is considered to produce unrealistically large errors since unless there was a real and consistent negative correlation between elements, in particular Mg and Fe. The second case is more realistic since it calculates errors in temperature assuming that errors on the analyses for each element are uncorrelated.

Attempts to constrain tectonic evolution through the use of geothermometers and geobarometers more often depends upon P-T differences rather than absolute P-T estimates (eg. P-T-t paths, establishing relative P-T differences between terranes or thrust blocks, etc.). There are two different approaches to estimate contrasting P-T conditions: 1. comparison of P-T results of a single geothermometer or geobarometer; or 2. comparison of P-T results of different geothermometers or geobarometers. Contrasting estimates of a single calibration only requires consideration of precision; all the results may be too high or low but, if all other variables are comparable, the relative differences will be preserved in spite of inaccurate estimates. The second method depends on the absolute estimates being correct so the estimation of P-T uncertainties must therefore take into account the uncertainties in both accuracy and precision.

Within individual terranes, where P-T estimates are predominantly determined by a single calibration, temperature and pressure differences greater than approximately 40° and .5 kbar are considered geologically significant and not the result of analytical

uncertainty. There is no definitive method for establishing the uncertainties in the P-T estimates for comparison between the Molson Lake and Lac Joseph Terranes where different geothermometric/geobarometric methods are utilized. The addition of the accuracy and precision uncertainties offers a maximum uncertainty of $\pm 90°$ for the two geothermometers and ± 1 and ± 2 kbar for the GASP and GADS geobarometers respectively. These maximum errors require that temperature and pressure differences must be in the order of 180° and 3 kbar respectively before the differences are outside the range of uncertainty. The upper estimation of the uncertainty by addition of indeterminate (accuracy) and determinate (precision) errors, where the result (K) is a quotient of two variables, will certainly overestimate errors. The lower limit for the uncertainties is calculated as the square root of the sum of the square of the errors, the method for calculating determinant errors of a result which is a quotient of the variables. This method yields uncertainties of $\pm 70°$ for the geothermometers and $\pm .7$ and ± 1.7 kbar for GASP and GADS geobarometers respectively.

Fe^{+2} and Fe^{+3} Assumptions

The geothermometers employed in this study are based on the temperature dependent exchange of Fe^{+2} and Mg^{+2} between two phases. The electon microprobe is unable to differentiate between Fe^{+2} and Fe^{+3}; lacking independent evidence concerning the oxidation state of Fe, Fe^{+2} is assumed to equal Fe^{TOTAL}, an assumption which may result in an over-estimation of Fe^{+2}.

Fe^{+3} may replace Al in the Y site of garnet to form andradite (see Appendix 2). However, since Al^{+3} typically fills or nearly fills the B site, Fe^{+3} substitution in garnet must be minimal. Similarly, Fe^{+3} replaces Al^{+3} in the Y site of clinopyroxene, coupled with Na in the X site to form acmite. By filling the structural sites as described in Appendix 2, the acmite component is not significant. Calculations where Fe^{+3} is calculated by site distribution and charge balance show no appreciable differences for the garnet-clinopyroxene geothermometer (Table A4.4).

Unlike garnet and clinopyroxene, which have a relatively simple structures and limited substitutions, Fe^{+3} in biotite is not easily assessed. Attempts to calculate Fe^{+3} by charge balance commonly results in an over-estimation due to real vacancies in the octahedral sites. In the absence of chemical analyses capable of distinguishing Fe^{+3} and Fe^{+2}, there is no satisfactory method to estimate Fe^{+3} in biotite on petrographic or mineralogical grounds. While allowing that Fe^{+3} in biotite would affect the temperature estimate, the relative differences between samples would be preserved if the oxygen fugacity were approximately similar throughout the Lac Joseph Terrane; the presence and relative constant modal percent of magnetite throughout the aluminosilicate-bearing pelites argues in favour of this condition.

Table A4-1: Analyses of electron microprobe standard SSHGNT.

STANDARD	NA2O	MGO	AL2O3	SIO2	K2O	CAO	TIO2	CR2O3	MNO	FEO	TOTAL
SSHGNT	0 00	11 51	21 15	38 87	0 00	4 05	0 01	0.02	0 64	22.40	98 60
SSHGNT	0 06	11 08	21 65	38 49	0 00	4 45	0.02	0.02	0 59	22 27	98 60
SSHGNT	0 00	11 42	21 84	38 58	0 00	4 36	0.02	0.03	0 60	21.98	98 80
SSHGNT	0 01	10.88	21 81	38 84	0 00	4 36	0 01	0 02	0 57	22.70	99 20
SSHGNT	0 01	10 88	21.81	38 84	0 00	4 36	0 01	0 02	0 57	22.70	99 20
SSHGNT	0 00	12.04	22 20	39 12	0 02	4 23	0 05	0 00	0 43	21.18	99 26
SSHGNT	0 06	12 02	22.68	38 79	0 00	3 78	0.07	0.00	0 52	21.35	99 35
SSHGNT	0 02	12 28	22.93	39 34	0 00	4 05	0.07	0 00	0 46	20.76	99 35
SSHGNT	0 03	11 28	22 13	38 39	0 00	4 39	0 01	0 00	0 61	22.61	99 40
SSHGNT	0 02	11 25	21 89	39 03	0 01	4 35	0 00	0 04	0 48	22 63	99 70
SSHGNT	0 05	11 83	23 14	38 72	0 07	3 85	0.03	0 00	0.52	21.48	99 88
SSHGNT	0 01	12 07	23 18	38 72	0 00	3 76	0.05	0 00	0 40	21.72	99 92
SSHGNT	0 07	12 16	23 32	37 95	0 11	4 30	0 09	0 00	0 32	21.75	100 08
SSHGNT	0 02	11 39	21 94	39 14	0.01	4 44	0.00	0 02	0 56	22.60	100 10
SSHGNT	0 02	11 39	21 94	39 14	0 01	4 44	0 00	0 02	0 56	22.60	100 10
SSHGNT	0 07	12 29	23 22	37 99	0 02	4 22	0.05	0 00	0 42	21 85	100 14
SSHGNT	0 05	11 75	22.35	38 70	0 00	4 42	0 00	0 02	0 57	22 41	100 20
SSHGNT	0 05	11 89	22.26	38 69	0 02	4 16	0 09	0 00	0 44	22 59	100 20
SSHGNT	0 10	12 14	22.76	38 72	0 08	4 13	0.04	0 00	0 45	22 14	100 57
SSHGNT	0 05	12.03	22 69	38 82	0 04	4 50	0 09	0 00	0 45	22.25	100 90
SSHGNT	0 09	11 98	23.05	39 55	0 00	3 56	0.06	0 00	0 52	22 30	101 10
SSHGNT	0 00	12.08	23 12	38 63	0 04	4 68	0 07	0 00	0 49	22 04	101 10
SSHGNT	0 05	12 28	23 10	38 39	0 05	4 00	0 02	0 00	0 34	22 91	101 14
SSHGNT	0 02	11 29	22.05	39 55	0 01	4 50	0 02	0 02	0 53	23 30	101 20
SSHGNT	0.00	12 20	23.19	39 19	0.03	3.88	0 06	0 00	0 38	22 54	101 44
SSHGNT	0 00	11 35	22 67	39 53	0 01	4 44	0 02	0 06	0 63	23.12	101 80
SSHGNT	0 02	12 47	22 88	39 41	0 02	4 11	0 07	0 00	0 50	22.35	101 84
SSHGNT	0 07	12 33	23 04	39 70	0 05	3.71	0 08	0 00	0.43	22.45	101 86
SSHGNT	0 00	12.25	23.13	39 09	0 01	4 71	0.05	0.00	0 46	22.21	101 93
AVERAGE		11.79								22 25	
1 SIGMA ERROR		0 46								0 56	
RELATIVE ERROR		3 92	%							2.52	%

Table A4-2: Modified microprobe analyses for error assessment for samples JNC-86-1073 and JNC-86-403. AOR = original; APM = modified analyses (Fe, Mg and/or Ca increased or decreased in proportion to the relative analytical errors calculated for electron microprobe data).

Sample:	1073	1073	1073	1073	1073	1073	403	403	403	403	403	403
Min:	GNT	GNT	BIO	BIO	PLG	PLG	GNT	GNT	CPX	CPX	PLG	PLG
Code:	AOR	APM	AOR	APM	AOR	APM	AOR	APM	AOR	APM	AOR	APM
SiO2	40 00	40 00	35 77	35 77	60 70	60 70	40 22	40 22	52 79	52 79	64 13	64 13
TiO2	0 00	0 00	3 80	3 80	0 00	0 00	0 00	0 00	0 18	0 18	0 00	0 00
Al2O3	21 47	21 47	16 60	16 60	24 28	24 28	21 04	21 04	2 59	2 59	20 84	20 84
Cr2O3	0 01	0 01	0 03	0 03	0 00	0.00	0 06	0 06	0 03	0 03	0 00	0 00
FeO	29 73	30 48	13 48	13 14	0 03	0 03	24 28	23 67	11 45	11 74	0 00	0 00
MnO	2 04	2 04	0 01	0 01	0 00	0 00	2 75	2 75	0 60	0 60	1 13	1 13
MgO	8 68	8 36	14 12	14 64	0 00	0 00	4 66	4 83	11 79	11 36	0 00	0 00
CaO	0 89	0 86	0 00	0 00	5 97	6 19	8 75	9 07	20 39	19 64	3 08	2 97
Na2O	0 02	0 02	0 06	0 06	8 63	8 63	0 04	0 04	1 35	1 35	9 30	9 30
K2O	0.00	0 00	9 06	9 06	0 14	0.14	0 00	0 00	0 01	0 01	0 25	0 25
Sum	102 84	103 24	92 93	93 11	99 75	99 97	101 80	101 68	101 18	100 29	98 73	98 62
Si	3.029	3 027	2 717	2 708	2 710	2 706	3 080	3 078	1 964	1 979	2 873	2 875
Ti	0 000	0 000	0 217	0 216	0 000	0 000	0 000	0 000	0 005	0 005	0 000	0 000
Al	1 916	1 915	1 486	1 481	1 278	1 276	1 899	1 898	0 114	0 114	1 101	1 101
Cr	0 001	0 001	0 002	0 002	0 000	0 000	0 004	0 004	0 001	0 001	0 000	0 000
Fe	1 883	1 929	0 856	0 832	0 001	0 001	1 555	1 515	0 356	0 368	0 000	0 000
Mn	0 131	0 131	0 001	0 001	0 000	0 000	0 178	0 178	0 019	0 019	0 043	0 043
Mg	0 980	0 943	1 598	1 652	0 000	0 000	0 532	0 551	0 654	0 635	0 000	0 000
Ca	0 072	0 070	0 000	0 000	0 286	0 296	0 718	0 744	0 813	0 789	0 148	0 143
Na	0 003	0 003	0 009	0 009	0 747	0 746	0 006	0 006	0 097	0 098	0 808	0 808
K	0 000	0 000	0 878	0 875	0 008	0 008	0 000	0 000	0 000	0 000	0 014	0 014
Sum	8 014	8 017	7 765	7 776	5 029	5 033	7 972	7 974	4 023	4 008	4 987	4 985
XMg	0 342	0 328	0 651	0 665	0 000	0 000	0 255	0 267	0 647	0 633	0 000	0 000
AlT	0 000	0 000	1 283	1 292	0 290	0 294	0 000	0 000	0 036	0 021	0 127	0 125
AlO	1 916	1 915	0 204	0 189	0 987	0 982	1 899	1 898	0 077	0 093	0 974	0 977

Table A4-3: Results of error calculations (ERR=error; ABS=absolute).

	PRESSURE	TEMPERATURE			
		ORIGINAL	WITH ERR		ABS ERR
FOR GNT-BIO:	2	750.63	711.15	+/-	39.48
	4	759.91	720.08	+/-	39.83
	6	769.20	729.01	+/-	40.19
	8	778.48	737.93	+/-	40.55
	10	787.77	746.86	+/-	40.91
FOR GNT-CPX:	2	787.42	820.33	+/-	32.92
	4	793.48	826.54	+/-	33.06
	6	799.54	832.74	+/-	33.20
	8	805.60	838.94	+/-	33.34
	10	811.66	845.15	+/-	33.49

Table A4-4: Comparison of P-T results for garnet-clinopyroxene geothermometery where FeTOT is assumed equal to Fe+2 (FeTOTAL) and where Fe+3 is calculated by charge balance (Fe+2/Fe+3).

SAMPLE	P (Kb)	TEMPERATURE (C)	
		FeTOTAL	Fe+2/Fe+3
403	2	815	816
424	2	740	740
5039	2	835	832

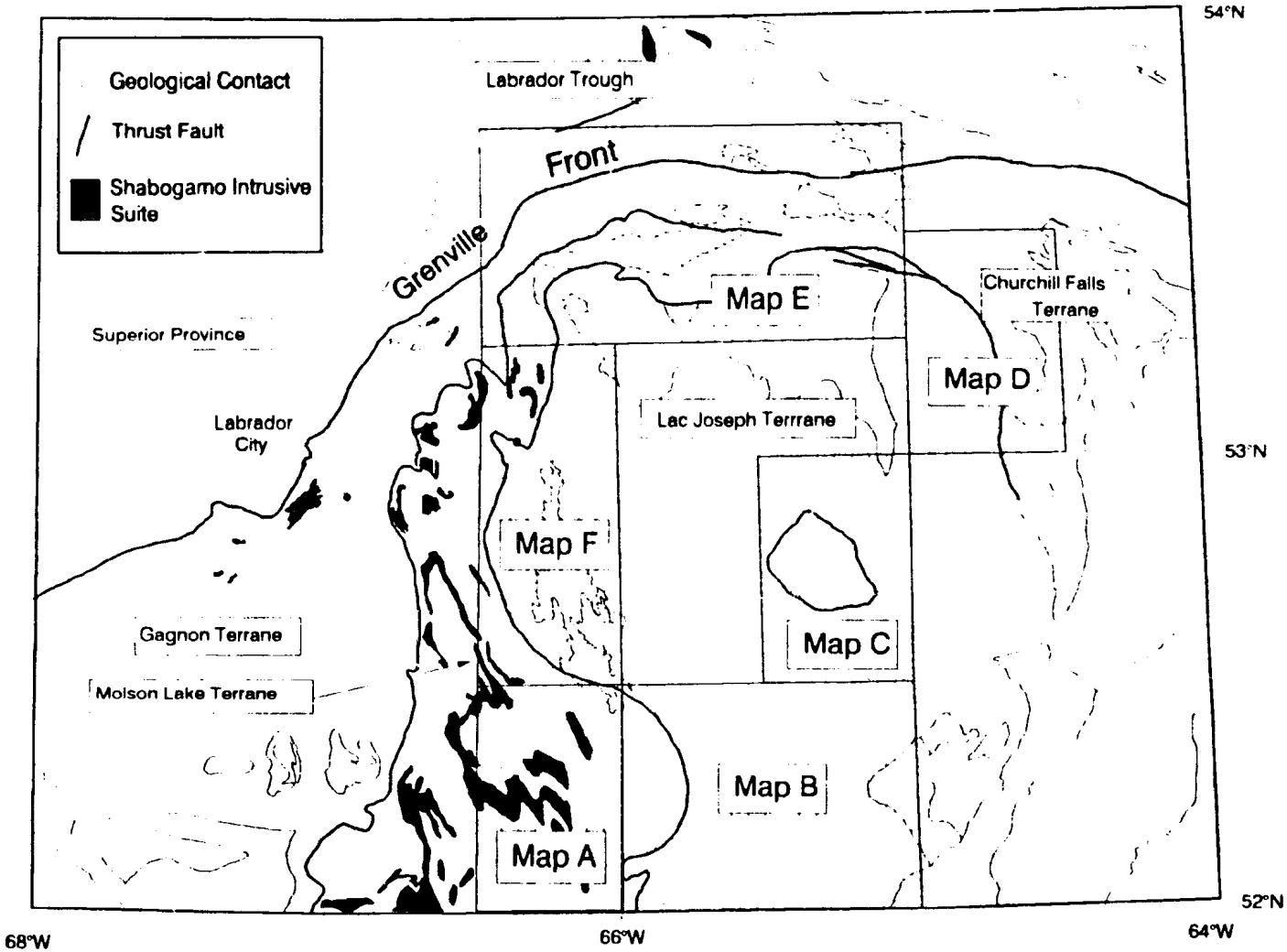

Location of field maps in back pocket; legends for maps are also in pocket.

LEGEND (all maps)

GRENVILLIAN OR YOUNGER (not shown on maps due to scale)

10. Diabase dykes; late, pristine dykes containing plagioclase - clinopyroxene

9. Granitoid pegmatite dykes

POST-LABRADORIAN TO PRE-GRENVILLIAN

8. Equigranular granitoid suite; small granitoid bodies intruding supracrustal rocks of the Lac Joseph Terrane; massive to strongly foliated, inclusions of mafic paragneiss

7. Fleur-de-May granitoid plutonic suite: marginal phase to the Atikonak Anorthosite Massive; equigranular to K-feldspar megacrystic

6. Shabogamo Intrusive Suite: gabbroic to gabbronoritic intrusive rocks apparently exclusive to the Molson Lake Terrane; characteristically coronitic with garnet and/or amphibole separating cores of clinopyroxene from surrounding plagioclase

LABRADORIAN OROGENY

5. Molson Lake Terrane equigranular granitoid suite: partially recrystallized, typically strongly foliated and lineated with accessory minerals dependent on local metamorphic grade

4. Basic intrusive suite including the Ossokmanuan Intrusive Suite: recrystallized and unrecrystallized massive to foliated basic intrusive rocks; local preservation of primary cumulate and ophitic textures

3. Rapakivi K-feldspar megacrystic granite suite; massive to foliated, contains accessory orthopyroxene, amphibole, biotite and magnetite

2. Equigranular granite; foliated, medium-grained granite containing biotite, garnet and sillimanite; indistinct contacts with host supracrustal rocks

1. Supracrustal rocks of the Lac Joseph Terrane: pelitic composition dominates with interlayered semipelites, psammites and mafic gneisses; 1a - pelitic paragneiss; 1a-m - pelitic paragneiss identical to 1a except muscovite has replaced sillimante in restite; 1b - semipelitic paragneiss locally interlayered with 1a; 1c - psammitic paragneiss; 1d - mafic gneiss; agmatic to strongly foliated gneiss; 1e - light coloured, medium grained, massive crystalline marble;

Geology of Maps A and B by J.N. Connelly and P. Scowen, 1986.
Geology of Maps C, D, E and F by J.N. Connelly and K. Manser

Geological cartography of Maps A and B by Cartography Department, Newfoundland Dept. of Mines.

Field work upon which these maps are based was financed under the Canada/Newfoundland Mineral Development Agreement (1984-1989).

SYMBOLS FOR MAPS A AND B

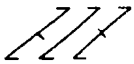
S1 gneissic layering (inclined, vertical, horizontal)

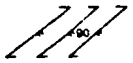
S2 foliation (inclined, vertical, horizontal)


F2 fold axial plane (inclined, vertical, horizontal)


S1 foliation/F2 fold axial plane (inclined, vertical, horizontal)


L1 lineation; mineral and extension lineations


L2 lineation


F2 minor fold axes


F2 fold axis/L1 lineation

Ductile mylonite zones

Late brittle faults

SYMBOLS FOR MAPS C, D, E AND F


S1 gneissic layering


Mylonitic planar fabrics


F2 fold axial plane


S1 gneissocity/F2 axial planes


F3 fold axial planes


L1 lineation


Mylonitic lineation


F2 fold axis


F2 fold axis/L1 lineation


F3 fold axis

SYMBOLS COMMON TO ALL MAPS


Thrust faults


Geological contacts

Map Scale: 1:100,000

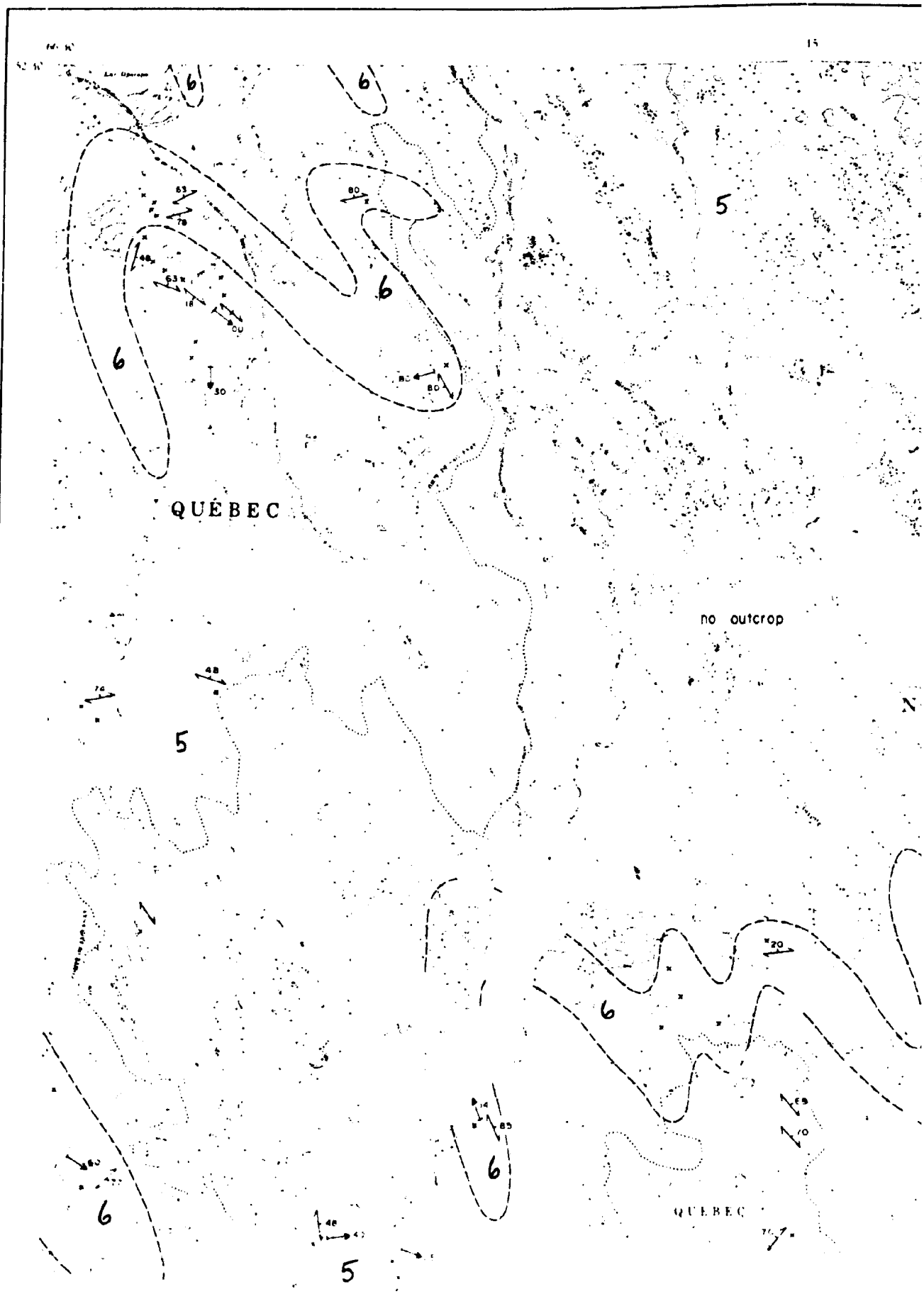
QUÉBEC
no outcrop
QUEBEC
N

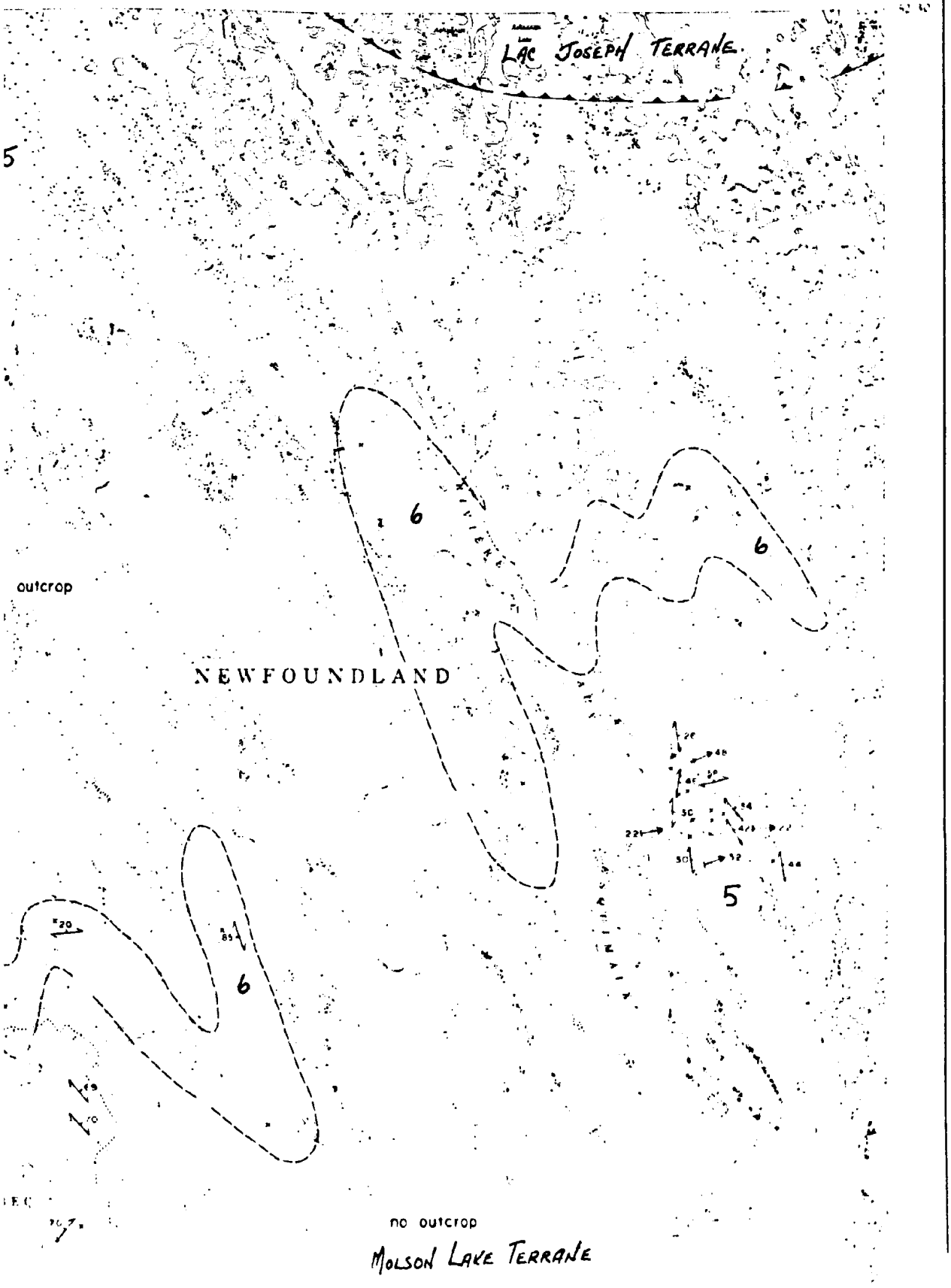
LAC JOSEPH TERRANE.
5
6
6
6
outcrop
NEWFOUNDLAND
5
no outcrop
MOLSON LAKE TERRANE

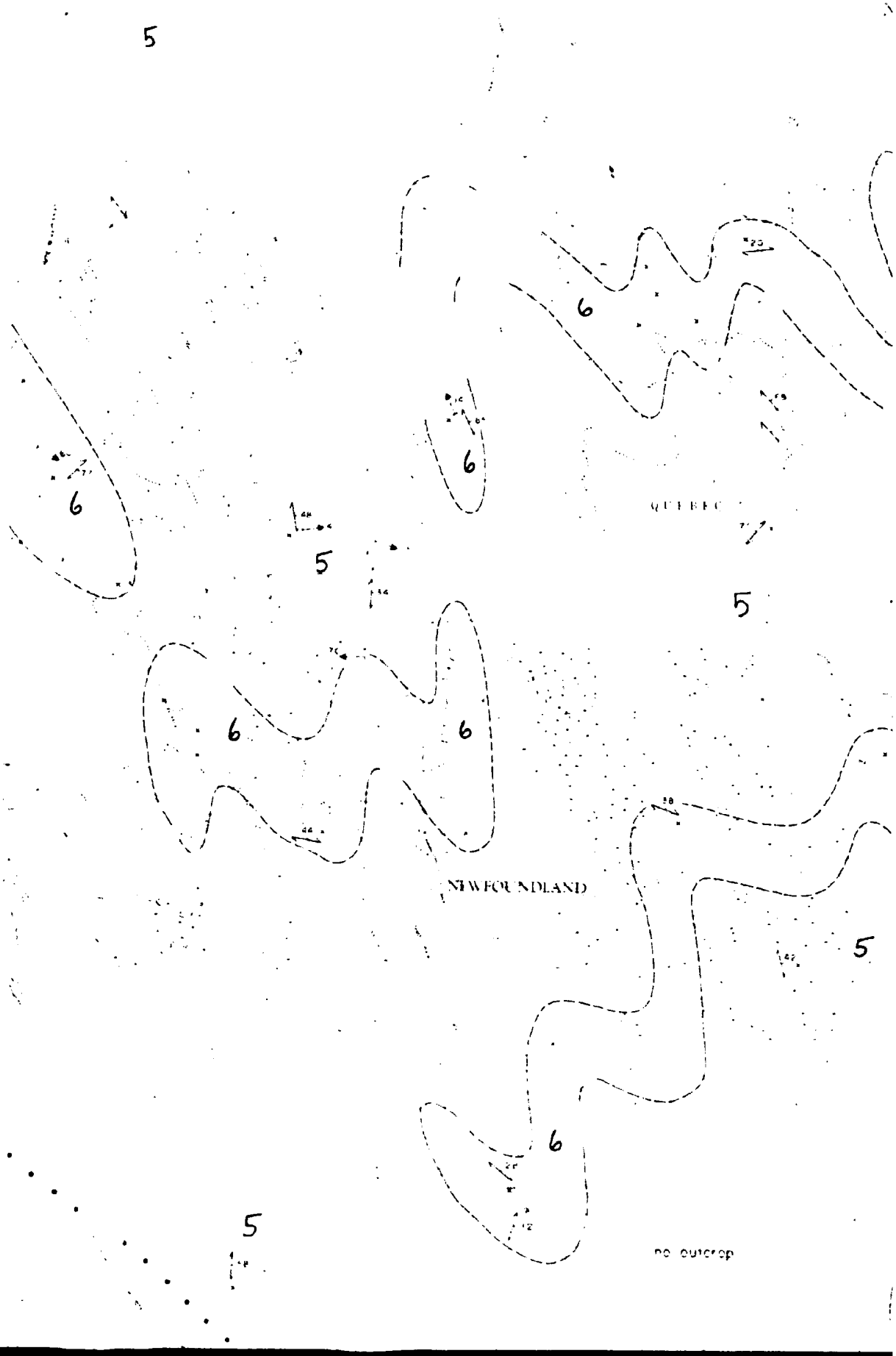
5
6
6
6
5
QUEBEC
5
6
6
NEWFOUNDLAND
5
6
5
PO outcrop

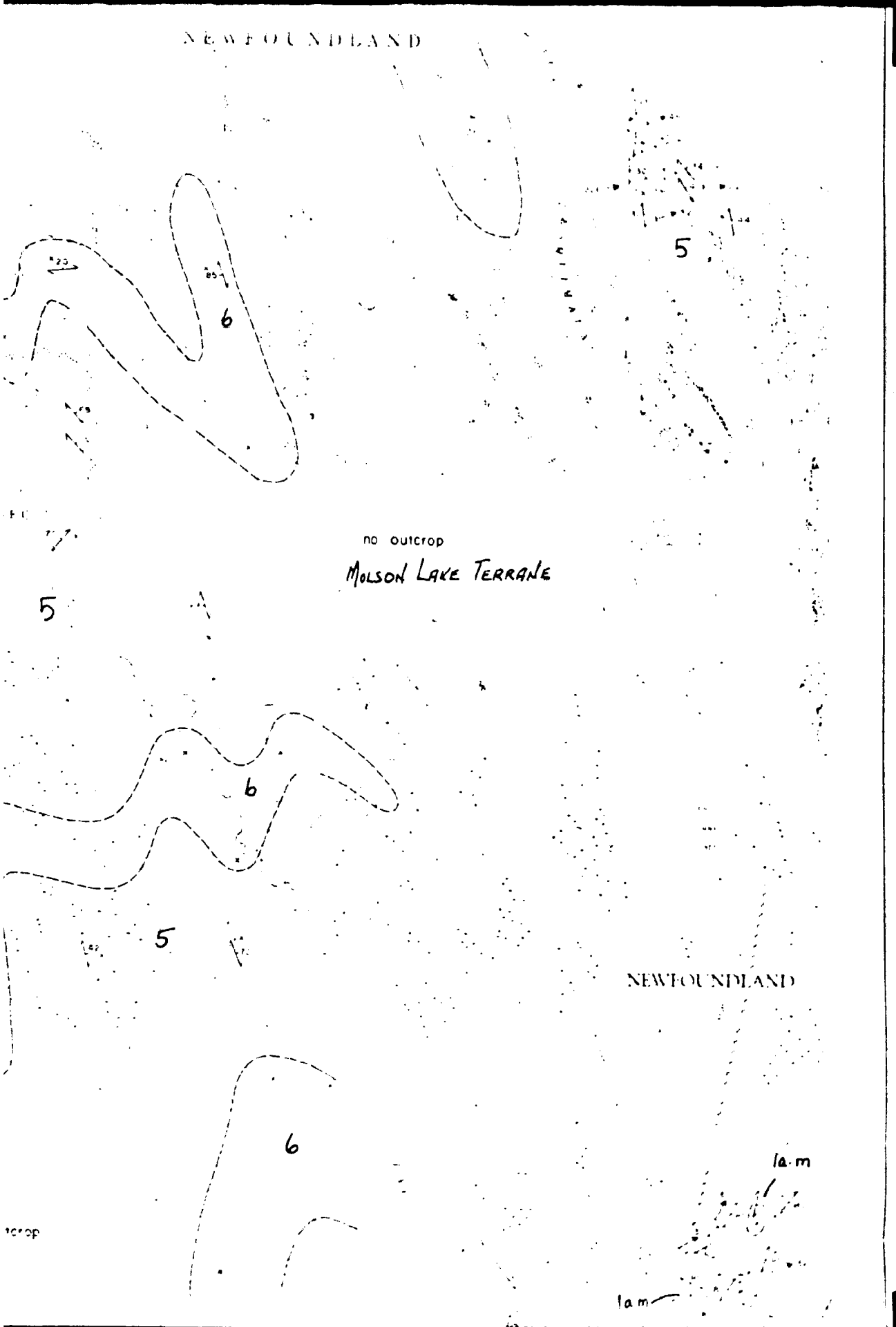
NEWFOUNDLAND
5
6
no outcrop
Molson Lake Terrane
5
6
5
NEWFOUNDLAND
6
1a-m
1a m

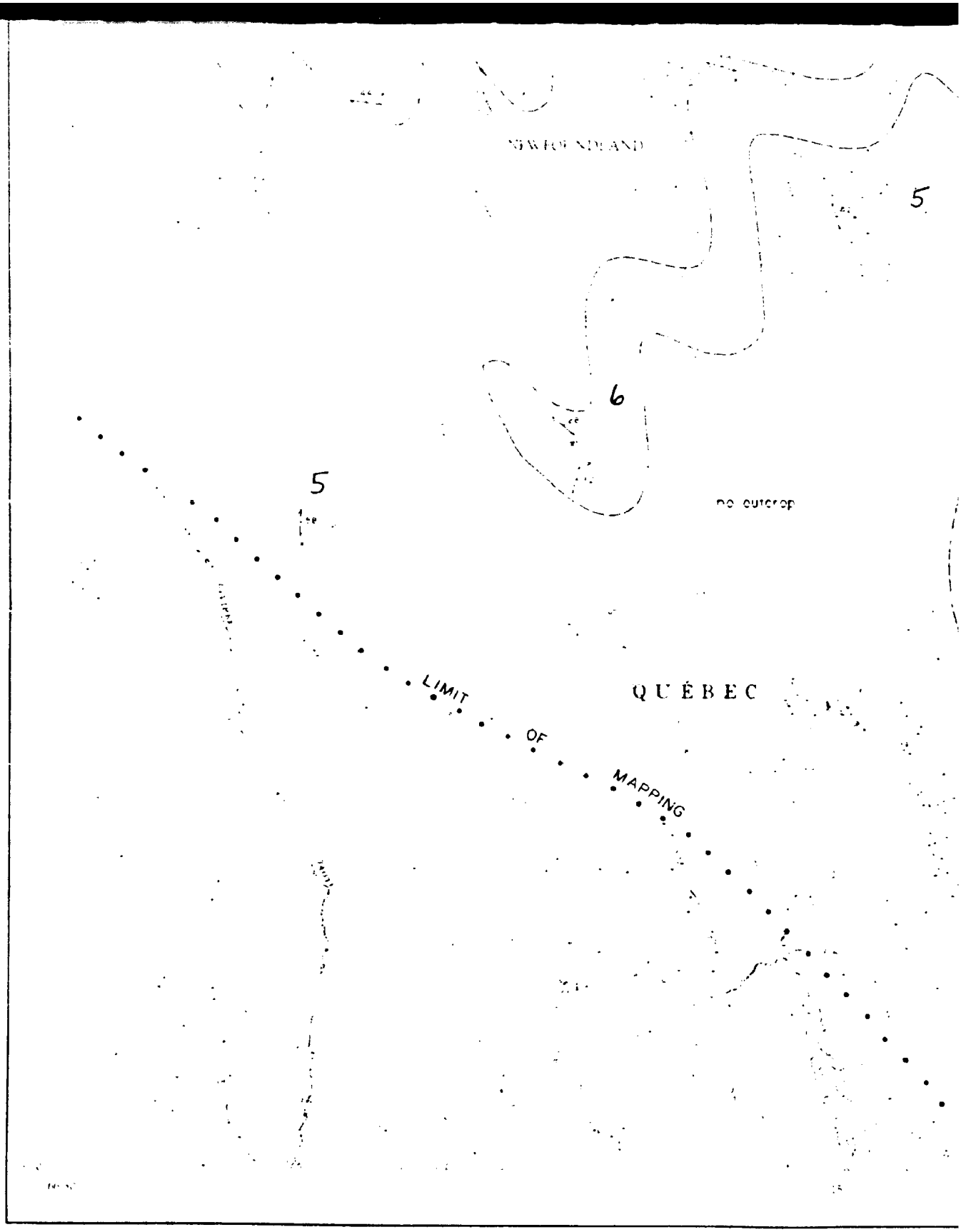
NEWFOUNDLAND
5
6
5
no outcrop
LIMIT
OF
MAPPING
QUÉBEC

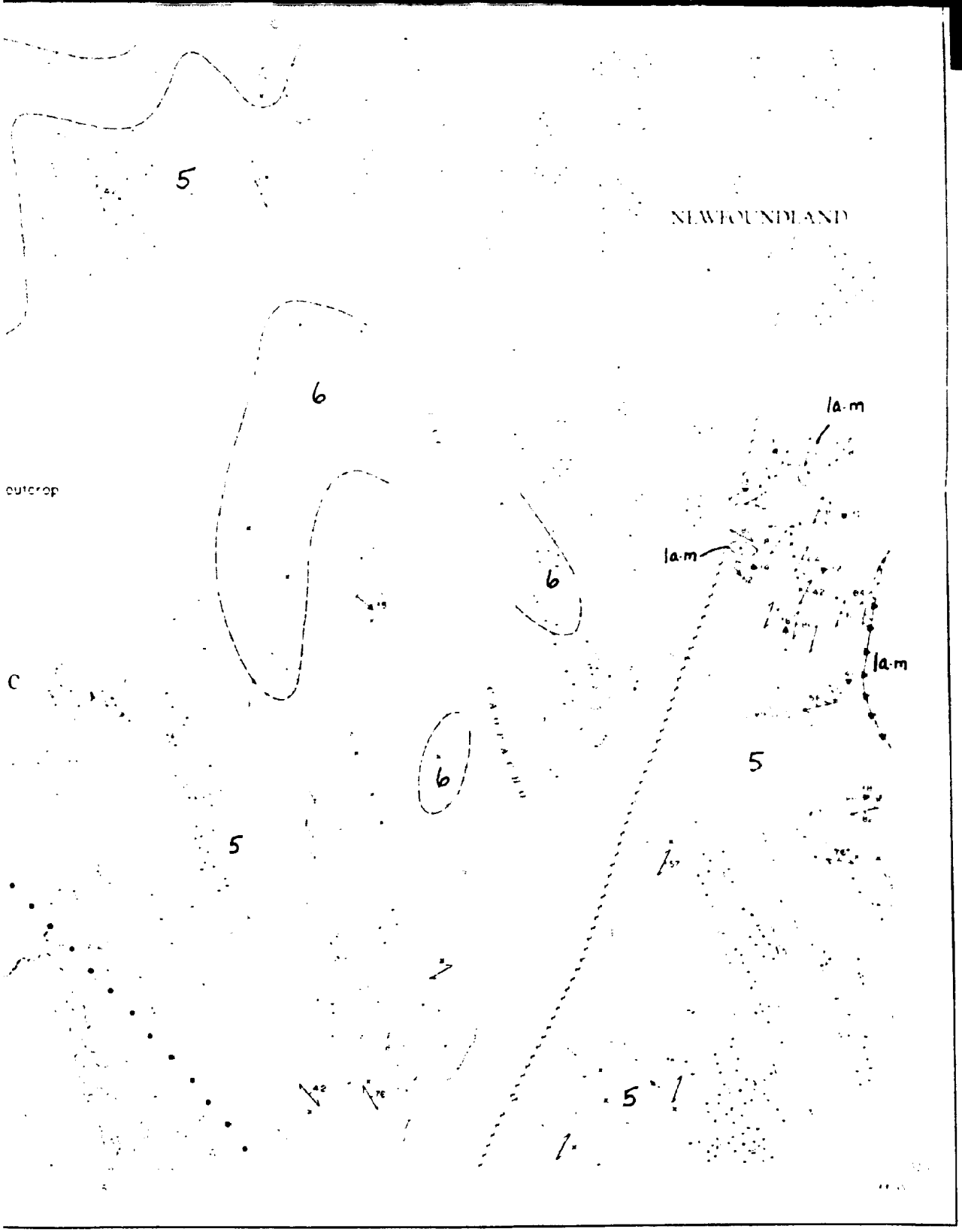
NEWFOUNDLAND
5
6
6
6
5
5
1a-m
1a-m
1a-m
5
5
1
1
outcrop
C

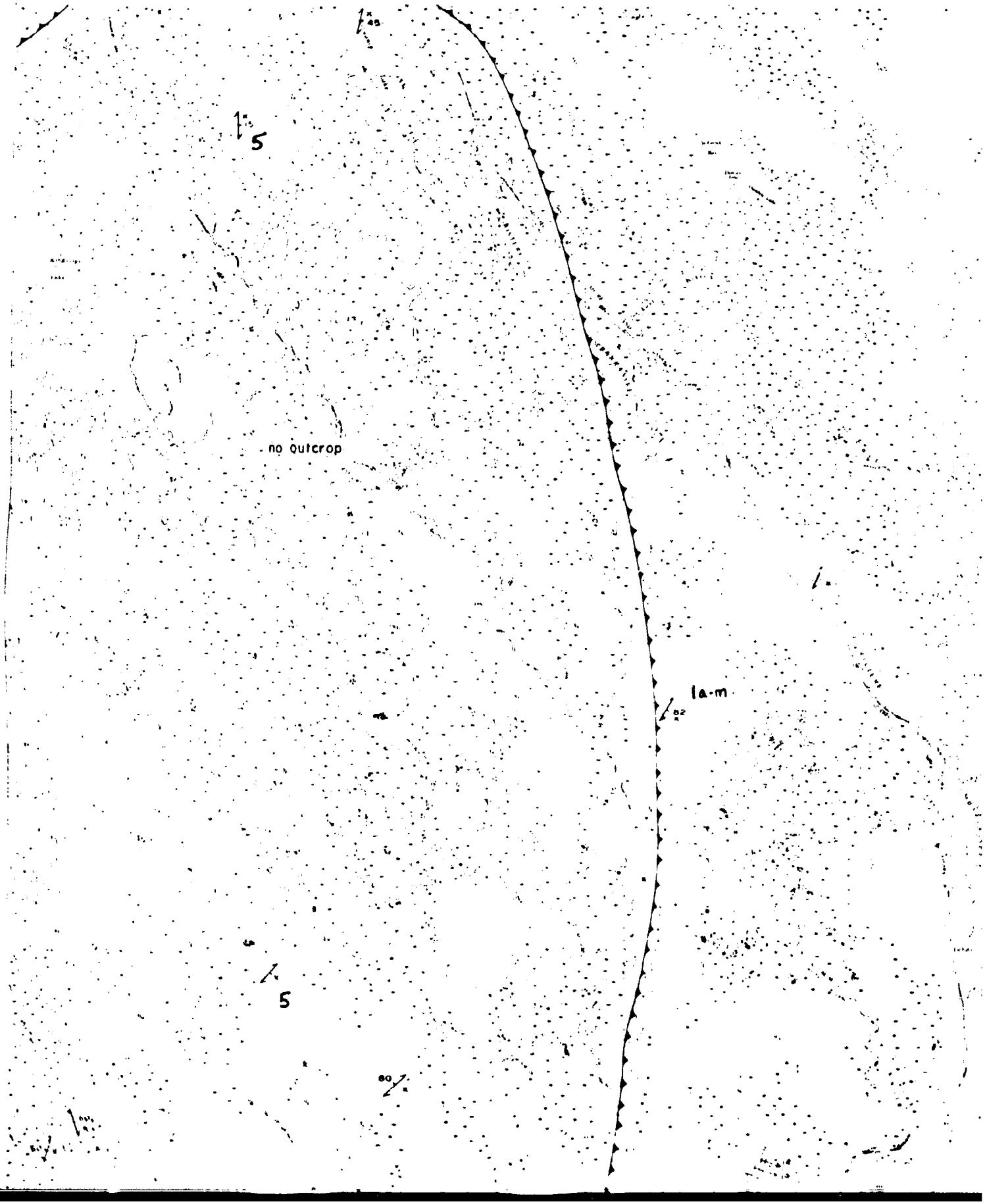
no outcrop
la-m
5
5
80

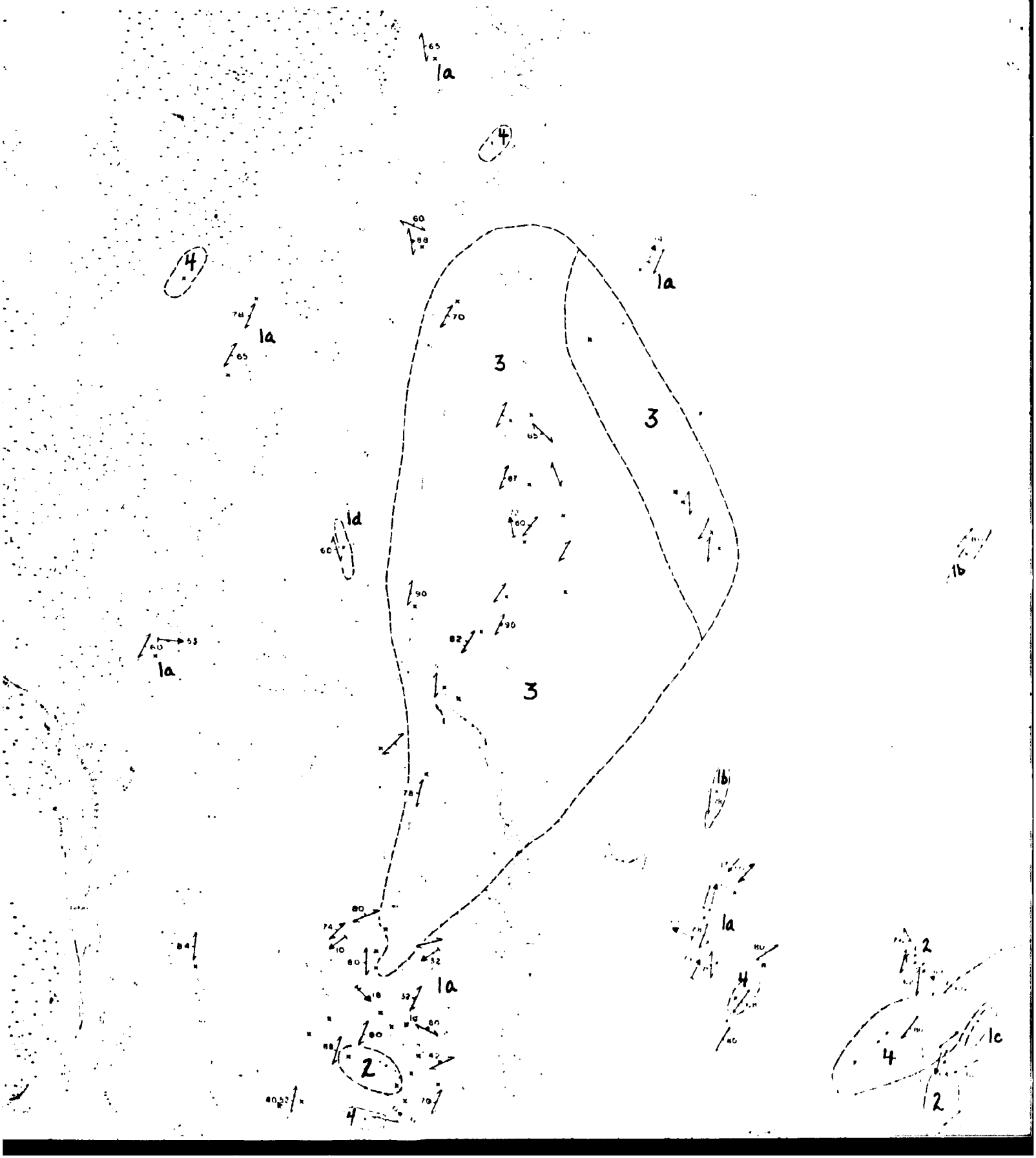
1a
4
3
1d
1b
2
1c

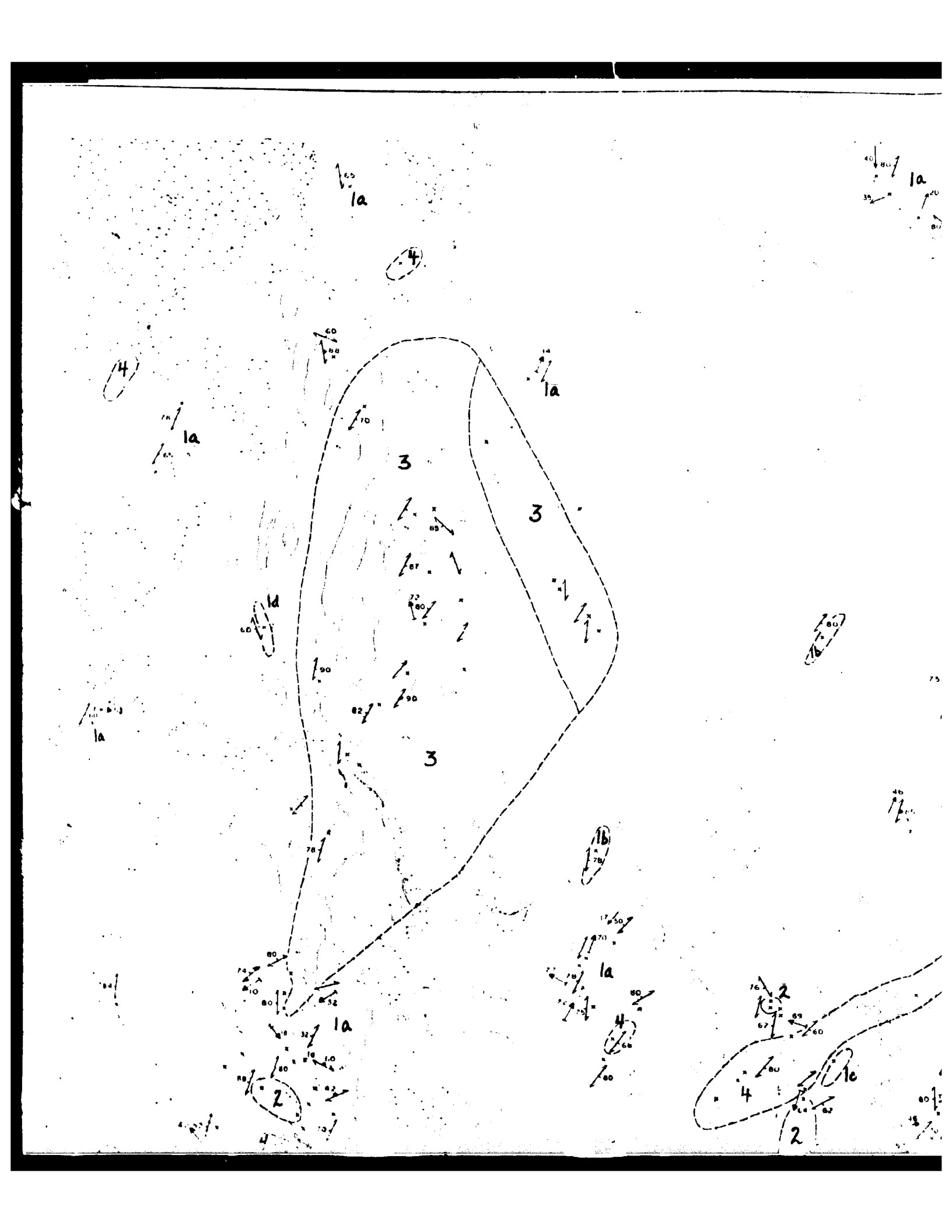
1a
4
3
1d
1b
2
1c

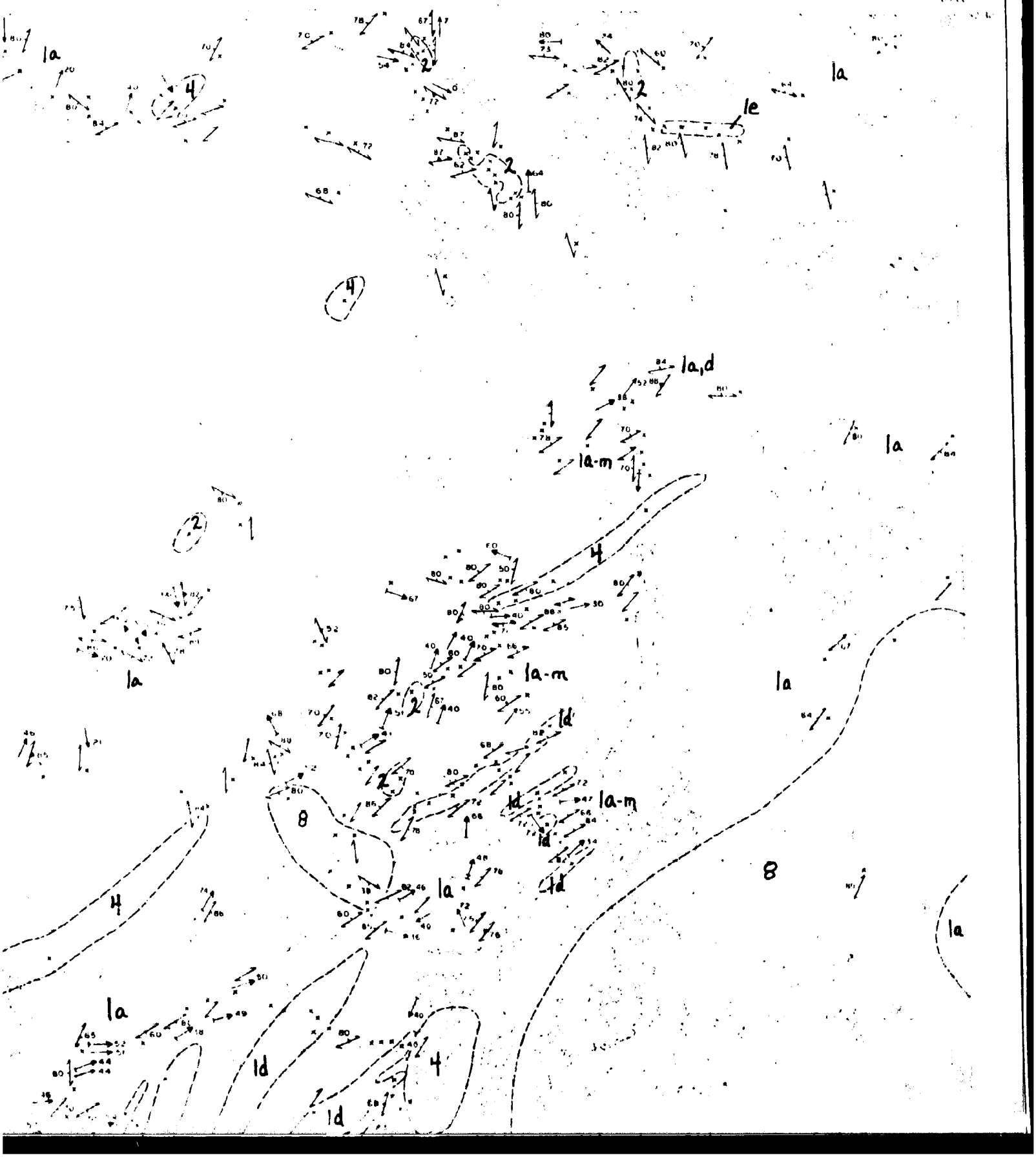
1a
1e
1a,d
1a-m
1d
2
4
8

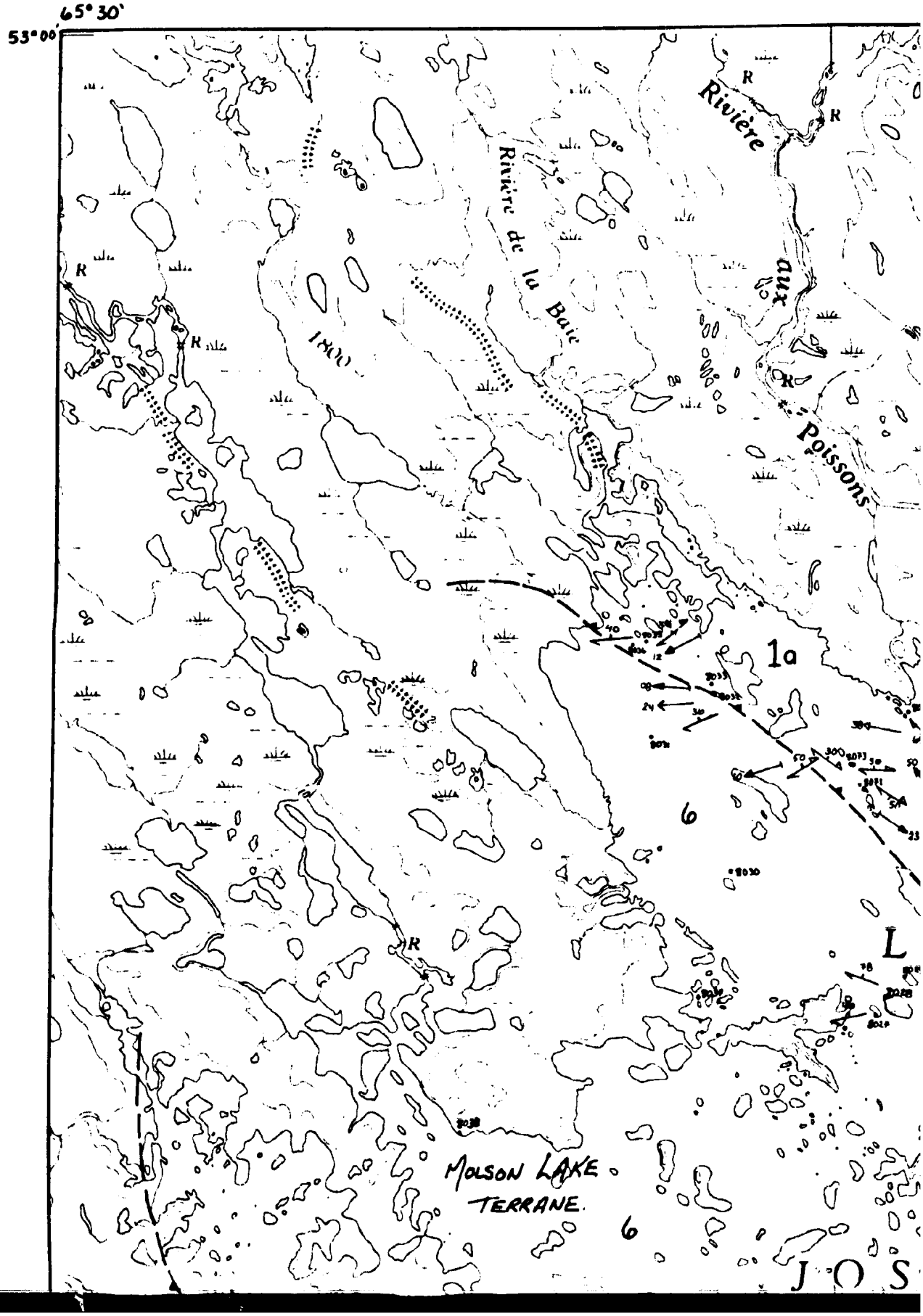
65° 30'
53° 00'
Rivière
Rivière de la Baie
aux
Poissons
1a
6
6
MOLSON LAKE
TERRANE.

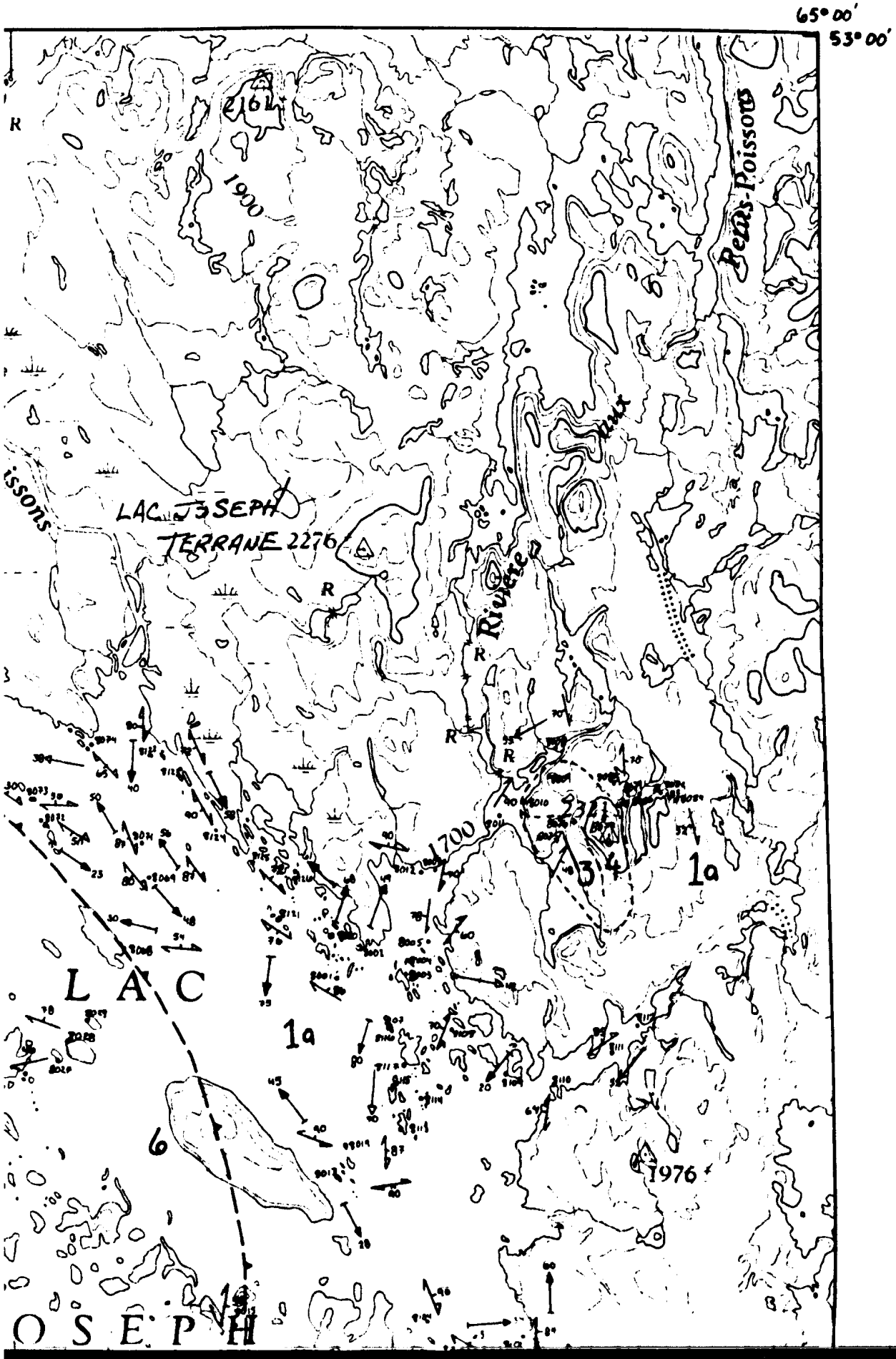
65° 00'
53° 00'
1900
1700
LAC JOSEPH
TERRANE 2276
Rivière
Rivière aux Rochers
Rivière aux Perdrix
Rivière aux Perdrix-Poissons
1a
1a
1976
6
L A C
O S E P H

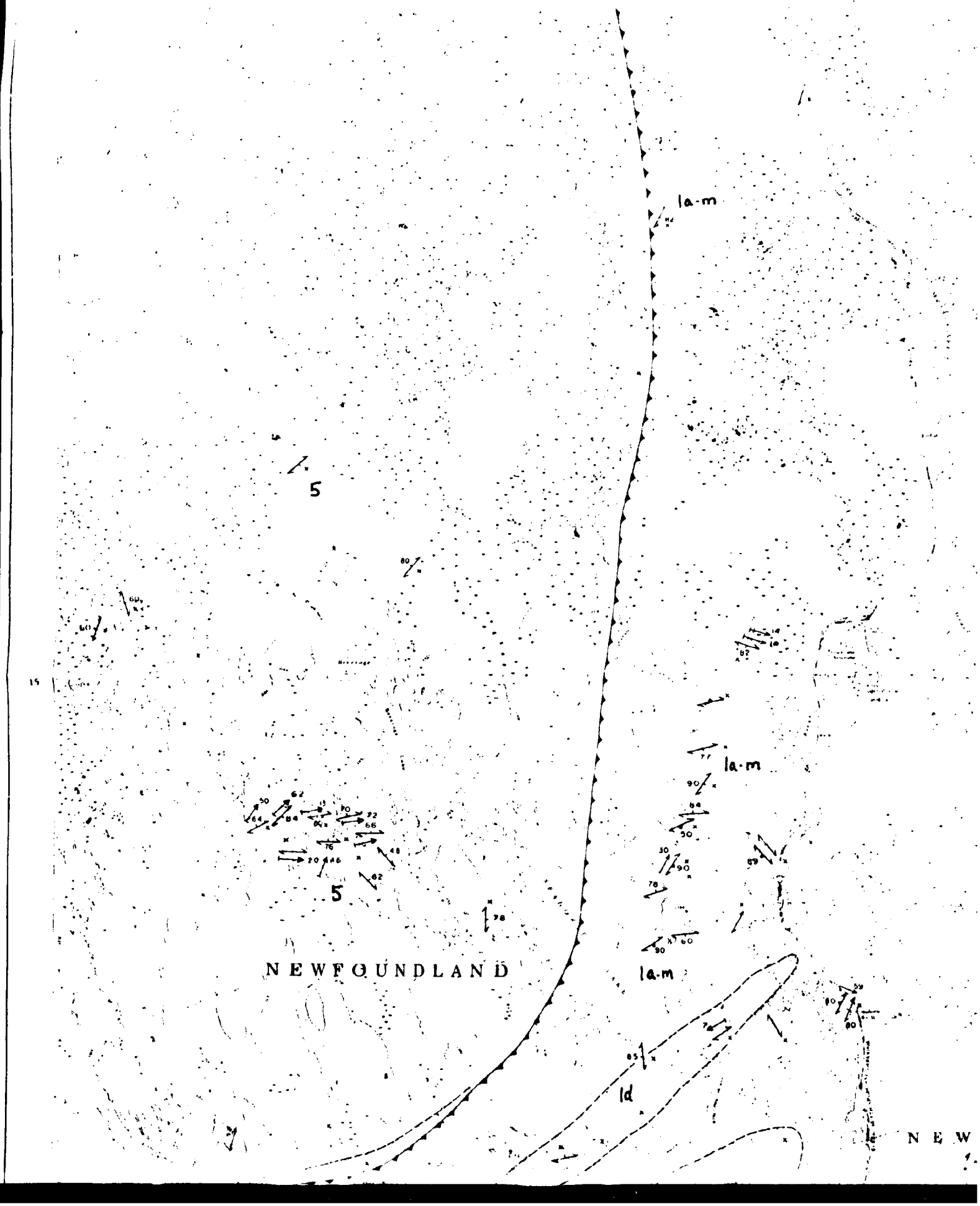
la-m
5
la-m
5
NEWFOUNDLAND
la-m
ld
N E W

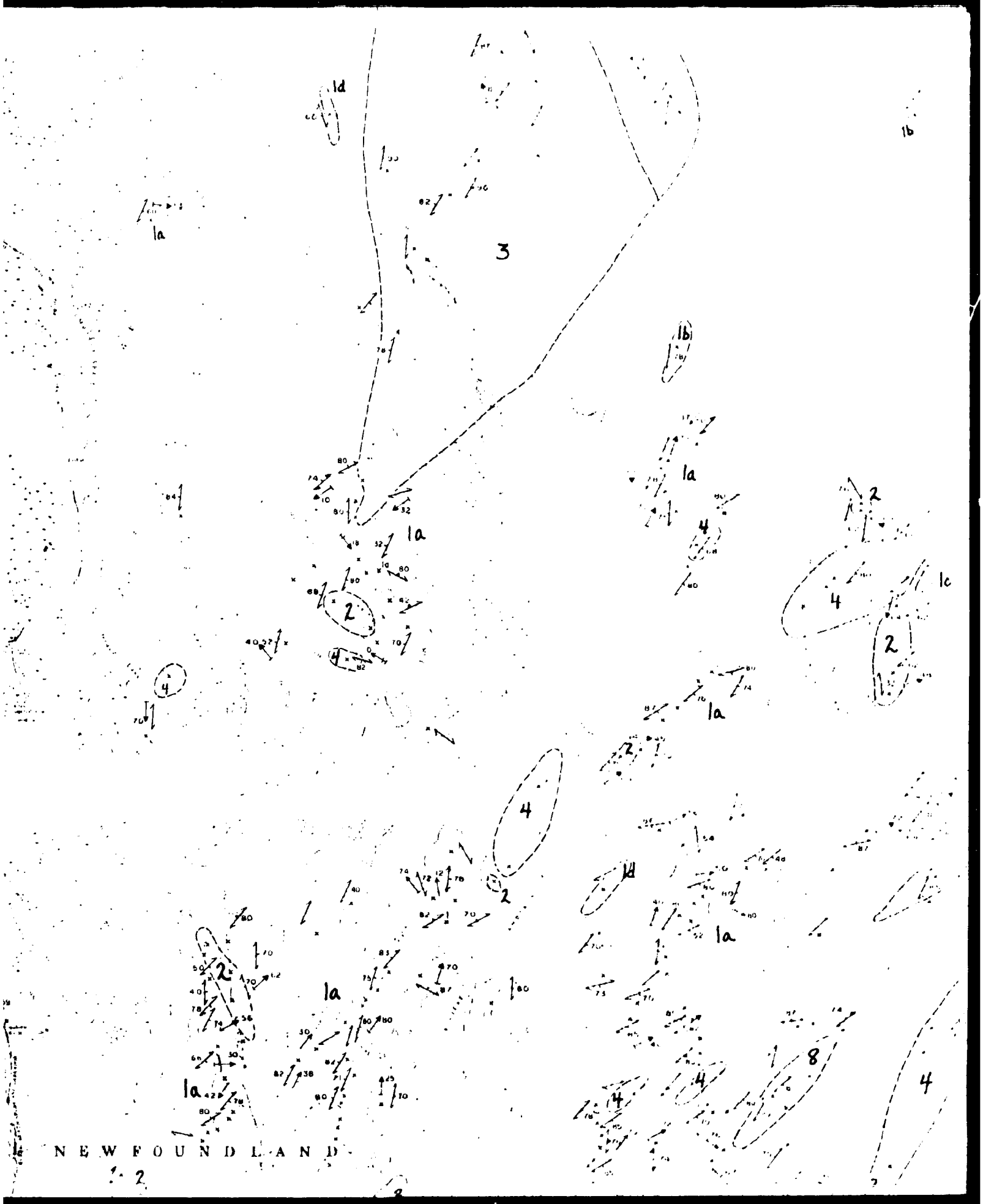
1d
1b
1a
3
1b
1a
1a
2
4
1c
4
2
1a
4
2
2
1a
4
1d
1a
2
1a
4
8
4
NEWFOUNDLAND

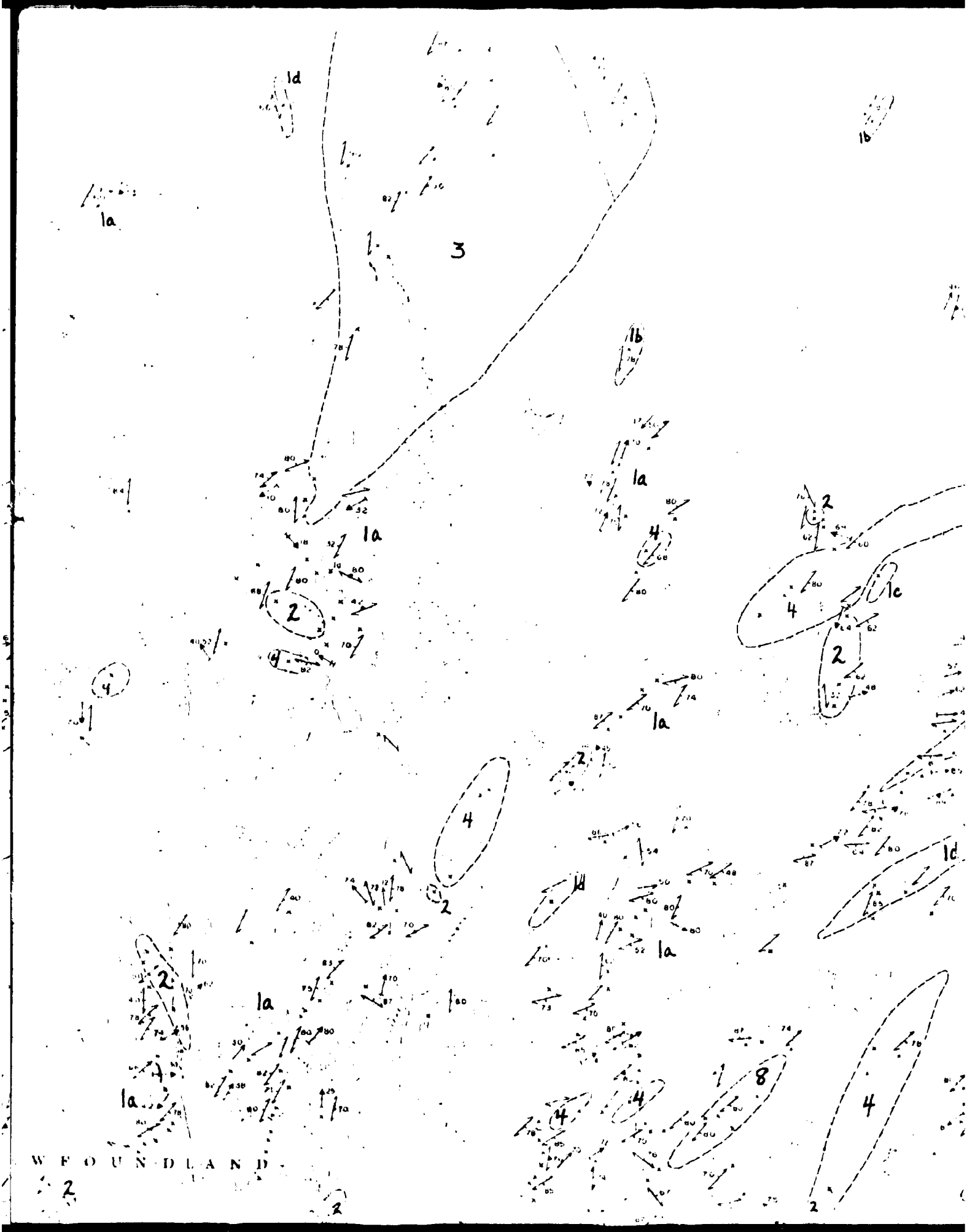
1d
1a
3
1b
1a
1b
1a
4
2
1a
4
2
1c
4
2
1a
2
4
2
1a
1d
1a
1a
2
1a
4
4
8
4
2
2
2
NEWFOUNDLAND

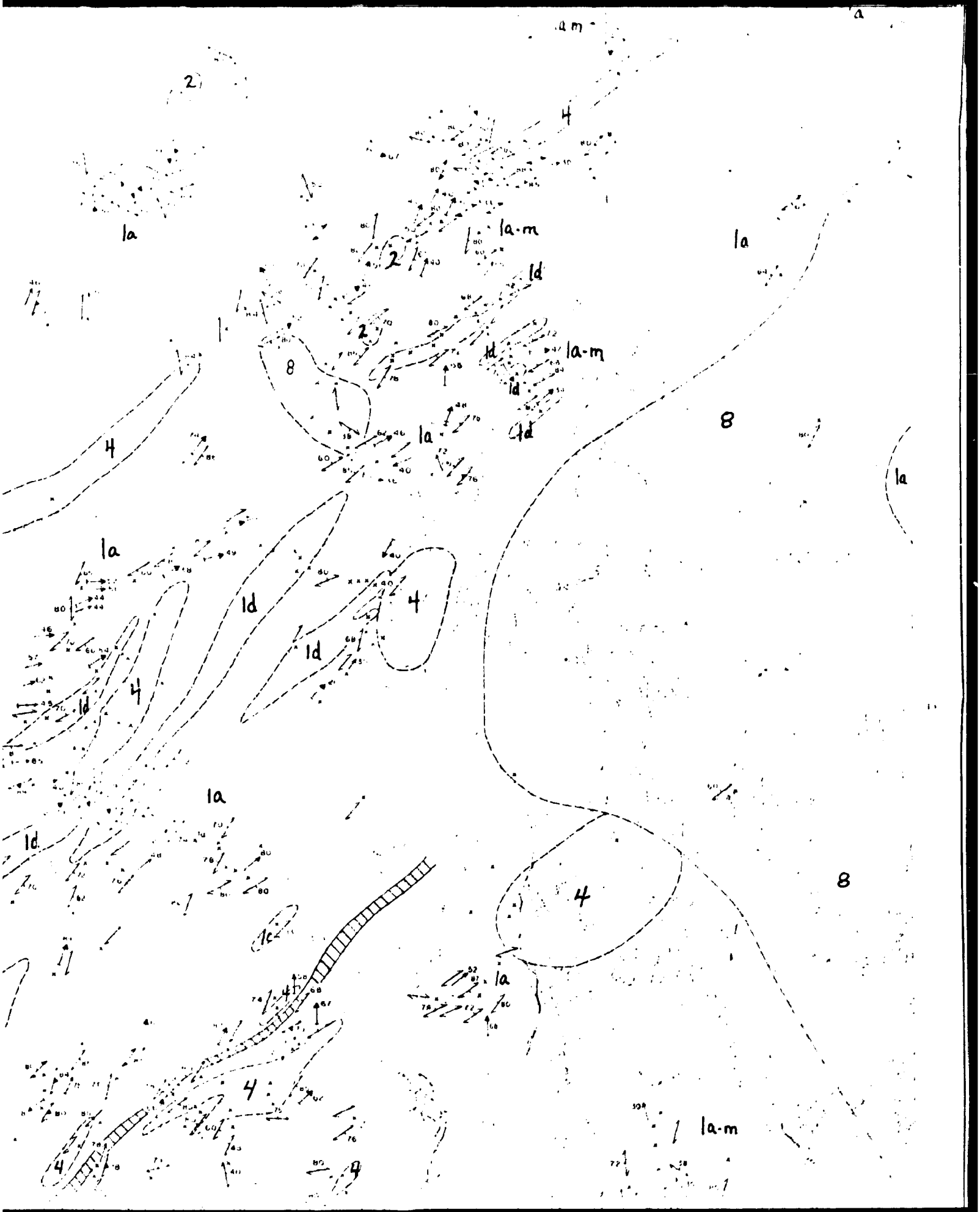
1a-m
2
4
1a
1a-m
1d
2
1d
1a-m
8
1d
1a
4
8
1a
1a
1d
4
1d
4
1d
1a
1d
4
8
1c
4
1a
1a-m
4
4
4

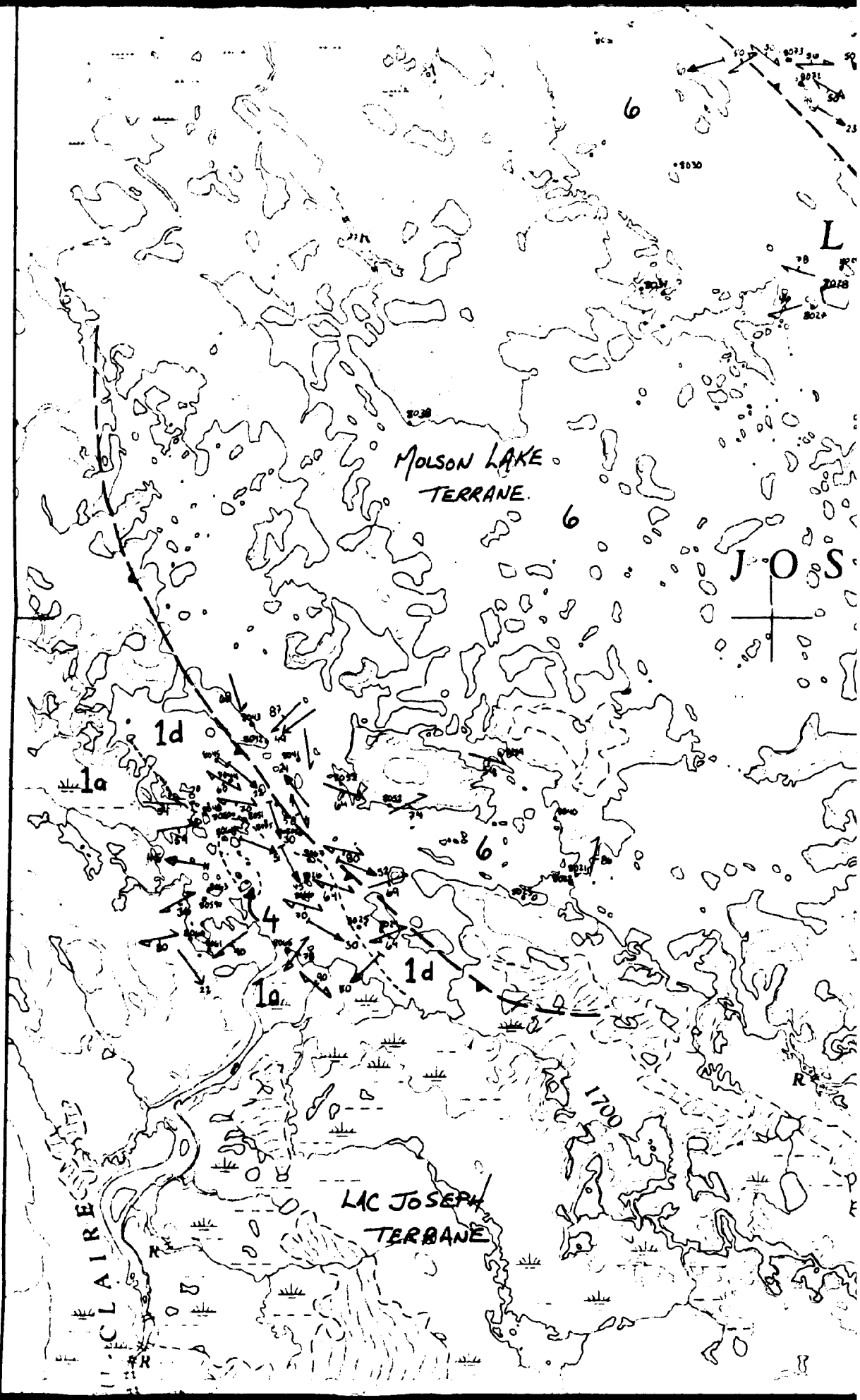
MOLSON LAKE
TERRANE
LAC JOSEPH
TERRANE
CLAIRE
1700
1d
1a
1d
1a
6
6
6
4
L
J O S

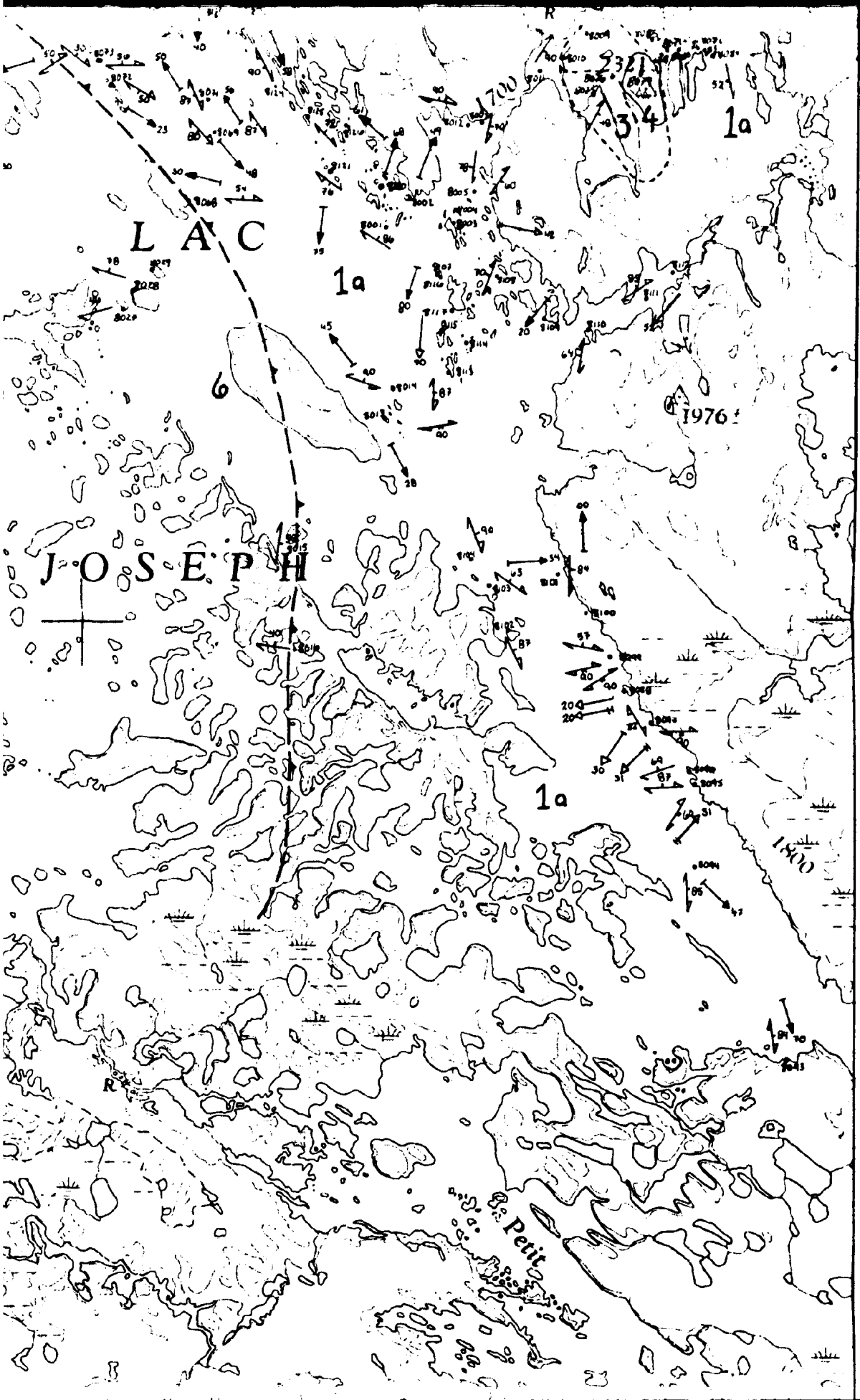
L A C
1a
6
J O S E P H
1a
1a
1976
Petit

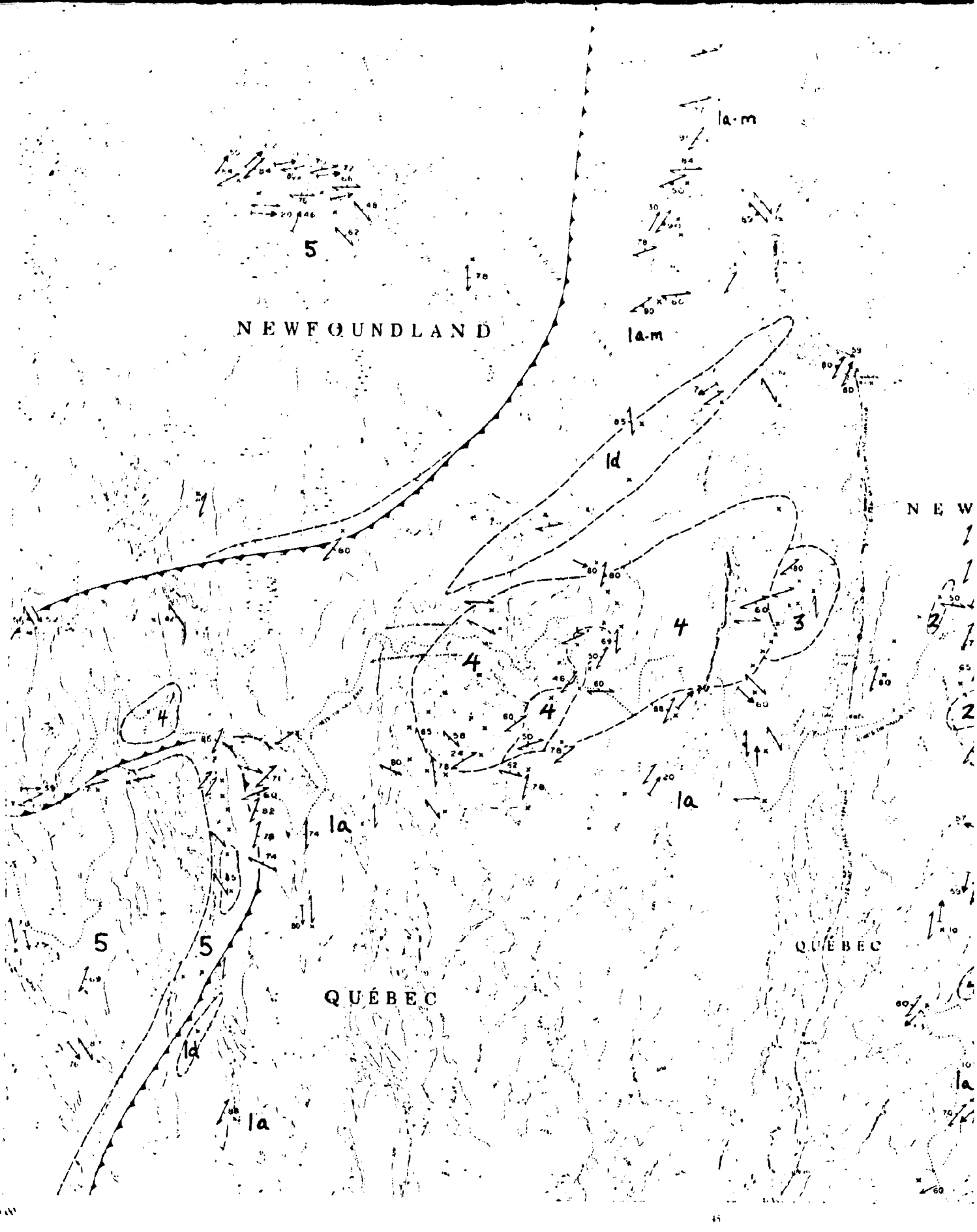
NEWFOUNDLAND
QUÉBEC
QUÉBEC
NEW
1a-m
1a-m
1d
1a
1a
1d
1a
5
5
5
4
4
4
4
3
3
2
1
1
1
1a

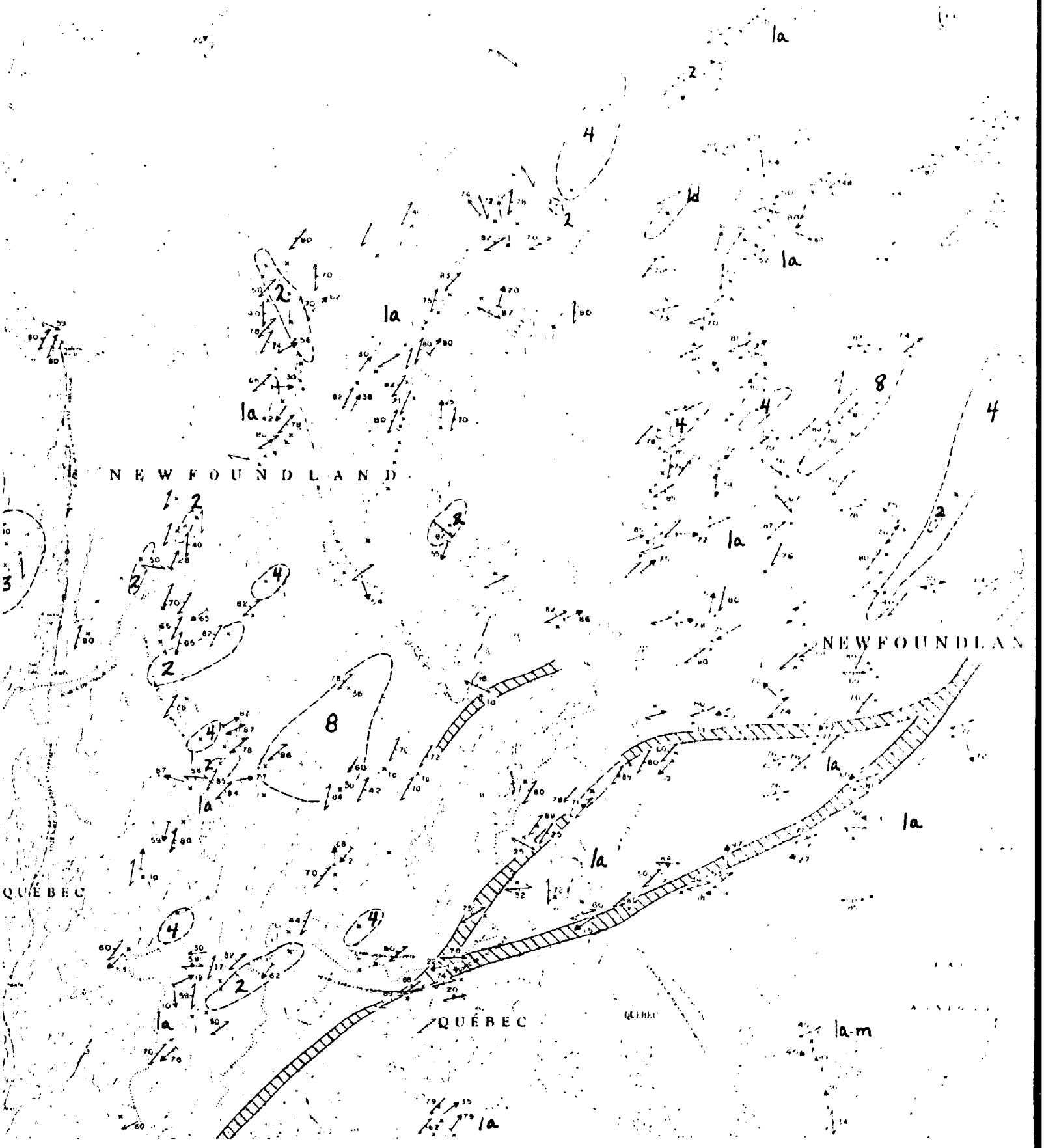
NEWFOUNDLAND
NEWFOUNDLAN
QUÉBEC
QUÉBEC
QUEBEC
1a
1a
1a
1a
1a
1a
1a
1a
1a
1a
1a-m
1d
2
2
2
2
2
2
2
2
2
2
2
3
4
4
4
4
4
4
4
4
8
8

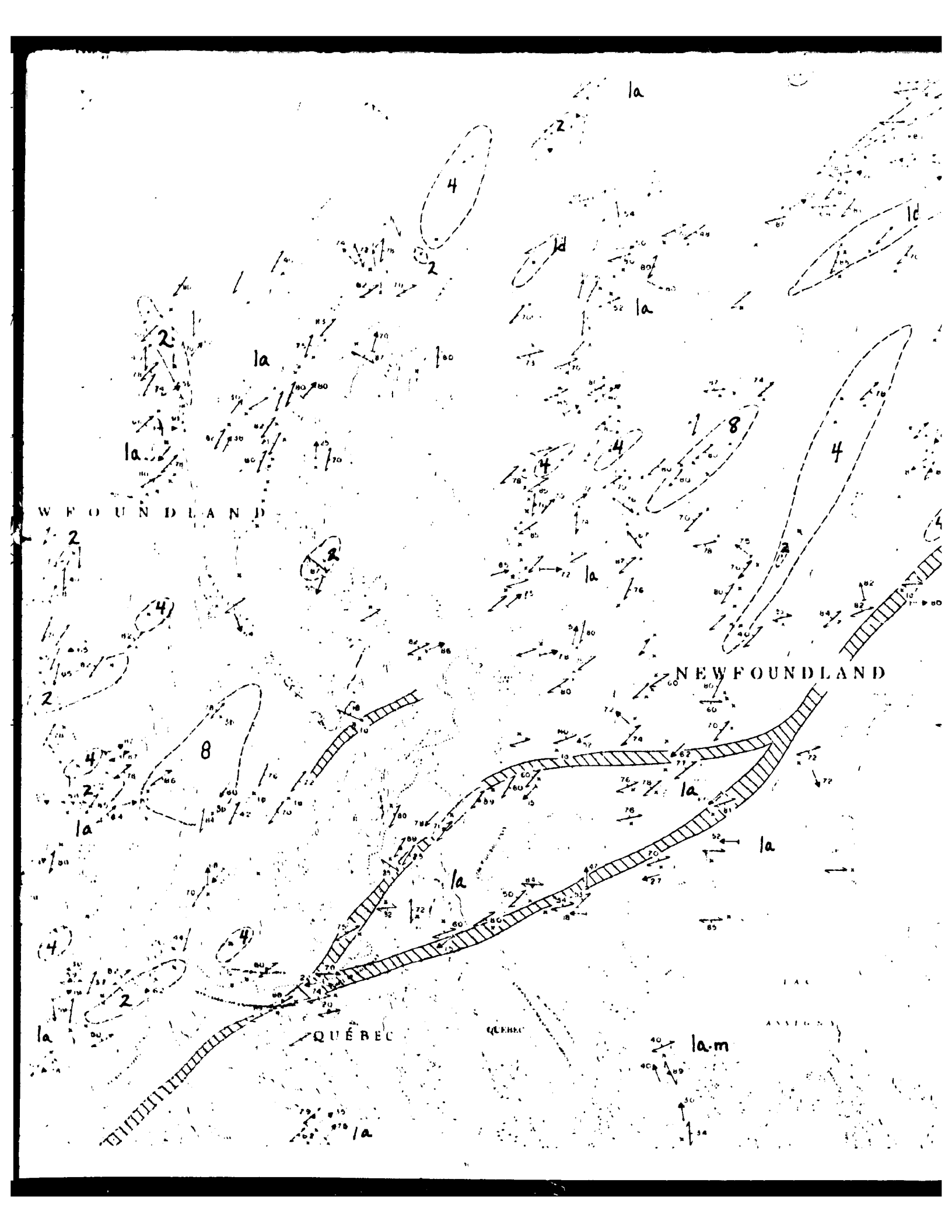
NEWFOUNDLAND
QUÉBEC
1a
1a-m
1d
2
4
8

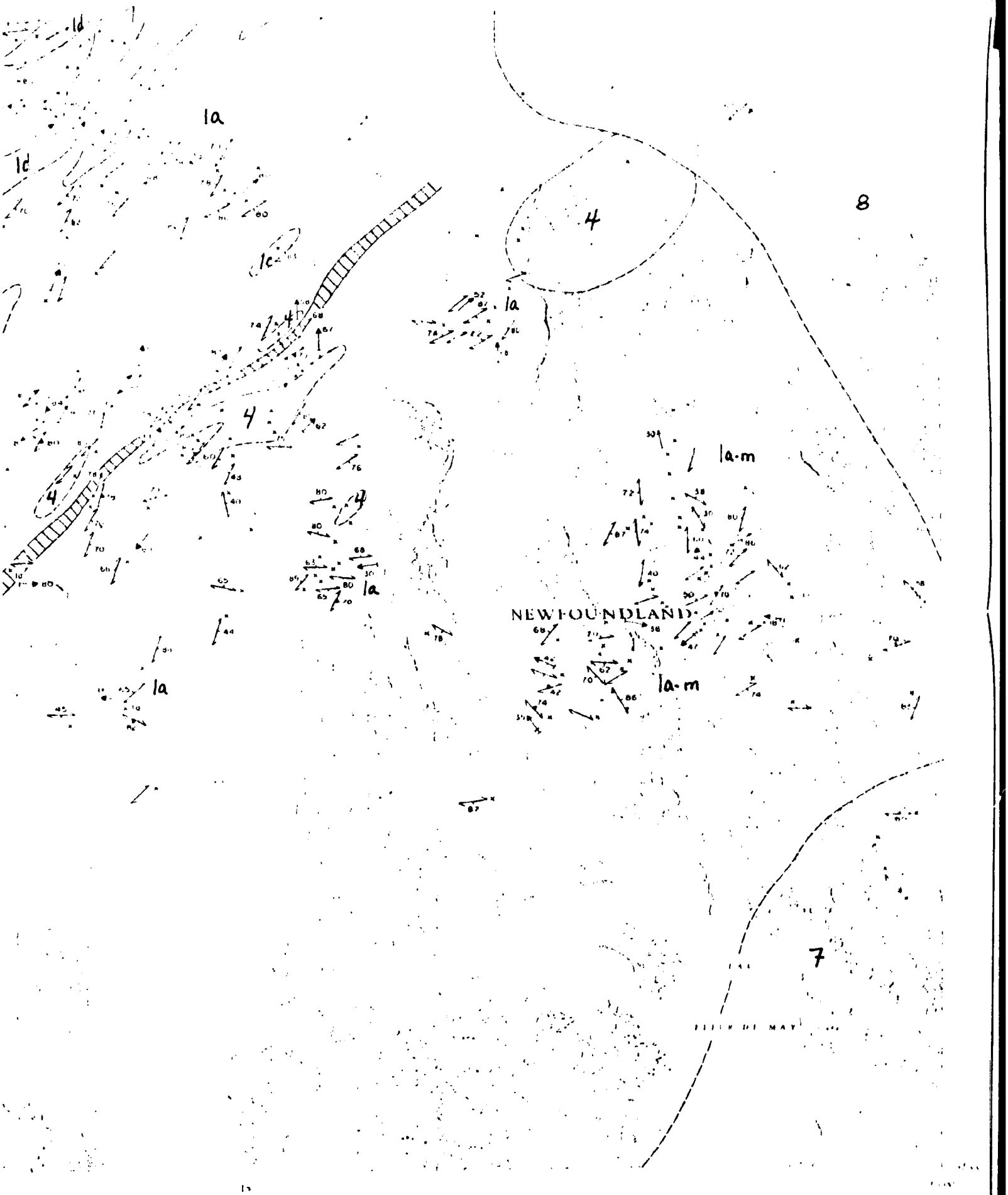
1d
1a
1d
1c
4
1a
4
8
4
4
1a-m
4
1a
NEWFOUNDLAND
1a
1a-m
7

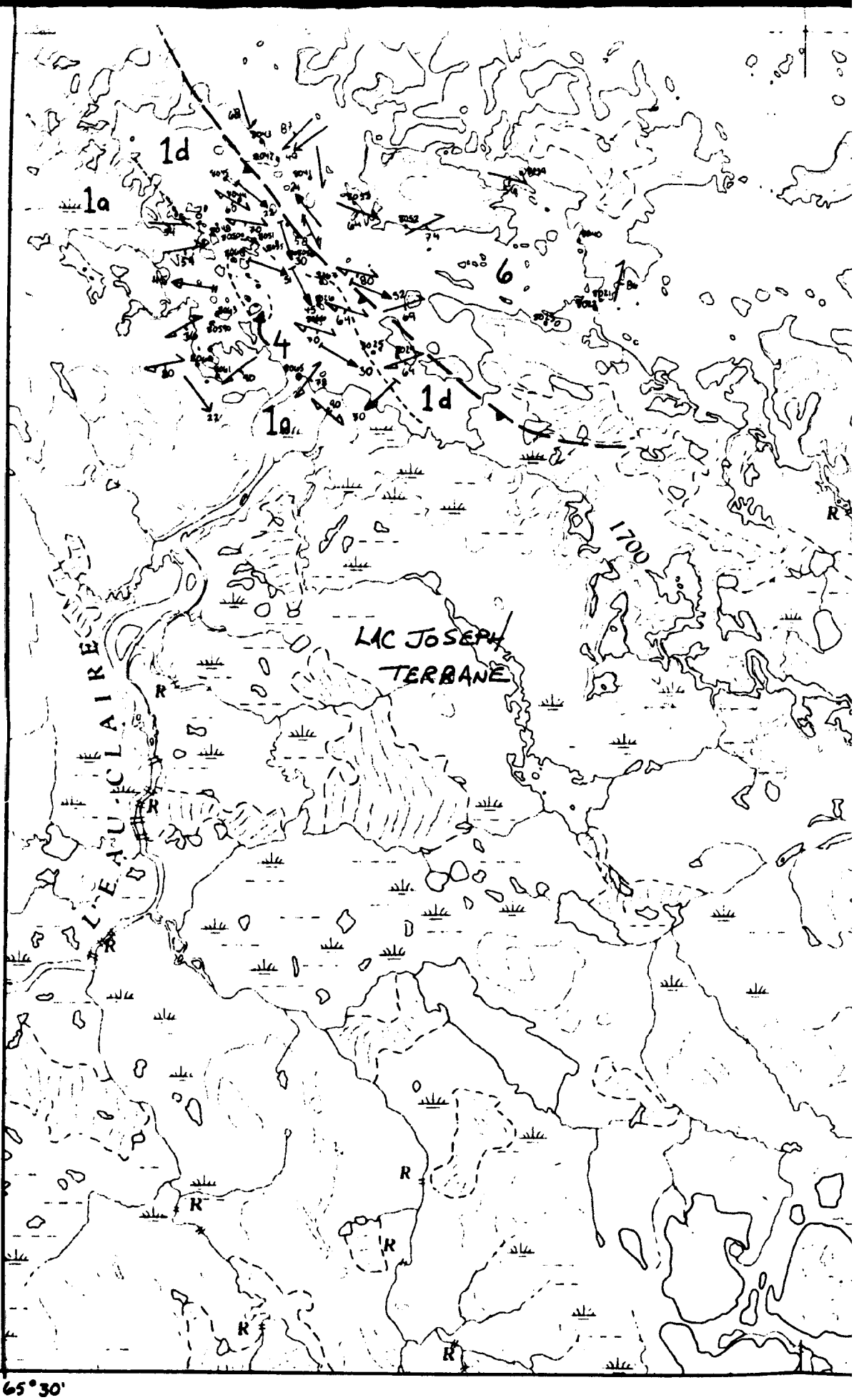
1d
1a
6
4
1a
1d
1700
LAC JOSEPH
TERRANE
L'EAU CLAIRE
R
52°30'
65°30'

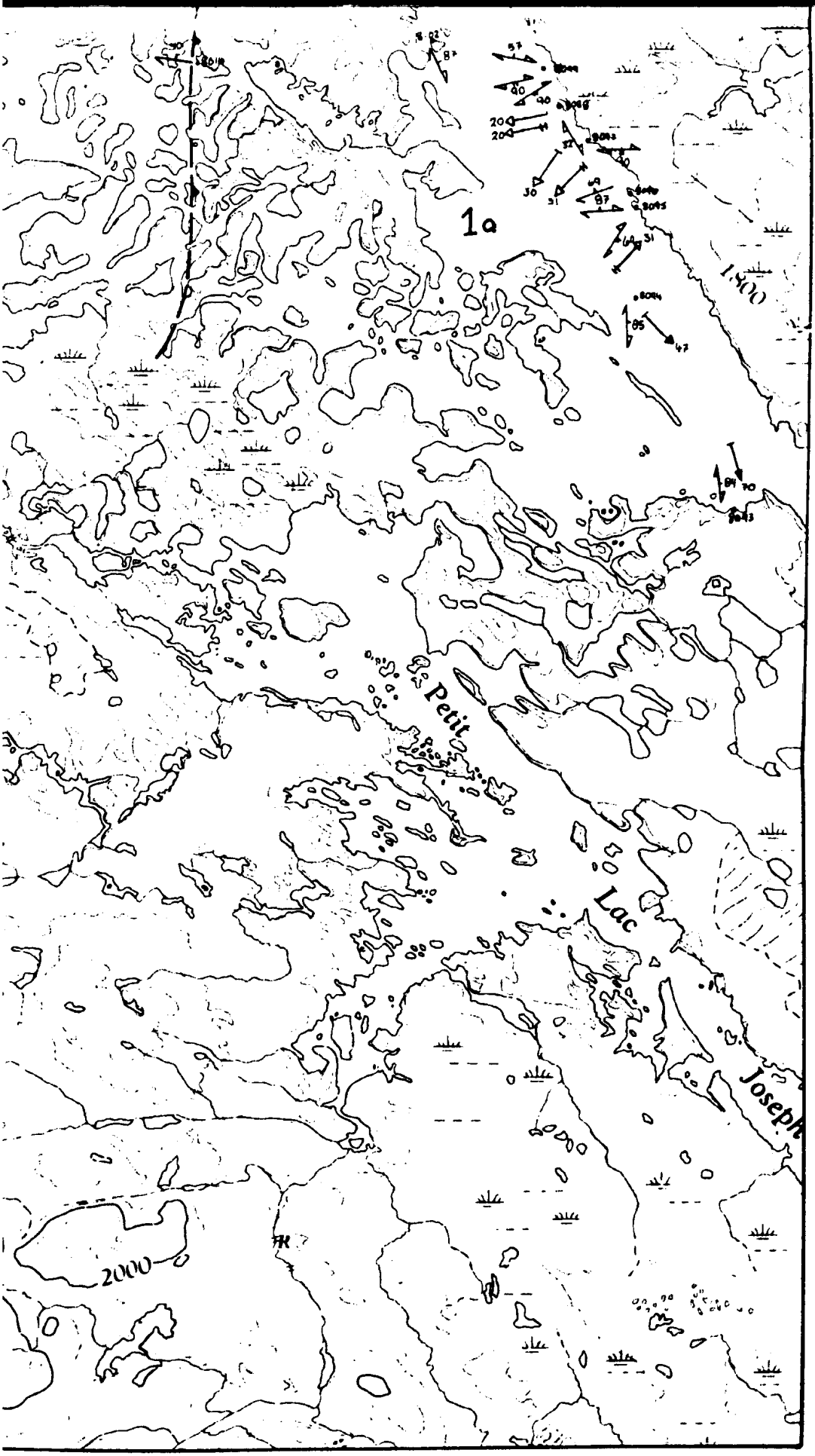
1a
1,400
Petit
Lac
Joseph
2000
52° 30'
65° 00'

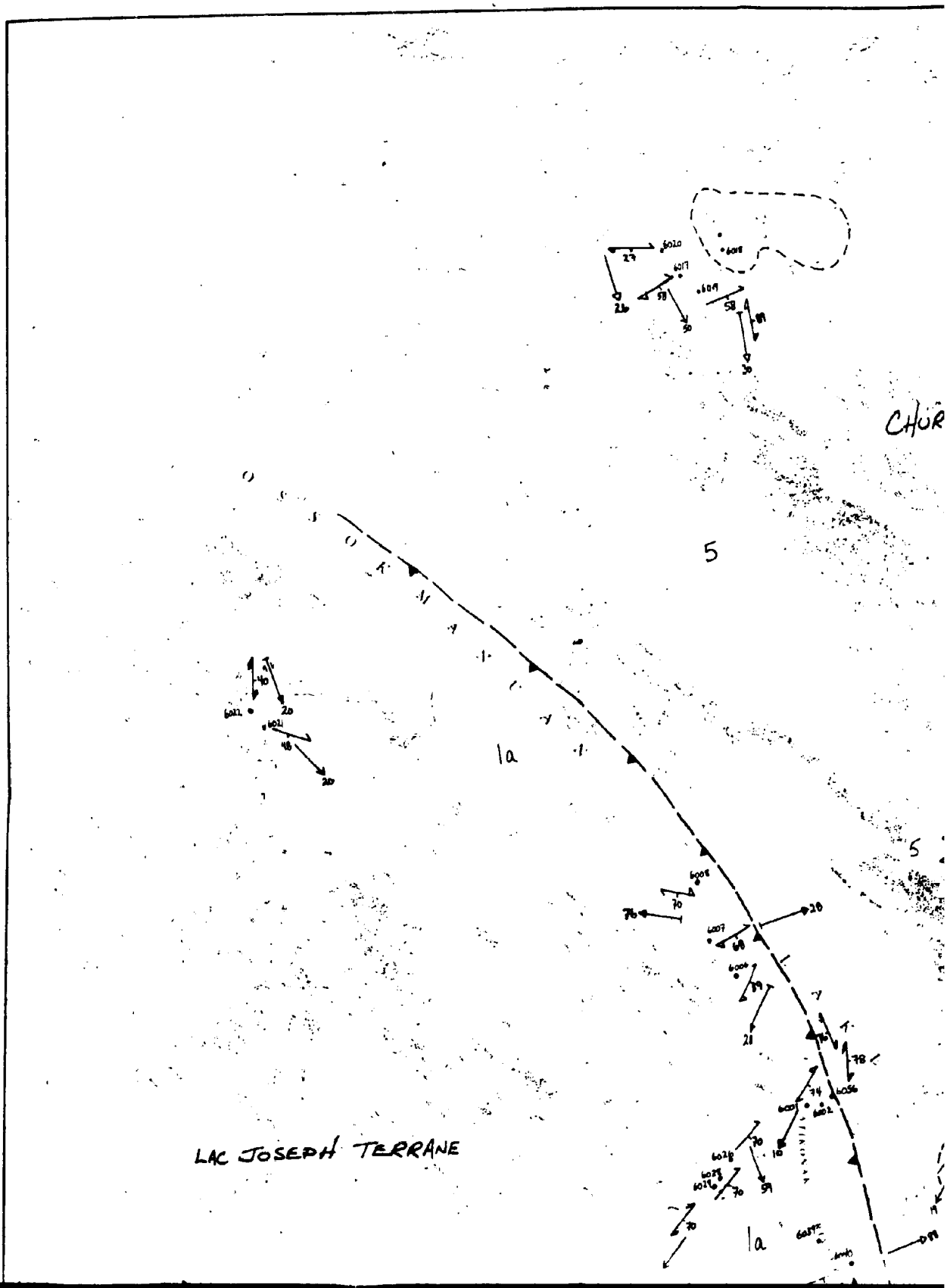
CHUR
5
1a
LAC JOSEPH TERRANE

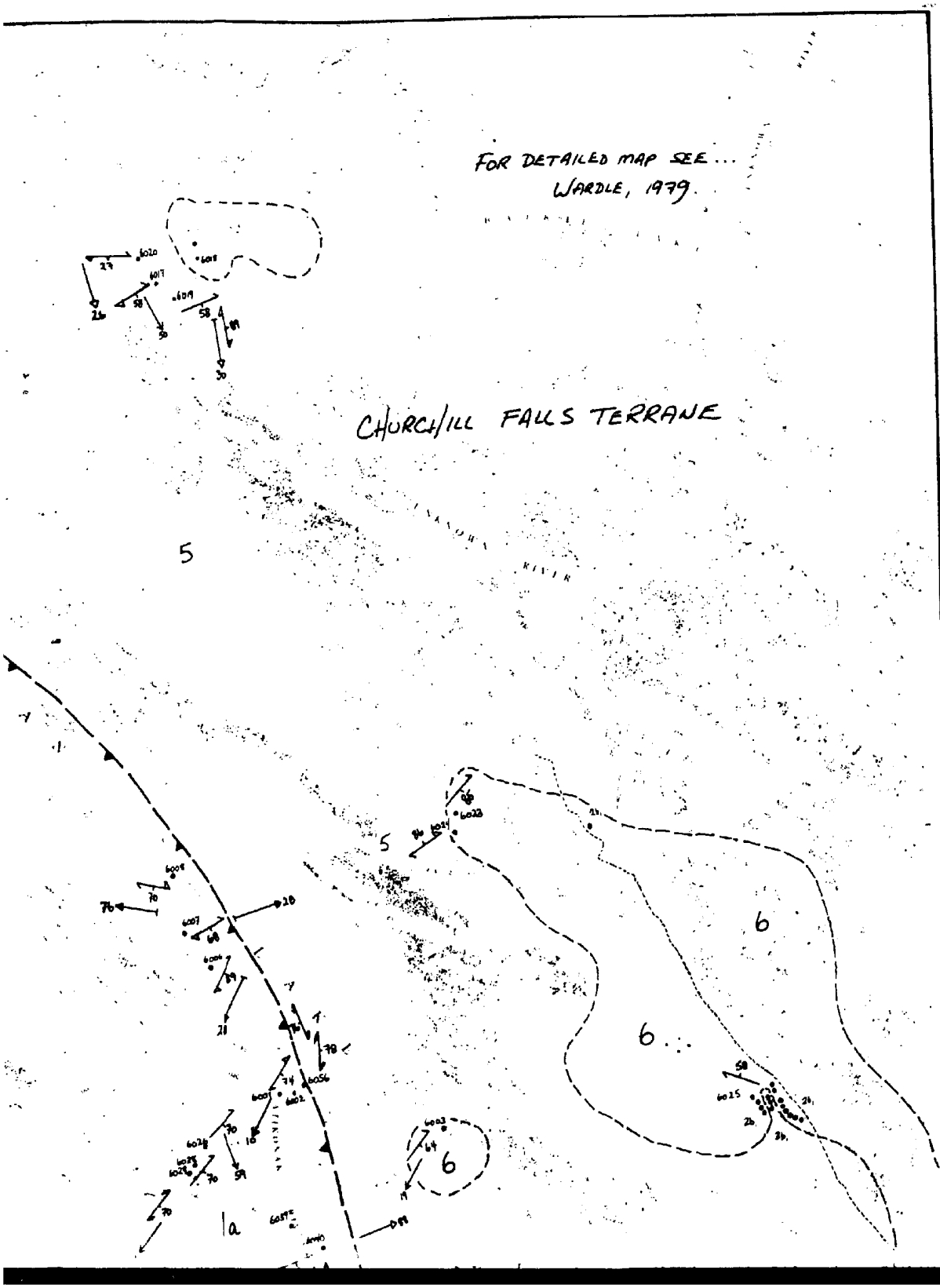
FOR DETAILED MAP SEE...
WARDLE, 1979.
CHURCHILL FALLS TERRANE
5
5
6
6
1a

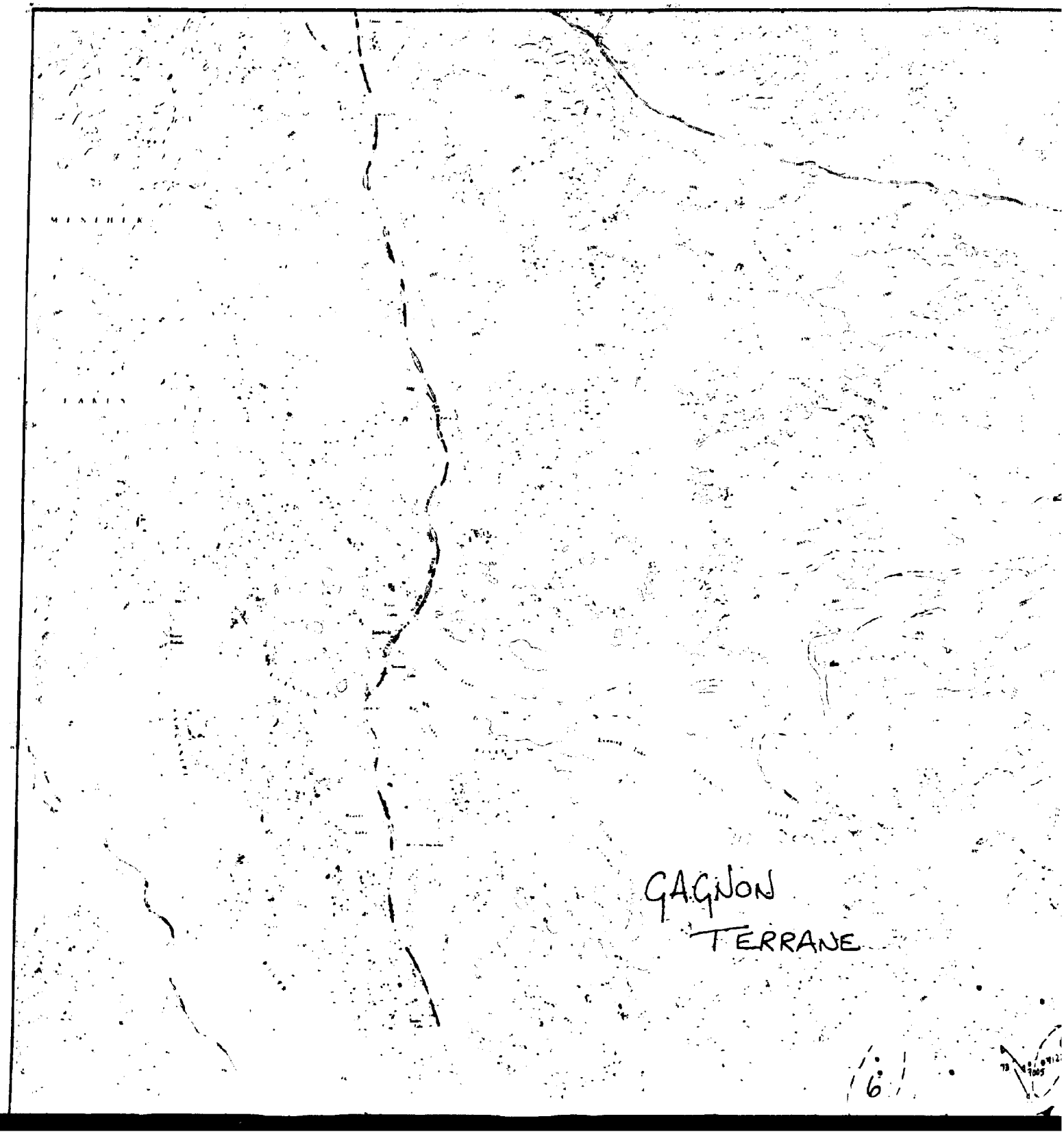
GAGNON
TERRANE

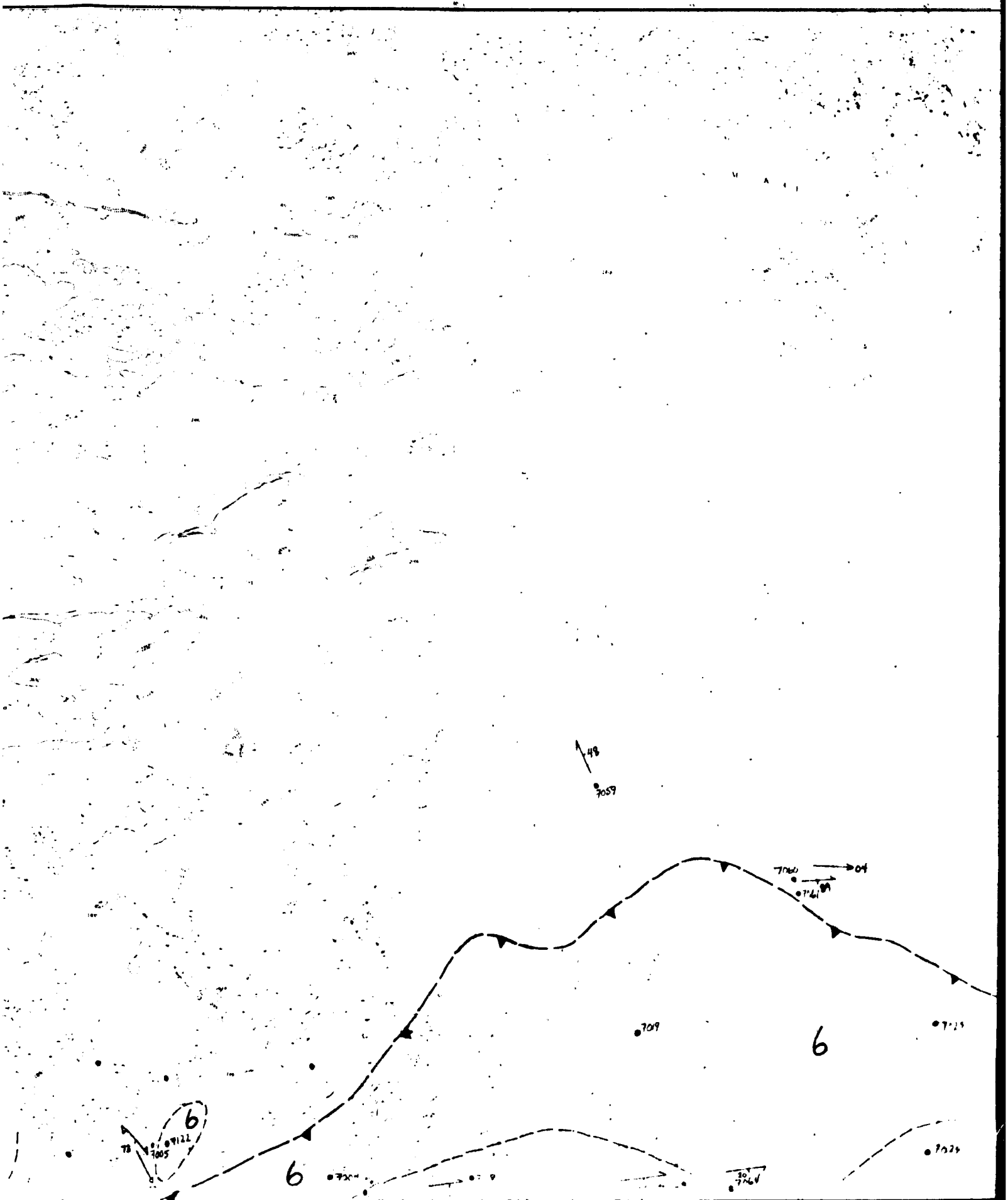
6
6
6

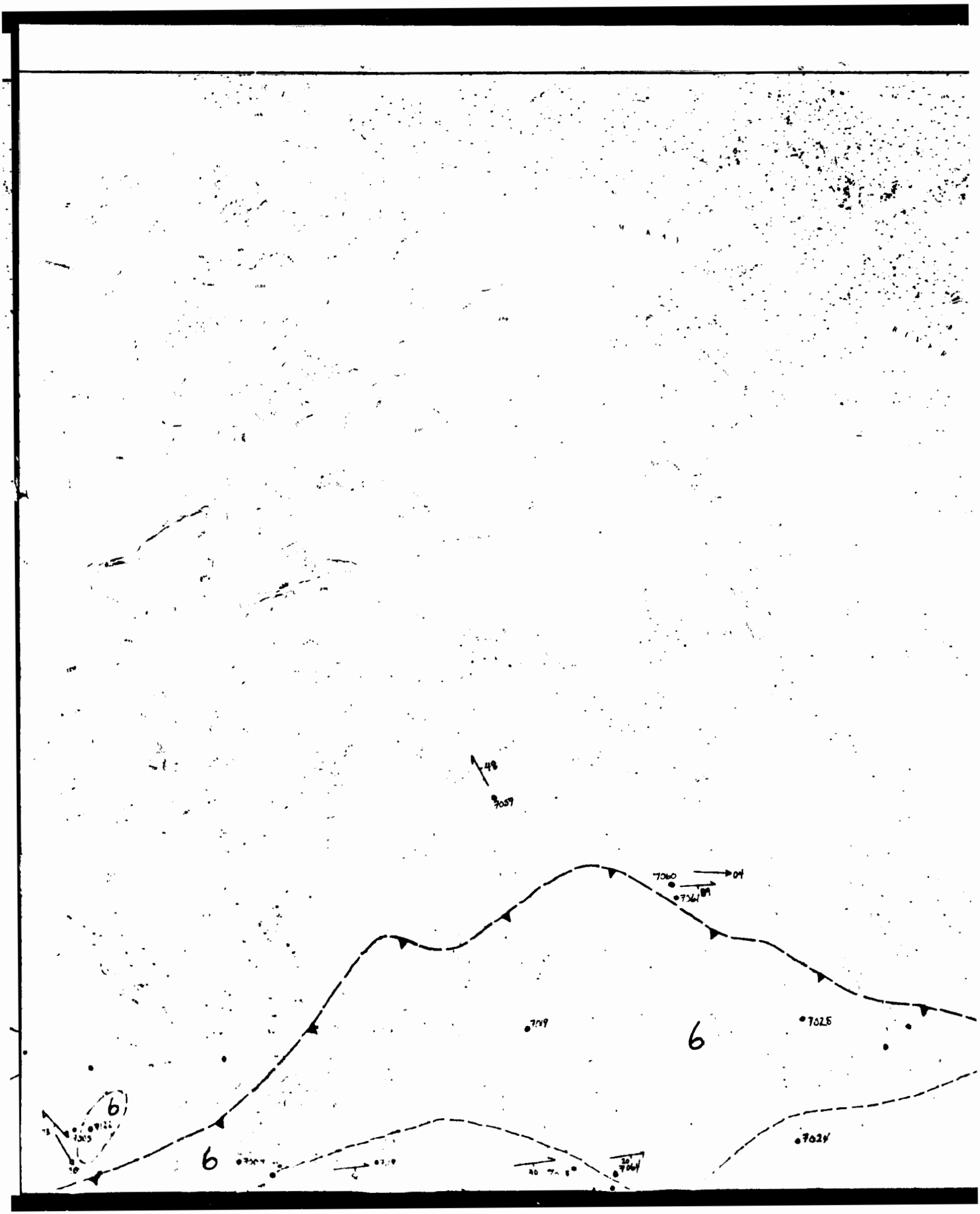
7059
7060
7061
7049
7025
7029
6
6
6

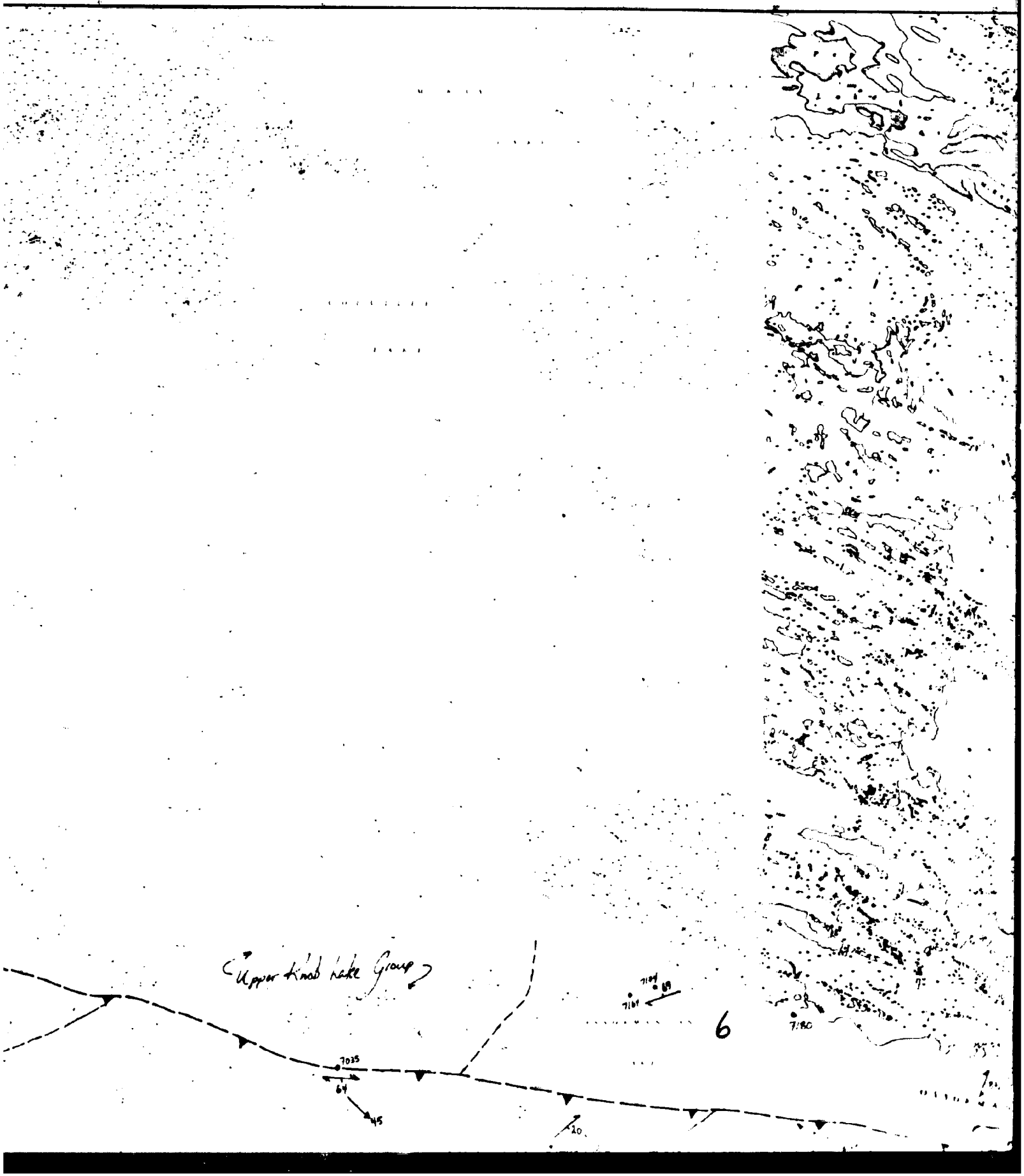
Upper Kinab Lake Group
7035
64
45
10
7184
69
7181
7180
6

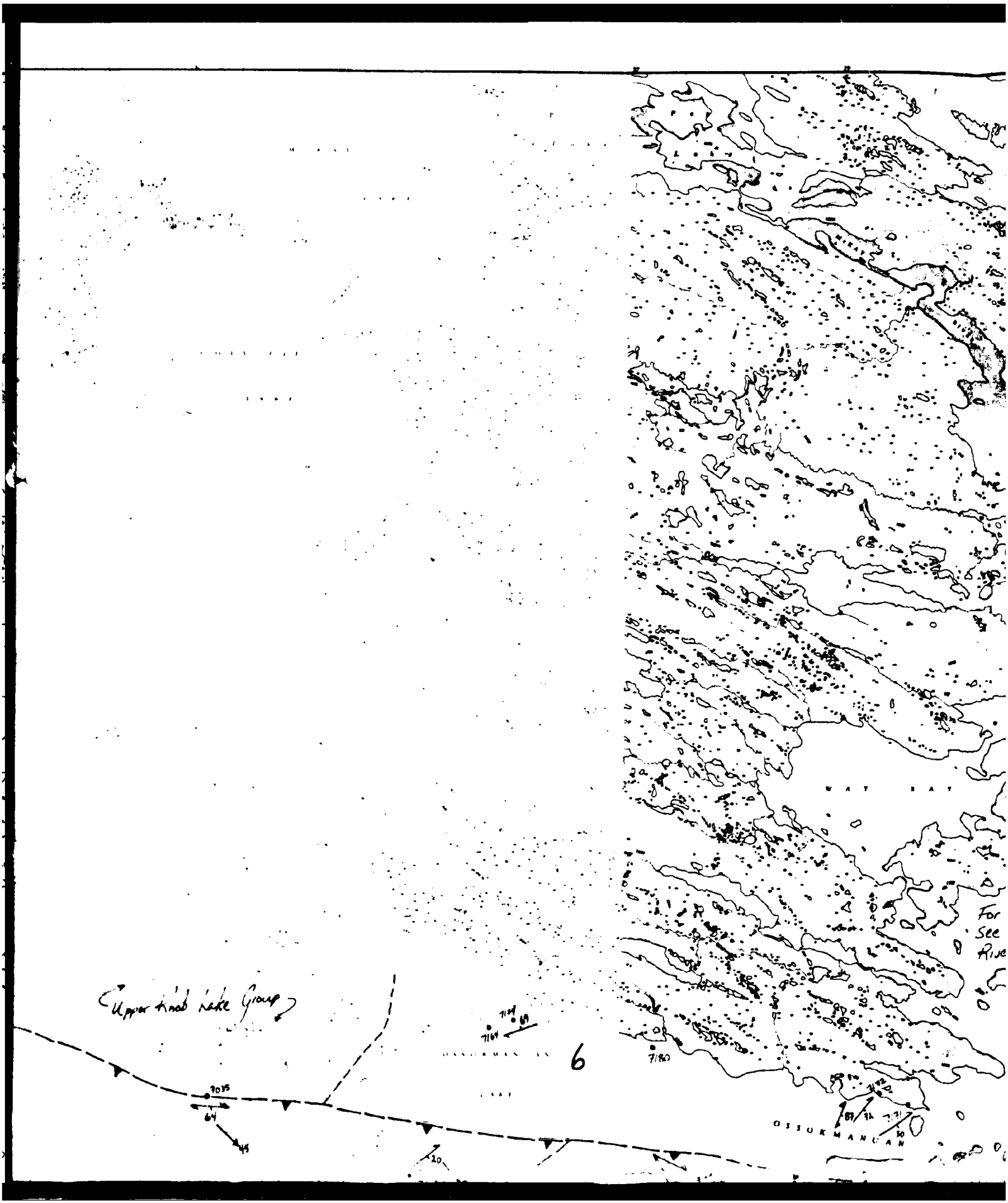
Upper Arab Lake Group
6
WAT BAY
OSSOKMANUAN
For
See
Rive

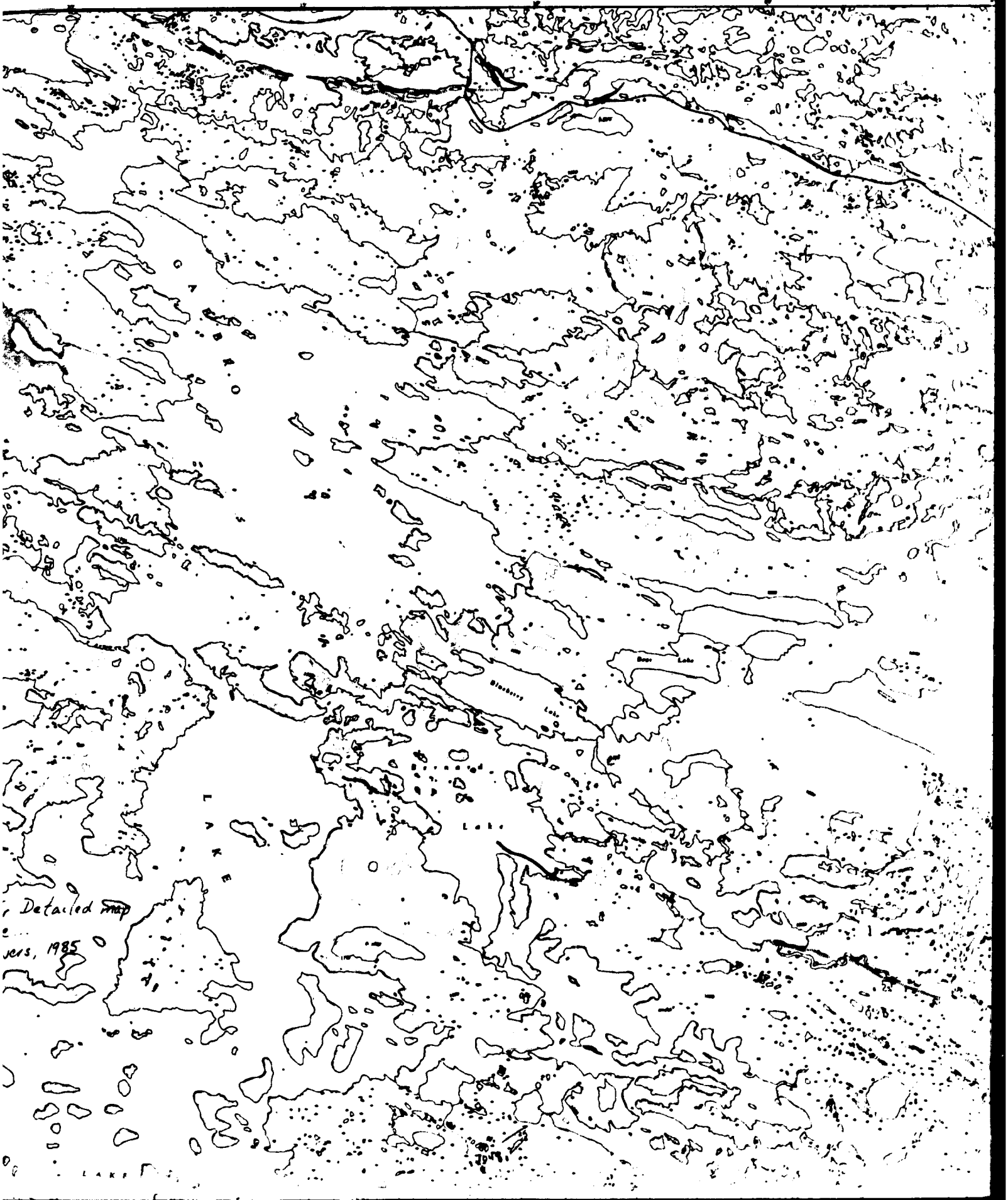
Detailed Map
1985

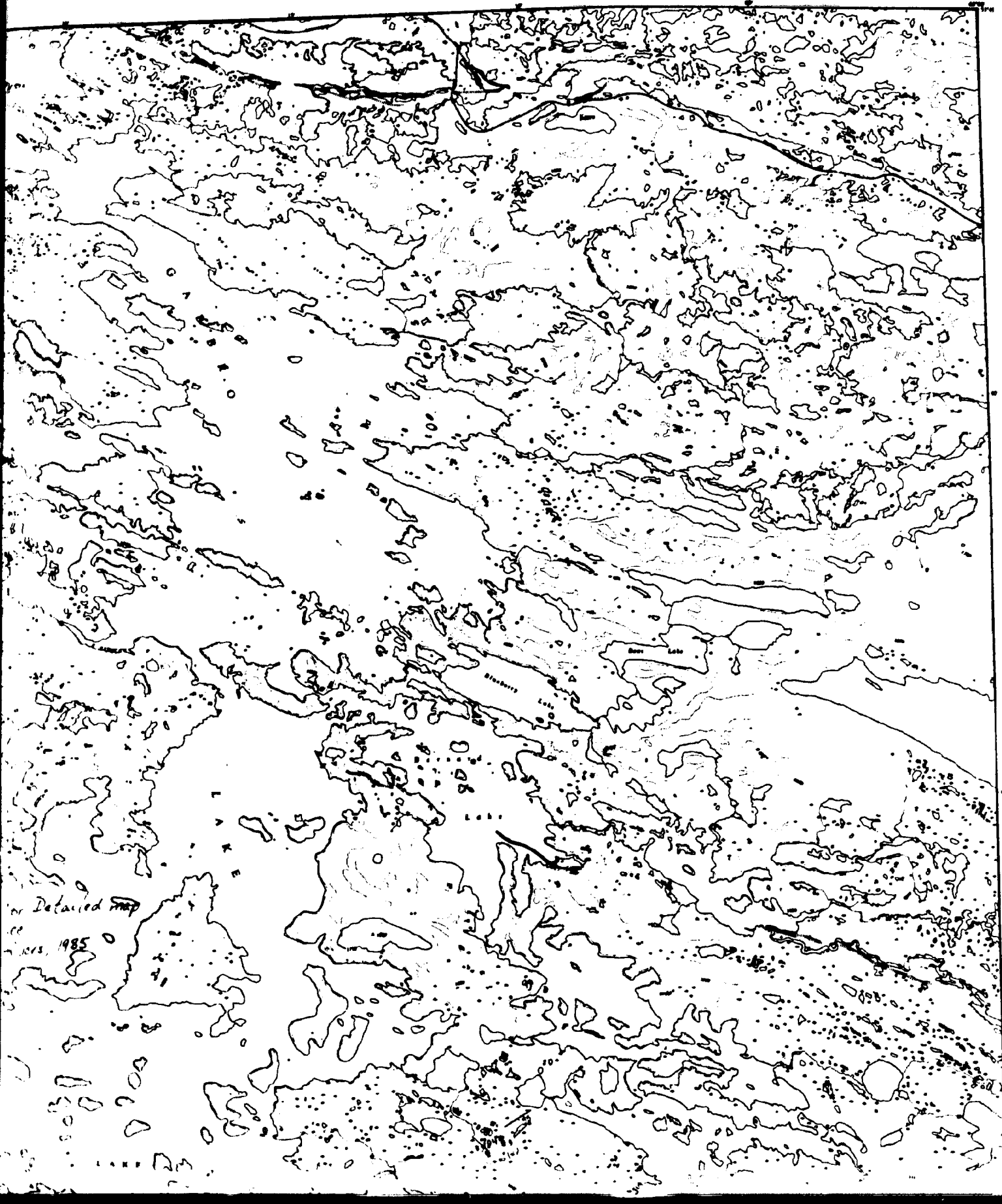
Bass Lake
Blackberry
LAKE
or Detailed Map
ers, 1985

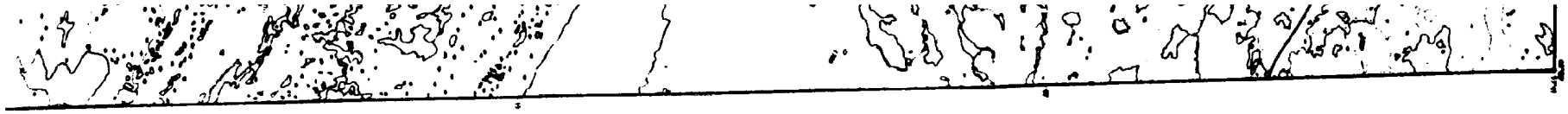

LAC JOSEPH TERRANE

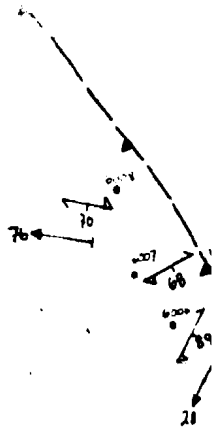

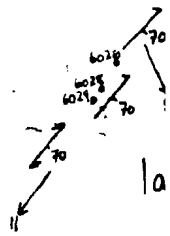

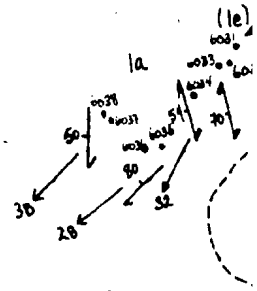

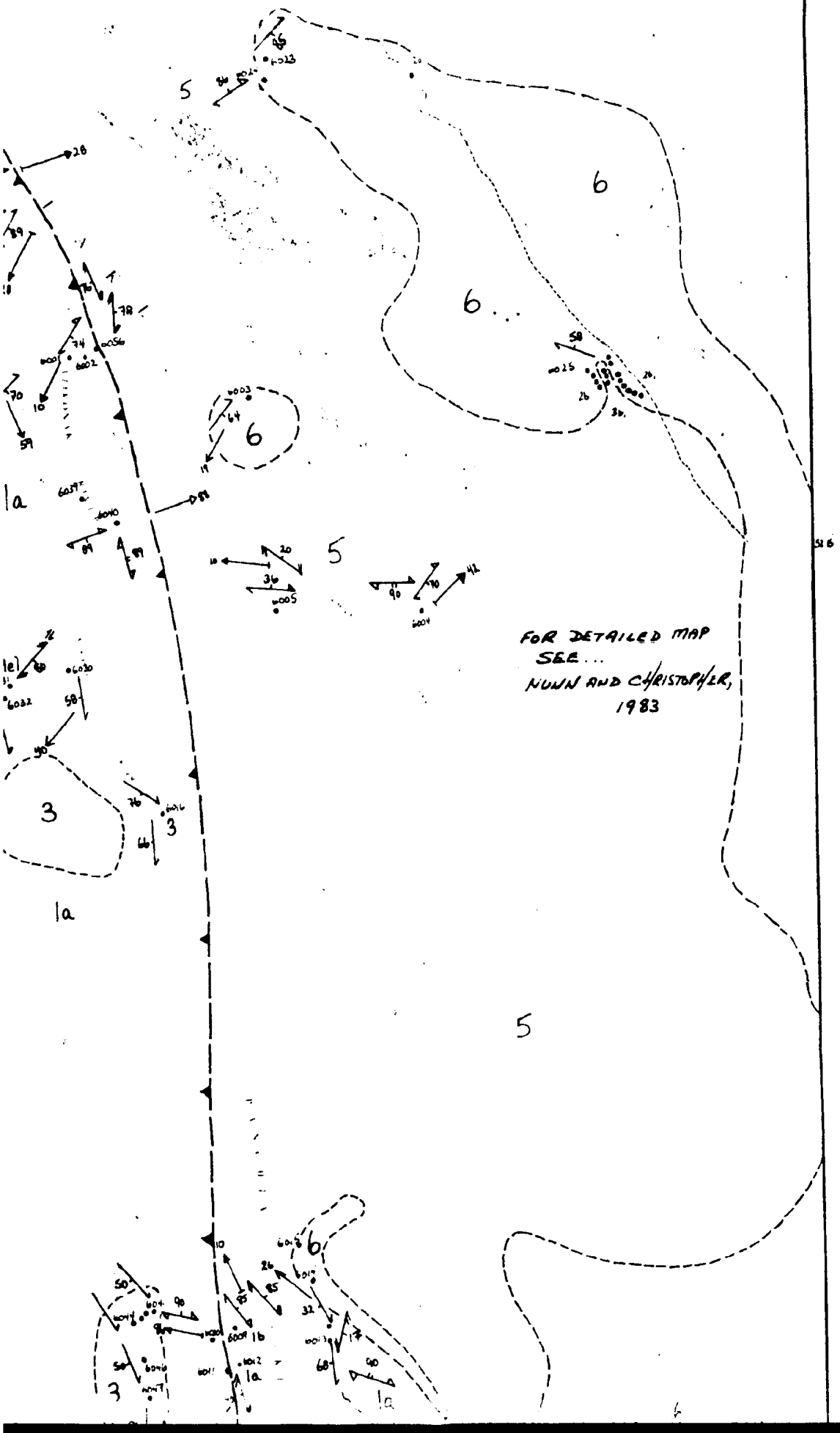
FOR DETAILED MAP
SEE...
NUNN AND CHRISTOPHER,
1983

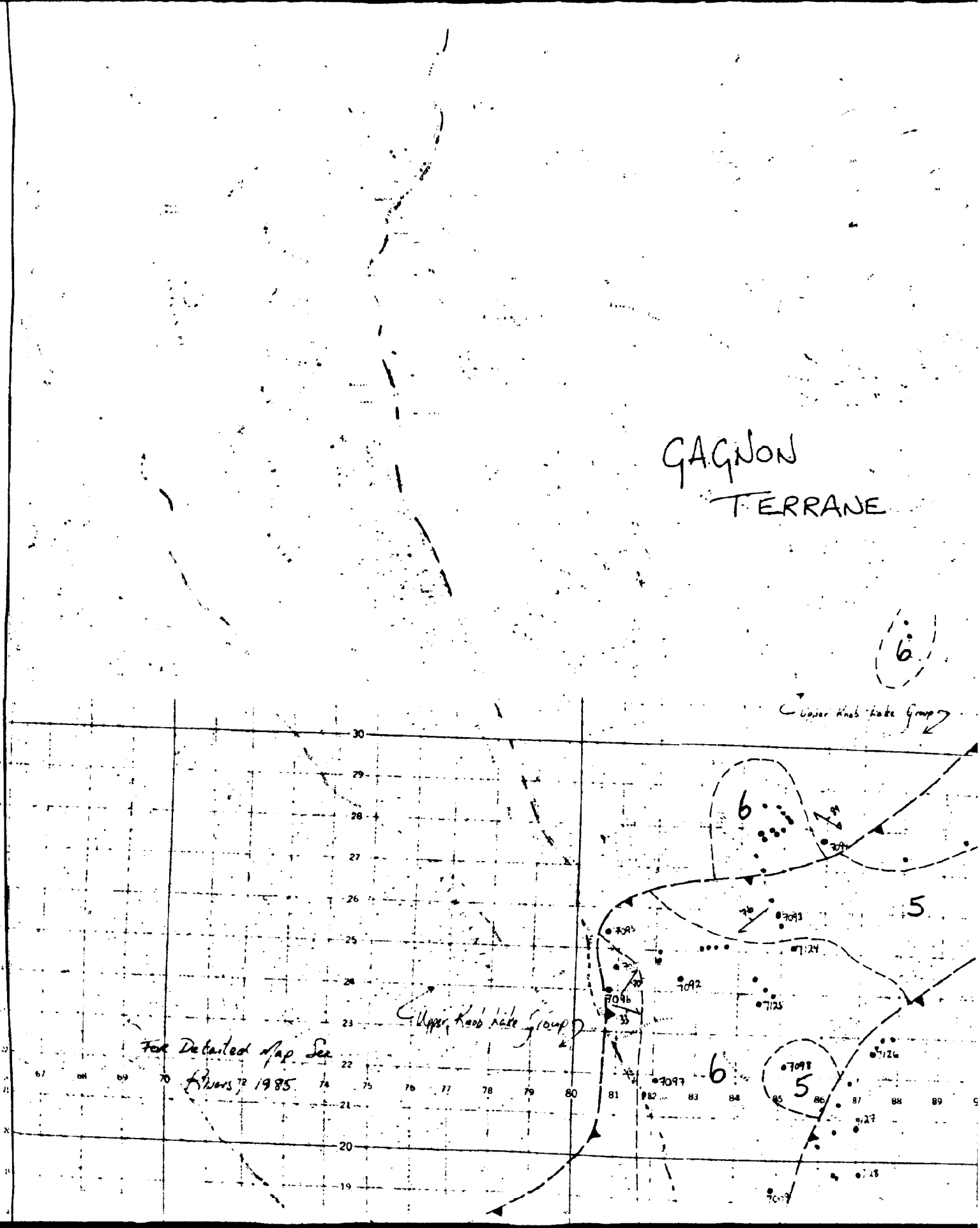
GAGNON
TERRANE
6
Upper Knob Lake Group
6
5
7092
7125
7096
7097
7098
5
6
Upper Knob Lake Group
For Detailed Map See
Rivers, 1985

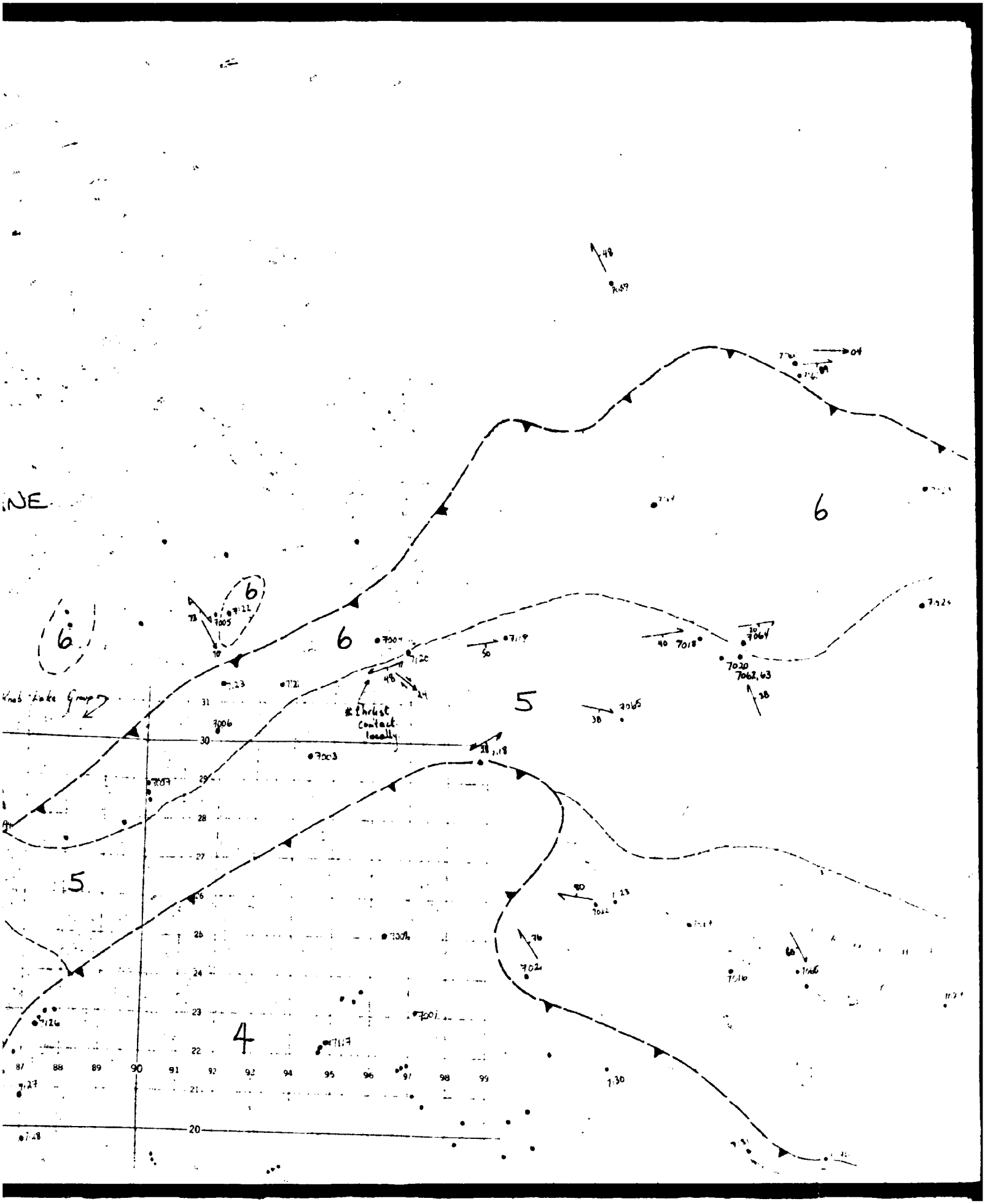
NE
6
6
6
5
5
4
Knob Lake Group
* Thrust contact locally
7005
7006
7003
7004
7007
7018
7020
7062,63
7065
7022
7024
7016
7001
30
29
28
27
26
24
23
22
21
20
87
88
89
90
91
92
93
94
95
96
97
98
99

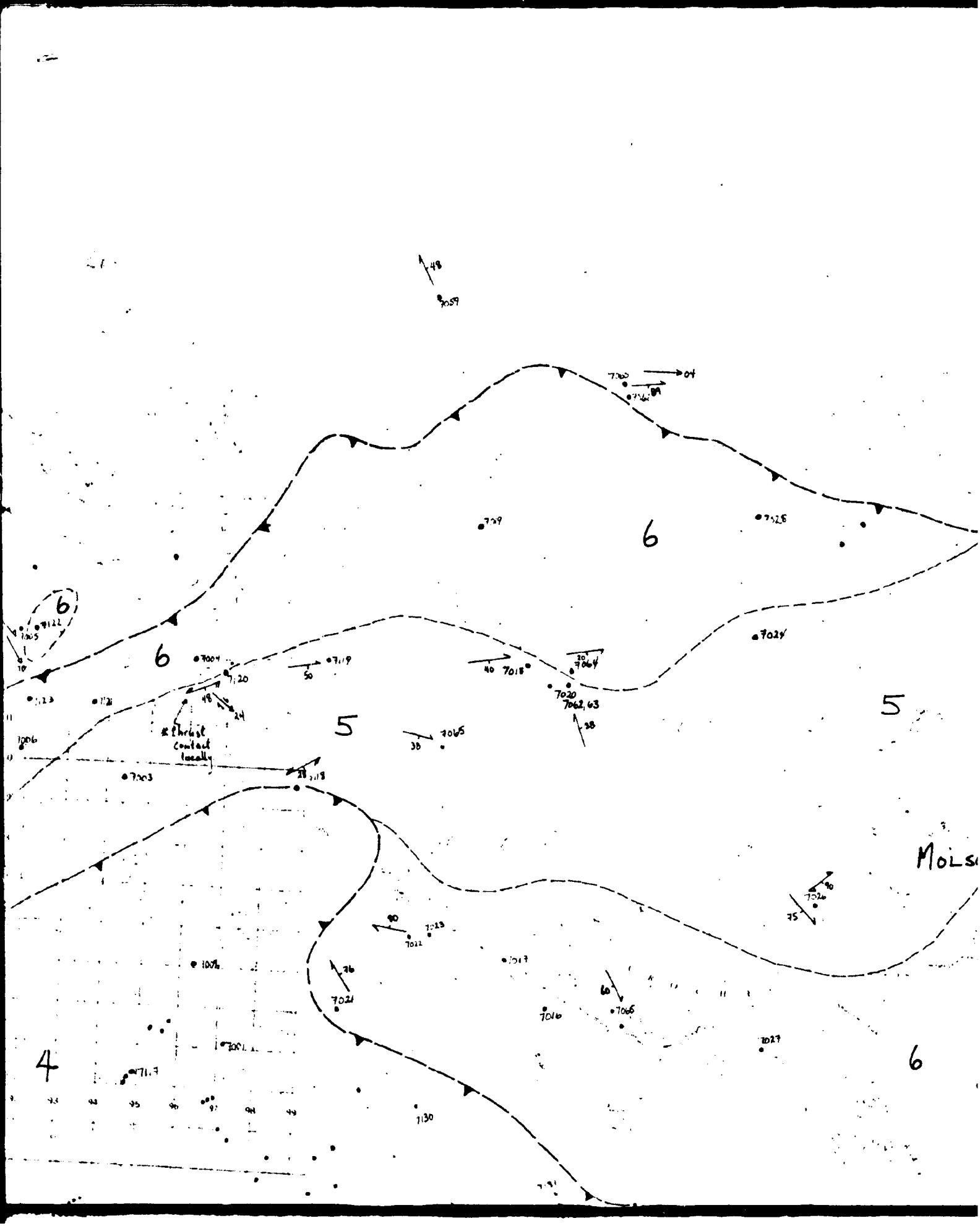
6
6
5
5
4
6
Christ
Contact
locally
Molso

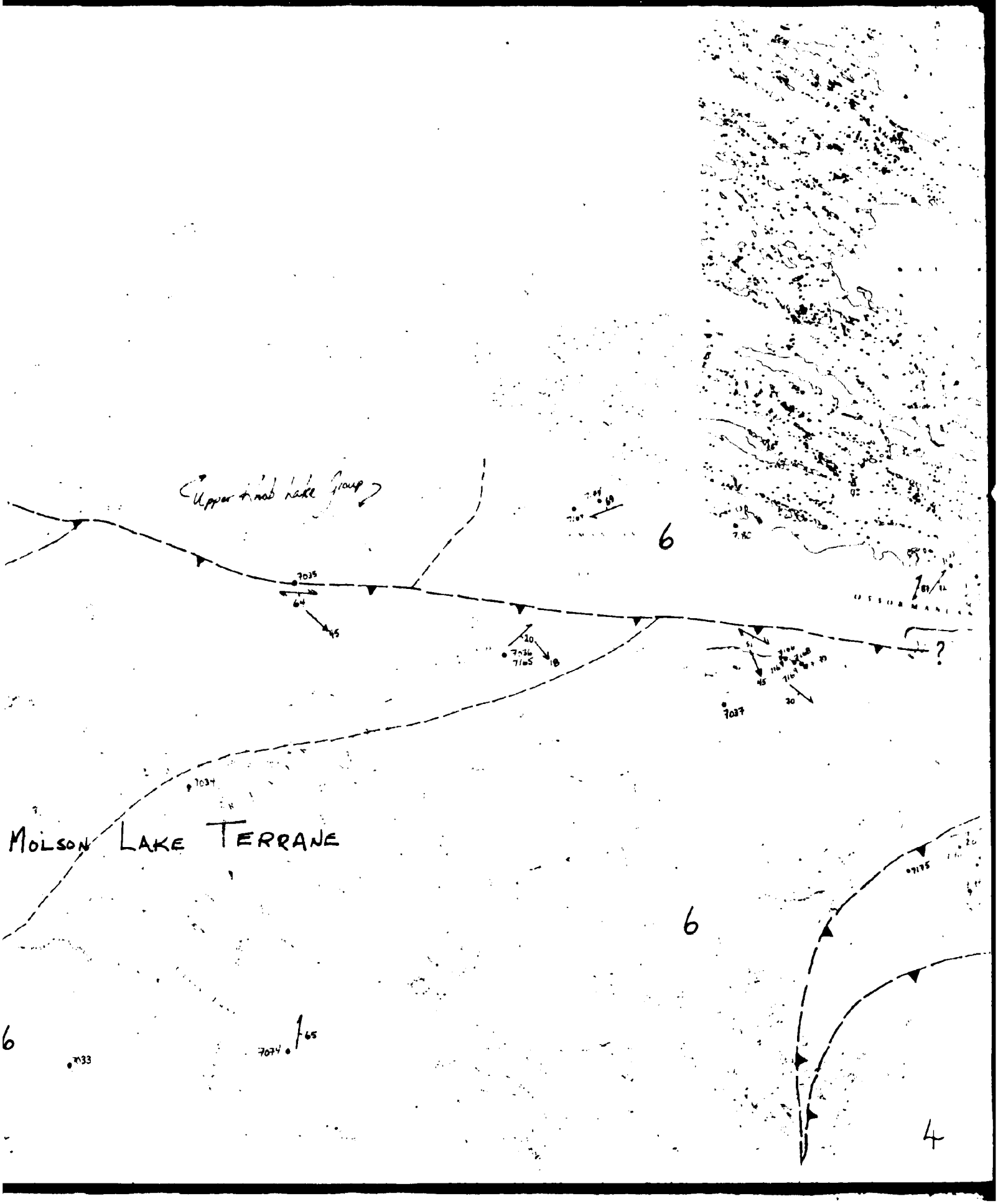
Upper Knob Lake Group?
MOLSON LAKE TERRANE
6
6
6
4
7035
7034
7037
7074
7033
7075
7076
7135
64
45
20
18
65
?

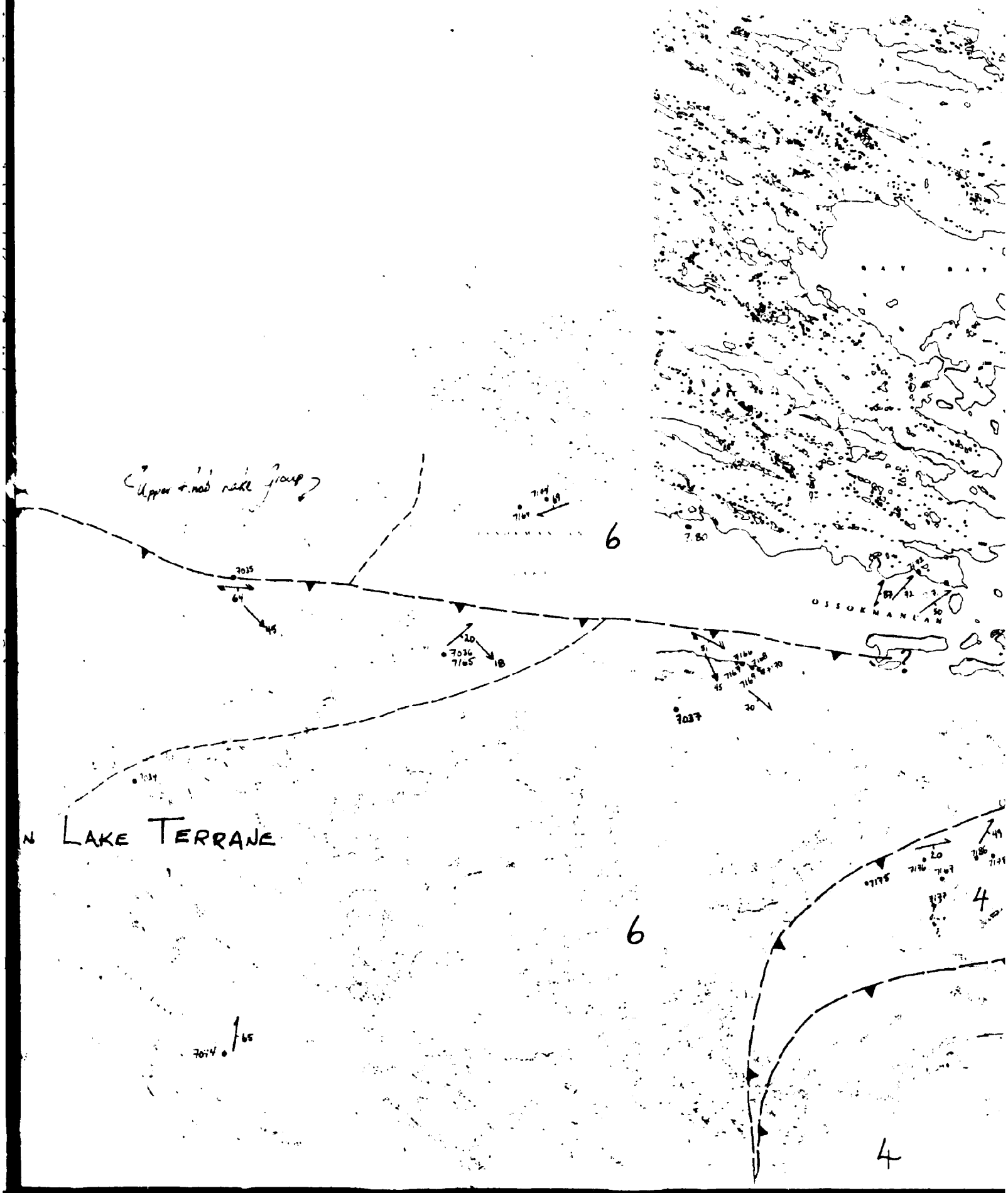
("Upper + mod mtn group")
7035
64
45
7036
7105
20
18
7164
69
6
7180
OSSOKMANIAN
7037
7034
N LAKE TERRANE
6
7165
7175
7176
7167
7177
7186
7179
49
20
4
4

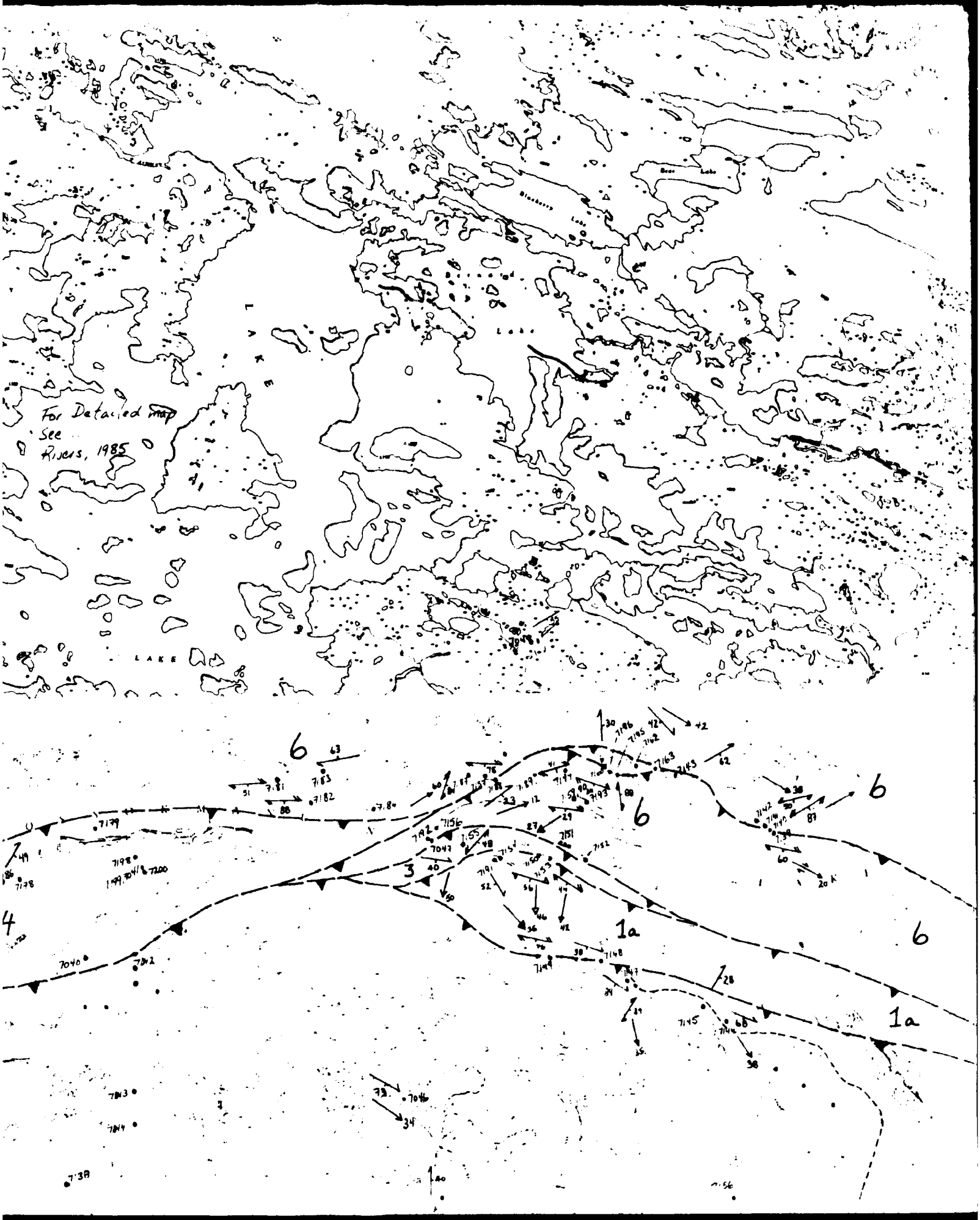
For Detailed map
See
Rivers, 1985
LAKE
6
1a
3
4

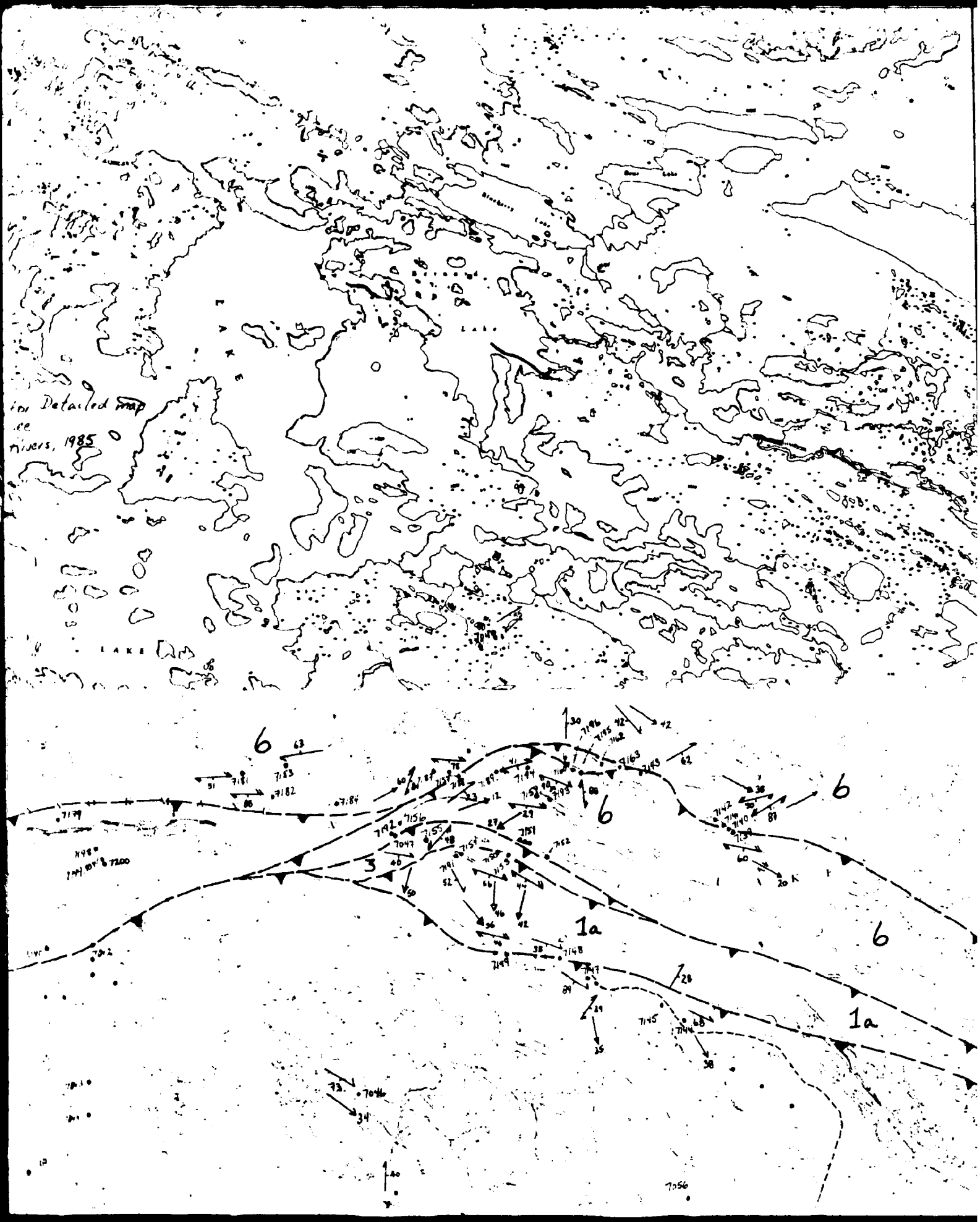
LAKE
LAKE
LAKE
6
6
6
6
3
1a
1a

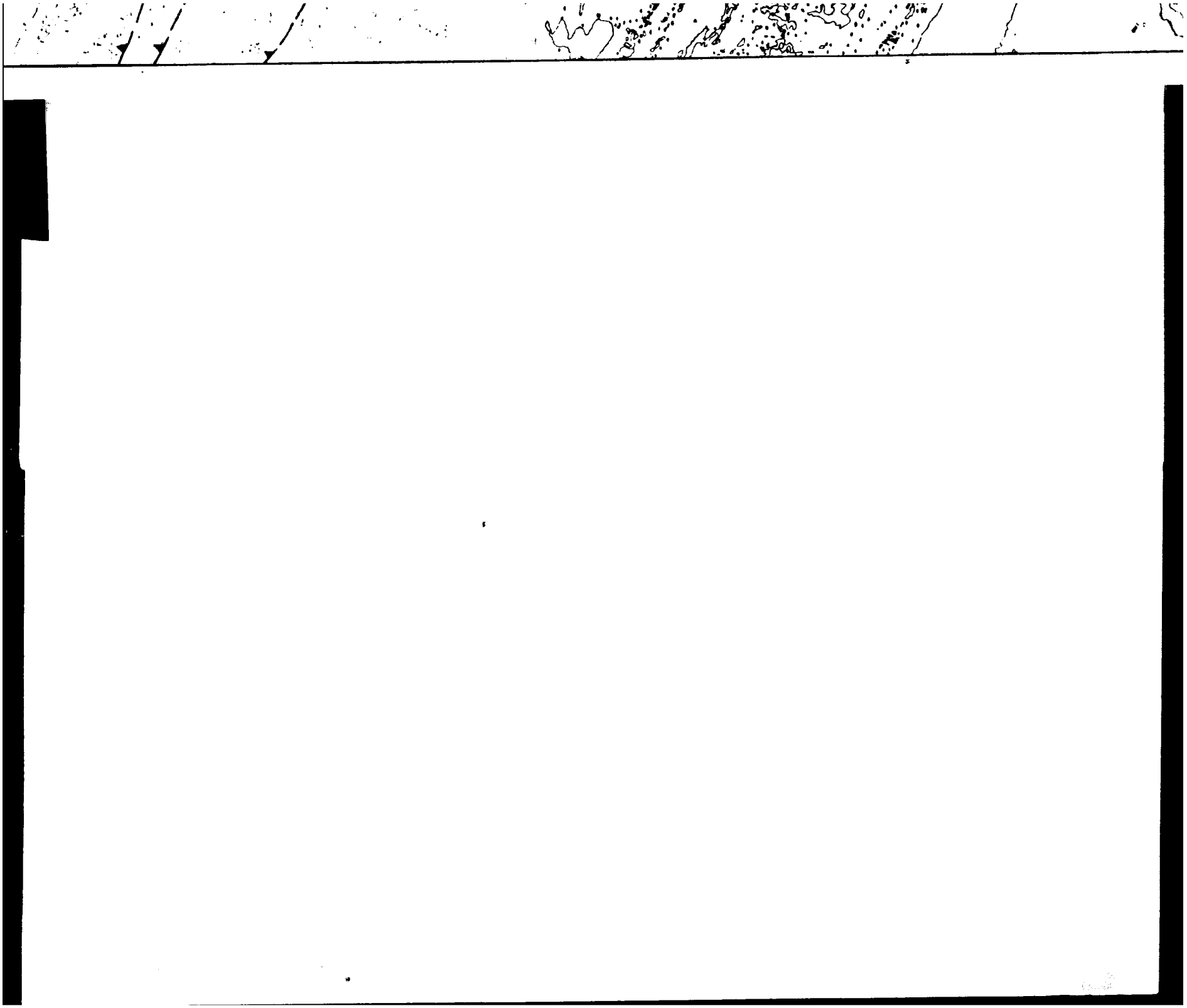

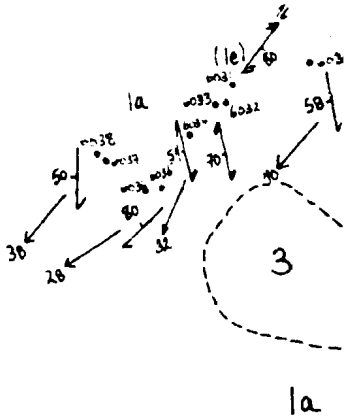

1a

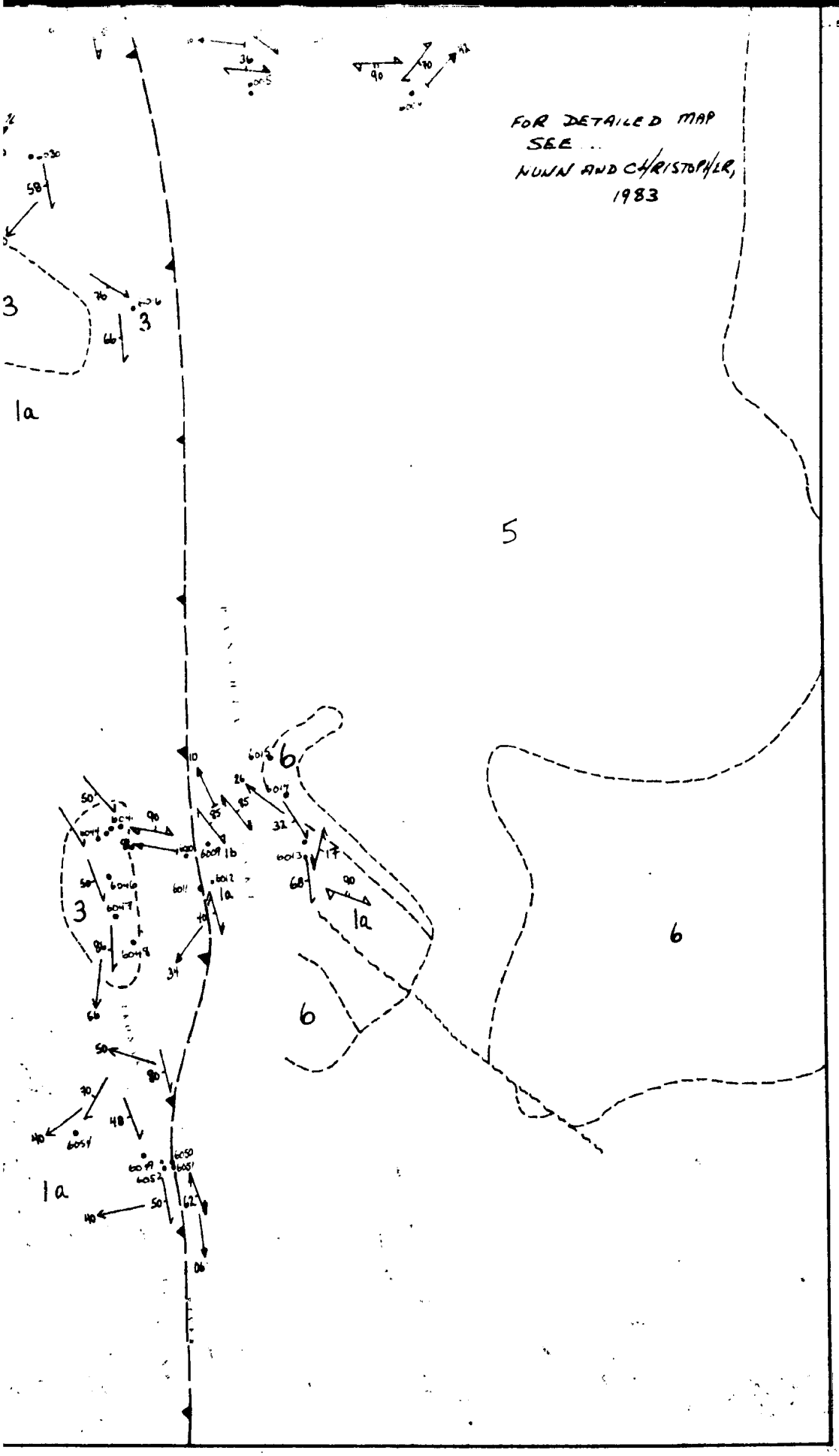
FOR DETAILED MAP
SEE ...
NUNN AND CHRISTOPHER,
1983
5
6
6
6
3
3
3
1a
1a
1a
1b
1a
1a

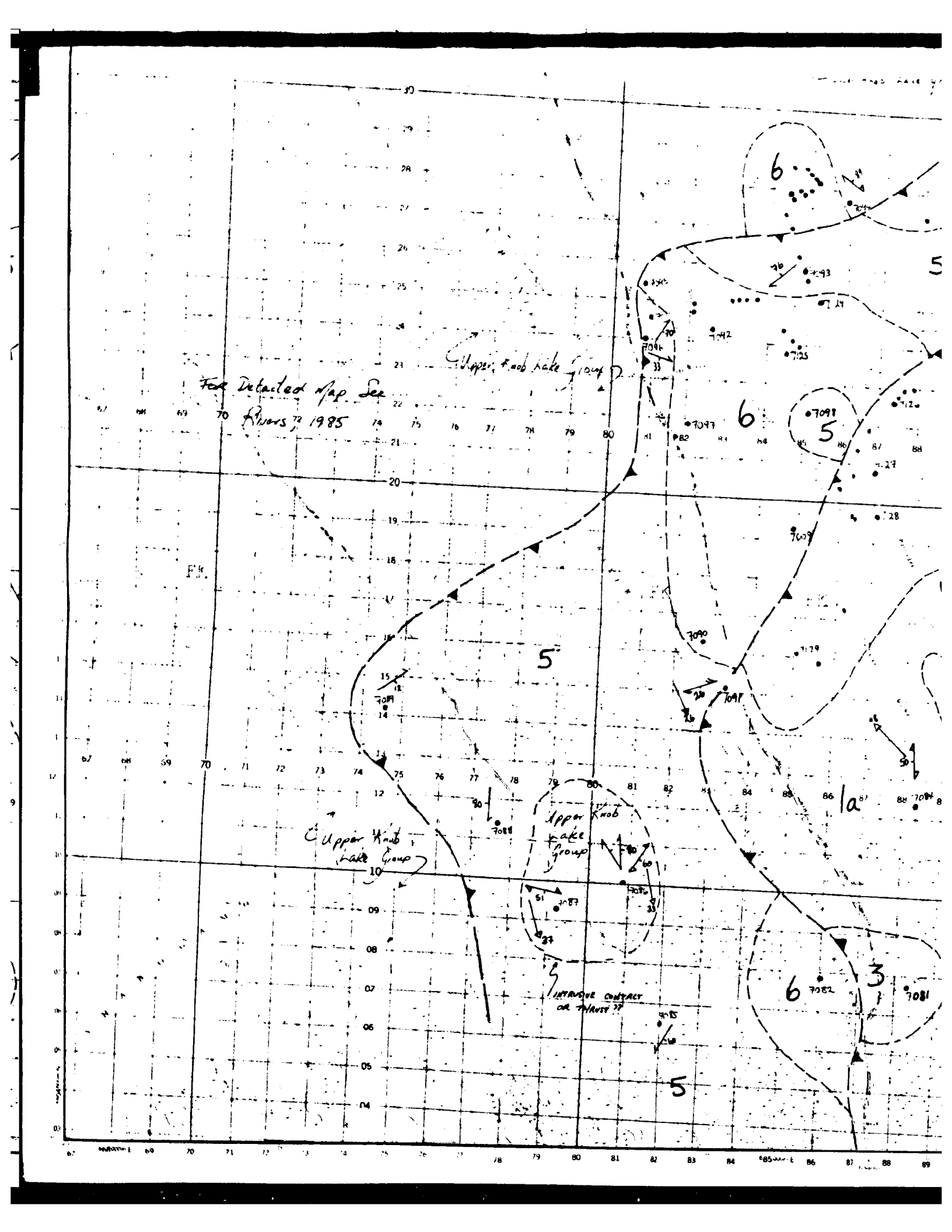
Upper Knob Lake Group
For Detailed Map See
Rivers, 1985
Upper Knob Lake Group
Upper Knob Lake Group
INTRUSIVE CONTACT OR THRUST ??
6
5
6
5
5
6
3
1a

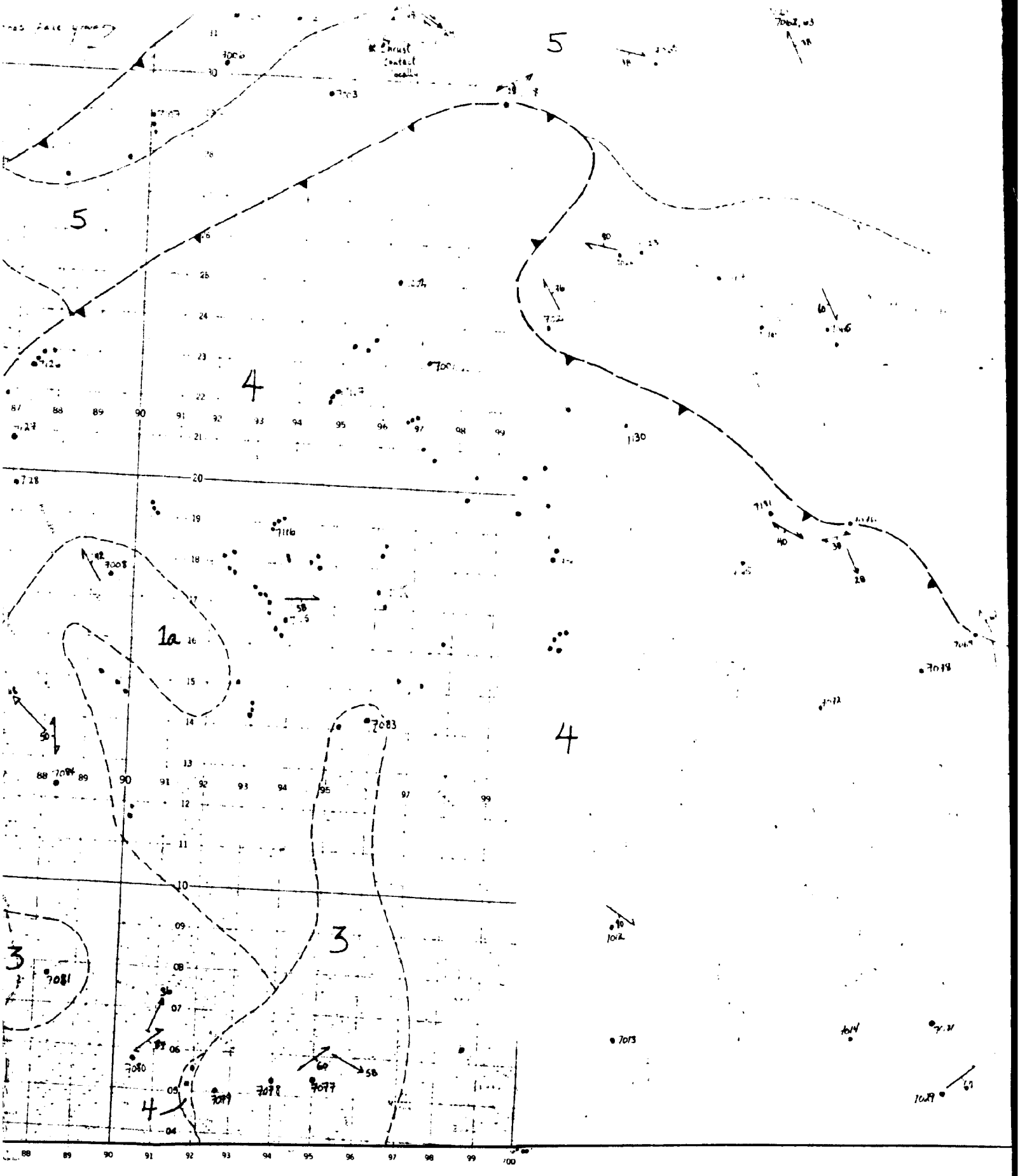
5
5
4
4
1a
3
3
4
7083
7081
7080
7079
7078
7077
7013
7014
7088
7084
7008
7116
7128
7130
7191
7022
7003
7000
7012
7049
7014
7049
Thrust
Central
Axis

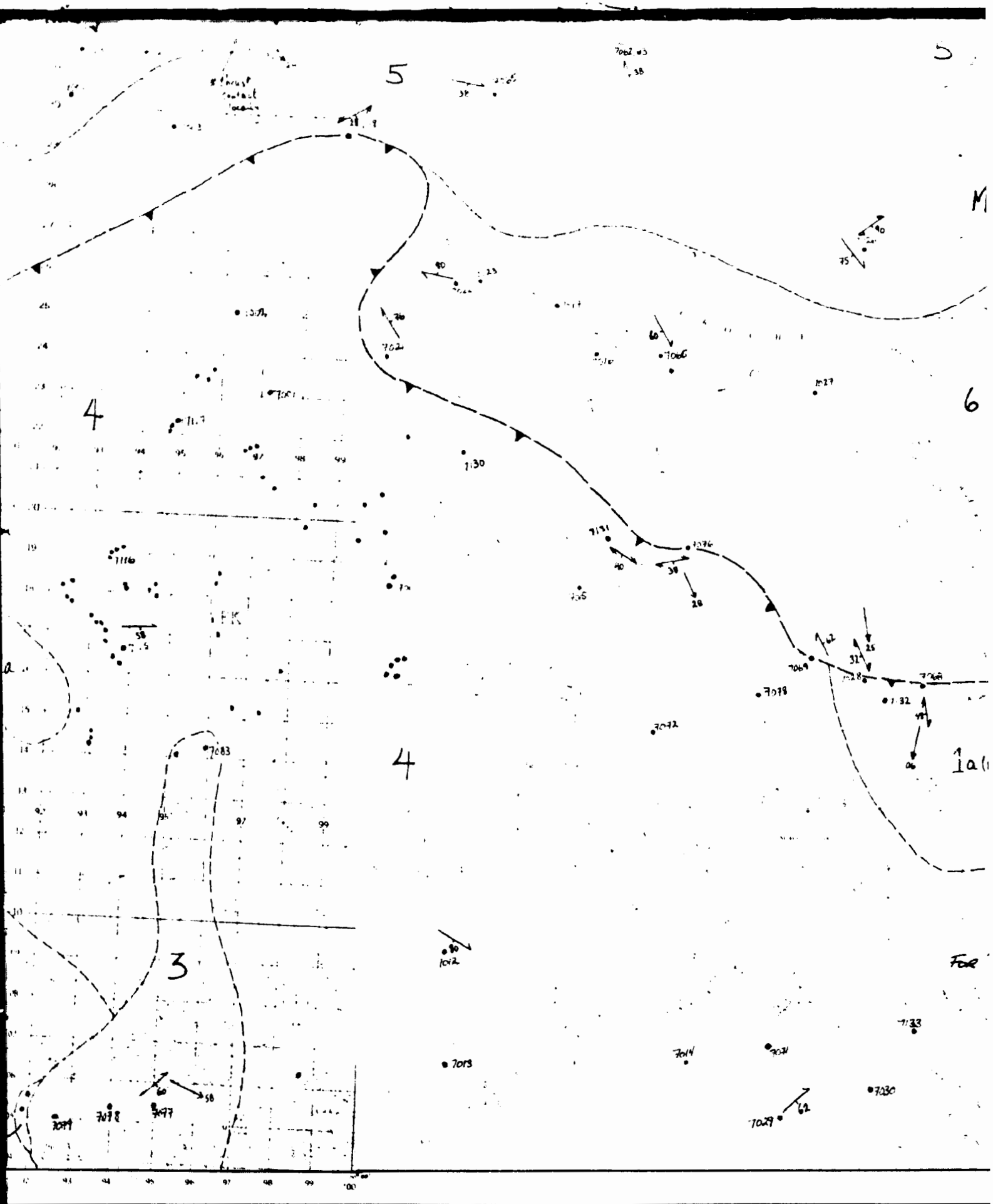
5
4
3
6
7130
7066
7072
7083
7078
7077
7013
7014
7030
7029
7133
7069
7068
7072
7076
7131
7116
7096
7078
7032
7031
7033
7062 #3
38
90
23
80
75
60
58
40
39
28
32
25
42
99
96
94
91
88
100

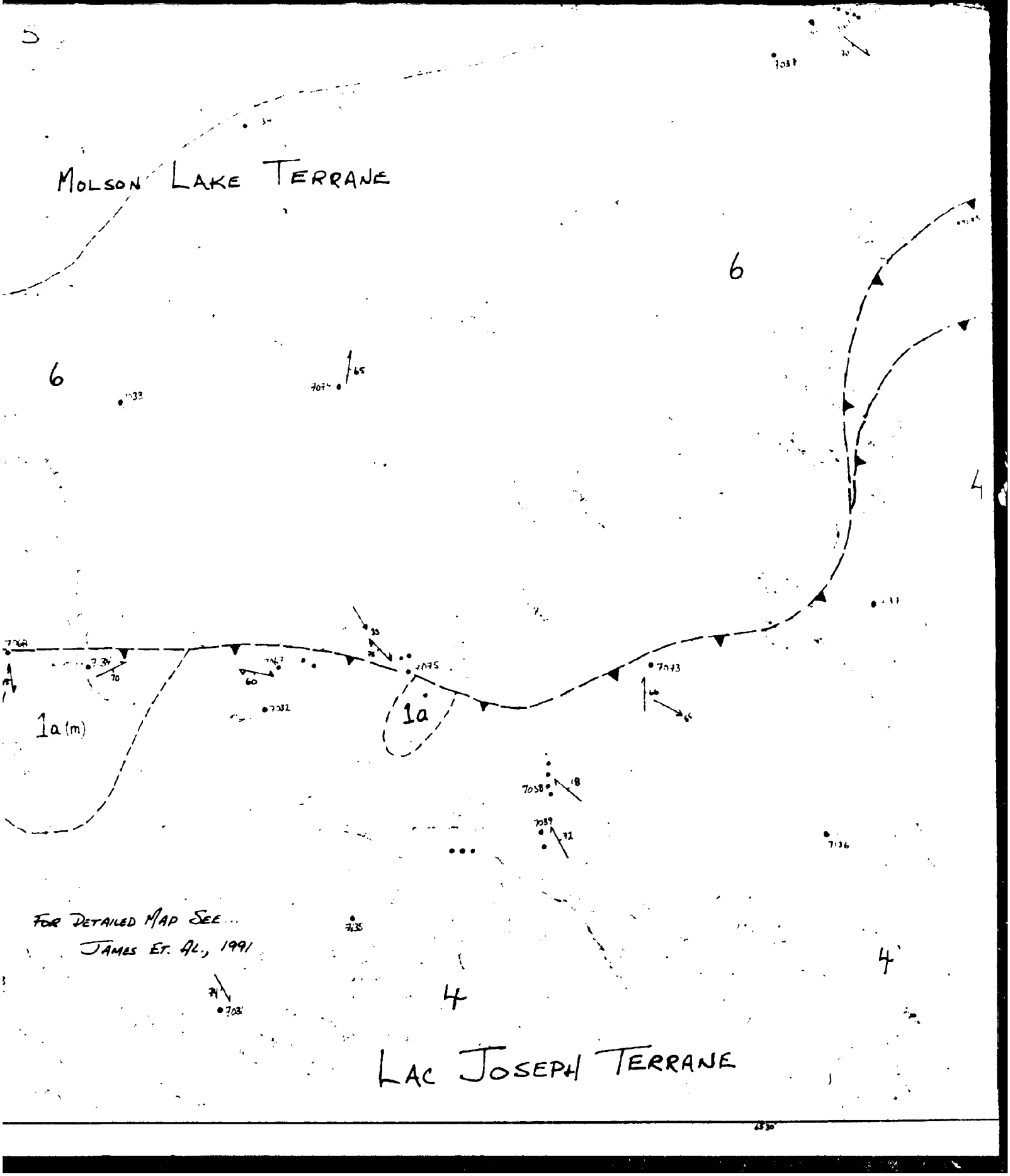
MOLSON LAKE TERRANE
6
6
4
4
4
1a (m)
1a
FOR DETAILED MAP SEE...
JAMES ET. AL., 1991
LAC JOSEPH TERRANE

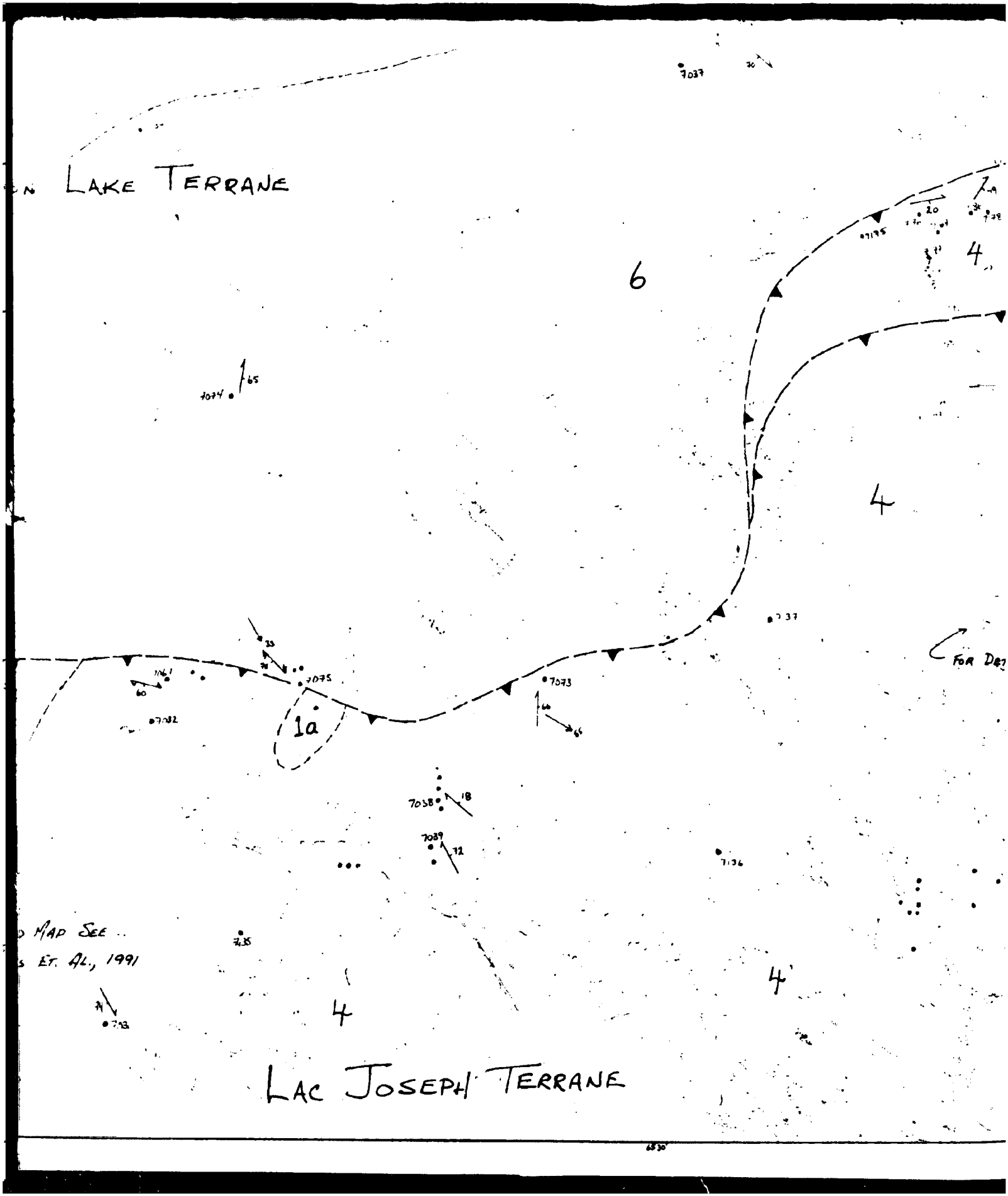
LAKE TERRANE
6
4
4
4
4
1a
7037
7074
7075
7073
7038
7039
7136
7138
7137
FOR DET
LAC JOSEPH TERRANE

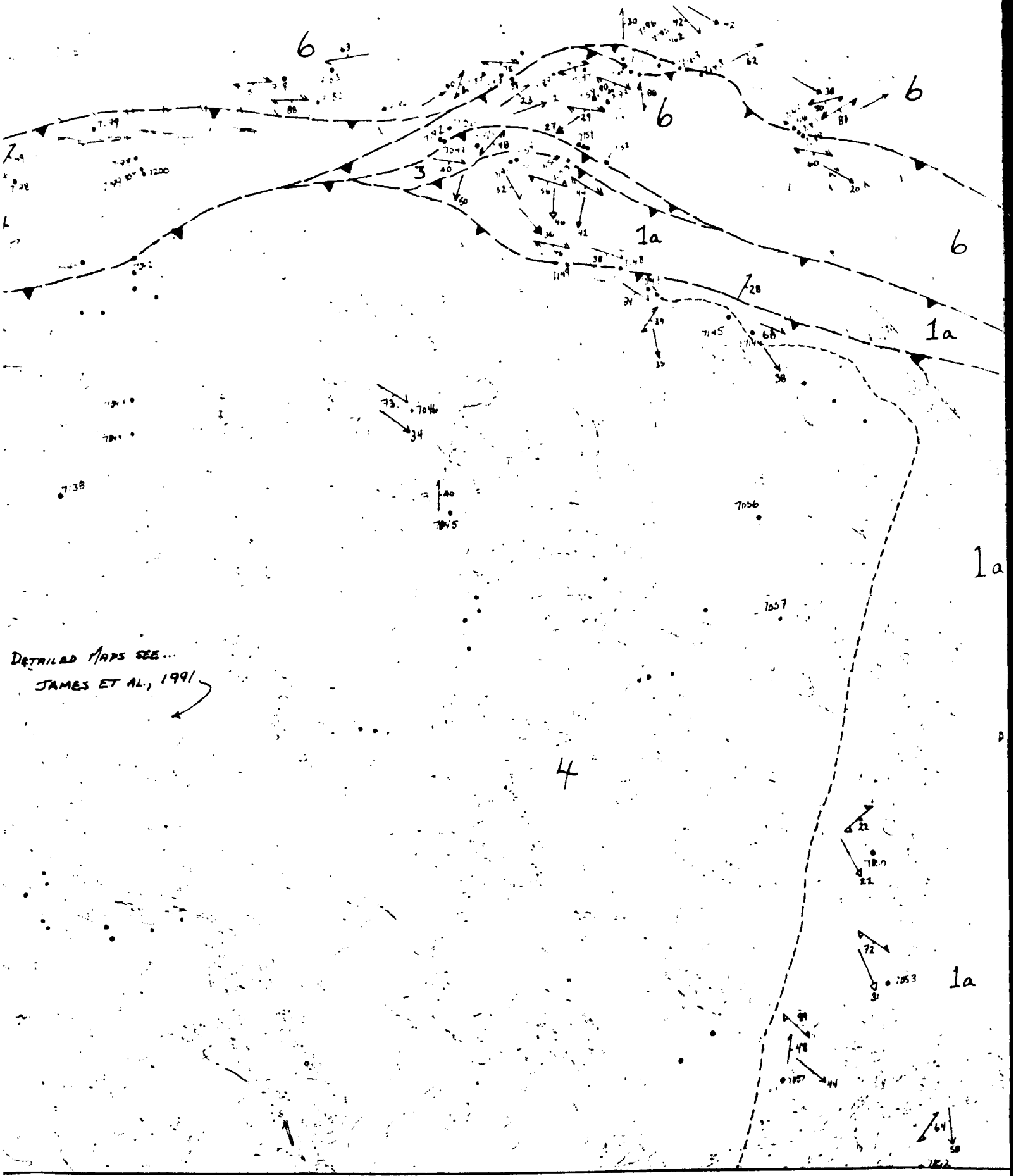
6
6
6
6
3
1a
1a
1a
4
DETAILED MAPS SEE...
JAMES ET AL., 1991

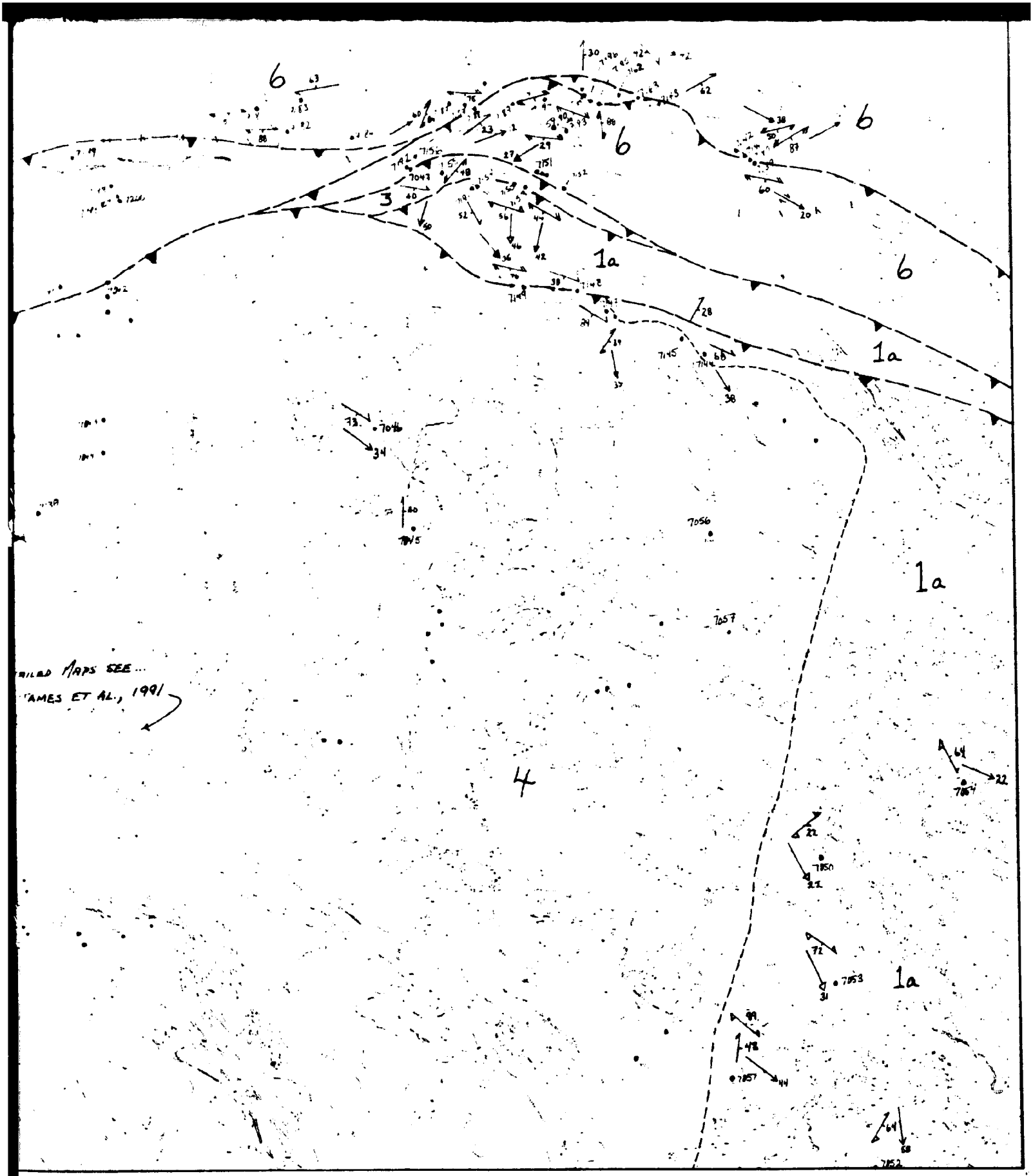
6
6
6
6
3
1a
1a
1a
1a
4
7046
7056
7057
7145
7151
7850
7853
7857
7852
TAILED MAPS SEE...
TAMES ET AL., 1991